



HAL
open science

Synthesis, structural and supramolecular studies of linear and cyclic 2 1- $[\alpha/\text{aza}]$ -oligomers

Ibrahim Mohamed Ibrahim Abdelmoneim

► To cite this version:

Ibrahim Mohamed Ibrahim Abdelmoneim. Synthesis, structural and supramolecular studies of linear and cyclic 2 1- $[\alpha/\text{aza}]$ -oligomers. Chemical and Process Engineering. Université de Lorraine, 2017. English. NNT : 2017LORR0159 . tel-01905002

HAL Id: tel-01905002

<https://hal.univ-lorraine.fr/tel-01905002>

Submitted on 27 Sep 2021

HAL is a multi-disciplinary open access archive for the deposit and dissemination of scientific research documents, whether they are published or not. The documents may come from teaching and research institutions in France or abroad, or from public or private research centers.

L'archive ouverte pluridisciplinaire **HAL**, est destinée au dépôt et à la diffusion de documents scientifiques de niveau recherche, publiés ou non, émanant des établissements d'enseignement et de recherche français ou étrangers, des laboratoires publics ou privés.



AVERTISSEMENT

Ce document est le fruit d'un long travail approuvé par le jury de soutenance et mis à disposition de l'ensemble de la communauté universitaire élargie.

Il est soumis à la propriété intellectuelle de l'auteur. Ceci implique une obligation de citation et de référencement lors de l'utilisation de ce document.

D'autre part, toute contrefaçon, plagiat, reproduction illicite encourt une poursuite pénale.

Contact : ddoc-theses-contact@univ-lorraine.fr

LIENS

Code de la Propriété Intellectuelle. articles L 122. 4

Code de la Propriété Intellectuelle. articles L 335.2- L 335.10

http://www.cfcopies.com/V2/leg/leg_droi.php

<http://www.culture.gouv.fr/culture/infos-pratiques/droits/protection.htm>



Thesis

Doctoral School RP2E
Science and Engineering, Resources, Processes, Products and Environment

Synthesis, structural and supramolecular studies of linear and cyclic 2:1- $[\alpha/\text{aza}]$ -oligomers

Presented and defended publically by

Mohamed Ibrahim ABDELMONEIM IBRAHIM

21 September, 2017

To obtain the degree of

Doctor of the Université de Lorraine

Specialty : Génie des Procédés et des Produits

Jury members

Maïté PATERNOSTRE	DR, I2BC, CEA de Saclay	Reviewer
Gilles SUBRA	Prof., IBMM, Université de Montpellier	Reviewer
Philippe LE GREL	MCF, ISCR, Université de Rennes 1	Examinator
Brigitte JAMART-GREGOIRE	Prof., LCPM, Université de Lorraine	Examinator
Marie-Christine AVERLANT-PETIT	CR, LCPM, Université de Lorraine	Director
Jacques BODIGUEL	MCF, LCPM, Université de Lorraine	Co-Director

Laboratoire de Chimie Physique Macromoléculaire (LCPM), UMR 7375, CNRS-UL
1 Rue Grandville, 54001 Nancy, France

Aknowledgements

After an intensive period of four years, today is the day to write this note of thanks and put the finishing touch on my dissertation. It has been a period of intense learning for me, not only in the scientific arena, but also on a personal level. Writing this dissertation has had a big impact on me. I would like to reflect on the people who have supported and helped me so much throughout this period.

First and foremost, I would like to express my sincere gratitude to my thesis advisor Dr. Marie-Christine Averlant-Petit. It has been an honor to be her Ph.D. student. You have been a tremendous mentor for me, thank you for encouraging my research and for allowing me to grow as a research scientist. Your advices on research as well as on my life have been priceless and helped me come up with the thesis topic. I would also like to express my special appreciation and thanks to my co-advisor Dr. Jacques Bodiguel for the continuous support of my Ph.D. study. Your guidance helped me in the most difficult times of research and writing of this thesis. You gave me the moral support and the freedom I needed to move on and to be a self-independent researcher. Both of you definitely provided me with the tools that I needed to choose the right direction and successfully complete my dissertation.

Besides my advisors, my gratitude is also dedicated to the evaluators of this thesis: Prof. Gilles Subra, Dr. Maité Paternostre, Dr. Philippe Le Grel, and Prof. Brigitte Jamart-Grégoire. It is indeed an honor to have them in the jury of the thesis. I truly appreciate the effort of all the juries to fulfill the task through their insightful and brilliant comments, suggestions and profound questions which incented me to widen my research from various perspectives, thanks to you.

I am also grateful to LCPM staff: Prof. Alain Durand (Director of LCPM), Samir Acherar (MC), Dr. Guillaume Pickaert (MC), Dr. Axelle Arault (MC), and Dr. Loic Stefan (CR), for their unfailing support and assistance during my Ph.D. research. In particular, my sincere thanks go to Dr. Régis Vanderesse, his precious encourages, advices and wisdom instructions had amazing help to achieve the goals of this work,

I praise the enormous amount of help by Mr. Olivier Fabre (LCPM) who had relentlessly entertained my needs for NMR analyses during this research. Thanks to Mrs Mathilde Achard (LCPM) for her assistance in mass analyses. I would especially like to thank Mr. Philippe Arnoux (LRGP) who helped me in photophysical analyses. I can not forget to express my grateful to Dr. Ludovic Colombeau (LRGP) for his wonderful collaboration, he supported me greatly and he was always willing to help me. All of these people have been there to support me when I recruited patients and collected data for my Ph.D. thesis.

I would like to thank my fellow doctoral students, lab mates, office mates and all the friends for their feedback, cooperation and of course friendship, as well as for the stimulating discussions, the sleepless nights we were working together before deadlines, and for all the fun we have had in the last four years.

This is a good chance to express my gratitude to everyone who supported me throughout the course of this research either by direct or indirect way. I am thankful for their aspiring guidance, invaluable constructive criticism and friendly advice during the work. I am sincerely grateful to them for sharing their truthful and illuminating views on a number of issues related to the work.

Last but not the least, I would like to send the fruit of this work to the souls of my parents, words can not express how grateful I am to my beloved family: my sisters, my nieces and my nephews for all of the sacrifices that you've made on my behalf. Thanks for supporting me spiritually throughout the last four years and my life in general. Your prayers for me were and are what sustained me thus far.

Thank you very much!

Merci beaucoup!

شكراً جزيلاً!

Mohamed Ibrahim

Table of Contents

Aknowledgements.....	1
Table of Contents	3
List of Figures.....	9
List of Schemes.....	15
List of Tables.....	16
List of Abbreviations.....	17
General Introduction	20
Objectives of Study	23
Part A Synthesis and Structural Studies of New Linear and Cyclic 2:1-[α /aza]-Oligomers.....	25
Chapter I. Bibliography of Pseudopeptides (Aza-Peptides) and Peptidomimetics.....	26
I.1. Introduction.....	27
I.2. Origin of Pseudopeptides, Peptidomimetics and Foldamers	27
I.3. Structural Features of Peptidic Backbone.....	28
I.4. Conformational Secondary Structures Aspects in Peptides and Pseudopeptides Series	30
I.4.1. Helices.....	31
I.4.2. β -sheets.....	32
I.4.3. β -Strands and β -Hairpins.....	34
I.4.4. Turns.....	34
I.4.4.1. γ -Turns or C_7	34
I.4.4.2. β -Turns or C_{10}	35
I.4.4.2.1. β -Turns in Substituted Diprolines	37
I.4.4.2.2. β -Turns in α , α -Disubstituted Glycine	37
I.4.4.2.3. β -Turns Induced by β - or γ -Amino Acids.....	38
I.5. Structure Modifications of Peptides	39
I.5.1. Pseudopeptides and Peptidomimetics	40
I.5.2. Side Chain Modifications	40
I.5.3. Backbone Modifications.....	40
I.6. Conformational Aspects in Pseudopeptides and Peptidomimetics Series	41
I.6.1. <i>N</i> -Amino peptides.....	41
I.6.2. Peptoids.....	42
I.6.3. β -Peptides.....	42
I.6.4. α -Aminoxypeptides	43
I.6.5. Aza- β^3 -peptides	44
I.6.6. Hydrazino peptides.....	45
I.6.7. Azapeptides.....	47

I.7. History and Biological Interests of Azapeptides.....	51
I.7.1. Preferred Conformations of Azapeptides.....	52
I.7.2 Influences of the Nature of Side Chain and Introducing of an Aza-Amino Acid on the Conformations of Pseudopeptides.....	53
I.7.3. Influence of the Position of Aza-Amino Acid Residue on Azapeptides Conformations...	55
I.7.4. Influence of the Nature of the Amino Acid Preceding the Aza-Amino Acid Residue on the Azapeptides Conformations	57
I.7.5. Relationship between the Configuration of N ^α and the Conformations of Azapeptides .	57
Chapter II. Synthesis and Methods of Analysis of 2:1-[α/aza]-Oligomers.....	60
II.1. Introduction	61
II.2. General Methods of Azapeptides Synthesis	61
II.2.1. Isocyanates Method	61
II.2.2. Activated Esters Method (Activated Carbazate or Carbamate).....	62
II.2.3. Method of Coupling with Acid Chlorides.....	62
II.2.4. Reaction of <i>N</i> -Azolides with Amine Partner	63
II.2.5. Ring Opening of 1,3,4-Oxadiazole-2-(3H)-one with Amine Partner.....	63
II.3. Methods of the Synthesis of Hydrazine Derivatives.....	65
II.4. Synthesis of Azapeptides Oligomers.....	68
II.4.1. Synthesis of Azadipeptides Boc-azaAA-AA-OMe	68
II.4.2. Synthesis of 2:1-[α/aza]-Oligomers	69
II.4.2.1. Synthesis of 2:1-[α/aza]-Trimers	69
II.4.2.2. Synthesis of of 2:1-[α/aza]-Hexamers	71
II.5. Methods for Conformational Analysis.....	72
II.5.1. Infrared Absorption Spectroscopy (IR)	72
II.5.2. Nuclear Magnetic Resonance Spectroscopy (NMR).....	74
II.5.3. X-ray Diffraction.....	77
II.5.4. Molecular Modelling	77
II.5.5. Circular Dichroism (CD).....	78
II.6. Conclusions.....	79
Chapter III. Structural Studies of 2:1-[α/aza]-Oligomers Possessing Lysine Residues	80
III.1. Introduction.....	81
III.2. Conformational Studies of New 2:1-[α/aza]-Trimers.....	82
III.2.1. NMR Spectroscopic Studies of 2:1-[α/aza]-Trimers.....	82
III.2.2. FTIR Spectroscopic Studies of 2:1-[α/aza]-Trimers.....	83
III.2.3. Molecular Dynamic Calculations of 2:1-[α/aza]-Trimers.....	84
III.3. Conformational Studies of 2:1-[α/aza]-Hexamers	88
III.3.1. NMR Spectroscopic Studies of 2:1-[α/aza]-Hexamers	88

III.3.2. FTIR Spectroscopic Studies of 2:1-[α /aza]-Hexamers.....	91
III.3.3. Molecular Dynamic Calculations of 2:1-[α /aza]-Hexamers.....	92
III.4. Conclusions.....	96
Experimental Section.....	97
Bibliographies.....	106
Chapter IV. Impact of C $^{\alpha}$ -Chirality on Supramolecular Self-Assembly of Cyclo-(<i>L</i> - / <i>D</i> -Phe-azaPhe-Ala) ₂ -Hexamers.....	114
Introduction.....	115
Abstract.....	116
IV.1. Introduction.....	116
IV.2. Results and Discussion.....	116
IV.3. Conclusions.....	122
IV.4. Experimental Section.....	122
IV.5. Acknowledgements.....	122
IV.6. References.....	122
Part B 2:1-[α /aza]-Oligomers as Low Molecular Weight Gelators.....	124
Chapter V. Bibliography of Gels and Low Molecular Weight Organo-/Hydro-Gelators.....	125
V.1. General Introduction.....	126
V.2. Review of Literature.....	126
V.2.1. Definition of Gel and Mechanism of Gelation.....	126
V.2.2. Classification of Gels.....	128
V.2.2.1. Classification Based on the Source (Origin).....	128
V.2.2.1.1. Natural Gels.....	128
V.2.2.1.2. Synthetic (Artificial) Gels.....	128
V.2.2.2. Classification Based on Medium of Gelation.....	129
V.2.2.3. Classification Based on the External Stimuli for Gelation.....	129
V.2.2.3.1. Thermo-Responsive Gels.....	129
V.2.2.3.2. pH-Responsive Gels.....	129
V.2.2.3.3. Ultrasonic-Responsive Gels.....	130
V.2.2.3.4. Photo- or Light-Responsive Gels.....	130
V.2.2.3.5. Catalytic and Enzyme-Responsive Gels.....	130
V.2.2.3.6. Magnetic and Electro-Responsive Gels.....	131
V.2.2.4. Classification of Gels Based on the Type of Secondary Interactions.....	131
V.2.3. Characterization of Gels.....	132
V.2.3.1. Visual Inspection.....	132
V.2.3.2. Microscopy.....	132
V.2.3.3. Oscillatory Rheometry and Differential Scanning Calorimetry.....	133

V.2.3.4. X-ray Diffraction	134
V.2.3.5. Other Physical Techniques.....	134
V.2.3.6. Molecular Modelling Methods	135
V.3. Structural Diversity of Low Molecular Weight Organo-Gelators (LMWOGs).....	136
V.3.1. LMWOGs Based on Hydrocarbons, Fatty Acids and Esters	136
V.3.2. LMWOGs Based on Ureas, Bis-ureas and Amides.....	136
V.3.3. LMWOGs Based on Steroids.....	140
V.3.4. LMWOGs Based on Saccharides and their Derivatives (Sorbitols).....	141
V.3.5. LMWOGs Containing Aromatic Moieties	142
V.3.6. LMWOGs Containing Macrocycles.....	144
V.3.7. LMWOGs Based Hybrid Systems.....	146
V.3.8. LMWOGs Based-Amino Acids, Peptides and their Cyclic Derivatives	147
V.3.9. LMWOGs Based on New Families Obtained by LCPM Group.....	151
V.4. Introduction of Low Molecular Weight Hydrogelators (LMWHGs)	153
V.4.1. Structural Diversity of Low Molecular Weight Hydro-Gelators.....	153
V.4.1.1. LMWHGs Based on Small Organic Molecules.....	153
V.4.1.2. LMWHGs Based on Long-Chain or Rigid Hydrocarbons.....	154
V.4.1.3. LMWHGs Based on Urea, Bisureas and Bisamids.....	155
V.4.1.4 Hydrogelators Containing Polyhydroxyl Groups.....	156
V.4.1.5. Bolaamphiphilic Hydrogelators	157
V.4.1.6. Hydrogelators Bearing a Cavity	158
V.4.1.7. Hydrogelators Containing a Polyaromatic Core.....	158
V.4.1.8. Other Homotypic Hydrogelators	159
V.4.1.9. Hydrogelators Composed of Two Components.....	160
V.4.2. Inorganic–Organic Hybrid Hydrogels.....	161
V.4.2.1. Hydrogelators Containing Carboxylic Groups as Ligands.....	162
V.4.2.2. Hydrogelators Coordinating <i>via</i> Nitrogen(s).....	162
V.4.3. Hydrogels Based on Amino Acids, Peptides and their Derivatives	163
V.4.3.1. Amino Acid Derivatives	163
V.4.3.1.1. Amino Acid Derivatives Containing Alkyl Chain(s)	163
V.4.3.1.2. Ionic Amino Acid Derivatives	164
V.4.3.1.3. Amino Acid Derivatives Containing Aromatic Group(s)	165
V.4.3.1.4. Amino Acid-Based Bolaamphiphiles.....	166
V.4.3.2. Peptides.....	166
V.4.3.3. Peptide Derivatives	169
V.4.3.3.1. Peptides with Capped <i>N</i> - and/or <i>C</i> -Terminals	169
V.4.3.3.2. Peptide Derivatives Containing Alkyl Chain(s)	170

V.4.3.3.3. Peptide Derivatives Containing Aromatic Group(s)	171
V.4.3.3.4. Peptide Derivatives Containing a Photoresponsive Group	173
V.4.3.3.5. Peptide Bolaamphiphiles.....	174
V.4.4. Hydrogels Based on Nucleobase Derivatives	174
V.4.4.1. Homotypic Hydrogels Based on Nucleobases.....	174
V.4.4.2. Multicomponent Hydrogels Based on Nucleobases	175
V.4.5. Hydrogels Based on Saccharides	176
V.4.5.1. Monosaccharide-Based Hydrogelators.....	176
V.4.5.2. Oligosaccharide-Based Hydrogelators.....	178
Chapter VI. Supramolecular Organogels Based on Heterochiral Cyclo-(<i>D</i>-Phe-azaPhe-Ala)₂-Hexamer.....	180
VI.1. Introduction.....	181
VI.2. Gelation Behaviors of Cyclo-(<i>D</i> -Phe-azaPhe-Ala) ₂ -Hexamer.....	181
VI.3. NMR Spectroscopic Studies of Cyclo-(<i>D</i> -Phe-azaPhe-Ala) ₂ -Hexamer.....	183
VI.3.1. At Diluted Conditions.....	183
VI.3.2. Concentration-Dependent ¹ H NMR Studies.....	183
VI.3.3. Temperature-Dependent ¹ H NMR Studies.....	185
VI.4. FTIR Spectroscopic Studies of Cyclo-(<i>D</i> -Phe-azaPhe-Ala) ₂ -Hexamer	188
VI.4.1. Concentration-Dependent FTIR Studies	188
VI.4.2. Temperature-Dependent FTIR Studies	190
VI.5. Rheological Studies.....	192
VI.6. Morphological Studies.....	196
VI.7. Experimental Section	197
Chapter VII. Supramolecular Hydrogels Based on 2:1-[α/aza]-Trimers	200
VII.1. Introduction	201
VII.2. Synthesis and Characterizations of Fmoc- <i>L</i> - or <i>D</i> -Phe-azaPhe-Ala-OH.....	202
VII.3. Structural and Conformational Studies of Fmoc- <i>L</i> - or <i>D</i> -Phe-azaPhe-Ala-OH.....	202
VII.3.1. X-ray Crystallographic Data.....	202
VII.3.2. NMR Spectroscopic Studies	206
VII.3.3. FTIR Spectroscopic Studies.....	209
VII.3.4. Molecular Dynamic Calculations (AMBER 12).....	210
VII.4. Characterization of Low Molecular Weight Hydrogels from 7a' and 7b'.....	211
VII.4.1. Gel Preparation and Minimum Gelation Concentrations (MGCs)	211
VII.4.2. UV-visible Absorption and Fluorescence Emission Spectroscopic Studies	213
VII.4.3. Circular Dichroism (CD) Spectroscopic Studies.....	215
VII.4.4. ATR-FTIR Spectroscopic Studies	216
VII.4.5. Rheological Studies	218

VII.4.6. Morphological Studies	221
VII.5. Conclusions.....	222
VII.6. Experimental Section.....	222
Bibliographies.....	226
Part C Applications Based on 2:1-[α/aza]-Oligomers.....	243
Chapter VIII. Evaluation of the 2:1-[α/aza]-Oligomers in Two Potential applications.....	244
VIII.1. General Introduction.....	245
VIII.2. Gases Separation.....	245
VIII.2.1. Introduction.....	245
VIII.2.2. Results and Discussion.....	246
VIII.2.3. Conclusions	249
VIII.3. Phase Selective Gelation (PSG)	249
VIII.3.1. Introduction.....	249
VIII.3.2. Results and Discussion.....	250
VIII.3.3. Conclusions	251
VIII.4. Experimental Section.....	252
Bibliographies.....	253
General Conclusions and Perspectives.....	255
Appendices.....	i
Résumé.....	xlv

List of Figures

Figure 1.1. Representation of the basic structures of proteins.....	27
Figure 1.2. Representation of the chemical structures of: (a) amino acid, and (b) peptide chain.....	27
Figure 1.3. Representation of: (a) peptide bond formation, (b) double bond character of peptide bond, and (c) torsion angles within the peptide backbone	29
Figure 1.4. Representation of: (a, b) the planar arrangement, and (c) <i>trans/cis</i> -isomerization within the peptide bond.....	29
Figure 1.5. Representation of the principle intramolecular hydrogen bonds in peptides backbones.....	30
Figure 1.6. Ramachandran diagram shows the allowed and disfavored values of phi and psi (ϕ , ψ) in proteins.....	30
Figure 1.7. (a-d) Representation of different views of helix structure, (e) Ramachandran diagram of α -helices in protein, and (f) principle intramolecular hydrogen bonds in different types of helices in <i>L</i> - α -peptides.....	31
Figure 1.8. Different types of β -amino acids.....	32
Figure 1.9. Representation of different types of helices in β -peptides.....	32
Figure 1.10. (a) Helix-14 in <i>trans</i> -ACHC, and (b) helix-12 in <i>trans</i> -ACPC.....	32
Figure 1.11. Representation of: (a, b) parallel β -sheet, and (c, d) antiparallel β -sheet.....	33
Figure 1.12. Ramachandran plot of β -sheets in peptides and proteins.....	33
Figure 1.13. (a) Representation of β -hairpin, and (b) hydrogen bonds between two antiparallel β -strands joined together by a loop	34
Figure 1.14. Types of γ -turns.....	35
Figure 1.15. (a) Representation of ($i \leftrightarrow i + 3$) hydrogen bonding interaction in β -turn, (b) distance between C^α (i) and C^α ($i + 3$) atoms in β -turn, and (c-f) representation of the common types of β -turns in peptides.....	35
Figure 1.16. The most common types of β -turns: (a) β I-turn, and (b) β II-turn.....	36
Figure 1.17. ORTEP views for: (a) Tos- <i>D</i> -Pro-(<i>trans</i> -3-Me)- <i>D</i> -Pro-NH ₂ , and (b) Tos- <i>D</i> -Pro-(<i>cis</i> -3-Me)- <i>D</i> -Pro-NH ₂ with crystallographic numbering system.....	37
Figure 1.18. Crystal structure of Boc- <i>L</i> -(α Me)Nva-Aib-Aib- <i>L</i> -(α Me)Nva-Aib-OMe.....	37
Figure 1.19. Crystal structures illustrating: (a) β -turn in Z-(Ac ₄ C) ₃ -Ot-Bu, and (b) 3_{10} -helix in Z-(Ac ₉ C) ₅ -Ot-Bu.....	38
Figure 1.20. β -turn conformation of the tripeptide cyclohexane- β , β -disubstituted β -amino acid in solid state.....	38
Figure 1.21. Crystal structure (X-ray) of the dipeptide 2, 4-disubstitued γ -amino acids.....	39
Figure 1.22. Selected examples of peptide modifications.....	39
Figure 1.23. (a) Crystal structure of Piv-Pro- <i>N</i> ^{α} (<i>N</i> ^{β} H ₂)-Gly-NH <i>i</i> -Pr, and (b) C ₈ -hydrogen bond formation in 1:1-[α / <i>N</i> -amino]-tetramer.....	41
Figure 1.24. Peptide <i>versus</i> peptoid sequences.....	42
Figure 1.25. Different types β -amino acids.....	42
Figure 1.26. Representaion of α -amino acid, β -amino acid and α -aminoxy acid.....	43
Figure 1.27. Examples of the N-O turn in three types of α -aminoxy derivatives.....	43
Figure 1.28. (a) NOE correlations in solution, and (b) crystal structure of α -aminoxytriamide... ..	44
Figure 1.29. NOE correlations observed in ROESY of 1:1-[α / α -aminoxy]-mer.....	44
Figure 1.30. Representation of aza- β^3 -peptide derivative of <i>N</i> ^{α} -substituted- <i>N</i> ^{β} -protected- α -hydrazinoacetic acid.....	44
Figure 1.31. (a) NOE correlations in solution of aza- β^3 -peptide amide monomer, and (b) crystal structure of aza- β^3 -peptide amide dimer.....	45
Figure 1.32. Representation of α -amino acid, β -amino acid and α -hydrazinoacid.....	45

Figure 1.33. Crystal structure of Piv-Pro-N ^β H-N ^α Bn-CH ₂ -CO-NH <i>i</i> -Pr.....	45
Figure 1.34. Possible hydrogen bonds network in hydrazinopeptides.....	46
Figure 1.35. The primary C ^α -substituted- α -hydrazinohexapeptides.....	46
Figure 1.36. Possible hydrogen bonds network in the octamer 1:1-[α / α -N ^α -Z-hydrazino]-ester.....	47
Figure 1.37. Crystal structure of Piv-Pro-azaAla-NH <i>i</i> -Pr.....	47
Figure 1.38. (a) Hydrogen bonds network in Boc-(Phe-azaAla-Ala) ₂ -OMe, and (b) molecular crystal structure of Boc-Phe-azaPhe-Ala-OMe.....	48
Figure 1.39. ROE correlations from 2D ROESY in solution for: (a) homochiral trimer, (b) heterochiral trimer. Molecular modelling calculations based on NMR structural constraints for: (c) homochiral trimer, and (d) heterochiral trimer; (Boc- <i>L</i> - or <i>D</i> -Phe-azaPhe-Ala-OMe).....	49
Figure 1.40. Models show the main conformations obtained by molecular modelling calculations based on NMR constraints for: (a) Boc-(Phe-azaPhe-Ala) ₂ -OMe, (b) Boc-(<i>D</i> -Phe-azaPhe-Ala) ₂ -OMe, (c and d) representations for the intramolecular hydrogen bonds in homo and heterohexamer Boc-(<i>L</i> - or <i>D</i> -Phe-azaPhe-Ala) ₂ -OMe, respectively.....	50
Figure 1.41. Representation of the main conformations adopted by Boc-(Phe-azaPhe-Ala) ₂ -OMe in solid state (X-ray).....	50
Figure 1.42. Azapeptide analog of angiotensin bovine II.....	51
Figure 1.43. Representation of atazanavir azapeptide inhibitor against HIV protease.....	51
Figure 1.44. Elements of azapeptide.....	52
Figure 1.45. Illustration of the torsion angles in: (a) For-azaXaa-NH ₂ (Xaa = Gly, Ala, Leu), and (b) Ac-azaPhe-NHMe.....	53
Figure 1.46. Superposition of the lowest energy structures for the tripeptides obtained by molecular dynamics based on NMR structural constraints.....	53
Figure 1.47. Crystal structures of the azapeptides: (a) <i>Z</i> -azaAsn(Me)-Pro-NH <i>i</i> -Pr, (b) <i>Z</i> -azaAsp(OEt)-Pro-NH <i>i</i> -Pr, and (c) Boc-azaAla-Pro-NH <i>i</i> -Pr.....	54
Figure 1.48. Solid state structure of Piv-Pro-azaAsn(Me)-NH <i>i</i> -Pr.....	55
Figure 1.49. Structural formula of the compound For-Ala-azaAla-NH ₂ and its most stable conformation at the HF/6-31G* theory level.....	55
Figure 1.50. (a) NOE correlations in Boc-Ala-Phe-azaLeu-Ala-OMe, and (b) superposition of the lowest energy structures obtained from molecular dynamic calculations based on NOE constraints.....	56
Figure 1.51. X-ray structures of: <i>Z</i> -azaAsn(Me)-Pro-NH <i>i</i> -Pr, and Piv-Pro-azaAsn(Me)-NH <i>i</i> -Pr.....	56
Figure 1.52. Superposition of the lowest energy structures of the tripeptides Boc-Xaa-azaPhe-Ala-OMe [(Xaa = Gly (1), Ala (2), Phe (3), Asp (4))]; obtained from molecular dynamics based on NOE constraints.....	57
Figure 1.53. Solid state structure of the compound <i>Z</i> -azaAsp(OEt)-Pro-NH <i>i</i> -Pr.....	58
Figure 1.54. Structural formula of 1:1-[α /aza]-oligomers and 2:1-[α /aza]-oligomers.....	58
Figure 2.1. Structural formula of 1:1-[α /aza]-oligomers and 2:1-[α /aza]-oligomers.....	61
Figure 2.2. Nomenclature of 1:1-[α /aza]-oligomers.....	68
Figure 2.3. Nomenclature of 2:1-[α /aza]-oligomers.....	69
Figure 2.4. FTIR spectra of an oligomer, n = 2 - 6, 8.....	73
Figure 2.5. Deconvolution of the experimental spectrum of Boc-Phe-azaPhe-Ala-OMe.....	73
Figure 2.6. Influence of the addition of DMSO- <i>d</i> ₆ on the chemical shifts of the NH protons of Boc-Phe-azaPhe-Ala-OMe.....	75
Figure 2.7. Values of $\Delta\delta$ in different primary amides.....	75
Figure 2.8. ROESY spectrum of Boc-Phe-azaPhe-Ala-OMe.....	76
Figure 2.9. Crystal structure of Boc-Phe-azaPhe-Ala-OMe.....	77
Figure 2.10. Structure of Boc-Phe-azaPhe-Ala-OMe using molecular dynamic calculations based on NMR structural constraints.....	78

Figure 2.11. The CD dataset of 4 standard secondary structures of (Poly- <i>L</i> -glutamic, ddH ₂ O): (a) helix, (b) sheet, (c) random coil, and (d) turn.....	79
Figure 3.1. Molecular structures of 2:1-[α /aza]-trimers and hexamers.....	81
Figure 3.2. Molecular structures of 2:1-[α /aza]-trimers for: (7c) left, and (7d) right.....	82
Figure 3.3. ROE correlations of β II- and β II'-turn conformations in 7c (left) and 7d (right), respectively; (300 MHz, 3.0 mmol. L ⁻¹ , CDCl ₃ , 300 K).	82
Figure 3.4. Chemical shift-variations (δ) of NH protons for: (a) 7c , and (b) 7d as a function of % [CDCl ₃ /DMSO- <i>d</i> ₆] mixtures.	83
Figure 3.5. FTIR spectra belong to the NH vibration stretching region for: (a) 7c , and (b) 7d (3.0 mmol. L ⁻¹ , CDCl ₃).....	83
Figure 3.6. FTIR spectra belong to the CO vibration stretching region for for: (a) 7c , and (b) 7d (3.0 mmol. L ⁻¹ , CDCl ₃).	84
Figure 3.7. Selected frames for molecule 7c issued of molecular dynamic simulations, illustrating different intramolecular hydrogen bonds.	86
Figure 3.8. Selected frames for molecule 8c issued of molecular dynamic simulations, illustrating different intramolecular hydrogen bonds.	87
Figure 3.9. Molecular structures of 2:1-[α /aza]-Hexamers for: (8c) left, and (8d) right.	88
Figure 3.10. ROE correlations of β -turn conformations in: (8c) left, and (8d) right; (300 MHz, 4.0 mmol. L ⁻¹ , CDCl ₃ , 300 K).....	89
Figure 3.11. Chemical shift-variations (δ) of NH protons for: (a) 8c , and (b) 8d as a function of % [CDCl ₃ /DMSO- <i>d</i> ₆] mixtures.	90
Figure 3.12. FTIR spectra belong to the NH (up spectra), and CO (bottom spectra) stretching regions for: (a & c) 8c , and (b & d) 8d ; (3.0 mmol. L ⁻¹ , CDCl ₃).	91
Figure 3.13. Selected frames for molecule 8c issued of molecular dynamic simulations, illustrating different intramolecular hydrogen bonds.	94
Figure 3.14. Selected frames for molecule 8d issued of molecular dynamic simulations, illustrating different intramolecular hydrogen bonds.	95
Figure 4.1. Models show the main conformations obtained by molecular modelling calculations based on NMR constraints for: (8a) left, (8b) right.....	115
Figure 4.2. Crystal molecular structure of compound 9a (X-ray): (a) top view, and (b) side view. Illustrating the intermolecular hydrogen bonds and intramolecular hydrogen bonds	118
Figure 4.3. View of compound 9b in the crystal state (X-ray): (a) top view, and (b) side view. Illustrating the intermolecular and intramolecular hydrogen bonds.....	118
Figure 4.4. ROE correlations observed in the two conformers: L (left), and M (right); (0.5 mmol. L ⁻¹ , CDCl ₃).....	119
Figure 4.5. (a) View of the crystal state from X-ray of compound 9a , <i>versus</i> (b) the model of the most energetically favorable monomer using Amber 10 program.....	119
Figure 4.6. Chemical shift-variations (δ) of NH protons for: (a) 9a , and (b) 9b as a function of % [CDCl ₃ /DMSO- <i>d</i> ₆ ; 3.0 mmol. L ⁻¹] mixtures.	119
Figure 4.7. FTIR spectra belong to the NH stretching region (left spectra), and CO stretching region (right spectra) for: (a) 9a , and (b) 9b ; (0.8 mmol. L ⁻¹ , CDCl ₃).....	121
Figure 4.8. Normalized concentration-dependent FTIR spectra for NH stretching region of: (a) 9a , and (b) 9b ; (1.0 to 8.0 mmol. L ⁻¹ , CDCl ₃).....	121
Figure 5.1. Schematic illustration of the gelation process.	127
Figure 5.2. LMWOGs based on alkanes, fatty acids and esters.....	136
Figure 5.3. LMWOGs based on ureas.....	137
Figure 5.4. LMWOGs based on bis-ureas and tris-ureas.....	138
Figure 5.5. LMWOGs based on bis-amides.....	139
Figure 5.6. LMWOGs based on steroids.	140

Figure 5.7. LMWOGs based on saccharides.....	141
Figure 5.8. LMWOGs based on sorbitols.....	142
Figure 5.9. LMWOGs based on aromatic cores.	143
Figure 5.10. LMWOGs containing macrocycles.	145
Figure 5.11. LMWOGs based-hybrid systems.....	146
Figure 5.12. LMWOGs based on α -amino acid (<i>L</i> -alanine).	147
Figure 5.13. LMWOGs based on acylated amino acids.	148
Figure 5.14. LMWOGs based on bis-amino acids.....	149
Figure 5.15. LMWOGs based cyclic Val-Gly dipeptide.	150
Figure 5.16. LMWOGs based on amino acid derivatives.....	151
Figure 5.17. LMWOGs based on cyclo-1:1-[α/α - <i>N</i> ^{α} -Bn-hydrazino]-mers.	151
Figure 5.18. Number of papers per year, searching by the topic of “hydrogels” from Web of Science database, Feb./2017.....	153
Figure 5.19. Molecular structures of long-alkyl-chain-containing hydrogelators 154	154
Figure 5.20. Molecular structures of rigid-hydrocarbons-containing hydrogelators.	154
Figure 5.21. LMWHGs based on urea and bisureas.	155
Figure 5.22. LMWHGs based on bisamides.	156
Figure 5.23. LMWHGs containing polyhydroxyl groups.....	156
Figure 5.24. LMWHGs based on bolaamphiphiles.....	157
Figure 5.25. LMWHGs possessing a cavity.....	158
Figure 5.26. LMWHGs possessing polyaromatic moities.....	158
Figure 5.27. Representative molecular structures of other homotypic LMWHGs.....	159
Figure 5.28. Representative molecular structures of the photosensitive LMWHG 160	160
Figure 5.29. Representative molecular structures of two-component LMWHGs.	160
Figure 5.30. Representative molecular structures of other two components LMWHGs.....	161
Figure 5.31. LMWHGs containing carboxylic group(s).	162
Figure 5. 32. Hydrogels based on coordination <i>via</i> nitrogen(s).....	163
Figure 5.33. Hydrogelators based on amino acid bearing long alkyl chain.	164
Figure 5.34. Hydrogelators based on ionic amino acid derivatives bearing long alkyl chain.	164
Figure 5.35. LMWHGs based on amino acid derivatives bearing aromatic moities.	165
Figure 5.36. Amino acid-based amphiphile as LMWHG.....	166
Figure 5.37. Representative molecular structures of LMWHGs based on different peptides.....	168
Figure 5.38. Molecular structures of peptidic LMWHGs with capped <i>N</i> -terminal.....	169
Figure 5.39. Representative molecular structures of LMWHGs based on peptide derivatives bearing long alkyl chain.	170
Figure 5.40. Representative molecular structures of LMWHGs based on peptide derivatives bearing aromatic moities.....	171
Figure 5.41. Representative molecular structures of LMWHGs based on peptide derivatives bearing pyrene as an aromatic moiety.....	172
Figure 5.42. LMWHGs based peptide derivatives bearing photosensitive azobenzene group....	173
Figure 5.43. Representative molecular structures of peptide-based amphiphiles as LMWHGs. 174	174
Figure 5.44. Examples of homotypic LMWHGs containing nucleobases.	175
Figure 5.45. Examples of multicomponents LMWHGs based on nucleobases.....	176
Figure 5.46. Molecular structures of monosaccharide based one-component LMWHGs.....	177
Figure 5.47. Other examples of monosaccharide based one-component LMWHGs.....	177
Figure 5.48. Molecular structures of some LMWHGs based on oligosaccharides.....	178
Figure 6.1. Molecular structure of heterochiral cyclo-(<i>D</i> -Phe-azaPhe-Ala) ₂ -hexamer (9b).....	181
Figure 6.2. (a) Gelation tests in different solvents, and (b) aerogel of 9b from toluene obtained under supercritical CO ₂ -drying condition.....	182

Figure 6.3. ROE correlations of β -turn conformations in the two conformers V and W from ROESY experiment in toluene- d_8 ; (1.0 mmol. L ⁻¹ , 293 K).....	183
Figure 6.4. Concentration-dependent ¹ H NMR (600 MHz) spectra show chemical shifts (δ ppm) of NH protons for compound 9b in toluene- d_8 ; (c = 0.1 to 6.0 mmol. L ⁻¹).....	184
Figure 6.5a. Temperature-dependent ¹ H NMR (300 MHz) of gelator 9b in toluene- d_8 ; (c = 0.5 wt%).....	185
Figure 6.5b. Temperature-dependent ¹ H NMR (300 MHz) of compound 9b in gel state; (0.5 wt% in benzene- d_6).....	186
Figure 6.5c. Temperature-dependent ¹ H NMR (300 MHz) of compound 9b in gel state; (0.5 wt% in chlorobenzene- d_5).....	186
Figure 6.5d. Temperature-dependent ¹ H NMR (300 MHz) of compound 9b in gel state; (0.5 wt% in <i>p</i> -xylene- d_{10}).....	187
Figure 6.6. Concentration-dependent FTIR of 9b in toluene- d_8 ; (c = 0.8 to 3.0 mmol. L ⁻¹).	188
Figure 6.7. Comparison of the ATR-FTIR spectra in the crystal, aerogel, and xerogel states for 9b : (a) NH stretching region, and (b) CO stretching region.....	189
Figure 6.8. Temperature-dependent FTIR spectra from 25 °C to 90 °C of toluene- d_8 gel from 9b at c = 0.5 wt%; (a) NH stretching region, and (b) CO stretching region.....	190
Figure 6.9a. Temperature-dependent FTIR spectra from 25 °C to 70 °C of benzene- d_6 gel from 9b at c = 0.5 wt%; NH stretching region (left), and CO stretching region (right).....	191
Figure 6.9b. Temperature-dependent FTIR spectra from 25 °C to 90 °C of chlorobenzene- d_5 gel from 9b at c = 0.5 wt%; NH stretching region (left), and CO stretching region (right).....	191
Figure 6.9c. Temperature-dependent FTIR spectra from 25 °C to 90 °C of <i>p</i> -xylene- d_{10} gel from 9b at c = 0.5 wt%; NH stretching region (left), and CO stretching region (right).....	191
Figure 6.10. Gel-to-sol transition temperature (T _g) using FTIR for toluene- d_8 gel from 9b at 0.5 wt%.....	192
Figure 6.11. Oscillatory stress sweep experiments (OSS) for organogels of 9b ; (c = 0.5 wt%, ω = 0.63 rad. s ⁻¹ , T = 25 °C).....	193
Figure 6.12. The rheogram shows the oscillatory time sweep experiments (OTS) for the organogels from 9b ; (c = 0.5 wt%, ω = 0.628 rad. s ⁻¹ , σ = 1.5 Pa, T = 25 °C).....	193
Figure 6.13. Oscillatory frequency sweep experiments (OFS) for organogels of 9b ; (c = 0.5 wt%, σ = 1.5 Pa, T = 25 °C).....	194
Figure 6.14. Oscillatory temperature sweep experiment shows the transition temperature of gel 9b from toluene at ~ 67 °C; (c = 0.5 wt%, σ = 1.5 Pa, ω = 0.628 rad. s ⁻¹).	195
Figure 6.15. Variations of T _g (°C) as a function of concentration (wt%) for the organogels of 9b from different gelified solvents.....	195
Figure 6.16. The rheogram of the oscillatory frequency sweep experiments (OFS), at the T _g of toluene gel from 9b ; (c = 0.5 wt %, T = 65 °C, σ = 1.5 Pa).....	196
Figure 6.17. (a-c) SEM images, and (d) TEM image of aerogel of 9b from toluene.....	196
Figure 6.18. SEM images of xerogels obtained from air-drying of organogels of 9b from: (a) toluene, (b) benzene, (c) chlorobenzene, and (d) <i>p</i> -xylene.....	197
Figure 7.1. Molecular structures of Fmoc-FazaFA (7a') and Fmoc- <i>D</i> -FazaFA (7b').....	202
Figure 7.2. Crystal molecular structure (X-ray) of the asymmetric unit of compound 7b' . Illustrating the intramolecular and intermolecular hydrogen bonds.....	203
Figure 7.3. Crystal molecular structure (X-ray) of the conformers P (left), and Q (right). Illustrating the intramolecular hydrogen bonds.....	203
Figure 7.4. View of the packing mode in compound 7b' in crystal state (X-ray) involving asymmetric units: (a) side view, and (b) top view.....	205
Figure 7.5. ROE correlations of β -turn in compound 7a' (left) and β' -turn conformation in compound 7b' (right); (4.0 mmol. L ⁻¹ , DMSO- d_6).....	206

Figure 7.6. Chemical shift-variations (δ) of NH protons for: (a) 7a' , and (b) 7b' as a function of % [CDCl ₃ /DMSO- <i>d</i> ₆] mixtures; (300 MHz, 4.0 mmol. L ⁻¹).....	207
Figure 7.7. Chemical shift-variations (δ) ppm of aromatic protons for: (a) 7a' , and (b) 7b' as a function of % [CDCl ₃ /DMSO- <i>d</i> ₆] mixtures; (300 MHz, 4.0 mmol. L ⁻¹).....	208
Figure 7.8. FTIR spectra belong to the NH stretching region for: (a) 7a' , and (b) 7b' ; (2.0 mmol. L ⁻¹ , CDCl ₃).....	209
Figure 7.9. FTIR spectra belong to CO stretching region for: (a) 7a' , and (b) 7b' ; (2.0 mmol. L ⁻¹ , CDCl ₃).....	209
Figure 7.10. Selected frame for molecule: 7a' (left), and 7b' (right) issued of the molecular dynamic simulations showing the intramolecular hydrogen bond.	210
Figure 7.11. Supramolecular hydrogels from 7a' , and 7b' induced by pH 7.0 and pH 10.0; (c = 1.0 wt%).....	212
Figure 7.12. Effect of insertion of aza-amino acid on the MGCs. Hydrogels obtained from compounds 7a' , and 7b' <i>versus</i> viscous solution from the corresponding peptides without aza-moitiey, Fmoc-FFA, and Fmoc- <i>D</i> -FFA; (1.0 wt%, pH 7.0 and 10.0).....	212
Figure 7.13. UV-visible spectra of: (a) Fmoc-FazaFA (7a') and, (b) Fmoc- <i>D</i> -FazaFA (7b').....	213
Figure 7.14. Concentration gradient fluorescence spectra of: (a) Fmoc-FazaFA (7a') and, (b) Fmoc- <i>D</i> -FazaFA (7b'); (λ_{ex} = 265 nm).....	214
Figure 7.15. Temperature-dependent fluorescence spectra of: (a) Fmoc-FazaFA (7a') and, (b) Fmoc- <i>D</i> -FazaFA (7b'); (25 °C and 90 °C, λ_{ex} = 265 nm).....	214
Figure 7.16. Normalized CD spectra of gel and viscous states for hydrogels from pH 7.0 of: (a) 7a' , and (b) 7b'	215
Figure 7.17. Comparison of the ATR-FTIR spectra in the CO stretching and NH bending regions for the dried gels from: (a) 7a' , and (b) 7b' at pH 7.0 and pH 10.0, <i>versus</i> their solid states.....	217
Figure 7.18. Comparison of the FTIR spectra in the NH stretching region between the solid states and solution states in CDCl ₃ for: (a) 7a' , and (b) 7b'	218
Figure 7.19. Oscillatory stress sweep experiments (OSS) for hydrogels from pH 7.0 of: (a) 7a' , and (b) 7b' ; (c = 2.0 wt%, ω = 0.63 rad. s ⁻¹ , T = 25 °C).	219
Figure 7.20. Oscillatory time sweep experiments (OTS) for hydrogels from pH 7.0 of: (a) 7a' , and (b) 7b' ; (c = 2.0 wt%, ω = 0.63 rad s ⁻¹ , σ = 0.01 Pa, T = 25 °C).	219
Figure 7.21. Oscillatory frequency sweep experiments (OFS) for hydrogels from pH 7.0 of: (a) 7a' , and (b) 7b' ; (c = 2.0 wt%, σ = 1.5 Pa, T = 25 °C).	220
Figure 7.22. SEM images of the dried hydrogels from pH 7.0 (up) and pH 10.0 (bottom) for: (a & c) 7a' and (b & d) 7b'	221
Figure 8.1. Representation of the two pathways followed in preparation of Pebax®-pseudopeptide membranes.	246
Figure 8.2. Chemical structures of the Pebax® co-polymer, and the PEDEGA polymer.....	247
Figure 8.3. Permeability of CO ₂ and selectivity $\alpha_{\text{CO}_2/\text{N}_2}$ for different Pebax®1074 membranes with additives of protected and deprotected pseudopeptides dimer, trimer and hexamer, determined by time-lag method.	248
Figure 8.4. PSG by gelator 9b ; (a) addition of the concentrated ethanolic solution of 9b (c = 12.5 w/v%) to organic/aqueous mixture, (b) gelation of the organic phase, and (c) separation of the organogel by filtration.	250
Figure 8.5. PSG by gelator 9b for individual organic solvent: (a) Toluene, (b) benzene, and (c) <i>p</i> -xylene; (c = 0.5 wt% with respect to the organic solvent).....	251

List of Schemes

Scheme 2.1. Synthesis of azapeptide by addition of hydrazine derivative to an isocyanate.....	62
Scheme 2.2. Synthesis of azapeptides by activated ester derivatives.....	62
Scheme 2.3. Synthesis of azapeptides by coupling with acid chlorides.....	62
Scheme 2.4. Synthesis of azapeptides with <i>N</i> -azolides.	63
Scheme 2.5. Synthesis of azapeptides by ring opening of 1,3,4-oxadiazole-2-(3H)-one.....	63
Scheme 2.6. General methods for the synthesis of azapeptides.....	64
Scheme 2.7. Synthesis of substituted hydrazine derivatives by William Lubell group.....	65
Scheme 2.8. Synthesis of <i>N</i> -(fluoren-9-yl-methyl)- <i>N'</i> -alkyl-carbazate by William Lubell group. .	65
Scheme 2.9. Synthesis of [aza-arylglycine] GHRP-6 analogs.....	66
Scheme 2.10. <i>N</i> -arylation in solution phase.....	67
Scheme 2.11. Proposed mechanism of Mitsunobu reaction for phthalimide derivatives.	67
Scheme 2.12. General steps for the synthesis of azadipeptide Boc-azaAA-AA-OMe.....	68
Scheme 2.13. Synthesis of 2:1-[α /aza]-trimers by acid fluoride method.....	70
Scheme 2.14. Synthesis of 2:1-[α /aza]-hexamers by the classical peptide coupling methods.....	71
Scheme 4.1. Stepwise synthesis of macrocycles 9a and 9b	117
Scheme 5.1. Classification of gels.	128
Scheme 7.1. Stepwise synthesis of 7a' and 7b' from the corresponding Boc-precursors.....	202
Scheme 8.1. Example for the preparation of Pebax®1074 membrane with an additive of azapeptide trimer (7c') after deprotection of the Z-groups using: (A) chemical pathway, and (B) direct mixing method.	247
Scheme 8.2. Synthesis of the azide-functionalized-PEDEGA polymer as described by LCPM polymeric group.	248

List of Tables

Table 1.1. Ideal torsion angles for different β -turn types	36
Table 2.1. Different coupling reagents trials in the synthesis of 2:1-[α /aza]-trimers.....	69
Table 2.2. Different 2:1-[α /aza]-trimers obtained by acid fluoride method.....	70
Table 2.3. Different 2:1-[α /aza]-hexamers obtained by the classical peptide coupling methods.....	71
Table 2.4. Selected techniques used in the conformational analysis of peptides and proteins.....	72
Table 3.1. Assignment of the CO groups in 7c and 7d (3.0 mmol. L ⁻¹ , CDCl ₃)	84
Table 3.2. Mean values of the bond distances and bond angles for the predicted intramolecular hydrogen bonds in 7c and 7d issued of the molecular dynamic simulations.....	85
Table 3.3. Mean values of dihedral angles of molecules 7c and 7d issued of the molecular dynamic simulations.....	88
Table 3.4. Mean values of bond distances and bond angles for the predicted intramolecular hydrogen bonds in 8c and 8d issued of the molecular dynamic simulation.....	92
Table 3.5. Mean dihedral angles of molecules 8c and 8d issued of the molecular dynamic simulations	93
Table 6.1. Minimum gelation concentrations (MGCs, wt%), and gel-to-sol transition temperature (T _{gs} , °C) of 9b in different organic solvents	182
Table 7.1. All the trials for hydrogel formation based on 2:1-[α /aza]-trimers (7)	201
Table 7.2. Intramolecular hydrogen bond distances and bond angles in conformers P and Q ..	203
Table 7.3. Intermolecular hydrogen bond distances and bond angles in the asymmetric unit of compound 7b' (X-ray).....	204
Table 7.4. Torsion angles in 7b' (X-ray)	204
Table 7.5. Intermolecular hydrogen bond distances and bond angles between conformers P and Q in packing mode.....	205
Table 7.6. Average intramolecular hydrogen bond distances and angles in 7a' and 7b' issued of molecular dynamic simulations.....	211
Table 7.7. Mean dihedral angles of molecules 7a' and 7b' issued of molecular dynamic simulations	211
Table 7.8. Minimum gelation concentrations of azapeptides (7a' and 7b') <i>versus</i> normal peptides (N1 and N2).....	213
Table 8.1. Description of the 2:1-[α /aza]-oligomers tested for gases separation.....	246
Table 8.2. % of recovered organic solvent(s) from (water/organic) mixture by 9b using phase selective gelation (PSG) method.....	251

List of Abbreviations

[θ]	Molar ellipticity (Deg. cm ² . dmol ⁻¹)
ΔA	$\Delta A = A_{\text{left}} - A_{\text{right}}$
AA	Amino acid residue
ACN / CH₃CN / MeCN	Acetonitrile
$\alpha\text{CO}_2/\text{N}_2$	Ideal selectivity for separation of (CO ₂ /N ₂) gases
AcOEt / EtOAc	Ethyl acetate
A_{left}	Left-handed circular polarization
A_{right}	Right-handed circular polarization
ATR	Attenuated total reflectance
azaAA	Aza-amino acid
Boc	<i>tert</i> -butyloxycarbonyl
Boc₂O	di- <i>tert</i> -butyl dicarbonate
BOP	Benzotriazol-1-yloxy-tris(dimethylamino)phosphonium hexafluorophosphate
Bzl	Benzoyl
COSY	Correlation spectroscopy
<i>D</i>	Diffusion coefficient (cm ² . s ⁻¹)
DAST	Diethylaminosulfurtrifluoride
DCC	<i>N, N'</i> -dicyclohexylcarbodiimide
DEAD	Diethyl azodicarboxylate
DIPEA	<i>N, N</i> -diisopropylethylamine
DMAP	4-(<i>N, N</i> -dimethylamino)pyridine
DMF	<i>N, N</i> -dimethylformamide
DMSO	Dimethyl sulfoxide
DMSO-<i>d</i>₆	Deuterated dimethyl sulfoxide
DSC	Differential scanning calorimetry
EDC	1-ethyl-3-(3-dimethylaminopropyl)carbodiimide
equiv.	Equivalent
Et	Ethyl
Flu	Fluorescence
Fmoc	9-fluorenylmethyloxycarbonyl
Fmoc-OSu	9-fluorenylmethyl <i>N</i> -succinimidyl carbonate
For	Formyl
FTIR	Fourier transform infrared
G'	Elastic rigidity modulus (Pa)
G''	Viscous rigidity modulus (Pa)
HATU	1-[bis(dimethylamino)methylene]-1 <i>H</i> -1,2,3-triazolo[4,5- <i>b</i>]pyridinium 3-oxid hexafluorophosphate
HBTU	2-(1 <i>H</i> -benzotriazol-1-yl)-1,1,3,3-tetramethyluronium hexafluorophosphate
hGly	Hydrazinoglycine
HOBT	<i>N</i> -hydroxybenzotriazole
HRMS (ESI)	High resolution mass spectrometry (electrospray ionization)
HRSEM	High resolution scanning electron microscopy
<i>i</i>-Bu	Isobutyl
<i>i</i>-Pr	Isopropyl

LCPM	Laboratoire de chimie physique macromoléculaire
LMOHG	Low molecular weight hydrogelator
LMWG	Low molecular weight gelator
LMWOG	Low molecular weight organogelator
LVR	Linear viscoelastic region
MGC	Minimum gelation concentration
MgSO₄	Magnesium sulfate
Napht	Naphthalimide
NMM	<i>N</i> -methylnmorpholine
NMR	Nuclear magnetic resonance
NOE	Nuclear Overhauser effect
NOESY	Nuclear Overhauser effect spectroscopy
OFS	Oscillatory frequency sweep
OSS	Oscillatory stress sweep
OTS	Oscillatory time sweep
P	Permeability (Barrer = 10 ⁻¹⁰ cm ³ (STP).cm ⁻¹ .cmHg ⁻¹ . s ⁻¹)
Pebax[®]1074	Co-polymer (polyamide12 45%wt : polyethylene oxide 55%wt)
PEDEGA	Poly(ethyl diethylene glycol acrylate)
p-ether	Petroleum ether
PFP	Pentafluorophenol
Ph	Phenyl
Pht	Phthalimide
Piv	Pivaloyl
PNP	<i>p</i> -nitrophenol (4-hydroxynitrobenzene)
POCl₃	Phosphoryl chloride
PSG	Phase selective gelation
Rdt	Yield
R_f	Retardation factor
ROESY	Rotating frame nuclear Overhauser effect spectroscopy
RT	Room temperature
S	Sorption coefficient (cm ³ (STP).cm ⁻³ . cmHg ⁻¹)
SAFIN	Self-assembled fibrillar network
SET-LRP	Single electron-transfer living radical polymerization
TBTU	<i>O</i> -(benzotriazol-1-yl)- <i>N, N, N', N'</i> -tetramethyluronium tetrafluoroborate
<i>t</i>-Bu	<i>tert</i> -butyl
Tg	Transition temperature or gelation temperature
THF	Tetrahydrofuran
TLC	Thin layer chromatography
TOCSY	Total correlation spectroscopy
XRD	X-ray diffraction
Z	Benzyloxycarbonyl group
ZOSu	Benzyloxycarbonyl- <i>N</i> -hydroxysuccinimide

General Introduction and Thesis Objectives

General Introduction

Naturally, enormous numbers of peptide and protein molecules are evolved from the covalent linkage (also known as amide linkage) between the well-defined 20 proteinogenic amino acid residues. Peptide and protein molecules are fundamentally different from each other by the number, nature and sequence of α -amino acids incorporated in their skeletons, consequently they reflect different biological and physiological functions in living organisms.¹

Peptides have been limited from direct use as therapeutic agents due to their (i) biodegradability by peptidases in the digestive system or in biological fluids, (ii) flexibility which leads to a multiplicity of actions as well as, (iii) hydrophilic character that may prevent them from crossing the physiological barriers.^{1,2} Accordingly, designing new analogs of these bioactive peptides have gained much prominence especially in the medicinal chemistry field. Chemists used the approach of introducing chemical changes in the peptide backbone and/or side chain in order to increase the biological activity, selectivity, stability against hydrolysis enzymes in addition to optimize the hydrophilic/hydrophobic ratio to allow their passage through the physiological barriers. These modifications in the peptide structures have risen the terms "Pseudopeptides and Peptidomimetics" which become well established families in the scientific community.

Among the modifications in the peptide structures recommended by pharmacologists, those introduced in the peptide backbone, particularly in the amide bond leaving the side chains without any modifications. Generally, side chains are necessary for the high recognition by the active sites of the target proteins. However, synthesis of new pseudopeptides is one of the interesting goals of chemists, the structure activity relationship (SAR) studies of peptides and proteins have increased rapidly and are in a progressive manner. This SAR may provide better understanding of the mechanisms of the various biological processes which are associated mainly with the compact conformational structures of peptides and proteins.

Owing to the complexity in studying tertiary and quaternary structures, researchers have given much interest to study the three dimensional secondary structures of proteins and peptides such as turns, helices and sheets which can be investigated by a number of available physico-chemical techniques. Moreover, chemists supposed that introducing modifications in the peptide structures may lead to change in the secondary structures of the peptides so that they can adopt conformations that allow better affinity, more stability and greater specificity with the receptors.

In recent decades, synthesis and development of new pseudopeptides have progressed rapidly due to their possibility to replace α -peptides to act as substrates for enzymes and also serve as receptors for proteins. They can also adopt well-defined secondary structures, a necessary feature which makes them excellent candidates for drug design. The most widely used methods to modify the peptide backbone involve: (i) insertion of isosteres or exchanged isoelectronic center in the peptide backbone such as peptoids, azapeptides, azatides, *etc.*, or (ii) introducing of an additional fragment in the peptide backbone as in hydrazinopeptides, β -peptides, α -aminoxy, oligo-ureas, *etc.*³

More recently, Gellman has found an interesting property of the synthetic oligomers as they show their abilities to self-organize in solution, so he proposed the term "foldamer".⁴ Most of the studies on foldamers focused primarily on the synthesis of oligomers comprising one type of monomeric subunits which were classified as homogeneous foldamers.⁵⁻⁸ In 1996, Gellman and Seebach have studied a homogeneous β -peptides which showed unexpected ability to adopt helical conformations with improved stability compared with those of α -peptides.^{5,8} Further studies on β -peptide revealed their stability against proteolytic degradation *in vitro* and *in vivo*.⁸⁻¹⁰

General Introduction and Objectives of Study

In recent years, synthesis of heterogeneous foldamers has gained considerable interest; they are hybrid or mixed oligomers which are built by alternating more than one type of amino acids such as α/β , β/γ or α/γ .¹¹⁻¹³ Heterogeneous foldamers showed many advantages over their homogeneous analogs. One of the advantages is the structural diversity when designing heterogeneous skeleton which could not be obtained by the homogenous series. This diversity is based on variations in the stoichiometry and the nature of the amino acid residue, which lead to many new molecular structures.^{11,12} For example, in case of heterogeneous foldamer composed of alternating α and β amino acids, there are different possible combinations α - β - α - β - α - β , α - α - β - α - β - α , α - β - β - α - β - β , α - β - α - β , *etc.* In this example, while a β residue provides a conformational pre-organization, the α residue permits the introduction of many various side chains at specific positions. Subsequently, each of these sequences potentially offers the opportunity to have different orientation of side chains in space, which therefore lead to specific activity.¹²

Furthermore, many researchers have showed their interests in the synthesis of homo- and heterocyclic foldamers which revealed much rigidity than their linear precursors. Interestingly, the studies investigated that the cyclic analogs possess intramolecular interactions and they exhibit improved activity through their strained and rigid structures.^{14,15}

Interestingly, some cyclofoldamers have shown their ability to self-assemble and stack together to produce 3D highly organized structures such as nanotubes, tubular, columnar structures. These structures result from the association of macrocycles through intermolecular interactions mainly hydrogen bonding and π -stacking. In 1993, Ghadiri and his collaborators demonstrated that cyclic oligomers comprising alternating *D*- and *L*-configurations of natural α -amino acids could arrange into 3D highly ordered constructions to form nanotubes *via* a network of continuous intermolecular hydrogen bonds.¹⁶ Other groups have concerned by modifying the physical and chemical properties of these nanotube (polarity, reactivity, *etc.*) through the synthesis of a number of new mixed heterogeneous cyclofoldamers, *e.g.*, cyclo-(1:1-[α /urea]-tetramer)¹⁷, cyclotetramer of [α/β]-peptides¹⁸ and [α/γ]-peptides¹⁹.

Creating new foldamers must satisfy the following criteria: (i) identify of new motifs that can induce folding in solution upon introducing them in the parent oligomer structure, so it is necessary to understand and predict the relation between the structure of the repeating monomers and the secondary structure of the resulting oligomer, (ii) foldamers should have an interesting chemical and/or biological functions through their structure activity relationship, (*e.g.*, secondary structure *versus* enzymatic stability), and (iii) foldamers must be synthesized effectively from their monomers in a high stereochemically pure forms.

"Laboratoire de Chimie Physique Macromoléculaire" group has interested in the design, synthesis, structural and conformational studies of bis-nitrogen compounds such as hydrazinopeptides²⁰⁻²² *N*-amino peptides²³ and azapeptides²⁴.

In our study, we are interested in the synthesis of new pseudopeptides, particularly azapeptides which are α -peptide analogs obtained by replacement of at least one carbon C $^{\alpha}$ atom of an α -amino acid by a nitrogen atom.

Several reasons have supported our choice for synthesizing and studying of new oligomers and cyclooligomeres containing aza-amino acid motif: (i) according to LCPM studies on bis-nitrogen pseudopeptides, the results showed that insertion of an additional nitrogen atom in the peptide backbone as in hydrazinopeptides²⁰⁻²² and *N*-aminopeptides^{23,25} enhances the resistance towards biodegradation²⁶, (ii) Kang-Bong Lee *et al.* showed that aza-amino acids have a preferred β -trun

General Introduction and Objectives of Study

conformation²⁷⁻²⁹ which leads to folding of the pseudopeptide enabling the *N*- and *C*-termini to be close from each other facilitating the cyclization process, in addition (iii) the side chain of the natural amino acid is conserved without any modification which is necessary for active site recognition in protein.

Michel Marraud in our laboratory was the first who succeeded to incorporate an aza-motif in short peptide sequences of one, two and three residues.²⁶ After that, our group has announced for the emerging of two azapeptide families of the sequences 1:1- and 2:1-[α /aza]-oligomers.²⁴ Firstly, Abbas-Quinternet *et al.* could optimize a general strategy for the synthesis of azapeptides in solution using Boc-chemistry and she succeeded to synthesize and study different linear and cyclic oligomers at their monomeric level.^{24,30} After that, Zhou *et al.* in the previous study have extended the studies on those two families focusing on the synthesis and structural studies of linear and cyclic oligomers of longer sequences at their 3D highly ordered constructions.^{31,32}

Gelation is a remarkable phenomenon which reflects the ability of gelator molecules to self-assemble into highly ordered hierarchical structures (*e.g.*, fibers, tubes, rods, ribbons, helices, *etc.*) which undergo further entanglement to afford three-dimensional cross-linked network that entraps and immobilizes the solvent phase within the spaces of the self-assembled matrix. The process of self-assembly is driven by different kinds of either chemical and/or physical intermolecular interactions between gelator molecules themselves or between gelator and solvent molecules in which the attractive and repulsive forces are so balanced.^{33,34} Gelation can be considered to be a competition between solubilization and phase separation.³⁴

Traditionally, gels were synthesized utilizing long chain polymers having a large hydrodynamic radius which upon external stimuli (*e.g.*, cooling or pHs), these chains interact/entangle with each other and form a continuous network with solid-like properties.³⁵ In the past decade, a new form of gel composed mainly of low molecular weight gelator molecules (LMWGs) has gained remarkable interest in which the monomeric gelator molecules must first self-assemble before entanglement and eventually gel the solvent molecules.³⁶⁻³⁹

Accordingly, gels can be classified in several ways based on their origin (natural or synthetic), constitution (macromolecular or molecular), the type of cross-linking that creates their 3D network (chemical or physical) and the medium of gelation (organo, hydro, xero or aero).⁴⁰

Self-assembly process which leads to molecular gels, has become an area of great interest in the field of supramolecular chemistry due to the extensive applications of these gels in various disciplines: biomedical and tissue engineering as anti-inflammatory agents, drug delivery matrices for topical and oral pharmaceuticals, light harvesting materials, enzyme immobilization matrices as well as in phase selective gelation and waste water treatment.^{39,41-43}

Recently, it was estimated that over than 1000 low molecular weight gelators have been reported.⁴⁴ Although there is a large structural diversity within LMWGs, they have a common feature that they gel solvent molecules through self-assembly phenomenon by a combination of intermolecular non-covalent interactions such as electrostatic, dipole-dipole, hydrogen bonding, hydrophobic, π - π stacking, van der Waals interactions and hydrophilic/lipophilic balance.^{41,43,45} LMWGs have been derived from various systems including hydrocarbons, fatty acids, saccharides, steroids, amides, amino acids, peptides, ureas, aromatic molecules, metal complexes and dendrimers.^{33,40,46-54}

General Introduction and Objectives of Study

In 2001, our group in LCPM has found serendipitously the formation of gel materials upon cooling refluxed amino acid derivatives from toluene. Structural studies and mechanism of gelation for these organogels have been established later.^{55,56} The group became interested in preparation of supramolecular gels from our pseudopeptides in order to be involved in some potential applications. More recently, our laboratory extended their interests to obtain molecular gels from the macrocyclic pseudopeptides. They gave the evidences of the ability of new two cyclic 1:1-[α/α -N ^{α} -Bn-hydrazino]-mers to self-assemble in cyclohexane and toluene forming 3D network which entrap the solvent molecules resulting in thermoreversible organogels. They reported that these supramolecular organogels are stabilized through intermolecular hydrogen bonds and π -stacking interactions between the aromatic moieties.⁵⁷

In Zhou Zhou thesis (2014), synthesis and structural studies of homo- and heterochiral cyclo-(2:1-[α/α]-L- or D-Phe-azaPhe-Ala)₂-hexamers have been investigated. The results revealed that while the homoanalog could give monocystals showing its ability for the formation of well-defined highly ordered 3D structure, no crystal structure has been reported for the heteroanalog however it showed a fascinating property for the formation of gel from toluene solvent.³¹ These interesting behaviors brought some questions and ideas at the beginning of the current work: (i) Is it possible to get monocystals and solve the crystal structure of the heteroanalog and compare it with the homoanalog?, (ii) How does the chirality affect the packing of those two macrocycles and permit only the heteroanalog to form organogel?, (iii) May we obtain organogels from both macrocycles in other solvents rather than toluene? and if yes, (iv) What are the characteristic properties of these organogels in terms of mechanical, thermal, morphology, *etc.*?, (v) May we get hydrogels by changing the side chains within the azapeptide sequences?, and (vi) Can the 2:1-[α/α]-family promise for some potential applications? These questions and their potential answers led us to the objectives of the current work:

Objectives of Study

- (1) Synthesis of new 2:1-[α/α]-oligomers possessing lysine amino acid residues in their sequences.
- (2) Structural studies of the synthesized oligomers using NMR, FTIR, X-ray diffraction as well as molecular dynamics calculations method, highlighting the effect of lysine side chains and backbone chain length on the conformations of these oligomers.
- (3) Structural modifications in the synthesized azapeptides in order to induce gelation from low molecular weight azapeptide molecules.
- (4) Structural studies and characterizations for the low molecular weight gelators and the formed gels using some physico-chemical techniques such as NMR, FTIR, CD, UV-vis, fluorescence, rheometer, SEM, X-ray diffraction and molecular dynamic calculations.
- (5) Evaluation of some potential applications for the 2:1-[α/α]-oligomers.

These objectives have been successfully achieved, and the results will be highlighted in three main parts:

➤ **Part A** “Synthesis and structural studies of new linear and cyclic 2:1-[α/α]-oligomers”

- Chapter I** : Bibliography of pseudopeptides (azapeptides) and peptidomimetics.
- Chapter II** : Synthesis and methods of analysis of 2:1-[α/α]-oligomers.
- Chapter III** : Structural studies of 2:1-[α/α]-oligomers possessing lysine residues.
- Chapter IV** : Impact of C ^{α} -chirality on supramolecular self-assembly of cyclo-(L- / D-Phe-azaPhe-Ala)₂-hexamers.

General Introduction and Objectives of Study

➤ **Part B** “2:1-[α /aza]-oligomers as low molecular weight gelators”

Chapter V : Bibliography of gels and low molecular weight organo-/hydrogelators.

Chapter VI : Supramolecular organogels based on heterochiral cyclo-(*D*-Phe-azaPhe-Ala)₂-hexamer.

Chapter VII : Supramolecular hydrogels based on 2:1-[α /aza]-trimers.

➤ **Part C** “Applications based on 2:1-[α /aza]-oligomers”

Chapter VIII : Evaluation of the 2:1-[α /aza]-oligomers in two potentials applications.

Part A
**Synthesis and Structural Studies of New Linear
and Cyclic 2:1-[α /aza]-Oligomers**

Chapter I. Bibliography of Pseudopeptides (Aza-Peptides) and Peptidomimetics

Part A

Chapter I. Bibliography of Pseudopeptides (Aza-Peptides) and Peptidomimetics

I.1. Introduction

Proteins and peptides exert a number of biological functions which based mainly on the three dimensional (3D) compact tertiary and quaternary structures of their polypeptide chains (Figure 1.1). Conformational studies of the 3D structures are the informative keys that can provide better understanding of the mechanisms of various biological processes. The difficulty to synthesize proteins and instability of the synthesized peptides *in vivo*, limit their potentials as drug candidates, and this was the cresset for emerging a new field which has been widely developed by chemical society, called “Foldamers”. They are synthetic oligomers have non-biological well-defined backbones.⁴

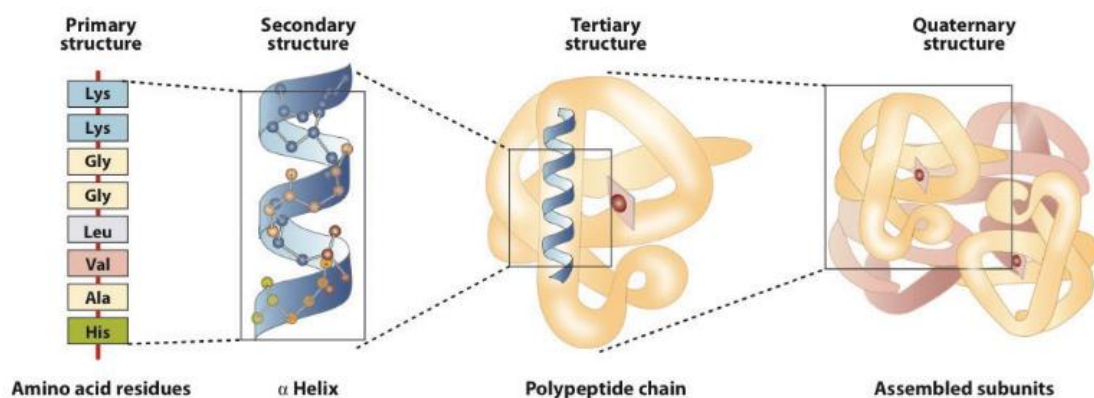


Figure 1.1. Representation of the basic structures of proteins; ([©]Nelson & Cox, *Lehninger Principles of Biochemistry*, 3rd ed.).

Indeed, chemists have succeeded to synthesize functionalized oligomers capable of self-organizing in solution in a controlled manner possessing defined structures with catalytic and biological behaviors that mimic natural peptides and proteins. Construction of such oligomers involves either modifying naturally occurring amino acids or synthesizing non-natural monomeric units taking into consideration the orientation of the side chains of the monomer subunits. These modifications could lead to constrained conformational structures for these oligomers which in turn stabilize their secondary structures.^{58,59}

I.2. Origin of Pseudopeptides, Peptidomimetics and Foldamers

α -amino acids are naturally occurring and biologically important organic compounds containing at least one amine ($-\text{NH}_2$) and one carboxylic acid ($-\text{COOH}$) functional groups, usually along with a side chain (R) group specific to each α -amino acid. They are considered the building block of natural peptides and proteins (Figure 1.2a).⁶⁰

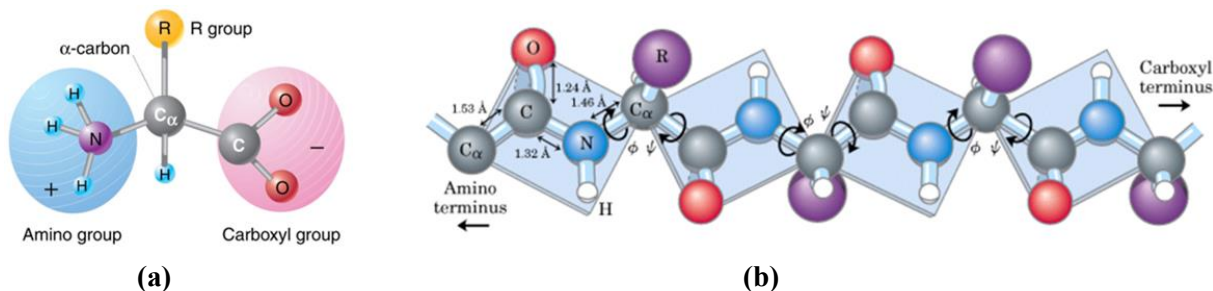


Figure 1.2. Representation of the chemical structures of: (a) amino acid, and (b) peptide chain; Fig. 1.2a ([©]2010 Peter. J. Russell, *iGenetics* 3rd ed.), and Fig. 1.2b ([©]Nelson & Cox, *Lehninger Principles of Biochemistry*, 3rd ed.).

Part A

Chapter I. Bibliography of Pseudopeptides (Aza-Peptides) and Peptidomimetics

Peptides are α -amino acid-derived compounds containing at least one peptide bond (Figure 1.2b). Peptides up to 15 α -amino acids are named oligopeptides, while the term polypeptide refers to peptides up to 50 α -amino acids, and the expression “protein” is used for derivatives containing more than 50 amino acids. Peptides include diverse structural types such as linear, cyclic, depsipeptides, *etc.*^{60,61}

Peptides have the potential to be potent pharmaceutical agents for the treatment of many diseases particularly of the Central Nervous System (CNS).^{62,63} The therapeutic efficacy of a peptide as drug candidate is basically controlled by several concepts: (i) physico-chemical properties such as the activity and selectivity at the specific receptor site, (ii) pharmacokinetic properties (adsorption, transport, ability to cross biological barriers, excretion), (iii) toxicity, (iv) lipophilicity/hydrophilicity ratio which related to the amino acid nature and peptide structure, (v) bioavailability, as well as (vi) the enzymatic stability of the peptides that depends particularly on the nature and sequence of the amino acids, overall size, flexibility, conformations and side chain metabolism.^{64,65}

Unfortunately, these promising drugs can only be applied to a very limited extent as pharmacologically active compounds due to their rapid degradation by proteases, low selectivity because their flexible conformations allow the interactions of these peptides with different receptors,⁶⁶⁻⁷² and the low membrane permeability due to their high hydrophilic character.⁶¹ Consequently, chemists have done their best efforts to develop pharmacologically active small bio-organic molecules through new chemical approaches including peptide modifications and the design of peptidomimetics from which two new families "Pseudopeptide and Peptidomimetics" have been evolved.⁶¹

Peptidomimetics (Section I.5.1) are compounds contain non-peptidic structural element, such as peptide bond-surrogates not cleaved by peptidases. They imitate the conformational structure and the biological action of a peptide in its receptor-bound conformation.^{60,63,73,74} Designing of peptidomimetics which demonstrate biological activity, conformational stability, bioavailability, stability against enzymatic degradation and high receptor selectivity, is the subject of major interest by pharmaceutical companies.

Pseudopeptides are modified peptides contain non-proteinogenic or modified amino acid building blocks (Section I.5.1). Chemists used the approach of introducing chemical changes in the peptide backbone or its side chain(s) in order to increase the biological activity, selectivity, stability against hydrolysis enzymes, in addition to optimize the hydrophilic/hydrophobic ratio to allow their passage through the physiological barriers.⁶¹

Interestingly, Gellman has found the ability of some synthetic oligomers to self-organize in solution giving stable and reproducible secondary structures that mimic protein secondary structures such as helices, sheets or turns, so he coined the term "Foldamers". The term "Foldamer" as proposed by Gellman consists of two words "folding + unnatural oligomer or polymer" which refers to unnatural polymer or oligomer that has strong tendency to self-organize into a predictable well-defined compact structure in solution that mimic the secondary structures of peptides and proteins.⁴

I.3. Structural Features of Peptidic Backbone

Peptide bond “amide bond” is the covalent linkage between the carbonyl group (CO) of an amino acid (i) and the NH group of the following amino acid (i+1) in peptides and proteins (Figure 1.3a). The free rotation about the (C–N) amide bond is drastically restricted due to delocalization and involvement of the non-bonding electron pair of the amide nitrogen in a resonance with the π -bound electrons of the carbonyl (C=O) group. This leads to the partial double bond character of the peptide

Part A

Chapter I. Bibliography of Pseudopeptides (Aza-Peptides) and Peptidomimetics

bond⁶⁰ (Figure 1.3b) and this behavior was proved by Pauling and Corey in 1951.⁷⁵ Based on the X-ray crystallography results of amino acids, they revealed that the (C–N) peptide bond length in peptides is shorter than a regular single bond, in addition the conformation of the peptide backbone is characterized by three torsion angles (ϕ , ψ and ω) correspond to the three bonds (NH–C ^{α}), (C ^{α} –CO) and (CO–NH) for the planes [C(=O)–N–C ^{α} ₁–C(=O)], [N–C ^{α} ₁–C(=O)–N] and [C ^{α} ₁–C(=O)–N–C ^{α} ₂], respectively as depicted in Figures 1.3b, c. The torsion angles (ϕ) and psi (ψ) vary from (-180° to +180°). The (R-group) substituent attached to the (C ^{α}) can also rotate around the (C ^{α}) and the (C ^{β}) of the side chain by other torsion angles.^{60,61,75}

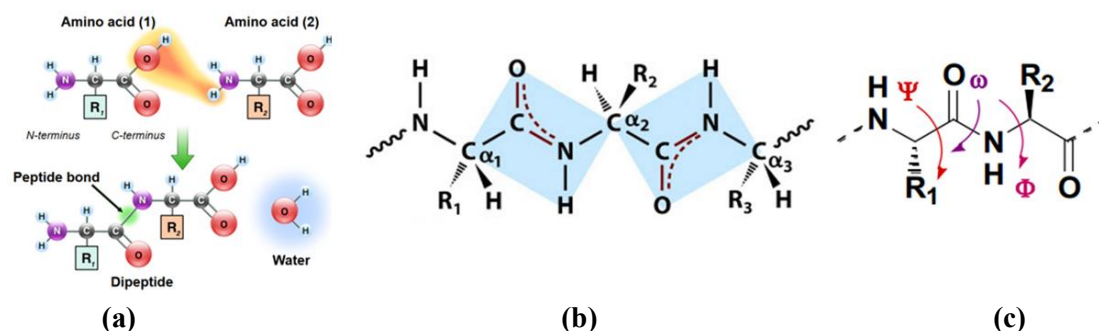


Figure 1.3. Representation of: (a) peptide bond formation, (b) double bond character of peptide bond, and (c) torsion angles within the peptide backbone; *Fig. 1.3a* (https://en.wikibooks.org/wiki/An_Introduction_to_Molecular_Biology/Function_and_structure_of_Proteins), and *Fig. 1.3b* (*Principles of Biochemistry*, 4/e ©2006 Pearson Prentice Hall, inc.)

The partial double bond character of the peptide bond leads to a planar arrangement in which the (N) and (C=O) of the amide bond acquire sp² hybridization and the six atoms of the amide bond [C ^{α} , C, O, N, H and C ^{α}] are in one plane (Figures 1.4a, b). This causes restrictions for the numbers of energy minima belong to amide bond torsion angle (ω) to have only the values of (0° or 180°). Subsequently, two rotamers of the peptide bond exist (Figure 1.4c): the *trans*-configured peptide bond ($\omega \approx 180^\circ$) which is energetically favored than the *cis*-configured peptide bond ($\omega \approx 0^\circ$) by 8 kJ mol⁻¹. The peptide bond exists preferentially in *trans* configuration, because *cis* configuration is thermodynamically unfavored by about 2 kcal mol⁻¹.⁶¹

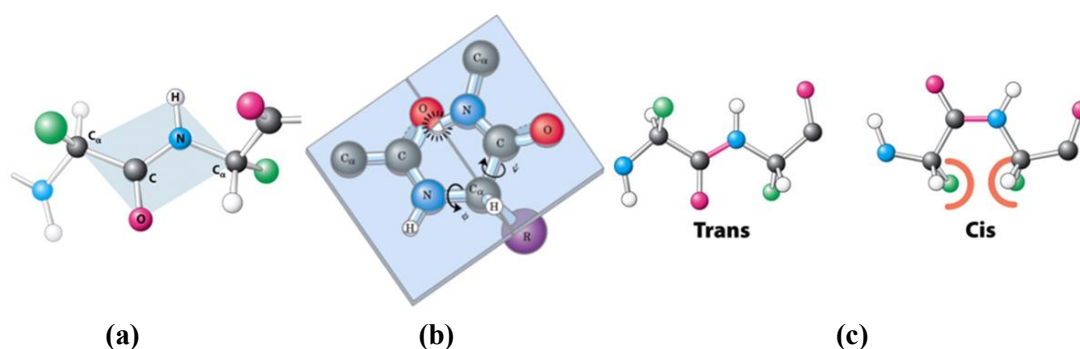


Figure 1.4. Representation of: (a, b) the planar arrangement, and (c) *trans/cis*-isomerization within the peptide bond; *Figs. 1.4a, c* (*Biochemistry, Seventh Edition* ©2012 W. H. Freeman and Company), and *Fig. 1.4b* (©Nelson & Cox, *Lehninger Principles of Biochemistry*, 3rd ed.).

Naturally, *trans*-isomer is found in most peptides except those containing proline, as the energy of the *trans*-configured Xaa-Pro bond is increased and hence the energy difference between the *cis*- and *trans*-isomers decreases.⁶¹

Part A

Chapter I. Bibliography of Pseudopeptides (Aza-Peptides) and Peptidomimetics

The complexity in studying tertiary and quaternary structures compelled the scientific community to orient their studies and interests toward the 3D secondary structures of peptides and proteins such as helices, sheets, turns, *etc.* which can be characterized by a number of available physico-chemical techniques.

I.4. Conformational Secondary Structures Aspects in Peptides and Pseudopeptides Series

The preferred peptide chain conformations under physiological conditions are dominated by the energetically favored torsion angles and stability enhanced by non-covalent interactions such as hydrogen bonds and hydrophobic contacts. Hydrogen bond is basically formed between the NH group (hydrogen bond donor) and the carbonyl oxygen atom (hydrogen bond acceptor) in peptide and protein structures and it is noted as ($i \leftrightarrow i + x$). The accepted hydrogen bond distances between the donor and acceptor atoms (N---O) should be between 2.6 Å and 3.5 Å, and the three atoms (H---N---O) are co-linear to have an angle between -30° and 30° .⁷⁶ The energy of hydrogen bond is quite low ($5 - 40 \text{ kJ mol}^{-1}$), compared to a covalent bond ($200 - 400 \text{ kJ mol}^{-1}$).⁶¹ Hydrogen bonding interaction leads to the formation of pseudocycle of n atoms, symbolized as C_n , which characterizes different types of the secondary structures (Figure 1.5).

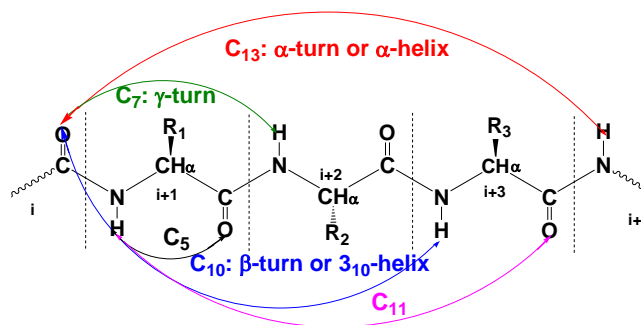


Figure 1.5. Representation of the principle intramolecular hydrogen bonds in peptides backbones.

Ramachandran plots (also known as a Ramachandran diagram, or $[\phi, \psi]$ plot), originally was developed by Ramachandran *et al.* in 1963.⁷⁷ It is a way to visualize the energetically allowed and favorable regions for backbone dihedral angles (ψ) against (ϕ) of amino acid residues in peptide and protein structures.⁷⁷ While the dihedral angle (ω) at the peptide bond is normally (0° or 180°), the dihedral angles (ϕ, ψ) can vary and take intermediate values between (-180° and 180°), however not all pairs of the angles (ϕ, ψ) are permitted sterically.^{75,77}

The plot shows the allowed regions in red which are the more favorable energetically structures adopted by the peptides or proteins. For example, right handed α -helices fall at ($-57^\circ, -47^\circ$) while left handed α -helices fall at ($+57^\circ, +47^\circ$). Parallel β -sheets have the values ($-119^\circ, +113^\circ$), while antiparallel β -sheets fall at ($-139^\circ, +135^\circ$), *etc.* White regions refer to sterically disallowed areas for all amino acids except glycine, and the yellow areas are outer limit regions (Figure 1.6).

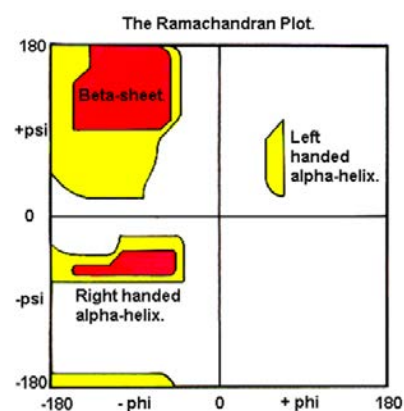


Figure 1.6. Ramachandran diagram shows the allowed and disfavored values of phi and psi (ϕ, ψ) in proteins; (The Fig. was drawn by Dr. Michael Wells, http://www.cryst.bbk.ac.uk/PPS95/course/3_geometry/rama.html).

Part A

Chapter I. Bibliography of Pseudopeptides (Aza-Peptides) and Peptidomimetics

I.4.1. Helices

Helix is a widely occurring secondary structure element comprising a screw like arrangement of the peptide backbone. It results from a repeating of pseudocycles or turns stabilized by intramolecular hydrogen bonds aligned in parallel way to the helix axis (Figures 1.7a-d). The most common types of helices in natural peptides and proteins, which were proposed by Pauling and Corey, are (3₁₀-helix, 3.6₁₃-helix or α -helix, 4.4₁₆-helix or π -helix, and 5.1₁₇-helix or γ -helix) (Figure 1.7f).⁷⁵

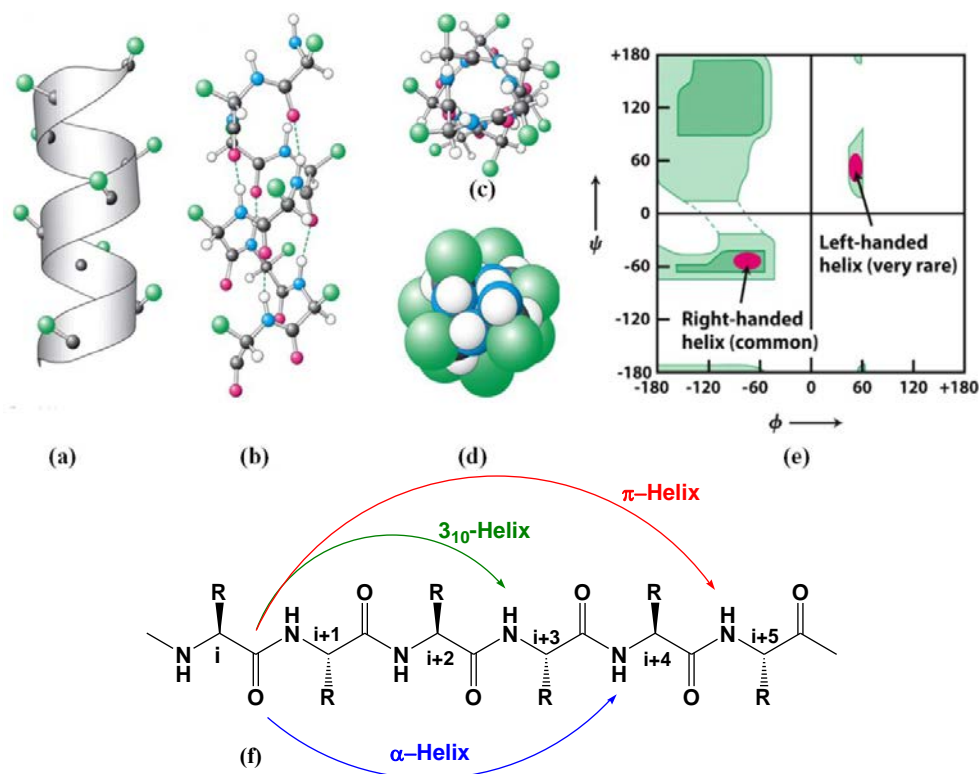


Figure 1.7. (a-d) Representation of different views of helix structure, (e) Ramachandran diagram of α -helices in protein, and (f) principle intramolecular hydrogen bonds in different types of helices in L - α -peptides; Figs. 1.7a-e (Biochemistry, Seventh Edition ©2012 W. H. Freeman and Company).

They are generally symbolized by (n_x -helix) where (n) is the number of amino acid residues per turn, and the subscript number (x) refers to the number of atoms involved in the formation of pseudocycle by the intramolecular hydrogen bond interaction. Helices are chiral objects, and characterized by the direction of the helical turn being clockwise defined by letters "P" (plus) or anticlockwise recognized by the letter "M" (minus).⁶¹

The nature of amino acid side chain is of crucial importance for helix stability.⁷⁸ According to statistic studies, the amino acids glycine, proline and hydroxyproline as well as other non-proteinogenic (e.g., N -alkylated amino acids) are not able to act as hydrogen bond donors and they display high helix breaking properties. In contrast, many other amino acids (Ala, Val, Leu, Phe, Trp, Met, His and Gln) are highly compatible with helical structures. There are some reasons responsible for the helices stability include: (i) steric requirements of the amino acid side chain, (ii) electrostatic interactions between charged amino acid side chain functionalities, (iii) interactions between distant amino acid side chains ($i \leftrightarrow i + 3$ or $i \leftrightarrow i + 4$), and (iv) the presence of proline residues.⁶¹ α -Helices can only be formed from homochiral building blocks containing exclusively D - or L -amino acids. The right-handed α -helix (from L -amino acids) is the preferred conformation for energetic and stereochemical reasons.⁶¹

Part A

Chapter I. Bibliography of Pseudopeptides (Aza-Peptides) and Peptidomimetics

In pseudopeptide series, Gellman⁵ and Seebach⁸ teams were interested in formation of helices based on β -amino acids (Figure 1.8) which are characterized by an additional carbon atom with the possibility of introducing one or more side chains at the second and/or the third positions with respect to the carboxyl group (Section I.6.3.).

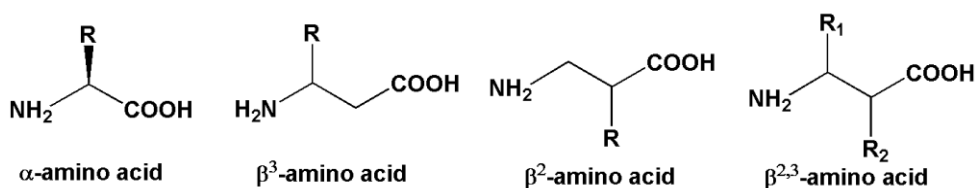


Figure 1.8. Different types of β -amino acids.

β -peptide backbone has great structural flexibility that has been exploited by Samuel Gellman and Dieter Seebach groups.^{4-9,79-83} They have identified six basic types of possible helices conformations in β -peptides (Figure 1.9). In addition, they reported that 3_{14} -helix is the most favorable type which is stabilized by a network of hydrogen bonds ($\text{CO}\cdots\text{NH}$) in opposite direction to those of the α -helices (Figure 1.7).

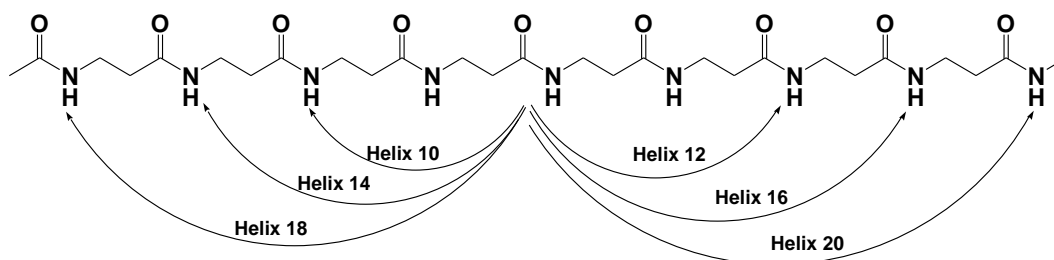


Figure 1.9. Representation of different types of helices in β -peptides.

Recently, Authors reported that helices secondary structures can be further stabilized by the presence of a cyclic substituent in the side chain. This cycle is managed to stabilize helix-14 in the *trans*-2-aminocyclohexane carboxylic acid (*trans*-ACHC) and helix-12 in the *trans*-2-amino cyclopentane carboxylic acid (*trans*-ACPC) as shown in Figure 1.10.⁸⁴

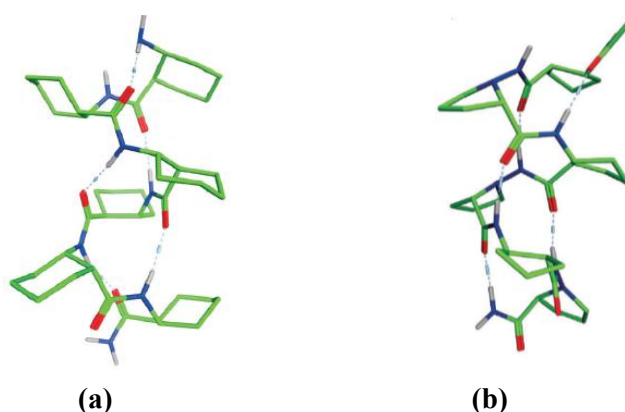


Figure 1.10. (a) Helix-14 in *trans*-ACHC, and (b) helix-12 in *trans*-ACPC.⁸⁴

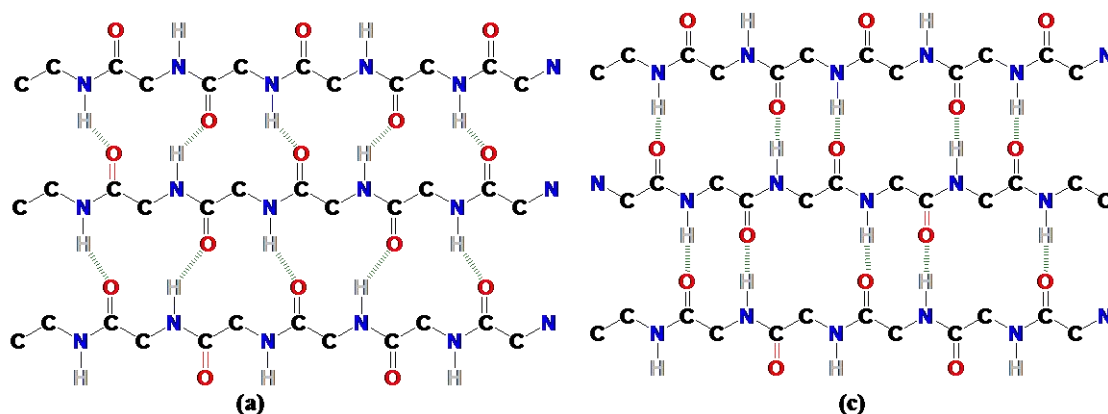
I.4.2. β -sheets

Hydrogen bond pattern of β -sheets differs fundamentally from that of helical structures since the hydrogen bonds are formed between two neighboring polypeptide chains (strands). Two main types of β -sheet structures may be distinguished. Parallel β -sheet, where the chains (β -strands) are

Part A

Chapter I. Bibliography of Pseudopeptides (Aza-Peptides) and Peptidomimetics

aligned in a parallel manner, and antiparallel β -sheet in which the two neighboring peptide chains are connected by hydrogen bonds and aligned in an antiparallel way (Figures 1.11).⁶¹



Figs. 11a and 11c (http://cbc.arizona.edu/classes/bioc462/462a/NOTES/Protein_Structure/secondary_structure.htm).

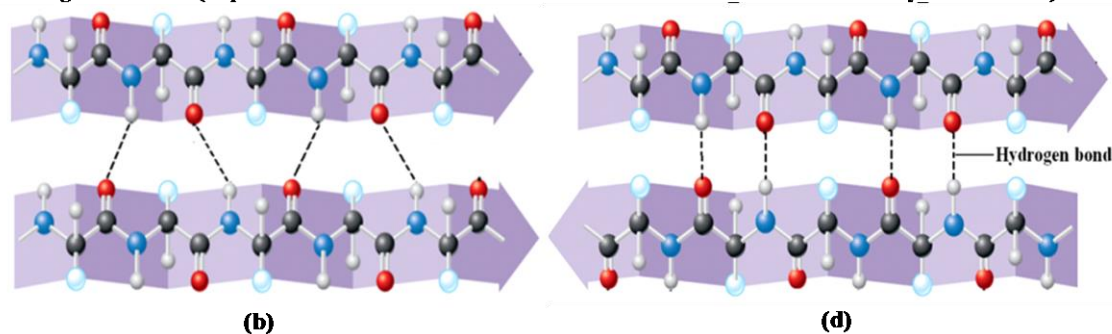


Figure 1.11. Representation of: (a, b) parallel β -sheet, and (c, d) antiparallel β -sheet, hydrogen bonds are illustrated by dashed line; Figs. 1.11b, d (©2011 Pearson Education, Inc.).

A hypothetical fully extended β -sheet structure is characterized by the angles ($\phi = -180^\circ$, $\psi = 180^\circ$). This structure can not be accommodated without distortion when side chains are present, leading to parallel or an antiparallel β -pleated sheet (Figure 1.11b, d) with torsion angles of ($\phi = -119^\circ$, $\psi = +113^\circ$) or ($\phi = -139^\circ$, $\psi = 135^\circ$), respectively (Figure 1.12). The side chains of the amino acids involved in β -sheet formation are aligned in an alternating manner toward both sides of the β -sheet.⁶¹ β -sheets may occur in a twisted, curled or back folded form⁸⁵ and they usually stabilized by non-bonding intra- and inter-strands interactions.⁶¹

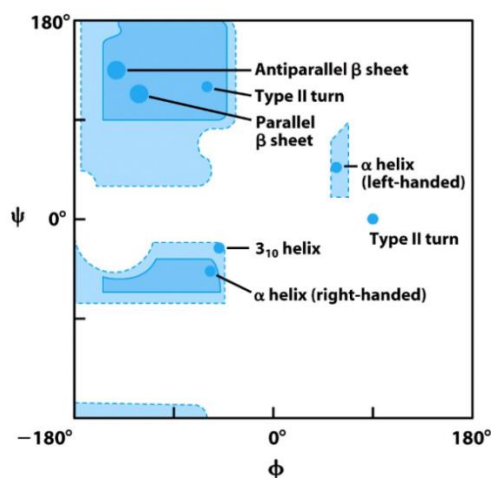


Figure 1.12. Ramachandran plot of β -sheets in peptides and proteins; (©2006 Pearson Prentice Hall, Inc).

I.4.3. β -Strands and β -Hairpins

A β -strand is a polypeptide chain that leads to the formation of β -sheets when two β -strands joined together in parallel or antiparallel manner. In 1994, Blanco has shown that small peptide chains of about 15 to 20 amino acids can fold into β -strand conformation in aqueous solution.⁸⁶ In the other hand, β -hairpin occurs frequently in all kinds of proteins and it is a simple protein motif structure composed of two β -strands oriented in an antiparallel direction (*N*-terminus of one sheet is adjacent to the *C*-terminus of the next), and the two strands are linked by a short loop or turn (Figure 1.13a) of two to six amino acids residues ($n = 2 - 6$). This loop allows the formation of multiple hydrogen bonds between the two antiparallel β -strands (Figure 1.13b).⁸⁷

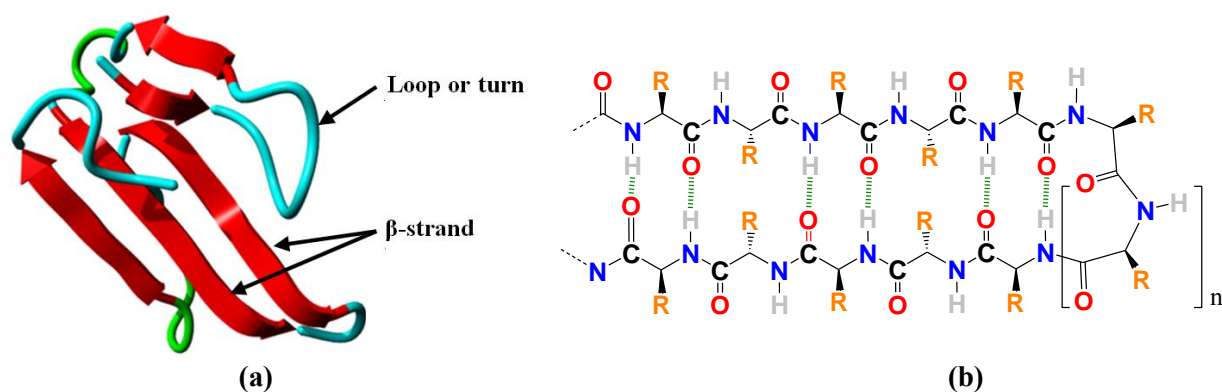


Figure 1.13. (a) Representation of β -hairpin, and (b) hydrogen bonds between two antiparallel β -strands joined together by a loop; Fig. 1.13a (http://curser.science.ru.nl/content-e/pub_NWI/Bioinformatics%20Summerschool%202006%20light%2003092006/documents/do_4271.htm).

I.4.4. Turns

Polypeptide chains can not fold into compact structure without involving tight turns that usually occur on the exposed surface of proteins.⁶¹ Hence, turns provide useful information about the architecture and bioactivity of the folded peptides and proteins for the design of new molecules such as drugs, antigens, *etc.*⁸⁸ Turns are stabilized by hydrogen bonds between amide groups in the peptide chain. Based on the number of amino acid residues involved, turns are classified into: γ -turns (three amino acids), β -turns (four amino acids), α -turns (five amino acids), or π -turns (six amino acids).^{85,89,90}

Whilst π -turn or C_{13} involves intramolecular hydrogen bonding interaction closing a pseudocycle of 13 atoms of the type ($i \leftrightarrow i + 5$), α -turns or C_{11} conformation is characterized by the presence of intramolecular hydrogen bond of the type ($i \leftrightarrow i + 4$) forming a pseudocycle of 11 atoms.⁸⁹ In fact, γ -turns and β -turns are more common in peptides and proteins⁹¹ and they are identified by features explained in the following sections.

I.4.4.1. γ -Turns or C_7

This conformation was highlighted during spectroscopic studies of dipeptides^{92,93} and proteins⁹⁴ in solution. It is characterized by the presence of intramolecular hydrogen bond of the type ($i \leftrightarrow i + 2$) forming stable pseudocycle of seven atoms. There are two forms of γ -turn conformation; the classical γ -turn (pseudo-axial orientation) with torsion angles ($\phi = +80^\circ$, $\psi = -65^\circ$), and the inverse γ -turn (pseudo-equatorial orientation) with torsion angles ($\phi = -80^\circ$, $\psi = +65^\circ$) with respect to the residue ($i + 1$) (Figure 1.14). It has been reported that inverse γ -turn is more stable than the classical one in peptides and proteins because of the favorable ϕ and ψ angles (Ramachandran plot).⁹⁵



Figure 1.14. Types of γ -turns.

I.4.4.2. β -Turns or C_{10}

The most known β -turns are characterized by the formation of a pseudocycle of ten atoms of the type ($i \leftrightarrow i + 3$) between the NH and CO groups. The general criteria for the existence of a β -turn are: (a) the hydrogen bond distance between the dipolar atoms (N---O) has a value between 2.8 Å and 3.5 Å, and (b) the distance between the C^α (i) and C^α ($i + 3$) atoms is smaller than 7 Å (Figure 1.15a, b).^{61,96,97}

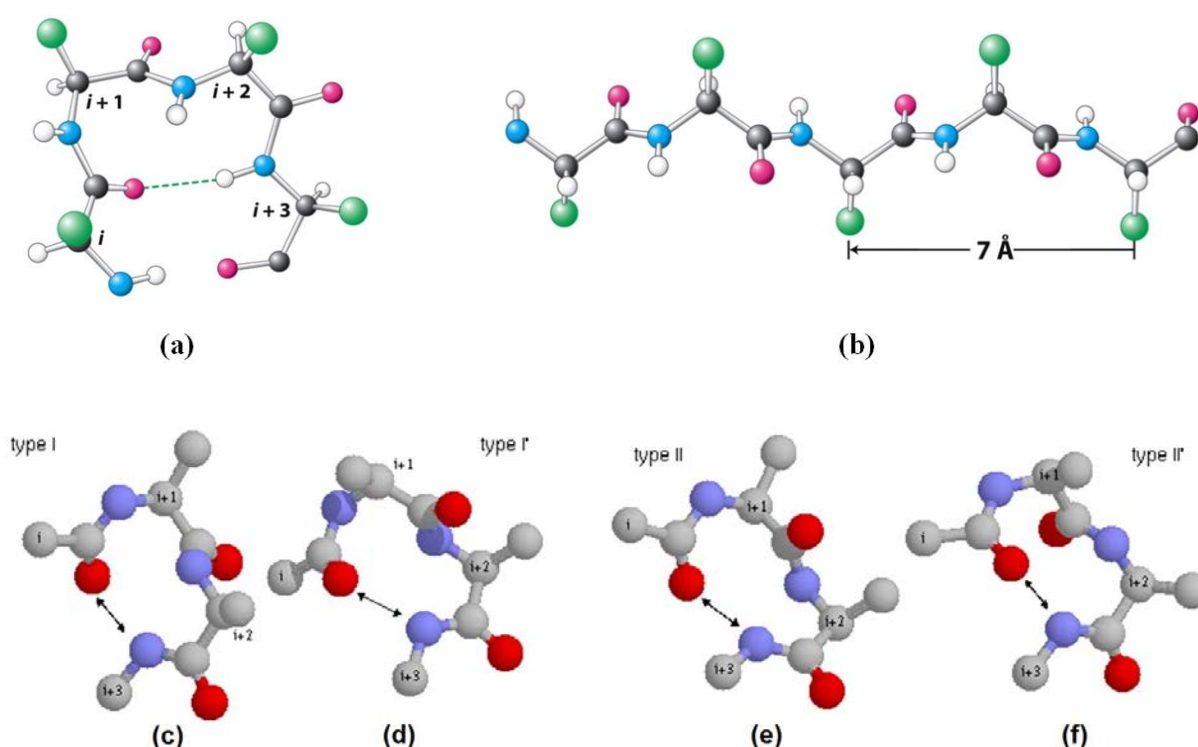


Figure 1.15. (a) Representation of ($i \leftrightarrow i + 3$) hydrogen bonding interaction in β -turn, (b) distance between C^α (i) and C^α ($i + 3$) atoms in β -turn, and (c-f) representation of the common types of β -turns in peptides; Figs. 1.15a, b (*Biochemistry, Seventh Edition* ©2012 W. H. Freeman and Company), Figs. 1.15c-f (http://www.cryst.bbk.ac.uk/PPS2/course/section8/ss-960531_16.html).

The most common types of β -turns in peptides and proteins are classified according to the characteristic dihedral angles of the second ($i + 1$) and the third ($i + 2$) amino acids (Figures 1.15c-f; Table 1.1).⁷⁶

Part A

Chapter I. Bibliography of Pseudopeptides (Aza-Peptides) and Peptidomimetics

Table 1.1. Ideal torsion angles for different β -turn types

Type	Residue (i + 1)		Residue (i + 2)		
	ϕ	ψ	ϕ	ψ	ω
β I	-60°	-30°	-90°	0°	180°
β I'	60°	30°	90°	0°	180°
β II	-60°	120°	80°	0°	180°
β II'	60°	-120°	-80°	0°	180°
β III	-60°	-30°	-60°	-30°	180°
β III'	60°	30°	60°	30°	180°
β V	-80°	80°	80°	-80°	180°
β V'	80°	-80°	-80°	80°	180°
β VIII	-60°	-30°	-120°	120°	180°
* β VIa1	-60°	120°	-90°	0°	0°*
* β VIa2	-120°	120°	-60°	0°	0°*
β VIb	-135°	135°	-75°	160°	0°*
β VI	-60°	120°	-120°	60°	180°
β IV	-61°	10°	-53°	17°	

(*) Types β VIa1-, β VIa2- and β VIb-turns are subjected to the additional condition that residue (i + 2) must be a *cis*-proline.

The existence of this conformation has been confirmed by many experimental and theoretical studies. β I- and β II-turns are the most often conformations found in α -amino acids (Figure 1.16).⁶¹

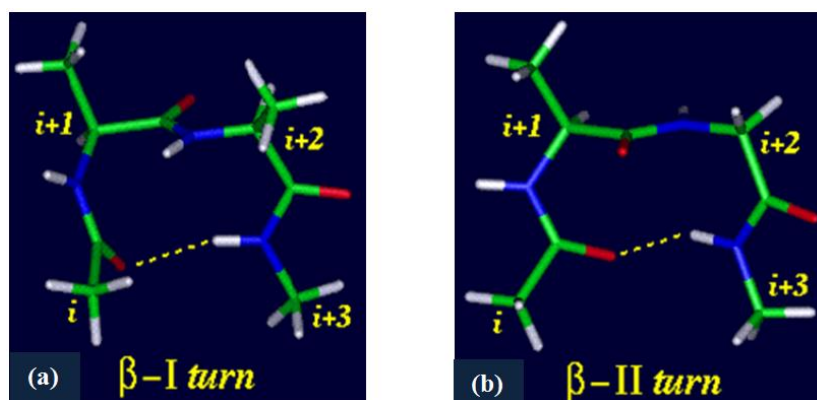


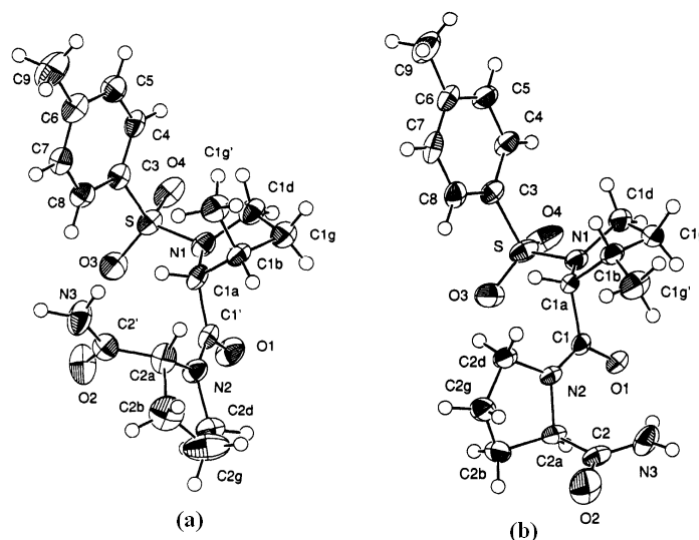
Figure 1.16. The most common types of β -turns: (a) β I-turn, and (b) β II-turn; (http://cbc.arizona.edu/classes/bioc462/462a/NOTES/Protein_Structure/secondary_structure.htm).

Proline has the highest tendency to occur in a reverse turn. Proline with a *trans*-configured peptide bond is found preferentially as β I- or β II-turns in position (i + 1). In the other side, proline with a *cis*-configured peptide bond adopts β VIa-turn in position (i + 2) which is also named proline turn. Mainly *D*-proline, but also *D*-amino acids generally have a high preference to adopt β II-turn when occupying position (i + 1).⁶¹

Owing to the importance of β -turns in receptor recognition process as they exist in the outer surface of globular proteins, many peptidomimetics with β -turns have been developed and incorporated into biologically active peptides.⁸⁸

I.4.4.2.1. β -Turns in Substituted Diprolines

In case of heterochiral (*L*, *D*) diprolines, 2-methyl-*D*-proline in position ($i + 2$) and a (*cis* or *trans*)-3-methyl-*L*-proline in position ($i + 1$) induce a β II-turn conformation similar to the conformation identified for the unsubstituted diprolines peptides. In contrast, homochiral diprolines (*D*, *D*), 2-methyl-*D*-proline in position ($i + 2$) and *cis*-3-methyl-*D*-proline in position ($i + 1$), seems to favor a different conformation compared to the unsubstituted analog, while the *trans*-3-methyl-*D*-proline appears to stabilize a β VI'-turn conformation (Figure 1.17).⁹⁸



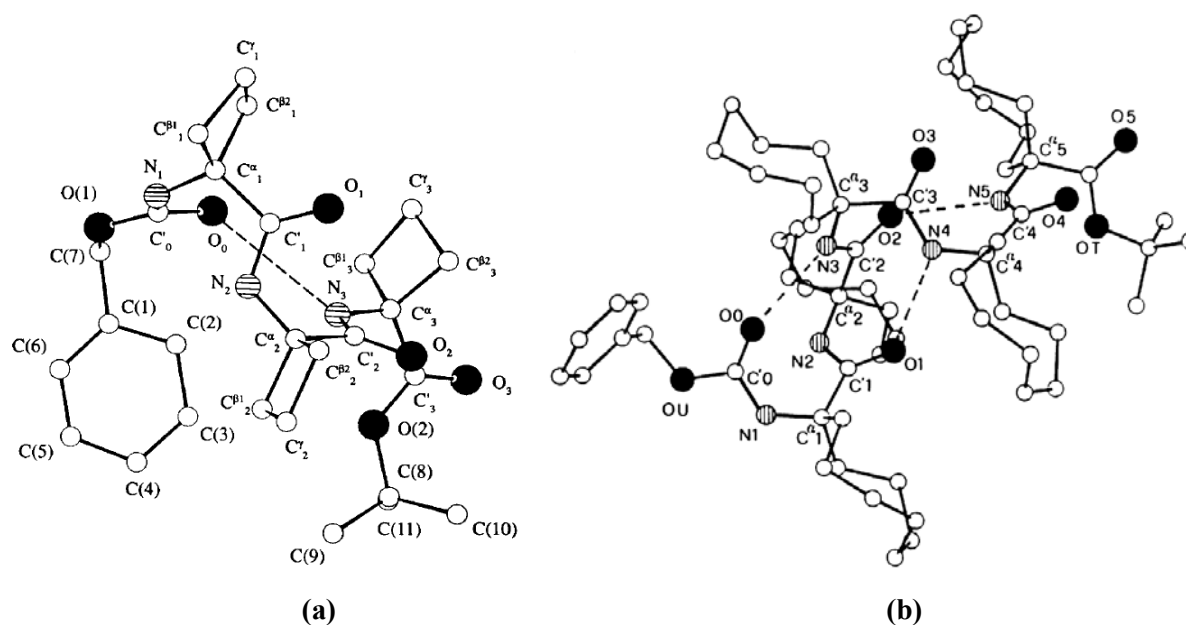


Figure 1.19. Crystal structures illustrating: (a) β -turn in Z -(Ac₄C)₃-Ot-Bu,¹⁰² and (b) 3_{10} -helix in Z -(Ac₉C)₅-Ot-Bu.¹⁰⁴

1.4.4.2.3. β -Turns Induced by β - or γ -Amino Acids

Seebach group has studied the formation of β -turns by β - and γ -amino acids. According to the X-ray diffraction, they reported that the tripeptide (cyclohexane- $\beta^{2,2}$ -disubstituted β -amino acid) exhibits β -turn conformation with the formation of a pseudocycle of 10 atoms (Figure 1.20).¹⁰⁶ In addition, NMR studies and molecular modelling method have shown that the β -derived peptide [(*S,S*)-*N*-acetyl- β^2 hVal β^3 hPhe-NHCH₃] displays β -turn conformaion.¹⁰⁷

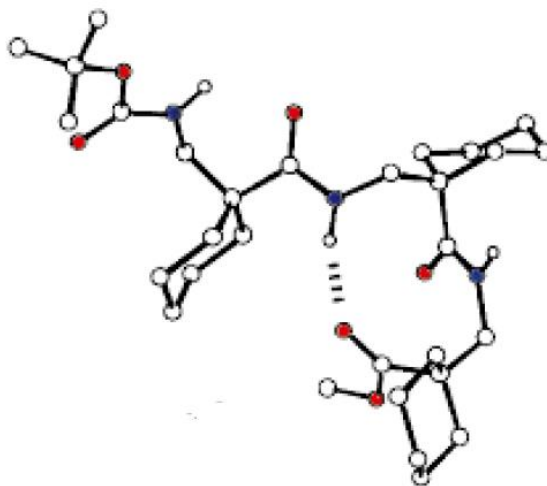


Figure 1.20. β -turn conformation of the tripeptide cyclohexane- $\beta^{2,2}$ -disubstituted β -amino acid in solid state.¹⁰⁶

Formation of β -turn by γ -amino acids depends on the absolute configuration of the asymmetric carbons. Seebach group has demonstrated by X-ray diffraction that the dipeptide (2, 4-disubstituted γ -amino acids) of inversed absolute configurations exists in β -turn conformation stabilized by an intramolecular hydrogen bond with the formation of a pseudocycle of 14 atoms (Figure 1.21).¹⁰⁸ The result was also confirmed by the NMR studies in CD₃OH.

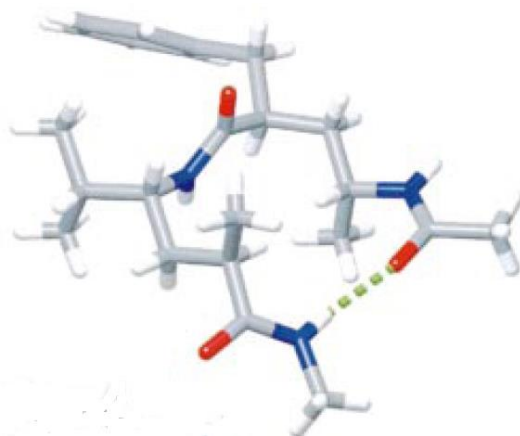


Figure 1.21. Crystal structure (X-ray) of the dipeptide 2, 4-disubstitued γ -amino acids.¹⁰⁸

I.5. Structure Modifications of Peptides

Designing new analogs that mimic the bioactive natural peptides has gained much interest especially in the medicinal chemistry field. Chemists used the approach of introducing chemical changes in the peptide skeleton or synthesizing peptidomimetics (Figure 1.22) in order to improve the physico-chemical properties of the peptides. These modifications were the start point of new two families termed “Pseudopeptides and Peptidomimetics”. Peptide analogs have been obtained by diverse approaches,¹⁰⁹ ranging from the simple replacement of the natural *L*-amino acids with their *D*-enantiomers, to the use of *N*-alkyl amino acids, α -substituted α -amino acids, β -substituted α -amino acids, proline analogs, γ - and β -amino acids, substituted α - or β -amino acids, *etc.*^{110,111}

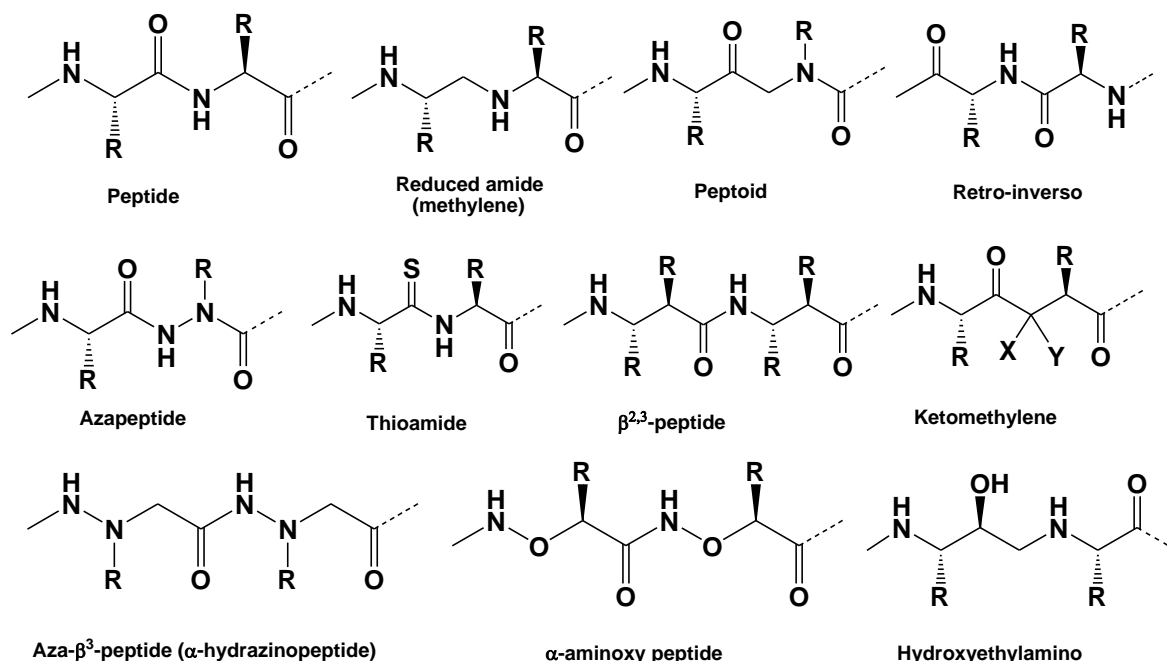


Figure 1.22. Selected examples of peptide modifications.

The main purpose of modifying or introducing specific moieties in peptide structure is to imitate secondary structure such as γ -turn, β -turn, β -sheet, α -helix, *etc.* that may lead to significant conformational differences compared with the native peptide and in such way it is no longer recognized by the protease of concern.^{58,59}

I.5.1. Pseudopeptides and Peptidomimetics

Designing of new peptidomimetics or pseudopeptides relies primarily on: (i) knowledge of the conformational, physico-chemical and electronic properties of the native peptide and its corresponding receptor,¹¹² (ii) introducing the appropriate structural effects (functional groups, polar or hydrophobic regions) into strategic positions to induce the required interactions with the receptors (hydrogen bond, hydrophobic interactions, *etc.*),⁸⁹ and (iii) the stabilization of conformation by introducing rigid elements^{113,114} must be taken into account. The major objective in the development of small molecules is to display pharmacological activity through mimicking the molecular interactions between natural proteins and their ligands.¹¹²

Peptidomimetics are peptide- and protein-derived compounds contain non-peptidic structural elements not cleaved by peptidases (Figure 1.22).⁷⁴ They can be obtained by structural modifications using unnatural amino acids. Peptoids, α -aminoxy peptides, hydrazinopeptides and β -peptides are examples of peptidomimetics (Figure 1.22). Peptidomimetic analog can imitate the conformational structure and the biological action of a natural peptide in its receptor-bound conformation.^{63,74}

Pseudopeptides are modified peptides contain non-proteinogenic or modified amino acid building blocks such as azapeptides, depsiptides, thiopeptides and ketomethylene peptides (Figure 1.22). Chemists used the approach of introducing chemical changes in the peptide backbone or side chain in order to increase the biological activity, selectivity, stability against hydrolysis enzymes in addition to optimize the hydrophilic/hydrophobic ratio to allow their passage through the physiological barriers.

I.5.2. Side Chain Modifications

The most straightforward approach for peptide modification is to introduce changes into the side chains of the amino acids. The strategy aims to introduce special functional groups to restrict the conformational flexibility of peptides or to enhance their metabolic stability. Introducing of *D*-configured amino acids, *N*-alkylated amino acids or *C*-dialkylated amino acids in the peptide structure are ways of these modifications (Figure 1.22).⁶¹

Incorporation of *D*-amino acids usually confers high metabolic stability on the peptide.^{115,116} Moreover, *D*-amino acids may also be used for the rational design of peptides with defined secondary structure because they stabilize a β II'-turn conformation when they exist in position (i + 1). Moreover, *D*-residues often enforce a different conformation of the peptide¹¹⁷ and strongly influence receptor affinity and selectivity.¹¹⁸ *N*-alkyl-substituted amino acids can favor the formation of turn structures because they often occur in position (i + 2) as β II-turn.¹¹⁹

I.5.3. Backbone Modifications

Among the modifications in the peptide structure recommended by pharmaco chemists, those introduced in the peptide backbone, particularly in the amide bond leaving the side chains without any modifications. Generally, side chains are necessary for high recognition by the active sites of the target proteins.¹²⁰ Peptide backbone can be modified in various ways either by extending the peptide chain by one more atom or by changing at least one peptide bond with an isosteric or isoelectronic surrogate (Figure 1.22). These modifications include:

- (i) The NH group of one or more amino acids within a peptide chain may be alkylated¹²¹ or exchanged by an oxygen atom (depsiptide), a sulfur atom (thioester), or a (CH₂) group (ketomethylene isoester).¹²²

Part A

Chapter I. Bibliography of Pseudopeptides (Aza-Peptides) and Peptidomimetics

- (ii) The CH moiety (C^α) may be exchanged in a similar manner by a nitrogen atom (azapeptide),^{123,124} by a C-alkyl group (C^α -disubstituted amino acid),¹²⁵ or by a BH⁻ group (borapeptide).
- (iii) The CO group may be replaced by thiocarbonyl group (endothiopeptide),¹²⁶ (CH₂) group (reduced amide bond),¹²⁷ (SO_n) groups (sulfnamides, n = 1; sulfonamides, n = 2), or (POOH) group (phosphoramides).
- (iv) The peptide bond (CO-NH) of one or more amino acid residues may be inverted giving retro peptides. In order to maintain the original side chain orientation, the retro modification has to be accompanied by inversion of the configuration at C^α to generate a new sequence called retro-inverso peptides.¹²⁸
- (v) Besides the previous isosteric replacements accompanied the peptide backbone, the peptide chain may also be modified by extending it with one more atom (O: aminoxy acid,¹²⁹ NH: hydrazino acid,^{130,131} CH₂: β -amino acid, *etc.*).^{132,133}

I.6. Conformational Aspects in Pseudopeptides and Peptidomimetics Series

I.6.1. N-Aminopeptides

N-aminopeptides are analogs of natural α -peptides. They are obtained when the NH proton of the peptide bond is replaced by a primary amine function (Figure 1.22). Marraud *et al.* have studied the structure of the (Piv-Pro- $N^\alpha(N^\beta H_2)$ -Gly-NHi-Pr) by X-ray diffraction and NMR spectroscopy (Figure 1.23a).

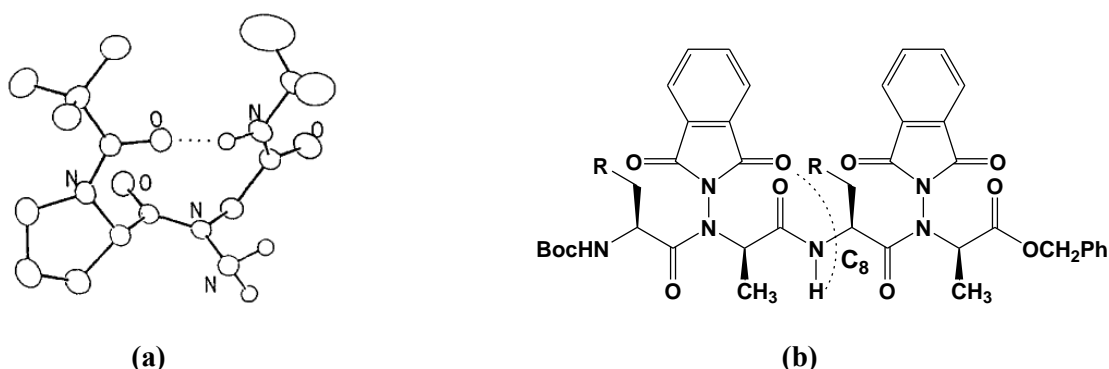


Figure 1.23. (a) Crystal structure of Piv-Pro- $N^\alpha(N^\beta H_2)$ -Gly-NHi-Pr,¹³⁵ and (b) C₈-hydrogen bond formation in 1:1-[α /N-amino]-tetramer.

The data highlighted the presence of an intramolecular hydrogen bond between the NH proton of the group NHi-Pr and the carbonyl oxygen atom of the Piv group of the type ($i \leftrightarrow i + 3$) closing a ring of 10 atoms (Figure 1.23a). The hydrogen bond distance (i -Pr) NH---OC (t -Bu) was 3.10 Å which is close to the value of the parent natural dipeptide (Piv-Pro-Gly-NHi-Pr) with a distance of 2.97 Å, suggesting the presence of β II-turn conformation.¹³⁴⁻¹³⁶

More recently, Dautrey *et al.* have studied the 1:1-[α /N-amino]-tetramer which is mixed pseudopeptide results from alternating of an amide bond with an N-amino link. The structure of this family is characterized by capping the amino (NH₂) group with a phthalimide moiety. They reported the ability of this pseudopeptide to self-organize in solution through an intramolecular hydrogen bond closing a ring of C₈ atoms between the carbonyl oxygen atom of the phthalimide group and the (NH) proton of the amide bond (Figure 1.23b).²⁵

I.6.2. Peptoids

In 1990, Bartlett defined peptoids as pseudopeptides containing *N*-alkylated glycines linked by peptide bonds.^{137,138} Formally, the nitrogen atoms of the peptide bonds are shifted to the C^α positions and the NH groups have been substituted by CH₂-groups (Figure 1.24).

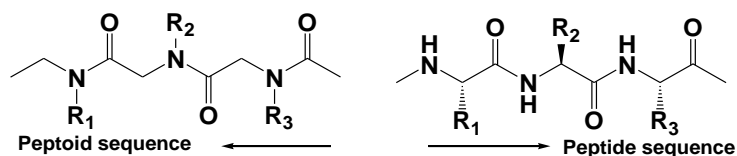


Figure 1.24. Peptide *versus* peptoid sequences.

These modifications result in: (i) sequence in a reverse direction to the native peptide (retro-sequence), and (ii) loss of the chirality of the α -carbons which decreases the probability of peptoids to adopt secondary structure,¹³⁹ however, some pentamers could adopt helical structure within various solvents.¹⁴⁰ Molecular dynamic calculations have predicted a stable helical structure with *cis*-configurations for all the amide bonds similar to the helical structure of polyproline.¹⁴¹ NMR studies have also confirmed these results and showed a helix with a pitch of 6.0 Å containing 3 residues.¹⁴²

I.6.3. β -Peptides

β -peptides are formed from the linkage of β -amino acids through amide bonds. β -amino acids are obtained by insertion of an additional (C) atom between the carboxyl group and C^α of a natural amino acid. Consequently, the side chains may be attached either to C^α (β^2 -peptide), C^β (β^3 -peptide), or to both C^α and C^β ($\beta^{2,3}$ -peptide) in which these modifications might exert an influence on the conformation of the resulted oligomer (Figure 1.25).¹⁴³

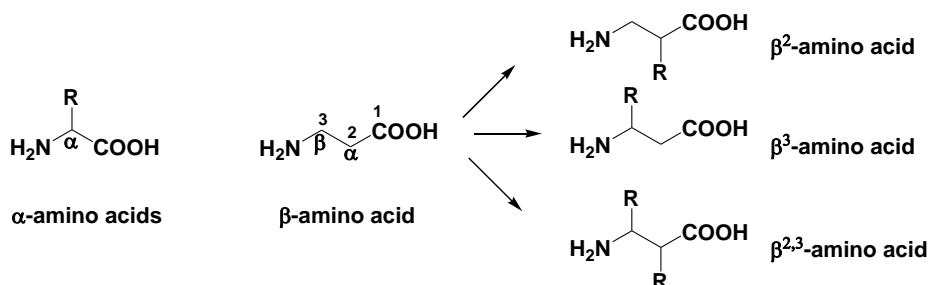


Figure 1.25. Different types β -amino acids.

β -peptides are one of the most important family in foldamers that have numerous studies related to Seebach, DeGrado and Gellman groups.^{4-9,79,81,82,143} They reported that in contrast to α -peptides, short- β peptides (less than six residues) could adopt well-defined secondary structures such as helices, sheets and turns. They concluded that the most favorable conformation is the 3_{14} -helix that obtained by forming a network of hydrogen bonds CO---HN in opposite direction to that of the α -helix (Figure 1.9).

The first structural investigations were performed on homo-oligomers of β -amino acids from about 55 years ago. Kovacs *et al.* postulated in 1965 that poly-(*L*- β -aspartic acid) forms a 3.4_{14} -P-helix [right-handed helix with 3.4 amino acid residues per turn] closing 14-membered ring by hydrogen bond between NH (*i*) and CO (*i*+2).¹⁴⁴ Gellman *et al.*^{5,79,145} and Seebach *et al.*^{9,146} profoundly examined the conformational behaviors of a series of different β -peptides. They investigated that these β -peptides could adopt predictable and reproducible helical conformations with hydrogen bond patterns

Part A

Chapter I. Bibliography of Pseudopeptides (Aza-Peptides) and Peptidomimetics

depending on the substituent position. Indeed, many β -peptides prefer 3_{14} -helices even in aqueous solutions^{9,81,147,148}. While formation of helices has been investigated in short β -peptides (hexamers), more than (10 - 12) amino acid residues are required to form a stable helix in the case of α -amino acids. An alternating combination of β^2 - and β^3 -amino acids leads to an irregular helix with 10- and 12-membered rings through intramolecular hydrogen bonds.¹⁴⁹

I.6.4. α -Aminoxypeptides

In 1996, Yang and Wu teams reported a new family of peptidomimetics called α -aminoxy peptide which is β -peptide analog obtained by the replacement of the β carbon by an oxygen atom (Figure 1.26). They found that introducing of α -aminoxy acid moiety in the peptide skeleton induced a particular conformation.¹⁵⁰ They performed theoretical calculations on the α -aminoxydiamide and they revealed that this molecule reflected the most favorably rigid structure through the formation a pseudocycle of eight membered ring. Moreover, the strength of the hydrogen bond was confirmed by the short O---H distance (2.02 Å) and the co-linearity of the N--H--O angle (159°).

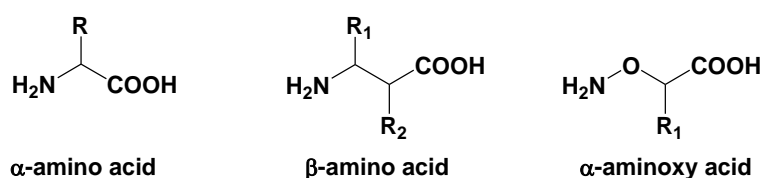


Figure 1.26. Representation of α -amino acid, β -amino acid and α -aminoxy acid.

NMR results in CDCl_3 and CD_2Cl_2 showed the involvement of each amidoxide NH proton in intramolecular hydrogen bond. Indeed, these NH protons were very sensitive to intermolecular interactions which also were confirmed by FTIR in three model types, two diamides and a triamide (Figure 1.27).¹⁵⁰

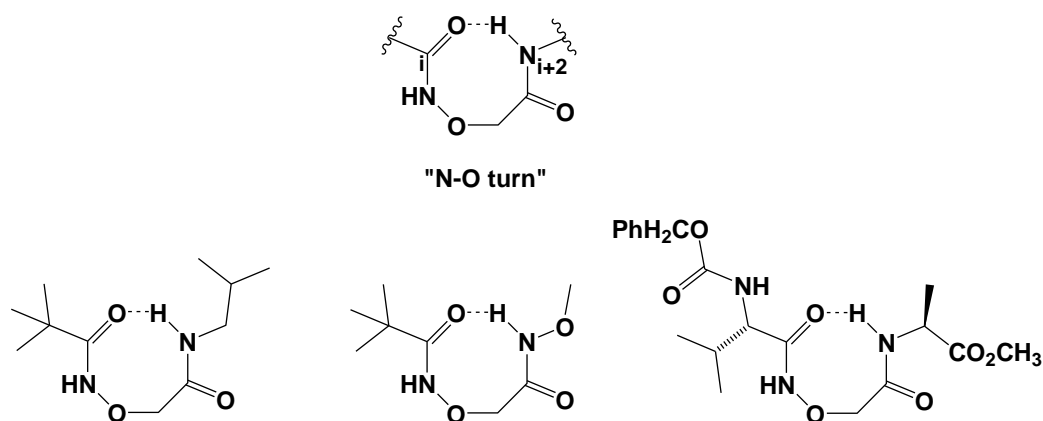


Figure 1.27. Examples of the N-O turn in three types of α -aminoxy derivatives.¹⁵⁰

ROESY experiments of the triamide, consisting of *D*-aminoxy leucine followed by *L*-aminoxy phenylalanine, showed the presence of strong dipolar coupling interaction between NH (i) and HC^α (i) protons, and weak interaction between NH (i) and HC^α (i - 1) protons (Figure 1.28a). These interactions suggested the formation of consecutive NO-turns closing pseudocycles of eight membered rings. X-ray diffraction of single crystals has demonstrated the same results as observed in the NMR experiments in solution (Figure 1.28b).¹⁵¹

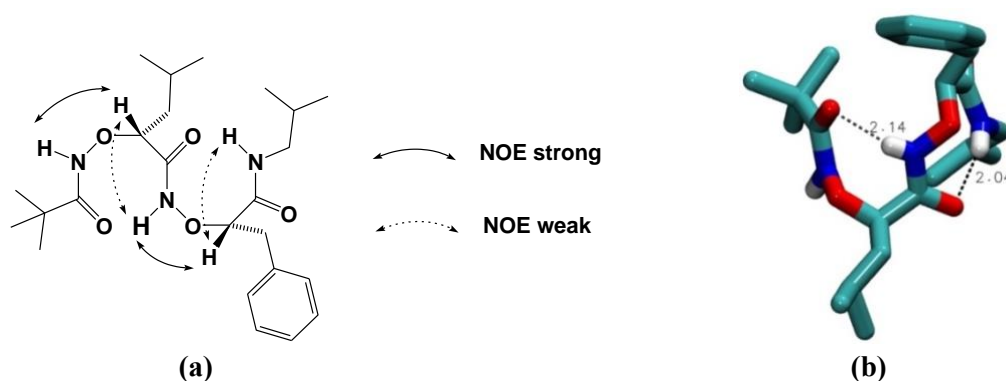


Figure 1.28. (a) NOE correlations in solution, and (b) crystal structure of α -aminoxytriamide.¹⁵¹

In 2003, the same group has designed new family of mixed oligomer of the type amide/ α -aminoxy since they suggested the possibility of this structure to induce γ -turn by the presence of NO-turn. The theoretical calculations of the amide/ α -aminoxy oligomers provided access to a new helical conformation.¹⁵² They reported that it is possible to induce a γ -turn in short peptide sequences by adding an α -aminoxy acid directly after a particular α -amino acid residue; between the NH ($i + 2$) of the α -aminoxy and C=O (i) of the α -amino acid residue. These theoretical studies were confirmed by 2D NMR studies in solution (Figure 1.29), however, the group reported that it was not possible to solve the crystal structures of these compounds.

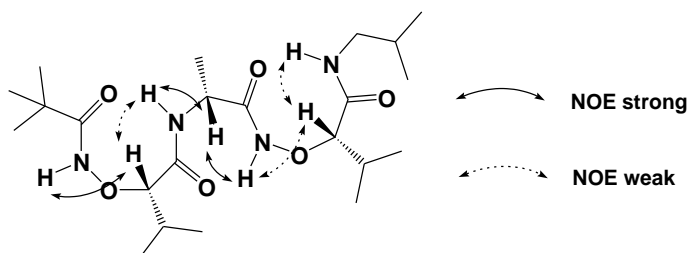


Figure 1.29. NOE correlations observed in ROESY of 1:1- $[\alpha/\alpha\text{-aminoxy}]$ -mer.¹⁵²

1.6.5. Aza- β^3 -peptides

More recently, Le Grel group was interested in studying a number of substituted N^α -hydrazinoacetic acid derivatives¹⁵³ which are more commonly called aza- β^3 -peptides. They are hydrazinopeptides in which chirality is carried by nitrogen atom (Figure 1.30).



Figure 1.30. Representation of aza- β^3 -peptide derivative of N^α -substituted- N^β -protected- α -hydrazinoacetic acid.

^1H NMR spectra of these compounds exhibited well-defined and discriminated NH signals, proposing that they adopt a specific structure in solution. Le Grel team suggested that the backbone of aza- β^3 -peptides could generate a network of hydrogen bonds based on succession of pseudocycles of eight membered rings similar to the case of α -aminoxy peptides.¹⁵¹ Structural studies of small primary amide units by 2D NMR allowed highlighting the NOE correlations in these molecules.

The results confirmed the presence of hydrazinoturn and network of bifid hydrogen bonds closing pseudocycles of C₅- and C₈-membered rings (Figure 1.31a).¹⁵⁴ X-ray crystallography confirmed the self-organization of the aza-β³-peptide amide dimer compounds by consecutive hydrazinoturns (Figure 1.31b).

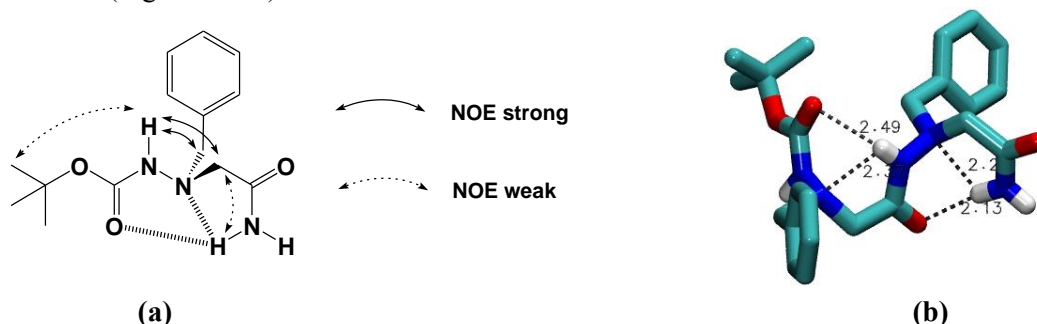


Figure 1.31. (a) NOE correlations in solution of aza-β³-peptide amide monomer, and (b) crystal structure of aza-β³-peptide amide dimer.¹⁵⁴

1.6.6. Hydrazinopeptides

Are analogs of β-peptides in which at least one of the β carbon atoms is replaced by nitrogen atom in β-peptide skeleton (Figure 1.32).

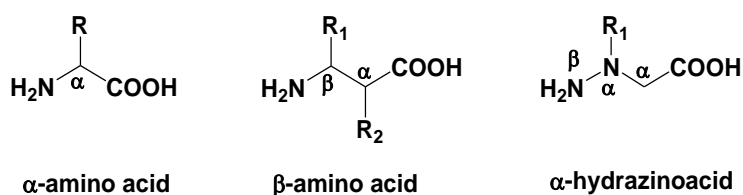


Figure 1.32. Representation of α-amino acid, β-amino acid and α-hydrazinoacid.

LCPM group in collaboration with Aubry's group have used X-ray diffraction for the structural studies of single crystals obtained from different hydrazinopeptides with two and three residues (Piv-Pro-Y-NHi-Pr; Y = azaGly or azaAla) to study the effect of the bis-nitrogen hydrazino bond on the conformation of peptides. They showed that these hydrazinopeptides, (*e.g.*, Piv-Pro-N^βH-N^αBn-CH₂-CO-NHi-Pr) where benzyl moiety is carried by the N^α atom, have adopted particular conformation (Figure 1.33).¹³⁴

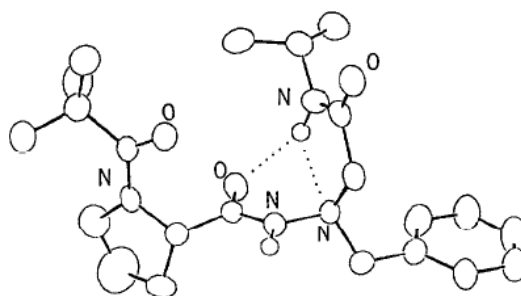


Figure 1.33. Crystal structure of Piv-Pro-N^βH-N^αBn-CH₂-CO-NHi-Pr.¹³⁴

The NHi-Pr proton had a bifurcated character forming two pseudocycles through intramolecular hydrogen bonds, the first with the carbonyl group of proline residue forming ring of C₈ atoms, and the second with the free lone pair of the nitrogen N^α atom (sp³ hybridization) closing a pseudocycle of C₅ atoms. So, the NHi-Pr linked by two intramolecular hydrogen bonds with the CO of proline and N^α of hydrazide, and this bifurcated bonds induce hydrazinoturns (Figure 1.33).¹³⁴

Part A

Chapter I. Bibliography of Pseudopeptides (Aza-Peptides) and Peptidomimetics

In 2001 and based on theoretical studies, Günther and Hofmann have extended the concept of β -peptides through the hydrazinopeptides.¹⁵⁵ They defined hydrazinopeptides as aza analogs of β -peptides because their skeleton composed mainly of hydrazinoacetic residues whose atoms are respectively assigned as C^α , N^α and N^β . The HN^α groups in this skeleton exhibit the possibilities to act as either hydrogen bond donor and/or acceptor through the classical interaction $CO\cdots HN$ and this induces a particular secondary structure. The authors suggested the entire possibilities of intramolecular hydrogen bonds network as well as the resulting conformations as illustrated in Figure 1.34. They reported that 3.3_{14} -helix and 1.75_8 -helix conformations have the lowest relative energy and are the most favorable conformations adopted by these hydrazinopeptides.¹⁵⁵

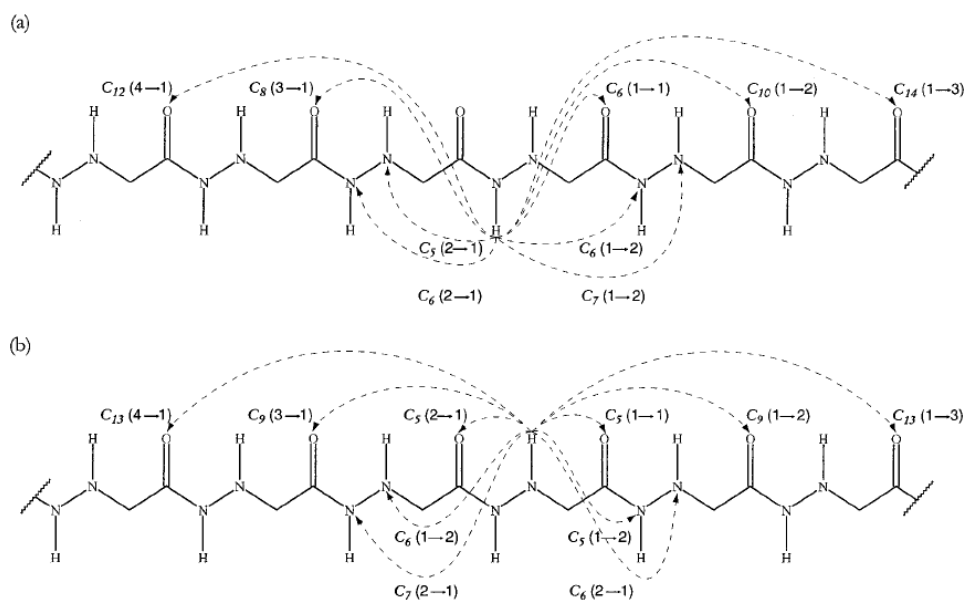


Figure 1.34. Possible hydrogen bonds network in hydrazinopeptides.¹⁵⁵

Indeed, the difficulty of obtaining enantiomerically pure α -hydrazinoacids and the lack of the effective methods for their incorporation into peptides, have limited for decades their uses as therapeutic agents. In 2003, Seebach and Lelais have succeeded in synthesis and studying the conformations of an enantiomerically pure α -substituted hydrazinohexapeptide in which the C^α bears the alkyl side chain (Figure 1.35). They proved by X-ray diffraction the folding of these β -peptide analogs through hydrazinoturns.¹⁰

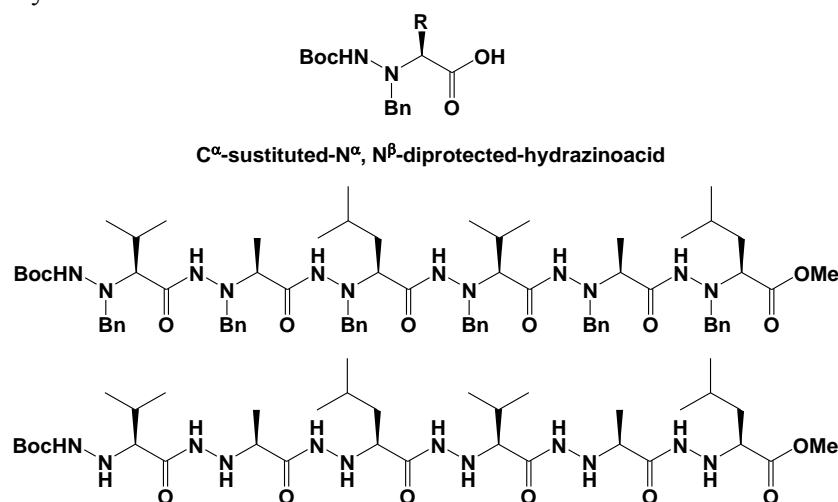


Figure 1.35. The primary C^α -substituted- α -hydrazinohexapeptides.

The thesis of Bouillon (2006) has concerned with the simulation and restrained molecular dynamics on mixed pseudopeptides, 1:1- $[\alpha/\alpha\text{-}N^{\alpha}\text{-}Z\text{-hydrazino}]$ -esters, in which the C^{α} is substituted by alkyl chain while N^{α} is protected by Z -group. The results showed that the folding by these molecules is stabilized by intramolecular hydrogen bond between HN^{β} of the residue (i) and the CO of Z -group of the residue (i + 2) leading to the formation of a pseudocycle of 12 atoms. The interesting behavior in these structures is the involvement of the CO of the Z -group and not of the peptide backbone in hydrogen bond formation (Figure 1.36). These results could not be confirmed by NMR studies in solution due to the broadness and poorly defined signals in the NMR spectra. In the other hand, FTIR studies confirmed the presence of intramolecular hydrogen bond within the molecule without sufficient information to conclude the exact conformation of the molecule under investigation.¹⁵⁶

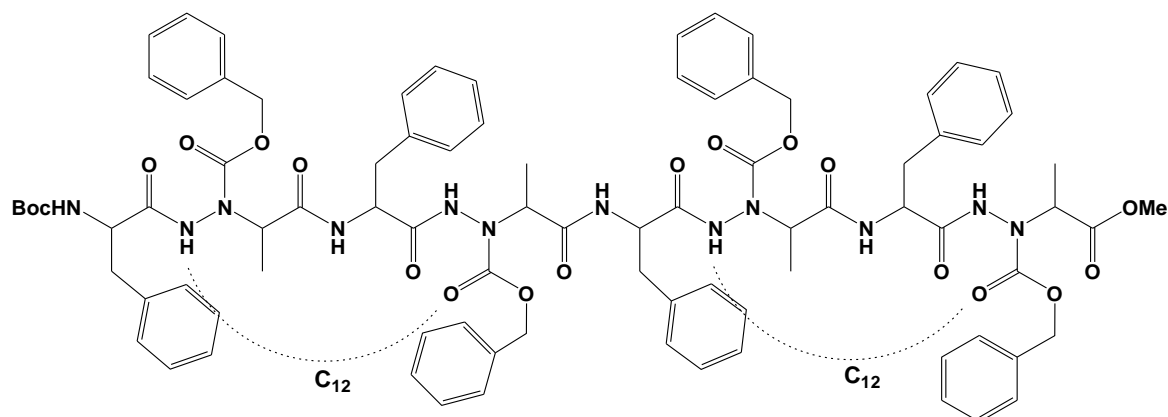


Figure 1.36. Possible hydrogen bonds in the octamer 1:1- $[\alpha/\alpha\text{-}N^{\alpha}\text{-}Z\text{-hydrazino}]$ -ester.¹⁵⁶

1.6.7. Azapeptides

Azapeptide analogs are derived by replacement of at least one carbon atom (C^{α}) of α -amino acid by a nitrogen atom (Figure 1.22).^{26,157} The structure of azapeptides has been studied by our laboratory in collaboration with the Laboratory of Crystallography, Magnetic Resonance and Modelling (CRM2) of Nancy. Indeed, Marraud *et al.* have synthesized azadipeptide (Piv-Pro-azaAla-NHi-Pr) which demonstrated its ability to adopt a β -turn conformation (Figure 1.37). Moreover, Aubry *et al.* have solved the crystal structure of this azadipeptide and they reported the formation of an intramolecular hydrogen bond closing a pseudocycle of C_{10} atoms with a distance (i -Pr) $\text{NH}\cdots\text{OC}$ (t -Bu) of 3.06 Å. This value is close to that obtained for normal peptides (i -Pr-CO-Pro- L -Ala-NHi-Pr; 3.05 Å) or (i -Pr-CO-Pro- D -Ala-NHi-Pr; 3.10 Å) in which they induce β -turn conformation.^{61,158}

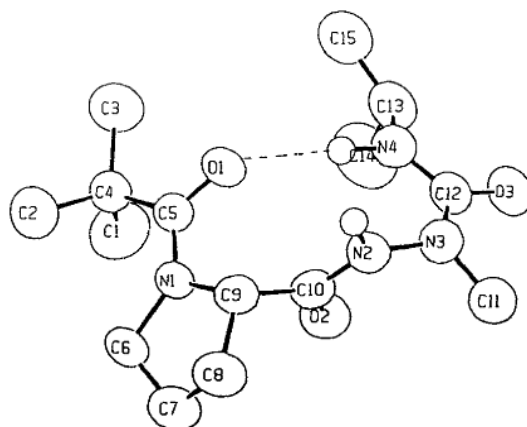


Figure 1.37. Crystal structure of Piv-Pro-azaAla-NHi-Pr.¹⁵⁸

Part A

Chapter I. Bibliography of Pseudopeptides (Aza-Peptides) and Peptidomimetics

Several studies have demonstrated that insertion of an aza-residue into the peptide backbone has intense effects not only on the geometrical structure of parent peptide, but also on its physico-chemical properties: (i) the CO-N amide bonds are elongated by 0.03 Å¹⁵⁹ while the N-N^α and N^α-CO bonds are shortened by 0.06 Å, compared to N-C^α and C^α-CO in natural peptides, (ii) the N-N^α-CO angle is larger by about 4 - 5° than the N-C^α-CO bond angle, (iii) the substituted nitrogen atom N^α adopts chiral property with a pyramidal nature of sp³ hybridization,^{26,159} (iv) reduction of the flexibility in the formed azapeptides compared with the parent one due to replacement of the rotatable C^α-C(O) bond by a more rigid urea N^α-C(O) structure, (v) electronic repulsion of the lone pairs of the two adjacent nitrogens restricts motion about the dihedral angle (ϕ),^{160,161} consequently (vi) conformational restrictions in the azapeptides have been predicted, which bend the peptide about the aza-amino acid residue away from a linear geometry.¹⁶²

Recently, Abbas-Quinternet *et.al.*^{24,30,163} have synthesized a new family of azapeptides of the type 2:1-[α/aza]-oligomers in which the aza-amino acid is connected to two normal amide linkages. They have proved that the aza-amino acid within the sequence (α-aza-α) induces a β-turn even in the absence of a proline residue which has already been reported by our group for the Pro-azaXaa-OH pseudopeptides (Xaa = Ala or Asn), in which the turn was only attributed due to the presence of the proline residue.⁹² FTIR and NMR studies of the homochiral hexamer Boc-(Phe-azaAla-Ala)₂-OMe in solution³⁰ as well as molecular dynamic calculations revealed the presence of three hydrogen bonds. Two hydrogen bonds between the NH protons of the two Ala residues and the (CO) carbonyl groups of the two Phe residues of the type (i ↔ i + 2) forming pseudocycles of C₇ atoms. The third hydrogen bond between the NH proton of Ala (i + 6) and the (CO) carbonyl group of the Ala (i + 3) from the type (i ↔ i + 3) closing a pseudocycle of C₁₀ atoms (Figure 1.38a).

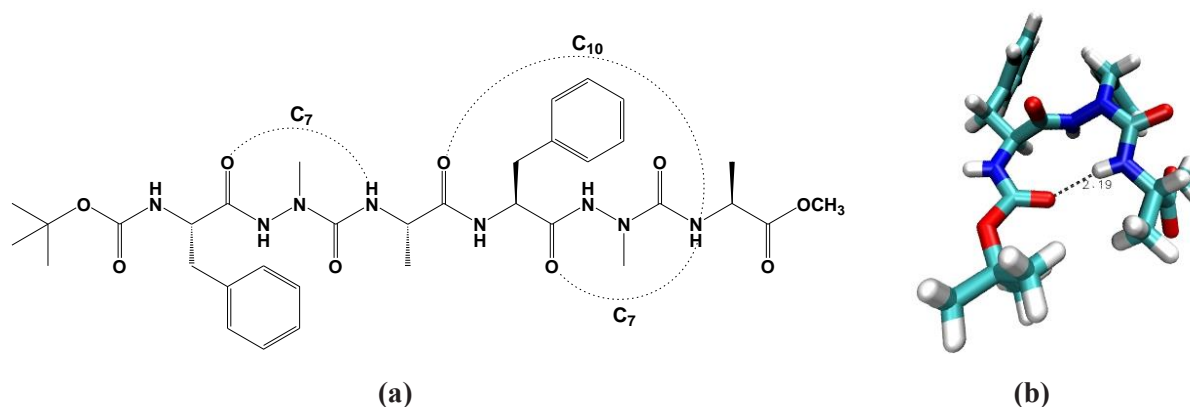


Figure 1.38. (a) Hydrogen bonds network in Boc-(Phe-azaAla-Ala)₂-OMe,³⁰ and (b) molecular crystal structure of Boc-Phe-azaPhe-Ala-OMe.²⁴

Moreover, they confirmed by X-ray diffraction analysis that the homochiral trimer Boc-Phe-azaPhe-Ala-OMe is folded by an (i ↔ i + 3) hydrogen bond between NH_{i+3} (Ala) and CO_i (Boc). All the amide bonds are *trans*-planar and the values of the torsional angles are typical of a βII-turn (Figure 1.38b).²⁴

More recently, further conformational and structural studies on the same azapeptide sequence, 2:1-[α/aza]-oligomers, were investigated by Zhou *et al.* in solution state.^{31,32} They have also studied the effect of introducing *D*-amino acid on the conformation of azapeptides. FTIR experiments together with molecular modelling based on NMR constraints of homo- and heterochiral trimers Boc-Y-azaPhe-Ala-OMe (Y = *L*-Phe or *D*-Phe) (Figure 1.39a, b), confirmed the possibility of hydrogen bond formation between the NH_{i+3} (Ala) and CO_i (Boc).

Part A

Chapter I. Bibliography of Pseudopeptides (Aza-Peptides) and Peptidomimetics

Structures were refined using molecular dynamic simulations and they clearly revealed the presence of a β IV-turn stabilized by a hydrogen bond between the amidic proton of the Ala and the carbonyl oxygen of the Boc group (Figure 1.39c, d).

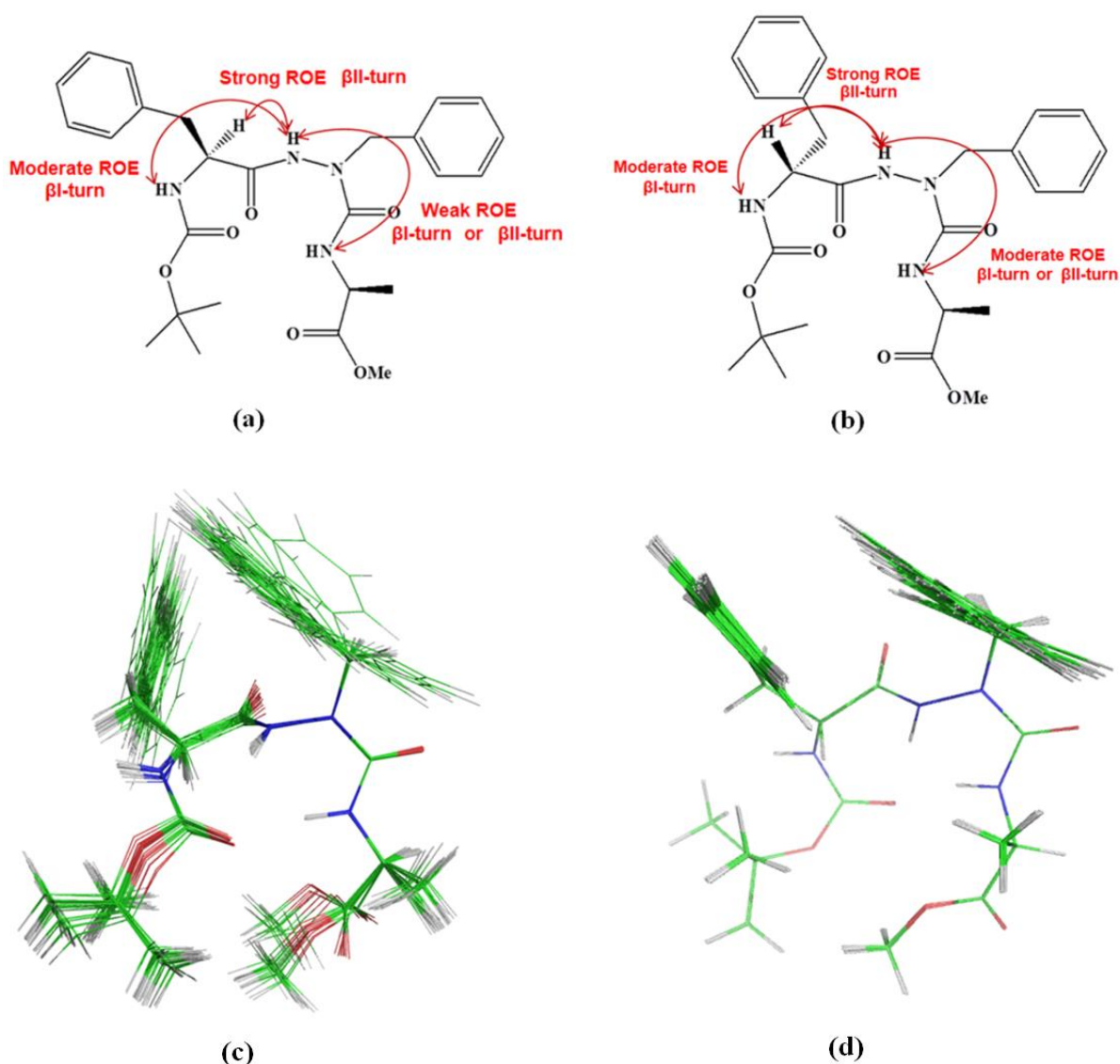


Figure 1.39. ROE correlations from 2D ROESY in solution for: (a) homochiral trimer, (b) heterochiral trimer. Molecular modelling calculations based on NMR structural constraints for: (c) homochiral trimer, and (d) heterochiral trimer; (trimer = Boc-*L*- or *D*-Phe-azaPhe-Ala-OMe).³¹

Zhou *et al.* have extended the structural studies on hexamers of the same azapeptides Boc-(Y-azaPhe-Ala)₂OMe (Y = *L*-Phe or *D*-Phe).^{31,32} Molecular modelling calculations based on NMR constraints of homo- and heterochiral hexamers showed that both oligomers exhibit a β IV-turn at the *N*-terminus stabilized by a hydrogen bond between CO_{*i*} (Boc) group and the NH_{*i+3*} (Ala). In the other side, the *C*-terminus demonstrated different conformations in the two oligomers. The homochiral oligomer displays two turns stabilized by hydrogen bonds between the CO_{*i+1*} (Phe) and NH_{*i+4*} (Phe) or/and NH_{*i+5*} (azaPhe) forming C₁₀ or/and C₁₃ pseudocycles, respectively (Figure 1.40a, c). The *C*-terminus of the heterochiral is characterized by C₇ or/and C₁₀ pseudocycles stabilized by hydrogen bonds between CO_{*i+3*} (Ala) and NH_{*i+5*} (azaPhe) or/and NH_{*i+6*} (Ala), respectively (Figure 1.40b, d).³²

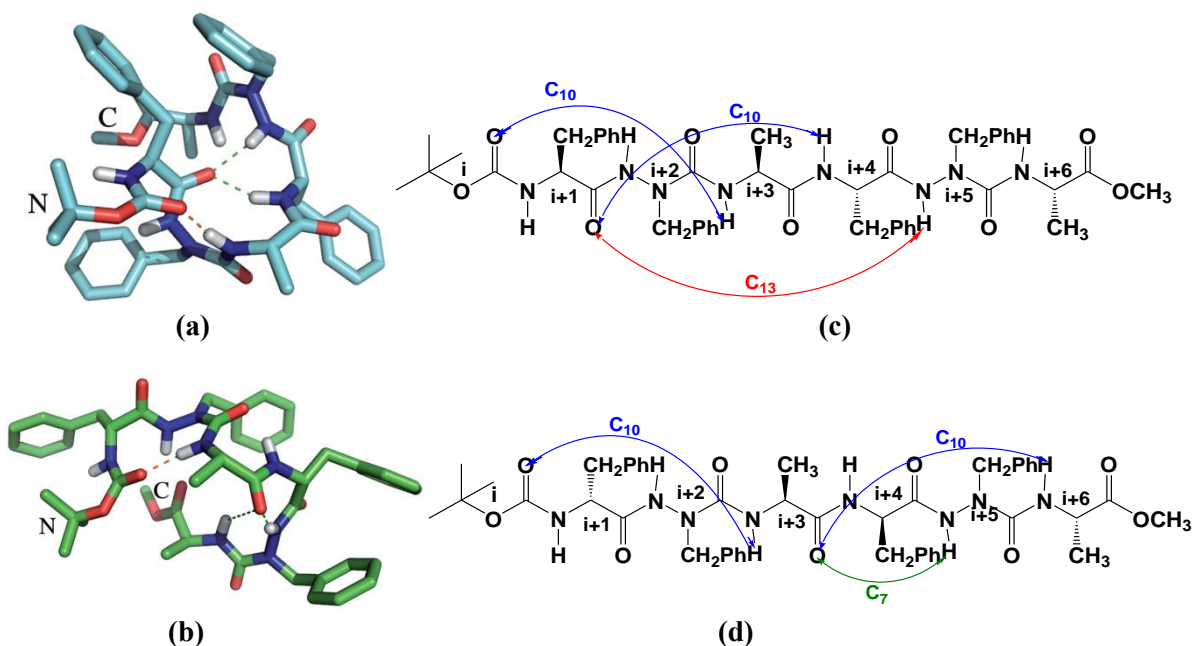


Figure 1.40. Models show the main conformations obtained by molecular modelling calculations based on NMR constraints for: (a) Boc-(Phe-azaPhe-Ala)₂-OMe, (b) Boc-(*D*-Phe-azaPhe-Ala)₂-OMe, (c and d) representations for the intramolecular hydrogen bonds in homo and heterohexamer Boc-(*L*- or *D*-Phe-azaPhe-Ala)₂-OMe, respectively.³²

The crystal structure of the homochiral oligomer (*SSSS*) Boc-(Phe-azaPhe-Ala)₂-OMe has been resolved by Abbas-Quinternet *et al.* confirming the presence of two β -turns of the types I and II through intramolecular hydrogen bonds of type ($i \leftrightarrow i + 3$) with the formation of pseudocycle of C₁₀ atoms (Figure 1.41).³² The difference in the conformations between the solid and solution states reveals that these compounds are not necessarily to adopt the same behaviors in solution and crystalline states.

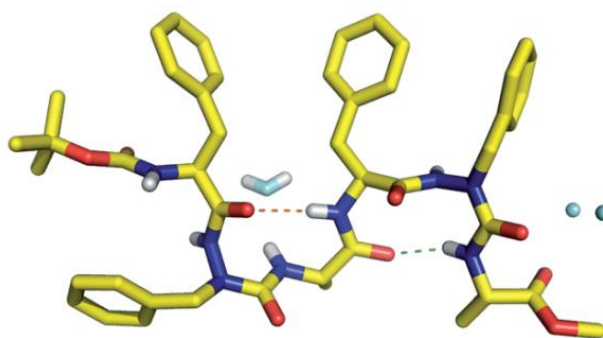


Figure 1.41. Representation of the main conformations adopted by Boc-(Phe-azaPhe-Ala)₂-OMe in solid state (X-ray), water molecules are represented in cyan.³²

Since we are interested in synthesis and studying of new peptide analogs containing azapeptide residues, the next sections will discuss in details the history, structural studies and conformational aspects of azapeptides and the effect of introduction aza-amino acids within the peptide sequence on inducing specific conformations in order to design new foldamers with potent potential applications.

Part A

Chapter I. Bibliography of Pseudopeptides (Aza-Peptides) and Peptidomimetics

I.7. History and Biological Interests of Azapeptides

Hans-Jürgen Hess and his collaborators were the first who have replaced an α -amino acid in a natural peptide chain with an aza-amino acid moiety in 1963.¹⁶⁴ They succeeded to incorporate an azaVal residue in position 3 forming an analog of the angiotensin bovine II (Figure 1.42).

The analog showed its biological activity by adjusting blood pressure through vasoconstriction process of the profound vessels.

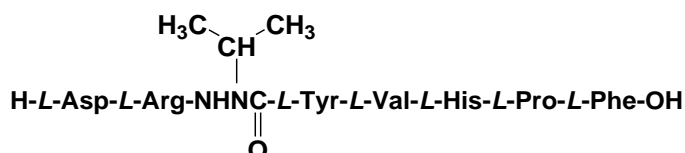


Figure 1.42. Azapeptide analog of angiotensin bovine II.¹⁶⁴

After that, azapeptides have been developed by several groups in order to synthesize analogs of hormones or inhibitors for the protease enzymes, *etc.*¹⁶⁵ Therapeutically, incorporation of certain aza-amino acids (serine and cysteine) in the peptide sequence has proved their efficacy in inhibition of the protease enzyme.¹²⁴ Example, atazanavir (BMS-232632) is a highly active azapeptide inhibitor against the HIV protease (Figure 1.43) and it has recently received approval for the human immunodeficiency virus (HIV) treatment.^{166,167}

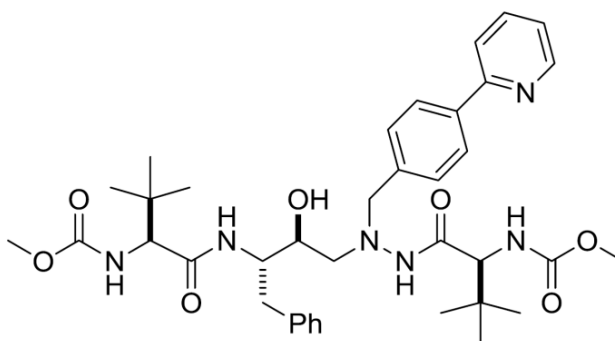


Figure 1.43. Representation of atazanavir azapeptide inhibitor against HIV protease.^{166,167}

Also agonists and antagonists analogs of the luteinizing hormone-releasing hormone (LHRH) have been prepared in order to produce or prevent ovulation.¹⁶⁸ ZOLADEX[®] is a product of this series and it has been applied as a medicine for the treatment of prostate cancer.¹⁶⁸

In our laboratory, Michel Marraud's group has synthesized a number of azapeptides of one, two and three residues.^{26,92,169-171} The dipeptides and tripeptides were developed with either azaAsp or azaAla residue then the group planned to study the effect of addition of proline residue in two different positions, before and after the aza moiety. The conformational analyses of these azapeptides have been investigated by X-ray diffraction, NMR and FTIR spectroscopies which demonstrated that:

Substitution of Asn/azaAsn or Ala/azaAla generates strong conformational changes. The nitrogen atom acquires *D*-chirality when the aza residue was positioned before the *L*-proline. As well as the nitrogen atom involved in β -folding whatever the aza residue in position ($i + 1$) or ($i + 2$). This conformation is not favorable in the natural peptides. There was ambiguity about the role of the aza-amino acids and proline in the β -folding, since both of them have proved their propensities to induce β -turn.

Part A

Chapter I. Bibliography of Pseudopeptides (Aza-Peptides) and Peptidomimetics

These azapeptide residues have been introduced into peptide sequences to study their biological activities. *N*-glycosylation is a biochemical process in which the carbohydrates are grafted on the peptidic chains to increase their tendency to enter the endoplasmic reticulum. Introducing an azaAsn within the sequence R-CO-Asn-Ala-Thr-NHR' increase the stability and encode the sequence to become unknown to the oligosaccharyltransferase (OST).

Myasthenia gravis is an autoimmune disease which arises when the antibodies block nicotinic acetylcholine receptors at the junction between the nerve and muscle. This prevents nerve impulses from triggering muscle contractions. In fact, auto-antibodies are mainly directed against an extracellular region of the acetylcholine receptor (AChR) which is called MIR (Main Immunogenic Region) which differs from that binds the acetylcholine itself. Substitution of Asn/azaAsn in the decapeptide MIR led to significant conformational changes in the *N*-terminal part resulting in total loss of the affinity towards the known anti-AChR antibodies. Substitution of Ala/azaAla in the MIR caused decreasing in the binding affinity for anti-AChR antibodies of torpedo fish.

William D. Lubell and collaborators studied azapeptides by performing "aza-scanning" on known peptides sequences in order to detect the biologically active compositions.^{58,172,173} The study based mainly on chemical modifications through consequence replacement of α -amino acid with an aza-amino acid in the peptide sequence, followed by studying the impact of each modification on the conformations and behaviors of the peptides. The synthesis and the chemical modifications were done on solid support. They have studied three biologically active peptides:⁵⁸ (i) the secretagogue growth hormone (which stimulates the production of organs), (ii) the agonist of the melanocortine receptor (which stimuli the production of the melanine in the cells of skin), and the antagonist of the human calcitonine peptidic hormone (hypocalcitonine and hypophosphoremiante hormone).^{172,173} The results showed that the formation of β II'-conformation in case of the aza analogs of the antagonist of the human calcitonine peptidic hormone has increased the power of the antagoniste. In the other hand, no data concerned the secretagogue growth hormone and the agonist of the melanocortine receptor have been published.

I.7.1. Preferred Conformations of Azapeptides

Azapeptides consist of two parts: a "hydrazine" part (blue) whose conformation is described by the twist angle ϕ and a "urea" element (red) with the dihedral angle ψ (Figure 1.44). The non-bound pair of the nitrogen is orienting perpendicular with the angle $\phi = \pm 90^\circ$, while the "urea" element tends to be planar. On the other hand, the presence of the N^α atom causes the loss of chirality either by the rapid inversion between the two pyramidal nitrogen geometries or by the planar structure around the N^α atom which is favored by conjugation effect.

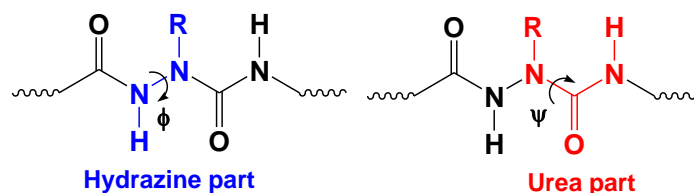


Figure 1.44. Elements of azapeptide.

To determine the role of an aza-amino acid in azapeptide sequence, the structural analyses of the azapeptides have been studied by some groups using either quantum chemistry and/or X-ray diffraction.^{174,175}

I.7.2 Influences of the Nature of Side Chain and Introducing of an Aza-Amino Acid on the Conformations of Pseudopeptides

Conformational disruption caused by insertion of aza-amino acid residue within a peptide chain was predicted by Lee's group using *ab initio* calculations.²⁸ They reported that the most stable conformation corresponding to the compositions For-azaXaa-NH₂ model (Xaa = Gly, Ala, Leu) (Figure 1.45a) is the β -folding with dihedral angles of $\phi = 90^\circ \pm 30^\circ$ for the N-N ^{α} bond and $\psi = 0^\circ \pm 30^\circ$ or $180^\circ \pm 30^\circ$ for the N ^{α} -C(O) bond. The calculations were done by taking into consideration the repulsion between the non-bound electron pair of the nitrogen and the partial double bond character of the N ^{α} -CO bond.

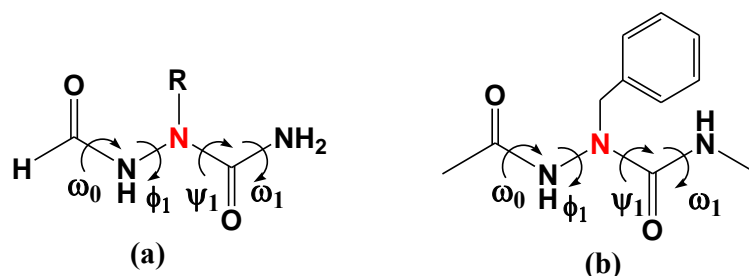


Figure 1.45. Illustration of the torsion angles in: (a) For-azaXaa-NH₂ (Xaa = Gly, Ala, Leu), and (b) Ac-azaPhe-NHMe.

Furthermore, the same group has performed *ab initio* calculations for the structure Ac-azaPhe-NHMe (Figure 1.45b). The dihedral angles corresponding to the most stable conformation were $\phi = \pm 91^\circ \pm 24^\circ$, and $\psi = \pm 18^\circ \pm 10^\circ$ (or $\pm 169^\circ \pm 8^\circ$).²⁷ Interestingly, these dihedral angles are similar to those calculated for the For-azaXaa-NH₂ compounds (Xaa = Gly, Ala, Leu). The values of the dihedral angles (ϕ , ψ) of the aza-amino acid residues in the compounds Ac-azaPhe-NHMe and For-azaXaa-NH₂ (Xaa = Gly, Ala, Leu) suggested that the incorporation of azaXaa residue in position ($i + 2$) peptide could stabilize β -turn. They confirmed this suggestion by using various methods including *ab initio* calculations, NMR, FTIR and molecular modelling to analyze the tripeptides Boc-Phe-azaLeu-Ala-OMe and Boc-Phe-azaPhe-Ala-OMe, Figure 1.46.

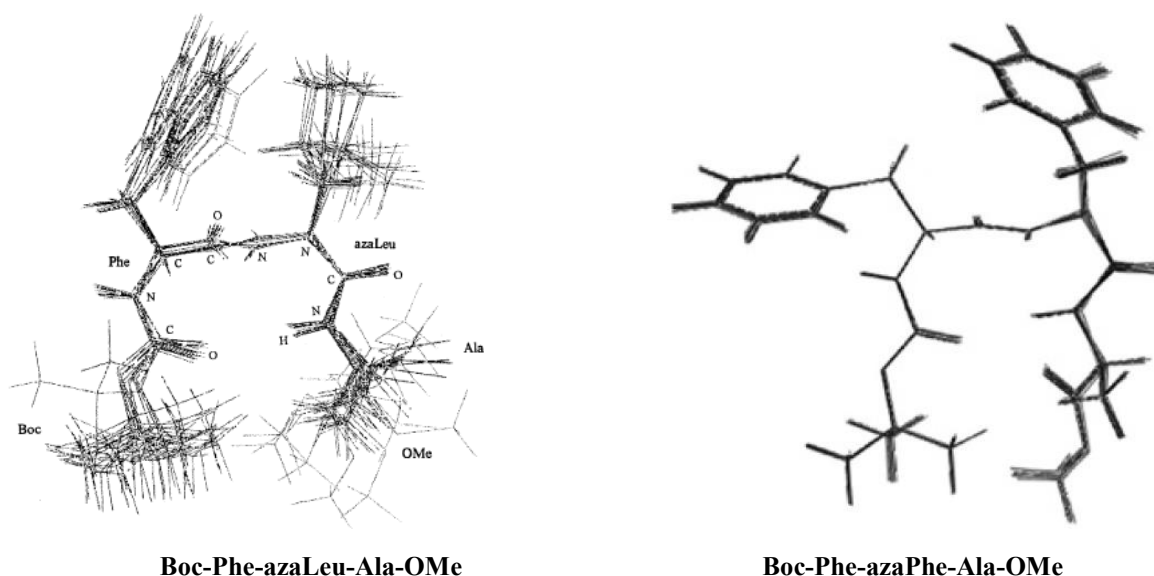


Figure 1.46. Superposition of the lowest energy structures for the tripeptides obtained by molecular dynamics based on NMR structural constraints.^{27,28}

The group reported the following:

- (i) Temperature dependent ^1H NMR indicated that the NH proton of residue Ala is involved in intramolecular hydrogen bond.
- (ii) By using FTIR, they observed a band between 3400 and 3200 cm^{-1} which corresponds to the stretching vibration when the NH proton is involved in hydrogen bonding
- (iii) The presence of certain NOE correlations indicates that the carbonyl group of the Boc group is engaged in intramolecular hydrogen bond to form a pseudocycle of C_{10} atoms.
- (iv) Constrained molecular modelling using NOE correlations showed that the two tripeptides adopt a βII -turn with an intramolecular hydrogen bond between the NH proton of Ala residue and the carbonyl (CO) of Boc group (Figure 1.46).

Michel Marraud *et al.* have synthesized and studied a number of azapeptides containing two and three residues.^{26,92,170,171} X-ray diffraction, NMR and FTIR spectroscopies have shown that the *Z*-azaAsn(Me)-Pro-NHi-Pr, *Z*-azaAsp(EtO)-Pro-NHi-Pr, Boc-azaAla-Pro-NHi-Pr, Piv-Pro-azaAsn(Me)-NHi-Pr, and Piv-Pro-azaAla-NHi-Pr (azaXaa is the aza-analog of amino acid residue) exist in β -turn conformation. Furthermore, the β -turn was not disturbed by the presence of hydrogen bond donor or hydrogen bond acceptor in the side chain as in the case of azaAsn or azaAsp, respectively. They explained that these molecules fold into β -turn by intramolecular hydrogen bonds between the NH proton (*C*-terminus residue) and CO (*N*-terminus residue) of the type ($i \leftrightarrow i + 3$).

According to X-ray results, they concluded that molecules with the sequence azaXaa-Pro adopt βI -turn, and the N^α atom acquires a *D*-configuration when the aza residue is linked to an *L*-proline (Figure 1.47). They investigated that the N^δH proton of (azaAsn) is involved in intramolecular hydrogen bond with the N^α of azaAsn residue forming a pseudocycle of C_5 atoms.²⁶

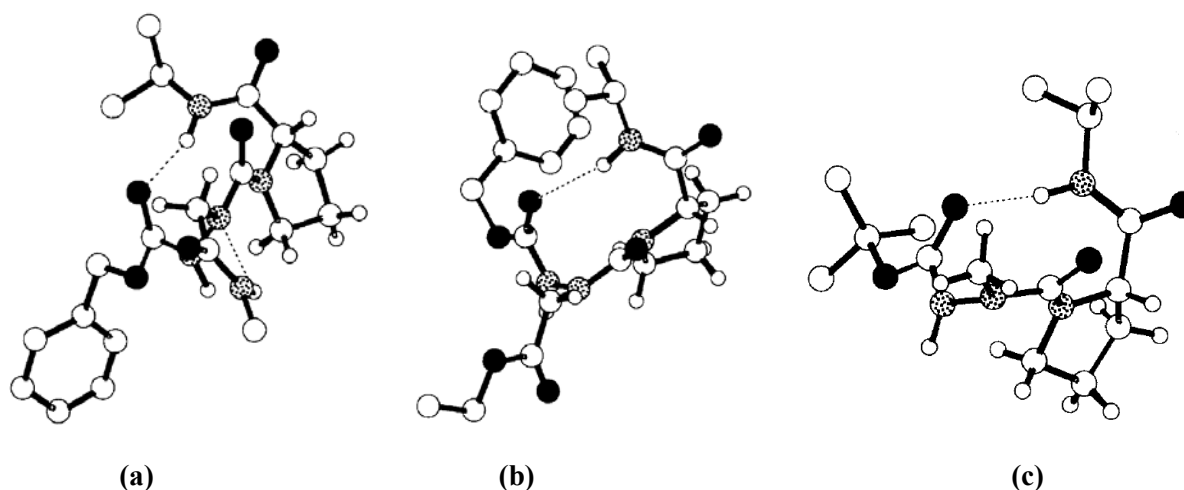


Figure 1.47. Crystal structures of the azapeptides: (a) *Z*-azaAsn(Me)-Pro-NHi-Pr, (b) *Z*-azaAsp(OEt)-Pro-NHi-Pr, and (c) Boc-azaAla-Pro-NHi-Pr.²⁶

In case of the sequence Pro-azaXaa, authors demonstrated that the two molecules induce βII -turn which stabilized through an intramolecular hydrogen bond between NH (*i*-Pr) and CO (Piv). Compared with the *Z*-azaAsn(Me)-Pro-NHi-Pr molecule, authors revealed that the NH of azaAsn of the molecule Piv-Pro-azaAsn(Me)-NHi-Pr is involved in a hydrazine turn which is characterized by bifid intramolecular interactions. The N^δH proton of the azaAsp ($i + 2$) interacts intramolecularly with both the carbonyl group (*i*) of the Pro residue, and with the electron pair of the nitrogen N^α of the azaAsp closing two pseudocycles of eight and five atoms, respectively (Figure 1.48).²⁶

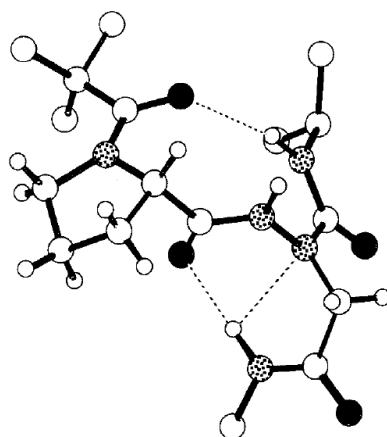


Figure 1.48. Solid state structure of Piv-Pro-azaAsn(Me)-NH-Pr.²⁶

1.7.3. Influence of the Position of the Aza-Amino Acid Residue on Azapeptides Conformations

In previous studies on azapeptides, our group showed that changing the position of the aza-amino acid residue resulted in structure variations. While the Ala-azaPro sequence favors β -turn conformation, azaPro-Ala sequence prefers an open structure. The difference in behavior has been explained as: the *cis*-configured conformation is more favorable for the amide bond in the sequence azaPro-Ala.¹⁷⁵

To investigate the role of the aza-amino acid residue in peptide structure and the influence of the chain length variation, Lee's group used the *ab initio* MO theory to calculate the dihedral angles corresponding to the most stable conformer of the compound For-Ala-azaAla-NH₂. The dihedral angles of the most stable conformer were ($\phi_1 = -61^\circ$, $\psi_1 = 131^\circ$, $\phi_2 = 79^\circ$, $\psi_2 = 15^\circ$) which belong to the β II-turn (Figure 1.49). They also reported that the NH (4) proton is involved in two intramolecular hydrogen bonds, one with the N (2) of azaAla residue with a distance of 2.39 Å, and the other with the O (1) of the formaldehyde group forming pseudocycle of C₁₀ atoms (Figure 1.49).²⁹

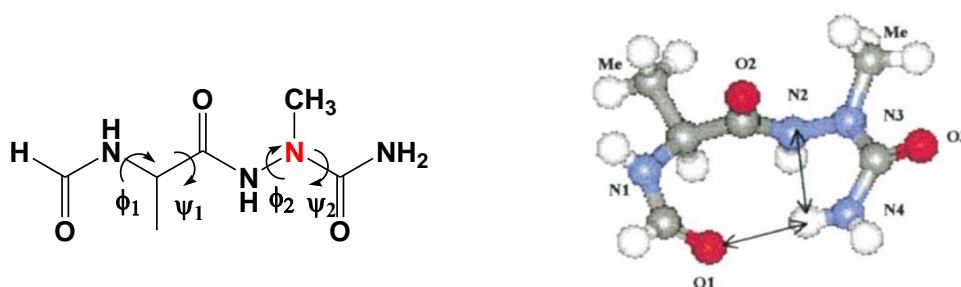


Figure 1.49. Structural formula of the compound For-Ala-azaAla-NH₂ and its most stable conformation at the HF/6-31G* theory level.²⁹

NMR and FTIR studies of the tetrapseudopeptide Boc-Ala-Phe-azaLeu-Ala-OMe showed that this pseudopeptide conserves the β -turn conformation in solution and the conformation is stabilized by the presence of intramolecular hydrogen bond between NH proton of Ala (4) residue and the CO group of the Ala (1) residue. In addition, the strong NOE correlation between C ^{α} H (Phe 2) and NH (azaLeu 3), and the weak NOE correlation between NH (azaLeu 3) and NH (Ala 4) indicated that this azapeptide may adopt a β II-turn conformation (Figure 1.50a).²⁹

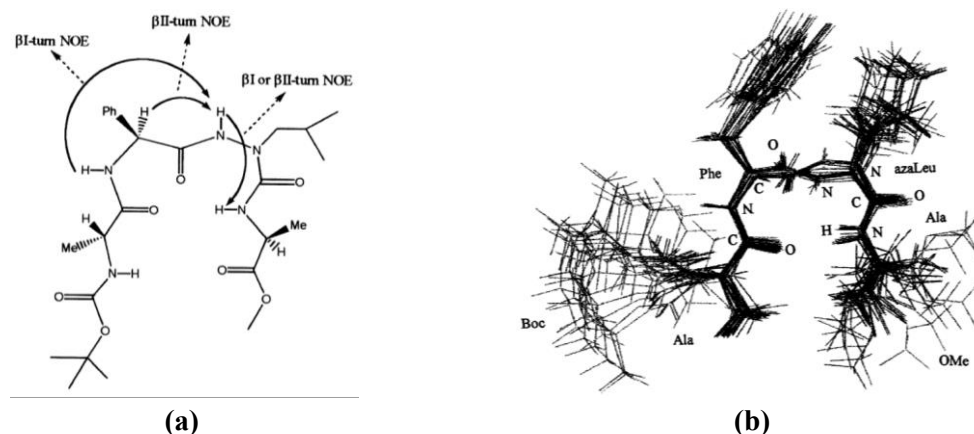


Figure 1.50. (a) NOE correlations in Boc-Ala-Phe-azaLeu-Ala-OMe, and (b) superposition of the lowest energy structures obtained from molecular dynamic calculations based on NOE constraints.²⁹

Moreover, molecular dynamic based on NOE restraints predicted that this tetrapeptide could adopt β II-turn stabilized by intramolecular hydrogen bond between NH proton of the Ala (4) residue and the CO group of Ala (1) residue (Figure 1.50b).

Finally, Lee's group documented that the tripeptide Boc-Phe-azaleu-Ala-OMe adopts the same conformation of the tetrapeptide Boc-Ala-Phe-azaLeu-Ala-OMe.^{27,29} These results reveal that the variation in chain length or changing the position of the aza-amino acid in the peptide chain has no much influence on the conformations of azapeptides.

Hofmann's group also studied the influence of the position of aza-amino acid on the azapeptides structures.¹⁷⁴ They studied two series of compounds of the sequences Ac-azaXaa-L-Ala-NHMe and Ac-L-Ala-azaXaa-NHMe with (azaXaa = azaGly and azaAla) in second and third positions. The *ab initio* calculations predicted that the most stable conformation for the two sequences is β I-turn when the aza-amino acid is at position (2), while it is β II-turn conformation when the aza-amino acid is incorporated in position (3).¹⁷⁴

These results were also confirmed by Michel Marraud's group in our laboratory, they demonstrated by X-ray diffraction that β I-turn is the preferred conformation for the azapeptides when the aza-amino acid in the second position, while it adopts the β II-turn conformation when the aza-amino acid occupying the third position (Figure 1.51).²⁶

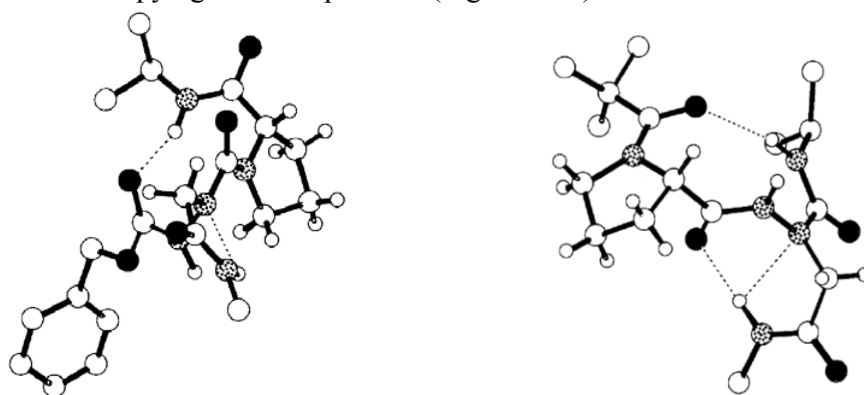


Figure 1.51. X-ray structures of: (left) Z-azaAsn(Me)-Pro-NHi-Pr, and (right) Piv-Pro-azaAsn(Me)-NHPr.²⁶

Therefore, we could conclude that changing the position of aza-amino acid may have an influence on the nature of β -turn conformation.

Part A

Chapter I. Bibliography of Pseudopeptides (Aza-Peptides) and Peptidomimetics

I.7.4. Influence of the Nature of the Amino Acid Preceding the Aza-Amino Acid Residue on the Azapeptides Conformations

Lee's group has synthesized tripeptides of the sequence Boc-Xaa-azaPhe-Ala-OMe [Xaa = Gly (1), Ala (2), Phe (3), Asn (4)] to study the influence of the nature of the amino acid preceding the aza-amino acid residue on the type of β -turn in solution.²⁷

They concluded from the NOE correlations results that the four tripeptides are all in the β -turn forms; mixed between β I- and β II-turns. FTIR and NMR spectroscopies showed that the NH Ala (3) is involved in an intramolecular hydrogen bond. In the other hand, molecular dynamic based on NMR restraints showed that the structures of these tripeptides (Boc-Xaa-azaPhe-Ala-OMe) induce β II-turn conformation (Figure 1.52).

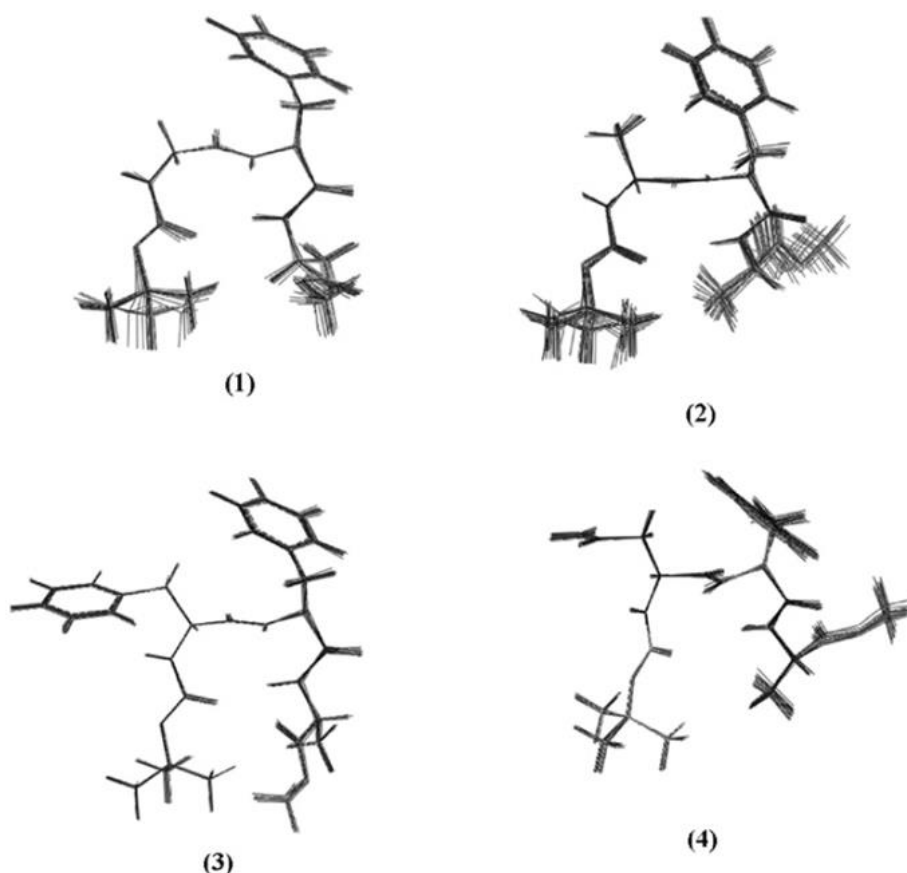


Figure 1.52. Superposition of the lowest energy structures of the tripeptides Boc-Xaa-azaPhe-Ala-OMe [(Xaa = Gly (1), Ala (2), Phe (3), Asp (4)]; obtained from molecular dynamics based on NOE constraints.²⁷

These results suggest that the nature of the amino acid residue preceding the azaPhe has little influence on the conformations of azapeptides.

I.7.5. Relationship between the Configuration of N^α and the Conformations of Azapeptides

In azapeptides, delocalization of non-bound pair of the N^α atom with the carbonyl group leads to a planar structure with nitrogen atom of sp^2 hybridization, however, this nitrogen atom showed a gap from the planar structure by tenths of angstroms reflecting its pyramidal character with sp^3 hybridization.^{30,31}

Part A

Chapter I. Bibliography of Pseudopeptides (Aza-Peptides) and Peptidomimetics

In solution, chirality in azapeptides has gained much attention because of possible inversion that can occur in the N^α atom affecting the conformation of the azapeptides. Therefore, orientation of side chains of aza-amino acids has gained an interesting subject of study to see its effect on the conformations of azapeptides.

According to the calculations by quantum chemistry for two series of azapeptides sequences Ac-azaXaa-L-Ala-NHMe and Ac-L-Ala-azaXaa-NHMe (azaXaa = azaGly and azaAla), Hofmann's group¹⁷⁴ reported that N^α atom is pyramidal and it adopts (*D*) configuration in the β I-turn conformation, and consequently they concluded that N^α would acquire (*L*) configuration in the β I'-turn. This configuration is independent of the position of the *L*-amino acid in the dipeptide. In contrast, in case of β II-turn, the configuration of the N^α atom depends on the position of the aza-amino acid. If aza-amino acid is in the second position, the N^α atom acquires (*D*) configuration, while it adopts (*L*) configuration in β II'-turn conformation. The situation is reversed for the aza-amino acid in third position.

These results were confirmed by the X-ray diffraction studies by our group. They showed that the N^α atom has a (*D*) configuration in β I-turn (Figure 1.53) for the azaXaa-Pro sequence.²⁶

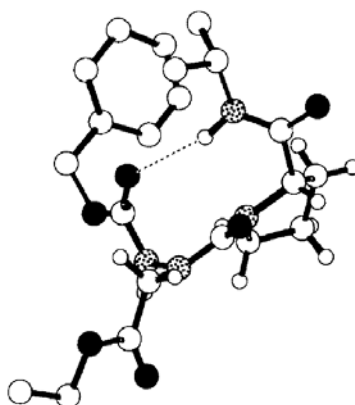


Figure 1.53. Solid state structure of the compound Z-azaAsp(OEt)-Pro-NHi-Pr.²⁶

In the previous studies, our group has succeeded to develop two new sequences based aza-amino acid: (a) the pseudodipeptide sequence α /aza, and (b) the pseudotripeptide sequence α /aza/ α . Moreover, the group was interested in their oligomerizations which generated two new families.

The nomenclature of these azapeptide families was established based on Gellman's principles for nomenclature of oligomers. Accordingly, the two families could be noted as 1:1- $[\alpha$ /aza]-oligomers and 2:1- $[\alpha$ /aza]-oligomers, where the first and second digits refer to the number of α -amino acid and aza residues in the repeating unit, respectively (Figure 1.54). The term oligomer indicates the total number of residues in the chain (dimer ---< two residues, trimer ---< three residues, tetramer ---< four residues, etc.).

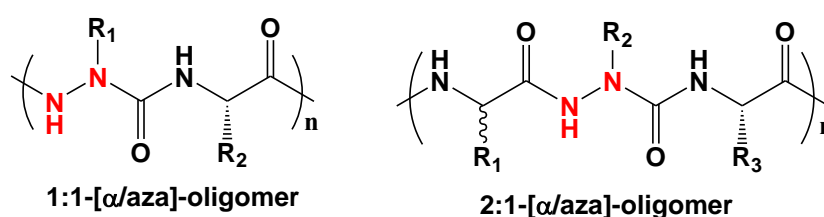


Figure 1.54. Structural formula of 1:1- $[\alpha$ /aza]-oligomers and 2:1- $[\alpha$ /aza]-oligomers.

Part A

Chapter I. Bibliography of Pseudopeptides (Aza-Peptides) and Peptidomimetics

Concerning the sequence 1:1-[α /aza]-oligomers, they are heterogeneous mixed oligomers (similar to 1:1-[α /NO]-oligomers),¹⁷⁶ it was found that their synthesis is quite problematic due to a lack of reactivity of the synthons. Furthermore, the structural studies of these compounds do not allow them to clearly define the type of folding as they showed their propensities to exist in equilibrium between many conformers. Consequently, the group directed towards studying the 2:1-[α /aza]-oligomers in which their oligomerization and structural studies are more accessible.

In the next chapter (II), we will mention the different methods for the synthesis of azapeptides evaluating the appropriate one for the synthesis of our 2:1-[α /aza]-oligomers. Then, we will describe the general strategy which has been used in the synthesis of new oligomers possessing lysine residues. Some physico-chemical techniques for the structural and conformational analyses will be also overviewed in this chapter. The structural and conformational studies of new linear and cyclic 2:1-[α /aza]-oligomers will be overviewed in chapters III and IV, respectively.

Chapter II. Synthesis and Methods of Analysis of 2:1-[α /aza]-Oligomers

II.1. Introduction

Synthesis and designing of new [α /aza]-oligomers have gained the interest of our group not only because of their various potential applications, but also to study their structural activity relationship (SAR). Accordingly, we decided to synthesize and study new azapeptides belong to the families 1:1- and 2:1-[α /aza]-oligomers (Figure 2.1).

We planned to use Boc chemistry because the residual by-products of Boc can be easily removed and it affords products in good yields.²⁴ Our strategy is based on the use of the benzyl moiety as the lateral chain carried by the N $^{\alpha}$ atom which has advantages of being the side chain of the phenylalanine amino acid residue that may: (i) support the folding and self-assembly phenomena, (ii) increase the stability of the final oligomers through π -interactions, (iii) increase rigidity and reducing flexibility by its phenyl ring, and (iv) increase hydrophobicity which is necessary for hydrogelation process. In our study, we suggested that the incorporation of basic amino acid (lysine) with supplementary nitrogen atom (N $^{\epsilon}$ H) in its side chain may: (i) produce oligomers with good selectivity in gases separation by membrane technology, and (ii) optimize the hydrophilicity/lipophilicity ratio of the final oligomers which may support the hydrogelation phenomenon.

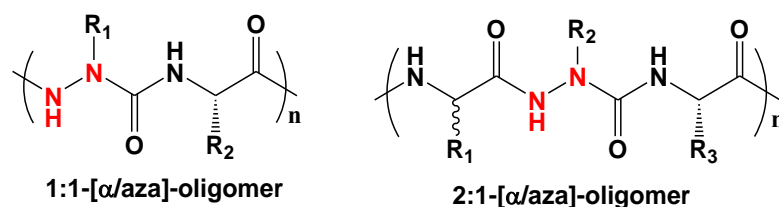


Figure 2.1. Structural formula of 1:1-[α /aza]-oligomers and 2:1-[α /aza]-oligomers.

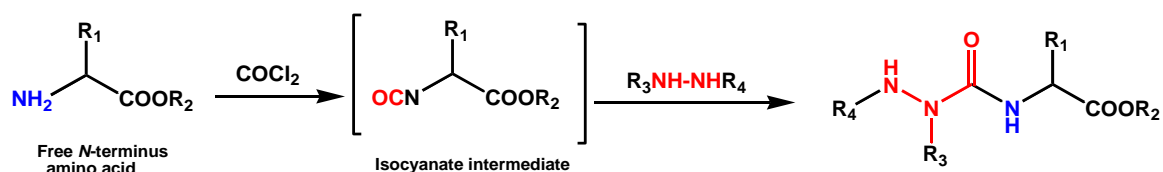
Concerning the sequence 1:1-[α /aza]-oligomers, they are heterogeneous mixed oligomers but their synthesis is quite problematic due to a lack of reactivity of the synthons similar to 1:1-[α /NO]-oligomers.¹⁷⁶ Furthermore, their structural studies showed that they could not clearly induce particular type of folding.^{24,32} Consequently, we have given our interests to study 2:1-[α /aza]-oligomers whose oligomerization and structural studies are more accessible.^{24,30-32}

II.2. General Methods of Azapeptides Synthesis

Incorporation of an aza-amino acid in peptide skeleton has been achieved by different methods similar to those used in the classical peptide coupling but derived from the semicarbazide chemistry. Principally, aza-amino acid is the product of the reaction between hydrazine or hydrazide derivative and a carbonyl group (activated carboxylic acid derivatives).¹⁵⁷ Generally, synthesis of azapeptides can be considered the result of the combination between peptides and hydrazine chemistry.

II.2.1. Isocyanates Method

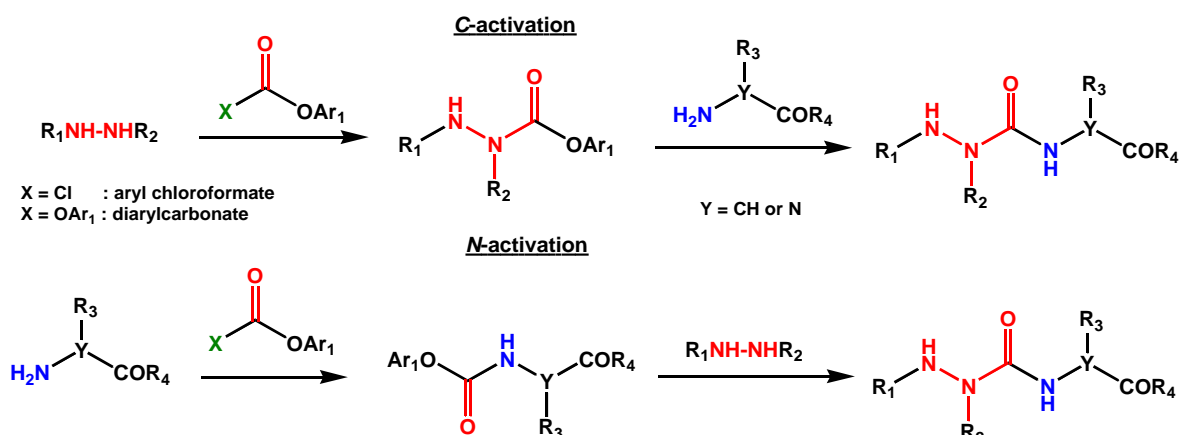
It is the most frequently protocol used in the synthesis of azapeptides. The method based on the reaction between protected hydrazine and an isocyanate which obtained by the action of phosgene on the free N-terminal of a protected amino acid in its C-terminal (Scheme 2.1). Addition reaction on the substituted nitrogen atom is the preferred pathway which leads to the formation of the interested substituted product at α nitrogen as a major product. The limitation of this method is that the isocyanate derivative is not very stable.



Scheme 2.1. Synthesis of azapeptide by addition of hydrazine derivative to an isocyanate.

II.2.2. Activated Esters Method (Activated Carbazate or Carbamate)

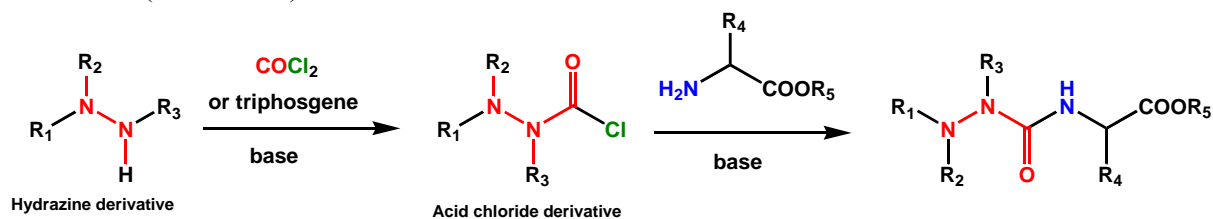
Activation of the *C*- or *N*-terminals can be accomplished through activated ester method. While *C*-activation is achieved by the reaction of hydrazide with aryl chloroformate or diarylcarbonate, *N*-activation is performed by the reaction between free *N*-terminal amine group of α -amino acid or aza-amino acid with the same reactants (Scheme 2.2).



Scheme 2.2. Synthesis of azapeptides by activated ester derivatives.

II.2.3. Method of Coupling with Acid Chlorides

Acid chlorides method is very common strategy in peptide coupling and it efficiently produces classical peptides in high yields. The method also has applied successfully in the synthesis of azapeptides series.^{28,92,171} Similar to the activated esters protocol, *C*- and *N*-activations can be prepared by acid chloride method but most of the applications use the *C*-activation protocol of the hydrazide derivatives (Scheme 2.3).

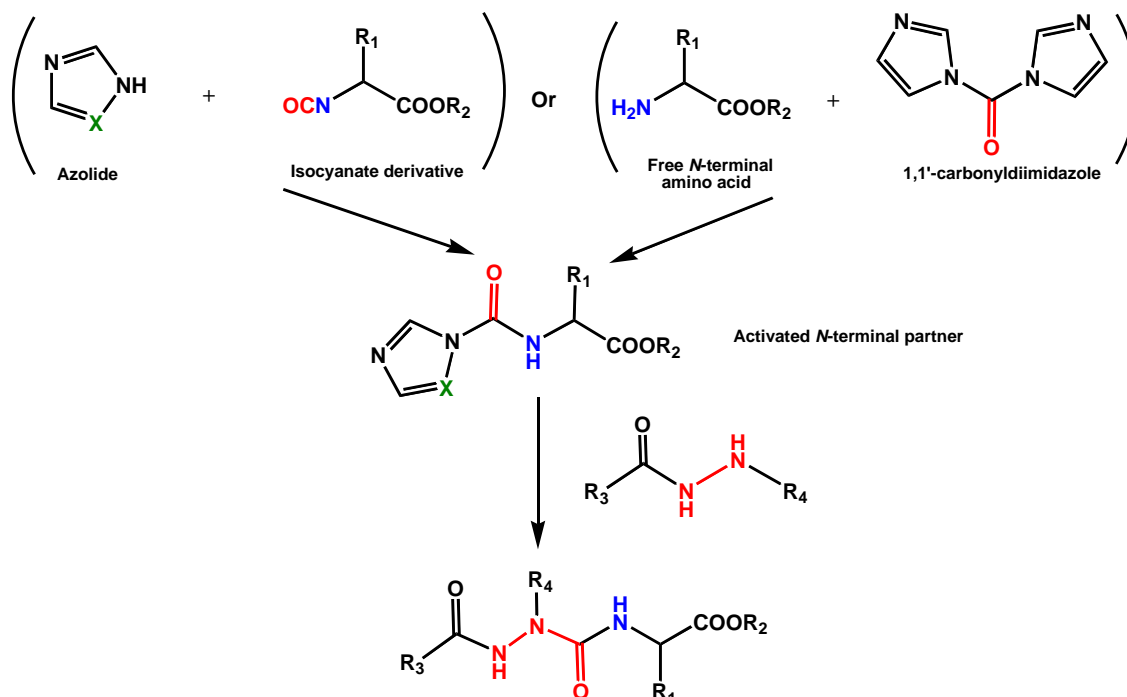


Scheme 2.3. Synthesis of azapeptides by coupling with acid chlorides.

Firstly the hydrazine or its derivative reacts with phosgene or triphosgene in the presence of base to give the corresponding acid chloride (can be isolated and stored at 4°C) which followed by coupling with the activated free *N*-terminal of an amino acid in the presence of base to yield the azapeptide of interest. This method is recommended for difficult couplings with secondary amines because the method is known with the formation of a strong active acid chloride intermediates which facilitate the second coupling step with the free amines.

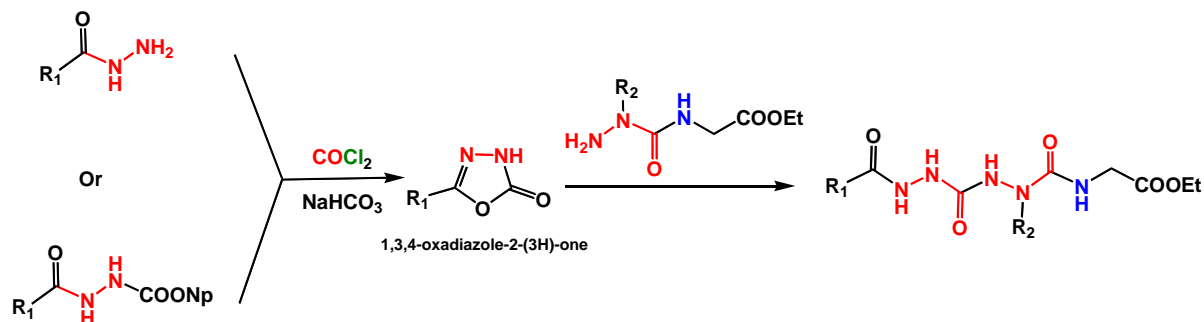
II.2.4. Reaction of *N*-Azolides with Amine Partner

N-activation of the azolides can be used in the synthesis of azapeptides by the same manner as the activated esters method. The activated *N*-partner is prepared either by the reaction between azolide and isocyanate derivative, or by the reaction between amino acid and 1,1'-carbonyldiimidazole.¹⁷⁷ The latter strategy is more interesting because it is easy to be accomplished and there is no formation of isocyanate intermediate which is toxic and less stable (Scheme 2.4).

Scheme 2.4. Synthesis of azapeptides with *N*-azolides.

II.2.5. Ring Opening of 1,3,4-Oxadiazole-2-(3H)-one with Amine Partner

Ring opening of 1,3,4-oxadiazole-2-(3H)-one by amine partner leads to formation of azapeptides. It proceeds *via* the reaction between 1,3,4-oxadiazole-2-(3H)-one, (substituted with alkyl, aryl or Z-group in position 5), with different azadipeptides having free amino group in their *N*-terminals (Scheme 2.5).¹⁷⁸ Opening the cycle leads directly to the formation of azatri- or azatetrapeptides. The heterocyclic 1,3,4-oxadiazole-2-(3H)-one can be obtained in basic condition by the action of phosgene on either the corresponding hydrazide or an aza-amino acid protected in its C-terminal with 4-nitophenyl group.

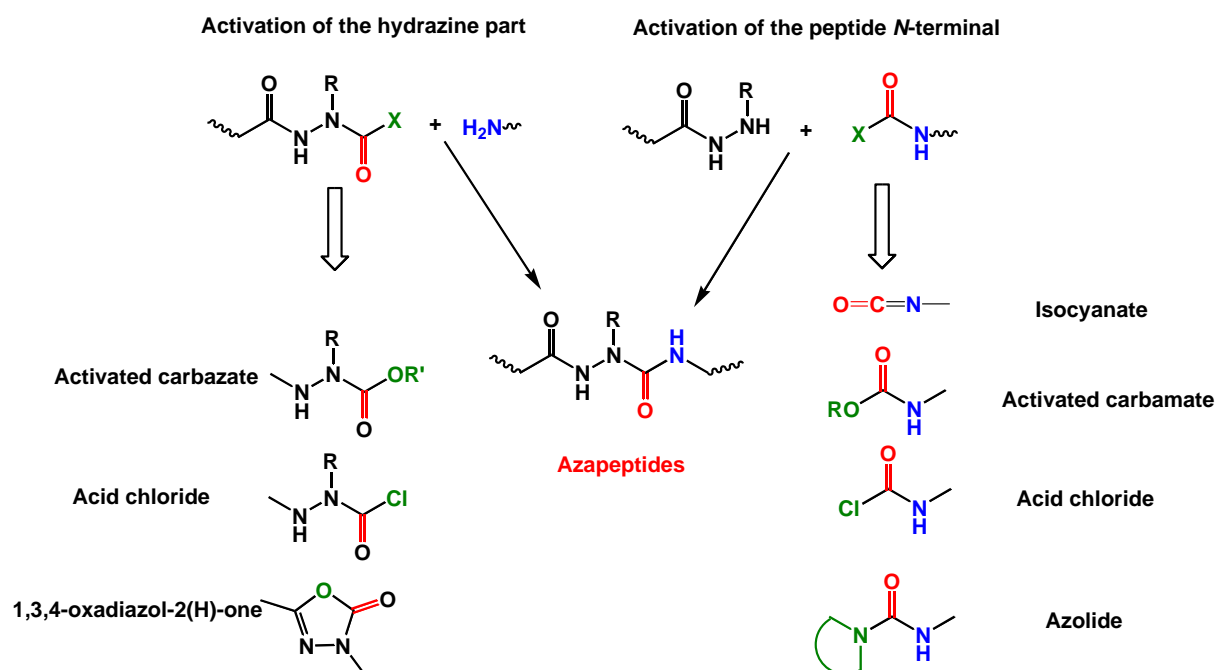


Scheme 2.5. Synthesis of azapeptides by ring opening of 1,3,4-oxadiazole-2-(3H)-one.

Part A

Chapter II. Synthesis and Methods of Analysis of New 2:1-[α /aza]-Oligomers

Among the aforementioned five methods for the synthesis of azapeptides, we could summarize and compare between them to choose the one that would be easy and effective in the synthesis of our azapeptides (Scheme 2.6).



Scheme 2.6. General methods for the synthesis of azapeptides.

- **Acid chlorides method:** It could not be applicable in the synthesis of peptides or azapeptides using Boc strategy as it leads to the liberation of the HCl, and Boc group can be removed under these conditions.
- **Isocyanates method:** it is considered to be the most rapid and appropriate method for obtaining azapeptide derivatives. The method has the advantage of the presence of little by-products at the end of the reaction, so the purification is easy and the yields are good. The drawbacks of this method are the toxicity and instability of the isocyanate intermediates.
- **Reaction of *N*-azolides with amine partner:** this method has not any advantage over the isocyanate method and it needs one more step to obtain the final azapeptides of interest.
- **Ring opening of 1,3,4-oxadiazole-2-(3H)-one by amine partner:** in this method, there is a necessity to prepare the heterocycle 1,3,4-oxadiazole-2-(3H)-one. Moreover, the efficiency of the reaction depends mainly on the reactivity of the amine partner which is controlled by the nature of the side chains.
- **Activated esters method:** azapeptide derivatives can be easily obtained by this method. It requires the use of substituted hydrazine at the beginning of the synthesis.

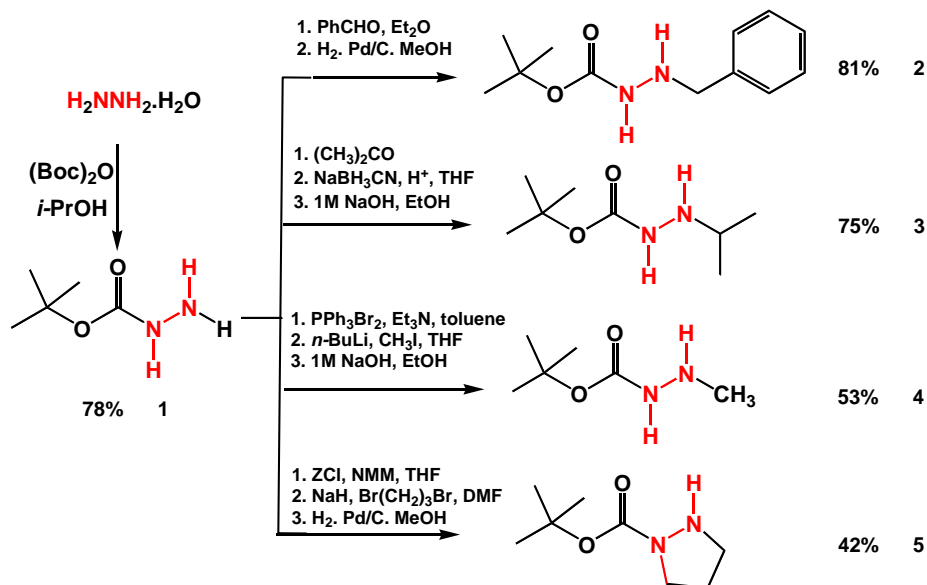
Since we can not use acid chlorides method because we have chosen to synthesize our 2:1-[α /aza]-oligomers by Boc strategy. So, the method of activated esters would be the best choice for the synthesis of our azapeptides if we could succeed in establishing a general protocol for the synthesis of substituted hydrazine derivatives.

Part A

Chapter II. Synthesis and Methods of Analysis of New 2:1-[α /aza]-Oligomers

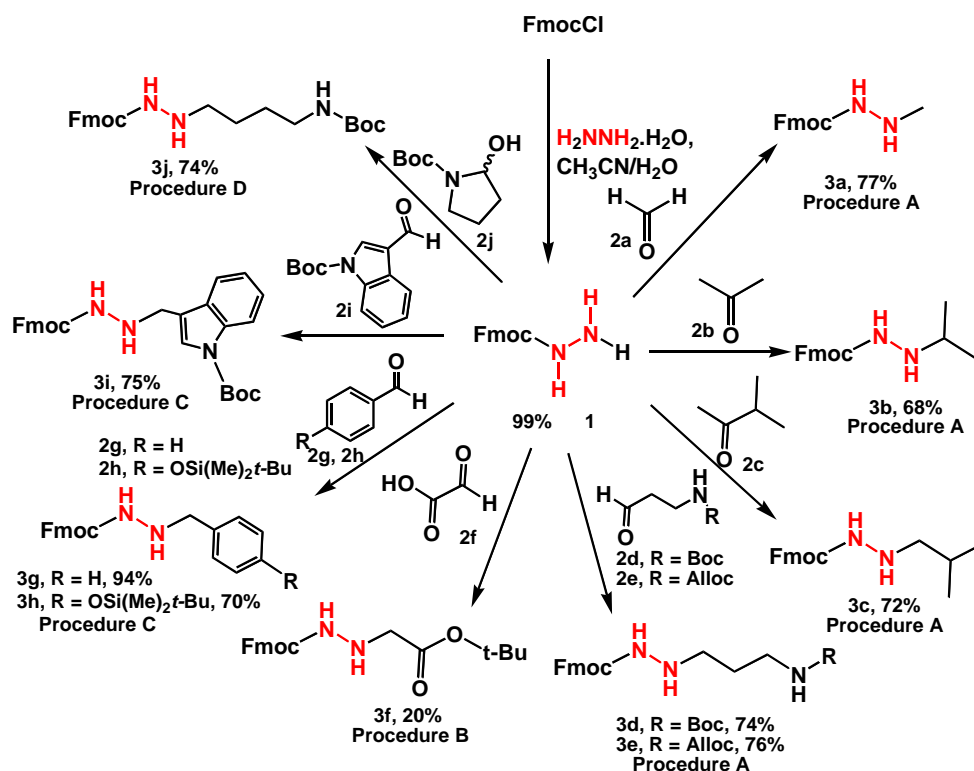
II.3. Methods of the Synthesis of Hydrazone Derivatives

William D. Lubell team has synthesized azapeptides and they succeeded to introduce them in a biologically active peptides.^{58,173} In Boc strategy, William D. Lubell and his collaborators have synthesized 4 types of substituted hydrazines (Scheme 2.7).



Scheme 2.7. Synthesis of substituted hydrazine derivatives reported by William D. Lubell *et al.*¹⁷³

Moreover, they have developed many azapeptides using Fmoc strategy and they have succeeded to synthesize a number of *N*-(fluoren-9-yl-methyl)-*N'*-alkyl-carbazate from 9-*H*-fluoren-9-yl-methyl-carbazate (Scheme 2.8).⁵⁹



Scheme 2.8. Synthesis of *N*-(fluoren-9-yl-methyl)-*N'*-alkyl-carbazate by William D. Lubell *et al.*⁵⁹

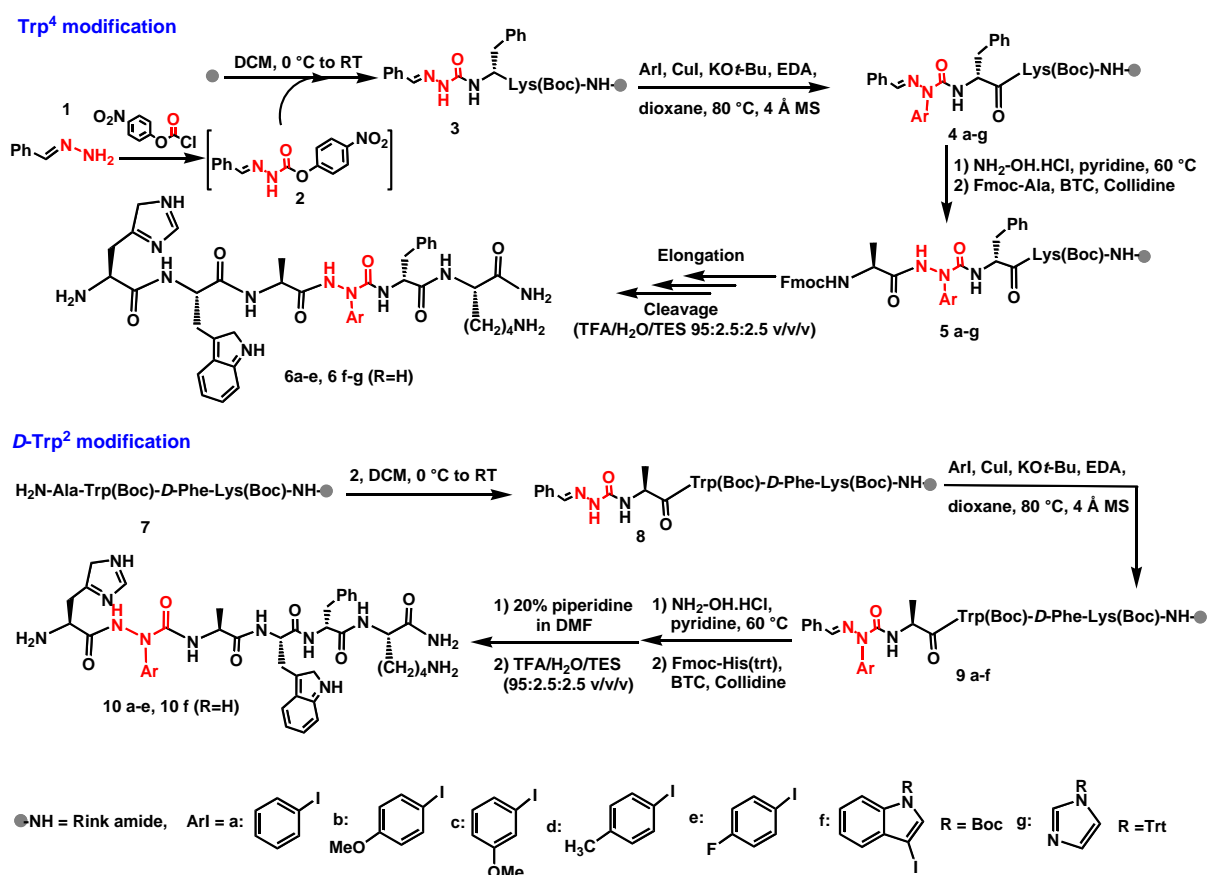
Part A

Chapter II. Synthesis and Methods of Analysis of New 2:1-[α /aza]-Oligomers

All of these precursors were incorporated in dipeptide synthesis with the general sequence P-azaAA-AA-OH (P = Boc or Fmoc) followed by further reaction in other peptide synthesis on solid phase strategy. Hence, it is possible to introduce different aza-amino acids in the peptide chain.

Unfortunately, there is no general protocol for the synthesis of substituted hydrazine derivatives to be the precursors for the azapeptides synthesis. As illustrated in Schemes 2.7 and 2.8, William D. Lubell group has proposed four protocols for the synthesis of different four substituted hydrazine derivatives through Boc strategy, and they also have proposed four different protocols for obtaining ten substituted hydrazine derivatives by Fmoc strategy.

William D. Lubell group has recently described a three-step process by exploiting the use of a semicarbazone fragment to achieve selective alkylation and incorporation of hydrazine fragments in peptides using solid phase strategy (Scheme 2.9).⁵⁹



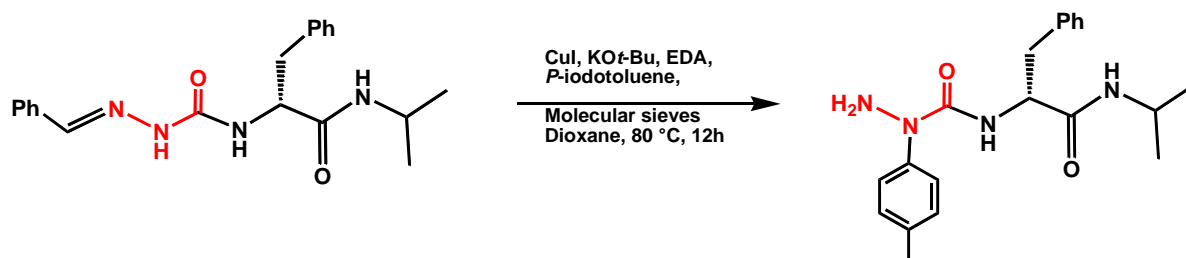
Scheme 2.9. Synthesis of [aza-arylglycine] GHRP-6 analogs.⁵⁹

In the solid phase, the yield of the reaction depends on the position of the modified residue. For the *D*-Trp² position, the yield is much lower compared to the modification in Trp⁴ position (aza moiety in position 4). The large difference in yields could be due to folding of the peptide which blocks the arylation reaction.

Moreover, the same group tested the reactivity of the semicarbazone in solution state. They reported that the *N*-arylation and the hydrazone deprotection reactions take place simultaneously. The overall reaction yield is low (20 %) which could be due to the elimination of hydrazone motif that would be initiated by ethylene diamine.¹⁷⁹

Part A

Chapter II. Synthesis and Methods of Analysis of New 2:1-[α /aza]-Oligomers

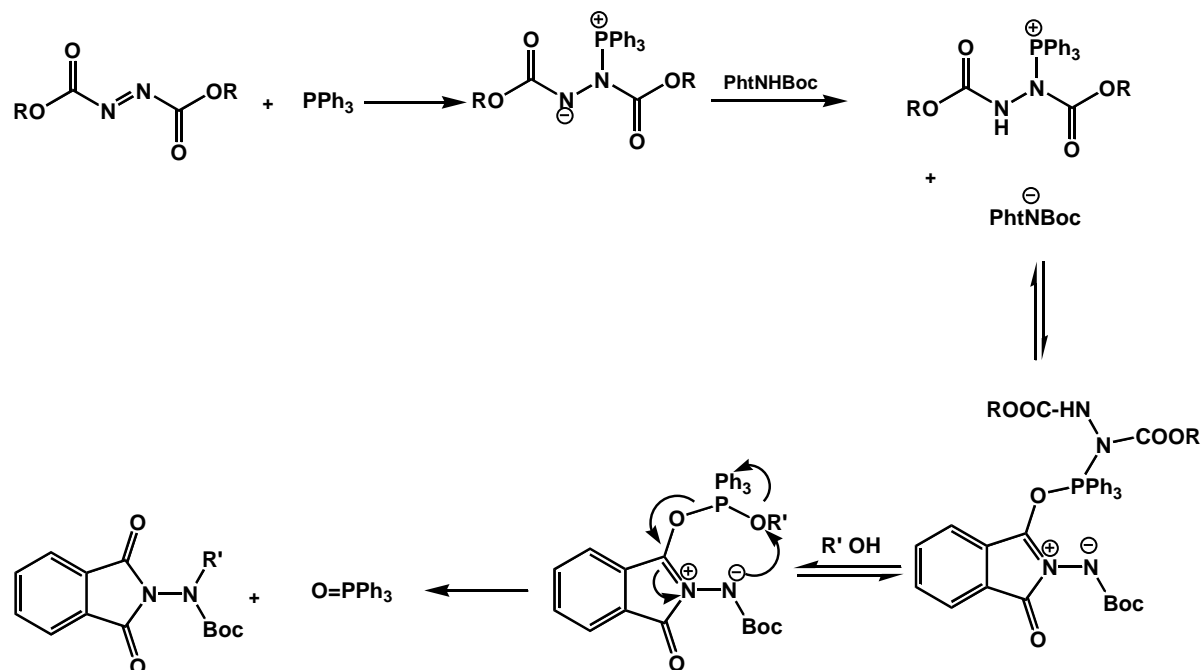


Scheme 2.10. *N*-arylation in solution phase.¹⁷⁹

The nature of the side chain to be selectively carried by the nitrogen is limited by the diversity of the methods of synthesis because it seems difficult to differentiate selectively between the two nitrogen atoms of the hydrazine moiety. Subsequently, the use of bulky protecting group may be a good solution for this problem which gives the chance for selective acylation for one of the two nitrogen.¹⁸⁰ The peptide coupling reaction between hydrazine and substituted peptide or activated amino acid is a regioselective acylation reaction for the α and β nitrogens of the substituted hydrazine.²⁴

In our laboratory, new acid partners for Mitsunobu reaction have been recommended, the *N*-alkyloxycarbonyl-*N*-aminophthalimides, which opened the way to a new way for preparing alkylhydrazines.^{181,182} These compounds can be considered as triprotected hydrazines which possess a steric hindrance by the presence of the cyclic phthalimide moiety. The only free hydrogen is particularly acidic ($pK_a \sim 11$) due to the presence of three carbonyl electron-withdrawing groups.

The *N*-alkyloxycarbonyl-*N*-aminophthalimide molecule can be easily alkylated through Mitsunobu reaction. This reaction allows the introduction of a varied number of alkyl groups by simply changing the used alcohol (ROH). Moreover, phthalimide moiety stabilizes the phosphorane intermediate, as the strong delocalization of the electron pair on the nitrogen atom of the phthalimide moiety forms zwitter ion which stabilized *via* resonance phenomenon (Scheme 2.11).



Scheme 2.11. Proposed mechanism of Mitsunobu reaction for phthalimide derivatives.

II.4. Synthesis of Azapeptides Oligomers

II.4.1. Synthesis of Azadipeptides Boc-azaAA-AA-OMe

We have used Gellman's principles for nomenclature of our mixed azapeptides (Figure 2.2).

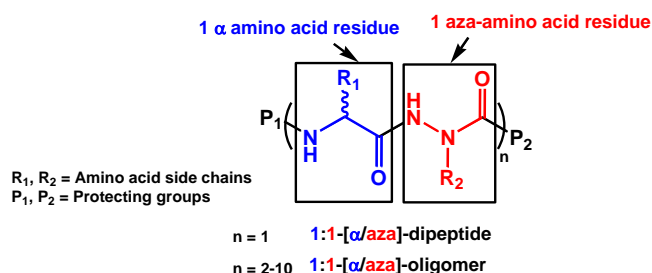
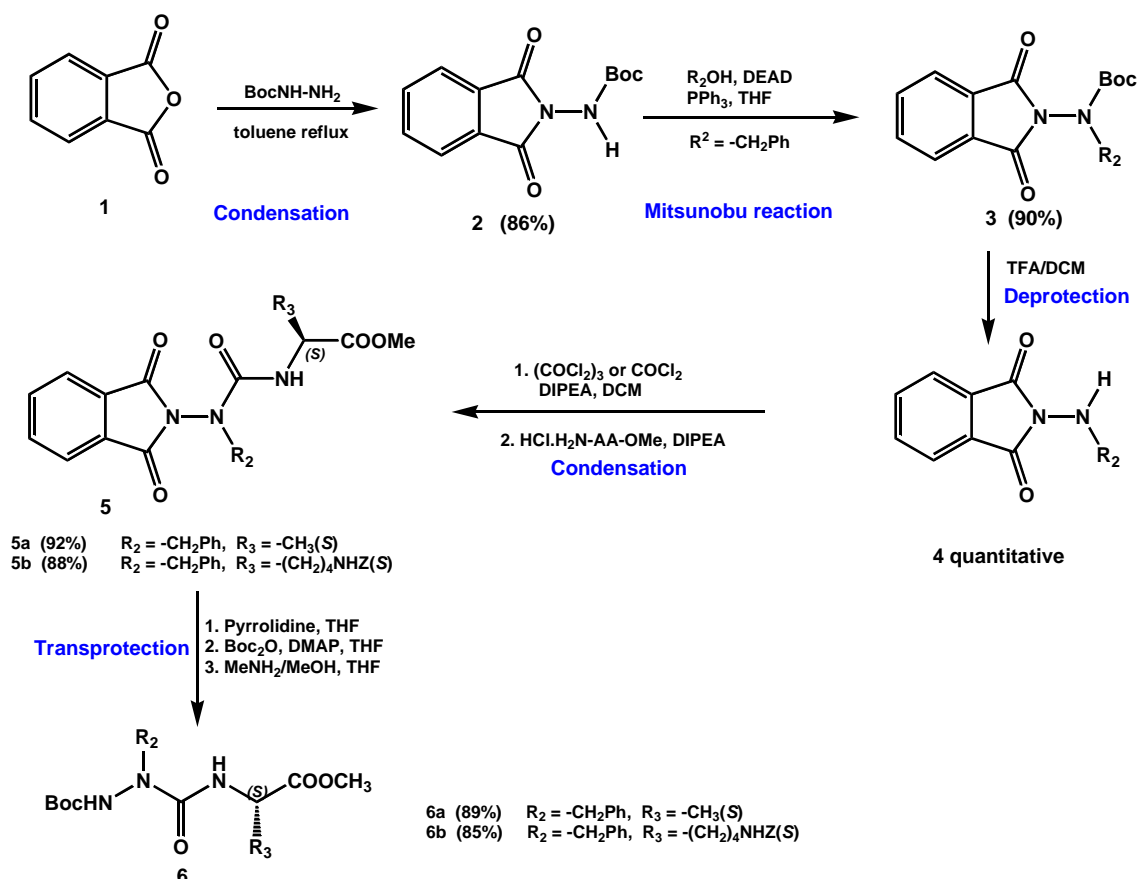


Figure 2.2. Nomenclature of 1:1-[α /aza]-oligomers.

In this study, we succeeded to synthesize new different dipeptides (**Boc-azaAA-AA-OMe**) in good yields based on the protocol that was developed by Cécile Abbas-Quinternet in solution phase.³⁰ This protocol involves five successive steps: first condensation, Mitsunobu reaction^{181,182}, deprotection, second condensation¹⁸³ and the protocol ends with a trans-protection step¹⁸⁴ as shown in Scheme 2.12.



Scheme 2.12. General steps for the synthesis of azadipeptide Boc-azaAA-AA-OMe (6).

This protocol not only allows incorporating different α -amino acid residues, but also different aza moieties can be prepared by using different alcohols in Mitsunobu reaction. Consequently, different azadipeptides of the sequence α /aza can be synthesized which is considered to be the base unit for the synthesis of our mixed α /aza/ α sequence.

Part A

Chapter II. Synthesis and Methods of Analysis of New 2:1-[α /aza]-Oligomers

In the current work, synthesis of the activated acyl chloride intermediate from product (4) has been achieved by phosgene (20% in toluene) instead of triphosgene (previous studies)^{24,32} as phosgene showed a lot of advantages: (i) efficient coupling, (ii) no side reactions if it is used in excess, (iii) the excess can be removed easily under ventilated hood, (iv) the reaction is faster than using triphosgene, and (v) the final products (5) are very pure in better yields than using triphosgene.

II.4.2. Synthesis of 2:1-[α /aza]-Oligomers

According to Gellman, the family of mixed α /aza/ α sequence could be named as in Figure 2.3.

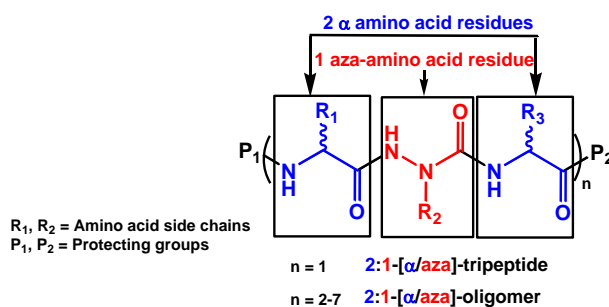


Figure 2.3. Nomenclature of 2:1-[α /aza]-oligomers.

II.4.2.1. Synthesis of 2:1-[α /aza]-Trimers

This coupling reaction is not easy due to the weak nucleophilicity of the nitrogen of the azadipeptide (amine partner) which may be attributed to the effect of the electron attracting carbonyl group adjacent to this nucleophilic center. Cécile Abbas has reported low yields of coupling upon using EDC/HOBt, and DCC/HOBt as coupling reagents. In contrast, good yields of different 2:1-[α /aza]-trimers were obtained when using cyanuric fluoride as activating reagent (Table 2.1).³⁰

In the current study, owing to the non-availability of cyanuric fluoride from the commercial supplier during certain period, we have tested other coupling reagents under different conditions of solvents, bases and temperature (Table 2.1). Unfortunately, none of the tested coupling reagents could give close yields as cyanuric fluoride except the DAST (diethylaminosulfurtrifluoride) which produced our interested trimers with acceptable yields as obtained by cyanuric fluoride.

Table 2.1. Different coupling reagents trials in the synthesis of 2:1-[α /aza]-trimers

Coupling reagents	Conditions	Yields (%)	Coupling reagents	Conditions	Yields (%)
EDC/HOBt*	DCM, DIPEA, RT	10 to 60 (not reproducible)	DCC/PFP	DCM, NMM, RT	16
EDC/HOBt	DCM, NaHCO ₃ , RT	12	DCC/PNP	EtOAc, DIPEA, RT	19
DCC/HOBt*	DCM, DIPEA, RT	14	SOCl ₂ /pyridine	DCM, NaHCO ₃ , RT	22
HBTU	CH ₃ CN, DIPEA, RT	20	POCl ₃ /pyridine	DCM, NaHCO ₃ , RT	15
HATU	DMF/DCM, DIPEA, RT	22	C ₃ F ₃ N ₃ /pyridine*	DCM, NaHCO ₃ , -20 to -10 °C	Good and reproducible yields (see Table 2.2)
HATU	DMF/DCM, NMM, RT	17	DAST/pyridine	DCM, NaHCO ₃ , -5 °C	
DCC/PFP	DCM, DIPEA, RT	21			

*Trials by Cécile Abbas in previous study.³⁰ All yields correspond to the synthesis of Boc-Phe-azaPhe-Ala-OMe.

Part A

Chapter II. Synthesis and Methods of Analysis of New 2:1-[α /aza]-Oligomers

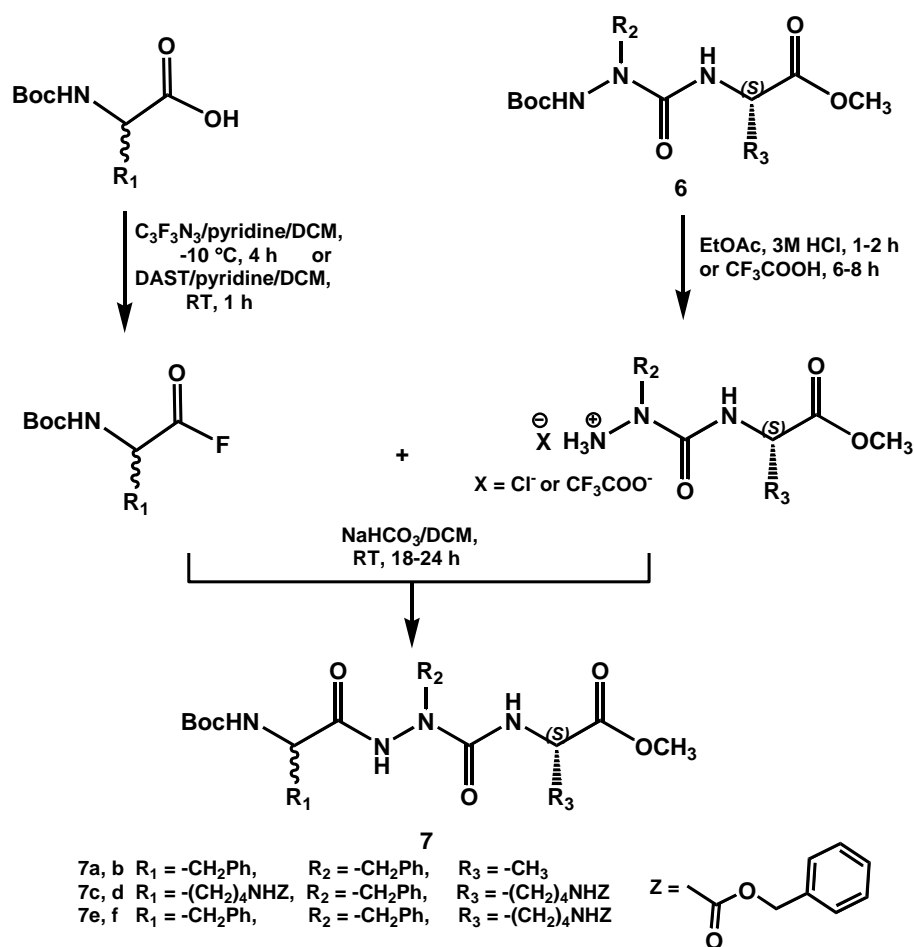
By using acid fluoride strategy, we could synthesize different 2:1-[α /aza]-trimers by varying the nature of the α -amino acid and also changing the absolute configuration of its asymmetric carbon (Table 2.2).

Table 2.2. Different 2:1-[α /aza]-trimers obtained by acid fluoride method

R ₁	Absolute configuration of R ₁	R ₃	Absolute configuration of R ₃	Yield (%) ^a	Product No.
CH ₂ Ph	<i>S</i>	CH ₃	<i>S</i>	74	7a
CH ₂ Ph	<i>R</i>	CH ₃	<i>S</i>	70	7b
(CH ₂) ₄ NHZ	<i>S</i>	(CH ₂) ₄ NHZ	<i>S</i>	63	7c
(CH ₂) ₄ NHZ	<i>R</i>	(CH ₂) ₄ NHZ	<i>S</i>	60	7d
CH ₂ Ph	<i>S</i>	(CH ₂) ₄ NHZ	<i>S</i>	58	7e
CH ₂ Ph	<i>R</i>	(CH ₂) ₄ NHZ	<i>S</i>	52	7f

^aAll yields have been calculated from pure isolated products based on the azadipeptides 6.

The yields of the different 2:1-[α /aza]-trimers using acid fluoride strategy are close (Table 2.2), and this reflects that the efficiency of this coupling reaction is not depend on the nature and absolute configuration of the α -amino acid. The method involves the coupling between free *N*-terminal of azadipeptide (6) acting as amine partner with a pre-activated α -amino acid in the acyl fluoride form acting as acid partner (Scheme 2.13).



Scheme 2.13. Synthesis of 2:1-[α /aza]-trimers by acid fluoride method.

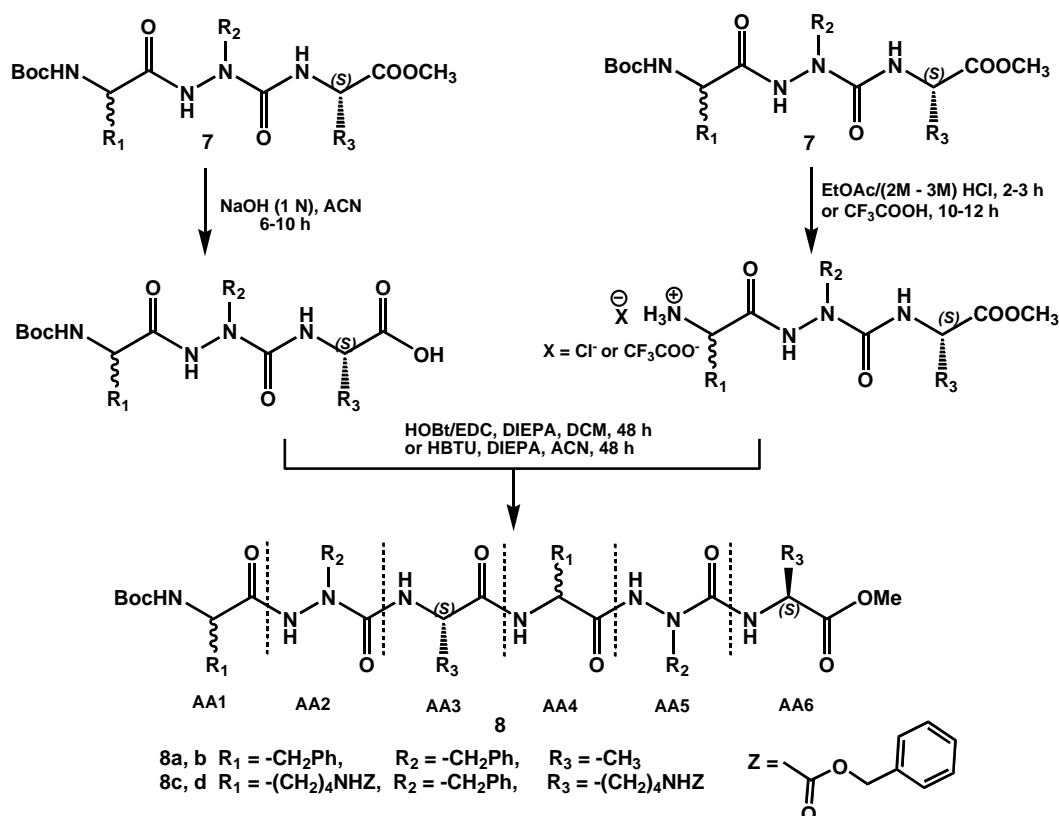
II.4.2.2. Synthesis of 2:1-[α /aza]-Hexamers

Synthesis of 2:1-[α /aza]-oligomers is based mainly on the 2:1-[α /aza]-trimers as a monomeric unit. The condensation between two trimer units leads to the formation of hexamer using the classical peptidic coupling reagents such as HOBt/EDC, HBTU/DIPEA, *etc.* Formation of 2:1-[α /aza]-hexamers is supposed to be easy to certain extent compared with the 2:1-[α /aza]-trimers where the *N*- and *C*-termini are a way from the modification that exists at position 2 (Table 2.3, Scheme 2.14).

Table 2.3. Different 2:1-[α /aza]-hexamers obtained by the classical peptide coupling methods

R ₁	R ₃	Absolute configuration AA1	Absolute configuration AA3	Absolute configuration AA4	Absolute configuration AA6	Yield (%) ^a	No.
CH ₂ Ph	CH ₃	<i>S</i>	<i>S</i>	<i>S</i>	<i>S</i>	87	8a
CH ₂ Ph	CH ₃	<i>R</i>	<i>S</i>	<i>R</i>	<i>S</i>	85	8b
(CH ₂) ₄ NHZ	(CH ₂) ₄ NHZ	<i>S</i>	<i>S</i>	<i>S</i>	<i>S</i>	64	8c
(CH ₂) ₄ NHZ	(CH ₂) ₄ NHZ	<i>R</i>	<i>S</i>	<i>R</i>	<i>S</i>	62	8d

^aAll yields have been calculated from pure isolated products based on the limiting acid partner reactant 2:1-[α /aza]-trimer (7).

Scheme 2.14. Synthesis of 2:1-[α /aza]-hexamers by the classical peptide coupling methods.

Deprotection of the Boc-group for trimers with Phe and Ala has been performed using (EtOAc/3M HCl), while more diluted condition (EtOAc/2M HCl) has been used in case of trimers with lysine residues to avoid the deprotection of the Z-protecting group in the N^H of lysine residues. Interestingly, better yields have been obtained for the hexamers possessing lysine residues (**8c**, **8d**) using HBTU as coupling reagent, while the yields revealed no much variations for hexamers with phenylalanine and alanine residues (**8a**, **8b**) upon using HOBt/EDC or HBTU.

II.5. Methods for Conformational Analysis

The three-dimensional secondary structure of peptides, proteins as well as pseudopeptides is the crucial parameter which participates to their biological activities.¹⁸⁵ These secondary structures can be established using some physico-chemical techniques (Table 2.4).

Table 2.4. Selected techniques used in the conformational analysis of peptides and proteins

Technique	Investigations	Structural information
Circular Dichroism Fluorescence	Interaction between chromophores, local conformation of chromophore	Existence of secondary structure (helix, sheet, turn, <i>etc</i>)
Infrared 1D NMR	Aggregation, interactions of weak energy (hydrogen bond, π -stacking)	Existence of interactions
2D NMR	Arrangement and correlations between the atoms in the molecular structure	Molecular structure of the compound, existence of secondary structure in solution
Ultraviolet-visible	Interaction between chromophores, local conformation of chromophore	Existence of interactions
Electronic microscope	Observation of the real spaces and folding of the structure in the solid state	Morphology of the ultrastructure of samples (crystalline, fibrous, <i>etc.</i>)
Microcalorimetry	Energy of structure	Thermodynamic properties
X-ray crystallography	3D arrangement of the atoms in solid state	Crystal structure of the compound

In addition to the aforementioned techniques, molecular dynamic calculations help to resolve the 3D structure in solution predicting the possible interactions and the most favorable conformation(s) adopted by the molecules. This method in many cases is based on the spectroscopic experimental data and/or X-ray results.

II.5.1. Infrared Absorption Spectroscopy (IR)

Nowadays, fourier transform infrared spectroscopy (FTIR) is commonly applied technique which is mainly used to estimate the content of secondary structure elements in peptides and proteins under various conditions (solvent composition, temperature, or changing concentration). The samples may be investigated in solution and solid states. In the latter case the technique of attenuated total reflectance (ATR) is often recommended¹⁸⁶ when the analyte displays low solubility or tends to associate in higher concentrations.

Infrared absorption (IR) spectra of peptides provide information related to the stretching vibrations and deformation of the amide bond. Indeed, the spectra are characterized by the presence of two main vibration regions correspond to the two vibrators of the amide bond:

- amide A includes the stretching vibration region 3200 - 3520 cm^{-1} : corresponds to the stretching of the NH vibrator and denoted as ν (N-H).
- amide I which includes the stretching vibration region 1580 - 1750 cm^{-1} : corresponds to the stretching of the C=O vibrator and denoted as ν (C=O).
- amide II corresponds to the bending vibration region 1510 - 1580 cm^{-1} : corresponds the bending of the NH vibrator and denoted as ν (N-H).

The formation of hydrogen bonds of the type N-H---O=C affects characteristically on the vibrations of the free amides mentioned above. Indeed, when those vibrators are involved in hydrogen bonds, red shifts to lower frequencies are noticed and the relative variations of frequencies reflect the

strength of the interactions involved. Moreover, previous study reported that the NH vibrator that is involved in hydrogen bond, appears at frequencies below 3400 cm^{-1} in the FTIR absorption spectrum.¹⁸⁷

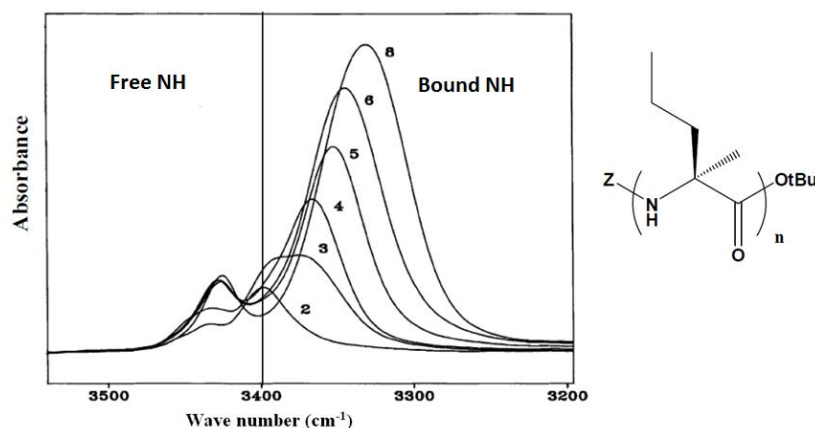


Figure 2.4. FTIR spectra of an oligomer, $n = 2 - 6, 8$.

Each spectra in Figure 2.4 shows a band at 3430 cm^{-1} corresponds to the free NH protons within each oligomer ($n = 2 - 6, 8$). The observed band around 3398 cm^{-1} (in dimer and trimer) is characteristic of weak hydrogen bond that generally observed in short oligomers. Longer than trimer, one NH bound band ($3368 - 3328\text{ cm}^{-1}$) appeared and became more intense and showed more red shift in the wave number. Increasing the intensities indicates that all the amide protons are bound, and the shift to shorter wave numbers reflects a strong hydrogen bonds formation.¹⁸⁷

This spectroscopic technique is limited to the use of transparency solvents within the interested frequency regions, and these solvent have the ability to solubilize the molecules. In certain cases, the possible folding and self-association of the molecules, the multiplicity and overlapping of NH and/or C=O bands cause difficulties to assign all the bands precisely. Thanks to computer programs and mathematical algorithms which help to overcome the overlapping problem through deconvolution.¹⁸⁸

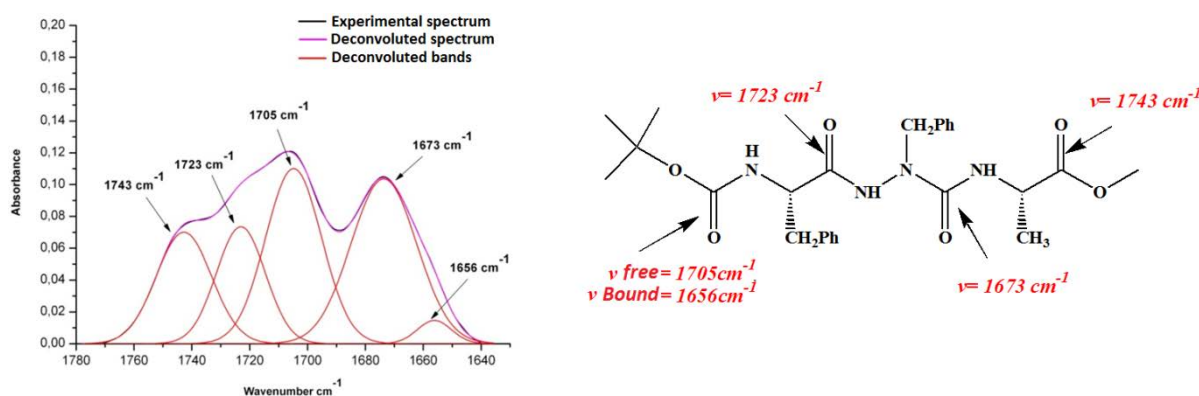


Figure 2.5. Deconvolution of the experimental spectrum of Boc-Phe-azaPhe-Ala-OMe.

While the experimental FTIR spectrum of Boc-Phe-azaPhe-Ala-OMe showed overlapped CO bands, five bands have been distinguished by applying the 2nd derivative deconvolution method (Figure 2.5). The bands at $1743, 1723, 1705$ and 1673 cm^{-1} were assigned to the free CO groups of Ala, Phe, Boc and azaPhe, respectively. In the other hand, the band at 1656 cm^{-1} was attributed to the bound CO of the Boc group indicating that this CO is involved in hydrogen bond interaction. Interestingly, authors suggested that Boc-Phe-azaPhe-Ala-OMe induces β -turn conformation in solution by the presence of the band at 1656 cm^{-1} .³²

Infrared through its very short experiment time can give idea of the presence of conformational phenomenon which is difficult to be detected in the same time scale by NMR.¹⁸⁸

To summarize, FTIR is a tool to highlight the interactions and to confirm the existence of a certain conformational structure.

II.5.2. Nuclear Magnetic Resonance Spectroscopy (NMR)

Nuclear magnetic resonance (NMR) spectroscopy is a highly versatile analytical technique used for structure elucidation. It can be applied either in solution or solid phases.¹⁸⁹ Moreover, NMR spectroscopy provides valuable information about the three-dimensional structure of the molecules, conformational dynamics and the involved intra- and/or intermolecular interactions in the molecules of interest⁶¹ through a number of experimental parameters:

- chemical shifts
- coupling constants
- nuclear Overhauser effect
- relaxation time

NMR spectroscopy can not detect different conformations involved in rapid equilibrium, but it gives an average signal between the populations of different conformers exist in solution.

Nowadays, beside the 1D NMR, more-dimensional NMR methods (2D NMR) are used routinely for the resonance assignment and structural analysis of peptides and small proteins.

a. One dimensional NMR (1D NMR)

Hydrogen bond interaction is one of the interesting information that can be obtained from 1D NMR spectroscopy upon studying peptides and proteins. It focuses primarily on chemical shifts of the amine or amide groups of the molecule that can be involved in intra- and/or intermolecular hydrogen bonds. There are several methods using NMR spectroscopy to confirm the existence of hydrogen bonds in solution:

- **effect of temperature:** this method is based on following the change in the chemical shifts of the NH protons of the peptide molecule upon raising temperature. The chemical shifts of the NH protons which are bound remain unaltered when increasing the temperature. This reveals the presence of hydrogen bond, and the applied thermal energy is not enough to break it.¹⁹⁰
- **effect of solvent:** it is a widely used method which involves the addition of polar solvent (DMSO- d_6 , CD₃OD) into the interested molecule dissolved in non-polar solvent (CDCl₃, CD₃CN).⁹² The method aims to study the effect of increasing polarity of the solvent mixture on the chemical shifts of the NH protons. When the NH protons are involved in hydrogen bonds, only a little change in their chemical shifts is shown by increasing the polarity of the mixture.

The following example in Figure 2.6 shows the effect of varying DMSO- d_6 concentration into a solution of Boc-Phe-azaPhe-Ala-OMe in CDCl₃. The results revealed that the NH protons of azaPhe and Phe suffer deshielding effect towards lower field upon addition of the DMSO- d_6 , this has been explained that the sulfoxide group of DMSO- d_6 can form intermolecular hydrogen bond with these protons. In contrast, NH proton of Ala residue showed a slight variation in its chemical shift upon the addition of DMSO- d_6 which reflects that this proton may be involved in intramolecular hydrogen bond.³¹

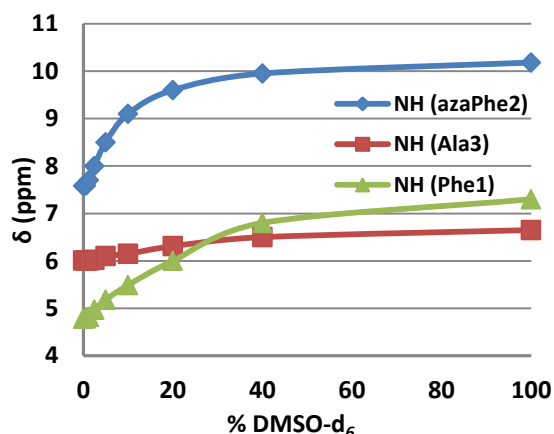


Figure 2.6. Influence of the addition of DMSO- d_6 on the chemical shifts of the NH protons of Boc-Phe-azaPhe-Ala-OMe.

• **effect of concentration:** this method is used to demonstrate which protons are involved in intra- or intermolecular hydrogen bonds in solution. When decreasing the concentration, NH protons that are involved in intramolecular hydrogen bonds are not sensitive to the concentration variations and their chemical shifts have almost no changes or vary very little. On the contrary, due to the effect of dilution, no intermolecular hydrogen bonds might be formed and then the chemical shifts of the NH protons change.

• **measurement of $\Delta\delta$:** Le Grel group has reported a few years ago that it is possible by measuring the chemical shift difference ($\Delta\delta$) between two protons of a terminal amide to get information about the presence of hydrogen bonds.¹⁹¹ The value of the chemical shift difference ($\Delta\delta$) reflects the states of the NH protons either involved in hydrogen bonds or exist freely in solution.

This method allowed better understanding the conformation “hydrazinoturn” in aza- β^3 -peptides where the value of ($\Delta\delta$) was considered as a function of the strength of the hydrogen bond and it gave an evidence of the bifurcated nature of the hydrazine turn (Figure 2.7).¹⁹¹

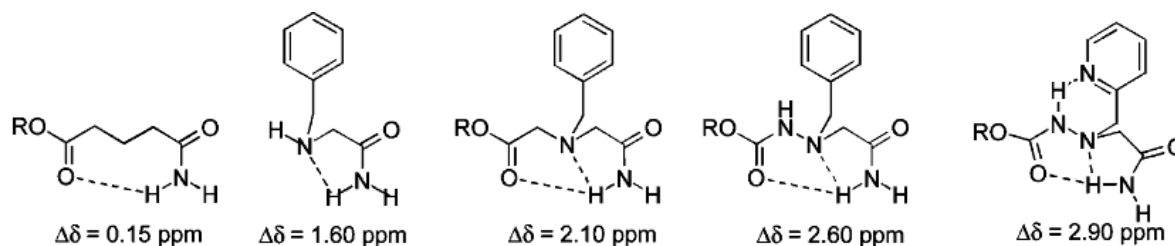


Figure 2.7. Values of $\Delta\delta$ in different primary amides.

b. Two dimensional NMR (2D NMR)

Owing to the superposition of signals of larger molecules in 1D NMR, assignment of signals for larger molecules is established through specific NMR techniques. Indeed, the assignment of the nuclei requires the use of 2D or higher dimension NMR.

COrrrelation SpectroscopY (COSY) shows the correlations of two nuclei separated by two or three bonds (2J , 3J), therefore the value of the coupling constant is not zero. It is used to assign the intra-residues spin systems, but the assignment becomes ambiguous when several identical residues are present.^{192,193} This experiment is often associated with a more sophisticated method; the TOCSY

(Total COReLation SpectroscopY) which allows the assignment of all the nuclei frequencies within the same spin system (2J , 3J , 4J , 5J).

For establishing the sequence of a peptide, ROESY (Rotating frame Overhauser Effect SpectroscopY) and NOESY (Nuclear Overhauser Effect SpectroscopY) are the methods of choice.¹⁹⁴ The Overhauser effect is based on the dipolar couplings (dipole-dipole) between nuclei through space. These dipolar correlations are only detectable in the ROESY/NOESY experiments if the interprotonic distance between the two nuclei is less than 5 Å. This technique provides information on the spatial relationship and the interatomic distances between two nuclei that are not covalently linked. Thus, the correlations $C^\alpha H_i/NH_i$ and $C^\alpha H_i/NH_{i+1}$ in a ROESY or NOESY spectrum provide the unique sequence of the peptide chain by the assignment of all the signals in the spectrum. These internuclear distances usually are indispensable for elucidation of the three-dimensional structure and are used together with other geometric constraints (covalent bond distances and angles) for the prediction of the three-dimensional peptide structure.

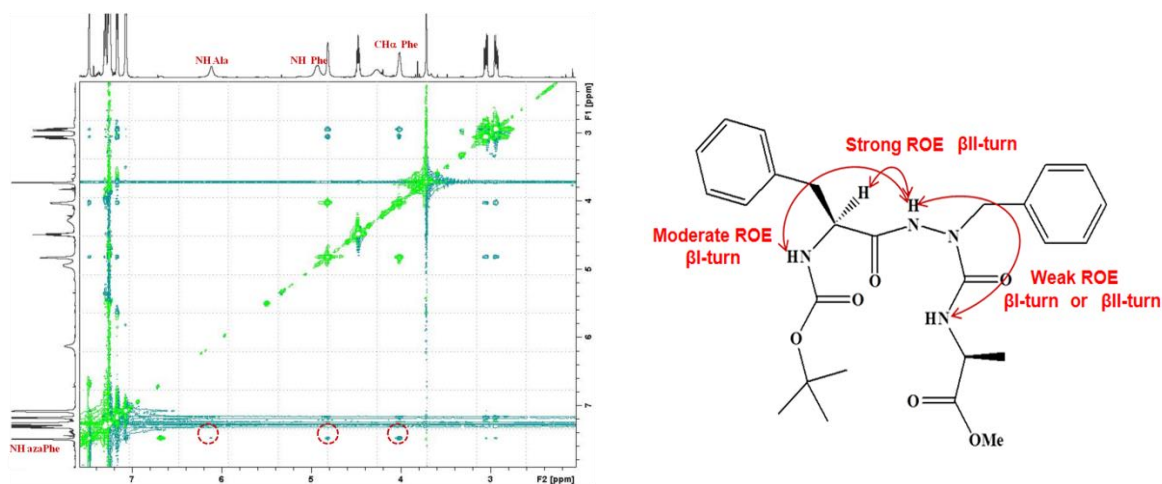


Figure 2.8. ROESY spectrum of Boc-Phe-azaPhe-Ala-OMe.

ROESY spectrum of Boc-Phe-azaPhe-Ala-OMe in Figure 2.8 shows that there are strong, moderate, and weak correlations between the proton of the NH (azaPhe) with the protons of $C^\alpha H$ (Phe), NH (Phe) and NH (Ala), respectively. These results give evidence that $C^\alpha H$ (Phe) proton is closer to NH proton of azaPhe than the others confirming the sequence of this azapeptide.³¹ In addition these correlations are characteristics of peptides adopt β -turn conformation.

The cross peak volume integrals of NOE spectra also provide valuable distance information for the corresponding nuclei. Calibration of these cross peak volumes with those of known internuclear distance (*e.g.*, geminal protons) leads to a direct conversion of the cross peak volume values to interproton distances where the cross peak volume is inversely proportional to the distance (d) between the two protons by the equation:

$$d_{ij} \approx \text{NOE}^{-1/6}$$

Where d_{ij} is the distance between two protons i and j , and NOE is the volume of the corresponding NOE peak.

The values of the coupling constants 3J give information about the values of the torsion angles using Karplus relation which helps to determine the conformation adopted by the molecule of interest.

II.5.3. X-ray Diffraction

X-ray crystallography permits the determination of the three-dimensional structure and packing of molecules in the crystal lattice.¹⁹⁵ It relies on the diffraction of an X-ray beam when passes through a single crystal lattice. The wavelength range of X-rays is correlated to the size of the diffracting structures (atomic radii and lattice constants), and the observed diffraction pattern resulted from a superposition of the diffracted beams.⁶¹ The rotating crystal method uses monochromatic X-rays at a constant wavelength with variation of the angle of incidence. Nowadays, intense, highly focused X-rays from integrated cyclotron radiation beam lines facilitate the traditionally tedious and time-consuming process of structural analysis.¹⁹⁶

The observed diffraction pattern provides very precise information on the 3D structure such as:

- the most favorable conformation(s) adopted by the molecule under investigation,
- the type of interactions either intra- and/or intermolecular (hydrogen bonds), and
- space group, symmetry of the crystal and other geometrical parameters such as the bond lengths, bond angles, and dihedral angles.

Once a suitable molecular model has been obtained, it is further refined, and then finally validated to provide the three-dimensional structure that is related as closely as possible to the electron density map obtained from X-ray diffraction.⁶¹

X-ray diffraction analysis depends mainly on obtaining single crystals of good quality. In addition, the conformation of a molecule in the crystal lattice depends on the stacking forces and the cohesion of the crystal which may distort the intramolecular interactions that exist in the isolated monomeric form or in diluted solution. Thus it is possible to observe different conformations for the same molecule between the solid and solution states. X-ray diffraction of single crystal of Boc-Phe-azaPhe-Ala-OMe confirmed that the molecule adopts β II-turn conformation and stabilized by intramolecular hydrogen bond between NH (i+3) and CO (i) forming a pseudocycle of C₁₀ atoms (Figure 2.9).^{24,32}

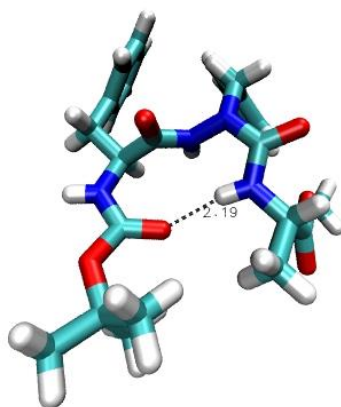


Figure 2.9. Crystal structure of Boc-Phe-azaPhe-Ala-OMe.

II.5.4. Molecular Modelling

Molecular modelling is a theoretical method which uses mathematical models to mimic or simulate the behaviors of the molecules by predicting the structure and reactivity of molecules. The technique is used in the fields of computational chemistry, drug design, computational biology and materials science for studying molecular systems ranging from small chemical systems to large biological molecules, in addition to material assemblies. There are different methods:

- **quantum methods:** they are applied to small systems not for large system due to the complexity increases with increasing number of atoms. They are mainly based on solving equations of quantum mechanics by using *ab initio* methods and semi-empirical methods.
- **molecular mechanics and molecular dynamics:** they are based on the use of classical mechanics laws to determine the behavior of a system. Parameters obtained from experimental techniques (spectroscopic analysis, X-ray diffraction or values obtained by *ab initio* methods), may be taken into consideration when operating calculations. Also, both the bonding and non-bonding interactions should be described and involved to define correctly the force field. For example, AMBER force fields are used to predict the conformation of the molecule in solution. It is very important to choose the adequate force field which gets the parameters of the compound such as bond angles, bond distances and dihedral angles. Molecular mechanics allow minimizing the total energies from bonds, angles and interactions (hydrogen bonds, van de Waals, *etc.*). Molecular dynamics explore the conformational space and give a panel of the molecular conformations adopted by molecules.

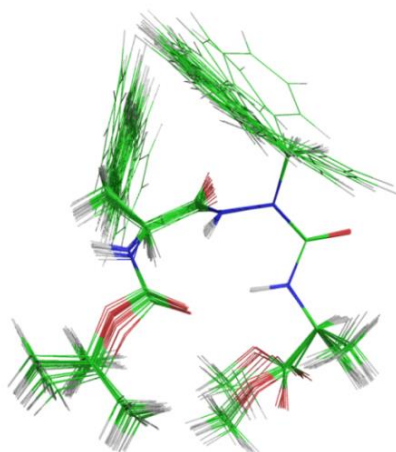


Figure 2.10. Structure of Boc-Phe-azaPhe-Ala-OMe using molecular dynamic calculations based on NMR structural constraints.

Modelling method of Boc-Phe-azaPhe-Ala-OMe (Figure 2.10) may predict the presence of the same intramolecular hydrogen bond with C₁₀ pseudocycle, as in the crystal state (Figure 2.9). In contrast, torsion angles calculations revealed that this compound adopted β I-turn conformation which is different from the solid state.³¹ Lee's group studied the same compound and they reported the presence of equilibrium between β I- and β II-turn conformations at certain NMR conditions (at definite temperature).²⁷ This reveals that it is not necessary for the same molecule to behave similarly in solution and solid states due to the different in the conditions of analysis in the both cases including temperature, solvent, *etc.*

II.5.5. Circular Dichroism (CD)

Circular dichroism is a highly sensitive spectroscopic technique which used for the conformational analysis of peptides and proteins. It is able to distinguish between α -helical, β -sheet and random coil conformations¹⁹⁷ when linear polarized light, (consists of two circular polarized components of opposite helicity but identical frequency, speed and intensity), passes through an optically active medium. The technique is based mainly on the ability of the enantiomerically pure or enriched optically active compounds to absorb both the left and right circularly polarized light in unequal way due to structural asymmetry. This results in elliptically in the polarized light wave.

CD spectroscopy detects the wavelength dependence of this ellipticity, and positive or negative CD bands are observed which known as Cotton effect.⁶¹ Racemic mixtures, optically inactive molecules or the absence of regular organization of the molecules chromophores lead to the absence of the circular dichroism response (signal of zero intensity).

The amide group is the most prominent chromophore in peptides and proteins to be observed by CD spectroscopy. Two electronic transitions of the amide chromophore have been characterized: the $n-\pi^*$ transition is usually quite weak and occurs as a negative band around 220 nm. The energy of the amide $n-\pi^*$ transition is sensitive to hydrogen bond formation. The $\pi-\pi^*$ transition usually is stronger, and is registered as a positive band around 192 nm and a negative band around 210 nm.

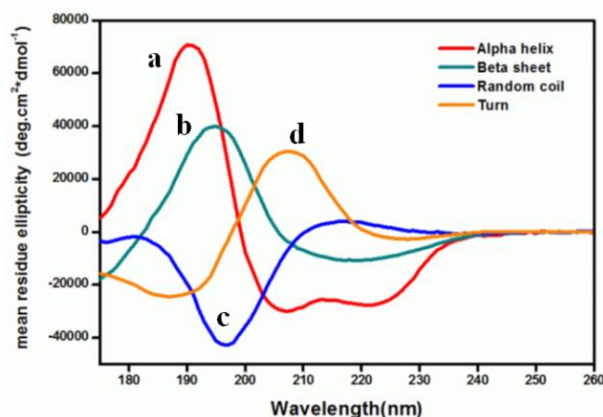


Figure 2.11. The CD dataset of 4 standard secondary structures of (Poly-*L*-glutamic, ddH₂O): (a) helix pH = 4 [red], (b) sheet [cyan], (c) random coil pH = 7 [blue], and (d) turn [orange]; (http://srcd_fit5.nsrcc.org.tw/).

The proportions of α -helical secondary structure, β -sheet conformation, turns and random coil can be determined by CD spectroscopy (Figure 2.11). An α -helical conformation usually is characterized by a negative band at 222 nm ($n-\pi^*$), a negative band at 208 nm, and a positive band at 192 nm.¹⁹⁸ β -sheets can be formed either in a parallel or antiparallel manner and they display a characteristic negative band at 216 nm and a positive band of comparable size close to 195 nm. Random coil conformations are usually characterized by a strong negative CD band just below 200 nm. This technique has also been used in the conformational studies of pseudopeptides such as peptoides¹⁴⁰, β -peptides⁸ and other oligomers¹⁹⁹.

II.6. Conclusions

In the first part of this chapter we overviewed the different methods for the synthesis of azapeptides. In addition, different 2:1-[α /aza]-trimers (**7**) and 2:1-[α /aza]-hexamers (**8**) with different absolute configurations have been synthesized in good yields giving different homo and heterochiral oligomers. The general strategy of the synthesis of 2:1-[α /aza]-oligomers based mainly on the synthesis of the monomeric trimer unit 2:1-[α /aza]-trimers (**7**) from the corresponding 1:1-[α /aza]-dipeptides (**6**).

In the second part, we conclude that establishment of the secondary structures of a molecule can not be confirmed using one technique since all the techniques are in fact complementary. Only the consistency of data obtained through the use of several tools can help to define the structure and the conformation of the molecules of interest.

Chapter III. Structural Studies of 2:1-[α /aza]- Oligomers Possessing Lysine Residues

III.1. Introduction

For several decades, the “Laboratoire de Chimie Physique Macromoléculaire” (LCPM) group has involved in the design, synthesis and conformational study of pseudopeptide oligomers.^{92,200,201} In recent years, the LCPM has focused on pseudopeptidic bis-nitrogen compounds such as the studies conducted on hydrazinopeptides^{21,22,202} and *N*-aminopeptides^{23,25,203}. More recently, the LCPM has extended the interests on the synthesis and conformational study of azapeptides^{24,32,163} in which the α -carbon of one or more of the amino acid residue(s) is/are replaced with one or more nitrogen atom(s) in the peptide sequence.^{72,123,157,204,205} Azapeptides have been studied since the early sixties and actively developed by Gante¹²³ and by Dutta and Morley²⁰⁶. Synthesis of azapeptides has been particularly investigated by Gante^{72,205} and our LCPM group^{158,201} in liquid-phase, and by Gray *et al.*²⁰⁷ in solid phase. Several spectroscopic,^{28,29,92,201,208} crystallographic,^{26,158,201,209,210} as well as computational^{28,29,174,211-213} studies have demonstrated the ability of azapeptides to induce β -turn conformations of type I, type II, and type VI when aza-residue occupying the position ($i + 1$) or ($i + 2$) in the peptide sequence stabilized by an intramolecular hydrogen bond.^{26,28,29,92,174,200,201,213}

In previous study²⁴ and recently Zhou *et al.*³² have proved, using FTIR and NMR spectroscopic techniques as well as molecular dynamic calculations, the propensity of the azapeptides (**7a**, **7b**, **8a**, and **8b**) to adopt β -turn conformations stabilized by intramolecular hydrogen bonds in the solid and solution states. There were no much studies concerned with studying the effect of introducing charged amino acid in the azapeptides sequences on their conformations. Consequently, our interest was to synthesize new 2:1-[α /aza]-oligomers containing charged amino acid moieties such as lysine. We suggested that incorporating of basic amino acid (lysine) with supplementary nitrogen atom N⁶H in their side chains may: (i) produce oligomers with good selectivity in gases separation, and (ii) increase the hydrophilicity of the final oligomers which may support the formation of hydrogels to be involved in promising environmental and medical applications.

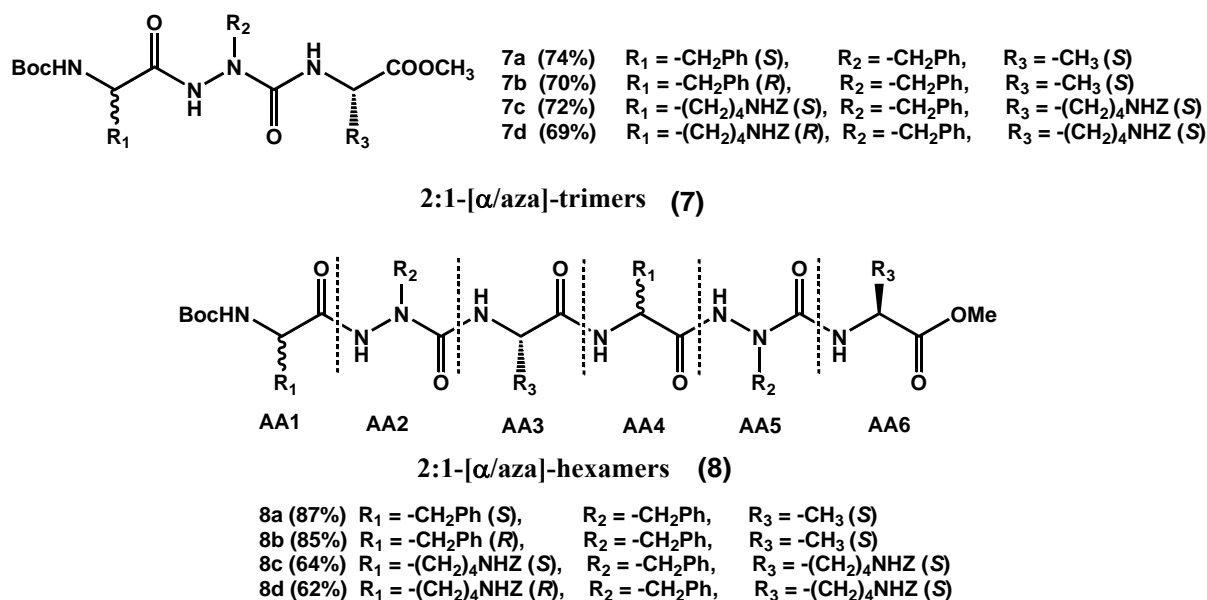


Figure 3.1. Molecular structures of 2:1-[α /aza]-trimers and hexamers.

In this chapter, we focus on the structural studies of new 2:1-[α /aza]-oligomers possessing lysine residues (**7c**, **7d**, **8c** and **8d**; Figure 3.1) in solution state using spectroscopic techniques (NMR and FTIR) as well as molecular dynamic calculations (Amber 12).

III.2. Conformational Studies of New 2:1-[α /aza]-TrimersIII.2.1. NMR Spectroscopic Studies of 2:1-[α /aza]-Trimers

^1H NMR studies for compounds **7c** and **7d** (Figure 3.2) were carried out at dilute concentration in CDCl_3 (3.0 mmol. L^{-1} , 300 K) to avoid intermolecular interactions. The spectra show well resolved signals and the CH_2 protons of the azaPhe moiety are non-equivalent chemically (Appendix 1, Figures S3.1 and S3.2).

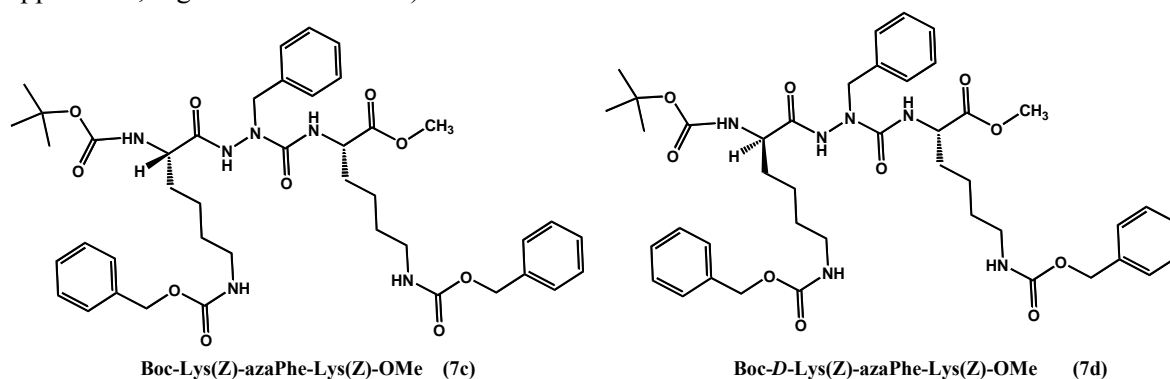


Figure 3.2. Molecular structures of 2:1-[α /aza]-trimers for: (**7c**) left, and (**7d**) right.

In addition, 2D NMR ROESY experiments were performed to determine the possible intramolecular correlations exist between the nuclei in space. ROE spectrum for compound **7c** (Appendix 1, Figure S3.3) reveals the presence of moderate correlation between the protons of $\text{C}^{\alpha}\text{H}_{i+1}$ (Lys1) and the NH_{i+2} (azaPhe), as well as weak correlation between the protons of NH_{i+2} (azaPhe) and NH_{i+3} (Lys2). The same ROE correlations have been observed for compound **7d** (Appendix 1, Figure S3.4); moderate correlation between $\text{C}^{\alpha}\text{H}_{i+1}$ (*D*-Lys1) and the NH_{i+2} (azaPhe) protons, and weak correlation between the NH_{i+2} (azaPhe) and NH_{i+3} (Lys2) protons. These intramolecular correlations give indication that the molecules **7c** and **7d** can induce βII - and $\beta\text{II}'$ -turn conformations in solution, respectively (Figure 3.3).^{27,32,174}

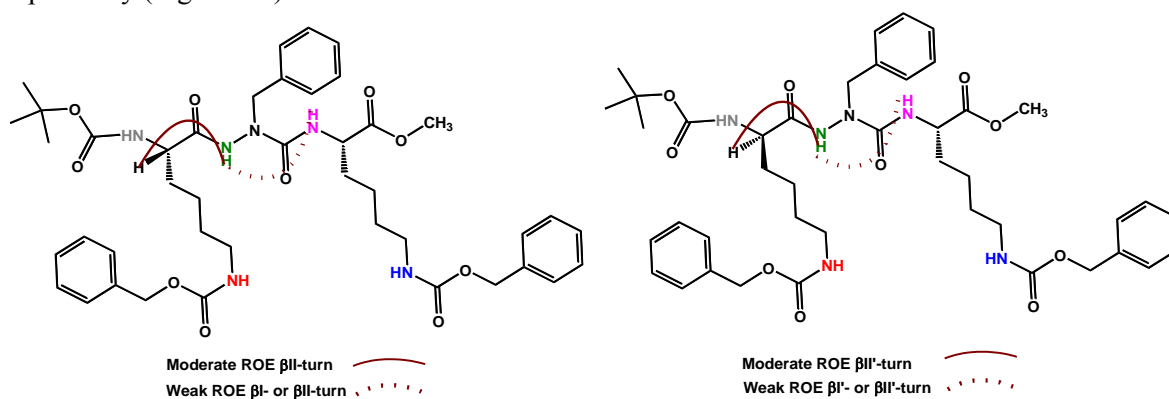


Figure 3.3. ROE correlations of βII - and $\beta\text{II}'$ -turn conformations in **7c** (left) and **7d** (right), respectively; (300 MHz, 3.0 mmol. L^{-1} , CDCl_3 , 300 K).

In order to verify if these β -turns are driven and stabilized by the presence of intramolecular hydrogen bond interactions, effect of solvent composition has been established using NMR technique. The method measures the sensitivity of the NH protons through their chemical shift variations as a function of $[\text{CDCl}_3/\text{DMSO-}d_6]$ composition.⁹² The results demonstrated that while most of NH protons of **7c** and **7d** are sensitive to the addition of $\text{DMSO-}d_6$ into their CDCl_3 solutions, the NH_{i+3} (Lys2) are weakly sensitive to the addition of the $\text{DMSO-}d_6$ (Figures 3.4a, b). These results suggest that only the

NH_{i+3} (Lys2) may be involved in intramolecular hydrogen bond, in contrast to the other NH protons including [NH_{i+1} (Lys1 or *D*-Lys1), NH_{i+2} (azaPhe), and N^εH of the side chains of both lysine residues] are free and not involved in any intramolecular hydrogen bond due to their high chemical shifts variations at high %DMSO-*d*₆ (Appendix 1, Figures S3.5a, b).⁹²

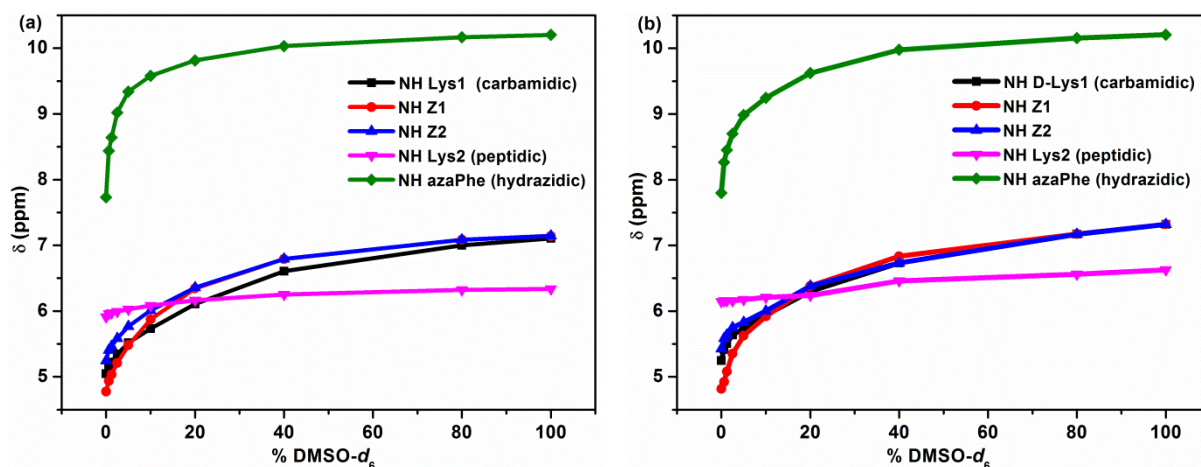


Figure 3.4. Chemical shift-variations (δ) of NH protons for: (a) **7c**, and (b) **7d** as a function of % [CDCl₃/DMSO-*d*₆] mixtures.

III.2.2. FTIR Spectroscopic Studies of 2:1-[α /aza]-Trimers

IR spectra were recorded for compounds **7c** and **7d** at dilute conditions (3.0 mmol. L⁻¹, CDCl₃) to avoid intermolecular interactions. To investigate the presence of certain conformation and the bound NH and CO groups, we focused mainly on two characteristic domains correspond to the stretching NH and CO regions.

For compound **7c**, the NH stretching region reveals the presence of free NH band around 3449 cm⁻¹ belongs to the free NH_{i+1} (Lys1), N^εH (Lys1 + Lys2) and NH_{i+2} (azaPhe), in addition the spectrum shows a very broad band with a maximum at 3378 cm⁻¹ which is related to the bound NH_{i+3} (Lys2) proton (Figure 3.5a). The NH stretching region of **7d** shows the presence of free band with maximum at 3449 cm⁻¹ corresponds to NH_{i+1} (Lys1), N^εH (*D*-Lys1 + Lys2) and NH (azaPhe_{i+2}), and also the spectrum reflects very broad band at 3375 cm⁻¹ belongs to the bound NH_{i+3} (Lys2). Moreover, there is additional bound band at 3302 cm⁻¹ which may be attributed to the involvement of the N^εH proton of the side chain of lysine residues in weak intramolecular hydrogen bond (Figure 3.5b). The assignments of the free and bound NH bands were based on solvent composition NMR experiments.

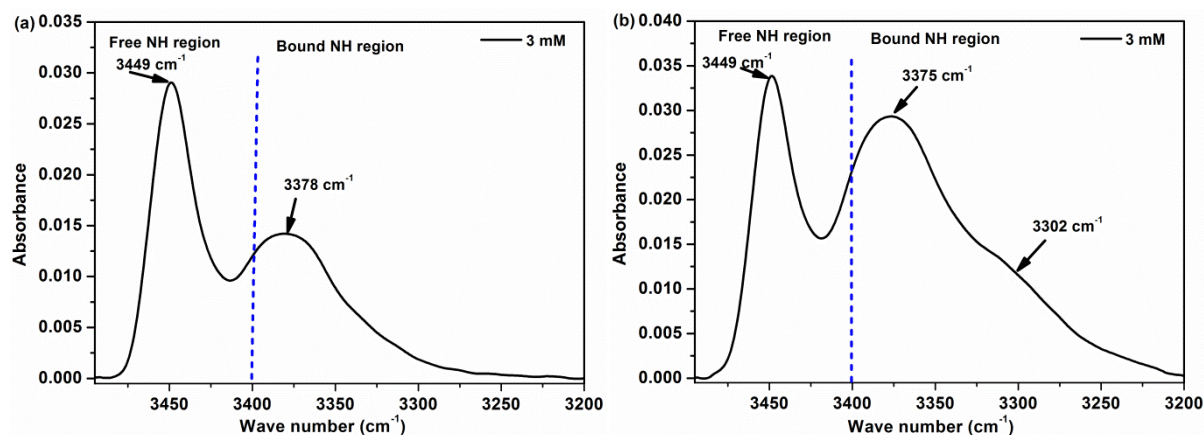


Figure 3.5. FTIR spectra belong to the NH vibration stretching region for: (a) **7c**, and (b) **7d** (3.0 mmol. L⁻¹, CDCl₃).

Part A

Chapter III. Structural Studies of 2:1-[α /aza]-Oligomers Possessing Lysine Residues

Regarding the CO vibration region, the two spectra are very similar and they show broadening and overlapping of the CO groups which have been solved by the help of the 2nd derivative deconvolution method (Figures 3.6a, b).

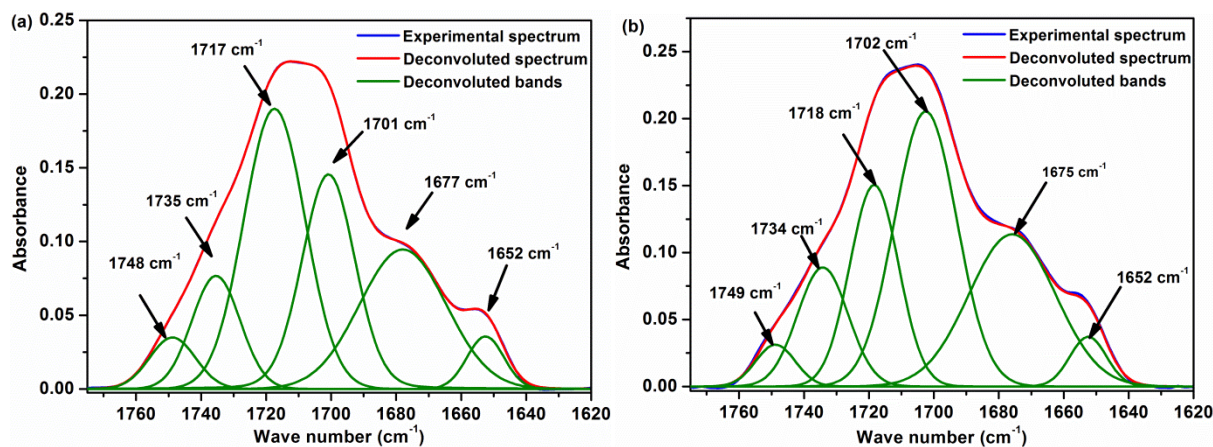


Figure 3.6. FTIR spectra belong to the CO vibration stretching region for for: (a) **7c**, and (b) **7d** (3.0 mmol. L⁻¹, CDCl₃).

The assignment of the CO groups of **7c** and **7d** were done based on shorter peptide sequences and on other oligomers belong to the same series that have been studied previously.³² Subsequently, we could assign six bands as summarized in Table 3.1, especially the band at 1652 cm⁻¹ which was assigned to the bound CO_i of the Boc group.³²

Table 3.1. Assignment of the CO groups in **7c** and **7d** (3.0 mmol. L⁻¹, CDCl₃)

CO Molecule 7c	Free methyl ester	Free Lys _{i+1}	Free CO(Z) (Lys _{i+1} +Lys _{i+3})	Free Boc _i	Free azaPhe _{i+2}	Bound Boc _i
Wave number	1748 cm ⁻¹	1735 cm ⁻¹	1717 cm ⁻¹	1701 cm ⁻¹	1677 cm ⁻¹	1652 cm ⁻¹
CO Molecule 7d	Free methyl ester	Free Lys _{i+1}	Free CO(Z) Lys _{i+3}	Free CO(Z) D-Lys _{i+1} +Boc _i	Free azaPhe _{i+2}	Bound Boc _i
Wave number	1749 cm ⁻¹	1734 cm ⁻¹	1718 cm ⁻¹	1702 cm ⁻¹	1675 cm ⁻¹	1652 cm ⁻¹

Accordingly, we could assume that the NH_{i+3} (Lys2) in both compounds **7c** and **7d** are involved in intramolecular hydrogen bonds with the CO_i (Boc-group) which stabilizes the β -turn conformation by closing a pseudocycle of 10 atoms, while the other CO groups are in free states in dilute solution as noticed from their higher wave numbers. These results are consistent with the previous studies on this series of azapeptides.^{24,32}

III.2.3. Molecular Dynamic Calculations of 2:1-[α /aza]-Trimers

In order to investigate the most conformational space as well as the possible intramolecular hydrogen bonds in our 2:1-[α /aza]-oligomers (trimers and hexamers), molecular dynamic calculations on the four molecules **7c**, **7d**, **8c** and **8d** were carried out according to the protocol described in experimental section.^{214,215}

Ptraj modulus of AMBER software suite²¹⁵ was employed for the analysis of 25,000 structures for each molecule separately in order to assess: (i) the possibility of hydrogen bond formation, and (ii) the average values of torsion angles to have an idea about the most favorable conformation(s) adopted by these oligomers.

Part A

Chapter III. Structural Studies of 2:1-[α /aza]-Oligomers Possessing Lysine Residues

In order to get information about the possible hydrogen bonds in the four molecules, we applied the most favorable parameters for hydrogen bond formation on the 25,000 simulated structures in which the bond angle (N---H---O) prefers to be greater than 120° and the hydrogen bond distance (O---NH) to be less than 3.2 Å.^{216,217}

In compound **7c**, the calculations predicted the presence of two hydrogen bonds: (i) between CO_i (Boc) and the NH_{i+2} (azaPhe) of 2.86 Å closing a pseudocycle of 7 atoms constructing the peptide backbone in γ -turn like conformation, and (ii) between CO_{i+2} (azaPhe) and the N^εH_{i+3} (Lys2) of 2.96 Å closing a pseudocycle of 10 atoms, with occurrences of 36% and 35%, respectively, Table 3.2 and Figure 3.7.

Table 3.2. Mean values of the bond distances and bond angles for the predicted intramolecular hydrogen bonds calculated from 25,000 structures in **7c** and **7d** issued of the molecular dynamic simulations

Molecule	Bond Ref.	Residue	Residue	Distance (Å) N-----O	Angle (°)	H-bond (%)
7c	i	CO (i)	NH (i + 2)	2.86	139.50	36
	ii	CO (i + 2)	N ^ε H (i + 3)	2.96	159.04	35
7d	i	CO(Z) (i + 3)	NH (i + 2)	2.89	162.01	40
	ii	CO(Z) (i + 3)	NH (i + 1)	2.91	158.44	26
	iii	CO (i)	N ^ε H (i + 1)	2.98	159.42	22

Regarding to compound **7d**, the calculations indicated the possible existence of three hydrogen bonds. The CO(Z)_{i+3} (Lys2) reflected its ability to form two hydrogen bonds: (i) with the NH_{i+2} (azaPhe) of 2.89 Å, and (ii) with NH_{i+1} (Lys1) of 2.91 Å, forming pseudocycles of 13 and 16 atoms, with occurrences of 40% and 26%, respectively. The third hydrogen bond (iii) exists with less occurrence of 22% between CO_i (Boc) and the N^εH_{i+1} (Lys1) of 2.98 Å closing a pseudocycle of 10 atoms, Table 3.2 and Figure 3.8. We could recognize that the three intramolecular hydrogen bonds occur between the side chains (N^εH or CO(Z)) and the peptide backbone, these interactions are sufficient to cause large deviations in the backbone dihedral angles from the classical values.

Molecular dynamic calculations are consistent with the infrared spectroscopy results by interpreting the additional bound NH bands. The FTIR spectra showed one broad bound band in case of **7c** and two broad bound bands in molecule **7d**.

We could also calculate that about 3197 frames (12.8%) in case of **7c** possess the two hydrogen bonds together (Figure 3.7). In the other side, the calculations for compound **7d** showed that about 6356 frames (25.4%) possess the first and second hydrogen bonds together, 3713 frames (14.8%) possess the first and third hydrogen bonds together, 1701 frames (6.8%) possess the second and third hydrogen bonds together, and only 1669 frames show the three hydrogen bonds together (Figure 3.8).

In order to investigate if these intramolecular hydrogen bonds that exist between the side chains (N^εH (Lys) and CO(Z)) and peptide backbone disturb the backbone dihedral angles, calculations of the average torsion angles in both molecules were done (next paragraphs).

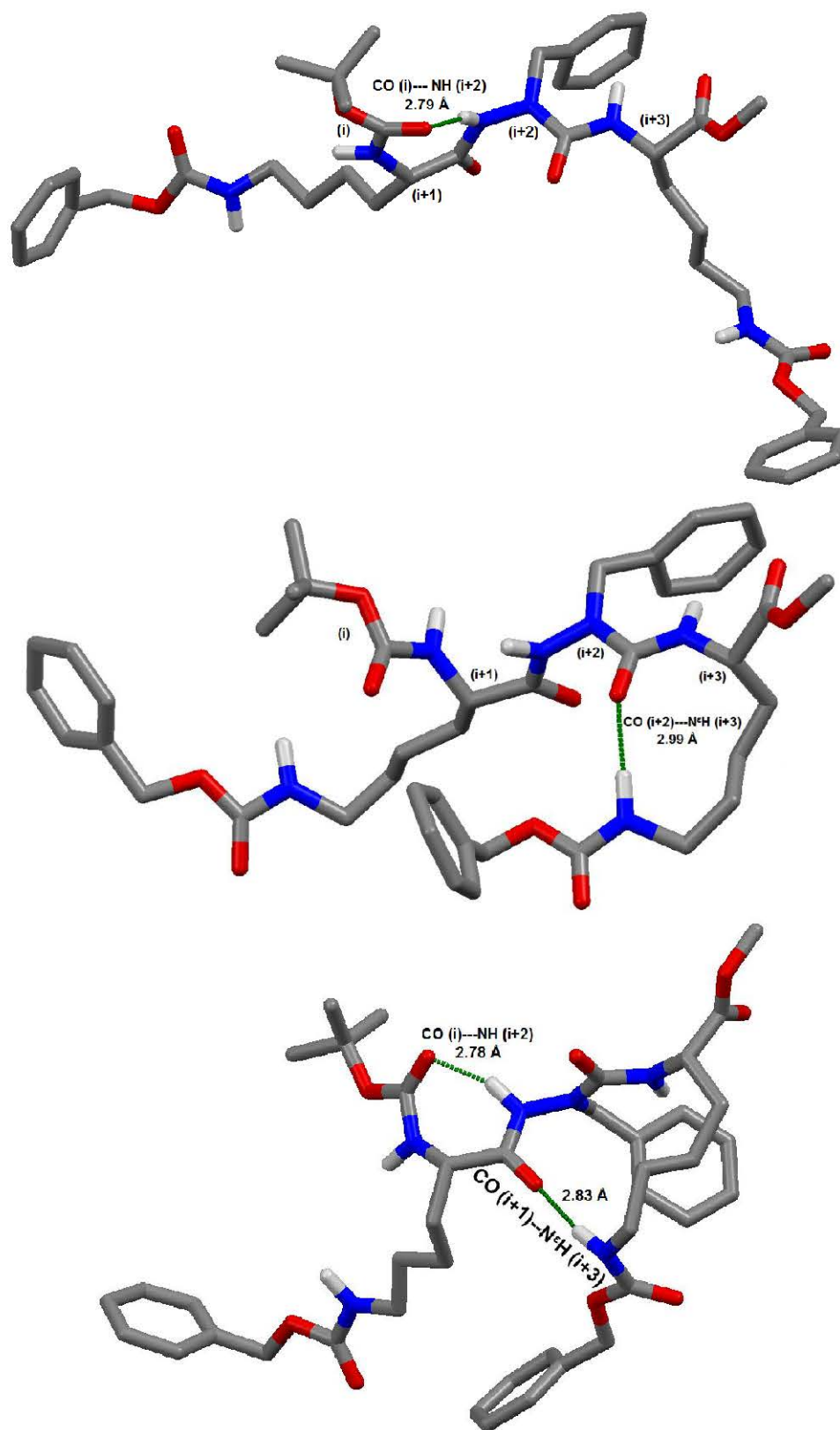


Figure 3.7. Selected frames for molecule 7c issued of molecular dynamic simulations, illustrating different intramolecular hydrogen bonds (green dots): top---type (i), middle---type (ii), and bottom---types (i & ii) together. The H atoms, except those of the NH groups, have been omitted for clarity.

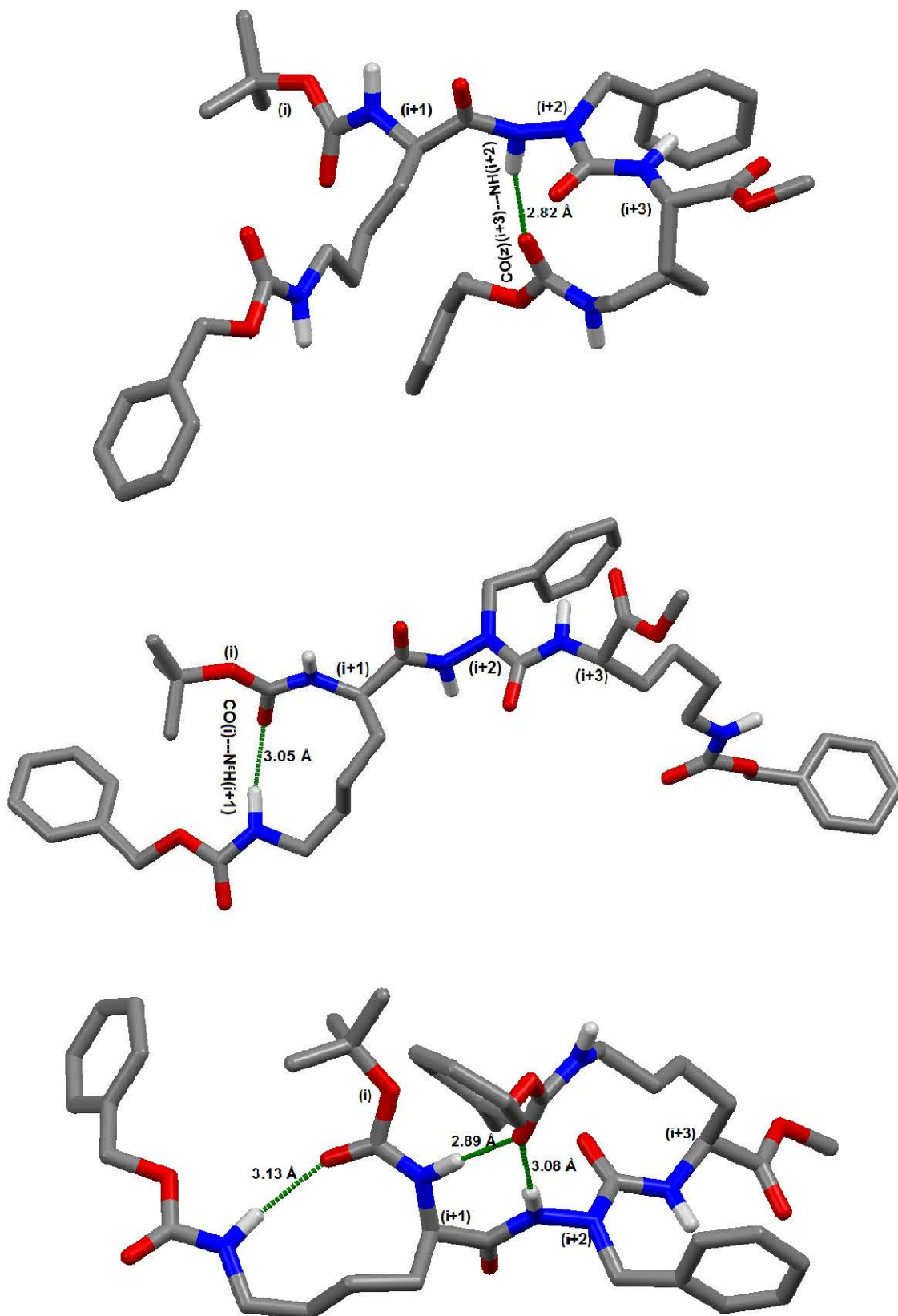
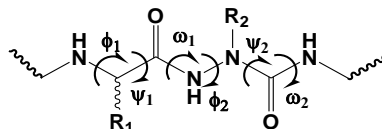


Figure 3.8. Selected frames for molecule **8c** issued of molecular dynamic simulations, illustrating different intramolecular hydrogen bonds (green dots); top---type (i), middle---type (iii), bottom---types (i, ii & iii). The H atoms, except those of the NH groups, have been omitted for clarity.

Part A

Chapter III. Structural Studies of 2:1-[α /aza]-Oligomers Possessing Lysine Residues

It has been reported that the secondary structure of azapeptide is based on its backbone structural elements which composed of the hydrazine and an urea constituent, in which the two parts are described by the torsion angles ϕ and ψ , respectively.¹⁷⁴ Identifying the most favorable conformations adopted by the 2:1-[α /aza]-trimers (**7c** and **7d**) required calculating the average values of the backbone torsion angles for all the simulated 25,000 structures as shown in Table 3.3.



Nomenclature used for the backbone dihedral angles of the four oligomers **7c**, **7d**, **8c** and **8d**.

Table 3.3. Mean values of dihedral angles of molecules **7c** and **7d** calculated from 25,000 structures issued of the molecular dynamic simulations

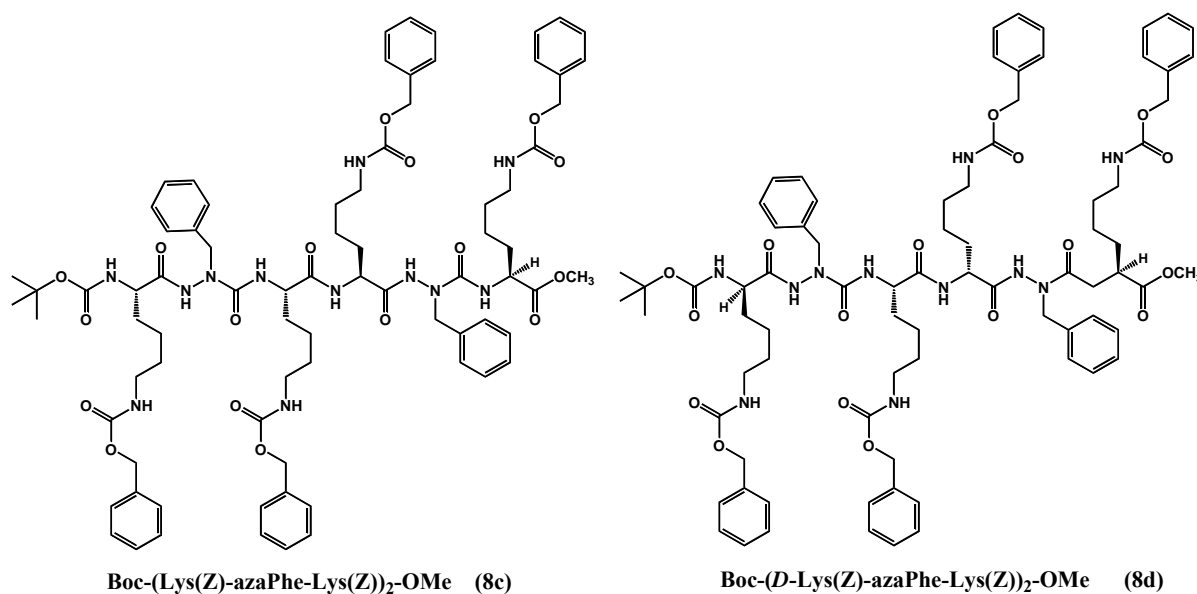
	ϕ_{i+1}	ψ_{i+1}	ϕ_{i+2}	ψ_{i+2}	ϕ_{i+3}	ψ_{i+3}
Molecule 7c	-29.7°	26.37°	-89.07°	47.89°	-138.6°	125.56°
Molecule 7d	128.4°	-64.94°	91.81°	38.83°	-146.91°	125.82°

It is clearly obvious from Table 3.3 that the deviation of the dihedral angles from the classical values (γ -, β -, or α -turn in peptides and proteins) in compound **7c** is less than in compound **7d**. These behaviors are confirmed by the ability of peptide backbone of **7c** to be constructed in γ -turn like conformation, while compound **7d** favors the formation of undefined folded structure. This may be interpreted by the presence of more intramolecular hydrogen bonds between the side chains and the peptide backbone in **7d** (three hydrogen bonds) that cause more distortion in its dihedral angles from the canonical values (Section I.4).

III.3. Conformational Studies of 2:1-[α /aza]-Hexamers

III.3.1. NMR Spectroscopic Studies of 2:1-[α /aza]-Hexamers

¹H NMR studies for compounds **8c** and **8d** (Figure 3.9) were carried out in CDCl₃ (4.0 mmol. L⁻¹, 300 K). The ¹H spectrum of **8d** shows well resolved signals compared with the spectrum of **8c** (Appendix 1, Figures S3.6 - S3.9). The spectra show that the CH₂ protons of the azaPhe moieties are non-equivalent chemically in both compounds.



Boc-(Lys(Z)-azaPhe-Lys(Z))₂-OMe (8c)

Boc-(D-Lys(Z)-azaPhe-Lys(Z))₂-OMe (8d)

Figure 3.9. Molecular structures of 2:1-[α /aza]-Hexamers for: (**8c**) left, and (**8d**) right.

In order to study the conformations favored by **8c** and **8d** in solution, 2D NMR (ROESY) experiments were performed in CDCl_3 (4.0 mmol. L^{-1} , 300 K). Unfortunately, no many correlations in the ROESY spectrum for compound **8c** have been observed (Appendix 1, Figure S3.10). We suggested that the high steric hindrance of the four lysine side chains with the same *S*-configuration in molecule **8c** allows the molecule to be more flexible adopting more energetically stable conformation and hence deviating from the classical β -turn conformations under these experimental conditions. Only the presence of weak correlation between $\text{C}^\alpha\text{H}_{i+6}$ (Lys4) and the NH_{i+5} (azaPhe), and the moderate correlation between the NH_{i+5} (azaPhe) and NH_{i+6} (Lys4) protons gives indication that the *C*-terminal amino acid residues of compound **8c** might be folded in β -turn conformation, Figure 3.10a.^{27,32,174}

In contrast, ROESY spectrum for compound **8d** (Appendix 1, Figure S3.11) is rich in the intramolecular correlations between the nuclei of the spin system. The strong correlations between NH_{i+2} (azaPhe) and both $\text{C}^\alpha\text{H}_{i+1}$ (*D*-Lys1) and NH_{i+3} (Lys2), and the moderate correlation between NH_{i+2} (azaPhe) and NH_{i+1} (*D*-Lys1) suggest that the *N*-terminal amino acid residues show an equilibrium between $\beta\text{I}'$ - and $\beta\text{II}'$ -turns, Figure 3.10b.^{27,32,174} Similarly, the strong correlations between NH_{i+5} (azaPhe) and either $\text{C}^\alpha\text{H}_{i+6}$ (Lys4) proton, NH_{i+4} (*D*-Lys3) and/or NH_{i+6} (Lys4) protons indicate that the *C*-terminal amino acid residues show also an equilibrium between $\beta\text{I}'$ - and $\beta\text{II}'$ -turns.^{27,32,174}

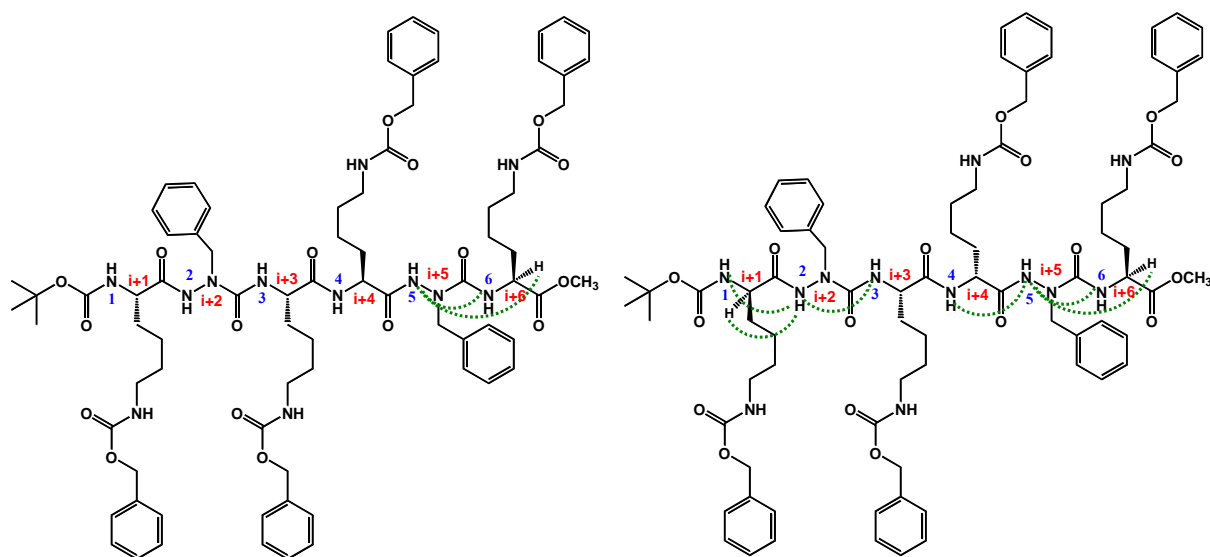


Figure 3.10. ROE correlations of β -turn conformations in: (**8c**) left, and (**8d**) right; (300 MHz, 4.0 mmol. L^{-1} , CDCl_3 , 300 K).

Concerning the solvent composition experiment by NMR technique, increasing %DMSO- d_6 in [DMSO- d_6 / CDCl_3] mixture shows that the NH1 (Lys1; **8c**) or (*D*-Lys1, **8d**) and all the NH protons of the lysine side chains (NH7 – NH10; except NH10 of **8d**) for both compounds are very sensitive to the addition of DMSO- d_6 and their chemical shifts vary largely with further increasing of %DMSO (Appendix 1, Figure S3.12). Accordingly, we suppose that these protons are free and not involved in any intramolecular hydrogen bond (except NH10 of **8d**) due to their high sensitivity upon the addition of DMSO- d_6 .⁹² In contrast, the NH protons of the NH3 (Lys2) and NH6 (Lys4) of both compounds **8c** and **8d** are not sensitive to the addition of the DMSO- d_6 (Figure 3.11). These results demonstrate that these protons [NH3 (Lys2) and NH6 (Lys4)] may be involved in strong intramolecular hydrogen bonds.⁹²

Part A

Chapter III. Structural Studies of 2:1-[α /aza]-Oligomers Possessing Lysine Residues

Regarding compound **8c**, the NH2 (azaPhe) is strongly affected by increasing %DMSO- d_6 which reflects the free state of this proton in solution (Appendix 1, Figure S3.12). Moreover, NH4 (Lys3) and NH5 (azaPhe2) are not sensitive to the increasing in DMSO- d_6 concentration till the range \sim (20 - 30%), then they become more affected with further increasing in %DMSO- d_6 . Accordingly, we proposed that these NH protons are probably involved in weak intramolecular hydrogen bonds (Figure 3.11a).⁹²

In case of compound **8d**, NH2 (azaPhe1) and NH5 (azaPhe2) are not sensitive to the initial addition of DMSO- d_6 , but their chemical shifts (ppm) show higher values by increasing the DMSO- d_6 concentration more than 40%. This reflects that these protons may be engaged in weak intramolecular hydrogen bonds (Figure 3.11b). In contrast, the chemical shift of the NH4 (*D*-Lys3) reflects large sensitivity through its chemical shift values (ppm) by increasing %DMSO- d_6 which indicates that this proton is free and not involved in intramolecular hydrogen bond (Appendix 1, S3.12). Interestingly, NH10 (Lys4) proton reveals weak dependence on %DMSO- d_6 till 5%, then its chemical shift acquires high values with increasing %DMSO- d_6 , this behavior supposes the possibility of this NH10 (Lys4) proton to form weak intramolecular hydrogen bond.

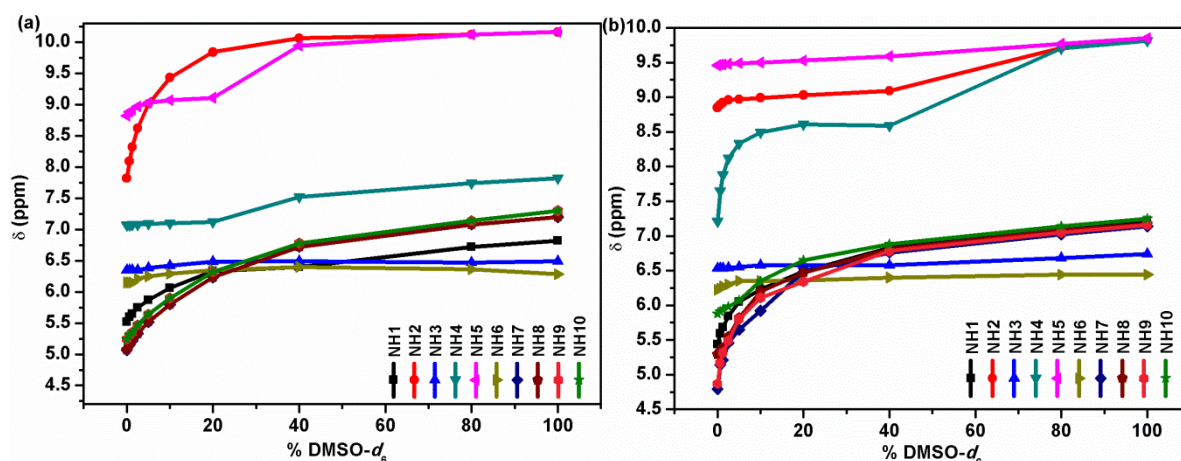
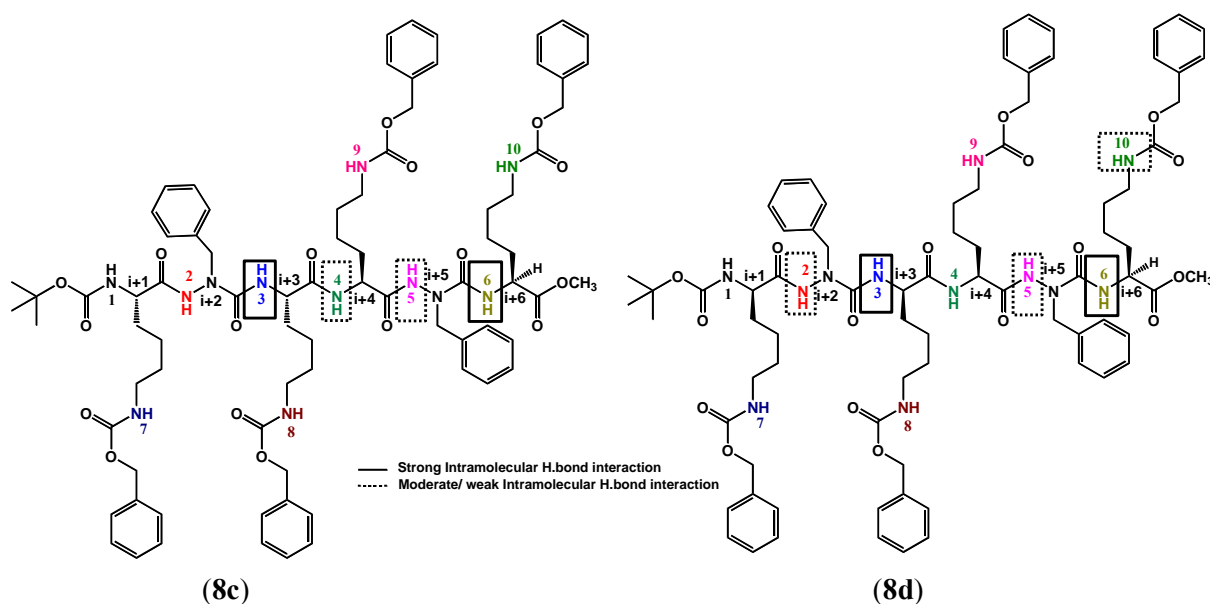


Figure 3.11. Chemical shift-variations (δ) of NH protons for: (a) **8c**, and (b) **8d** as a function of % [$\text{CDCl}_3/\text{DMSO-}d_6$] mixtures.



III.3.2. FTIR Spectroscopic Studies of 2:1-[α / α]-Hexamers

IR spectra were recorded for compounds **8c** and **8d** at dilute conditions (3.0 mmol. L⁻¹, CDCl₃). Both compounds (**8c** and **8d**) show similar NH stretching regions as their trimers (**7c** and **7d**), respectively. The NH stretching domain of both compounds demonstrated a band in the free NH region corresponds to the free NH protons. In addition, there is a broad band in the bound NH region around 3345 cm⁻¹ in the both molecules which should belongs mainly to the bound NH protons of NH3 (Lys2) and NH6 (Lys4) according to the solvent composition NMR experiments, (Figures 3.12a, b). Interestingly, there is an additional broad bound band in the far NH stretching region [(3235 – 3280 cm⁻¹) in **8c**, and (3180 – 3230 cm⁻¹) in **8d**] which may be related to other intramolecular hydrogen bonds. Finally, one can notice that the bound NH bands in **8d** have more intensities, broadening and lower frequencies than those of the **8c**, reflecting the presence of more number and stronger intramolecular hydrogen bonds in molecule **8d** than in molecule **8c**, (Figures 3.12a, b). These results are consistent with the solvent composition studies by NMR technique.

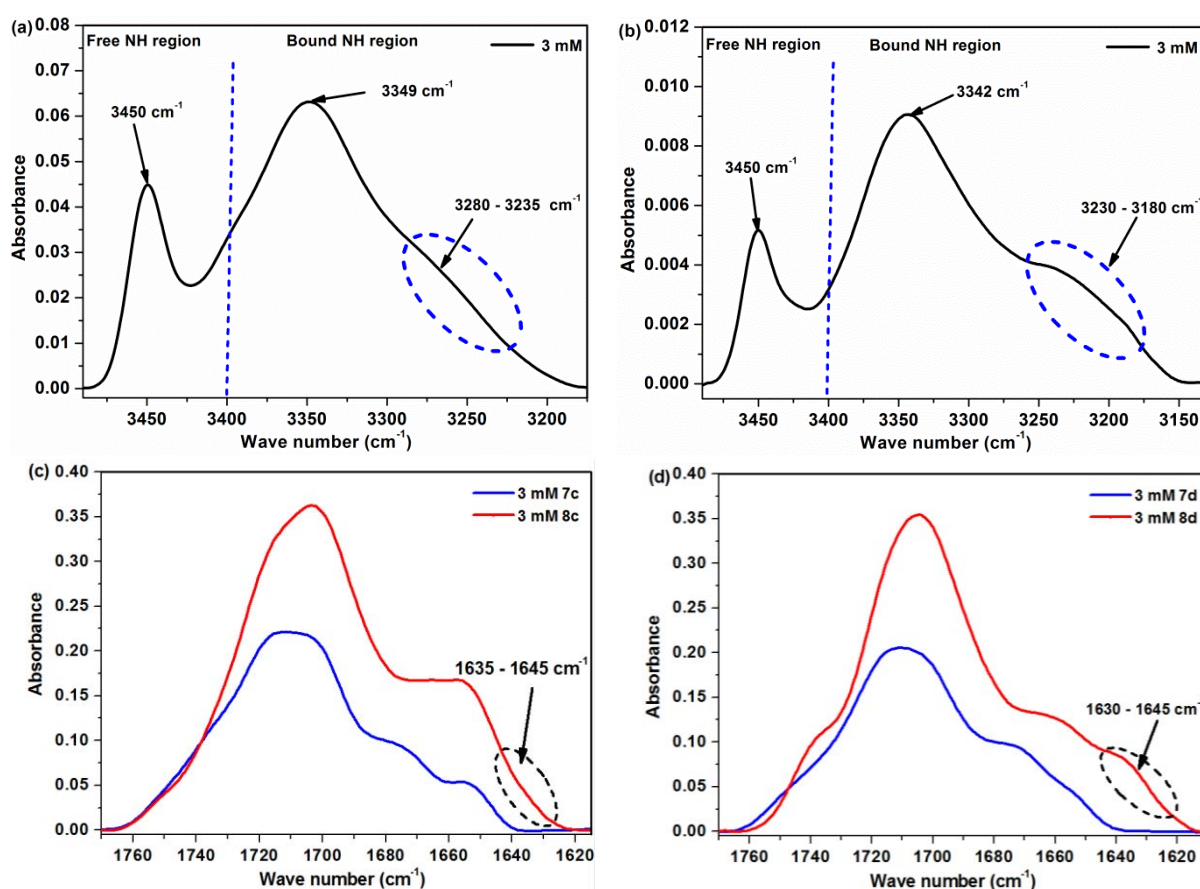


Figure 3.12. FTIR spectra belong to the NH (up spectra), and CO (bottom spectra) stretching regions for: (a & c) **8c**, and (b & d) **8d**; (3.0 mmol. L⁻¹, CDCl₃).

Regarding the CO stretching domain, the two spectra are very similar to their trimers and they show broadening and overlapping of the CO bands that caused an obstacle to assign all the bands even with the help of 2nd derivative deconvolution method. So we could not identify which carbonyl groups are involved in intramolecular hydrogen bonds. By comparing the CO spectra of the trimer and the corresponding hexamer (Figures 3.12c, d), we can notice that **8c** and **8d** molecules exhibit new broad band at (1635 - 1645 cm⁻¹) and (1630 - 1645 cm⁻¹), respectively which is characteristic for the presence of β -turn and these results are consistent the NMR studies, particularly for compound **8d**.²¹⁸

Based on the spectroscopic results, we suppose that both NH3 (Lys2) and NH6 (Lys4) in both compounds **8c** and **8d** are involved in strong intramolecular hydrogen bonds while some other NH protons are weakly involved. We could not succeed to know which carbonyl groups are involved in intramolecular hydrogen bonds. 2D ROESY experiments demonstrated that only C-terminal in **8c**, and the both N- and C-termini in **8d** might be folded in β -turn conformations.

III.3.3. Molecular Dynamic Calculations of 2:1-[α /aza]-Hexamers

Analyses of the results obtained from the molecular dynamic simulations for the two hexamers (**8c** and **8d**) were more complicated than for their trimers (**7c** and **7d**). The complexity comes from the elongation of the peptide chain (6 residues) which increases the flexibility of the molecule to adopt and exist in many conformations. In addition, the presence of long side chains of four lysine moieties in **8c** and **8d** compete in forming intramolecular hydrogen bonds with the peptide backbone and this may lead to undefined folded conformations in these oligomers.

It was interesting to assess the existence of hydrogen bonds within these hexamers. The calculations for both molecules predicted a number of intramolecular hydrogen bonds as summarized in Table 3.4.

Table 3.4. Mean values of bond distances and bond angles for the predicted intramolecular hydrogen bonds calculated from 25,000 structures in **8c** and **8d** issued of the molecular dynamic simulation

Molecule	Bond Ref.	Residue	Residue	Distance (Å) N-----O	Angle (°)	H-bond (%)
8c	i	CO (i+2)	NH (i + 4)	2.78	146.35	90.8
	ii	CO (i + 1)	N ^ε H (i + 4)	2.91	157.18	64.9
	iii	CO (i)	NH (i + 2)	2.89	140.85	48.9
	iv	CO (i+2)	NH (i + 5)	3.02	147.36	32.9
8d	i	CO (i + 1)	NH (i + 5)	2.97	149.60	59.1
	ii	CO(Z) (i + 6)	NH (i + 1)	2.90	156.03	58.7
	iii	CO (i + 2)	NH (i + 4)	2.94	137.64	38.8
	iv	CO (i)	NH (i + 2)	2.84	143.62	29.5
	v	CO(Z) (i + 4)	N ^ε H (i + 1)	2.95	159.04	26.9
	vi	CO (i + 5)	N ^ε H (i + 3)	2.94	155.21	23.0

In compound **8c**, the calculations indicated the possibility of 4 different hydrogen bonds between: (i) CO_{i+2} (azaPhe1) and NH_{i+4} (Lys3) closing a pseudocycle of 7 atoms (γ -turn) occurring as 90% of the simulated frames, (ii) CO_{i+1} (Lys1) and N^εH_{i+4} (Lys3) closing a pseudoring of 16 atoms with 64.9%, (iii) CO_i (Boc) and NH_{i+2} (azaPhe1) closing a pseudocycle of 7 atoms (γ -turn) with 48.9%, and (iv) CO_{i+2} (azaPhe1) and NH_{i+5} (azaPhe2) closing a pseudocycle of 10 atoms (β -turn) with occurrence of 32.9%. Accordingly, the peptide backbone is structured in β - and/or γ -turn like conformation(s).

In the other side, the calculations for compound **8d** predicted the possibility of 6 different hydrogen bonds as illustrated in Table 3.4. The hydrogen bonds are: (i) CO_{i+1} (*D*-Lys1) and NH_{i+5} (azaPhe2) closing a pseudocycle of 13 atoms (α -turn) occurring as 59.1% of the simulated frames, (ii)

Part A

Chapter III. Structural Studies of 2:1-[α /aza]-Oligomers Possessing Lysine Residues

CO(Z)_{i+6} (Lys4) and NH_{i+1} (*D*-Lys1) closing a pseudocycle of 25 atoms with 58.7%, (iii) CO_{i+2} (azaPhe1) and NH_{i+4} (*D*-Lys3) closing a pseudocycle of 7 atoms (γ -turn) with occurrence of 38.9%, (iv) CO_i (Boc) and NH_{i+2} (azaPhe1) closing a pseudocycle of 7 atoms (γ -turn) with 29.5%, (v) CO(Z)_{i+4} (*D*-Lys3) and N^εH_{i+1} (*D*-Lys1) closing a pseudocycle of 23 atoms with occurrence of 26.9%, and (vi) CO_{i+5} (azaPhe2) and N^εH_{i+3} (Lys2) closing a pseudocycle of 15 atoms with occurrence of 23.0%. Subsequently, the peptide backbone is structured in γ - and/or α -turn like conformation(s).

These results are consistent with solvent composition ¹H NMR results as we supposed that the protons of NH4 and NH5 may be involved in weak hydrogen bonds in case of **8c**. Similarly, we suggested that protons NH2 and NH5 in compound **8d** are involved in weak intramolecular hydrogen bonds at low %DMSO-*d*₆. In addition, the results are consistent with the 2D NMR studies in solution because molecule **8c** showed weak correlations between the nuclei (less folded) compared with **8d** in which the 2D spectrum reflects more intramolecular correlations between the nuclei of the spin system (more folded). Moreover, molecular dynamic calculations interpreted the broad bound bands in the far NH and CO regions in both molecules due to the presence of several intramolecular hydrogen bonds.

By applying the most favorable parameters for hydrogen bond formation,^{216,217} we could calculate average percentages of the intramolecular hydrogen bonds in both molecules, (Appendix 1, Tables S3.1 and S3.2). Some selected frames representing for the molecules **8c** and **8d** are shown in Figures 3.13 and 3.14, respectively. The Figures illustrate different types of intramolecular hydrogen bonds particularly the intramolecular interactions between the side chains and peptide backbone. In both hexamers, we suppose that the presence of intramolecular hydrogen bonds between the side chain (N^εH or CO(Z)) and peptide backbone will affect the backbone dihedral angles deviating from the well known values for the secondary structures in peptides and proteins (next paragraphs).

Based on the average calculated values of the torsion angles for all the simulated 25,000 structures in the two oligomers **8c** and **8d** (Table 3.5), we could suggest that both hexamers exist in equilibrium between many conformations stabilized by the aforementioned intramolecular hydrogen bonds.

Table 3.5. Mean dihedral angles of molecules **8c** and **8d** calculated from 25,000 structures issued of the molecular dynamic simulations

Compound	ϕ_{i+1}	ψ_{i+1}	ϕ_{i+2}	ψ_{i+2}	ϕ_{i+3}	ψ_{i+3}	ϕ_{i+4}	ψ_{i+4}	ϕ_{i+5}	ψ_{i+5}
8c	-85.81°	23.79°	86.23°	-68.93°	-66.15°	26.77°	-129.05°	13.11°	-88.26°	21.62°
8d	83.43°	-27.38°	79.51°	-112.39°	-68.92°	5.67°	131.28°	30.66°	97.04°	-9.78°

The values of the dihedral angles (Table 3.5.) are distorted from the classical values of the secondary structures in peptides and proteins (Section I.4). The deviation from the classical torsion angles values may be due to the involvement of the side chains (N^εH or CO(Z)) in intramolecular hydrogen bonds with peptide backbone.

We can conclude that although the strong impact of the nature and chirality of the lysine residues on the conformations of azapeptides, the aza-motif still exerting its vital role in constraining and constructing the peptide backbone. Based on the molecular dynamic calculations for trimers and hexamers, we noticed that changing the chirality of the lysine amino acid(s) from (*S*) to (*R*) has led to increasing the possibility of folding. Furthermore, it allows the side chain (N^εH or CO(Z)) to engage in more intramolecular hydrogen bonds with the peptide backbone (**7d** < **7c** & **8d** < **8c**).

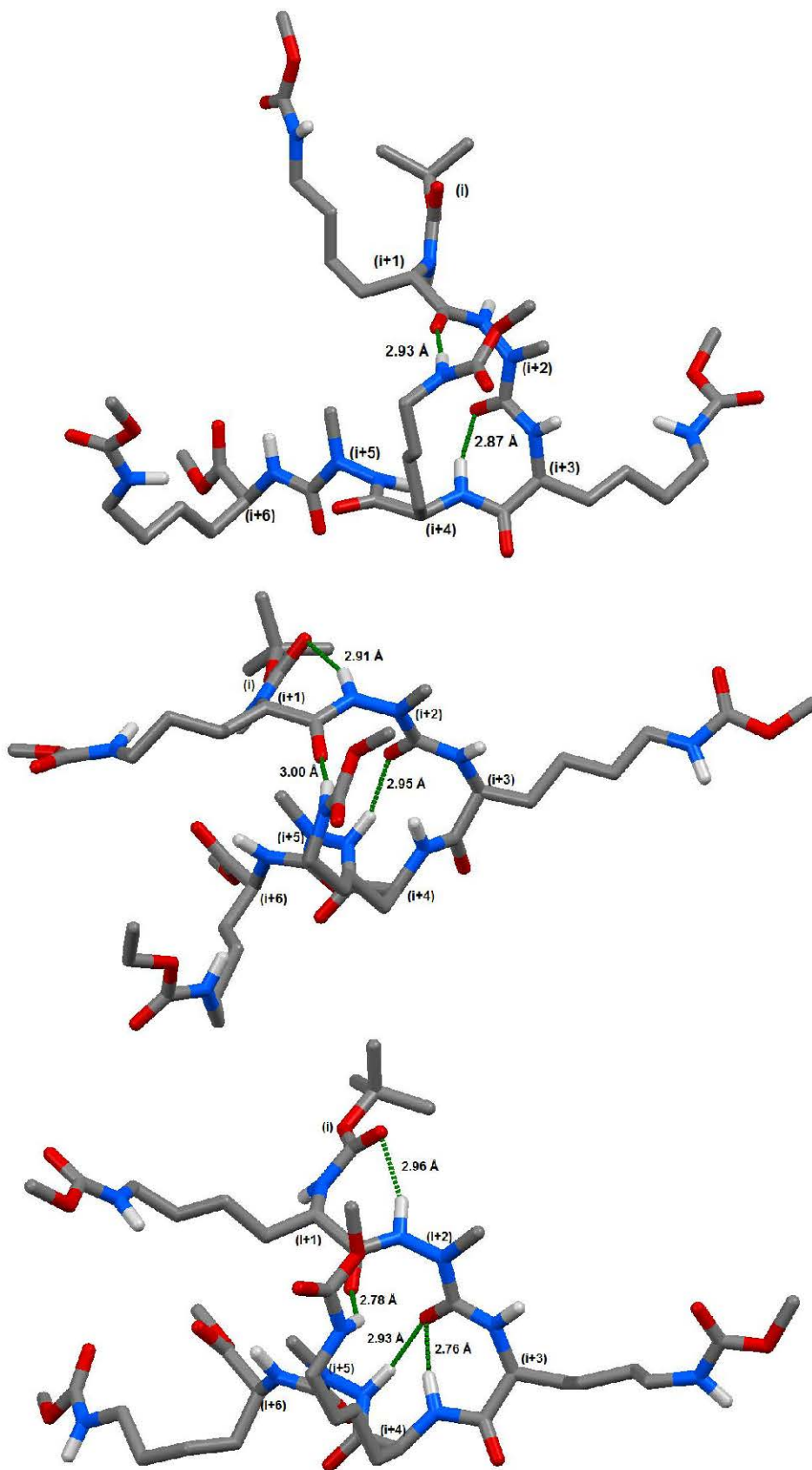


Figure 3.13. Selected frames for molecule **8c** issued of molecular dynamic simulations, illustrating different intramolecular hydrogen bonds (green dots). The H atoms, except those of the NH groups, and the phenyl groups have been omitted for clarity.

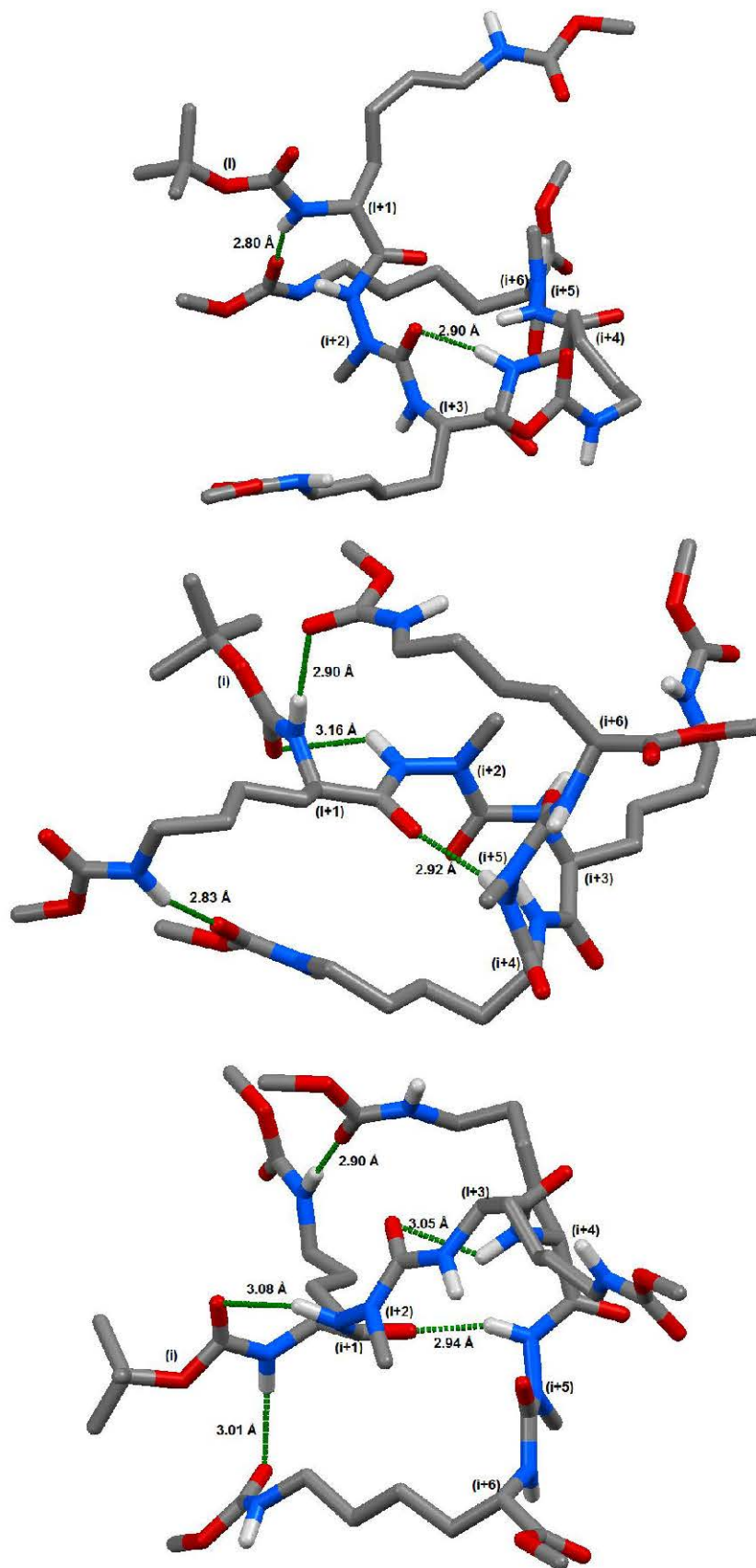


Figure 3.14. Selected frames for molecule **8d** issued of molecular dynamic simulations, illustrating different intramolecular hydrogen bonds (green dots). The H atoms, except those of the NH groups, and the phenyl groups have been omitted for clarity.

III.4. Conclusions

New 2:1-[α /aza]-oligomers (trimers and hexamers) possessing lysine amino acid residues have been synthesized in good yields. The study aimed to investigate the influence of the chirality, chain length and the role of N^εH of lysine side chain on the conformation of these oligomers. NMR and FTIR results indicated that the β -turn conformation is conserved in trimers. Increasing the chain length led to increase the steric hindrance, particularly in homo-hexamer (**8c**) which increased the flexibility of the molecule and became less folded compared with the heteroanalog. Interestingly, alternating the chirality between *R* and *S* produced hetero-hexamer oligomer (**8d**) with less steric hindrance than the homo analog (**8c**), and it revealed conservation of the β -turn conformations in its both termini. In the other hand, molecular dynamic calculations for trimers and hexamers demonstrated that although the side chains (N^εH lysine or CO(Z)) exert strong impact on the conformation of these azapeptides by involving in intramolecular hydrogen bonds with peptide backbone affecting their torsion angles, the aza-motifs still play vital roles in constructing and constraining the peptide backbone to adopt defined conformation(s).

Part A
Experimental Section

Part A

Experimental Section

General: Unless otherwise stated, all chemicals and reagents were purchased from commercial suppliers (Sigma-Aldrich, Fluka, Merck or Alfa-Aesar). Dry CH_2Cl_2 was obtained by distillation over P_2O_5 under an argon atmosphere, MeOH was purchased in anhydrous form, and other reagent-grade solvents were used without further purification as received. Reactions were monitored by thin layer chromatography (TLC) using aluminum-backed silica gel plates. TLC spots were viewed under UV light or/and by heating the plate after treatment with a staining solution of phosphomolybdic acid. Flash chromatography was carried out on silica gel 60 (0.04 – 0.063 μm Mesh ASTM). All yields were calculated from pure isolated products. Electron spray ionization mass spectra (HRMS-ESI) were recorded with a Bruker MicroTof-Q HR spectrometer in the “Service commun de Spectrométrie de Masse”, Faculté des Sciences et Technologies, Vandoeuvre-lès-Nancy, France. All melting points (mp) were uncorrected.

NMR spectroscopy: 1D (^1H and ^{13}C) and 2D (ROESY) NMR spectra were recorded using a Bruker Advance NMR spectrophotometer (300 MHz) in CDCl_3 , CD_3CN and $\text{DMSO}-d_6$ as solvents at room temperature with chemical shifts of 7.26, 1.94 and 2.50 ppm, respectively. The chemical shifts were reported in ppm (δ) relative to tetramethylsilane (TMS) served as an internal standard ($\delta = 0$ ppm) for ^1H NMR, while CDCl_3 ($\delta = 77.16$ ppm), CD_3CN ($\delta = 1.32$ & 118.26 ppm) and $\text{DMSO}-d_6$ ($\delta = 39.5$ ppm), were used as an internal standards for ^{13}C NMR. Multiplicities are reported as follows: s = singlet, d = doublet, q = quartet, m = multiplet, br = broad, arom = aromatic.

Fourier Transform Infrared Spectroscopy: FTIR spectra for all products in CDCl_3 were recorded with Bruker Tensor 27 over 128 scans and referenced to the residual solvent resonances. In addition, attenuated total reflectance (ATR-FTIR) measurements have been performed on solids for some products. All the ATR-FTIR spectra were recorded on Bruker Tensor 27 spectrometer equipped with a trough plate comprising of a germanium single crystal where the samples were loaded over it. Spectra were acquired in the 4000 - 400 cm^{-1} range with a resolution of 4.0 cm^{-1} over 128 scans, taken into consideration the background subtraction from each spectra to correct for atmospheric interference.

Molecular Dynamic Calculations (AMBER 12): Calculations on molecules **7c**, **7d**, **8c**, and **8d** were carried out according to the protocol: 0.5 μs with 2fs steps molecular dynamics simulations were calculated in explicit solvent (chloroform; CHCl_3 box) without any ROE constraints under constant pressure periodic boundary conditions, pressure relaxation time of 0.5 μs , and constant temperature 300 K, using the package of molecular dynamics simulation programs AMBER 12. The starting molecules were constructed using MarvinSketch (ChemAxon), Antechamber and Xleap from AMBER program suite. Molecular simulation was done with Sander program with general AMBER force field (GAFF) and included amino acid parameters (ff99SB). Ptraj was employed for the analysis of 25,000 structures.^{214,215}

Synthesis and Characterizations of products (2 – 5):

***N*-tert-butylloxycarbonylaminophthalimide (2):** Phthalic anhydride (1.0 equiv.) and *tert*-butylcarbazate (1.0 equiv.) were dissolved in toluene in a monocol with a Dean-Stark. The suspension was refluxed for 12h. The mixture was cooled and the *N*-tert-butylloxycarbonylaminophthalimide **2** precipitated. The solid was filtered off and recrystallized from EtOAc.

Characterization data: *N*-tert-butylloxycarbonylaminophthalimide **2** was obtained as white crystals (yield 86%) after recrystallization from ethyl acetate; m.p. 214 - 216 $^\circ\text{C}$; ^1H NMR (300 MHz, CDCl_3 , 8.0 mmol. L^{-1}) δ_{H} 1.49 (2 s, 9H, $\text{C}(\text{CH}_3)_3$), 6.61 (br s, 1H, NH), 7.76-7.79 (m, 2H, H arom Phth), 7.89-7.92 (m, 2H, H arom Phth). ^{13}C NMR (75 MHz, CDCl_3 , 8.0 mmol. L^{-1}) δ_{C} 28.4 ($\text{C}(\underline{\text{C}}\text{H}_3)_3$), 83.81 ($\underline{\text{C}}(\text{CH}_3)_3$), 124.65 (CH arom Phth), 130.68 (C arom Phth), 135.37 (CH arom Phth), 154.07 (N- $\underline{\text{C}}\text{OOt}$ -

Part A

Experimental Section

Bu), 166.13 (O=C-Pht). **IR (KBr)** $\tilde{\nu}_{\max}$ = 3395 cm^{-1} (NH); 1706 cm^{-1} , 1740 cm^{-1} , 1783 cm^{-1} (C=O). **HRMS (ESI)** for $[\text{C}_{13}\text{H}_{14}\text{N}_2\text{O}_4]$: calculated $[\text{M}+\text{H}]^+$ (m/z) 263.0954; found, 263.1034.

***N*-benzyl-*N*-*tert*-butyloxycarbonylaminophthalimide (3):** To a solution of *N*-*tert*-butyloxycarbonylaminophthalimide **2** (1.0 equiv.), PPh_3 (1.5 equiv.) and benzyl alcohol (3.0 equiv.) in dry THF, DEAD (1.5 equiv.) was added in one portion under N_2 and stirring at (0 - 5 $^\circ\text{C}$). The resulting solution was stirred overnight (monitored by TLC until completion) and concentrated under vacuum. The residue was triturated in EtOAc, placed in refrigerator and most of the triphenylphosphine oxide was precipitated which then removed by filtration. The filtrate was evaporated and the residue was purified by column chromatography on silica gel.

Characterization data: *N*-benzyl-*N*-*tert*-butyloxycarbonylaminophthalimide **3** was obtained as white solid (yield 90%) after flash chromatography (0.04 – 0.063 μm) using (15% ethyl acetate : 85% petroleum ether) as eluent; m.p. 107 - 109 $^\circ\text{C}$; **^1H NMR** (300 MHz, CDCl_3 , 8.0 mmol. L^{-1}) δ_{H} 1.37 and 1.52 (2 s, 9H, $\text{C}(\text{CH}_3)_3$), 4.85 and 4.89 (2 s, 2H, NCH_2), 7.27 - 7.44 (2 m, 5H, H arom Ph), 7.73-7.84 (m, 4H, H arom Phth). **^{13}C NMR** (75 MHz, CDCl_3 , 8.0 mmol. L^{-1}) δ_{C} 28.59 and 28.86 ($\text{C}(\underline{\text{C}}\text{H}_3)_3$), 53.35 and 55.32 (NCH_2), 83.17 and 83.95 ($\underline{\text{C}}(\text{CH}_3)_3$), 124.41 (CH arom Phth), 128.58 (CH arom Ph), 129.02 (CH arom Ph), 129.20 (CH arom Ph), 129.73 (CH arom Ph), 130.44 (C arom), 130.64 (C arom), 135.20 (CH arom Phth), 154.18 ($\text{N}-\underline{\text{C}}\text{OO}t\text{-Bu}$), 165.71 (O=C-Pht). **IR (NaCl)** $\tilde{\nu}_{\max}$ = 1737 cm^{-1} , 1796 cm^{-1} (C=O). **HRMS (ESI)** for $[\text{C}_{20}\text{H}_{20}\text{N}_2\text{O}_4]$: calculated $[\text{M}+\text{Na}]^+$ (m/z) 375.1321; found, 375.1314.

***N*-alkylaminophthalimide (4):** To a solution of *N*-alkyl-*N*-*tert*-butyloxycarbonylaminophthalimide **3** (1.0 equiv.) in CH_2Cl_2 , trifluoroacetic acid (10.0 equiv., 8.0% in CH_2Cl_2) was added at 0 $^\circ\text{C}$. The mixture was stirred overnight (monitored by TLC). The solution was concentrated under vacuum, and then the residue was dissolved in CH_2Cl_2 , neutralized with a saturated solution of NaHCO_3 (pH = 7) and extracted three times with CH_2Cl_2 . The combined organic layers were dried over MgSO_4 and evaporated under vacuum giving a yellow solid which was immediately used without further purification.

Characterization data: *N*-alkylaminophthalimide **4** was obtained as pure yellow solid (quantitative 100%) without purification; m.p. 109 - 110 $^\circ\text{C}$; **^1H NMR** (300 MHz, CDCl_3 , 8.0 mmol. L^{-1}) δ_{H} 4.22 (s, 2H, NCH_2), 4.56 (br, 1H, NH), 7.27-7.47 (m, 5H, H arom Ph), 7.71-7.83 (m, 4H, H arom Phth). **^{13}C NMR** (75 MHz, CDCl_3 , 10.0 mmol. L^{-1}) δ_{C} 55.97 (NCH_2), 124.07 (CH arom Phth), 128.73 (CH arom Ph), 129.22 (CH arom Ph), 129.89 (CH arom Ph), 130.92 (C arom Phth), 134.87 (CH arom Phth), 136.69 (C arom Ph), 167.06 (O=C-Phth). **IR (NaCl)** $\tilde{\nu}_{\max}$ = 3290 cm^{-1} (NH); 1774 cm^{-1} , 1719 cm^{-1} (C=O). **HRMS (ESI)** for $[\text{C}_{15}\text{H}_{12}\text{N}_2\text{O}_2]$: calculated $[\text{M}+\text{H}]^+$ (m/z) 253.0977; found, 253.0963.

Pht-azaPhe-Ala-OMe (5a): To a mixture of *N*-alkyl-aminophthalimide **4** (1.0 equiv.) and DIPEA (2.2 equiv.) in dry CH_2Cl_2 , phosgene 20% in toluene (1.5 equiv.) was added. After 15 min stirring, the toluene solvent and excess of phosgene gas were removed by rotary evaporator under ventilated hood. The white acid chloride residue was re-dissolved in dry CH_2Cl_2 , then solution of alanine methyl ester hydrochloride (1.0 equiv.) and DIPEA (1.5 equiv.) in dry CH_2Cl_2 was added in one portion. The reaction mixture was stirred for 1h at RT. The solvent was evaporated to dryness, diluted with CH_2Cl_2 , washed with aqueous HCl (1M), aqueous NaHCO_3 (1M) and brine, dried over MgSO_4 and evaporated. Compound **5a** was obtained in pure form after precipitation in cold diethyl ether.

Characterization data: Pht-azaPhe-Ala-OMe **5a** was obtained as pure white solid (yield 92%) after trituration with cold diethyl ether; m.p. 158 - 161 $^\circ\text{C}$; **^1H NMR** (300 MHz, CDCl_3 , 8.0 mmol. L^{-1}) δ_{H} 1.38 and 1.40 (d, 3H, CH_3), 3.72 (s, 3H, COOCH_3), 4.53 (m, 1H, $\text{C}^{\alpha}\text{H}$), 4.86–4.97 (m, 2H, CH_2), 5.31 and 5.37 (d, 1H, NH), 7.23-7.42 (m, 5H, H arom Ph), 7.75-7.85 (m, 4H, H arom Phth). **^{13}C NMR** (75

Part A

Experimental Section

MHz, CDCl_3 , 10.0 mmol. L^{-1}) δ_{C} 19.60 (CH_3), 50.19 ($\text{C}^{\alpha}\text{H}$), 53.14 (COOCH_3), 53.62 (NCH_2), 124.62 (CH arom Phth), 128.89 (CH arom Ph), 129.20 (CH arom Ph), 129.80 (C arom Phth), 135.33 (C arom Ph), 135.51 (CH arom Phth), 156.15 ($\text{O}=\text{C}-\text{NH}$), 165.84 ($\text{O}=\text{C}-\text{Phth}$), 174.32 (COOCH_3). **IR (ATR)** $\tilde{\nu}_{\text{max}} = 3353 \text{ cm}^{-1}$ (NH); 1647 cm^{-1} , 1677 cm^{-1} , 1736 cm^{-1} , 1751 cm^{-1} ($\text{C}=\text{O}$). **HRMS (ESI)** for $[\text{C}_{20}\text{H}_{19}\text{N}_3\text{O}_5]$: calculated $[\text{M}+\text{Na}+\text{MeOH}]^+$ (m/z) 436.1479; found, 436.1457.

Pht-azaPhe-Lys(Z)-OMe (5b): To a mixture of *N*-alkyl-aminophthalimide **4** (1.0 equiv.) and DIPEA (2.2 equiv.) in dry CH_2Cl_2 , phosgene 20% in toluene (1.5 equiv.) was added. After 15 min stirring, the toluene solvent and excess of phosgene gas were removed by rotary evaporator under ventilated hood. The white acid chloride residue was further re-dissolved in dry CH_2Cl_2 , then solution of lysine(Z) methyl ester hydrochloride (1.0 equiv.) and DIPEA (1.5 equiv.) in dry CH_2Cl_2 was added in one portion. The reaction mixture was stirred for 1h at RT. The solvent was evaporated to dryness, diluted with CH_2Cl_2 , washed with aqueous HCl (1M), aqueous NaHCO_3 (1M) and brine, dried over MgSO_4 and evaporated. Compound **5b** was obtained in pure form after precipitation in cold EtOAc.

Characterization data: Pht-azaPhe-Lys(Z)-OMe **5b** was obtained as pure white solid (yield 88%) after precipitation with cold ethyl acetate; m.p. 134 - 135 °C; **^1H NMR** (300 MHz, CDCl_3 , 8.0 mmol. L^{-1}) δ_{H} 1.23-1.86 (m, 6H, ($\text{C}^{\beta}\text{H}_2$, $\text{C}^{\gamma}\text{H}_2$, $\text{C}^{\delta}\text{H}_2$)), 3.13-3.15 (m, 2H, $\text{C}^{\epsilon}\text{H}_2$), 3.66 (s, 3H, COOCH_3), 4.47-4.54 (m, 1H, $\text{C}^{\alpha}\text{H}$), 4.87 (s, 2H, NCH_2), 5.01 (br s, 1H, $\text{NH}(\text{Z})$), 5.06 (s, 2H, $\text{CH}_2(\text{Z})$), 5.42 and 5.44 (d, 1H, NH), 7.20-7.38 (m, 10H, H arom Ph), 7.68-7.81 (m, 4H, H arom Phth). **^{13}C NMR** (75 MHz, CDCl_3 , 10.0 mmol. L^{-1}) δ_{C} 22.68 ($\text{C}^{\gamma}\text{H}_2$), 29.82($\text{C}^{\delta}\text{H}_2$), 33.01 ($\text{C}^{\beta}\text{H}_2$), 41.39 ($\text{C}^{\epsilon}\text{H}_2$), 53.14 (OCH_3), 53.82 (NCH_2), 53.97 ($\text{C}^{\alpha}\text{H}$), 67.23 (OCH_2), 124.71 (CH arom Phth), 128.70 (CH arom Ph), 128.94 (CH arom Ph), 129.18 (CH arom Ph), 129.24 (CH arom Ph), 129.80 (CH arom Ph), 130.15 (C arom Phth), 130.22 (C arom Phth), 135.37 (C arom Ph), 135.54 (CH arom Phth), 137.42 (C arom Ph), 156.35 ($\text{O}=\text{C}-\text{NH}$), 157.16 (COOCH_2Ph), 165.82 ($\text{O}=\text{C}-\text{Phth}$), 165.99 ($\text{O}=\text{C}-\text{Phth}$), 173.67 (COOCH_3). **IR (ATR)** $\tilde{\nu}_{\text{max}} = 3336 \text{ cm}^{-1}$, 3405 cm^{-1} (NH); 1698 cm^{-1} , 1672 cm^{-1} , 1735 cm^{-1} , 1752 cm^{-1} ($\text{C}=\text{O}$). **HRMS (ESI)** for $[\text{C}_{31}\text{H}_{32}\text{N}_4\text{O}_7]$: calculated $[\text{M}+\text{Na}]^+$ (m/z) 595.2169; found, 595.2170; calculated $[\text{M}+\text{K}]^+$ (m/z) 611.3254; found, 611.1909.

Synthesis and Characterizations of Boc-azaPhe-YY-OMe (6):

Boc-azaPhe-Ala-OMe (6a): To a solution of Phth-azaPhe-Ala-OCH₃ **5a** (1.0 equiv.) in THF, pyrrolidine (3.0 equiv.) was added at RT. The mixture was stirred at RT until completion (4h, monitored by TLC). The solvent and the excess of amine were removed under vacuum giving foam residue. The obtained residue was dissolved in THF, then Boc_2O (1.5 equiv.) and a catalytic amount of DMAP (0.15 equiv.) were added. The mixture was stirred at RT until completion (12h, monitored by TLC). The solvent was removed under vacuum, the residue was dissolved in THF and a freshly prepared solution of methylamine (1.5 equiv., 2M in MeOH) was added at RT. The mixture was stirred at RT until completion (12h, monitored by TLC), the solvent and the excess of amine were removed under vacuum and the residue was purified by column chromatography on silica gel.

Characterization data: Boc-azaPhe-Ala-OMe **6a** was obtained as pure white solid (yield 89%) after flash chromatography (0.04 – 0.063 μm) using (30% ethyl acetate : 70% petroleum ether) as eluent; m.p. 90 - 91 °C; **^1H NMR** (300 MHz, CDCl_3 , 8.0 mmol. L^{-1}) δ_{H} 1.42-1.47 (m, 12H, CH_3 and $\text{C}(\text{CH}_3)_3$), 3.76 (s, 3H, COOCH_3), 4.50-4.60 (m, 1H, $\text{C}^{\alpha}\text{H}$), 4.85 (br s, 2H, NCH_2), 5.91 and 5.94 (d, 1H, NH), 5.97 (br s, 1H, NHBoc), 7.26-7.37 (m, 5H, H arom Ph). **^{13}C NMR** (75 MHz, CDCl_3 , 10.0 mmol. L^{-1}) δ_{C} 19.70 (CH_3), 28.75 ($\text{C}(\text{CH}_3)_3$), 49.84 ($\text{C}^{\alpha}\text{H}$), 51.25 (NCH_2), 52.99 (COOCH_3), 83.04 ($\text{C}(\text{CH}_3)_3$), 128.53 (CH arom Ph), 129.45 (CH arom Ph), 129.59 (CH arom Ph), 136.73 (C arom Ph), 154.90 ($\text{COO}t\text{-Bu}$), 157.61 ($\text{O}=\text{C}-\text{NH}$), 174.75 (COOCH_3). **IR (ATR)** $\tilde{\nu}_{\text{max}} = 3207 \text{ cm}^{-1}$, 3415 cm^{-1} (NH); 1647 cm^{-1} , 1723 cm^{-1} , 1732 cm^{-1} ($\text{C}=\text{O}$). **HRMS (ESI)** for $[\text{C}_{17}\text{H}_{25}\text{N}_3\text{O}_5]$: calculated $[\text{M}+\text{H}]^+$ (m/z) 352.1872; found, 352.1878.

Part A

Experimental Section

Boc-azaPhe-Lys(Z)-OMe (6b): To a solution of Phth-azaPhe-Lys(Z)-OCH₃ **5b** (1.0 equiv.) in THF, pyrrolidine (3.0 equiv.) was added at RT. The mixture was stirred at RT until completion (5h, monitored by TLC). The solvent and the excess of amine were removed under vacuum giving foam residue. The obtained residue was dissolved in THF, then Boc₂O (1.5 equiv.) and a catalytic amount of DMAP (0.15 equiv.) were added. The mixture was stirred at RT until completion (12h, monitored by TLC). The solvent was removed under vacuum, the residue was re-dissolved in THF and a freshly prepared solution of methylamine (1.5 equiv., 2M in MeOH) was added at RT. After a night and by TLC monitoring, the solvent and the excess of amine were removed under vacuum and the residue was purified by column chromatography on silica gel.

Note: The volume of the THF during the second step (addition of Boc₂O) was twice the volume used for the first and third steps (pyrrolidine or methyl amine) to inhibit the reactivity of the N^εH of lysine in concentrated condition avoiding the formation of **Boc-azaPhe-Lys(Boc & Z)-OMe**.

Characterization data: Boc-azaPhe-Lys(Z)-OMe **6b** was obtained as an oily sticky product (yield 85%) after flash chromatography (0.04 – 0.063 μm) using (45% ethyl acetate : 55% petroleum ether) as eluent; ¹H NMR (300 MHz, CDCl₃, 8.0 mmol. L⁻¹) δ_H 1.40-1.90 (m, 15H, (C^βH₂, C^γH₂, C^δH₂) and C(CH₃)₃), 3.15-3.21 (m, 2H, C^εH₂), 3.73 (s, 3H, COOCH₃), 4.51-4.58 (m, 1H, C^αH), 4.99 (br s, 2H, NCH₂), 5.07 (s, 2H, CH₂(Z)), 5.89 and 5.92 (d, 1H, NH), 6.02 (br s, 1H, NHBoc), 7.22-7.33 (m, 10H, H arom Ph). ¹³C NMR (75 MHz, CDCl₃, 10.0 mmol. L⁻¹) δ_C 22.89 (C^γH₂), 28.73 (C(CH₃)₃), 29.82(C^δH₂), 33.33 (C^βH₂), 41.39 (C^εH₂), 51.39 (NCH₂), 53.00 (OCH₃), 53.61 (C^αH), 67.23 (OCH₂), 83.10 (C(CH₃)₃), 128.56 (CH arom Ph), 128.70 (CH arom Ph), 128.76 (CH arom Ph), 129.15 (CH arom Ph), 129.46 (CH arom Ph), 129.59 (CH arom Ph), 136.72 (C arom Ph), 137.38 (C arom Ph), 154.87 (COO^t-Bu), 156.17 (O=C-NH), 157.86 (COOCH₂Ph), 174.13 (COOCH₃). IR (ATR) $\tilde{\nu}_{\max}$ = 3331 cm⁻¹, 3439 cm⁻¹ (NH); 1656 cm⁻¹, 1701 cm⁻¹, 1718 cm⁻¹, 1735 cm⁻¹ (C=O). HRMS (ESI) for [C₂₈H₃₈N₄O₇]: calculated [M+Na]⁺ (m/z) 565.2638; found, 565.2643; calculated [M+K]⁺ (m/z) 581.3723; found, 581.2377.

Synthesis and Characterizations of 2:1-[α/aza]-Trimers

General Protocol for the Synthesis of Trimers (7):

Boc deprotection: To a stirred solution of Boc protected compound **6** (1.0 equiv.) in CH₂Cl₂, ethyl acetate/3M HCl was added at 0 °C. The resulting solution was stirred until completion (1 - 2h, monitored by TLC) and concentrated under vacuum. The excess hydrochloride acid was co-evaporated with CH₂Cl₂ (4 times). The residue was used in coupling reaction without further purification.

Acid fluoride preparation: To a stirred solution of Boc-AA-OH (1.5 equiv., AA = Phe, *D*-Phe, Lys(Z), or *D*-Lys(Z)) in dry CH₂Cl₂ and pyridine (1.5 equiv.) kept under a N₂ atmosphere, cyanuric fluoride (3.0 equiv.) was added dropwise at -20 °C. The solution was stirred at -10°C during 4h, a precipitate or emulsion formed and its amount gradually increased. After 4h, crushed ice was added along with an additional CH₂Cl₂. The organic layer was separated and the aqueous layer extracted with cold CH₂Cl₂. The combined organic layers were washed with ice-cold water and dried over MgSO₄, and the solvent was removed with a rotary evaporator at room temperature to yield the acyl fluoride intermediate product which was directly used in the coupling reaction.

Coupling reaction: Boc-*D*- or *L*-AA-F (1.5 equiv., AA = Phe, or Lys(Z)) in CH₂Cl₂ was added dropwise to a stirred solution of HCl, H-azaPhe-AA-OMe (1.0 equiv., AA = Ala, or Lys(Z)) in CH₂Cl₂ and NaHCO₃ (2.0 equiv.), pH = 7 - 8. The mixture was stirred at RT overnight monitoring by TLC. Then, the organic layer (CH₂Cl₂) was washed twice with HCl (1M), NaHCO₃ (1M) and saturated NaCl, and then was dried over MgSO₄ and the solvent was removed under vacuum and the residue was purified by column chromatography on silica gel.

Part A

Experimental Section

Characterization data for 2:1-[α /aza]-Trimers (7):

Boc-Phe-azaPhe-Ala-OMe 7a was obtained as a white solid (yield 74%) after flash chromatography (0.04 – 0.063 μ m) using (50% ethyl acetate : 50% petroleum ether) as eluent; m.p. 149 - 150 °C; $^1\text{H NMR}$ (300 MHz, CDCl_3 , 10.0 mmol. L^{-1}) δ_{H} 1.37-1.43 (m, 12H, CH_3 and $\text{C}(\text{CH}_3)_3$), 2.88-2.95 and 3.01-3.08 (m, 2H, CH_2), 3.71 (s, 3H, COOCH_3), 4.03 (m, 1H, CH), 4.28 (br s, 1H, NHBoc), 4.43-4.51 (m, 1H, CH), 4.90-4.95 (br m, 2H, NCH_2), 6.2 (br s, 1H, NH), 7.06-7.30 (m, 10H, H arom Ph), 7.73 (br s, 1H, NH). $^{13}\text{C NMR}$ (75 MHz, CDCl_3) δ_{C} 18.71 (CH_3), 28.88 ($\text{C}(\underline{\text{CH}}_3)_3$), 37.83 (CH_2), 50.11 ($\text{C}^{\alpha}\text{H}$), 52.01 (NCH_2), 52.86 (COOCH_3), 56.0 ($\text{C}^{\alpha}\text{H}$), 81.55 ($\text{C}(\underline{\text{CH}}_3)_3$), 128.05 (CH arom Ph), 128.25 (CH arom Ph), 129.15 (CH arom Ph), 129.42 (CH arom Ph), 129.63 (CH arom Ph), 129.85 (CH arom Ph), 136.45 (C arom Ph), 137.10 (C arom Ph), 156.43 ($\text{COO}t\text{-Bu}$), 157.57 ($\text{O}=\text{C}-\text{NH}$), 171.08 ($\text{O}=\text{C}-\text{NH}$), 174.88 (COOCH_3). **IR** (CDCl_3) $\tilde{\nu}_{\text{max}}$ = 3370 cm^{-1} , 3440 cm^{-1} (NH); 1656 cm^{-1} , 1673 cm^{-1} , 1705 cm^{-1} , 1723 cm^{-1} , 1743 cm^{-1} (C=O). **HRMS (ESI)** for [$\text{C}_{26}\text{H}_{34}\text{N}_4\text{O}_6$]: calculated [$\text{M}+\text{Na}$] $^+$ (m/z) 521.2376; found, 521.2344.

Boc-D-Phe-azaPhe-Ala-OMe 7b was obtained as a white solid (yield 70%) after flash chromatography (0.04 – 0.063 μ m) using (50% ethyl acetate : 50% petroleum ether) as eluent; m.p. 72 - 73 °C; $^1\text{H NMR}$ (300 MHz, CDCl_3 , 8.0 mmol. L^{-1}) δ_{H} 1.39-1.41 (m, 12H, CH_3 and $\text{C}(\text{CH}_3)_3$), 2.82-2.89 and 3.09-3.16 (m, 2H, CH_2), 3.71 (s, 3H, COOCH_3), 4.09-4.16 (m, 1H, $\text{C}^{\alpha}\text{H}$), 4.42-4.49 (br m, 1H, $\text{C}^{\alpha}\text{H}$), 4.67 (br s, 2H, NCH_2), 4.79 (br d, 1H, NHBoc), 6.04 (br s, 1H, NH), 7.12-7.35 (m, 10H, H arom Ph), 7.52 (br s, 1H, NH). $^{13}\text{C NMR}$ (75 MHz, CDCl_3 , 10.0 mmol. L^{-1}) δ_{C} 18.57 (CH_3), 28.88 ($\text{C}(\underline{\text{CH}}_3)_3$), 37.90 (CH_2), 50.03 ($\text{C}^{\alpha}\text{H}$), 51.86 (NCH_2), 52.85 (COOCH_3), 56.27 ($\text{C}^{\alpha}\text{H}$), 81.96 ($\text{C}(\underline{\text{CH}}_3)_3$), 128.16 (CH arom Ph), 128.35 (CH arom Ph), 129.23 (CH arom Ph), 129.56 (CH arom Ph), 129.75 (CH arom Ph), 129.82 (CH arom Ph), 136.30 (C arom Ph), 137.18 (C arom Ph), 156.69 ($\text{COO}t\text{-Bu}$), 157.54 ($\text{O}=\text{C}-\text{NH}$), 170.90 ($\text{O}=\text{C}-\text{NH}$), 174.67 (COOCH_3). **IR** (CDCl_3) $\tilde{\nu}_{\text{max}}$ = 3372 cm^{-1} , 3439 cm^{-1} (NH), 1657 cm^{-1} , 1674 cm^{-1} , 1705 cm^{-1} , 1721 cm^{-1} , 1741 cm^{-1} (C=O). **HRMS (ESI)** for [$\text{C}_{26}\text{H}_{34}\text{N}_4\text{O}_6$]: calculated [$\text{M}+\text{Na}$] $^+$ (m/z) 521.2376; found, 521.2389.

Boc-Lys(Z)-azaPhe-Lys(Z)-OMe 7c was obtained as a white foam (yield 72%) after flash chromatography (0.04 – 0.063 μ m) using (60% dichloromethane : 38.5% ethyl acetate : 1.5% methanol) as eluent; $^1\text{H NMR}$ (300 MHz, CDCl_3 , 8.0 mmol. L^{-1}) δ_{H} 1.31 (s, 9H, $\text{C}(\text{CH}_3)_3$), 1.32-1.78 (m, 12H, 2*($\text{C}^{\beta}\text{H}_2$, $\text{C}^{\gamma}\text{H}_2$, $\text{C}^{\delta}\text{H}_2$)), 2.98-3.04 (m, 2H, $\text{C}^{\epsilon}\text{H}_2$), 3.07-3.14 (m, 2H, $\text{C}^{\epsilon}\text{H}_2$), 3.62 (s, 3H, COOCH_3), 3.73 (br m, 1H, $\text{C}^{\alpha}\text{H}$), 4.45-4.47 (m, 1H, $\text{C}^{\alpha}\text{H}$), 4.78 (br s, 1H, NHZ), 4.36 and 4.86 (m, 2H, NCH_2), 4.99 (s, 2H, $\text{CH}_2(\text{Z})$), 5.00 (s, 2H, $\text{CH}_2(\text{Z})$), 5.06 (br, 1H, NHBoc), 5.24 (br s, 1H, NHZ), 5.91 (br s, 1H, NH), 7.17-7.26 (m, 15H, H arom Ph), 7.75 (br s, 1H, NH). $^{13}\text{C NMR}$ (75 MHz, CDCl_3 , 10.0 mmol. L^{-1}) δ_{C} 22.79 ($\text{C}^{\gamma}\text{H}_2$), 22.93 ($\text{C}^{\gamma}\text{H}_2$), 29.01 ($\text{C}(\underline{\text{CH}}_3)$), 29.51($\text{C}^{\delta}\text{H}_2$), 29.98 ($\text{C}^{\delta}\text{H}_2$), 31.23 ($\text{C}^{\beta}\text{H}_2$), 32.41 ($\text{C}^{\beta}\text{H}_2$), 40.70 ($\text{C}^{\epsilon}\text{H}_2$), 41.32 ($\text{C}^{\epsilon}\text{H}_2$), 51.91 (NCH_2), 52.92 (OCH_3), 53.76 ($\text{C}^{\alpha}\text{H}$), 54.02 ($\text{C}^{\alpha}\text{H}$), 67.33 (OCH_2), 67.43 (OCH_2), 81.27 ($\text{C}(\underline{\text{CH}}_3)_3$), 128.40 (CH arom Ph), 128.75 (CH arom Ph), 128.85 (CH arom Ph), 129.19 (CH arom Ph), 129.30 (CH arom Ph), 129.35 (CH arom Ph), 137.20 (C arom Ph), 156.69 ($\text{COO}t\text{-Bu}$), 157.29 ($\text{O}=\text{C}-\text{CH}_2\text{Ph}$), 157.68 ($\text{O}=\text{C}-\text{NH}$), 172.20 ($\text{O}=\text{C}-\text{NH}$), 174.06 (COOCH_3). **IR** (CDCl_3) $\tilde{\nu}_{\text{max}}$ = 3378 cm^{-1} , 3449 cm^{-1} (NH), 1652 cm^{-1} , 1677 cm^{-1} , 1701 cm^{-1} , 1717 cm^{-1} , 1735 cm^{-1} , 1748 cm^{-1} (C=O). **HRMS (ESI)** for [$\text{C}_{42}\text{H}_{56}\text{N}_6\text{O}_{10}$]: calculated [$\text{M}+\text{Na}$] $^+$ (m/z) 827;3956 found, 827.3978; calculated [$\text{M}+\text{K}$] $^+$ (m/z) 843.3695 found, 843.3715.

Boc-D-Lys(Z)-azaPhe-Lys(Z)-OMe 7d was obtained as a white foam (yield 69%) after flash chromatography (0.04 – 0.063 μ m) using (60% dichloromethane : 38.5% ethyl acetate : 1.5% methanol) as eluent; $^1\text{H NMR}$ (300 MHz, CDCl_3 , 8.0 mmol. L^{-1}) δ_{H} 1.41 (s, 9H, $\text{C}(\text{CH}_3)_3$), 1.42-1.87 (m, 12H, 2*($\text{C}^{\beta}\text{H}_2$, $\text{C}^{\gamma}\text{H}_2$, $\text{C}^{\delta}\text{H}_2$)), 3.06-3.11 (m, 2H, $\text{C}^{\epsilon}\text{H}_2$), 3.16-3.20 (m, 2H, $\text{C}^{\epsilon}\text{H}_2$), 3.68 (s, 3H, COOCH_3), 3.80 (m, 1H, $\text{C}^{\alpha}\text{H}$), 4.41-4.44 (m, 1H, $\text{C}^{\alpha}\text{H}$), 4.48 and 5.00 (m, 2H, NCH_2), 4.82 br s, 1H, NHZ), 5.05 (s, 2H, $\text{CH}_2(\text{Z})$), 5.08 (s, 2H, $\text{CH}_2(\text{Z})$), 5.24 (br, 1H, NHBoc), 5.43 (br s, 1H, NHZ), 6.15

Part A

Experimental Section

and 6.16 (br d, 1H, NH), 7.26-7.34 (m, 15H, H arom Ph), 7.83 (br s, 1H, NH). ^{13}C NMR (75 MHz, CDCl_3 , 10.0 mmol. L^{-1}) δ_{C} 22.51 ($\text{C}^{\gamma}\text{H}_2$), 23.13 ($\text{C}^{\gamma}\text{H}_2$), 28.99 ($\text{C}(\underline{\text{C}}\text{H}_3)$), 29.43 ($\text{C}^{\delta}\text{H}_2$), 30.21 ($\text{C}^{\delta}\text{H}_2$), 30.92 ($\text{C}^{\beta}\text{H}_2$), 31.71 ($\text{C}^{\beta}\text{H}_2$), 40.27 ($\text{C}^{\epsilon}\text{H}_2$), 40.91 ($\text{C}^{\epsilon}\text{H}_2$), 51.96 (NCH_2), 52.82 (OCH_3), 54.18 ($\text{C}^{\alpha}\text{H}$), 55.36 ($\text{C}^{\alpha}\text{H}$), 67.09 (OCH_2), 67.48 (OCH_2), 81.81 ($\underline{\text{C}}(\text{CH}_3)_3$), 128.35 (CH arom Ph), 128.65 (CH arom Ph), 128.83 (CH arom Ph), 128.91 (CH arom Ph), 129.15 (CH arom Ph), 129.23 (CH arom Ph), 129.59 (CH arom Ph), 137.10 (C arom Ph), 137.39 (C arom Ph), 137.55 (C arom Ph), 157.25 ($\underline{\text{C}}\text{OO}t\text{-Bu}$), 157.41 ($\text{O}=\underline{\text{C}}\text{-CH}_2\text{Ph}$), 157.63 ($\text{O}=\underline{\text{C}}\text{-CH}_2\text{Ph}$), 157.97 ($\text{O}=\text{C-NH}$), 171.82 ($\text{O}=\text{C-NH}$), 174.28 ($\underline{\text{C}}\text{OOCH}_3$). IR (CDCl_3) $\tilde{\nu}_{\text{max}}$ = 3302 cm^{-1} , 3375 cm^{-1} , 3449 cm^{-1} (NH), 1652 cm^{-1} , 1675 cm^{-1} , 1702 cm^{-1} , 1718 cm^{-1} , 1734 cm^{-1} , 1749 cm^{-1} (C=O). HRMS (ESI) for [$\text{C}_{42}\text{H}_{56}\text{N}_6\text{O}_{10}$]: calculated [$\text{M}+\text{Na}$] $^{+}$ (m/z) 827.3956 found, 827.3986; calculated [$\text{M}+\text{K}$] $^{+}$ (m/z) 843.3695 found, 843.3714.

Boc-Phe-azaPhe-Lys(Z)-OMe 7e was obtained as a white foam (yield 65%) after flash chromatography (0.04 – 0.063 μm) using (70% dichloromethane : 29% ethyl acetate : 1.0% methanol) as eluent; ^1H NMR (300 MHz, CDCl_3 , 10.0 mmol. L^{-1}) δ_{H} 1.38 (s, 9H, $\text{C}(\text{CH}_3)_3$), 1.48-1.85 (m, 6H, ($\text{C}^{\beta}\text{H}_2$, $\text{C}^{\gamma}\text{H}_2$, $\text{C}^{\delta}\text{H}_2$)), 2.74-2.80 and 2.94-3.01 (m, 2H, CH_2), 3.18-3.26 (m, 2H, $\text{C}^{\epsilon}\text{H}_2$), 3.69 (s, 3H, COOCH_3), 3.97 (m, 1H, $\text{C}^{\alpha}\text{H}$), 4.02 (br s, 1H, NHBoc), 4.48-4.54 (m, 1H, $\text{C}^{\alpha}\text{H}$), 5.02 and 5.03 (br d, 2H, NCH_2), 5.08 (s, 2H, $\text{CH}_2(\text{Z})$), 5.40 (br s, 1H, NHZ), 5.97 and 5.99 (br d, 1H, NH), 6.97-7.34 (m, 15H, H arom Ph), 7.58 (br s, 1H, NH). ^{13}C NMR (75 MHz, CDCl_3 , 10.0 mmol. L^{-1}) δ_{C} 22.89 ($\text{C}^{\gamma}\text{H}_2$), 28.96 ($\text{C}(\underline{\text{C}}\text{H}_3)$), 29.49 ($\text{C}^{\delta}\text{H}_2$), 32.33 ($\text{C}^{\beta}\text{H}_2$), 37.61 (CH_2Ph), 41.23 ($\text{C}^{\epsilon}\text{H}_2$), 52.12 (NCH_2), 52.80 (OCH_3), 53.75 ($\text{C}^{\alpha}\text{H}$), 55.91 ($\text{C}^{\alpha}\text{H}$), 67.28 (OCH_2), 81.61 ($\underline{\text{C}}(\text{CH}_3)_3$), 128.01 (CH arom Ph), 128.28 (CH arom Ph), 128.74 (CH arom Ph), 128.90 (CH arom Ph), 129.18 (CH arom Ph), 129.36 (CH arom Ph), 129.57 (CH arom Ph), 129.93 (CH arom Ph), 136.55 (C arom Ph), 137.07 (C arom Ph), 137.35 (C arom Ph), 156.46 ($\underline{\text{C}}\text{OO}t\text{-Bu}$), 157.19 ($\text{O}=\underline{\text{C}}\text{-CH}_2\text{Ph}$), 157.45 ($\text{O}=\text{C-NH}$), 171.20 ($\text{O}=\text{C-NH}$), 173.87 ($\underline{\text{C}}\text{OOCH}_3$). IR (CDCl_3) $\tilde{\nu}_{\text{max}}$ = 3374 cm^{-1} , 3444 cm^{-1} (NH), 1653 cm^{-1} , 1674 cm^{-1} , 1706 cm^{-1} , 1721 cm^{-1} , 1744 cm^{-1} (C=O). HRMS (ESI) for [$\text{C}_{37}\text{H}_{47}\text{N}_5\text{O}_8$]: calculated [$\text{M}+\text{Na}$] $^{+}$ (m/z) 712.3322 found, 712.3339; calculated [$\text{M}+\text{K}$] $^{+}$ (m/z) 728.3062 found, 728.3042.

Boc-D-Phe-azaPhe-Lys(Z)-OMe 7f was obtained as a white foam (yield 62%) after flash chromatography (0.04–0.063 μm) using (70% dichloromethane : 29% ethyl acetate : 1.0% methanol) as eluent; ^1H NMR (300 MHz, CDCl_3 , 10.0 mmol. L^{-1}) δ_{H} 1.37 (s, 9H, $\text{C}(\text{CH}_3)_3$), 1.23-1.87 (m, 6H, ($\text{C}^{\beta}\text{H}_2$, $\text{C}^{\gamma}\text{H}_2$, $\text{C}^{\delta}\text{H}_2$)), 2.71-2.79 and 2.93-3.00 (m, 2H, CH_2), 3.18-3.23 (m, 2H, $\text{C}^{\epsilon}\text{H}_2$), 3.68 (s, 3H, COOCH_3), 4.11-4.14 (m, 1H, $\text{C}^{\alpha}\text{H}$), 4.37-4.44 (m, 1H, $\text{C}^{\alpha}\text{H}$), 4.55 and 4.68 (br, 2H, NCH_2), 4.75 (br s, 1H, NHBoc), 5.02 (s, 2H, $\text{CH}_2(\text{Z})$), 5.24-5.31 (br m, 1H, NHZ), 6.08 and 6.10 (br d, 1H, NH), 7.10-7.33 (m, 15H, H arom Ph), 7.78 (br s, 1H, NH). ^{13}C NMR (75 MHz, CDCl_3 , 10.0 mmol. L^{-1}) δ_{C} 23.37 ($\text{C}^{\gamma}\text{H}_2$), 28.90 ($\text{C}(\underline{\text{C}}\text{H}_3)$), 29.51 ($\text{C}^{\delta}\text{H}_2$), 31.70 ($\text{C}^{\beta}\text{H}_2$), 37.81 (CH_2Ph), 41.01 ($\text{C}^{\epsilon}\text{H}_2$), 52.07 (NCH_2), 52.78 (OCH_3), 54.18 ($\text{C}^{\alpha}\text{H}$), 56.18 ($\text{C}^{\alpha}\text{H}$), 67.13 (OCH_2), 81.09 ($\underline{\text{C}}(\text{CH}_3)_3$), 128.15 (CH arom Ph), 128.30 (CH arom Ph), 128.69 (CH arom Ph), 129.17 (CH arom Ph), 129.52 (CH arom Ph), 129.73 (CH arom Ph), 136.11 (C arom Ph), 137.36 (C arom Ph), 156.95 ($\underline{\text{C}}\text{OO}t\text{-Bu}$), 157.22 ($\text{O}=\underline{\text{C}}\text{-CH}_2\text{Ph}$), 157.85 ($\text{O}=\text{C-NH}$), 171.10 ($\text{O}=\text{C-NH}$), 174.04 ($\underline{\text{C}}\text{OOCH}_3$). IR (CDCl_3) $\tilde{\nu}_{\text{max}}$ = 3376 cm^{-1} , 3444 cm^{-1} (NH), 1652 cm^{-1} , 1673 cm^{-1} , 1707 cm^{-1} , 1720 cm^{-1} , 1744 cm^{-1} (C=O). HRMS (ESI) for [$\text{C}_{37}\text{H}_{47}\text{N}_5\text{O}_8$]: calculated [$\text{M}+\text{Na}$] $^{+}$ (m/z) 712.3322 found, 712.3327; calculated [$\text{M}+\text{K}$] $^{+}$ (m/z) 728.3062 found, 728.3028.

Synthesis and Characterizations of 2:1-[α /aza]-Oligomers

General Protocol for the Synthesis of Hexamers (8):

Homo and heterochiral 2:1-[α /aza]-hexamers **8** were obtained by classical peptidic coupling based on the monomeric building blocks of 2:1-[α /aza]-trimers **7**.

Part A

Experimental Section

Boc deprotection: To a stirred solution of Boc protected trimer (**7**, 1.0 equiv.) in CH₂Cl₂, ethyl acetate/2-3M HCl was added at 0 °C. The resulting solution was stirred until completion monitored by TLC (2 - 4h) and concentrated under vacuum. The excess of hydrochloric acid was co-evaporated with CH₂Cl₂ (4 times). The residue was used in coupling reaction without further purification.

Methyl ester deprotection: To a stirred solution of methyl ester protected trimer (**7**, 1.0 equiv.) in CH₃CN, an aqueous solution of NaOH 1M (2.0 equiv.) was added at 0 °C. The resulting solution was stirred until completion monitored by TLC (4 - 10h), then aqueous HCl (2M) was added under vigorously stirring (pH = 2). The aqueous layer was extracted twice with CH₂Cl₂, then the combined organic layers were dried over MgSO₄ and evaporated. The residue was used in coupling reaction without further purification.

Coupling reaction: To a stirred solution of the Boc-deprotected trimer (amine partner, 1.0 equiv.) in CH₂Cl₂ were successively added at RT; DIPEA (2.2 equiv.), deprotected methyl ester trimer (acid partner, 1.1 equiv.) and HOBt (1.2 equiv.). After a night to 24h, the mixture was diluted with aqueous HCl (1M) under vigorously stirring (pH = 2). The organic layer was washed with water, aqueous NaHCO₃ (0.5M), brine, dried over MgSO₄ and evaporated. The residue was purified by column chromatography on silica gel.

Note: Better yields of hexamers possessing lysine residues (**8c** and **8d**) were obtained upon carrying the coupling reaction in CH₃CN using HBTU/DIPEA.

Characterization data for 2:1-[α /aza]-Hexamers (**8**):

Boc-(Phe-azaPhe-Ala)₂-OMe 8a was obtained as a white solid (yield 87%) after flash chromatography (0.04 – 0.063 μ m) using (60% ethyl acetate : 40% petroleum ether) as eluent; m.p. 132 - 133 °C; ¹H NMR (300 MHz, CD₃CN, 8.0 mmol. L⁻¹) δ_{H} 1.18 and 1.21 (d, 3H, CH₃), 1.34-1.38 (m, 12H, CH₃ and C(CH₃)₃), 2.77-2.84 (m, 1H, CH₂), 2.96-3.04 (m, 2H, CH₂), 3.18-3.24 (m, 1H, CH₂), 3.62 (s, 3H, COOCH₃), 3.89-3.98 (m, 1H, C ^{α} H), 4.02-4.09 (m, 1H, C ^{α} H), 4.20-4.29 (m, 2H, 2*C ^{α} H), 4.48-4.84 (br m, 4H, 2*NCH₂), 5.62 (br s, 1H, NH), 6.37 (br s, 1H, NH), 6.53 (br s, 1H, NH), 7.17-7.32 (m, 21H: 20H, arom Ph, and 1H, NH), 9.01 (br s, 2H, 2*NH). ¹³C NMR (75 MHz, CD₃CN, 10.0 mmol. L⁻¹) δ_{C} 17.33 (CH₃), 18.02 (CH₃), 28.62 (C(CH₃)₃), 37.46 (CH₂), 37.59 (CH₂), 50.52 (C ^{α} H), 50.66 (C ^{α} H), 52.75 (C ^{α} H and COOCH₃), 52.94 (NCH₂), 53.32 (NCH₂), 54.63 (C ^{α} H), 81.3 (C(CH₃)₃), 127.81 (CH arom Ph), 128.30 (CH arom Ph), 128.78 (CH arom Ph), 129.19 (CH arom Ph), 129.34 (CH arom Ph), 129.53 (CH arom Ph), 129.70 (CH arom Ph), 129.83 (CH arom Ph), 130.20 (CH arom Ph), 130.28 (CH arom Ph), 130.37 (CH arom Ph), 130.68 (CH arom Ph), 137.61 (C arom Ph), 138.01 (C arom Ph), 138.52 (C arom Ph), 139.91 (C arom Ph), 158.03 (O=C-NH), 159.41 (O=C-NH), 171.4 (O=C-NH), 175.33 (COOCH₃). IR (CDCl₃) $\tilde{\nu}_{\text{max}}$ = 3259 cm⁻¹, 3351 cm⁻¹, 3401 cm⁻¹, 3438 cm⁻¹ (NH), 1665 cm⁻¹, 1700 cm⁻¹, 1741 cm⁻¹ (C=O). HRMS (ESI) for [C₄₆H₅₆N₈O₉]: calculated [M+Na]⁺ (m/z) 887.4062 found, 887.4068.

Boc-(D-Phe-azaPhe-Ala)₂-OMe 8b was obtained as a white solid (yield 85%) after flash chromatography (0.04 – 0.063 μ m) using (60% ethyl acetate : 40% petroleum ether) as eluent; m.p. 172 - 173 °C; ¹H NMR (300 MHz, CD₃CN, 8.0 mmol. L⁻¹) δ_{H} 1.28 and 1.30 (d, 3H, CH₃), 1.34 (s, 9H, C(CH₃)₃), 1.35 and 1.37 (d, 3H, CH₃), 2.73-2.81 (m, 1H, CH₂), 2.91-2.98 (m, 1H, CH₂), 3.06-3.10 (m, 1H, CH₂), 3.17-3.23 (m, 1H, CH₂), 3.62 (s, 3H, COOCH₃), 3.89-4.08 (m, 2H, 2*C ^{α} H), 4.10-4.24 (m, 2H, 2*C ^{α} H), 4.33-4.67 (br m, 4H, 2*NCH₂), 5.62 (br s, 1H, NH), 6.45-6.57 (br, 2H, 2NH), 7.12-7.31 (m, 21H: 20H, arom Ph, and 1H, NH), 8.73 (s, 1H, NH), 9.13 (br s, 1H, NH). ¹³C NMR (75 MHz, CD₃CN, 10.0 mmol. L⁻¹) δ_{C} 17.11 (CH₃), 18.11 (CH₃), 28.70 (C(CH₃)₃), 36.81 (CH₂), 37.36 (CH₂), 50.52 (C ^{α} H), 52.27 (NCH₂), 52.64 (C ^{α} H and COOCH₃), 52.86 (NCH₂), 55.63 (C ^{α} H), 56.43 (C ^{α} H), 81.18 (C(CH₃)₃), 127.83 (CH arom Ph), 127.96 (CH arom Ph), 128.13 (CH arom Ph), 128.43 (CH

Part A

Experimental Section

arom Ph), 129.20 (CH arom Ph), 129.28 (CH arom Ph), 129.61 (CH arom Ph), 129.77 (CH arom Ph), 130.35 (CH arom Ph), 137.95 (C arom Ph), 138.41 (C arom Ph), 138.96 (C arom Ph), 158.32 (O=C-NH), 159.12 (O=C-NH), 171.26 (O=C-NH), 176.38 (COOCH₃). **IR** (CDCl₃) $\tilde{\nu}_{\max}$ = 3240 cm⁻¹, 3351 cm⁻¹, 3423 cm⁻¹ (NH), 1635 cm⁻¹, 1665 cm⁻¹, 1704 cm⁻¹, 1741 cm⁻¹ (C=O). **HRMS (ESI)** for [C₄₆H₅₆N₈O₉]: calculated [M+Na]⁺ (m/z) 887.4062 found, 887.4066.

Boc-(Lys(Z)-azaPhe-Lys(Z))₂-OMe 8c was obtained as a white foam (yield 64%) after flash chromatography (0.04 – 0.063 μ m) using (50% dichloromethane : 48% ethyl acetate : 2% methanol) as eluent; **¹H NMR** (300 MHz, CD₃CN, 8.0 mmol. L⁻¹) δ_{H} 1.37 (s, 9H, C(CH₃)), 1.38-1.78 (m, 24H, 4*(C ^{β} H₂, C ^{γ} H₂, and C ^{δ} H₂)), 3.02-3.09 (m, 8H, 4*(C ^{ϵ} H₂)), 3.64 (s, 3H, COOCH₃), 3.66-3.69 (br m, 1H, C ^{α} H), 3.93-3.99 (m, 2H, 2*C ^{α} H), 4.13-4.20 (m, 1H, C ^{α} H), 4.32-4.95 (br m, 4H, 2*NCH₂), 5.02 (s, 2H, CH₂(Z)), 5.04 (s, 2H, CH₂(Z)), 5.68 (br s, 2H, 2*NHZ), 5.76 (br s, 1H, NHZ), 5.83 (br s, 1H, NHZ), 5.93 (br, 1H, NHBoc), 6.29 and 6.31 (d, 1H, NH), 6.53 (br s, 1H, NH), 7.03 (d, 1H, NH), 7.16-7.34 (m, 30H, H arom Ph), 8.91 (br s, 1H, NH), 9.02 (br s, 1H, NH). **¹³C NMR** (75 MHz, CD₃CN, 10.0 mmol. L⁻¹) δ_{C} 23.21 (C ^{γ} H₂), 24.06 (C ^{γ} H₂), 28.77 (C(CH₃)), 30.29 (C ^{δ} H₂), 31.11 (C ^{δ} H₂), 31.49 (C ^{β} H₂), 32.19 (C ^{β} H₂), 40.88 (C ^{ϵ} H₂), 41.43 (C ^{ϵ} H₂), 41.49 (C ^{ϵ} H₂), 41.62 (C ^{ϵ} H₂), 52.09 (NCH₂), 52.56 (OCH₃), 53.02 (NCH₂), 54.91 (C ^{α} H), 66.74 (OCH₂), 66.79 (OCH₂), 66.88 (OCH₂), 66.94 (OCH₂), 81.15(C(CH₃)₃), 128.22 (CH arom Ph), 128.60 (CH arom Ph), 128.73 (CH arom Ph), 128.83 (CH arom Ph), 128.89 (CH arom Ph), 128.95 (CH arom Ph), 129.33 (CH arom Ph), 129.52 (CH arom Ph), 130.22 (CH arom Ph), 138.50 (C arom Ph), 138.59 (C arom Ph), 138.67 (C arom Ph), 138.81 (C arom Ph), 157.50 (COO*t*-Bu), 157.81 (O=C-CH₂Ph), 158.56 (O=C-CH₂Ph), 159.80 (O=C-NH), 159.98 (O=C-NH), 172.07 (O=C-NH), 174.69 (COOCH₃). **IR** (CDCl₃) $\tilde{\nu}_{\max}$ = 3256 cm⁻¹, 3349 cm⁻¹, 3450 cm⁻¹ (NH), 1651 cm⁻¹, 1667 cm⁻¹, 1699 cm⁻¹, 1712 cm⁻¹, 1724 cm⁻¹, 1740 cm⁻¹ (C=O). **HRMS (ESI)** for [C₇₈H₁₀₀N₁₂O₁₇]: calculated [M+Na]⁺ (m/z) 1499.7227, found, 1499.7181; calculated [M²⁺+Na] (m/z) 761.3615, found 761.3664.

Boc-(D-Lys(Z)-azaPhe-Lys(Z))₂-OMe 8d was obtained as a white foam (yield 62%) after flash chromatography (0.04 – 0.063 μ m) using (50% dichloromethane : 48% ethyl acetate : 2% methanol) as eluent; **¹H NMR** (300 MHz, CDCl₃, 8.0 mmol. L⁻¹) δ_{H} 1.36 (s, 9H, C(CH₃)), 1.37-1.77 (m, 24H, 4*(C ^{β} H₂, C ^{γ} H₂, and C ^{δ} H₂)), 3.03-3.14 (m, 8H, 4*(C ^{ϵ} H₂)), 3.46 (s, 3H, COOCH₃), 3.70-3.75 (br m, 1H, C ^{α} H), 3.87-3.93 (m, H, C ^{α} H), 4.04-4.08 (m, 1H, C ^{α} H), 4.56-4.60 (m, 1H, C ^{α} H), 4.21 (d) and 5.23 (br s) (2H, NCH₂), 4.40 (d) and 4.64 (br s) (2H, NCH₂), 4.82-4.87 (br s, 2H, 2*NHZ), 5.05 (s, 2H, CH₂(Z)), 5.07 (s, 2H, CH₂(Z)), 5.10 (s, 2H, CH₂(Z)), 5.11 (s, 2H, CH₂(Z)), 5.3 (br s, 1H, NHZ), 5.46 (br, 1H, NHBoc), 5.88 (br s, 1H, NHZ), 6.21 and 6.23 (d, 1H, NH), 6.54 (br s, 1H, NH), 7.16-7.34 (m, 31H; 30H arom Ph and 1H, NH), 8.85 (br s, 1H, NH), 9.46 (br s, 1H, NH). **¹³C NMR** (75 MHz, CDCl₃, 10.0 mmol. L⁻¹) δ_{C} 21.66 (C ^{γ} H₂), 22.42 (C ^{γ} H₂), 23.24 (C ^{γ} H₂), 23.56 (C ^{γ} H₂), 29.27 (C(CH₃)), 29.58 (C ^{δ} H₂), 30.23 (C ^{δ} H₂), 30.39 (C ^{δ} H₂), 31.77 (C ^{β} H₂), 32.18 (C ^{β} H₂), 40.75 (C ^{ϵ} H₂), 40.83 (C ^{ϵ} H₂), 40.85 (C ^{ϵ} H₂), 40.99 (C ^{ϵ} H₂), 51.67 (NCH₂), 52.29 (NCH₂), 52.59 (OCH₃), 53.45 (C ^{α} H), 55.32 (C ^{α} H), 56.59 (C ^{α} H), 56.93 (C ^{α} H), 66.93 (OCH₂), 67.12 (OCH₂), 67.44 (OCH₂), 67.74 (OCH₂), 81.65(C(CH₃)₃), 127.81 (CH arom Ph), 128.20 (CH arom Ph), 128.66 (CH arom Ph), 128.82 (CH arom Ph), 129.00 (CH arom Ph), 129.09 (CH arom Ph), 129.15 (CH arom Ph), 129.30 (CH arom Ph), 130.16 (CH arom Ph), 136.36 (C arom Ph), 136.91 (C arom Ph), 137.15 (C arom Ph), 137.52 (C arom Ph), 137.81 (C arom Ph), 157.17 (COO*t*-Bu), 157.44 (O=C-CH₂Ph), 157.79 (O=C-CH₂Ph), 157.96 (O=C-CH₂Ph), 158.21(O=C-NH), 159.41 (O=C-NH), 171.13 (O=C-NH), 171.62 (O=C-NH), 175.8 (COOCH₃). **IR** (CDCl₃) $\tilde{\nu}_{\max}$ = 3212 cm⁻¹, 3342 cm⁻¹, 3450 cm⁻¹ (NH), 1637 cm⁻¹, 1652 cm⁻¹, 1667 cm⁻¹, 1690 cm⁻¹, 1705 cm⁻¹, 1718 cm⁻¹, 1738 cm⁻¹ (C=O). **HRMS (ESI)** for [C₇₈H₁₀₀N₁₂O₁₇]: calculated [M+Na]⁺ (m/z) 1499.7227, found, 1499.7153; calculated [M²⁺+Na] (m/z) 761.3615, found 761.3592.

Part A
Bibliographies

Part A

Bibliographies

Bibliographies

- (1) Fauchere, J.-L.; Thuriéau, C. *Adv. Drug Res.* **1992**, *23*, 127-159.
- (2) Dutta, A. S. *Adv. Drug Res.* **1991**, *21*, 145-286.
- (3) Goodman, M.; Toniolo, C.; Moroder, L.; Felix, A.: Houben-Weyl Methods in Organic Chemistry, Volume E22, Synthesis of Peptides and Peptidomimetics, Volumes 1-5 (Workbench Edition). Thieme Medical Publishers Inc., **2004**.
- (4) Gellman, S. H. *Acc. chem. Res.* **1998**, *31*, 173-180.
- (5) Appella, D. H.; Christianson, L. A.; Karle, I. L.; Powell, D. R.; Gellman, S. H. *J. Am. Chem. Soc.* **1996**, *118*, 13071-13072.
- (6) Seebach, D.; Fritz, M. G. *Int. J. Biol. Macromol.* **1999**, *25*, 217-236.
- (7) Dado, G. P.; Gellman, S. H. *J. Am. Chem. Soc.* **1994**, *116*, 1054-1062.
- (8) Seebach, D.; Overhand, M.; Florian, N.; Kuhnle, M.; Martinoni, B.; Oberer, L.; Hommel, U.; Widmer, H. *Helv. chim. Acta.* **1996**, *79*, 913-941.
- (9) Seebach, D.; Matthews, J. L. *Chem. Commun.* **1997**, 2015-2022.
- (10) Lelais, G.; Seebach, D. *Helv. Chim. Acta* **2003**, *86*, 4152-4168.
- (11) Roy, A.; Prabhakaran, P.; Baruah, P. K.; Sanjayan, G. J. *Chem. Commun.* **2011**, *47*, 11593-11611.
- (12) Horne, W. S.; Gellman, S. H. *Acc. Chem. Res.* **2008**, *41*, 1399-1408.
- (13) Vasudev, P. G.; Chatterjee, S.; Shamala, N.; Balaram, P. *Acc. Chem. Res.* **2009**, *42*, 1628-1639.
- (14) Li, X.; Wu, Y. D.; Yang, D. *Acc. chem. Res.* **2008**, *41*, 1428-1438.
- (15) Le Grel, P.; Salaün, A.; Potel, M.; Le Grel, B.; Lassagne, F. *J. Org. Chem.* **2006**, *71*, 5638-5645.
- (16) Ghadiri, M. R.; Granja, J. R.; Milligan, R. A.; McRee, D. E.; Khazanovich, N. *Nature* **1993**, *366*, 324-327.
- (17) Fischer, L.; Decossas, M.; Briand, J. P.; Didierjean, C.; Guichard, G. *Angew. Chem., Int. Ed.* **2009**, *48*, 1625-1628.
- (18) Karle, I. L.; Handa, B. K.; Hassall, C. H. *Acta Cryst. B, Struct. Sci.* **1975**, *31*, 555-560.
- (19) Chapman, R.; Danial, M.; Koh, M. L.; Jolliffe, K. A.; Perrier, S. *Chem. Soc. Rev.* **2012**, *41*, 6023-6041.
- (20) Bouillon, I.; Brosse, N.; Vanderesse, R.; Jamart-Grégoire, B. *Tetrahedron Lett.* **2004**, *45*, 3569-3572.
- (21) Bouillon, I.; Brosse, N.; Vanderesse, R.; Jamart-Grégoire, B. *Tetrahedron* **2007**, *63*, 2223-2234.
- (22) Bouillon, I.; Vanderesse, R.; Brosse, N.; Fabre, O.; Jamart-Grégoire, B. *Tetrahedron* **2007**, *63*, 9635-9641.
- (23) Felten, A.-S.; Vanderesse, R.; Brosse, N.; Didierjean, C.; Jamart-Grégoire, B. *Tetrahedron Lett.* **2008**, *49*, 156-158.
- (24) Abbas, C.; Pickaert, G.; Didierjean, C.; Grégoire, B. J.; Vanderesse, R. *Tetrahedron Lett.* **2009**, *50*, 4158-4160.
- (25) Felten, A.-S.; Dautrey, S.; Bodiguel, J.; Vanderesse, R.; Didierjean, C.; Arrault, A.; Jamart-Grégoire, B. *Tetrahedron* **2008**, *64*, 10741-10753.
- (26) André, F.; Boussard, G.; Bayeul, D.; Didierjean, C.; Aubry, A.; Marraud, M. *J. Pept. Res.* **1997**, *49*, 556-562.
- (27) Lee, H.-J.; Park, H.-M.; Lee, K.-B. *Biophys. Chem.* **2007**, *125*, 117-126.
- (28) Lee, H.-J.; Ahn, I.-A.; Ro, S.; Choi, K.-H.; Choi, Y.-S.; Lee, K.-B. *J. Pept. Res.* **2000**, *56*, 35-46.
- (29) Lee, H.-J.; Choi, K.-H.; Ahn, I.-A.; Ro, S.; Jang, H.; Choi, Y.-S.; Lee, K.-B. *J. Mol. Struct.* **2001**, *569*, 43-54.
- (30) Abbas-Quinternet, C. Thesis: Synthèse et études structurales de nouveaux 2:1-[α /aza]-oligomères, vers de nouveaux foldamères. INPL-Nancy, **2009**.
- (31) Zhou, Z. Thesis: Synthèse et études structurales de nouveaux [a/aza]-oligomères et cyclooligomères, vers de nouveaux foldamères. LCPM-Lorraine University, **2014**.

Part A

Bibliographies

- (32) Zhou, Z.; Deng, C.; Abbas, C.; Didierjean, C.; Averlant-Petit, M.-C.; Bodiguel, J.; Vanderesse, R.; Jamart-Grégoire, B. *Eur. J. Org. Chem.* **2014**, 7643-7650.
- (33) Piepenbrock, M. O. M.; Lloyd, G. O.; Clarke, N.; Steed, J. W. *Chem. Rev.* **2010**, *110*, 1960-2004.
- (34) Schmidt, R. H. *Am. Chem. Soc.* **1981**, 131-146.
- (35) Rogers, M. A.; Kim, J. H. *J. Food Res. Int.* **2011**, *44*, 1447-1451.
- (36) Fleming, S.; Debnath, S.; Frederix, P. W. J. M.; Tuttlea, T.; Ulijn, R. V. *Chem. Commun.* **2013**, *49*, 10587-10589.
- (37) Adhikari, B.; Palui, G.; Banerjee, A. *Soft Matter* **2009**, *5*, 3452-3460.
- (38) Ryan, D. M.; Anderson, S. B.; Senguen, F. T.; Youngman, R. E.; Nilsson, B. L. *Soft Matter* **2010**, *6*, 475-479.
- (39) Reddy, S. M. M.; Shanmugam, G.; Durairandy, N.; Kiran, M. S.; Mandal, A. B. *Soft Matter* **2015**, *11*, 8126-8140.
- (40) Sangeetha, N. M.; Maitra, U. *Chem. Soc. Rev.* **2005**, *34*, 821-836.
- (41) Kar, T.; Mukherjee, S.; Das, P. K. *New J. Chem.* **2014**, *38*, 1158-1167.
- (42) Feng, G. L.; Chen, H. H.; Cai, J. H.; Wen, J. W.; Liu, X. B. *Soft Mater.* **2014**, *12*, 403-410.
- (43) Bachl, J.; Oehm, S.; Mayr, J.; Cativiela, C.; Marrero-Tellado, J. J.; Diaz, D. D. *Int. J. Mol. Sci.* **2015**, *16*, 11766-11784.
- (44) van Esch, J. H. *Langmuir* **2009**, *25*, 8392-8394.
- (45) Erdogan, H.; Sakalak, H.; Yavuz, M. S.; Demirel, G. *Langmuir* **2013**, *29*, 6975-6982.
- (46) Zinic, M.; Vogtle, F.; Fages, F.: Cholesterol-based gelators. In *Low Molecular Mass Gelators: Design, Self-Assembly, Function*; Fages, F., Ed.; Topics in Current Chemistry, **2005**; Vol. 256; pp 39-76.
- (47) Weiss, R. G.; Terech, P.: Molecular Gels: Materials with Self-Assembled Fibrillar Networks. Springer, **2006**.
- (48) Terech, P.; Weiss, R. G. *Chem. Rev.* **1997**, *97*, 3133-3159.
- (49) Hirst, A. R.; Smith, D. K.: Dendritic gelators. In *Low Molecular Mass Gelators: Design, Self-Assembly, Function*; Fages, F., Ed.; Topics in Current Chemistry, **2005**; Vol. 256; pp 237-273.
- (50) Fages, F.; Vogtle, F.; Zinic, M.: Systematic design of amide- and urea-type gelators with tailored properties. In *Low Molecular Mass Gelators: Design, Self-Assembly, Function*; Fages, F., Ed.; Topics in Current Chemistry, **2005**; Vol. 256; pp 77-131.
- (51) Estroff, L. A.; Hamilton, A. D. *Chem. Rev.* **2004**, *104*, 1201-1217.
- (52) Du, X. W.; Zhou, J.; Shi, J. F.; Xu, B. *Chem. Rev.* **2015**, *115*, 13165-13307.
- (53) Banerjee, S.; Das, R. K.; Maitra, U. *J. Mater. Chem.* **2009**, *19*, 6649-6687.
- (54) Abdallah, D. J.; Weiss, R. G. *Adv. Mater.* **2000**, *12*, 1237-1247.
- (55) Brosse, N.; Barth, D.; Jamart-Grégoire, B. *Tetrahedron Lett.* **2004**, *45*, 9521-9524.
- (56) Pham, Q. N.; Brosse, N.; Frochot, C.; Dumas, D.; Hocquet, A.; Jamart-Grégoire, B. *New J. Chem.* **2008**, *32*, 1131-1139.
- (57) Moussodia, R. O.; Acherar, S.; Romero, E.; Didierjean, C.; Jamart-Grégoire, B. *J. Org. Chem.* **2015**, *80*, 3022-3029.
- (58) Boeglin, D.; Lubell, W. D. *J. Comb. Chem.* **2005**, *7*, 864-878.
- (59) Proulx, C.; Picard, É.; Boeglin, D.; Pohankova, P.; Chemtob, S.; Ong, H.; Lubell, W. D. *J. Med. Chem.* **2012**, *55*, 6502-6511.
- (60) Jakubke, H.-D.; Sewald, N. Peptides from A to Z. *Wiley-VCH* **2008**.
- (61) Sewald, N.; Jakubke, H.-D. Peptides: Chemistry and Biology. *Wiley-VCH* **2002**.
- (62) Gentilucci, L. *Curr. Topics Med. Chem.* **2004**, *4*, 19-38.
- (63) Gentilucci, L.; Tolomelli, A.; Squassabia, F. *Curr. Med. Chem.* **2006**, *13*, 2449-2466.
- (64) Lee, V. H. L.; Yamamoto, A. *Adv. Drug Deliv. Rev.* **1990**, *4*, 171-207.
- (65) Bocci, V. *Adv. Drug Deliv. Rev.* **1990**, *4*, 149-169.
- (66) Morgan, B. A.; Gainor, J. A. *Annu. Rep. Med. Chem.* **1989**, *24*, 243-252.
- (67) Liskamp, R. M. J. *Recl. Trav. Chim. PaysBas* **1994**, *113*, 1-19.
- (68) Hruby, V. J. *Biopolymers* **1993**, *33*, 1073-1082.
- (69) Giannis, A.; Kolter, T. *Angew. Chem., Int. Ed. Engl.* **1993**, *32*, 1244-1267.
- (70) Wiley, R. A.; Rich, D. H. *Med. Res. Rev.* **1993**, *13*, 327-384.
-

Part A

Bibliographies

- (71) Spatola, A. F.: *Methods in Neurosciences*. Conn, P. M., Ed.: Academic Press, San Diego, **1993**, Vol. 13; pp 19-42.
- (72) Gante, J. *Angew. Chem., Int. Ed. Engl.* **1994**, *33*, 1699-1720.
- (73) Ripka, A. S.; Rich, D. H. *Curr. Opin. Chem. Biol.* **1998**, *2*, 441-452.
- (74) Hruby, V. J.; Matsunaga, T. O.: *Synthetic peptides*. 2nd ed.; Grant, G. A., Ed.: New York: Oxford University, **2002**.
- (75) Pauling, L.; Corey, H. R.; Branson, H. R. The Structure of Proteins: Two Hydrogen-Bonded Helical Configurations of the Polypeptide Chain". *Proc. Natl. Acad. Sci. USA* **1951**, *37*, 205-211.
- (76) Venkatachalam, C. M. *Biopolymers* **1968**, *6*, 1425-1436.
- (77) Ramachandran, G. N.; Ramakrishnan, C.; Sasisekharan, V. *J. Mol. Bio.* **1963**, *7*, 95-99.
- (78) Obrecht, D.; Altorfer, M.; Bohdal, U.; Daly, J.; Huber, W.; Labhardt, A.; Lehmann, C.; Müller, K.; Ruffieux, R.; Schönholzer, P.; Spiegler, C.; Zumbunn, C. *Biopolymers* **1997**, *42*, 575-626.
- (79) Appella, D. H.; Christianson, L. A.; Klein, D. A.; Powell, D. R.; Huang, X.; Barchi, J. J.; Gellman, S. H. *Nature* **1997**, *387*, 381-384.
- (80) Krauthäuser, S.; Christianson, L. A.; Powell, D. R.; Gellman, S. H. *J. Am. Chem. Soc.* **1997**, *119*, 11719-11720.
- (81) Appella, D. H.; Barchi, J. J.; Durell, S. R.; Gellman, S. H. *J. Am. Chem. Soc.* **1999**, *121*, 2309-2310.
- (82) Appella, D. H.; Christianson, L. A.; Karle, I. L.; Powell, D. R.; Gellman, S. H. *J. Am. Chem. Soc.* **1999**, *121*, 6206-6212.
- (83) Seebach, D.; Kimmerlin, T.; Šebesta, R.; Campo, M. A.; Beck, A. K. *Tetrahedron* **2004**, *60*, 7455-7506.
- (84) Martinek, T. A.; Fülöp, F. *Chem. Soc. Rev.* **2012**, *41*, 687-702.
- (85) Rose, G. D.; Gierasch, L. M.; Smith, J. A. *Adv. Protein Chem.* **1985**, *37*, 1-109.
- (86) Blanco, F. J.; Rivas, G.; Serrano, L. *Nat. Struct. Biol.* **1994**, *1*, 584-590.
- (87) Lee, J.; Shin, S. *J. Biophys.* **2001**, *81*, 2507-2516.
- (88) Tyndall, J. D. A.; Pfeiffer, B.; Abbenante, G.; Fairlie, D. P. *Chem. Rev.* **2005**, *105*, 793-826.
- (89) Smith, J. A.; Pease, L. G.; Koppke, K. D. *Crit. Rev. Biochem. Mol. Biol.* **1980**, *8*, 315-399.
- (90) Kuntz, I. D. *J. Am. Chem. Soc.* **1972**, *94*, 4009-4012.
- (91) Santa, H.; Ylisirnio, M.; Hassinen, T.; Laatikainen, R.; Perakyla, M. *Protein Eng.* **2002**, *15*, 651-657.
- (92) André, F.; Vicherat, A.; Boussard, G.; Aubry, A.; Marraud, M. *J. Pept. Res.* **1997**, *50*, 372-381.
- (93) Boussard, G.; Marraud, M.; Aubry, A. *Biopolymers* **1979**, *18*, 1297-1331.
- (94) Milner-White, E.; Ross, B. M.; Ismail, R.; Belhadj-Mostefa, K.; Poet, R. *J. Mol. Biol.* **1988**, *204*, 777-782.
- (95) Motta, A.; Reches, M.; Pappalardo, L.; Andreotti, G.; Gazit, E. *Biochemistry* **2005**, *44*, 14170-14178.
- (96) Némethy, G.; Scheraga, H. A. *Biochem. Biophys. Res. Commun.* **1980**, *95*, 320-327.
- (97) Zalkin, A.; Forrester, J. D.; Templeton, D. H. *J. Am. Chem. Soc.* **1966**, *88*, 1810-1814.
- (98) Baures, P. W.; Ojala, W. H.; Gleason, W. B.; Johnson, R. L. *J. Pept. Res.* **1997**, *50*, 1-13.
- (99) Kennedy, D. F.; Crisma, M.; Toniolo, C.; Chapman, D. *Biochemistry (Mosc.)* **1991**, *30*, 6541-6548.
- (100) Moretto, A.; Peggion, C.; Formaggio, F.; Crisma, M.; Toniolo, C.; Piazza, C.; Kaptein, B.; Broxterman, Q. b.; Ruiz, I.; Diaz-de-Villegas, M. d.; Galvez, J. a.; Cativiela, C. *J. Pept. Res.* **2000**, *56*, 283-297.
- (101) Saviano, M.; Lacovino, R.; Menchise, V.; Benedetti, E.; Bonora, G. M.; Gatos, M.; Graci, L.; Formaggio, F.; Crisma, M.; Toniolo, C. *Biopolymers* **2000**, *53*, 200-212.
- (102) Gatos, M.; Formaggio, F.; Crisma, M.; Toniolo, C.; Bonora, G. M.; Benedetti, Z.; Di Blasio, B.; Lacovino, R.; Santini, A.; Saviano, M.; Kamphuis, J. *J. Pept. Sci.* **1997**, *3*, 110-122.
- (103) Moretto, V.; Formaggio, F.; Crisma, M.; Bonora, G. M.; Toniolo, C.; Benedetti, E.; Santini, A.; Saviano, M.; Di Blasio, B.; Pedone, C. *J. Pept. Sci.* **1996**, *2*, 14-27.
- (104) Gatos, M.; Formaggio, F.; Crisma, M.; Valle, G.; Toniolo, C.; Bonora, G. M.; Saviano, M.; Lacovino, R.; Menchise, V.; Galdiero, S.; Pedone, C.; Benedetti, E. *J. Pept. Sci.* **1997**, *3*, 367-382.

Part A

Bibliographies

- (105) Moretto, A.; Formaggio, F.; Crisma, M.; Toniolo, C.; Saviano, M.; Benedetti, E.; Lacovino, R.; Vitale, R. M. *J. Pept. Res.* **2001**, *57*, 307-315.
- (106) Seebach, D.; Abele, S.; Sifferlen, T.; Hänggi, M.; Gruner, S.; Seiler, P. *Helv. Chim. Acta* **1998**, *81*, 2218-2243.
- (107) Peter, C.; Rueping, M.; Wörner, H. J.; Jaun, B.; Seebach, D.; Van Gunsteren, W. F. *Chem. - Eur. J.* **2003**, *9*, 5838-5849.
- (108) Brenner, M.; Seebach, D. *Helv. Chim. Acta* **2001**, *84*, 2155-2166.
- (109) Cardillo, G.; Gentilucci, L.; Tolomelli, A. *Aldrich Acta* **2003**, *36*, 39-50.
- (110) Perdih, A.; Dolenc, M.; Sollner. *Curr. Org. Chem.* **2007**, *11*, 801-832.
- (111) Cardillo, G.; Gentilucci, L.; Tolomelli, A. *Mini Rev. Med. Chem.* **2006**, *6*, 293-304.
- (112) Horwell, D. C. *Trends Biotechnol.* **1995**, *13*, 132-134.
- (113) Kessler, H. *Angew Chem., Int. Ed.* **1982**, *2*, 512-523.
- (114) Cowell, S. M.; Lee, Y. S.; Cain, J. P.; Hruby, V. J. *Curr. Med Chem.* **2004**, *11*, 2785-2798.
- (115) Manning, M.; Balaspiri, L.; Agosta, M. *J. Med. Chem.* **1973**, *16*, 975-978.
- (116) Luthman, K.; Hacksell, U.: Textbook of drug design and discovery. 3rd ed.; Krogsgaard-Larsen, P., Liljefors, T., Madsen, U., Eds.: London: Taylor & Francis, **2002**; pp 459-485.
- (117) Durani, S. *Acc. Chem. Res.* **2008**, *41*, 1301-1308.
- (118) Gentilucci, L.; Cardillo, G.; Squassabia, F.; Tolomelli, A.; Spampinato, S.; Sparta, A.; Baiula, M. *Bioorg. Med. Chem. Lett.* **2007**, *17*, 2329-2333.
- (119) Takeuchi, Y.; Marshall, G. R. *J. Am. Chem. Soc. Rev.* **1998**, *120*, 5363-5372.
- (120) De Marco, R. Thesis: Synthesis of Modified Amino Acids and Insertion in Peptides and Mimetics, Structural Aspects and Impact on Biological Activity. Bologna University, **2012**.
- (121) Manavalan, P.; Momany, F. A. *Biopolymers* **1980**, *19*, 1943-1973.
- (122) Vara Prasad, J. V. N.; Rich, D. H. *Tetrahedron Lett.* **1990**, *31*, 1803-1806.
- (123) Gante, J. *Synthesis* **1989**, 405-413.
- (124) Magrath, J.; Abeles, R. H. *J. Med. Chem.* **1992**, *35*, 4279-4283.
- (125) Balaram, P.; Sudha, T. S. *Int. J. Peptide Protein Res.* **1983**, *21*, 381-388.
- (126) Clausen, K.; Thorsen, M.; Lawesson, S. O.; Spatola, A. F. *J. Chem. Soc., Perkin Trans. 1* **1984**, 785-798.
- (127) El Masdouri, L.; Aubry, A.; Sakarellos, C.; Gomex, E. J.; Cung, M. T.; Marraud, M. *Int. J. Peptide Protein Res.* **1988**, *31*, 420-428.
- (128) Chorev, M.; Goodman, M. *Acc. Chem. Res.* **1993**, *26*, 266-273.
- (129) Yang, D.; Qu, J.; Li, B.; Ng, F.-F.; Wang, X.-C.; Cheung, K. K.; Wang, D.-P.; Wu, Y.-D. *J. Am. Chem. Soc.* **1999**, *121*, 589-590.
- (130) Aubry, A.; Mangeot, J.-P.; Vidal, J.; Collet, A.; Zerkout, S.; Marraud, M. *Int. J. Peptide Protein Res.* **1994**, *43*, 305-311.
- (131) Cheguillaume, A.; Lehardy, F.; Bouget, K.; Baudy-Floc'h, M.; Le Grel, P. *J. Org. Chem.* **1999**, *64*, 2924-2927.
- (132) Müller, A.; Vogt, C.; Sewald, N. *Synthesis* **1998**, 837-841.
- (133) Müller, A.; Schumann, F.; Kokschi, M.; Sewald, N. *Lett. Peptide Sci.* **1997**, *4*, 275-281.
- (134) Marraud, M.; Dupont, V.; Grand, V.; Zerkout, S.; Lecoq, A.; Boussard, G.; Vidal, J.; Collet, A.; Aubry, A. *Biopolymers* **1993**, *33*, 1135-1148.
- (135) Lecoq, A.; Marraud, M.; Aubry, A. *Tetrahedron Lett.* **1991**, *32*, 2765-2768.
- (136) Aubry, A.; Bayeul, D.; Mangeot, J.; Vidal, J.; Sterin, S.; Collet, A.; Lecoq, A.; Marraud, M. *Biopolymers* **1991**, *31*, 793-801.
- (137) Zuckermann, R. N.; Kerr, J. M.; Kent, S. B. H.; Moos, W. H. *J. Am. Chem. Soc.* **1992**, *114*, 10646-10647.
- (138) Kessler, H. *Angew. Chem., Int. Ed. Engl.* **1993**, *32*, 543-544.
- (139) Simon, R. J.; Kania, R. S.; Zuckermann, R. N.; Huebner, V. D.; Jewell, D. A.; Banville, S.; Ng, S.; Wang, L.; Rosenberg, S.; Marlowe, C. K. *Proc. Natl. Acad. Sci. USA* **1992**, *89*, 9367-9371.
- (140) Kirshenbaum, K.; Barron, A. E.; Goldsmith, R. A.; Armand, P.; Bradley, E. K.; Truong, K. T. V.; Dill, K. A.; Cohen, F. E.; Zuckermann, R. N. *Proc. Natl. Acad. Sci. USA* **1998**, *95*, 4303-4308.
- (141) Armand, P.; Kirshenbaum, K.; Falicov, A.; Dunbrack, J. R. L.; Dill, K. A.; Zuckermann, R. N.; Cohen, F. E. *Folding and Design* **1997**, *2*, 369-375.
-

Part A

Bibliographies

- (142) Armand, P.; Kirshenbaum, K.; Goldsmith, R. A.; Farr-Jones, S.; Barron, A. E.; Truong, K. T. V.; Dill, K. A.; Mierke, D. F.; Cohen, F. E.; Zuckermann, R. N.; Bradley, E. K. *Proc. Natl. Acad. Sci. USA* **1998**, *95*, 4309-4314.
- (143) Cheng, R. P.; Gellman, S. H.; DeGrado, W. F. *Chem. Rev.* **2001**, *101*, 3219-3232.
- (144) Kovacs, J.; Ballina, R.; Rodin, R.; Balasubramanian, O.; Applequist, J. *J. Am. Chem. Soc.* **1965**, *87*, 119-120.
- (145) Kirshenbaum, K.; Zuckermann, R. N.; Dill, K. A. *Curr. Opin. Struct. Biol.* **1999**, *9*, 530-535.
- (146) Seebach, D.; Ciceri, P. E.; Overhand, M.; Jaun, B.; Rigo, D.; Oberer, L.; Hommel, U.; Amstutz, R.; Widmer, H. *Helv. Chim. Acta* **1996**, *79*, 2043-2066.
- (147) Arvidsson, P. I.; Rueping, M.; Seebach, D. *J. Chem. Soc., Chem. Commun.* **2001**, 649-650.
- (148) Cheng, R. P.; DeGrado, W. F. *J. Am. Chem. Soc.* **2001**, *123*, 5162-5163.
- (149) Seebach, D.; Gademann, K.; Schreiber, J. V.; Matthews, J. L.; Hintermann, T.; Jaun, B.; Oberer, L.; Hommel, U.; Widmer, H. *Helv. Chim. Acta* **1997**, *80*, 2033-2038.
- (150) Yang, D.; Ng, F.-F.; Li, Z.-J.; Wu, Y.-D.; Chan, K. W. K.; Wang, D.-P. *J. Am. Chem. Soc.* **1996**, *118*, 9794-9795.
- (151) Yang, D.; Qu, J.; Li, W.; Wang, D.-P.; Ren, Y.; Wu, Y.-D. *J. Am. Chem. Soc.* **2003**, *125*, 14452-14457.
- (152) Yang, D.; Li, W.; Qu, J.; Luo, S.-W.; Wu, Y.-D. *J. Am. Chem. Soc.* **2003**, *125*, 13018-13019.
- (153) Cheguillaume, A.; Doubli-Bounoua, I.; Baudy-Floc'h, M.; Le Grel, P. *Syn. lett.* **2000**, 331-334.
- (154) Cheguillaume, A.; Salaün, A.; Sinbandhit, S.; Potel, M.; Gall, P.; Baudy-Floc'h, M.; Le Grel, P. *J. Org. Chem.* **2001**, *66*, 4923-4929.
- (155) Günther, R.; Hofmann, H.-J. *J. Am. Chem. Soc.* **2001**, *123*, 247-255.
- (156) Bouillon, I. Thesis: Synthèse d'alpha-hydrazinopeptides. INPL-Nancy, **2006**.
- (157) Zega, A.; Urleb, U. *Acta Chim. Slov.* **2002**, *49*, 649-662.
- (158) Benatalah, Z.; Aubry, A.; Boussard, G.; Marraud, M. *Int. J. Peptide Protein Res.* **1991**, *38*, 603-605.
- (159) Benedetti, E.: Peptides. Goodman, M., Meienhofer, J., Eds.: Wiley, New York, 1977; pp 257-273.
- (160) Lee, H.-J.; Lee, M.-H.; Choi, Y.-S.; Park, H.-M.; Lee, K.-B. *J. Mol. Struct.* **2003**, *631*, 101-110.
- (161) Reynolds, C. H.; Hormann, R. E. *J. Am. Chem. Soc.* **1996**, *118*, 9395-9401.
- (162) Caroline Proulx, C.; Sabatino, D.; Hopewell, R.; Jochen Spiegel, J.; Yésica García Ramos, Y. G.; Lubell, W. D. *Future Med. Chem.* **2011**, *3*, 1139-1164.
- (163) Abbas, C.; Jamart-Grégoire, B.; Vanderesse, R.; Didierjean, C. *Acta Crystallogr. Sect. E, Struct. Rep. Online* **2009**, *E65*, 3079.
- (164) Hess, H.-J.; Moreland, W. T.; laubach, G. D. *J. Am. Chem. Soc.* **1963**, *85*, 4040-4041.
- (165) Gante, J.; Krug, M.; Lauterbach, G.; Weitzel, R.; Hiller, W. *J. Pept. Sci.* **1995**, *1*, 201-206.
- (166) Orrick, J. J.; Steinhart, C. R. *Ann. Pharmacother* **2004**, *38*, 1664-1674.
- (167) Von Hentig, N.; Johann, W. *Drugs Today* **2008**, *44*, 103-132.
- (168) Dutta, A. S.; Furr, B. J. A.; Denis, M. B. *Annu. Rep. Med. Chem., Academic Press* **1985**, 203-214.
- (169) André, F.; Boussard, G.; Marraud, M.; Didierjean, C.; Aubry, A. *Lett. Peptide Sci.* **1995**, *2*, 239-242.
- (170) André, F.; Marraud, M.; Boussard, G.; Didierjean, C.; Aubry, A. *Tetrahedron Lett.* **1996**, *37*, 183-186.
- (171) André, F.; Marraud, M.; Tsouloufis, T.; Tzartos, S. J.; Boussard, G. *J. Pept. Sci.* **1997**, *3*, 429-441.
- (172) Boeglin, D.; Hamdan, F. F.; Melendez, R. E.; Cluzeau, J.; Laperriere, A.; Heroux, M.; Bouvier, M.; Lubell, W. D. *J. Med. Chem.* **2007**, *50*, 1401-1408.
- (173) Melendez, R. E.; Lubell, W. D. *J. Am. Chem. Soc.* **2004**, *126*, 6759-6764.
- (174) Thormann, M.; Hofmann, H.-J. *J. Mol. Struct. (Theochem)* **1999**, *469*, 63-67.
- (175) Didierjean, C.; Duca, V. D.; Benedetti, E.; Aubry, A.; Zouikri, M.; Marraud, M.; Boussard, G. *J. Pept. Res.* **2009**, *50*, 451-457.
- (176) Li, X.; Yang, D. *Chem. Commun.* **2006**, 3367-3369.
-

Part A

Bibliographies

- (177) Wiczerak, E.; Drabik, P.; Lankiewicz, L.; Oldziej, S.; Grzonka, Z.; Abrahamson, M.; Grubb, A.; Bromme, D. *J. Med. Chem.* **2002**, *45*, 4202-4211.
- (178) Gray, C. J.; Ireson, J. C.; Parker, R. C. *Tetrahedron* **1977**, *33*, 739-743.
- (179) Proulx, C.; Lubell, W. D. *Org. Lett.* **2012**, *14*, 4552-4555.
- (180) Ragnarsson, U. *Chem. Soc. Rev.* **2001**, *30*, 205-213.
- (181) Brosse, N.; Pinto, M.-F.; Bodiguel, J.; Jamart-Grégoire, B. *J. Org. Chem.* **2001**, *66*, 2869-2873.
- (182) Brosse, N.; Pinto, M.-F.; Jamart-Grégoire, B. *J. Org. Chem.* **2000**, *65*, 4370-4374.
- (183) Majer, P.; Randad, R. S. *J. Org. Chem.* **1994**, *59*, 1937-1938.
- (184) Brosse, N.; Jamart-Grégoire, B. *Tetrahedron Lett.* **2002**, *43*, 249-251.
- (185) Sunyaev, S.; Lathe III, W.; Bork, P. *Curr. Opin. Struct. Biol.* **2001**, *11*, 125-130.
- (186) Oberg, K.; Fink, A. L. *Anal. Biochem.* **1998**, *256*, 92-106.
- (187) Formaggio, F.; Crisma, M.; Toniolo, C.; Broxterman, Q. B.; Kaptein, B.; Corbier, C.; Saviano, M.; Palladino, P.; Benedetti, E. *Macromolecules* **2003**, *36*, 8164-8170.
- (188) Gardner, R. B.; Liang, G. B.; Gellman, S. H. *J. Am. Chem. Soc.* **1999**, *121*, 1806-1816.
- (189) Montelione, G. T.; Zheng, D.; Huang, Y. J.; Gunsalus, K. C.; Szyperski, T. *Nature Struct. Biol., Struct. Genomics Suppl.* **2000**, 982-985.
- (190) Iqbal, M.; Balaram, P. *Biopolymers* **1982**, *21*, 1427-1433.
- (191) Salaün, A.; Favre, A.; Le Grel, B.; Potel, M.; Le Grel, P. *J. Org. Chem.* **2006**, *71*, 150-158.
- (192) BAX, A. *J. Magn. Reson.* **1981**, *42*, 164-168.
- (193) Bax, A.; Freeman, R. *J. Magn. Reson.* **1969**, *44*, 542-561.
- (194) Bothner-By, A. A.; Stephens, R. L.; Lee, J.; Warren, C. D.; Jeanloz, R. W. *J. Am. Chem. Soc.* **1984**, *106*, 811-813.
- (195) Berman, H. M.; Westbrook, J.; Feng, Z.; Gilliland, G.; Bhat, T. N.; Weissig, H.; Shindyalov, I. N.; Bourne, P. E. *Nucleic Acids Res.* **2000**, *28*, 235-242.
- (196) Abola, E.; Kuhn, P.; Earnest, T.; Stevens, R. C. *Nature Struct. Biol., Struct. Genomics Suppl.* **2000**, 973-977.
- (197) Woody, R. W.: Circular Dichroism, Principles and Applications. Nakanishi, K., Berova, N., Woody, R. W., Eds.: VCH, New York, **1994**.
- (198) Nelson, J. W.; Kallenbach, N. R. *Proteins Struct. Funct. Genet.* **1986**, *1*, 211-217.
- (199) Violette, A.; Averlant-Petit, M.-C.; Semetey, V.; Hemmerlin, C.; Casimir, R.; Graff, R.; Marraud, M.; Briand, J.-P.; Rognan, D.; Guichard, G. *J. Am. Chem. Soc.* **2005**, *127*, 2156-2164.
- (200) Vanderesse, R.; Grand, V.; Limal, D.; Vicherat, A.; Marraud, M.; Didierjean, C.; Aubry, A. *J. Am. Chem. Soc.* **1998**, *120*, 9444-9451.
- (201) Lecoq, A.; Boussard, G.; Marraud, M.; Aubry, A. *Tetrahedron Lett.* **1992**, *33*, 5209-5212.
- (202) Moussodia, R. O.; Acherar, S.; Bordessa, A.; Vanderesse, R.; Jamart-Grégoire, B. *Tetrahedron* **2012**, *68*, 4682-4692.
- (203) Brosse, N.; Grandeury, A.; Jamart-Grégoire, B. *Tetrahedron Lett.* **2002**, *43*, 2009-2011.
- (204) Marraud, M.; Aubry, A. *Biopolymers* **1996**, *40*, 45-83.
- (205) Gante, J.; Krug, M.; Lauterbach, G.; Weitzel, R.: Peptides: Chemistry and Biology. Hodges, R. S., Smith, J. A., Eds.: Proceedings of the 13th American Peptide Symposium, ESCOM, Leiden, The Netherlands, **1994**; pp 299-301.
- (206) Dutta, A. S.; Morley, J. S. *J. Chem. Soc., Perkin Trans.* **1975**, *1*, 1712-1720.
- (207) Gray, C. J.; Quibell, M.; Beggett, N.; Hammerk, T. *Int. J. Peptide Protein Res.* **1992**, *40*, 351-362.
- (208) Zouikri, M.; Vicherat, A.; Aubry, A.; Marraud, M.; Boussard, G. *J. Pept. Res.* **1998**, *52*, 19-26.
- (209) Didierjean, C.; Del Duca, V.; Benedetti, E.; Aubry, A.; Zouikri, M.; Marraud, M.; Boussard, G. *J. Pept. Res.* **1997**, *50*, 451-457.
- (210) Lecoq, A.; Boussard, G.; Marraud, M.; Aubry, A. *Biopolymers* **1993**, *33*, 1051-1059.
- (211) Lee, H.-J.; Song, J.-W.; Choi, Y.-S.; Ro, S.; Yoon, C. *J. Phys. Chem. Chem. Phys.* **2001**, *3*, 1693-1698.
- (212) Zhang, W. J.; Berglund, A.; Kao, J. L.-F.; Couty, J. P.; Gershengorn, M. C.; Marshall, G. R. *J. Am. Chem. Soc.* **2003**, *125*, 1221-1235.

Part A

Bibliographies

- (213) Lee, H.-J.; Song, J.-W.; Choi, Y.-S.; Park, H.-M.; Lee, K.-B. *J. Am. Chem. Soc.* **2002**, *124*, 11881-11893.
- (214) Case, D. A.; Cheatham, T.; Darden, T.; Gohlke, H.; Luo, R.; Merz, K. M. J.; Onufriev, A.; Simmerling, C.; Wang, B. J. *Computat. Chem.* **2005**, *26*, 1668-1688.
- (215) Pearlman, D. A.; Case, D. A.; Caldwell, J. W.; Ross, W. S.; Cheatham, T. E.; DeBolt, S.; Ferguson, D.; Seibel, G.; Kollman, P. *Comp. Phys. Commun.* **1995**, *19*, 1-41.
- (216) Jeffrey, G. A. Review of hydrogen bonding: An Introduction to Hydrogen Bonding. *Oxford University Press: New York* **1997**.
- (217) Horne, W. S.; Stout, C. D.; Ghadiri, M. R. *J. Am. Chem. Soc.* **2003**, *125*, 9372-9376.
- (218) Vass, E.; Kurz, M.; Konat, R. K.; Hollósi, M. *Spectrochim. Acta. A. Mol. Biomol. Spectrosc.* **1998**, *54*, 773-786.

**Chapter IV. Impact of C^α-Chirality on
Supramolecular Self-Assembly of Cyclo-(*L*- / *D*-
Phe-azaPhe-Ala)₂-Hexamers**

Chapter IV. Impact of C^α-Chirality on Supramolecular Self-Assembly in Cyclo-2:1-[α /aza]-Hexamers (*L*-/*D*-Phe-azaPhe-Ala)₂

Introduction

In the previous study, molecular dynamic calculations based on NMR constraints have shown that the linear 2:1-[α /aza]-hexamers Boc-(*L*- or *D*-Phe-azaPhe-Ala)₂-OMe (**8a** and **8b**) adopt an almost closed cyclic shape which reflected the close proximity of the *N*- and *C*-termini enhancing macrocyclization greatly (Figure 4.1).^[1] Accordingly, our group proposed the synthesis of the corresponding macrocyclic derivatives of these linear hexamers to evaluate their propensities to form 3D highly ordered supramolecular structures.

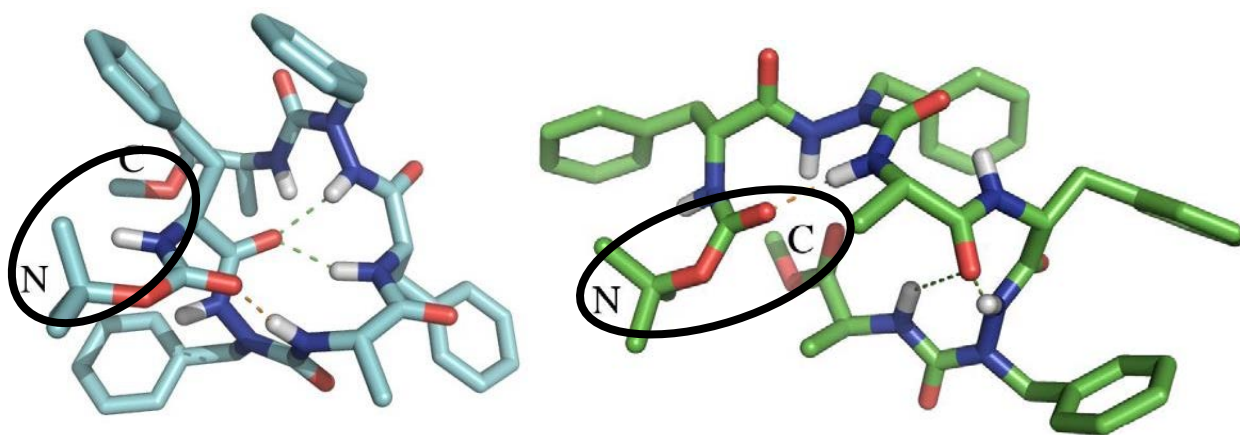
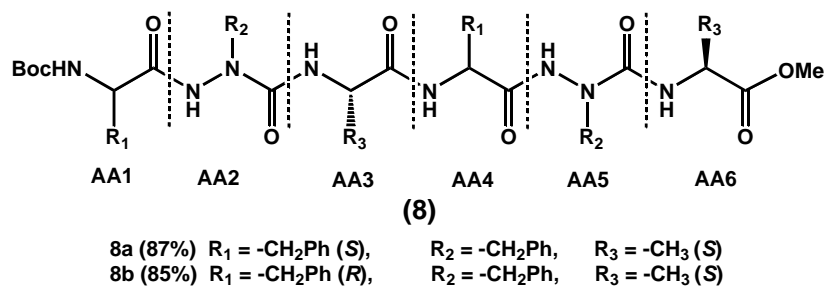


Figure 4.1. Models show the main conformations obtained by molecular modelling calculations based on NMR constraints for: (**8a**) left, (**8b**) right illustrating the proximity of the two *N*- and *C*-termini from each other.^[1]

In this chapter, we will report and compare the conformational behaviors of new homo- and hetero cyclo 2:1-[α /aza]-hexamers (**9a** and **9b**) in the solid and solution states at the monomeric and supramolecular levels. This work has been published under the title “Impact of C^α-Chirality on Supramolecular Self-Assembly in Cyclo-2:1-[α /aza]-Hexamers (*L*- / *D*-Phe-azaPhe-Ala)₂” in european journal of organic chemistry, **2017**, 4703–4712, DOI: 10.1002/ejoc.201700555.

Impact of C α -Chirality on Supramolecular Self-Assembly in Cyclo-2:1-[α /aza]-Hexamers (*L*-/*D*-Phe-azaPhe-Ala)₂

Mohamed Ibrahim Abdelmoneim Ibrahim^{[a, b]§}, Zhou Zhou^{[a]§}, Cheng Deng^[a], Claude Didierjean^[c], Régis Vanderesse^[a], Jacques Bodiguel^[a], Marie-Christine Averlant-Petit^{*[a]} and Brigitte Jamart-Grégoire^{*[a]}

Abstract: The design of new cyclic pseudopeptides of the sequence 2:1-[α /aza]-hexamers containing aza-amino acid motifs has gained much prominence to be involved in several potential applications. X-ray, FTIR, and NMR studies showed the ability of this series to adopt β -turn conformation in solid state, while in solution; equilibrium between the monomeric states (stabilized by β -turns through intramolecular hydrogen bonds), and supramolecular construction (stabilized by intermolecular hydrogen bonds and π - π stacking) predominates. Furthermore, both homo- and heterochiral 2:1-[α /aza]-cyclohexamers **9a** and **9b**, respectively can self-assemble into organized 3D structures with increasing concentration favoring the supramolecular construction where the macrocycles are stacking over each other and stabilized by several non-covalent intermolecular interactions.

IV.1. Introduction

Recently, design of cyclic pseudopeptides has gained considerable interest owing to: (1) their wide environmental and biomedical potential applications,^[2] (2) their rigid structures may result in greater stability against enzymatic degradation,^[3] enhanced receptor affinity, increased selectivity and bioavailability compared to the parent linear precursors,^[4] and (3) cyclic pseudopeptides have demonstrated self-assembly capacity into well-organized 3D hierarchical structures stabilized by numerous non-covalent weak interactions such as hydrogen bonds, π -stacking, electrostatic or van der Waals interactions, etc.^[5]

The design of self-assembling cyclic peptides (CPs) was first evolved from a report by Hassal *et al.*^[5a] in 1972 which predicted the formation of hollow cylindrical structure by the cyclic tetrapeptide [*L*-Ser(OtBu)- β -Ala-Gly- β -Asp(OMe)]-. The supramolecular structure of this tetrapeptide was confirmed two years later where X-ray data revealed that the macrocycles are stacking over each other through two of four inter-subunits hydrogen bonds.^[5a]

In 1993, Ghadiri *et al.* have given the evidence for the formation of hollow tubular structures of cyclic *D*, *L*- α -peptides using different physico-chemical techniques.^[5b] They demonstrated that the peptide solution of cyclo-[*D*-Ala-Glu-*D*-Ala-Glu]₂-] can self-assemble and lead to a supramolecular nanotubular architecture, stabilized by intermolecular hydrogen bonds.

[a] Laboratoire de Chimie-Physique Macromoléculaire (LCPM), UMR 7375, CNRS, Université de Lorraine, 1 rue Grandville, BP 20451, 54001 Nancy, France.

[b] Marine Chemistry Department, National Institute of Oceanography and Fisheries (NIOF), Qayet-Bey, El-Anfoushy, 21557, Alexandria, Egypt.

[c] Laboratoire de Cristallographie, Résonance Magnétique et Modélisation (CRM2), UMR 7036, CNRS, Université de Lorraine, Boulevard des Aiguillettes, 56506 Vandoeuvre-lès-Nancy, France.

§ Equal contribution to this work

E-mail: marie.averlant@univ-lorraine.fr, brigitte.jamart@univ-lorraine.fr
lcpm.univ-lorraine.fr

This article has been published in: *Eur. J. Org. Chem.* **2017**, 4703–4712, DOI: 10.1002/ejoc.201700555

Molecular modelling analysis predicts that cyclic homochiral β^3 -peptides could adopt planar, disc-like conformations when amino acid side chains are directed toward the exterior of the peptide ring. These anticipated structural features allow the peptide subunits to stack in a parallel way through intermolecular hydrogen-bonding leading to the formation of hollow peptide nanotubes.^[5b, 6] Shimizu *et al.* showed the formation of tubular structure from bis-urea macrocycle. The presence of the phenyl group not only induced rigidity for the cycle but also stabilized the nanotube structure through π - π stacking with a distance of 3.568 Å.^[7]

More recently, formation of hollow supramolecular structures particularly nanotubes have been extended to cyclic pseudopeptides containing β -amino acids^[8] alternating α - and β -amino acids,^[5d] vinylogous δ -amino acids,^[9] and oligoureas.^[10] Among the pseudopeptidic macrocycles, hydrazinopeptides and azapeptides developed by our group have been investigated to be promising candidates for construction of supramolecular structure. The presence of supplementary nitrogen in these two pseudopeptidic families offers a less flexibility in the backbone by involving in new secondary structure conformation called hydrazinoturn.^[11] In regards to the hydrazinopeptides family, X-ray, FTIR and NMR studies have confirmed the ability of cyclotetramer and cyclohexamer of heterochiral 1:1-[α / α -N^Q-Bn-hydrazino]-mers to self-assemble into nanotubular structures in the solid state. In solution an equilibrium between monomeric and nanotubular states has been observed.^[11i]

In the previous work concerning the azapeptides family,^[11h] our group has concluded that the linear 2:1-[α /aza]-oligomers could adopt β -turn conformations stabilized *via* intramolecular hydrogen bonds as assessed by X-ray data, NMR, FTIR experiments as well as the theoretical studies. This result is in accordance with a variety of theoretical,^[12] spectroscopic,^[11c, 12a, 13] and crystallographic studies^[11b, d, 14] of other reported azapeptides. Although several linear azapeptides have been scanned by systematic substitution of aza-residues for each amino acid in the sequence,^[15] only few aza-cyclopeptides have been so far reported in the literature.^[16] Moreover, molecular dynamic calculations based on NMR constraints have shown that the linear 2:1-[α /aza]-hexamers adopted an almost closed cyclic shape which reflected the close proximity of the *N*- and *C*-termini enhancing macrocyclization greatly.^[11h] Accordingly, our group proposed the synthesis of the corresponding macrocyclic derivatives of these linear hexamers to evaluate their propensities to form supramolecular assemblies.

In this work, we report and compare the conformational behaviors of new homo- and hetero cyclo 2:1-[α /aza]-hexamers in the solid and solution states at monomeric and supramolecular levels.

IV.2. Results and Discussion

The general stepwise strategy used to synthesize the homo- and heterochiral cyclo 2:1-[α /aza]-hexamers **9a** and **9b** is described in Scheme 4.1. Linear homochiral hexamer **8a** and heterochiral hexamer **8b** were obtained by classical coupling reactions using conditions previously described.^[11h] The corresponding macrocycles **9a** and **9b** were obtained

Part A

Chapter IV. Impact of C $^{\alpha}$ -Chirality on Supramolecular Self-Assembly in Cyclo-2:1-[α /aza]-Hexamers (*L*-/*D*-Phe-azaPhe-Ala) $_2$

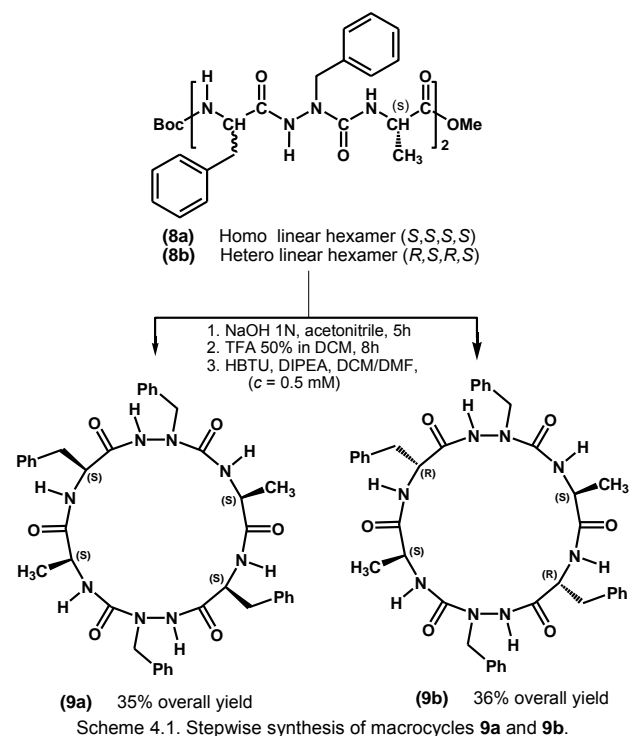
from the deprotected precursors by reaction with an excess of HBTU (HBTU = *O*-(Benzotriazol-1-yl)-*N,N,N',N'*-tetramethyluronium hexafluorophosphate) in DCM/DMF at 0.5 mmol. L $^{-1}$. They were isolated with high purity in overall yields of 35 %.

The conformation analysis was started in solid phase state. Single crystals of compounds **9a** and **9b** suitable for X-ray crystallographic analysis were grown by slow evaporation from EtOAc/DIP and EtOH/DIP (DIP = diisopropyl ether) solution, respectively. While the hexacycle **9a** crystallizes in the space group *P2* with one conformer in the asymmetric unit (two asymmetric units in the unit cell (*Z* = 2)), the hexacycle **9b** crystallizes in the space group *P1* with eight conformers (**A** \rightarrow **H**) in the asymmetric unit cell (*Z* = 1), (Appendix 2, Table S4.1, Figures S4.5 and S4.6).

In compound **9a**, the hexamacrocycle is not symmetric. Indeed the N $^{\alpha}$ atom of the azaPhe (*i* + 2) residue showed a slight pyramidal character with a distance of 0.202 Å from the plane and it has *D*-configuration, while the N $^{\alpha}$ atom of the azaPhe (*i* + 5) residue also shows a pyramidal character but with *L*-configuration and is located out of the plane by 0.232 Å. This inversion of configuration may be due to the interconversion from intramolecular to intermolecular hydrogen bonding with increasing concentration which has been already observed in literature, and we will discuss this later in this paper.^[17] Moreover, X-ray diffraction experiments revealed that the interatomic distance between the polar sites (NH $_{i+3}$ \cdots O $_i$) is 2.83 Å which is an adequate value for intramolecular hydrogen bond interaction^[18] leading to the formation of pseudocycle of 10 atoms between the (CO $_i$) Ala and (NH $_{i+3}$) Ala from the type (*i* + 3 \rightarrow *i*) as shown in Figure 4.2, (Appendix 2, Table S4.2). In addition, the distance between C $^{\alpha}$ of residues (*i*) and (*i* + 3) of the pseudocycle is less than 7 Å which supports the existence of β -turn conformation.^[19] Finally each macrocyclic subunit is stabilized by intramolecular orthogonal π -stacking between the benzyl group of the azaPhe and the benzyl group of the Phe of the same macrocycle. While the values of the torsion angle (ω) range from 168.54 $^{\circ}$ to 179.32 $^{\circ}$ confirm *Z*-configuration for all the peptide bonds, the torsion angles (ϕ , ψ) help in the characterization of the turn.^[12b, d] The torsion angles of molecule **9a** are ($\phi_{i+1} = -51.63^{\circ}$, $\psi_{i+1} = 125.9^{\circ}$), ($\phi_{i+2} = 77.71^{\circ}$, $\psi_{i+2} = -5.93^{\circ}$), ($\phi_{i+4} = -100.67^{\circ}$, $\psi_{i+4} = 103.38^{\circ}$), and ($\phi_{i+5} = 81.52^{\circ}$, $\psi_{i+5} = 12.24^{\circ}$) which confirm the presence of two turns, and both of them are β II-turn (Appendix 2, Table S4.3).^[12b, d]

On the other side, the asymmetric unit of compound **9b** is composed of two arrays; each contains four parallel conformers (Figure 4.3). Some of the N $^{\alpha}$ atoms of the conformers within the asymmetric unit adopt pyramidal character with either *D*- or *L*-configuration and they are out of the plan by distances summarized in Table S4.4 (Appendix 2). Moreover, all the conformers are characterized by the presence of one intramolecular hydrogen bond (Figure 4.3a) with accepted interatomic distances values between the polar sites.^[18] Bond distances range from 3.04 to 3.47 Å have been measured either between (CO $_i$) Ala and (NH $_{i+3}$) Ala in conformers **A**, **C**, **D**, **G** and **H** or between (CO $_{i+3}$) Ala and (NH $_i$) Ala in **B** and **E**. Conformer **F** reflects the both kinds of hydrogen bonding interactions. All the previous intramolecular interactions lead to the formation of pseudocycles of 10 atoms which are characteristic of a β -turn conformation (Figure 4.3a).^[11h, 19a, 20] The values of the bond distances and bond angles for the corresponding intramolecular hydrogen bonds are given in Table S4.5 (Appendix 2). The torsion angles (ϕ , ψ) of the eight conformers have been measured within the following ranges; ($\phi_{i+1} = 57.54^{\circ}$ to 90.17° , $\psi_{i+1} = -116.57^{\circ}$ to -103.79°), ($\phi_{i+2} = -121.38^{\circ}$ to -88.93° , $\psi_{i+2} = -12.66^{\circ}$ to 7.6°), ($\phi_{i+4} = 79.34^{\circ}$ to 106.84° , $\psi_{i+4} = -120.69^{\circ}$ to -104.61°), and ($\phi_{i+5} = -122.68^{\circ}$ to -92.0° , $\psi_{i+5} = -5.53^{\circ}$ to

5.73 $^{\circ}$), (Appendix 2, Table S4.6). These values reflect that the main conformation adopted by all the conformers is β II'-turn.^[12b, d]



The next step was to analyze the supramolecular packing in both compounds. For compound **9a**, we could recognize that three out of six carbonyl groups are oriented up and down perpendicularly while the others are projected equatorially to the plane of the cycle (Figure 4.2a). This is consistent with the analysis of other cyclic hexapeptidic structures deposited in the Cambridge Structural Database (version 5.38) which reveals that one-half or less of the carbonyl groups are oriented along the ring axis (Appendix 2, Figure S4.7). The alignment of the carbonyl groups allows the stacking of the aromatic rings and consequently the macrocycles reinforced by three intermolecular hydrogen bonds between (NH $_{i+2}$) azaPhe, (CO $_{i+3}$) Ala and (NH $_{i+5}$) azaPhe of one macrocycle and the (CO $_{i+1}$) Phe, (NH $_{i+4}$) Phe and (CO $_{i+4}$) Phe of another macrocycle respectively. This supports the formation of supramolecular structure held by an antiparallel hydrogen-bonding network (Figure 4.2b).^[2g, 5b, e, 21] The interatomic distances between the polar sites of these hydrogen bonds are 3.19, 3.06, and 3.00 Å, while the bond angles are 161.32 $^{\circ}$, 158.39 $^{\circ}$, and 152.17 $^{\circ}$ for the three hydrogen bonds respectively (Appendix 2, Table S4.7), which are accepted values as hydrogen bonds.^[18]

Similarly, all the conformers of compound **9b** have three out of six carbonyl groups oriented up and down along the plane of the pseudopeptidic macrocycle while the others are projected equatorially (Figure 4.3a). The alignment of the carbonyl groups allows self-assembly of the molecules as shown in Figure 4.3b. Indeed, each two overlaid macrocycles, for examples (**A/C**) from array 1 and (**D/F**) from array 2 are interconnected through three intermolecular hydrogen bonds (in orange, Figure 4.3b) between (CO $_{i+2}$) azaPhe, (NH $_{i+4}$) *D*-Phe, and (CO $_{i+4}$) *D*-Phe groups of one macrocycle and the (NH $_{i+2}$) azaPhe, (CO $_{i+3}$) Ala and (NH $_{i+5}$) azaPhe groups of the other macrocycle. This supports the formation of supramolecular organization stabilized by antiparallel hydrogen bonds network (Figure 4.3b).^[2g, 5b, e, 21] The interatomic distances between the polar sites of these intermolecular hydrogen bonds are within a range of 2.79 Å to 2.97 Å, and the bond angles are within a range of 132.25 $^{\circ}$ to 169.19 $^{\circ}$ (Appendix 2, Table S4.8).

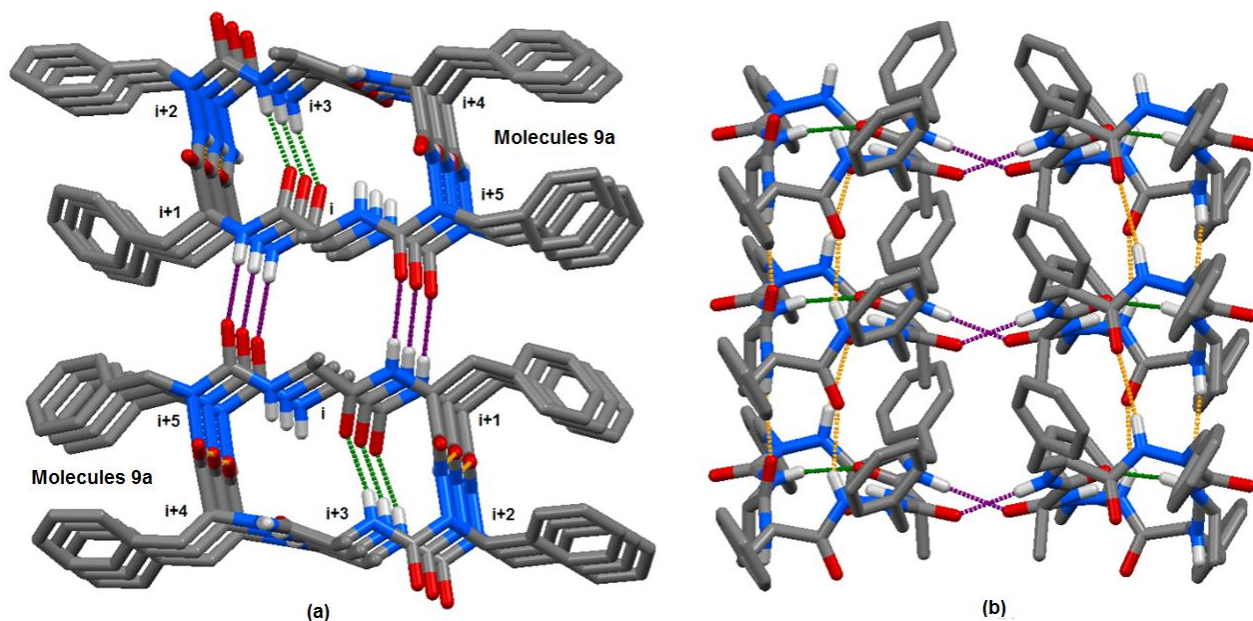
Chapter IV. Impact of C^α-Chirality on Supramolecular Self-Assembly in Cyclo-2:1-[α /aza]-Hexamers (*L*-/*D*-Phe-azaPhe-Ala)₂

Figure 4.2. Crystal molecular structure of compound **9a** (X-ray): (a) top view, and (b) side view. The intermolecular hydrogen bonds (orange and purple) and intramolecular hydrogen bonds (green) are illustrated as dotted lines. The H atoms, except amide protons have been omitted for clarity.

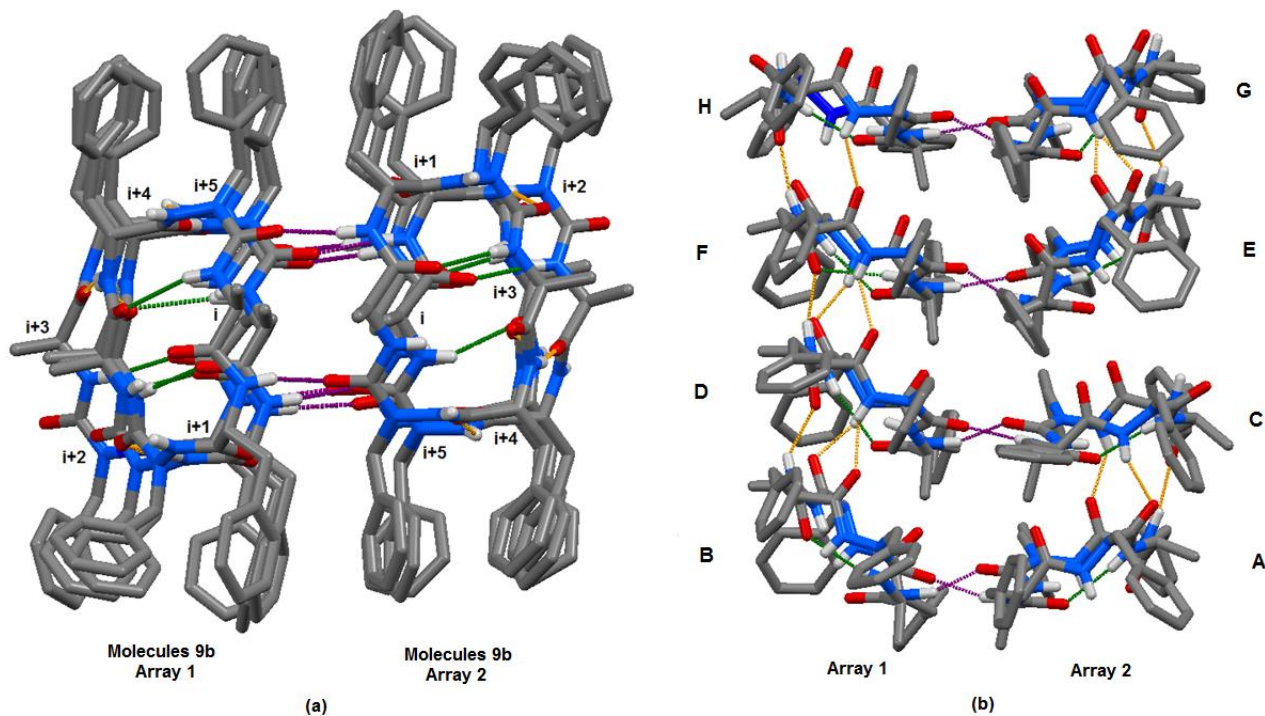


Figure 4.3. View of compound **9b** in the crystal state (X-ray): (a) top view, and (b) side view. The intermolecular hydrogen bonds (yellow and purple) and intramolecular hydrogen bonds (green) are marked as dashed lines. The H atoms, except amide protons, and all water molecules have been omitted for clarity.

The supramolecular assembly of both compounds **9a** and **9b** is not only held by the aforementioned intermolecular hydrogen bonds, but also by the parallel π - π stacking between the benzyl rings of each two stacked macrocycles with a distance of less than 5.5 Å.^[7] In addition to all the previously described intermolecular hydrogen bonds network, interestingly compounds **9a** and **9b** show two identical intermolecular hydrogen bonds between each two neighboring molecules, between the (NH_{i+1}) [Phe (**9a**) or *D*-Phe (**9b**)], and (CO_{i+5}) azaPhe groups of one molecule and (CO_{i+5}) azaPhe, and (NH_{i+1}) [Phe (**9a**) or *D*-Phe (**9b**)] groups of the adjacent molecule, respectively, (in purple, Figures 4.2 and 4.3). The bond distances between the polar sites range from 2.786 Å to 2.994 Å and angles of these hydrogen bonds close to the co-linear value (from 155.55° to 178.0°). These

values refer to strong intermolecular hydrogen bonds capable of stabilizing the supramolecular arrangement for both compounds (Appendix 2, Table S4.9).^[18] Finally, the internal cavities within the macrocycles of **9a** and **9b**, taking into account the van der Waal radii of the atoms, are collapsed and not large enough to accommodate water or small ions^[29, 8a] (Appendix 2, Figures S4.8a, b) which indicate a columnar structure more than a nanotubular structure for this size of pseudopeptidic macrocycles.

X-ray studies have corroborated that, although changing the configuration of one asymmetric C^α has only little effect on the conformation of each macrocycle (β -turns), it causes a great effect on the supramolecular packing within the unit cell. While compound **9a** has only one conformer (β II-

Chapter IV. Impact of C $^{\alpha}$ -Chirality on Supramolecular Self-Assembly in Cyclo-2:1-[α /aza]-Hexamers (*L*-/*D*-Phe-azaPhe-Ala) $_2$

turn) possessing only two intramolecular and two intermolecular hydrogen bonds in the unit cell ($Z = 2$), X-ray structure of compound **9b** shows eight conformers (all β II'-turn) and each unit cell ($Z = 1$) is characterized by the presence of nine intramolecular and twenty-two intermolecular hydrogen bonds. The results demonstrate the supramolecular arrangement in both compounds; while compound **9a** expands unidimensionally in the unit cell, compound **9b** shows a three dimensional supramolecular assembly within its unit cell stabilized by a 3D hydrogen-bonds network.

To go further with our investigations, compounds **9a** and **9b** were subjected to solution phase ^1H NMR studies. The experiments were carried out at dilute concentrations in CDCl_3 (0.8 mmol. L^{-1} for compound **9a** and 0.5 mmol. L^{-1} for compound **9b**) to avoid intermolecular interactions, and at low temperatures (253 K for compound **9a** and 278 K for compound **9b**) which provided the best spectral resolutions. The spectra of **9a** and **9b** reflect high C_2 -symmetry in solution and this is noticed from the signals of the six residues of the macrocycle, the residues are environmentally identical two by two (Appendix 2, Figure S4.9). While the spectrum of compound **9a** shows splitting of the peaks indicating the presence of equilibrium between two conformers ($\text{X} \rightleftharpoons \text{Y}$) with a ratio of 48 % and 52 % respectively (Appendix 2, Figure S4.9a), spectrum of compound **9b** demonstrates the existence of equilibrium between three conformers ($\text{L} \rightleftharpoons \text{M} \rightleftharpoons \text{N}$) with a ratio of (45 % : 44 % : 11 %), respectively (Appendix 2, Figure S4.9b).

2D NMR (ROESY) experiment was operated for compound **9b** at concentration 0.5 mmol. L^{-1} and temperature 278 K to determine its 3D conformation in solution (Appendix 2, Figure S4.10). It was difficult to determine the structure of minor conformer **N** because the NH protons are superimposed with the aromatic protons. However, conformers **L** and **M** adopt two consecutive β -turns as assessed from the ROE cross peaks (Figure 4.4). Strong correlation between CH^{α} (*D*-Phe) and NH (azaPhe), and moderate correlation between the NH (azaPhe) and NH (Ala) indicate that the conformer **M** adopts a β II'-turn conformation.^[12b, d] From the structural studies of acyclic series,^[11h] and based on our X-ray studies for **9a** and **9b**, we can notice that changing the absolute configuration of the Phe residue from (*S*) to (*R*), led to a change in the conformation from β II to β II', so conformer **M** presents two β II'-turn secondary structures.

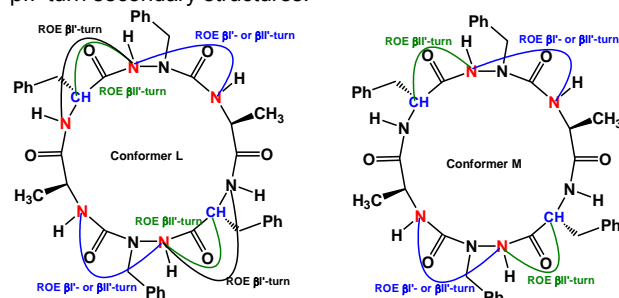


Figure 4.4. ROE correlations observed in the two conformers: **L** (left), and **M** (right); (0.5 mmol. L^{-1} , CDCl_3).

In the case of conformer **L**, the presence of a weak correlation between NH (*D*-Phe) and NH (azaPhe) suggests that conformer **L** adopts partially β I'-turn (in equilibrium with the β II'-turn conformation) which forces the NH protons not to be perpendicular to the macrocycle plane interfering with the stacking mechanism.^[12b, d]

Unfortunately, the NH protons of the Phe residues of compound **9a** are overlapped with the aromatic protons, which was an obstacle to find correlation from ROESY spectrum and determine the type of turn in solution. However, in order to know the most stable conformation of compound **9a** in dilute condition, modelling using Amber 10

program was recommended.^[22] Based on the results obtained from X-ray diffraction on the monomeric unit of **9a** which then placed in explicit solvent conditions followed by molecular dynamic simulations, the obtained models of compound **9a** showed that the two NH protons of the Ala residues (i and $i + 3$) are involved in intramolecular hydrogen bonds with the two carbonyl groups of Ala ($i + 3$ and i) with distances of 2.11 Å and 1.96 Å respectively, and are defining pseudocycles of ten atoms that induce a β II'-turn (Figure 4.5).^[11h, 19a, 20] Molecular dynamics simulations revealed the presence of a new intramolecular hydrogen bond between the two Ala moieties ($\text{CO}_{i+3} \rightarrow \text{NH}_i$) compared with the X-ray results, which will be confirmed by studying the effect of the $\text{CDCl}_3/\text{DMSO}-d_6$ solvent mixture using ^1H NMR spectroscopy.

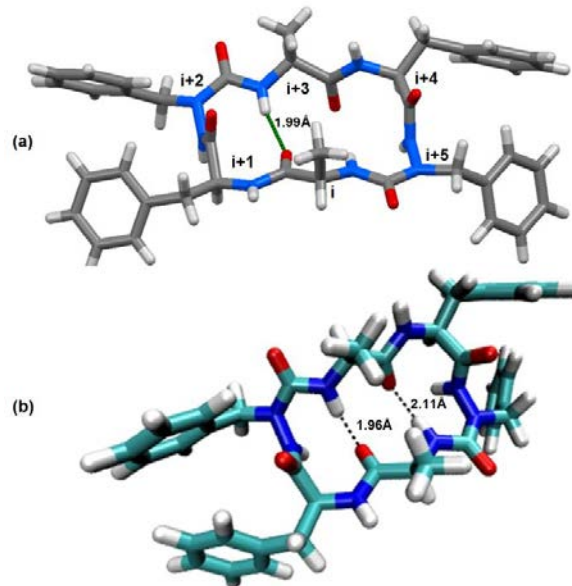


Figure 4.5. (a) View of the crystal state from X-ray of compound **9a**, versus (b) the model of the most energetically favorable monomer using Amber 10 program.

Indeed, the existence of hydrogen bonds may be investigated in solution using mixture solvent effect through NMR experiments. It harnesses the sensitivity of the NH protons to the change in environment (hydrogen bond for instance) and the impact on their chemical shifts as a function of variations of relative concentrations of CDCl_3 and $\text{DMSO}-d_6$ in solvent mixture with a total concentration of 3.0 mmol. L^{-1} .^[11c] At this point, we can notice that for the five conformers of compounds **9a** and **9b**, while the chemical shifts of all the NH protons of Phe, *D*-Phe, and azaPhe are greatly sensitive to the addition of $\text{DMSO}-d_6$, the NH protons of the Ala residues are weakly affected (Figure 4.6).

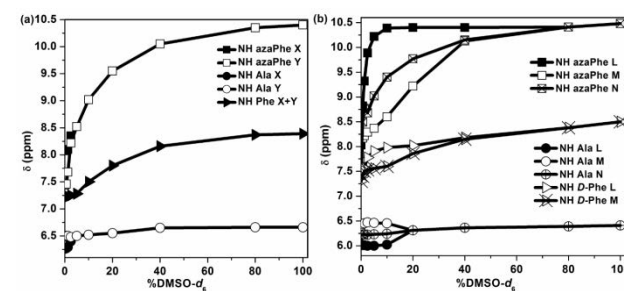


Figure 4.6. Chemical shift-variations (δ) of NH protons for: (a) **9a**, and (b) **9b** as a function of % [$\text{CDCl}_3/\text{DMSO}-d_6$, 3.0 mmol. L^{-1}] mixtures.

These results suggest that only the NH protons of Ala are involved in intramolecular hydrogen bonds, and this is consistent with the molecular dynamics calculations and X-ray results. Interestingly, increasing the percentage of $\text{DMSO}-d_6$ in solvent mixture led to the coalescence for the

Chapter IV. Impact of C α -Chirality on Supramolecular Self-Assembly in Cyclo-2:1-[α /aza]-Hexamers (*L*-/*D*-Phe-azaPhe-Ala)₂

signals of the conformers in both compounds (Appendix 2, Figure S11). This phenomenon has been also observed by Luis *et al.* who explained that the addition of polar solvent (*i.e.* methanol-*d*₄) into the solution of nonpolar solvent (*i.e.* CDCl₃) induces the rupture of the intramolecular hydrogen bonds and the formation of intermolecular hydrogen bonds with polar solvent molecules which leads to rapid equilibrium between the conformers resulting in coalescence of the signals.^[23]

To take the analysis one step further, concentration dependent NMR studies gave evidences on the formation of intermolecular hydrogen bonds. Generally, the chemical shift of NH proton involved in an intermolecular hydrogen bonding is sensitive to the change in concentration and then shows a shielding effect when decreasing concentration. In contrast, the variation of the concentration has no effect on the chemical shift of a NH proton involved in intramolecular hydrogen bond.^[24] ¹H NMR spectra were recorded at different concentrations: from 1.0 mmol. L⁻¹ to 8.0 mmol. L⁻¹ (solubility limit) for compound **9a** (Appendix 2, Figure S4.12a), and from 0.5 mmol. L⁻¹ to 10.0 mmol. L⁻¹ for compound **9b** (Appendix 2, Figure S4.12b). All the spectra were recorded at 278 K. For compound **3**, increasing the concentration from 1.0 to 4.0 mmol. L⁻¹ (Appendix 2, Figure S4.12a) leads to emergence of new signals (conformer **Z**). Moreover, the signals intensities increase (compared to conformers **X** and **Y**) when increasing the concentration (not all the signals of conformer **Z** were assigned due to overlapping with conformers **X** and **Y**). Furthermore, when increasing concentration from 4.0 mmol. L⁻¹ to 8.0 mmol. L⁻¹, the chemical shift of the NH protons of azaPhe residues in conformer **Z** shifts towards down field which indicates that these protons are involved in intermolecular hydrogen bonds.^[24] The chemical shift of the NH protons of Ala residues of this conformer remains unchanged and is located close to NH protons signals of Ala residues of conformers **X** and **Y** for which no shift is observed indicating their involvement in intramolecular hydrogen bonds.

For compound **9b**, increasing concentration (Appendix 2, Figure S4.12b) leads to a decrease of the intensities of most of the signals of the third conformer **N** which appears then as a minor conformer. Indeed, increasing concentration from 0.5 mmol. L⁻¹ to 10.0 mmol. L⁻¹, all NH protons of the minor conformer **N** are deshielded and their signals are loosely resolved. Regarding the conformer **L**, the chemical shifts of the NH protons of Ala and azaPhe residues do not show large change in their values suggesting that conformer **L** keeps the β I'-turn conformation (as observed in dilute conditions) with NH protons not perpendicular to the plane of the macrocycle which disadvantage the supramolecular organization.^[5b, e, 21b] In contrast to conformer **L**, the chemical shifts of the NH protons of *D*-Phe and azaPhe residues of conformer **M** are deshielded from 6.94 to 7.08 ppm and from 7.5 to 8.15 ppm respectively. Moreover, the NH protons of Ala residues, which are involved in intramolecular hydrogen bonds, are shielded from 6.41 to 6.19 ppm. We assume that some of intramolecular hydrogen bonds are broken when increasing the concentration to promote the formation of intermolecular bonds and the construction of supramolecular network (Appendix 2, Figure S4.12b). Finally, we have observed a shielding effect for the aromatic protons of the azaPhe residues of conformer **M** from 7.09 to 6.94 ppm suggesting the π - π stacking between the aromatic rings of two macrocycles.^[25]

2D ROESY spectrum of compound **9b** in CDCl₃ at 5.0 mmol. L⁻¹ (Appendix 2, Figure S4.13) has shown correlations between the NH protons of *D*-Phe residues and the β CH₂ of the azaPhe residues (conformer **M**) suggesting a β II'-turn conformation.^[12b, d] Based on ROESY experiments of compound **9b** at dilute and high concentrations, we can assume that the β II'-turn conformation for at least one conformer is not impacted by the formation of supramolecular

construction but there is an equilibrium between the monomeric state and supramolecular structure at high concentration.

Subsequently, we can summarize from 1D NMR experiments that: (i) conformer **L** adopts β I'-turn which does not support the formation of supramolecular structure^[5b, e, 21], (ii) conformer **M** adopts a β II'-turn conformation where the NH protons of the azaPhe, are perpendicular to the plan of the pseudopeptidic macrocycle. This conformation favors the formation of intermolecular hydrogen bonds with the CO groups of the *D*-Phe residues of another macrocycle facing to it.^[5b, e, 21]

Moreover, the concentration dependent NMR experiments reveal that increasing concentration leads to the deshielding of the NH protons of the azaPhe (conformer **Z**), and the deshielding of the NH protons of the *D*-Phe and azaPhe moieties (conformer **M**). As a consequence, the equilibrium between monomers and the supramolecular structure drifts to the latter which is stabilized by intermolecular hydrogen bonds. This result is in accordance with infrared results (next paragraphs) showing a decrease of the intensities of the free bands and an increase of the intensities of the bound bands when increasing concentration.

To complete this study, infrared spectroscopy (FTIR) analysis has been carried out for both compounds **9a** and **9b** at dilute condition (0.8 mmol. L⁻¹) to avoid the intermolecular interaction. We have focused our attention to the characteristic amide A, amide I and amide II domains that correspond to the CO and NH vibration regions. For compound **9a**, the NH stretching band around 3430 cm⁻¹ is characteristic of free NH amide (NH Phe and NH azaPhe), in addition to a broad band at 3343 cm⁻¹ which corresponds to the bound NH proton of Ala. Regarding the CO vibration region, four bands were observed and their assignments were based on previous results obtained from FTIR analysis of the corresponding linear precursors.^[11h] We observed that the CO of Ala is involved in an intramolecular hydrogen bond (characterized by a band at 1651 cm⁻¹), while the other CO groups are non-bound in dilute solution as assessed by their higher frequencies; 1717 cm⁻¹, 1699 cm⁻¹, and 1674 cm⁻¹, which correspond to the free CO of Phe, Ala and azaPhe residues, respectively (Figure 4.7a).

Similarly, spectrum of compound **9b** (0.8 mmol. L⁻¹) showed a band around 3402 cm⁻¹ in the stretching NH region which corresponds to a non-bound NH group (NH *D*-Phe and NH azaPhe), and a band around 3340 cm⁻¹ which corresponds to the bound NH proton of Ala. Regarding the CO vibration region, four bands were assigned as following: 1) the CO band of Ala involved in intramolecular hydrogen bond at 1651 cm⁻¹, 2) three other bands at higher wave numbers (1715 cm⁻¹, 1702 cm⁻¹, and 1674 cm⁻¹) correspond to the non-bound CO of *D*-Phe, Ala and azaPhe residues, respectively (Figure 4.7b). Experiments aiming the assignment of the four CO bands for each conformer using the 2nd derivative method were performed unsuccessfully. This can be explained by the FTIR time scale (10 – 100 fs) that is shorter than the conformational interconversion time.^[19b] Consequently, all the conformers of **9a** or **9b** have been detected simultaneously and they appeared as overlapped bands in infrared spectra. These FTIR studies are in agreement with the NMR studies in CDCl₃/DMSO-*d*₆ mixture.

Other experimental studies described in the literature indicate that not only the 1690 - 1660 cm⁻¹ region, but also the 1645 - 1635 cm⁻¹ region is characteristic for β -turn conformation in small peptides.^[26] Accordingly, 2nd derivative method was helpful to confirm the presence of a band at 1635 cm⁻¹ and 1637 cm⁻¹ correspond to the intramolecular hydrogen bonds in compounds **9a** and **9b**, respectively (Appendix 2, Figure S14a, b).

Part A

Chapter IV. Impact of C $^{\alpha}$ -Chirality on Supramolecular Self-Assembly in Cyclo-2:1-[α /aza]-Hexamers (*L*-/*D*-Phe-azaPhe-Ala) $_2$

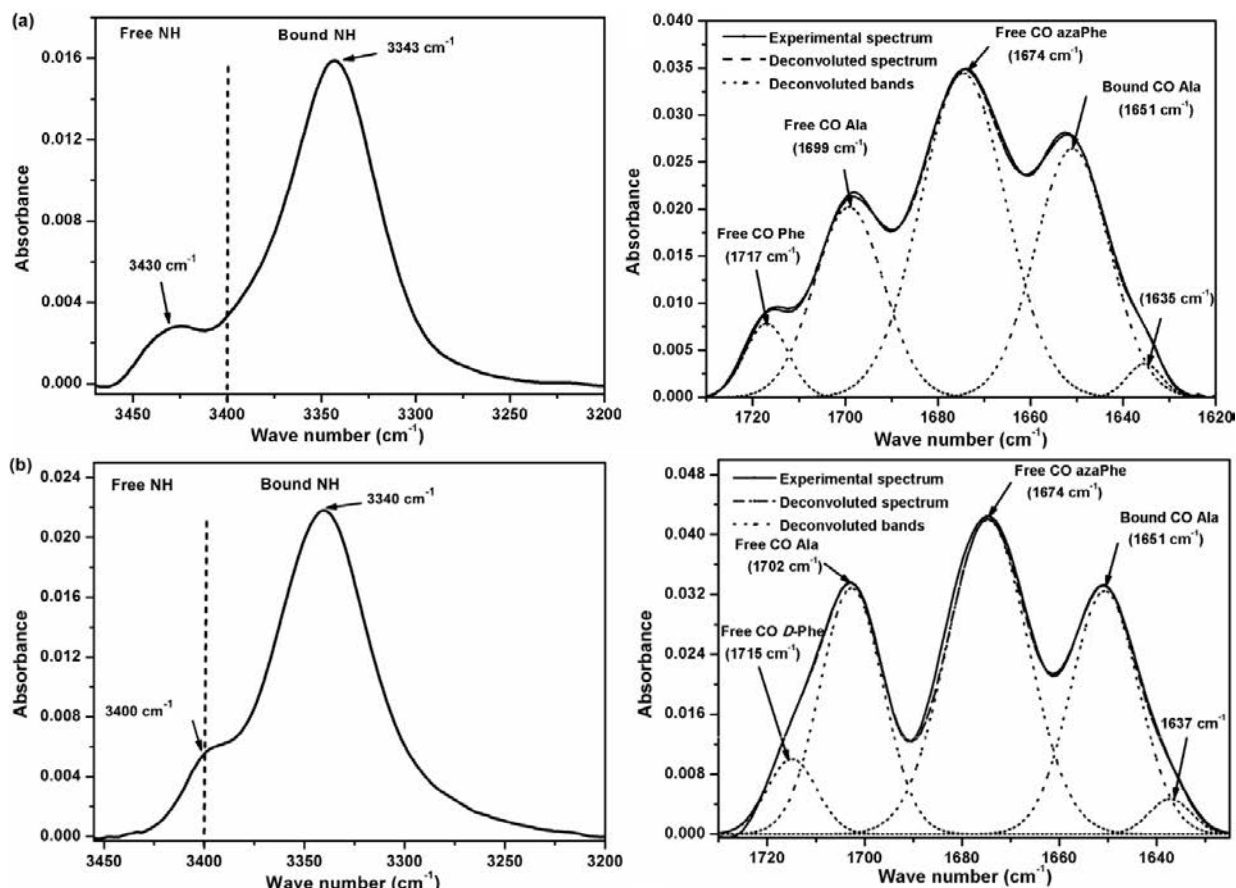


Figure 4.7. FTIR spectra belong to the NH stretching region (left spectra), and CO stretching region (right spectra) for: (a) **9a**, and (b) **9b**; (0.8 mmol. L $^{-1}$, CDCl $_3$).

From these results, we can conclude that at least one of the two conformers in case of compound **9a** or one of the three conformers in case of compound **9b** induces a β -turn conformation which is in agreement with the NMR results.

To complete the comparison with NMR experiments, FTIR spectra were also recorded at different concentrations ranged from 1.0 mmol. L $^{-1}$ to 8.0 mmol. L $^{-1}$ for compounds **9a** and **9b** (Figure 4.8). For compound **9a**, the variation of the concentration does not affect the band located at 3430 cm $^{-1}$ corresponding to the free NH protons of Phe and azaPhe (Figure 4.8a). In contrast, the intensities of the signals of the NH protons of *D*-Phe and azaPhe of compound **9b** (3402 cm $^{-1}$) decrease when increasing concentration. Unexpectedly, the intensities of the bands corresponding to

bound NH protons of Ala residues in compound **9a** (3343 cm $^{-1}$), and compound **9b** (3339 cm $^{-1}$) decrease when increasing concentrations (Figure 4.8). Interestingly, new bands (3165 - 3185 cm $^{-1}$) and (3270 - 3230 cm $^{-1}$) in strongly bound NH region were noticed in the spectra of compounds **9a** and **9b** (Figure 4.8) and their intensities increase with increasing concentration. These bands may be assigned to the intermolecular hydrogen bonds formed at high concentration.

In conclusion, the results obtained from FTIR experiments are consistent with NMR results, and confirm at high concentrations the self-assembly processes are stabilized by intermolecular hydrogen bonds of both compounds **9a** and **9b**. These intermolecular interactions are established to the detriment of the intramolecular hydrogen bonds which stabilize the monomeric form.

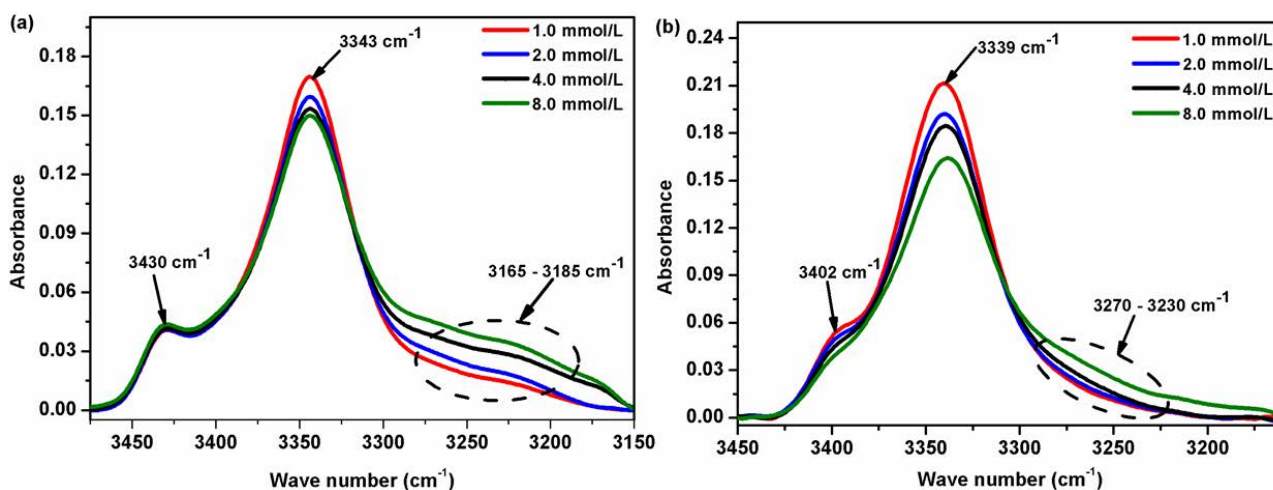


Figure 4.8. Normalized concentration-dependent FTIR spectra for NH stretching region of: (a) **9a**, and (b) **9b**; (1.0 to 8.0 mmol. L $^{-1}$, CDCl $_3$).

Chapter IV. Impact of C^α-Chirality on Supramolecular Self-Assembly in Cyclo-2:1-[α /aza]-Hexamers (*L*-/*D*-Phe-azaPhe-Ala)₂

IV.3. Conclusions

General strategy for the synthesis of new mixed cyclic 2:1-[α /aza]-oligomers has been investigated in this work which is considered one of few works concerning the structural and conformational studies of cyclic azapeptides in solution and solid states. X-ray, FTIR, and NMR studies showed the ability of **9a** and **9b** to adopt β -turn conformation of the type (*i*+3) closing a pseudocycle of 10 atoms and the conformation is stabilized not only by intramolecular hydrogen bonds, but also through π - π stacking interactions within the same macrocycle. In addition, our study shows the ability of both compounds **9a** and **9b** to self-assemble into highly organized 3D structures when increasing the concentration. The supramolecular structure is stabilized by several intermolecular hydrogen bonds between the amide groups of the macrocyclic subunits. Finally, the study gives the evidences of the self-assembling process which can be used further to design new self-assembled pseudopeptidic soft materials in the coming work.

IV.4. Experimental Section

Unless otherwise stated, all chemicals and reagents were purchased from commercial suppliers (Sigma-Aldrich, Merck or Alfa-Aesar). Dry CH₂Cl₂ was obtained by distillation over P₂O₅ under an argon atmosphere, MeOH was purchased in anhydrous form, and other reagent-grade solvents were used without further purification as received.

Reactions were monitored by thin layer chromatography (TLC) using aluminum-backed silica gel plates. TLC spots were viewed under UV light or/and by heating the plate after treatment with a staining solution of phosphomolybdic acid. Flash chromatography was carried out on silica gel 60 (0.04 – 0.063 μ m Mesh ASTM). All yields were calculated from pure isolated products. 1D (¹H, ¹³C) and 2D ROESY NMR spectra were recorded using a Bruker Advance NMR spectrophotometer at 300 MHz (300 K, for the characterization of compounds) or 600 MHz (253 K, or 278 K, for the structural studies) in CDCl₃ or DMSO-*d*₆ as solvents. The chemical shifts were reported in ppm (δ) relative to tetramethylsilane (TMS) served as an internal standard (δ = 0 ppm) for ¹H NMR, while CDCl₃ (δ = 77.0 ppm) or DMSO-*d*₆ (δ = 39.5 ppm), was used as an internal standard for ¹³C NMR. Multiplicities are reported as follows: s = singlet, d = doublet, q = quartet, m = multiplet, br = broad, arom = aromatic. IR spectra were recorded with Bruker Tensor 27 over 256 scans and referenced to the residual solvent resonances. Electron spray ionization mass spectra (ESI-MS) were recorded with a Bruker MicroTof-Q HR spectrometer in the "Service commun de Spectrométrie de Masse", Faculté des Sciences et Technologies, Vandoeuvre-lès-Nancy, France. All melting points (mp) were uncorrected.

GENERAL METHYL ESTER DEPROTECTION PROCEDURE

To a solution of methyl ester-protected **8a** or **8b** (1.0 equiv., 2.3 mmol.) in CH₃CN (20 mL), a solution of 1M NaOH (2.0 equiv., 4.6 mmol.) was added at 0 °C. The mixture was vigorously stirred for 6 – 8h at room temperature until reaction completion (as monitored by TLC). The aqueous phase was cooled to 0 °C and acidified with 2M HCl to pH 2 and extracted with CH₂Cl₂ (3 \times 10 mL). The combined organic layers were dried over MgSO₄, filtered, and evaporated under vacuum to give quantitatively the corresponding carboxylic acid which was used in the next step without further purification.

GENERAL BOC DEPROTECTION AND MACROCYCLIZATION PROCEDURES

To a stirred solution of Boc-protected compound from the previous step (1.0 equiv., 2.2 mmol.) in DCM, a TFA/DCM mixture (40/60 v:v) was added and the mixture was stirred overnight without any control by TLC. The solution was concentrated under vacuum, and the excess of TFA was co-evaporated with toluene (3 times), Et₂O (3 times) and DCM (2 times), affording the corresponding trifluoroacetate salt compound as a white foam in quantitative yield.

The crude residue (1.0 equiv., 2.0 mmol.) was dissolved in DCM, and DIPEA was added (4.0 equiv., 8.0 mmol.). The solution

was added dropwise into a solution of HOBT (1.1 equiv., 2.2 mmol.) and EDC.HCl (1.1 equiv., 2.2 mmol.) in DCM (the concentration was almost 0.5 mmol. L⁻¹ in the mixture). This slow addition was run during 7h, and then the reaction mixture was stirred at room temperature under nitrogen for 48 h. The volume was reduced to around 100 mL, and the solution was washed successively with 1M HCl (2 \times 20 mL), saturated NaHCO₃ (2 \times 20 mL), H₂O (2 \times 20mL), brine (2 \times 20 mL). The organic layer was dried over MgSO₄ and evaporated under vacuum and the resulting crude material was purified to give the corresponding cyclic product **9a** or **9b** as a white solid.

Homochiral Cyclohexamer [*L*-Phenylalanine-azaPhenylalanine-*L*-Alanine]₂ (**9a**).

Cyclo-(*L*-Phe-azaPhe-*L*-Ala)₂ **9a** was isolated as white powder (510 mg, yield 35%) after flash chromatography (0.04 – 0.063 μ m) using (96% CH₂Cl₂ : 4% MeOH) as eluent. Characterization data: m.p. 211 – 212 °C. ¹H NMR (300 MHz, DMSO-*d*₆, 5.0 mmol. L⁻¹) δ _H 1.17 and 1.19 (d, 6H, 2 \times CH₃), 2.90 – 2.93 (m, 4H, 2 \times CH₂), 3.50 (d, 2H, 2 \times NCH₂), 4.10 – 4.14 (m, 2H, 2 \times CH), 4.32 (m, 2H, 2 \times CH), 4.91 (d, 2H, 2 \times NCH₂), 6.63 (br s, 2H, 2 \times NH), 6.98 – 7.25 (m, 20H, H arom Ph), 8.33 (br s, 2H, 2 \times NH), 10.33 (br s, 2H, 2 \times NH). ¹³C NMR (75 MHz, DMSO-*d*₆, 8.0 mmol. L⁻¹) δ _C 19.75 (CH₃), 35.59 (CH₂) 48.75 (CH), 51.38 (NCH₂), 53.28 (CH), 126.48, 127.91, 128.01, 128.17 and 129.14 (CH arom Ph), 136.73 and 138.10 (C arom Ph), 156.41 (O=C-NH), 170.07 (O=C-NH), 171.76 (O=C-NH). IR (CDCl₃) $\tilde{\nu}$ _{max} = 3343 cm⁻¹, 3430 cm⁻¹ (NH), 1652 cm⁻¹, 1674 cm⁻¹, 1698 cm⁻¹, 1716 cm⁻¹ (C=O). HRMS (ESI) (m/z) for [C₄₀H₄₄N₈O₆Na]: calculated 755.3384; found, 755.3349 [M + Na]⁺.

Heterochiral Cyclohexamer [*D*-Phenylalanine-azaPhenylalanine-*L*-Alanine]₂ (**9b**).

Cyclo-(*D*-Phe-azaPhe-*L*-Ala)₂ **9b** was isolated as white powder (525 mg, yield 36%) after flash chromatography (0.04 – 0.063 μ m) using (98% CH₂Cl₂ : 2% MeOH) as eluent. Characterization data: m.p. 220 – 221 °C; ¹H NMR (300 MHz, DMSO-*d*₆, 5.0 mmol. L⁻¹) δ _H 1.10 and 1.12 (d, 6H, 2 \times CH₃), 2.71 – 2.87 (m, 4H, 2 \times CH₂), 3.61 and 3.66 (d, 2H, NCH₂), 4.18 – 4.25 (m, 4H, 4 \times CH) 4.86 and 4.91 (d, 2H, NCH₂), 6.36 (br d, 2H, 2 \times NH), 6.98 – 7.21 (m, 20H, H arom Ph), 8.48 (br s, 2H, 2 \times NH), 10.40 (br s, 2H, 2 \times NH). ¹³C NMR (75 MHz, DMSO-*d*₆, 8.0 mmol. L⁻¹) δ _C 20.05 (CH₃), 36.14 (CH₂) 49.21 (CH), 51.18 (NCH₂), 52.92 (CH) 126.51, 126.82, 127.95, 128.15 and 129.01 (CH arom Ph), 136.62 and 137.74 (C arom Ph), 156.05 (O=C-NH), 170.38(O=C-NH), 171.97 (O=C-NH). IR (CDCl₃) $\tilde{\nu}$ _{max} = 3340 cm⁻¹, 3400 cm⁻¹ (NH), 1651 cm⁻¹, 1674 cm⁻¹, 1702 cm⁻¹, 1716 cm⁻¹ (C=O). HRMS (ESI) (m/z) for [C₄₀H₄₄N₈O₆Na]: calculated 755.3384; found, 755.3283 [M + Na]⁺.

IV.5. Acknowledgements

The authors thank Emmanuel Wenger from Laboratoire de Cristallographie, Résonance Magnétique et Modélisations (CRM2), Université de Lorraine. Thanks to X-ray facilities and NMR facilities, Faculté des Sciences et Technologies, Université de Lorraine.

Keywords: Cyclic pseudopeptides • azapeptides • β -turn • Supramolecular self-assembly • Chirality

IV.6. References

- [1] Z. Zhou in *Thesis: Synthèse et études structurales de nouveaux [a/aza]-oligomères et cyclooligomères, vers de nouveaux foldamères*, Vol. LCPM-Lorraine University, 2014.
- [2] a) K. Moteshareh and M. R. Ghadiri, *J. Am. Chem. Soc.* **1997**, *119*, 11306-11312; b) S. Fernandez-Lopez, H.-S. Kim, E. C. Choi, M. Delgado, J. R. Granja, A. Khasanov, K. Kraehenbuehl, G. Long, D. A. Weinberger, K. M. Wilcoxon and M. R. Ghadiri, *Nature* **2001**, *412*, 452-456; c) Walsh and Wright, *Chem. Rev.* **2005**, *105*, 391-394; d) J. R. Granja and M. R. Ghadiri, *J. Am. Chem. Soc.* **1994**, *116*, 10785-10786; e) J. Sánchez-Quesada, H. Sun Kim and M. R. Ghadiri, *Angew. Chem., Int. Ed.* **2001**, *113*, 2571-2574; f) J. Couet, J. D. J. S. Samuel, A. Kopyshhev, S. Santer and M. Biesalski, *Angew. Chem., Int. Ed.* **2005**, *44*, 3297-

Part A

Chapter IV. Impact of C^α-Chirality on Supramolecular Self-Assembly in Cyclo-2:1-[α /aza]-Hexamers (*L*-/*D*-Phe-azaPhe-Ala)₂

- 3301; g) T. D. Clark, L. K. Buehler and M. R. Ghadiri, *J. Am. Chem. Soc.* **1998**, *120*, 651-656.
- [3] a) D. P. Fairlie, J. D. A. Tyndall, R. C. Reid, A. K. Wong, G. Abbenante, M. J. Scanlon, D. R. March, D. A. Bergman, C. L. L. Chai and B. A. Burkett, *J. Med. Chem.* **2000**, *43*, 1271-1281; b) A. Giannis and T. Kolter, *Angew. Chem., Int. Ed.* **1993**, *32*, 1244-1267.
- [4] a) R. L. A. Dias, R. Fasan, K. Moehle, A. Renard, D. Obrecht and J. A. Robinson, *J. Am. Chem. Soc.* **2006**, *128*, 2726-2732; b) L. K. Henchey, J. R. Porter, I. Ghosh and P. S. Arora, *Chem. Bio. Chem.* **2010**, *11*, 2104-2107.
- [5] a) P. De Santis, S. Morosetti and R. Rizzo, *Macromolecules* **1974**, *7*, 52-58; b) M. R. Ghadiri, J. R. Granja, R. A. Milligan, D. E. McRee and N. Khazanovich, *Nature* **1993**, *366*, 324-327; c) C. H. Hassall, *Chem. Biol. Pept., Proc. 3rd Am. Pept. Symp.* **1972**, 153-157; d) I. L. Karle, B. K. Handa and C. H. Hassall, *Acta Crystallogr., Sect. B* **1975**, *31*, 555-560; e) J. Montenegro, M. R. Ghadiri and J. R. Granja, *Acc. Chem. Res.* **2013**, *46*, 2955-2965.
- [6] M. R. Ghadiri, K. Kobayashi, J. R. Granja, R. K. Chadha and D. E. McRee, *Angew. Chem., Int. Ed.* **1995**, *34*, 93-95.
- [7] L. S. Shimizu, M. D. Smith, A. D. Hughes and K. D. Shimizu, *Chem. Commun.* **2001**, 1592-1593.
- [8] a) D. Seebach, J. L. Matthews, A. Meden, T. Wessels, C. Baerlocher and L. B. McCusker, *Helv. Chim. Acta* **1997**, *80*, 173-182; b) F. Fujimura, T. Hirata, T. Morita, S. Kimura, Y. Horikawa and J. Sugiyama, *Biomacromolecules* **2006**, *7*, 2394-2400; c) K. Gademann, M. Ernst, D. Hoyer and D. Seebach, *Angew. Chem., Int. Ed.* **1999**, *38*, 1223-1226; d) B. Jagannadh, M. S. Reddy, C. L. Rao, A. Prabhakar, B. Jagadeesh and S. Chandrasekhar, *Chem. Commun.* **2006**, 4847-4849.
- [9] D. Gauthier, P. Baillargeon, M. Drouin and Y. L. Dory, *Angew. Chem., Int. Ed.* **2001**, *40*, 4635-4638.
- [10] a) V. Semetey, C. Didierjean, J.-P. Briand, A. Aubry and G. Guichard, *Angew. Chem., Int. Ed.* **2002**, *41*, 1895-1898; b) L. Fischer, M. Decossas, J.-P. Briand, C. Didierjean and G. Guichard, *Angew. Chem., Int. Ed.* **2009**, *48*, 1625-1628.
- [11] a) R. Günther and H.-J. Hofmann, *J. Am. Chem. Soc.* **2001**, *123*, 247-255; b) M. Marraud, V. Dupont, V. Grand, S. Zerkout, A. Lecoq, G. Boussard, J. Vidal, A. Collet and A. Aubry, *Biopolymers* **1993**, *33*, 1135-1148; c) Z. Benatalah, A. Aubry, G. Boussard and M. Marraud, *Int. J. Protein Res.* **1991**, *38*, 603-605; d) M. Marraud and A. Aubry, *Biopolymers* **1996**, *40*, 45-83; e) F. André, A. Vicherat, G. Boussard, A. Aubry and M. Marraud, *J. Pept. Res.* **1997**, *50*, 372-381; f) A. Zega and U. Urleb, *Acta Chim. Slov.* **2002**, *49*, 649-662; g) G. Lelais and D. Seebach, *Helv. Chim. Acta* **2003**, *86*, 4152-4168; h) Z. Zhou, C. Deng, C. Abbas, C. Didierjean, M. C. Averlant-Petit, J. Bodiguel, R. Vanderesse and B. Jamart-Gregoire, *Eur. J. Org. Chem.* **2014**, 7643-7650; i) R. O. Moussodia, S. Acherar, E. Romero, C. Didierjean and B. Jamart-Gregoire, *J. Org. Chem.* **2015**, *80*, 3022-3029.
- [12] a) H. J. Lee, K. H. Choi, I. A. Ahn, S. Ro, H. G. Jang, Y. S. Choi and K. B. Lee, *J. Mol. Struct. (Theochem)* **2001**, *569*, 43-54; b) M. Thormann and H. J. Hofmann, *J. Mol. Struct. (Theochem)* **1999**, *469*, 63-76; c) H. J. Lee, K. B. Lee, I. A. Ahn, S. Ro, K. H. Choi, Y. S. Choi and K. B. Lee, *J. Pept. Res.* **2000**, *56*, 35-46; d) H. J. Lee, H. M. Park and K. B. Lee, *Biophys. Chem.* **2007**, *125*, 117-126.
- [13] M. Zouikri, A. Vicherat, A. Aubry, M. Marraud and G. Boussard, *J. Pept. Res.* **1998**, *52*, 19-26.
- [14] a) A. Lecoq, G. Boussard, M. Marraud and A. Aubry, *Biopolymers* **1993**, *33*, 1051-1059; b) J. Gante, M. Krug, G. Lauterbach, R. Weitzel and W. J. Hiller, *J. Pept. Sci.* **1995**, *2*, 201-206; c) F. André, G. Boussard, D. Bayeul, C. Didierjean, A. Aubry and M. Marraud, *J. Pept. Res.* **1997**, *49*, 556-562.
- [15] a) R. E. Melendez and W. D. Lubell, *J. Am. Chem. Soc.* **2004**, *126*, 6759-6764; b) D. Boeglin and W. D. J. Lubell, *Comb. Chem.* **2005**, *7*, 864-878; c) D. Boeglin, Z. Xiang, N. B. Sorenson, M. S. Wood, C. HaskellLuevano and W. D. Lubell, *Chem. Biol. Drug Des.* **2006**, *67*, 275-283; d) D. Sabatino, C. Proulx, S. Klocek, C. B. Bourguet, D. Boeglin, H. Ong and W. D. Lubell, *Org. Lett.* **2009**, *11*, 3650-3653; e) N. S. Freeman, Y. Tal-Gan, S. Klein, A. Levitzki and C. Gilon, *J. Org. Chem.* **2011**, *76*, 3078-3085; f) D. Sabatino, C. Proulx, P. Pohankova, H. Ong and W. D. Lubell, *J. Am. Chem. Soc.* **2011**, *133*, 12493-12506.
- [16] a) H. Dyker, J. Scherkenbeck, D. Gondol, A. Goehrt and A. Harder, *J. Org. Chem.* **2001**, *66*, 3760-3766; b) S. L. Goodman, G. Hölzemann, G. A. G. Sulyok and H. Kessler, *J. Med. Chem.* **2002**, *45*, 1045-1051.
- [17] P. Le Grel, A. Salaün, M. Potel, B. Le Grel and F. Lassagne, *J. Org. Chem.* **2006**, *71*, 5638-5645.
- [18] a) G. A. Jeffrey in *Review of hydrogen bonding: An Introduction to Hydrogen Bonding, Vol.* New York, Oxford University Press, **1997**; b) W. S. Horne, C. D. Stout and M. R. Ghadiri, *J. Am. Chem. Soc.* **2003**, *125*, 9372-9376.
- [19] a) G. Némethy and H. A. Scheraga, *Biochem. Biophys. Res. Commun.* **1980**, *95*, 320-327; b) H. H. Mantsch, A. Perczel, M. Hollósi and G. D. Fasman, *Biopolymers* **1993**, *33*, 201-207.
- [20] a) A. Aubry, D. Bayeul, J. Mangeot, J. Vidal, S. Sterin, A. Collet, A. Lecoq and M. Marraud, *Biopolymers* **1991**, *31*, 793-801; b) A. Lecoq, M. Marraud and A. Aubry, *Tetrahedron Lett.* **1991**, *32*, 2765-2768.
- [21] a) D. C. Thomas, K. B. Lukas and M. Reza Ghadir, *J. Am. Chem. Soc.* **1998**, *120*, 651-656; b) K. Rosenthal-Aizman, G. Svensson and A. Unden, *J. Am. Chem. Soc.* **2004**, *126*, 3372-3373.
- [22] T. A. D. Case, T. E. Cheatham III, C. L. Simmerling, J. Wang, R. E. Duke, R. Luo, M. Crowley, R. C. Walker, W. Zhang, K. M. Merz, B. Wang, S. Hayik, A. Roitberg, G. Seabra, I. Kolossváry, K. F. Wong, F. Paesani, J. Vanicek, X. Wu, S. R. Brozell, T. Steinbrecher, H. Gohlke, L. Yang, C. Tan, J. Mongan, V. Hornak, G. Cui, D. H. Mathews, M. G. Seetin, C. Sagui, V. Babin and P. A. Kollman, *AMBER 10* **2008**, University of California, San Francisco.
- [23] I. Alfonso, M. I. Burguete and S. V. Luis, *J. Org. Chem.* **2006**, *71*, 2242-2250.
- [24] A. Salaün, A. Favre, B. Le Grel, M. Potel and P. Le Grel, *J. Org. Chem.* **2006**, *71*, 150-158.
- [25] F. Allix, P. Curcio, Q. N. Pham, G. Pickaert and B. Jamart-Grégoire, *Langmuir* **2010**, *26*, 16818-16827.
- [26] E. Vass, M. Kurz, R. K. Konat and M. Hollósi, *Spectrochim. Acta. A. Mol. Biomol. Spectrosc.* **1998**, *54*, 773-786.

Part B
**2:1-[α /aza]-Oligomers as Low Molecular Weight
Gelators**

Chapter V. Bibliography of Gels and Low Molecular Weight Organo-/Hydro-Gelators

V.1. General Introduction

Molecular self-assembly is a fascinating process for the design of new supramolecular hierarchical structures. In certain cases, the self-assembly process leads to molecular gels, which has become an area of great interest in the field of supramolecular chemistry.¹ Gels are composed of a 3D network where organic (organogel)² or aqueous (hydrogel)³ solvent molecules are trapped.¹ First gels were obtained from polymers and during the last two decades authors have reported molecular gels obtained from low molecular weight gelators (LMWGs) (M.wt > 2000 Da).⁴⁻⁷ LMWGs have attracted much interest due to their practical implications as new soft materials and their extensive potential applications in a wide range of fields, such as solar cells,^{8,9} production of new semiconductors,¹⁰⁻¹² biomedical engineering and tissue engineering as anti-inflammatory agents, drug delivery matrices for topical and oral pharmaceuticals,¹³ as well as LMWGs have provided high efficiency in the biphasic selective gelation and waste water treatment processes.¹⁴⁻²¹

Recently, it was estimated that over than 1000 low molecular weight gelators have been reported.²² Although the large structural diversity within LMWGs, they have a common feature that they gelate solvent molecules through self-assembly phenomenon by a combination of non-covalent interactions such as electrostatic, charge-transfer, dipole-dipole, hydrogen bonding, hydrophobic, π - π stacking, van der Waals interactions and hydrophilic/lipophilic balance.²³⁻²⁷ Additionally, gelation is triggered by different external stimuli such as temperature,^{2,28-32} pH change,^{5,33-38} light,³⁹⁻⁴¹ ultrasound,^{42,43} ions,^{44,45} enzymes,^{46,47} *etc.*, which are generally used to manipulate the structure and function of the gel. Several reviews describing various systems of LMWGs have been published, including hydrocarbons, fatty acids, saccharides, steroids, amides, amino acids, peptides, ureas, aromatic molecules, metal complexes and dendrimers.^{2,3,16,32,48-52}

More recently, LMWGs form pseudopeptides or their cyclic analogs have got greater advantages as they can be easily synthesized, multiple responsive, control over their physical and chemical properties. A brief overview on low molecular weight organogelators (LMWOGs) and low molecular weight hydrogelators (LMWHGs) will be overviewed in this chapter describing the various types of LMWGs and the interactions that drive the self-assembly and gel formation.

V.2. Review of Literature

V.2.1. Definition of Gel and Mechanism of Gelation

Many attempts have been evolved over more than 150 years to have a descriptive definition for a “Gel” in a few words but the definition is still somehow illegible scientifically.

Lipowitz was one of the pioneers who has recognized the formation of gel from aqueous solutions of lithium urate in 1841.⁵³ In 1861 Thomas Graham⁵⁴ stated the following loose description: “While the rigidity of the crystalline structure shuts out external expressions, the softness of the gelatinous colloid partakes of fluidity, and enables the colloid to become a medium for liquid diffusion, like water itself”.

In 1926 Dorothy Jordon Lloyd⁵⁵ stated that the gel is colloid system which is easier to recognize than to define and settled the following statement: “Only one rule seems to hold for all gels which is, they must be built up from two components, one of which is a liquid at the temperature under consideration, and the other which is a solid; the gelling substance (gelator). The gel itself has the mechanical properties of a solid, *i.e.* it can maintain its form under the stress of its own weight, and under any mechanical stress it shows the phenomenon of strain”.

Part B

Chapter V. Bibliography of Gels and Low Molecular Weight Organo-/Hydro-Gelators

The previous exclusive definition did not recognize that not all colloids are gels and not all the gels are colloids.⁵⁶ So, by 1949, Hermans⁵⁷ described the gel system as “(i) Gels are coherent colloid dispersed systems of at least two components, (ii) they exhibit mechanical properties characteristic of the solid state, and (iii) both the dispersed component and the dispersion medium extend themselves continuously throughout the whole system.”

Later, Ferry avoided using a detailed definition, so he offered a more descriptive one: “A gel is a substantially diluted system which exhibits no steady state flow”.⁵⁸

Recently, Weiss⁴⁹ and Terech gave general criteria to classify a substance as a gel if it: (i) has a continuous microscopic structure with macroscopic dimensions that is permanent on the time scale of an analytical experiment and (ii) is solid-like in its rheological behavior despite being mostly liquid.

Macroscopically and for the screening purposes, the definition of Lloyd is still practical: if it looks like a "Jell-O", it must be a gel.⁵⁵

When a mixed solution (solvent and gelator molecules) is triggered by external stimuli, the molecules start to condense and three situations are possible: (i) crystallization with a highly ordered crystals aggregation, (ii) a random aggregation resulting in an amorphous precipitate, or (iii) gelation which is an intermediate aggregation process between the first two processes.

Gelation is a phenomenon which reflects the ability of gelator molecules to organize into highly ordered hierarchical structures including tubes, rods, ribbons, fibrils, *etc.* Once formed, these nanostructures undergo further entanglement, bundling and crosslinking that lead to the formation of three-dimensional interconnected network structures entrapping and immobilizing the solvent phase within the interstices of the self-assembled matrix to give what is recognized at the macroscopic level as gel, Figure 5.1.^{15,59-61} The process of self-assembled gelation is driven by different kinds of intermolecular forces either chemical and/or physical interactions between gelator molecules themselves or between gelator and solvent molecules in which the attractive and repulsive forces are so balanced.⁶²

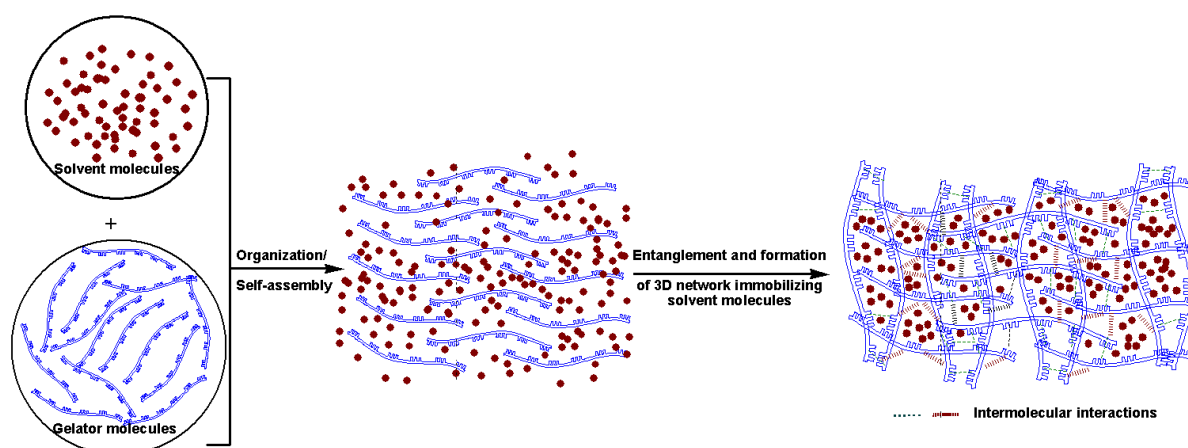


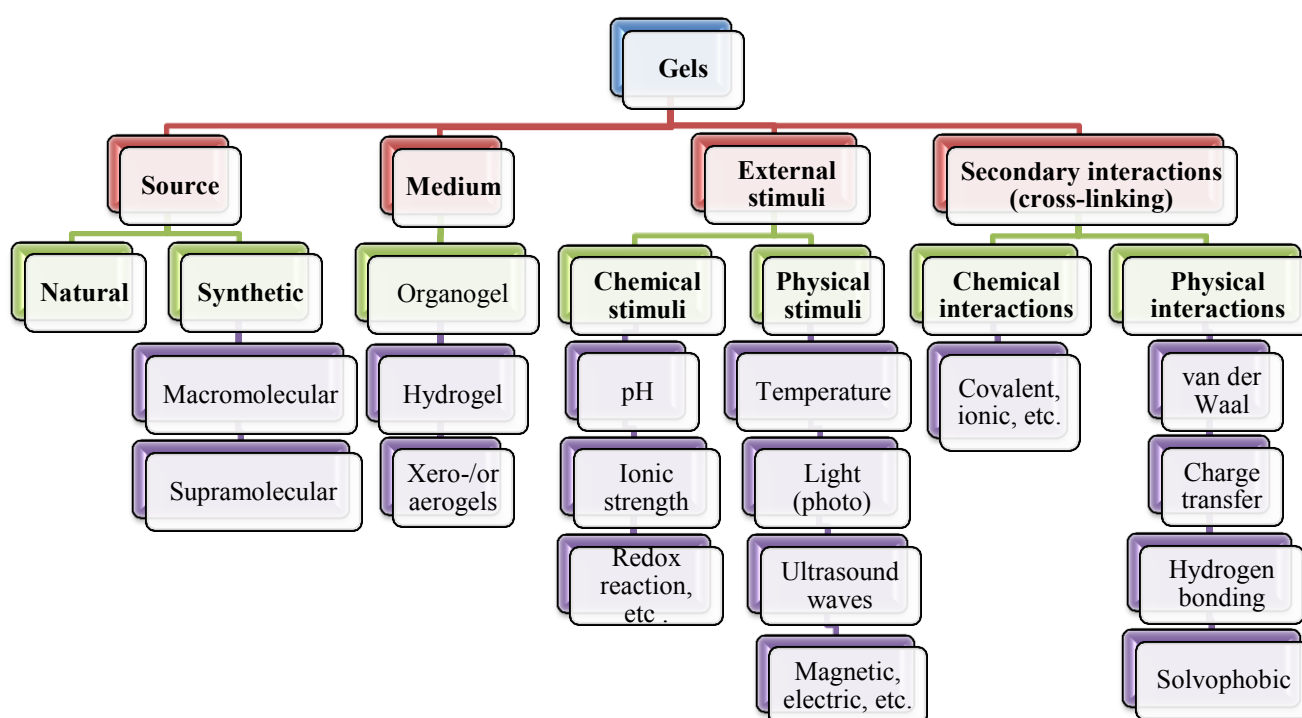
Figure 5.1. Schematic illustration of the gelation process.

In other words, gelation can be considered as the equilibrium state between solubility and phase separation (precipitation) at which balance between the intermolecular attractive and repulsive forces is achieved.^{51,62}

Nowadays, the discovery of gelators remains serendipitous. The major challenge in the rational design and synthesis of new gelator molecules is to understand the relative contributions that are required by the various intermolecular interactions to achieve gelation and how the solvent itself affects these contributions.^{63,64}

V.2.2. Classification of Gels

Gels can be classified in several ways based on their origin (natural or synthetic), constitution (macromolecular or molecular), the type of cross-linking that creates their 3D network (chemical or physical) and the medium they entrap [(organogels ---< organic media), (hydrogels ---< aqueous media), and (xero- and aerogels ---< no medium)], Scheme 5.1.^{50,65}



Scheme 5.1. Classification of gels.

V.2.2.1. Classification Based on the Source (Origin)

V.2.2.1.1. Natural Gels

Most of the naturally occurring gelators like gelatin, collagen, agar and starch are macromolecular compounds and they form gels by physical cross-linking mainly hydrogen bonding interactions.⁶⁶

V.2.2.1.2. Synthetic (Artificial) Gels

They can be subcategorized based on their constitution into:

(i) Macromolecular gels (polymer): traditionally, gels were synthesized from long chain polymers (macromolecular compounds) having a large hydrodynamic radius, which upon external stimuli (*e.g.*, cooling, pH change, *etc.*), they can immobilize large volume of solvent molecules in their three dimensional network. This 3D network is formed from the interaction/entanglement of the long chains with themselves, either through chemical (covalent) cross-linking or physical interactions (*e.g.*, polyester, polyamide, polyacrylate, *etc.*).⁶⁷

Part B

Chapter V. Bibliography of Gels and Low Molecular Weight Organo-/Hydro-Gelators

(ii) **Molecular or supramolecular gels:** during the past decade, a new form of gel has been gained remarkable interest instead of polymers, where the new soft materials are now generated from low molecular weight monomers. These supramolecular gels are formed through self-organization of the small gelator molecules to form entangled Self-Assembled Fibrillar Networks (SAFINs) through a combination of non-covalent physical interactions, entrapping the solvent molecules within the pores and spaces of the networks. 12-hydroxystearic acid,²⁸ bisamide- and bisurea-cyclohexyl based gelators,⁶⁴ Fmoc-functionalized *L*-lysine amino acids,¹ and 1:1-[α/α -*N* ^{α} -Bn-hydrazino]-mers series³⁰, are examples of this gel category.

Accordingly, supramolecular gelation process might be distinguished into six steps:^{51,68} (i) dimerization of two individual molecules, (ii) oligomer formation by interaction of dimers with further molecules, (iii) formation of fibrils of approximately the same width as the molecular building blocks (*ca.* 1 - 2 nm) by extension of the oligomers, (iv) fiber formation by bundling of fibrils (*ca.* 20 - 50 nm width), (v) interactions of fibers to give an effectively infinite, interconnected network (matrix) spanning the entire sample, and (vi) immobilization of the solvent by the fiber network, generally by surface tension effects.

V.2.2.2. Classification Based on Medium of Gelation

Gels can be classified based on the medium entrapped within the interconnected fibers network into: (i) **hydrogels:** gels obtained from aqueous media,³ (ii) **organogels:** are formed when the gelified medium is organic solvents² like hexane, toluene, *etc.*, and (iii) **aero-/xerogels:** there is no medium at all in both xerogels and aerogels. These gels are resulted from drying the hydro- and/or organogels using sophisticated techniques in order to study the morphology of the 3D network of the gels by removing the solvent effects, (usually drying occurs by supercritical CO₂ or slow air evaporation to obtain aero- or xerogels, respectively).^{69,70}

V.2.2.3. Classification Based on the External Stimuli for Gelation

Gels can also be classified into different categories depending on their fascinating property that they can exert upon exposure to either physical stimuli (*e.g.*, temperature, applying ultrasound, *etc.*) or chemical stimuli (*e.g.*, pH change, chemical or photochemical reactions, *etc.*).^{49,52} Some of these interesting categories are mentioned briefly in the following sections.

V.2.2.3.1. Thermo-Responsive Gels

Thermo-responsive gels are the most commonly studied class of stimuli-responsive for both hydro- and organogels systems,^{71,72} in which gels exhibit the (gel-to-sol) transition phenomenon reversibly by the influence of temperature. A unique property of temperature-responsive gels is the presence of a critical gelation temperature (T_g), which is the temperature at which the gel-to-sol phase transition occurs.⁷² Gelation temperature can be determined by multiple methods, including the “dropping ball” experiment,^{3,69,73} differential scanning calorimetry (DSC), spectroscopic techniques, and rheological measurements.⁷³ Many examples are related to this gel category such as polyacrylamide hydrogels,⁷⁴ polyurethane,⁷⁵ *L*-phenylalanine-dihydrazide derivatives,⁷⁶ cyclic dipeptides (diketopiperazines-DKPs),⁷⁷ and cyclo-1:1-[α/α -*N* ^{α} -Bn-hydrazino]-mers series.³⁰

V.2.2.3.2. pH-Responsive Gels

pH-responsive property is more characteristics for hydrogels and is the most effective and the simplest chemical method to trigger gelation. Gelator molecules containing acidic or alkaline functional groups require adjusting the pH of the solution around the pK_a value of these functional

Part B

Chapter V. Bibliography of Gels and Low Molecular Weight Organo-/Hydro-Gelators

groups. This will result in ionization of the groups and the generated electrostatic repulsive interactions may lead to change in the hydrodynamic resulting in hydrogels formation. The degree of gelation of these molecules depends on the degree of ionization of the functional groups. Poly(*L*-lysine),⁷⁸ poly(*L*-histidine),^{79,80} Fmoc-functionalized *L*-lysine amino acids¹ are typical examples of pH-sensitive hydrogels.

Formation of supramolecular peptide-based-hydrogels derivatives depends mainly on the change in pH which may result in three different kinds of hydrogels: (i) *N*-terminal-blocked peptides or peptide derivatives form hydrogels at low pH,⁸¹ (ii) amphiphilic peptide derivatives can form stable hydrogels at physiological pH, and they usually are suitable for certain biological applications,⁸²⁻⁸⁴ and (iii) some peptides or peptide derivatives possessing a very hydrophobic group or primary amine groups could self-assembly to give hydrogel at a high pH.^{85,86}

V.2.2.3.3. Ultrasonic-Responsive Gels

Ultrasound force has gained much attention as pioneering external stimuli in inducing gelation, where gels (hydro- or organo-) respond rapidly and reversibly upon exposure to the ultrasonic waves.⁸⁷ The ultrasound waves readily re-organize the aggregation of molecules by breaking the intramolecular hydrogen bonds or π -stacking to form interlocked structures through intermolecular interactions (*e.g.*, polylactide,⁸⁸ tetrapeptides based azobenzene moiety).⁵⁹

Recently, Feng *et al.* have reported that cyclo-(*L*-Tyr-*L*-Lys) can form hydrogel under the influence of ultrasound waves although it normally precipitates in water, and gels a number of polar organic solvents including *N,N*-dimethylformamide (DMF) and dimethyl sulfoxide (DMSO).⁸⁹ In addition, Gu *et al.* concluded that ultrasound accelerates the gelation process of an *L*-lysine-based hydrogelator by inducing the self-assembly of fibrils and their entanglement to form 3D networks.⁹⁰

V.2.2.3.4. Photo- or Light-Responsive Gels

Light is a simple external stimulus which may induce the gel-to-sol phase transition where it activates the reactants and starts a chemical transformation.^{91,92} Light-derived gels have received increasing attention for broad biomedical applications that include drug delivery, wound healing, tissue engineering, and construction of high-density cell arrays.^{93,94} Some gels systems based on aromatic moieties exhibit a reversible change in certain property in response to light trigger.

AuNP-embedded Phe-Phe-based organogel shows de-gelation process by laser illumination.⁶¹ Moreover, gelators containing azobenzene moiety,^{95,96} spirobenzopyran^{97,98} have been observed for their photoresponsive behavior. Wang *et al.* reported that light irradiation catalyzes the conversion of tyrosine to dityrosine of peptide-based ruthenium-complex to yield hydrogel with a very high mechanical stability with storage modulus of about 100 kPa for a concentration of 0.5 wt%.⁹⁹

V.2.2.3.5. Catalytic and Enzyme-Responsive Gels

Catalysis and enzymes have investigated their important roles in the generation and applications of supramolecular hydrogelators. van Esch *et al.* reported the formation of trishydrazone hydrogel from two water-soluble precursors, an oligoethylene-functionalized benzaldehyde and a cyclohexane-derived trishydrazide in the presence of acid or aniline as a catalyst, thus tuning the gelation time and mechanical properties of the final gels.^{100,101}

The first case of enzymatic formation of supramolecular hydrogels is the use of an alkaline phosphatase to dephosphorylate Fmoc-tyrosine phosphate under slightly basic conditions to form a hydrogelator which self-assembles in water to form a supramolecular hydrogel.¹⁰²

V.2.2.3.6. Magnetic and Electro-Responsive Gels

Magnetic-responsive gels are actually described in the literature as colloidal system composed of magnetic nanoparticles (with a typical size of about 10 nm) dispersed within a chemically cross-linked polymeric network. These systems respond reversibly under the effect of an applied external magnetic field due to sensitivity of the nanoparticles to the magnet effect. The magnetic field subsequently disturbs and distorts the macroscopic structure of the gel (switch on), and by removing the effect, re-construction of the macroscopic structure occurs (switch off) (e.g., poly(*N*-vinylcaprolactam-co-acetoacetoxyethyl methacrylate)).^{103,104}

Electro-responsive gels are most common for polymeric hydrogels, where under the influence of an electric field, the electro-responsive hydrogels undergo gel-to-sol transition.^{105,106} Poly(2-acrylamido-2-methyl propane sulfonic acid) (PAMPS) gel was observed to undergo worm-like mobility under the influence of electric field.^{107,108}

V.2.2.4. Classification of Gels Based on the Type of Secondary Interactions

Depending on the type of the cross linking and interactions between the entangled fibrils to form the interconnected networks which imprison the solvent molecules within the interstices, gels can be classified into two categories: (i) **chemical gels** which are formed by strong chemical bonds (covalent bonds, ionic bonds, *etc.*) and the gelation is irreversible (e.g., polyester, polyamide, poly(vinyl alcohol), polyethylene, and inorganic oxides),^{50,109} and (ii) **physical gels** which are formed by weak non-covalent interactions such as hydrogen bonding, solvophobic forces, π -stacking, electrostatic interactions, donor-acceptor interactions, metal coordination, ion-ion interactions, dipole-dipole interactions, London dispersion forces, and van der Waals interactions, hence the gelation is reversible.^{18,32,110-112}

Since we are interested in supramolecular gels which are constructed mainly through non-covalent interactions, in the next sections we will present briefly the four fundamental forces that support and stabilize the gel state. These forces are (a) van der Waals force, (b) charge transfer, (c) hydrogen bonding, and (d) solvophobic interactions. These forces control the behaviors of most of the physical gels:

(a) van der Waals interactions

Are attractive or repulsive forces between molecules or atomic groups, which do not arise from a covalent bond or electrostatic interactions that arise either between ionic groups or between ions and neutral molecules.^{113,114} Accordingly, these forces can be classified into three sub-classes (1 - 10 kJ mol⁻¹)

- i) **Dipole-dipole interactions** (Keesom force): (2 - 10 kJ mol⁻¹)
- ii) **Dipole-induced dipole interactions** (Debye force): (1 - 5 kJ mol⁻¹)
- iii) **Induced dipole-induced dipole interactions** (London dispersion force): (1 - 5 kJ mol⁻¹), the interactions between the alkyl chains.

(b) Charge transfer interactions

Occur either between two or more molecules, or between different moieties in a macromolecule when the electronic charge transfers between the molecular entities. The resulting electrostatic attraction provides a stabilizing force for the molecular complex. The source molecule from which the charge is transferred is called the electron donor and the receiving species is called the electron acceptor.

Part B

Chapter V. Bibliography of Gels and Low Molecular Weight Organo-/Hydro-Gelators

In **Inorganic chemistry**, most charge-transfer complexes involve electron transfer between the molecular orbitals (MO) of metal atoms and ligands ($\pm 20 \text{ kJ mol}^{-1}$), while in **Organic chemistry**, the interactions happen between aromatic nuclei or between conjugated systems (π - π stacking, 5 - 10 kJ mol^{-1}).¹¹⁵⁻¹¹⁷

(c) Hydrogen bond interactions

They are electrostatic attractions between polar groups, and occur when a hydrogen (H) atom located between two highly electronegative atoms such as nitrogen (N), oxygen (O) or fluorine (F), *etc.* These hydrogen-bond attractions can be intermolecular or intramolecular. Based on the geometry and environmental conditions, the energy of the hydrogen bond may have the range 5 – 40 kJ mol^{-1} . Hydrogen bond is stronger than van der Waals, but weaker than covalent or ionic bonds. This type of bond can be identified within inorganic molecules such as water, and in organic molecules like DNA, proteins or small molecules as peptides.¹¹⁸

(d) Solvophobic interactions

These types of interactions occur between non-polar solutes and polar solvents. Polar solvents are characterized by relatively strong cohesive forces between the solvent molecules due to hydrogen bonding or other polar interactions. In order to increase the solubility of the non-polar solutes, these solvent-solvent binding interactions must be overcome firstly.¹¹⁶

V.2.3. Characterization of Gels

Owing to the enormous number of gels that are being produced in an increased rate, more information about molecular gels at both the nanoscale and supramolecular levels are required. This can be achieved by doing more accurate analyses and characterizations which may help researchers better understanding how the small molecules are arranged and organized in the matrices of gels. Consequently, new approaches may be developed not only for rational design of new supramolecular gelators but also for the development of various functional molecular biomaterials.

V.2.3.1. Visual Inspection

Vial inspection is the “zero-order” characterization technique. The classic “inverting-vial” method is still the simplest way to initially assess a gel.^{119,120} It depends mainly on flipping the vial upside down, and this provides a first impression on the shape and strength of the gels. Hence, the material can easily be classified as a solution, viscous liquid, half-gel, or solid-like gel.

V.2.3.2. Microscopy

Microscopy techniques are used to study the morphology of micro- and nanostructures of the matrices of gel systems. Among all the microscopy techniques:

- (i) **polarizing light techniques:** despite their relatively low resolution, they do not require manipulation of the sample, allowing the native structure of the aggregates to be observed.¹²¹⁻¹²³
- (ii) **electron microscopies (AFM, TEM, SEM, *etc.*):** are high-resolution techniques allow imaging of features with resolution up to 0.2 nm, therefore they provide valuable information about the morphology of the aggregates that result in gelation.

a) Atomic force microscopy (AFM) or scanning force microscopy (SFM): is a high-resolution scanning probe microscopies, they can achieve a resolution on the order of fractions of a nanometer,

Part B

Chapter V. Bibliography of Gels and Low Molecular Weight Organo-/Hydro-Gelators

which is 1000 times more than the optical diffraction limit. AFM may analyze hydrated (solvated) samples *in situ* under high humidity conditions or even without dehydration.^{124,125} In addition, it is possible to measure the roughness of a sample surface at a high resolution, which helps to classify a sample based on its mechanical properties (*e.g.*, hardness and roughness).

b) Electron microscopy techniques: they include transmission (**TEM**) and scanning (**SEM**) microscopies. They utilize a beam of accelerated electrons as a source of illumination. Since the wavelength of an electron is short, electron microscopy has the capacity to reveal the structures of small objects with resolution up to a nanometer.^{126,127} Electron microscopy can provide valuable information about the morphology of the molecular aggregates/nanofibrils leading to gelation. SEM and TEM techniques need completely dried samples under the operating conditions (*e.g.*, high vacuum).¹²⁸ Furthermore, some staining agents (*e.g.*, uranyl acetate, phosphotungstate, or osmium tetroxide) are used for TEM samples, while gold coating are operated for SEM samples in order to increase the electron density of the samples to improve the quality/contrast of the images.³

Recently, cryogenic techniques have already been used in TEM and have applied for gel systems for studying the self-assembled structures. In order to use cryo-electron microscopy (cryo-EM), samples are studied at cryogenic temperatures (generally liquid nitrogen temperatures) through creation of thin vitrified ice films. Cryo-EM has the advantage of reducing or eliminating the artifacts and making nanometer resolution images of the native gel state feasible.¹²⁹

V.2.3.3. Oscillatory Rheometry and Differential Scanning Calorimetry

The macroscopic properties of a gel are derived primarily from the tertiary and to some extent to the secondary structure. The rheological and thermodynamic properties of gels can be investigated using techniques such as rheometry and differential scanning calorimetry (DSC). They provide useful information about the mechanical strength, thermal stability and flexibility of the gel that allow us to evaluate its potential for practical applications.¹³⁰⁻¹³²

Oscillatory rheometry becomes a routine technique to characterize the viscoelastic materials such as supramolecular gels. Rheology studies the flow of gels, and can provide tertiary structural information about the type and strength of the networks responsible for the observed gelation.¹³³ It is a convenient method that facilitates classification of gels between “strong” and “weak”.¹³⁴ Strictly speaking, “weak” gels do not fulfill the mechanical requirements of a true gel¹³⁵ since their flow properties depend upon gelator concentration and angular frequency (ω).

The temperature of gelation (T_g) is one of the most often studied characteristics for a gel, which is determined by the point at which the non-covalent cross-links are broken by thermal energy. Multiple methods can be used to determine this value, including the “dropping ball” experiment in which a small ball is placed on top of a gel while it is being heated. The temperature at which the ball breaks through the gel (deformation of the tertiary structure) is recorded as the T_g .^{3,69,73}

The values indicated by spectroscopic measurements can differ significantly from the rheological ones. Spectroscopic T_g values do not correlate with cessation or initiation of flow, since the methods measure microscopically the structural modifications of strand organization within a colloid, the formation or dissolution of individual strands, *etc.* The difference between transition temperatures measured *via* rheology and spectroscopy is smallest when the change in gelator solubility with temperature is greatest.²

Differential scanning calorimetry (DSC) is a well-established characterization method that can provide better defined T_g that corresponds to the breaking of cross-links or molecular arrangements, especially when there is a sharp phase transition associated with gelation.¹³⁶

V.2.3.4. X-ray Diffraction

There are two diffraction techniques, small-angle X-ray (SAXS) and small-angle neutron scattering (SANS). They have been applied to gel systems to investigate the suprastructures formed by the fibers (tenth of nanometers).¹³⁷⁻¹⁴⁰

Small-angle X-ray scattering (SAXS), mainly provides average information on the matrices of gel samples by measuring the spatiality of the matrices. In addition, wide-angle X-ray powder diffraction (XRD) has great potential for the elucidation of the molecular organization and nanostructures of many organogels.^{123,141-145} The spacing (d) of subsequent peaks can be used to distinguish lamellar (1, 1/2, 1/3) from hexagonal (1, 1/x2, 1/x3) packing.^{146,147} The long (d) spacing obtained from XRD represents the longest repeat distance in the ordered structures, which may provide insight into the packing of the monomeric molecules in either an extended or a bent conformation. Much of this work has been on dried samples, however it was difficult to draw direct conclusions about the structure of the gel in its native state.

Although the small-angle neutron scattering (SANS)^{148,149} is a specialized technique to which researchers have limited access, SANS is able to provide useful information about the average sizes and shapes of the nanostructures in gels systems.^{150,151} In addition, SANS has resolution approximately close to that of TEM which in turns can focus on the local morphology of gels matrices.

Rigorous mathematical analysis is required to interpret the results of these techniques. First, a model is chosen for the type of aggregate (*e.g.*, rod-like micelles) and then using the appropriate parameters, the data are fitted to this model. Information on the type of packing (cubic, hexagonal, *etc.*) of the rod-like aggregates can be determined.¹⁵²⁻¹⁵⁴

V.2.3.5. Other Physical Techniques

Spectroscopic techniques can help in determining the primary structure of small gelator molecules. Various spectroscopic techniques have been applied to gels systems, including NMR, fluorescence, UV, CD, and IR spectroscopies. All of which can provide information on the molecular organization of the gels through detection of the molecule-molecule or molecule-solvent interactions in primary or secondary structures. Since many of these techniques are temperature-sensitive, they provide additional methods for determining T_g. The melting temperatures determined by spectroscopy will often be different from those determined from rheometry, since they detect changes in primary rather than tertiary structure.⁷³

Solution-state NMR can be used to identify the formation of hydrogen bonds during gelation,^{142,155,156} and the changes in the aggregation process from the solution state to the gel state by analyzing the chemical shift variations.¹⁵⁷ Solid-state magic angle spinning NMR (MAS NMR), is used for characterizing structures of protein or peptide aggregates. It may be useful for elucidating the structures of gel systems by identifying the chemical shift variations from the solution state, indicating a change in aggregation.^{158,159}

FTIR spectroscopy is suitable for confirming the presence of hydrogen bonds in gel systems.^{122,155,160,161} Some peaks of interest (such as the NH stretch) are obscured by the OH stretch of water in case of hydrogels, subsequently the studies are done with dehydrated samples. In addition the technique helps in studying the nature of the self-assembled structures within the gel system.

Circular dichroism (CD) has a wide range of applications in many different fields, such as the study of the secondary structures of proteins, or the investigation of charge transfer transitions. In the cases of soft materials such as hydro- or organogels, some examples have been reported for the use of

the CD to study the self-assembled suprastructures in the gel phase or at the gel-to-sol transition.^{162,163} However, it always remains a challenge to make a precise conclusion from the CD spectra alone, which means that it is better to combine CD with other techniques for studying secondary structures of supramolecular gels.

UV-vis absorption and fluorescence emission are spectroscopic techniques used for investigating π - π stacking (aromatic-aromatic interactions) or metal coordination in the process of gelation.¹⁶⁴⁻¹⁶⁶ UV-vis and fluorescence methods in combination with CD may provide information about the molecular arrangements in gels.¹⁶⁰

V.2.3.6. Molecular Modelling Methods

On the basis of the molecular structural data collected from several of the complementary techniques discussed above, it is possible to use modelling for proposing a plausible arrangement of the molecular organization in gel state.¹⁴³ Actually, researchers have already developed some relevant model systems using higher level energy minimization and molecular dynamic calculations to model the primary structure of gels to simulate the gelation process of gelators in organic solvents.¹⁶⁷⁻¹⁶⁹ Indeed, few modelling approaches are currently reliable in describing the self-assembly of small molecules in both aqueous^{130,155,170} and organic solvents.^{167-169,171}

V.3. Structural Diversity of Low Molecular Weight Organo-Gelators (LMWOGs)

V.3.1. LMWOGs Based on Hydrocarbons, Fatty Acids and Esters

Long *n*-alkanes are structurally the simplest LMWOGs and their gels in organic solvents are considered to be the simplest class of organogels. Abdallah and Weiss reported that long *n*-alkanes have the ability to gel many organic solvents such as alcohols (ethanol, 1-octanol), aromatic solvents (benzene, toluene), and apolar solvents (dichloromethane, ethyl acetate) as well as silicon oil.³² They concluded that the main driving force for the gelation is London dispersion forces, and the gel stability increases with increasing the length of the alkane chain ($C_{24} < C_{28} < C_{36}$) due to increasing the opportunities for the London forces between the long chains. XRD analysis revealed that *n*-hexatriacontane **1** (Figure 5.2) assembles in wafers leading to an orthorhombic lamellar stacking in the gel state.^{172,173}

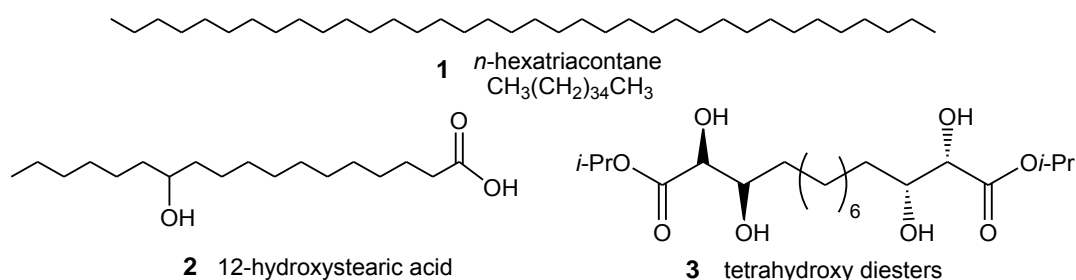


Figure 5.2. LMWOGs based on alkanes, fatty acids and esters.

Fatty acids are known by their amphiphilic property as they are characterized by the presence of hydrophilic hydroxyl groups to form hydrogen bonds and hydrophobic alkyl chains necessarily for van der Waals interactions. Gel formation by fatty acids are controlled by: (i) the balance between hydrophilic/hydrophobic ratio, and (ii) the ability of fatty acids to self-assemble in solvents to form a 3D network structure.¹⁷⁴ 12-hydroxystearic acid **2** (HSA) (Figure 5.2) is an example of this series which displays a remarkably improved gelation ability to form thermoreversible gels in a number of aromatic (benzene, toluene), and chlorinated (dichloromethane, chloroform, carbon tetrachloride) solvents.^{28,174,175} In addition to van der Waals forces, X-ray and FTIR studies revealed that the HSA fibers in hydrocarbon gels are also enforced by intermolecular hydrogen bonds between the hydroxyl groups forming a zigzag sequences along the fiber axis and “head to head” contacts within the orthogonal plane between carboxylic acid groups.^{28,175}

CD analysis of the gel in CCl_4 for the chiral 12-hydroxystearic acid **2** suggested a helical structure with a negative sign for the *R*-enantiomer (right-handed helix), and a positive sign for the *S*-enantiomer (left-handed helix) with a definite CD band at 370 nm. X-ray diffraction results confirmed the helical twisted fibers structure.^{175,176}

Compound **3** with eight methylene connections (Figure 5.2), belongs to the tetrahydroxy diesters series, has proved its gelation efficiency at low concentration for polar and non-polar solvents including toluene, cyclohexane and water through hydrogen bonding interactions.¹⁷⁷

V.3.2. LMWOGs Based on Ureas, Bis-ureas and Amides

As illustrated in Section V.3.1, London dispersion forces alone could stabilize the gels formed by LMWOGs based *n*-alkanes. It has been suggested that introducing of one heteroatom (*e.g.*, nitrogen, oxygen or sulfur atom) within the *n*-alkane chain may provide organogelators efficient for

Part B

Chapter V. Bibliography of Gels and Low Molecular Weight Organo-/Hydro-Gelators

gelling various organic liquids because the London dispersion forces are supported by intermolecular hydrogen bonding and dipolar forces.^{178,179}

Urea **4** and some of its short-chained derivatives are more efficient gelators than the longer-chained ureas and thioureas **5**. The main driving forces responsible for the molecular packing arrangements within the gel fibrils are hydrogen bonding and London dispersion interactions.^{180,181} *N*-alkyl and *N,N'*-dialkyl substituted ureas and thioureas are efficient gelators for a variety of organic liquids. In fact, *N,N'*-dimethylurea **6** (Figure 5.3), which is known as the lowest molecular weight organogelator (M.wt ~ 88 Da), can gel silicone oil and carbon tetrachloride.¹⁸²

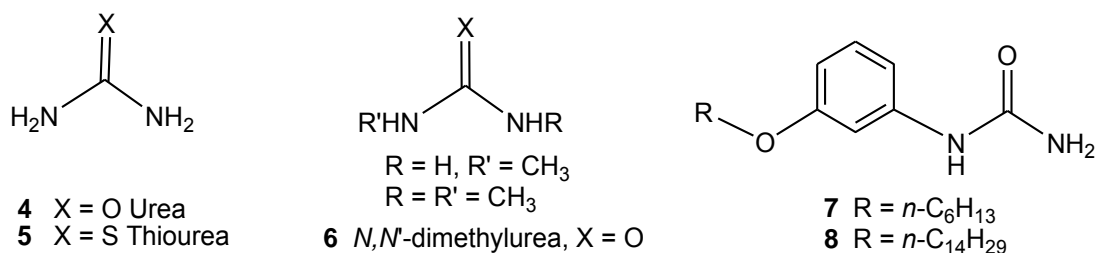


Figure 5.3. LMWOGs based on ureas.

Moreover, the monourea derivative **7** (Figure 5.3) acts as LMWOG and showed the ability to gel water and various solvents including cyclohexane, benzene, toluene and CCl₄. Compound **8** with longer alkyloxy chain, not only can gel the aforementioned solvents, but also it gels polar solvents such as methanol, acetone and dioxane. Temperature dependent ¹H NMR studies revealed that both hydrogen bonding between the amide groups and π -stacking interactions are the main driving forces in the gelation process.¹⁸³

Bis-ureas have been found to be more effective organogelators than the corresponding monourea derivatives for a variety of organic solvents, including alkanes, esters and alcohols. SEM analysis of the areogels for most of the bis-urea derivatives showed fibrous and sheet-like morphologies depending on the structure of the gelators, the solvent and the concentration. It has been recognized that the presence of long alkyl chain is essential for effective gelation. In contrast, incorporation of branched methacrylate groups have led to disruption of the packing of the hydrocarbon tail enhancing the solubility.¹⁸⁴

Bis-urea **9** (Figure 5.4) forms a three-dimensional gel network through hydrogen bonds between the urea moieties in hexadecane, *p*-xylene, tetralin, cyclohexanone and *n*-butyl acetate.¹⁷¹ In addition tris-urea derivatives, such as compound **10**, are efficient LMWOGs for a wide variety of organic solvents.¹⁸⁵⁻¹⁸⁷

Bis-urea compounds derived from 1,2-diaminobenzene **11** - **13** or from optically pure *trans*-1,2-diaminocyclohexane **16** - **19** (Figure 5.4) possessing aliphatic, aromatic or ester groups in their structures have demonstrated their efficient gelation for organic solvents such as aliphatic and aromatic hydrocarbons, esters, ketones and alcohols at concentrations lower than 1.0 (w/v)%. Authors reported that the gelation capability for the different solvents and the minimum gelation concentrations do not depend largely on the nature of the R group.¹⁸⁸

In contrary, the *meta*- and *para*-substituted analogs **14** and **15**, failed to gel any of the solvents investigated (except for **14** with hexadecane), and the same behavior has also been reported for the *cis*-compound **20**, which could not gel any of the solvents investigated and it gave viscous solution or it precipitated upon cooling the heated solution.¹⁸⁸

Infrared studies showed that the aggregation is accompanied by the formation of a hydrogen-bound network between urea moieties. X-ray studies confirmed that the molecules assemble into sheets and lamella stabilized by the formation of intermolecular hydrogen bonds between the urea groups of adjacent molecules. The authors have reported that the molecular arrangement in the gels is most likely similar to that in the crystal, but the complete interpretation of the molecular arrangement in gels is complicated due to polymorphism property of these compounds during aggregation.¹⁸⁸

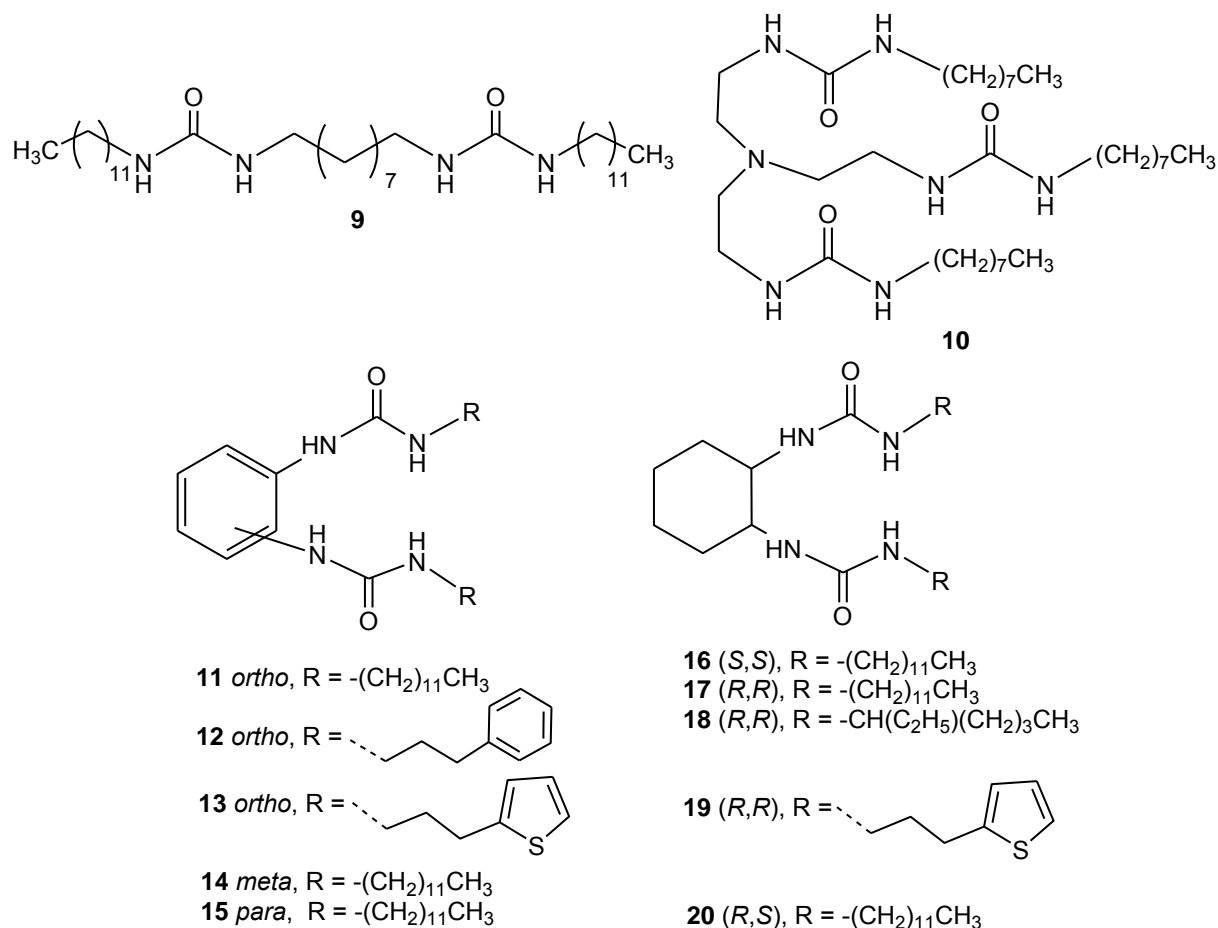


Figure 5.4. LMWOGs based on bis-ureas and tris-ureas.

The enantiomerically pure *trans*-1,2-bis(3-dodecylureido)cyclohexane (**16**) forms stable gels with a variety of solvents including alcohols (1-propanol, 1-butanol, 1-hexanol and 1-octanol). Light and electron microscopic studies revealed that the gels are birefringent with well-ordered structures. The gelator molecules are aggregated into elongated fibers of about tenths of micrometers long with diameters up to 100 nm, which undergo further association to form an entangled 3D network that immobilize the solvent molecules. Many of the fibers are twisted to form left-handed helices.¹⁸⁹ Rheology measurements showed that bis-urea **16** forms rigid gels up to concentrations of at least 50 mmol. L⁻¹ with alcohols.

The phase diagrams and DSC experiments of these gel systems revealed that the thermal stability of gels from **16** increases in the order 1-octanol < 1-hexanol < 1-butanol < 1-propanol with increasing polarity of the solvent which is counterintuitive result. The results were interpreted as the solvophobic interactions (owing to the presence of the two dodecyl chains) become dominant over hydrogen bonding interactions for the aggregation of **16** in more polar solvents.¹⁸⁹

Part B

Chapter V. Bibliography of Gels and Low Molecular Weight Organo-/Hydro-Gelators

Bis-amides are characterized by possessing two amide groups in their structures which increase the possibility of hydrogen bonding interactions. Xuzhong Luo reported that the diamide amphiphiles, (oxamide derivatives) monoalkyloxamide **24** - **26** containing no chiral centers, can form ordered bilayer aggregates in a number of organic solvents leading to gel formation.¹⁹⁰ Indeed, the oxamide crystal is known by its triclinic layer structure and the molecules within the layers are linked together by hydrogen bonds.¹⁹¹

XRD and FTIR results of the gel **24** (Figure 5.5) from toluene revealed that the gel aggregates consist of a repeating bilayer unit which bears the head-to-head packing model and highly tilted alkyl chains relative to the bilayer normal. The gel is maintained through intra- and inter-layer hydrogen bonds that connect the amphiphiles within the bilayer unit.¹⁹⁰

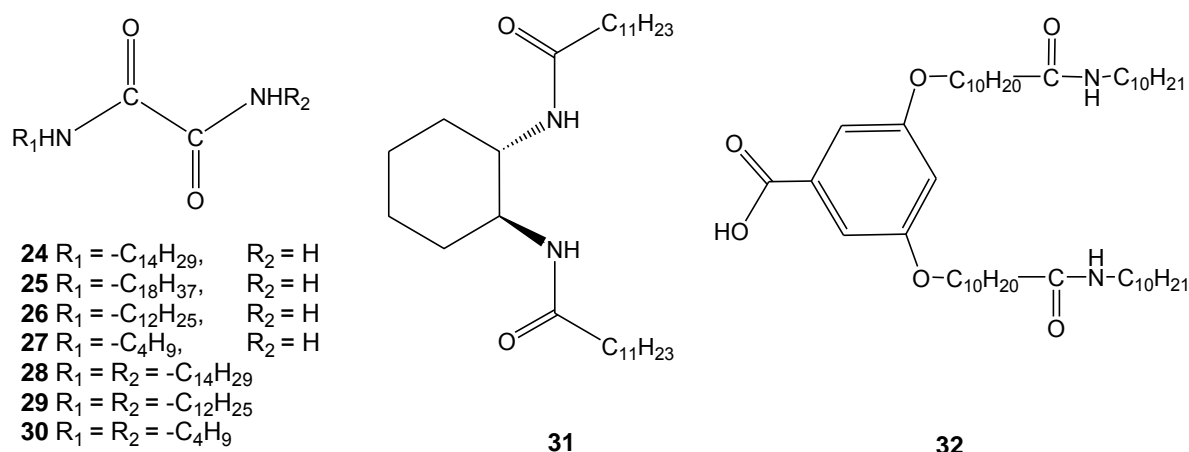


Figure 5.5. LMWOGs based on bis-amides.

Surprisingly, *N,N*-disubstituted oxamides **28** - **30** (Figure 5.5) exhibit no gelling ability due to the substitution of one of the two hydrogen atoms of the primary amides by an alkyl chain, and this inhibits the formation of interlayer hydrogen bonds between the head-to-head arrangements. It has been noticed that the presence of long lipophilic chain is essential for gelation through van der Waals interactions and this was recognized from the non-gelling ability of the monosubstituted oxamide **27** compared with the gelling behavior of **24** - **26**. The authors concluded that gelling ability strongly depends on the oxamido-group which plays an important role in stabilizing the ordered bilayer aggregates through hydrogen bonds, also the hydrophile-lipophile balance in the gelator molecule is a determinant factor for gelation process.¹⁹⁰

The hydrogen bonds between the amide groups of adjacent molecules and van der Waals interactions between the long alkyl chains have induced the enantio-pure *trans*-isomers (1*R*, 2*R* and 1*S*, 2*S*) of bis-amide derivative **31** (Figure 5.5) to gel various solvents like hydrocarbons, alcohols, ketones, esters and mineral oil.^{192,193} The corresponding *cis*-isomers could not form gel with any of the solvents that have been gelled by the *trans*-isomers.

Aromatic bis-amide derivative **32** showed its gelation ability for solvents like benzene, toluene and *p*-xylene, but not hexane due to insolubility.¹⁹⁴ The analog of **32** without the amide groups could not gel these aromatic solvents and this reflects that hydrogen bonding interactions between the amide groups are necessarily for gelation process.

V.3.3. LMWOGs Based on Steroids

Steroids are a class of naturally occurring lipids. The first steroid based LMWOGs for hydrocarbon solvents is *D*-3 β -hydroxy-17,17-dipropyl-17 α -azahomoandrostanyl-17 α -oxy (STNO) **33** and its amino analog (Figure 5.6).¹⁹⁵ ALS gelators are compounds consist of an aromatic group (A) connected by a linker (L) to a steroid (S) based molecule.² Various ALS-type organogelators have been reported possessing anthracene,^{196,197} azobenzene,¹⁹⁸ porphyrine,¹⁹⁹ bile acids²⁰⁰ and stilbene²⁰¹ as aromatic nucleus.

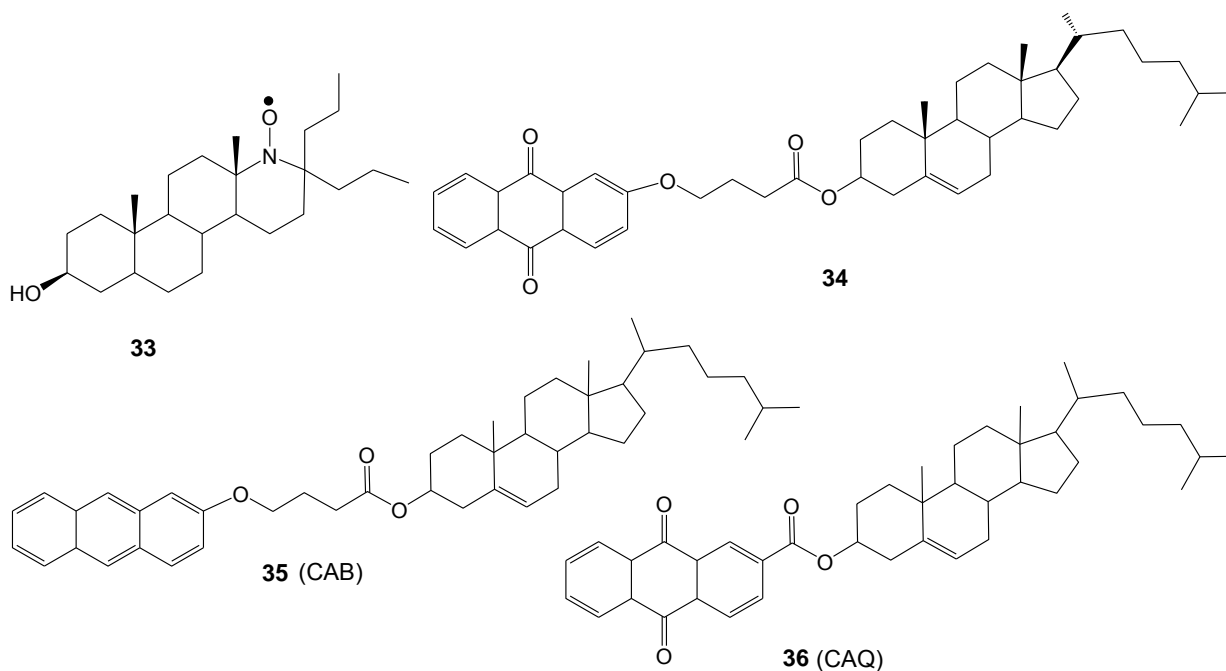


Figure 5.6. LMWOGs based on steroids.

Mukkamala and Weiss²⁰² prepared a series of anthraquinone-steroid based LMWOGs and they found that the functionality and the length of the linker group between anthraquinone and steroid have a strong effect on the gelation ability. Compound **34** (Figure 5.6) is one example of ALS molecules that is able to gel various hydrocarbons, alcohols, acrylates and silicone oil.

Serendipitously, small amounts (< 1.0 wt%) of cholesteryl 4-(2-anthryloxy)butyrate (CAB) **35** (Figure 5.6) was found to cause reversible gelation of a wide variety of organic liquids including alkanes, alkenes, alcohols, aldehydes, carboxylic acids, esters and amines. It has been reported that these gels exhibit solid-like behavior and nearly translucent, and the gelation process is mainly driven by the weak van der Waals interactions. Circular dichroism of gel **35** from *n*-dodecane (0.72 wt%) proved the helical stacking of anthracenyl units.¹⁹⁶

In fact, cholesteryl anthraquinone-2-carboxylate (CAQ) **36** was found to be effective gelator for a variety of organic solvents as well as silicon fluid at low concentrations (< 2.0 wt%). (CAQ)-silicone gel was found to be more stable thermally than the corresponding CAQ-hydrocarbon gels at equal concentration. Authors attributed this behavior to the lower solubility of the gelator **36** in silicone fluid at all temperatures, and once its fibrous network is formed, it is difficult to break it down. Optical and electron microscopy revealed that all the silicone gel demonstrated three dimensional and interlocking fibrous bundles generated from central points. Cryogenic scanning electron microscopy (SEM) showed the presence of "endless" fibers that intertwine to form a 3D networks immobilizing the silicone fluid *via* weak intermolecular forces forming the gel.²⁰³

V.3.4. LMWOGs Based on Saccharides and their Derivatives (Sorbitols)

Many saccharides based LMWOGs are able to form gels in both organic solvents and aqueous mixtures through intermolecular hydrogen bonds. The monosaccharide derivatives can be divided into three groups based on their structures (Figure 5.7): openchain²⁰⁴ (**37**, **38**), cyclic²⁰⁵ (**39**) and acetal-protected cyclic monosaccharides²⁰⁶⁻²⁰⁸ (**40**, **41**). Disaccharide derivatives²⁰⁹ and acetylated cyclodextrins²¹⁰ have also been reported to function as organogelators.

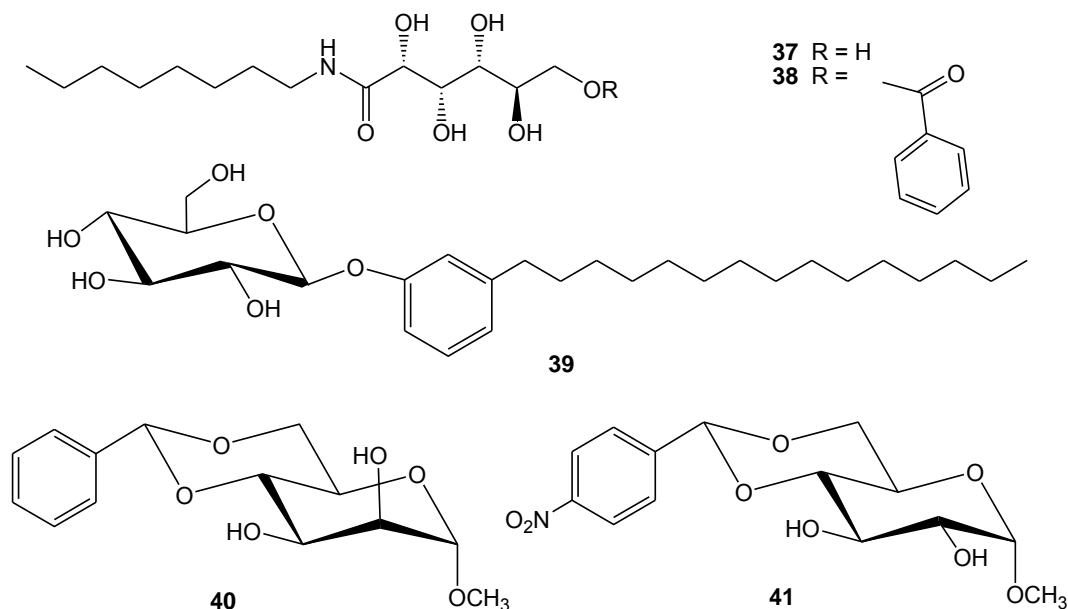


Figure 5.7. LMWOGs based on saccharides.

Glucose derivative of open-chain monosaccharide **37** (Figure 5.7) can gel 1,2-xylene. Furthermore addition of a benzoyl group yields **38**, which forms a thermoreversible gels in various solvents such as alcohols, acetonitrile, acetone, chloroform as well as in aromatic solvents that reflected the most thermally stable gels.²⁰⁴

Cyclic saccharide compound **39** gels cyclohexane and several aromatic solvents through hydrogen bonding and solvophobic interactions. It can not form gels from acetone, DMF, DMSO, alcohols or water, however, the gels form at a 1:1 mixtures (solvent/water).²⁰⁵ In case of the acetal-protected cyclic monosaccharide including methyl 4,6-benzylidene derivatives **40** and **41** (Figure 5.7); the α -manno derivative **40** forms colorless gels in alkanes, aromatic solvents, carbon disulfide, diphenyl ether and water.²⁰⁶ FTIR, NMR and X-ray diffraction analyses indicated that gelation occurs through hydrogen bonding, π -stacking and van der Waals interactions. The α -glucopyranoside derivative **41** gels alcohols beside all the solvents that are gelled by the derivative **40** with the exception from alkanes, since no gel is formed.²⁰⁷

1,3:2,4-di-O-benzylidene-*D*-sorbitol (DBS) **42** (Figure 5.8) was first synthesized by Thomas and Sibi upon the condensation product of benzaldehyde and sorbitol in 1926.²¹¹ DBS is an unusual excellent gelling agent for organic solvents as it is a relatively small (M.wt \sim 358 Da). It can readily self-assemble at relatively low concentrations through intermolecular hydrogen bonds to form a three-dimensional network in organic²¹² and inorganic²¹³ solvents.

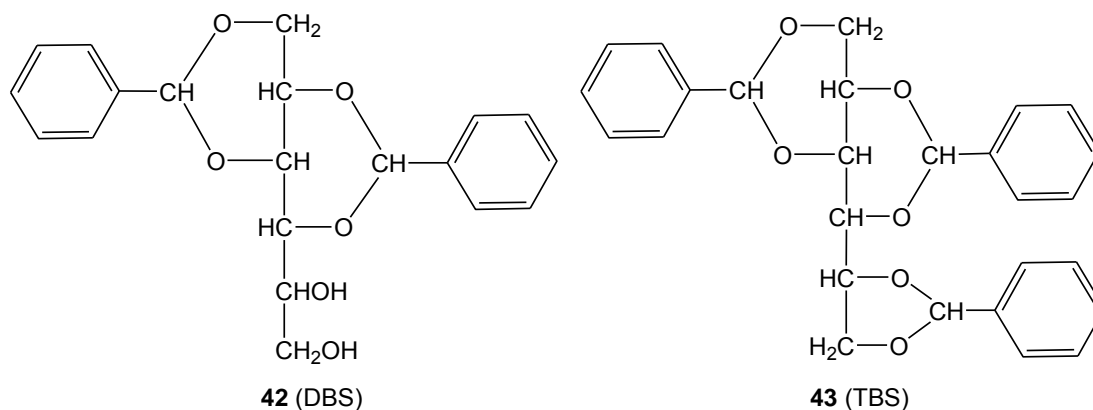


Figure 5.8. LMWOGs based on sorbitols.

Yamamoto discovered the gelation of DBS (**42**) in alcoholic solvents in 1942.²¹⁴ Mineo Watase *et al.* have investigated the thermal and fluorescence properties of gels formed from DBS (**42**) and 1,3:2,4:5,6-tri-O-benzylidene-*D*-sorbitol (TBS, **43**) (Figure 5.8) in ethylene glycol (EG), glycerol (GL) and other alcoholic solvents. They concluded based on the photophysical results that DBS molecules (**42**) can readily self-aggregate in alcoholic solutions such as EG and GL to form microcrystals or fibers even at concentrations lower than 0.05 %. Moreover, these aggregates can further interact with solvents molecules and form gel network which is stabilized by π -stacking between the two aromatic groups. In addition, they assumed that the two benzylidene groups are in a parallel configuration and separated by a distance of at most 0.35 nm.²¹⁵

V.3.5. LMWOGs Containing Aromatic Moieties

Gelation phenomenon from LMWOGs containing aromatic groups (*e.g.*, benzene, pyridine, anthracene and porphyrin) is supported mainly by π - π stacking among aromatic moieties which can be considered as the major driving force for gelation. One of the simplest LMWOG based on aromatic molecules, is the di-*n*-alkoxy-benzene derivatives **44** (Figure 5.9) which is able to gel acetonitrile, propylene carbonate, DMF, and dimethylacrylamide through π - π stacking, dipole-dipole, and van der Waals interactions.²¹⁶ Substitution of the benzene moiety with a naphthalene moiety **45**,²¹⁷⁻²¹⁹ an anthracene moiety **46**, or an anthraquinone moiety²²⁰ **47** yields an efficient organogelator for hydrocarbons and alcohols (Figure 5.9).

2,3-Didecyloxyanthracene (DDOA) **46** (Figure 5.9) can gel large variety of organic solvents at very low concentrations by forming a three-dimensional network of fibers stabilized by van der Waals interactions between the alkyl chains and π - π stacking between the anthracene moieties. X-ray diffraction experiments on xerogels and aerogels of DDOA could not provide any Bragg diffraction patterns.

A model of the molecular arrangement of the DDOA molecules within the fibers was proposed from *ab initio* calculations combined with FTIR, fluorescence and dichroism experiments performed on oriented bundles of aerogel fibers which revealed that the DDOA molecules are arranged along helicoidal coils in concentric cylinders.²²¹

Perylene bis-imide **48** is a semiconductor, ables to gel various organic solvents including aliphatic and aromatic solvents, ethers and triethylamine at low concentrations.^{222,223} The three dimensional fibrous network is generated from the self-assembly of **48** through hydrogen bonds between the benzamide groups and strong π - π stacking interactions.

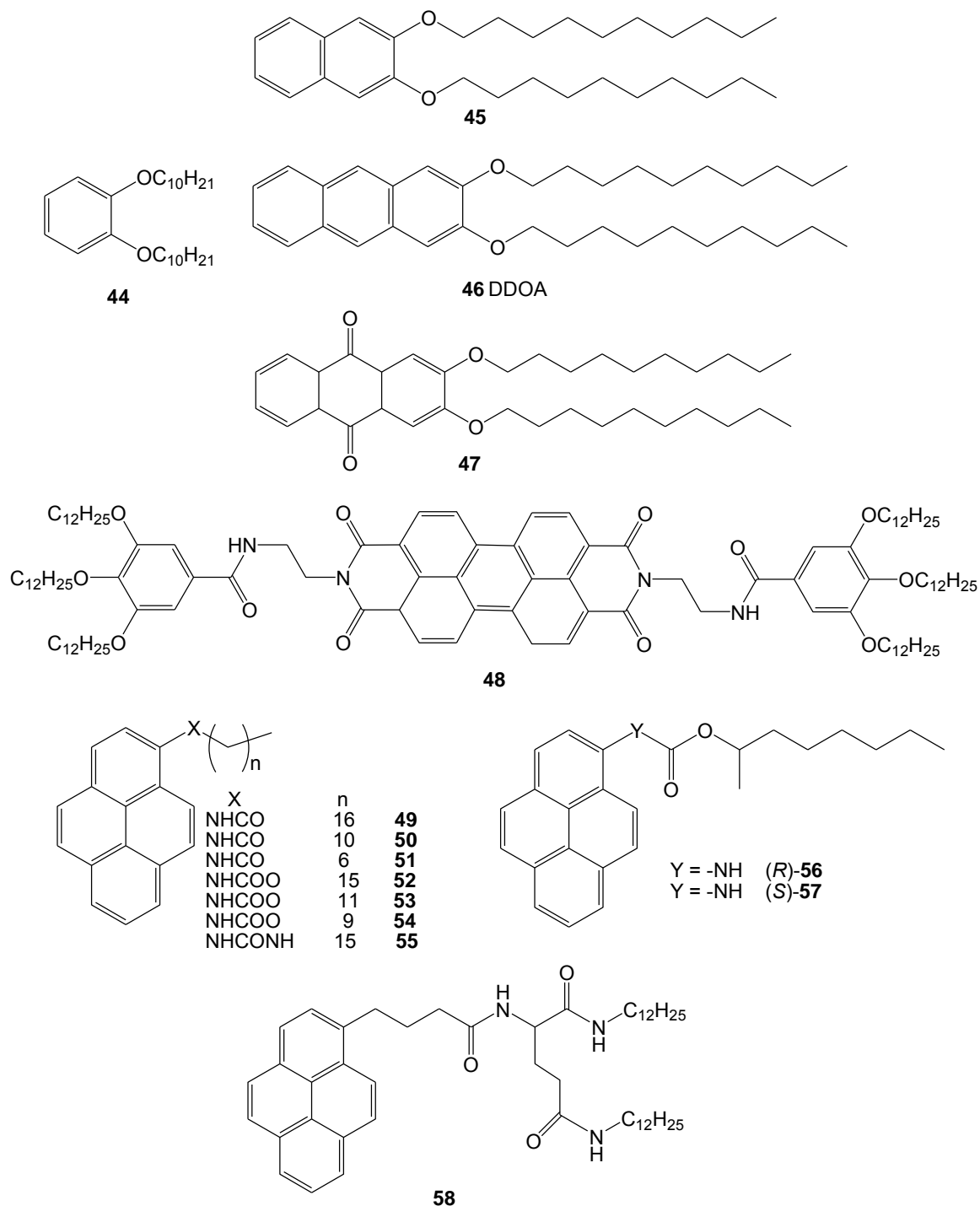


Figure 5.9. LMWOGs based on aromatic cores.

Maitra group has synthesized and studied the gelation ability of alkyl based-pyrene derivatives (Figure 5.9): (i) reverse amides **49 - 51** in which the bond orientation of the linker is NHCO which is in reverse direction compared to the amide -CONH group, (ii) urethanes **52 - 54**, and (iii) urea **55**.²²⁴⁻²²⁸ They have demonstrated that these compounds are one component organogelators can form helical aggregates *via* a combination of hydrogen bonds, π -stacking between pyrene nuclei and van der Waals interactions supported by alkyl chains which provide the balance between solubility and crystallization. The minimum gelation concentrations of these materials are lower than 1.0 wt% and

Part B

Chapter V. Bibliography of Gels and Low Molecular Weight Organo-/Hydro-Gelators

the gel melting points are typically between 60 - 80°C. The gels are thermally reversible and they remain stable for several months at room temperature.²²⁵

FTIR studies gave evidence that the amide groups in most of the pyrene based LMWOGs are bound through strong hydrogen bonds in the gel state similar to the solid state.²²⁵ Variable temperature absorption spectral analysis indicated the de-stacking of the pyrene moieties during heating the gels. Molecular modelling (INSIGHT II) predicted that in order to maintain both the intermolecular hydrogen bonds and stacking of the aromatic groups, the pyrene units must adopt a helical organization.²²⁷

Alkyl chain length plays a fundamental role in gelation process as reported by the disability of compounds **51** and **54** to gel any solvents that are gelled by analogs with longer alkyl chains. In addition, π -surface area is very important interactions enforcing gel formation as confirmed by the disability of a naphthyl group to enhance gelation when substitutes the pyrene moiety in compound **49**.

Compounds **56** and **57** (Figure 5.9) with urethane linker and chiral side chain can only gel hydrocarbons. Formation of chiral aggregates was observed with optical rotation in circular dichroism. CD analysis for the (*R*)-enantiomer **56** showed helical aggregates, while its (*S*)-enantiomer **57** had optical rotation and CD signals with opposite signs.^{225,227} X-ray crystal structure of chiral gelator indicated that the supramolecular structure is stabilized by the presence of the π - π stacking, hydrogen bonding and van der Waals interactions.²²⁸

Pyrene substituted dialkyl *L*-glutamine derivative **58** (Figure 5.9) demonstrated its ability to gel benzene and cyclohexane.²²⁹ Fluorescence and FTIR spectroscopies indicated the formation of fibers *via* π -interactions between the pyrenes in addition to the hydrogen bonds among the amide groups. Other examples of efficient LMWOGs containing large aromatic groups include porphyrins^{230,231} and phthalocyanine²³²⁻²³⁴ derivatives have also been reported.

V.3.6. LMWOGs Containing Macrocycles

Phthalocyanines (PCS) belong to a class of macrocyclic compounds that form coordination complexes with most elements of the periodic table. They have potential applications in functional nanostructures. Phthalocyanines substituted with long, flexible hydrocarbon chains can self-assemble to form columnar mesophases,²³⁵⁻²³⁹ Langmuir-Blodgett (LB) multilayers,²³⁹⁻²⁴⁶ or aggregates in solution.²⁴⁶⁻²⁴⁹

Tetrakis[4', 5'-bis(decoxy)benzo-18-crown-6]phthalocyanine **59** is an example of macrocycles that self-assembles in chloroform solution to form gel (Figure 5.10). The driving forces for the formation of spontaneous supramolecular entangled structure are mainly due to: (a) the high degree of shape anisotropy of the PCS, which favors their packing into columnar assemblies, and (b) the fact that the molecules are strongly held together by van der Waals and π - π interactions between the PC cores and also between the peripheral benzene units.

UV-vis spectroscopy revealed that the molecules are most likely stacked in an eclipsed conformation. CPK molecular modelling and TEM microscopic techniques showed that the gelator molecules display dense network of large fibers consisting of bundles of single parallel strands. The length of the fibers is of the order of a few micrometers.²³²

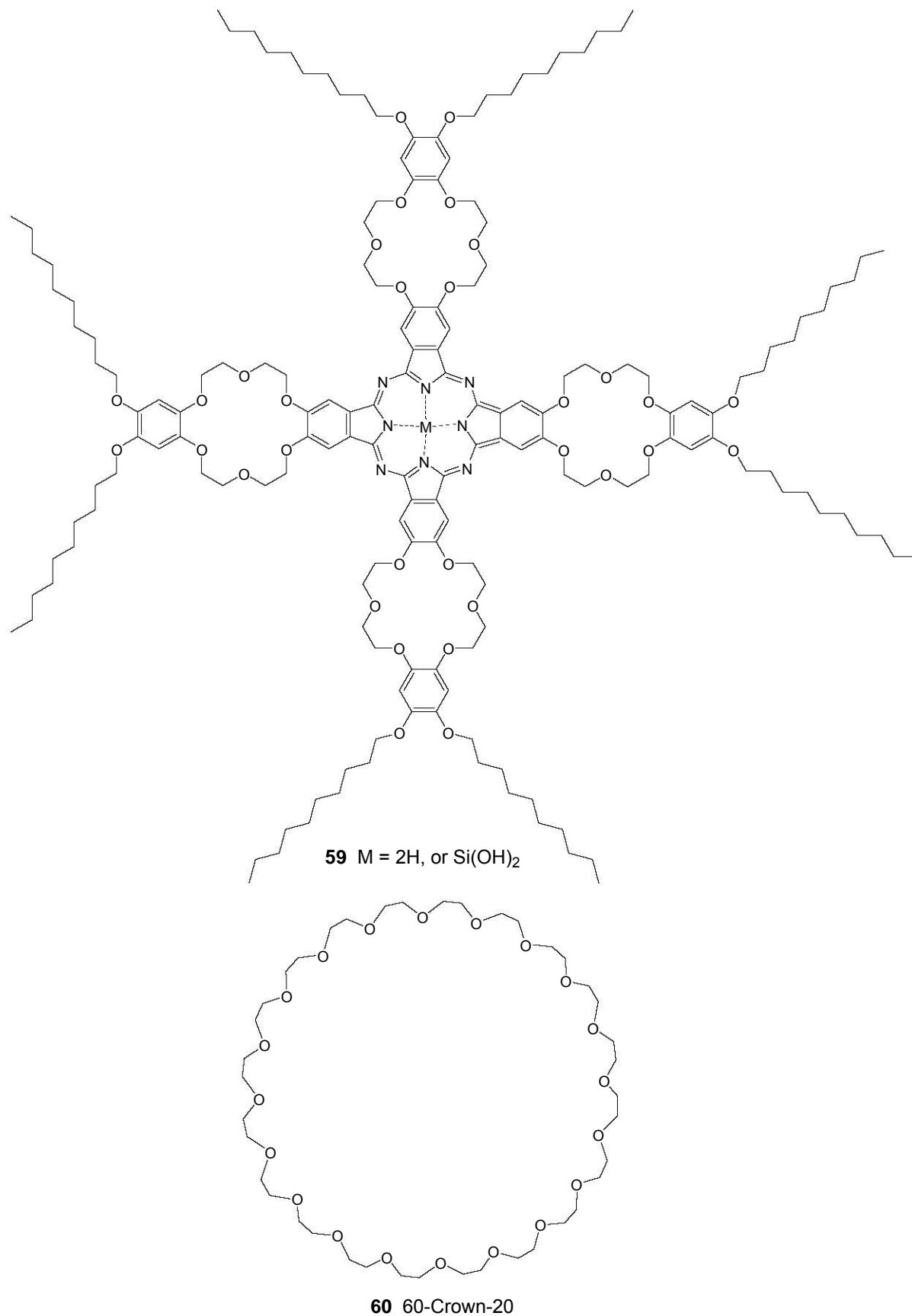


Figure 5.10. LMWOGs containing macrocycles.

In 1991, Prasad *et al.* found that the driving force that induces the gelation of 60-Crown-20 (**60**) in carbon tetrachloride (CCl₄) or acetone is mainly van der Waals interactions (Figure 5.10). By utilizing XRD analysis, they have proposed that the gelator molecules in the dried gel assemble in the same manner as in the crystal state through London dispersion forces.²⁵⁰

V.3.7. LMWOGs Based Hybrid Systems

One of the well-known LMWOGs hybrid systems are those composed mainly of metal ion linked to ligands as a linker. Binding of a metal ion to a gelator can affect the self-assembly modes and tune the gelation process.²⁵¹ One of the earlier gelling complexes is copper(II) β -diketonate (**61**) containing eight alkyl chains which could form green gels in cyclohexane (Figure 5.11).²⁵² The role of the copper in the gelation and the kinetics of aggregation were studied by electron paramagnetic resonance (EPR).

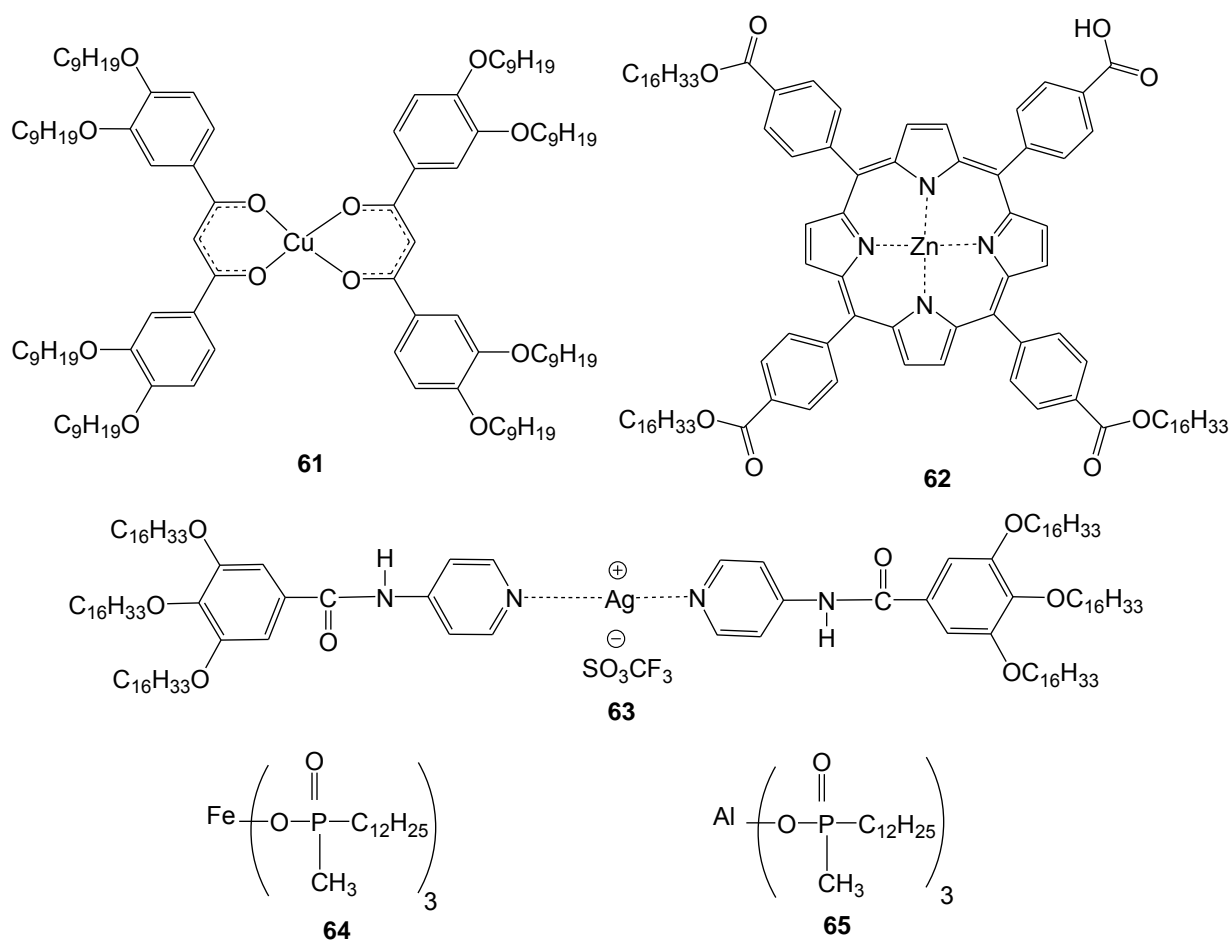


Figure 5.11. LMWOGs based-hybrid systems.

Trisubstituted zinc(II) porphyrin gelator (**62**) with three long ester linked alkyl chains and one carboxylic acid group, can gel efficiently cyclohexane at low concentration (Figure 5.11).²⁵³ The main driving forces necessarily for gelation are the presence of both the free carboxylic acid and the metal center, since the corresponding tetraester does not show gelation phenomenon.²⁵⁴

Authors have designed a symmetrical organo-metallic structure (**63**) bearing a pyridyl group for Ag⁺ coordination and an amide group for the formation of intermolecular hydrogen bonds (Figure 5.11). The complex showed a good gelation property in various mixed solvents such as mixtures of

Part B

Chapter V. Bibliography of Gels and Low Molecular Weight Organo-/Hydro-Gelators

chloroform with acetone, ethanol, or other polar solvents. Interestingly, complexes of other metal cations such as Co^{2+} , Cu^{2+} and Ni^{2+} with the same ligand could not provide gels.²⁵⁵

UV-vis absorption spectra have been employed to determine the stoichiometry of the complex gel. SEM of the xerogel and AFM of the solution showed that the complex gel composed of a belt-like fibrous structure of 50 - 300 nm in width and several tens of micrometers in length weave into 3D network.

In addition, XRD of the xerogel revealed that the belt-like fiber possesses a lamellar structure of the complex with a layer spacing of 6.3 nm. FTIR confirmed the existence of strong hydrogen bonds between amide groups (NH---OC) which together with the van der Waals interactions (hydrophobic interactions) between the alkyl chains were the main driving forces in gel formation.²⁵⁵⁻²⁵⁷

Iron(III) **64** and aluminum(III) **65** complexes of dodecylmethylphosphinic acid represent non-aromatic organogelators and they reveal their abilities to form gel in dodecane.²⁵⁸

V.3.8. LMWOGs Based-Amino Acids, Peptides and their Cyclic Derivatives

Several LMWOGs based amino acids provide the formation of gel fibers through hydrogen bonds, dipole-dipole, π -stacking and van der Waals interactions. The gelation ability depends on the structure of the amino acid residue and the gelation efficiency increases when a molecule includes more than one peptide unit.²⁵⁹ The solvent also has significant effect on the gel fiber network structure as well as on the properties of the gel.²⁶⁰ Compound **66** (Figure 5.12) is a fatty acid amide includes *L*-alanine amino acid, could gel various aliphatic and aromatic hydrocarbons.²⁶¹ FTIR studies showed that the gelation by **66** occurs *via* hydrogen bonds that are significantly affected by the polarity and nature of the solvent. Elongation of the fatty acid chain increases van der Waals interactions as well as mechanical strength and thermal stability of the gel.²⁶¹

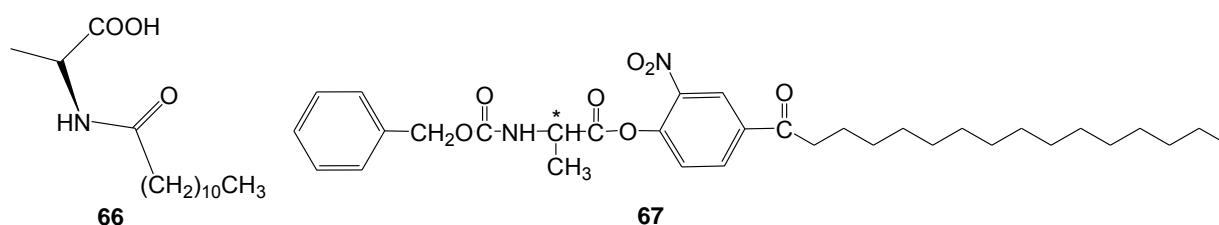


Figure 5.12. LMWOGs based on α -amino acid (*L*-alanine).

Hanabusa *et al.* have reported that *N*-benzyloxycarbonyl-*L*-alanine-4-hexadecanoyl-2-nitrophenyl ester **67** (Figure 5.12) can form strong thermoreversible gels at less than 1.0 wt% in methanol or cyclohexane. TEM and SEM of gels revealed rod-like fibers and huge aggregates with branched structure. FTIR studies confirmed the presence of intermolecular hydrogen bonds between N-H and C=O of the urethane moieties. In addition, they concluded the gelation ability of the molecule is further supported from the dipole-dipole interaction between NO₂ and C=O, as well as the hydrophobic interaction of the long hydrocarbon chain, since the structurally related molecules without NO₂ at the 2-position, C=O at the 4-position, or a long hydrocarbon chain could not act as gelling agents.²⁶²

Authors have studied the chiral structure **67** of the aggregates in a loose gels (0.1 wt%) using circular dichroism (CD) in cyclohexane. The CD spectrum for the *L*-alanine ester at 25 °C revealed a strong negative peak due to the nitrophenylene unit; $[\Theta]_{294} = -6.65 \times 10^4 \text{ g dm}^{-3}$. In contrast, the spectrum for the *D*-alanine ester at 25 °C was characterized by a positive peak; $[\Theta]_{292} = +6.71 \times 10^4 \text{ g}$

Part B

Chapter V. Bibliography of Gels and Low Molecular Weight Organo-/Hydro-Gelators

dm⁻³. These strong CD peaks disappeared at 50 °C as the loose gel transformed to an isotropic solution. Furthermore, a racemic *D, L*-alanine ester did not show any CD bands and could not act as a gelling agent.²⁶²

Mieden-Gundert *et al.* have reported that *N*-acyl-1,ω-amino acid derivative compounds **68 - 81** (have similar structural features to 12-HAS) can exert gelation ability, particularly those derivatives containing long aliphatic chain as spacer between the terminal carboxylic functionality and amide, urethane, or urea group (Figure 5.13). They concluded that the gel formation is mainly driven through van der Waals and hydrogen bonding interactions.¹⁷⁴

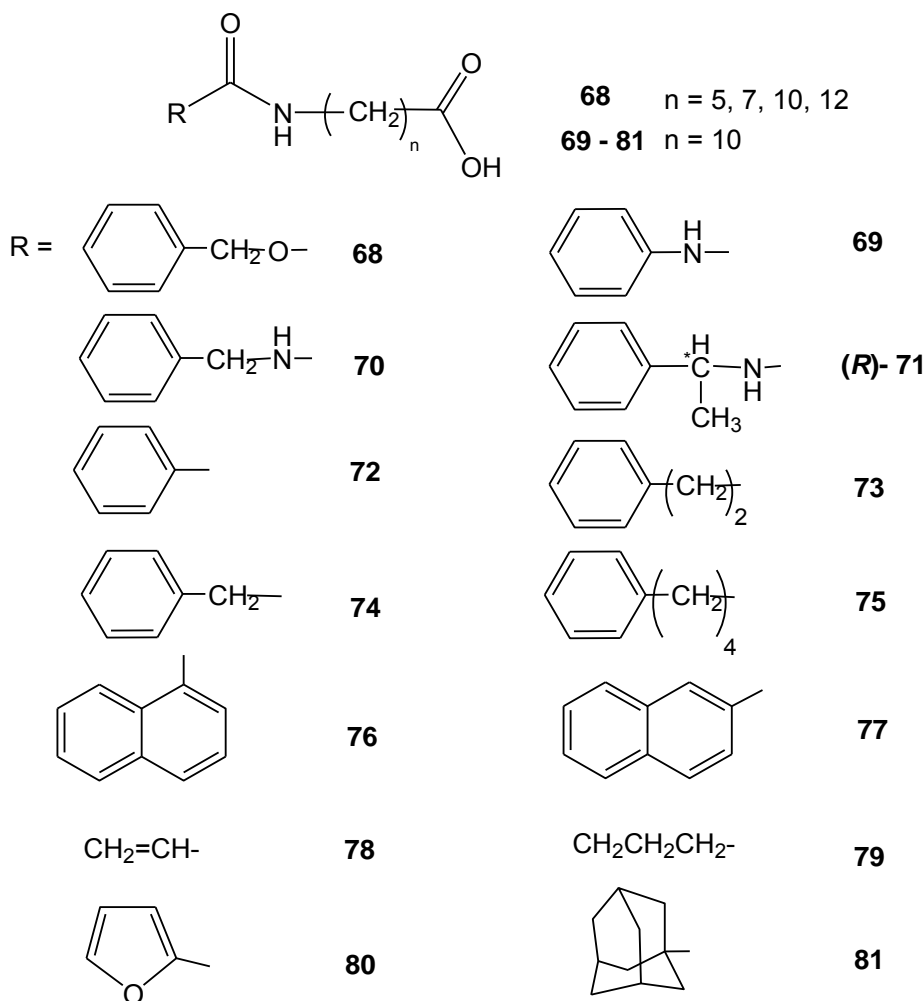


Figure 5.13. LMWOGs based on acylated amino acids.

They have investigated that most of the neutral carboxylic acid derivatives were found to be insoluble in hot CCl₄ and very soluble in DMF at room temperature (> 20 mg mL⁻¹). Only compounds **78** and **79** (Figure 5.13) were observed to gel toluene at a concentration of 0.2 mmol. L⁻¹.

Indeed, they also reported that some of the sodium carboxylate salts have the ability to gel a number of aprotic polar solvents (DMF, DMSO, propylene carbonate, or *N, N*-dimethylacrylamide), for example they have observed the gelation phenomenon for the chiral urea (*R*)-Na **71** but not for the achiral analog 3-Na **70** which lacks the methyl substituent. Consequently, it is clearly remarked that sodium cation coordination and hydrogen bond formation play a major role in the establishment of the gels.¹⁷⁴

Part B

Chapter V. Bibliography of Gels and Low Molecular Weight Organo-/Hydro-Gelators

Janja Makarevic *et al.* have studied three different bis(amino acid) oxalamide gelators (Figure 5.14) capable of forming not only thermoreversible gels with various organic solvents, but also form gels of exceptional thermal stability with some solvents of low and medium polarities.²⁶³

Bis(LeuOH) oxalamide **82** forms thermoreversible gels with high polar solvents such as water, EtOH and other alcohols. Moreover, it forms gels of exceptional thermal stability with some solvents of medium (acetone, butan-2-one, EtOAc, THF) and low (CCl₄) polarities, however the racemate and meso-diastereoisomer of **82** are not act as gelator molecules (Figure 5.14).²⁶³

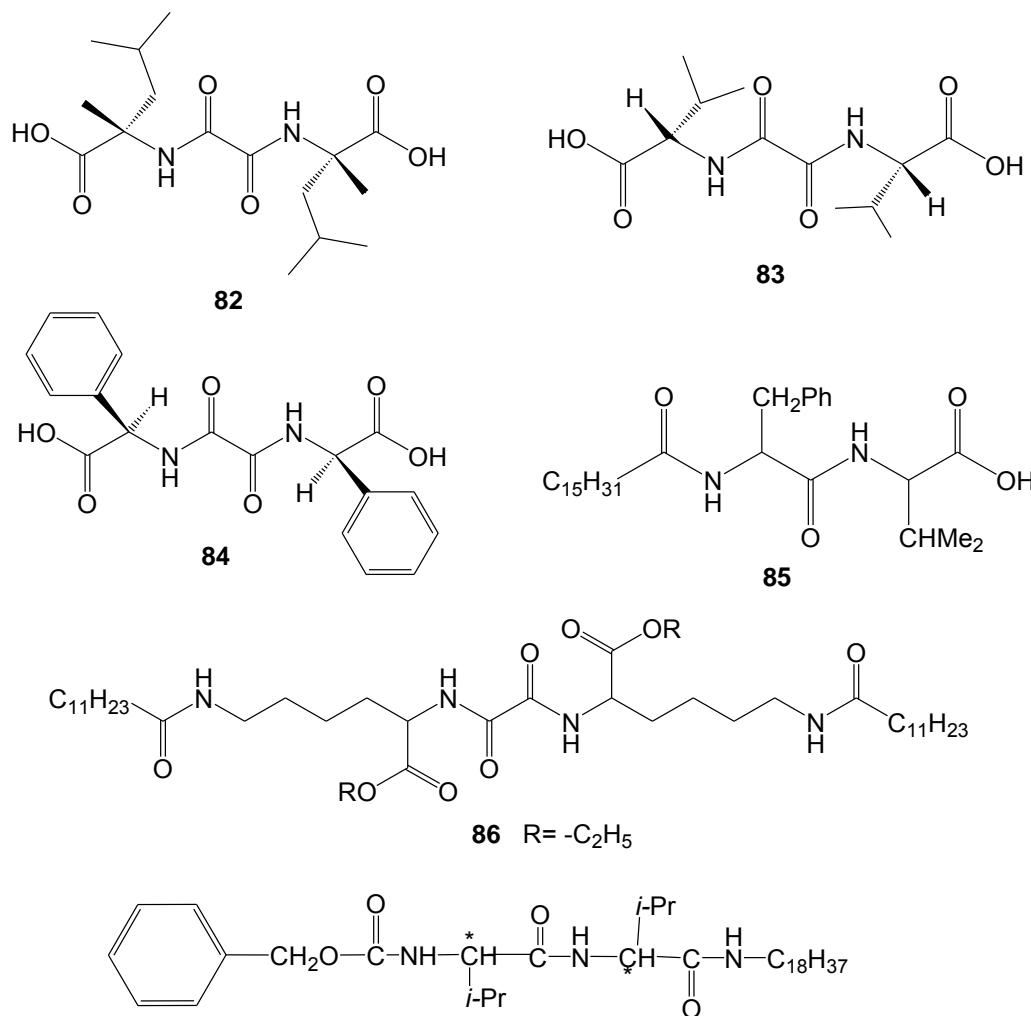


Figure 5.14. LMWOGs based on bis-amino acids.

Temperature-dependent FTIR spectrum of the thermoreversible bis(LeuOH) gel **82** from EtOH investigated that the driving force for the self-assembly is the hydrogen bonds between the amide and carboxylic groups. In addition, temperature-dependent ¹H NMR experiments revealed that only the free or weakly aggregated gelator molecules could be observed at low temperature.^{155,264} In the other hand, the signals of molecules assembled in the rigid gel network could not be observed due to strong broadening induced by long correlation times.^{265,266} By increasing the temperature, the bound gelator signals became more refined due to network disassembly process. The exceptional higher thermal stability of the gel **82** in solvents of low (CCl₄) and medium (acetone) polarities than of higher solvent polarity (EtOH) was explained by the very low gelator solubility in the former solvents which prevent network disassembly even at higher temperatures (Figure 5.14).²⁶³

Part B

Chapter V. Bibliography of Gels and Low Molecular Weight Organo-/Hydro-Gelators

Bis(ValOH) derivative **83** was found to form a thermostable gel only with CCl_4 , while the related aromatic (*R*-phenylglycine) amino acid derivative **84** was not able to form gels with any of the tested solvents, giving precipitates in most cases.²⁶³

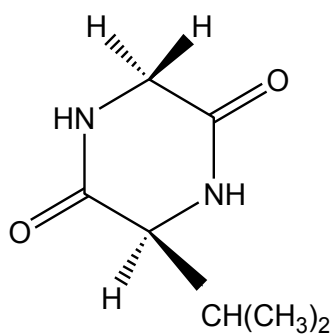
Another dipeptide example is **85** (Figure 5.14) which possesses free carboxylic group, long alkyl chain and a phenyl group in its structure. It forms stable gels in various aromatic solvents and CCl_4 .²⁶⁷ The corresponding sodium salt of **85** showed enhanced gelling efficiency in aromatic solvents but could not gel CCl_4 . There are also other examples of linear amino acid have been reported including *N*-alkanoyl-alanine derivatives²⁶⁸ and terminally protected tripeptides^{168,269} which act as low molecular weight organogelators.

Serendipitously, it has been found that the geminal compound **86** consisting of two oxalyl amides functioned as good organogelator. FTIR and ^1H NMR studies of **86** gel from chloroform indicated that the driving forces of the self-assembly into nanofibers are through inter- and intramolecular hydrogen bonding interactions. TEM images revealed that the gels consist of a 3D network structure formed by entanglement of the self-assembled nanofibers with a diameter of 20 - 40 nm (Figure 5.14).²⁷⁰

N-benzyloxycarbonyl-*L*-valyl-*L*-valine-octadecylamide **87** is an excellent gelling agent, hardening a wide variety of organic liquids including alkanes, alcohols, esters, ketones, aromatics, mineral oils and edible oils. FTIR spectra and the thermodynamic parameters of the gel from cyclohexane suggested that the gel is built up through intermolecular hydrogen bonds between the N-H and C=O groups of both the amide and urethane bonds. TEM of the gels from cyclohexane or ethyl acetate showed that the networks are consisted of numerous intertwined fibres of diameter 10 - 30 nm which are interlocked by van der Waals and hydrogen bonding interactions (Figure 5.14).²⁷¹

According to the aforementioned previous studies, it has been reported that: (i) the gelation ability of LMWOGs based on amino acids strongly depends on the structure and nature of the amino acid residues, (ii) racemic molecules are unsuitable for gelation, (iii) the balance between the hydrophile/lipophile properties is a determinant factor for gelation, and (iv) the gelation ability increases with increasing the number of peptide bonds (more than one amino acid).²⁷¹

Cyclic amino acid compounds such as valine containing cyclophanes²⁷² and cyclo-dipeptides³¹ have shown their gelation ability. Compound **88** (Figure 5.15) represents an example of cyclic dipeptide of glycine and valine, which is able to immobilize organic solvents like ethanol, methoxybenzene, soybean and silicone oil. FTIR and X-ray studies indicated that solvents are gelled through hydrogen bonds between the amide groups.



88

Figure 5.15. LMWOGs based cyclic Val-Gly dipeptide.

V.3.9. LMWOGs Based on New Families Obtained by LCPM Group

Serendipitously in 2001, our laboratory LCPM has announced the first LMWOG based on amino acid derivative **89** which has been obtained after cooling a refluxed solution of leucine amino acid linked to naphthalimide group in toluene. The group has showed the ability of this organogelator to form gel even at low concentration (Figure 5.16). ^1H NMR and FTIR studies confirmed that the gelation process of **89** is supported by hydrogen bonding and π -stacking interactions.²⁷³ The group has reported that the organogelation behavior of the derivative **89** possessing a naphthalimide group in the C-terminal part was higher than those of the phthalimide derivative **90** (Figure 5.16).

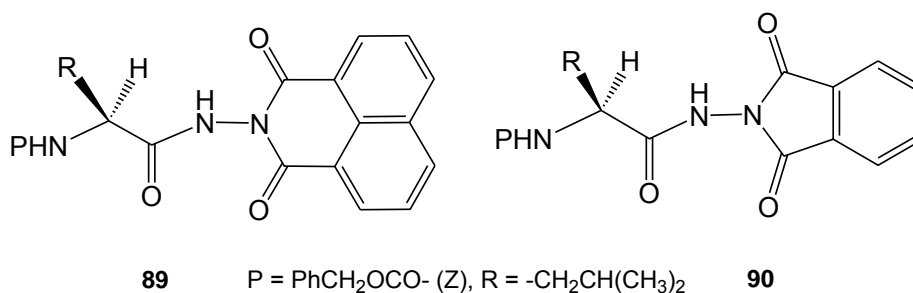


Figure 5.16. LMWOGs based on amino acid derivatives.

This observation gives an evidence of the importance of the π -surface of stacking that involves in the gelation process. They also illustrated that the structural variations of the side chain of the amino acid affect the solubility and the efficiency of the intermolecular entanglement of the aggregates. Thus, the π -stacking appears to be an important contributor to the gelation phenomenon in aromatic solvents, whereas the presence of aliphatic moiety seems to enhance the gelation of aliphatic solvents. SEM image of the dried gel **89** from toluene showed aggregates ranged from a fibrous to a lamellar morphology. The group assumed two steps of the formation of gel fibers from **89** gelator based-leucine amino acid in toluene: firstly, the molecules are stacked up head-to-tail by hydrogen bonds and subsequently the columns are assembled into aggregates through intercolumnar π - π stacking interactions leading to gel fibers networks.^{273,274}

Recently, our laboratory extended their interests to obtain supramolecular gels from linear and macrocyclic pseudopeptides. They gave the evidences of the ability of new two cyclic 1:1-[α/α -N^{*α*}-Bn-hydrazino]-mers **91** and **92** to self-assemble in cyclohexane and toluene forming 3D networks entrapping solvent molecules resulting in thermoreversible gels. They reported that these gels are stabilized by intermolecular hydrogen bonds and π -stacking interactions between the aromatic moieties (Figure 5.17).³⁰

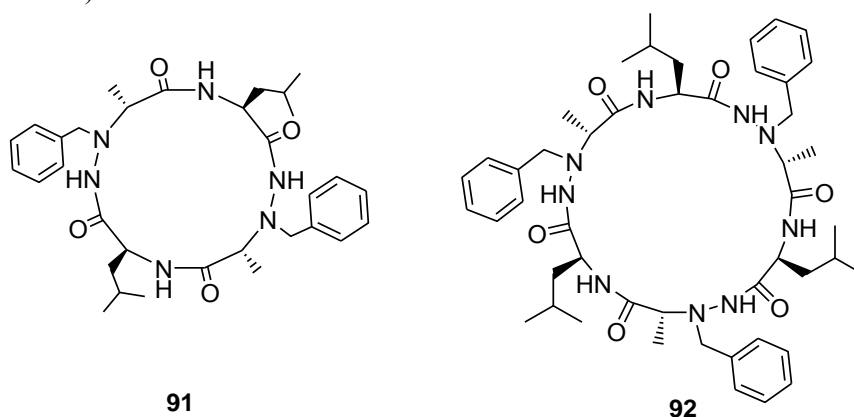


Figure 5.17. LMWOGs based on cyclo-1:1-[α/α -N^{*α*}-Bn-hydrazino]-mers.

¹H NMR and FTIR studies of **91** and **92** have confirmed that the supramolecular structures are stabilized through π - π stacking between the aromatic moieties and the hydrogen bonds between the amide groups in the gels. SEM analysis of the aerogels from **91** and **92** confirmed the presence of non-twisted fibers of diameter 220 nm for compound **91** (from toluene) and 150 nm for compound **92** (from cyclohexane). ATR-FTIR spectra of the crystal and xerogel from **91** showed similar signatures suggesting that the same nanotubular structure exists in the crystal and the xerogel which in turn would be the same in the organogel. XRD data for the aerogel of **91** showed a stacking pattern that was very similar to the one observed in the crystal structure, indicating that the molecules in the gel state adopt similar packing mode (nanotubular structure) as in the crystal structure. Similarly, ATR-FTIR spectra of the xerogel and the crystal of **92** demonstrated the same FTIR signature for the two states revealing that compound **92** self-assembles in the same manner in gel and crystal states.³⁰

V.4. Low Molecular Weight Hydrogelators (LMWHGs)

The demands for novel hydrogels have been increased rapidly in the last 30 years as shown in Figure 5.18, because they are involved in many different disciplines. Recently, hydrogelation phenomenon based on small organic molecules has gained extensive interests particularly in supramolecular chemistry. Synthesis and design of new low molecular weight organic molecules, exhibiting the ability to gel aqueous solvents, have become the goal of many research groups due to their possible promising applications in tissue engineering,²⁷⁵ vehicles for controlled drug release,^{276,277} and pollutants capture and removal.²⁷⁸ In medical and pharmaceutical applications, low molecular weight hydrogelators (LMWHGs) are characterized by their biodegradability and they can control drug release compared with polymeric gels, because LMWHGs are derived from biocompatible components and are held together by weak non-covalent forces which facilitate their degradation in the body.²⁷⁹

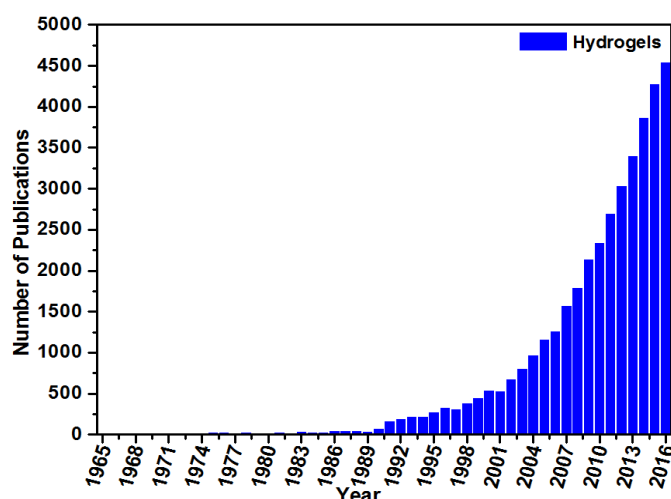


Figure 5.18. Number of papers per year, searching by the topic of “hydrogels” from Web of Science database, Feb./2017.

As we have discussed in the Section V.2.1 that gelation process is the equilibrium state between the tendency of the molecules to dissolve or to aggregate. More precisely, hydrogelator molecules self-assemble in aqueous phase to form three-dimensional supramolecular networks that encapsulate a large amount of aqueous solvent molecules leading to hydrogel formation. Unlike the polymeric hydrogels that are mainly based on covalently cross-linked networks, supramolecular hydrogels are formed *via* the self-assembly of small molecules through non-covalent interactions between the hydrogelator molecules.²⁸⁰ In addition to the role of hydrogen bonds in hydrogels formation, hydrophobic interactions play a vital part in the stability of the formed hydrogels. The most efficient hydrogelator refers to the one that occupies the lowest volume fraction to form a hydrogel (*i.e.*, ables to gel aqueous system at low concentrations).²⁸¹

V.4.1. Structural Diversity of Low Molecular Weight Hydro-Gelators

V.4.1.1. LMWHGs Based on Small Organic Molecules

In recent years, large numbers of supramolecular hydrogels based on small organic molecules have been discovered.^{3,52} Hydrogelators under this category can be sub-classified either as: (i) supramolecular hydrogels made of homotypic hydrogelators, or (ii) hydrogels consisting of mixed components of small molecules.⁵²

V.4.1.2. LMWHGs Based on Long-Chain or Rigid Hydrocarbons

As shown in Figure 5.19, Schmidt *et al.* synthesized a series of derivatives of *N*-amidated 3- and 4-aminobenzoic acids with linear alkyl chains ranging between 3 and 13 methylene units. They discovered the ability of 4-(octanoylamino)benzoic acid sodium salt **93** to form supramolecular thermoreversible hydrogel in 1M NaOH at a concentration of 1.0 wt%. Based on the SEM, XRD and cryo-TEM analysis, the authors have proposed the mechanism of the formation of nanofibers of **93**, which involves the transformation of spherical micelles into ribbons and platelets of multiple stacks of bilayers of the sodium salt derivative of **93**.²⁸²

Kawai *et al.* found that **94** (Figure 5.19) which consists of three amide moieties and one alkyl chain, is pH responsive hydrogelator. Authors reported that **94** self-assembles at pH 9.0 to form 3D network that entraps solvent molecules forming hydrogel at MGC value of 0.3 wt%. The hydrogel of **94** exhibits high sensitivity to the pH change, since decreasing the pH of the gels leads to a gel-sol transition due to the protonation of the ternary amine. On the basis of X-ray diffraction and FTIR analyses, the authors concluded that **94** forms lamellar-like aggregates in the hydrogel and the gel is stabilized by strong intermolecular hydrogen bonds between the amide moieties.²⁸³

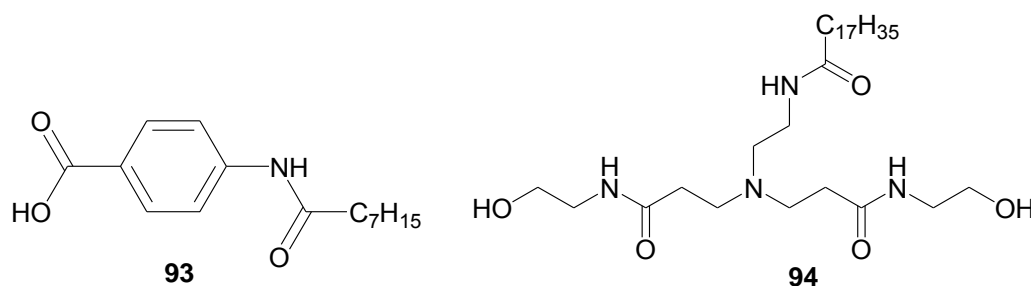


Figure 5.19. Representative molecular structures of long-alkyl-chain-containing hydrogelators.

As shown in Figure 5.20, Galantini and Tato *et al.* reported an interesting hydrogelator of a bile salt derivative that forms a hydrogel in bicarbonate buffer (pH 10.0) at a concentration of 0.18 wt%.²⁸⁴

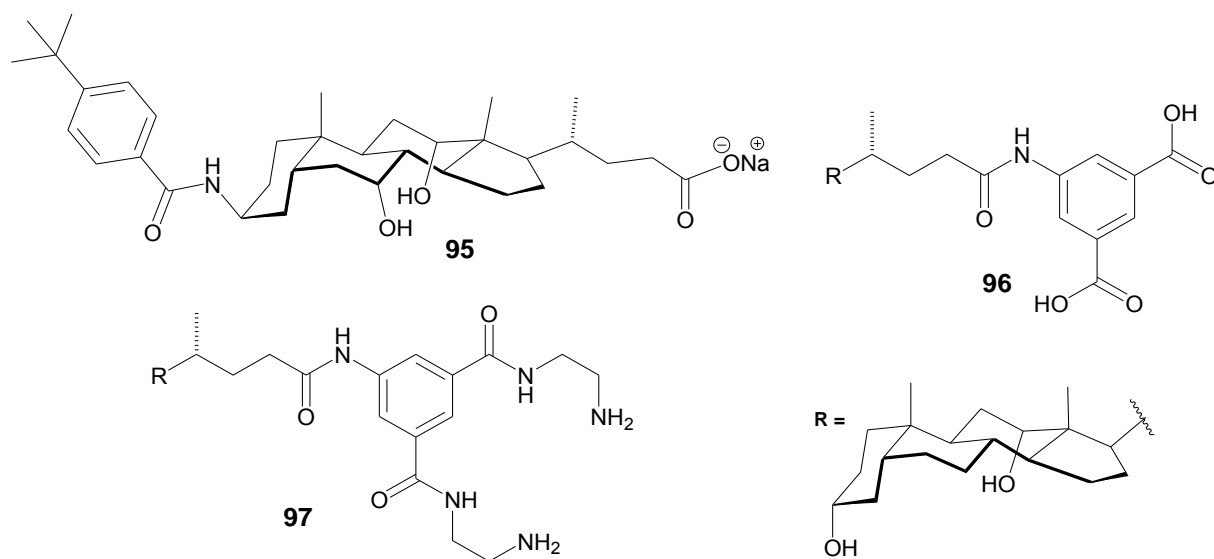


Figure 5.20. Representative molecular structures of rigid-hydrocarbons-containing hydrogelators.

By the help of CD, SAXS, TEM and optical microscopies techniques, the authors concluded that **95** self-assembles in buffer and forms supramolecular nanotubes. According to the authors, the tubule formation starts with the aggregation of the fibrils, followed by a slow transformation and ordering of the tubule walls in well-spaced layers.^{285,286}

Galantini *et al.* obtained compounds **96** and **97** (Figure 5.20) by introducing a diamine or a dicarboxylic aromatic residue on the lateral of a natural bile acid. They reported that while **97** forms a hydrogel at a MGC of 0.16 wt%, a mixture of **96** and **97** results in a hydrogel at a MGC of 0.05 wt%. Accordingly, they concluded that the presence of the electrostatic interaction promotes the hydrogelation from more diluted samples, suggesting that cationic and anionic mixtures enhance the efficiency of the gelators.²⁸⁷

V.4.1.3. LMWHGs Based on Urea, Bisureas and Bismids

Dastidar *et al.* synthesized a small hydrogelator **98** (Figure 5.21) which is able to form hydrogel in water or mixed solvents of water/ethylene glycol with a MGC of 0.8 wt%.^{288,289} The authors have found that the hydrogel is formed only if the urea group at the para position of the pyridine. The crystals formed from water/ethylene glycol system revealed the presence of both water and ethylene glycol, and this provides valuable details about the intermolecular interactions that involve **98**, water and ethylene glycol. Scanning electron microscopy (SEM) confirms the self-assembly by showing the formation of fibrils by **98**. The fibrils of this hydrogelator formed in water are much thinner than the fibrils formed in water/ethylene glycol, suggesting that the addition of ethylene glycol promotes the interfibrillar interactions.

Steed *et al.* reported the gelation ability of a series of chiral bisurea gelators **99** (Figure 5.21).²⁹⁰ Molecule **99** can form hydrogels when (n) is an even number (1.0 wt%) in a mixed solvent (*e.g.*, CHCl₃-MeCN-DMSO : H₂O = 7 : 1), but it fails to act as gelator when (n) is an odd number. On the basis of crystal packing diagrams, authors concluded that the antiparallel urea tape motif appears to be necessary for the formation of hydrogel.

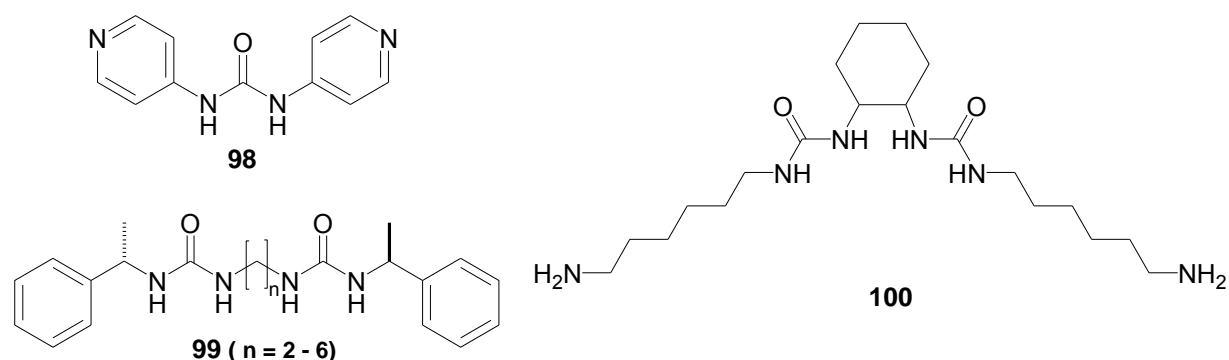


Figure 5.21. LMWHGs based on urea and bisureas.

Furthermore, van Esch *et al.* reported a class of efficient hydrogelators based on a simple connection between hydrophilic hydroxyl or amino functionalities with cyclohexane bisurea organogelators. They reported that **100** in 1.0 M NaOH forms a hydrogel with a MGC of 0.5 wt%. Authors found that the hydrogel formed from the pure enantiomer **100** (Figure 5.21) is more stable than that obtained from racemic at the same concentration.²⁹¹

As we described in Section V.3.2 that bisamides are organic compounds have two amide groups in their structures which increase the possibility of hydrogen bonding interactions and these may support gelation process. Jong Hwa Jung *et al.* reported that aldopyranoside-based compounds act as efficient gelators due to their ability to form gels in various organic solvents and water at extremely low concentrations. On the basis of electron microscopy, the authors revealed that compounds **101** and **102** (Figure 5.22) self-assemble in aqueous system and adopt film-like lamellar structures with 50 ± 100 nm thickness and lengths of up to several micrometers at extremely low concentration of 0.05 wt% which lead to the formation of transparent thermoreversible hydrogels.¹⁴²

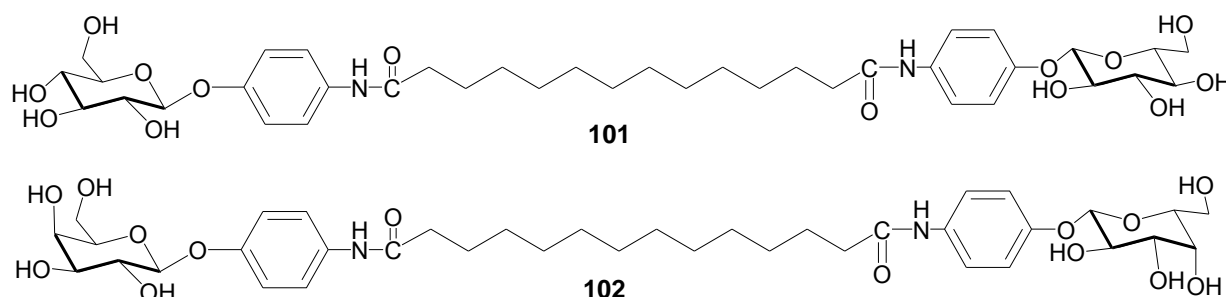


Figure 5.22. LMWHGs based on bisamides.

Based on the results of powder XRD experiments, authors investigated that the bolaamphiphilic-based gelators could form well-ordered monolayered aggregates. XRD, ¹H NMR and FTIR experiments afforded evidences that the self-assembly of these aldopyranoside gelators are stabilized by a combination of different intermolecular forces: (i) hydrogen bonds between amide groups, (ii) π - π stacking between the aromatic groups, and (iii) hydrophobic forces among the fibers through van der Waals forces. The balance between these forces is essential to successfully design the aqueous and the organic gel systems. They also reported that the aromatic units induce rigidity in the structure and support the formation of hydrogels with the help of linear arrangement.¹⁴²

V.4.1.4 Hydrogelators Containing Polyhydroxyl Groups

Song *et al.* studied the effect of NaCl salt on the hydrogelation of 2,4-(3,4-dichlorobenzylidene)-*D*-sorbitol (DCBS, **103**, Figure 5.23) which could form a hydrogel at a concentration of 1.0 wt%. While SEM indicates that the hydrogel consists of globular aggregates, the addition of NaCl to the aqueous medium not only accelerates the gelation, but also results in network of long fibers.²⁹²

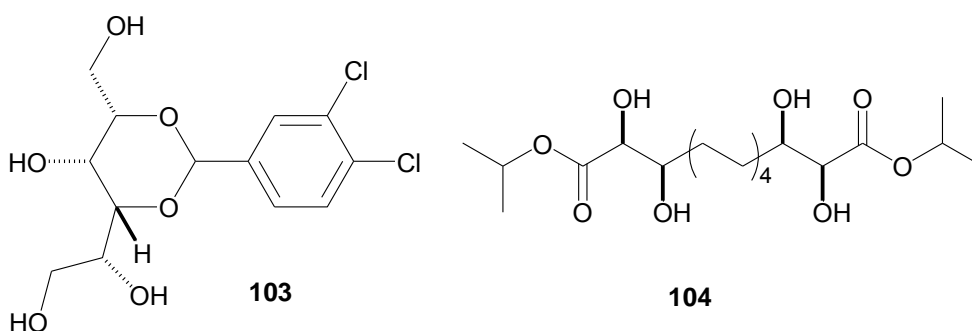


Figure 5.23. LMWHGs containing polyhydroxyl groups.

UV-vis and fluorescence emission revealed that the extensive aggregation of the phenyl rings is responsible for the gelation. Furthermore, temperature-dependent ^1H NMR spectra demonstrated that addition of NaCl salt enhances the π - π interactions. Wide-angle X-ray diffraction showed that the hydrogel has a layered structure. The authors also used density functional theory (DFT) calculations to support the proposed molecular packing of the gelator in the nanofibers.²⁹²

Griffiths *et al.* found that bis- α,β -dihydroxyl esters are able to gel thermoreversibly a wide range of solvents.²⁹³ They reported that **104** (Figure 5.23) can gel a water-rich (75 %) ethanol/water mixture at a concentration of 0.18 wt%. On the basis of SANS, Ohseido *et al.* suggested that in the gelation mechanism, the bis- α,β -dihydroxyl ester motif forms rod-like structure.^{294,295}

V.4.1.5. Bolaamphiphilic Hydrogelators

Bolaamphiphiles are a class of hydrogelators composed of two terminal hydrophilic groups linked by a hydrophobic backbone/chain. The ability of the bolaamphiphiles to self-assemble to give hydrogels and the properties of the formed supramolecular soft materials depend basically on the structures of the “head group” and the “linker” of bolaamphiphiles.⁵²

As shown in Figure 5.24, Blume *et al.* have demonstrated in several studies the efficient hydrogelation belongs to a class of symmetric long chain bolaamphiphiles.^{149,296-306} For example, they reported the ability of dotriacontane-1,19-diylbis[2-(dimethylammonio)ethyl phosphate] (**105**) to form a clear hydrogel at pH 5.0 of concentration 0.1 wt%. Morphological study using TEM analysis revealed that the hydrogelator forms a dense network of helically structured nanofibrils with a diameter of 3 – 4 nm. At pH 5.0, **105** self-assembles to form nanofibrils that are stable up to 75 °C. The authors observed that there is no gelation occurs at pH 10.0, however the nanofibrils are formed and they become fragmented at 75 °C.²⁹⁷

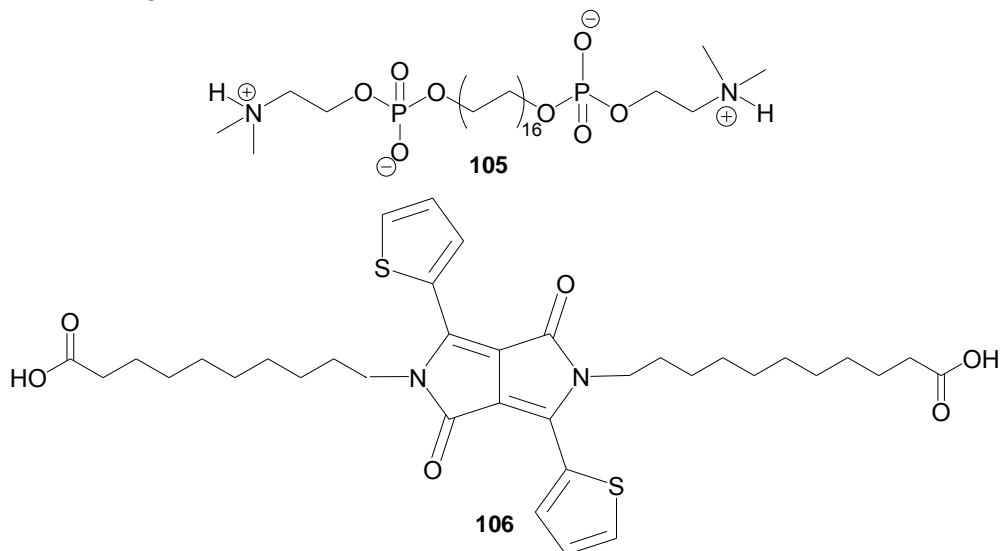


Figure 5.24. LMWHGs based on bolaamphiphiles.

Zhang *et al.* developed a bolaamphiphile **106** (Figure 5.24) that has two carboxylic acid ends and a diketopyrrolopyrrole chromophore in the center. On the basis of the color change associated with the self-assembly process, the authors concluded that the π - π stacking of the central parts and the hydrogen bonds between the ends are responsible for the formation of the nanofibrils of **106** in water. Although **106** self-assembles at a concentration as low as 0.06 wt% in water, the formation of a hydrogel has not been reported by the authors.³⁰⁷

V.4.1.6. Hydrogelators Bearing a Cavity

Jiang *et al.* developed a class of supramolecular hydrogelators possessing a cavity and their structures are mainly based on the cyclotrimeratrylene (CTV). By introducing deprotonable COOH or protonable NH₂ as terminal groups into the rigid and hydrophobic CTV backbones, the authors successfully obtained **107** and **108** (Figure 5.25). These molecules form supramolecular hydrogels with MGCs of 1.0 and 1.5 wt%, respectively. The hydrogels of **107** and **108** are luminescent and exhibit reversibly pH-responsive gel-sol transitions.³⁰⁸

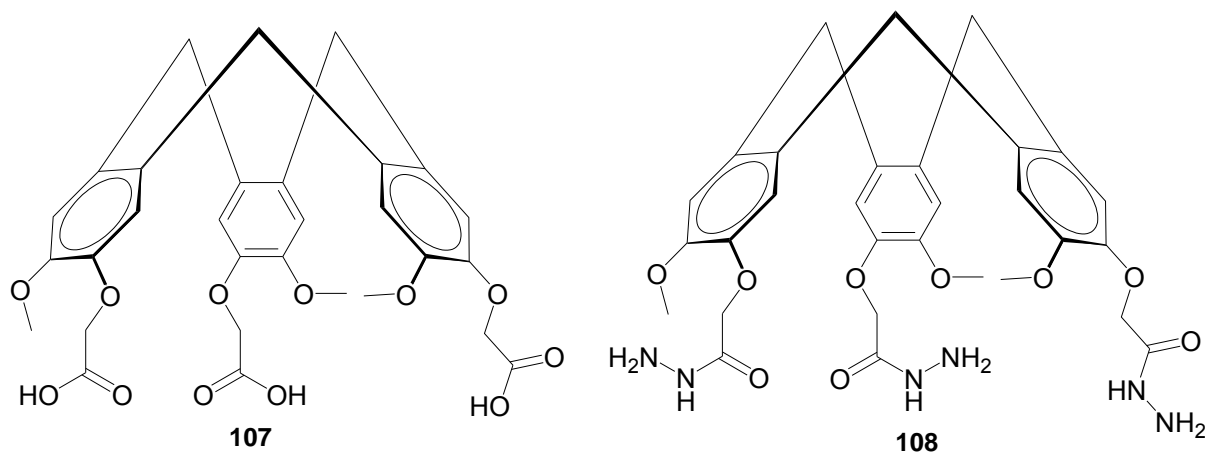


Figure 5.25. LMWHGs possessing a cavity.

V.4.1.7. Hydrogelators Containing a Polyaromatic Core

As shown in Figure 5.26, Banerjee *et al.* found that introducing of *L*-tyrosine into the perylenebisimide core generates a hydrogelator **109** that forms stable, semiconducting, photoresponsive, and pH-sensitive hydrogels. The authors reported that the MGC value of **109** is about 0.27 wt% at pH 5.0. TEM analysis indicates that the self-assembly of **109** starts at 8.8 μ M, which is exceptionally low. On the basis of the impressive photoswitching behavior of this hydrogel, the authors suggested that such a high photoresponse value could lead to soft photodetectors.³⁰⁹

Zang *et al.* reported that a perylenebisimide derivative **110** (Figure 5.26) self-assembles to form hydrogel upon pH triggering. The authors found that addition of hydrochloric acid in the 4.4 mM solution of **110** (in the presence of 26.4 mM triethylamine) results in a dark red hydrogel³¹⁰ which confirms the presence of charge transfer interaction.³¹¹

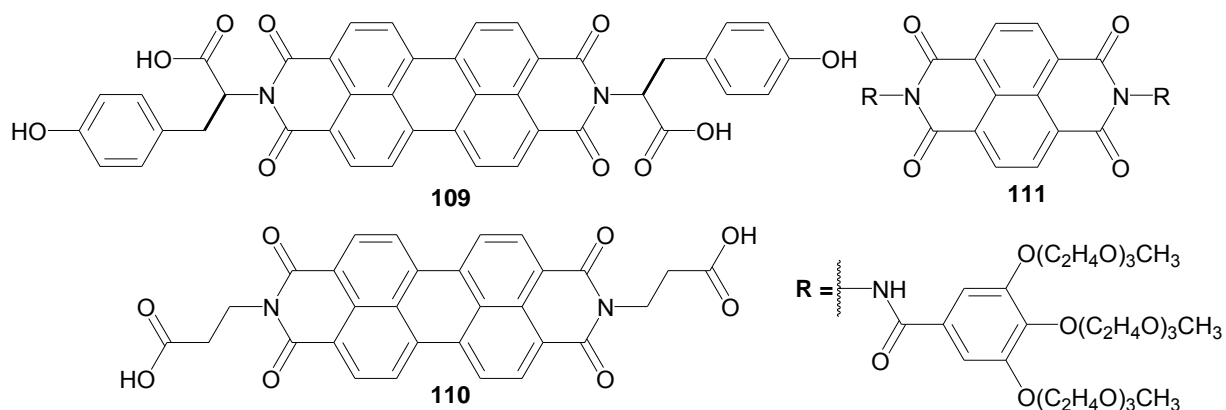


Figure 5.26. LMWHGs possessing polyaromatic moities.

Ghosh *et al.* developed a non-ionic bolaamphiphile **111** (Figure 5.26) which has a naphthalenediimide as the core and ethylene glycol as the side chains. Authors reported that the bolaamphiphil starts to aggregate at 0.05 wt% and forms vesicles. As an electron-deficient core-based bolaamphiphile, **111** forms donor-acceptor (DA) charge-transfer (CT) interactions with pyrene, a water-insoluble electron-rich donor. This interaction ruptures the membrane vesicles to form 1D fibers, thus producing CT-mediated hydrogels with a MGC of 0.3 wt%.³¹²

V.4.1.8. Other Homotypic Hydrogelators

Based on the physico-chemical/structure relationship and the earlier studies concerning the bis(amino acid) oxalamides,^{313,314} Zinic *et al.* found that (*S, S*)-bis(tyrosinol) oxalamide **112** (Figure 5.27) forms hydrogel at concentration of 1.33 (w/v)% upon rapid cooling.³¹⁵

Feng *et al.* have suggested that the carbonyl groups in amino acids play a critical role in hydrogels formation. They developed two C₂-symmetric benzene-based hydrogelators (**113** and **114**, Figure 5.27).³¹⁶ They reported that **113** forms a hydrogel at pH 2.0 with a MGC of 0.25 wt%. In the other hand, the more efficient hydrogelator **114** is obtained by capping the C-terminal of **113** by ethylene glycol and it forms a hydrogel at 0.1 wt%. The authors found unique layered porous structures in the hydrogel of **113** and fibrous structures in the hydrogel of **114**.

Wang *et al.* discovered the hydrogelation ability of tripeptoids. They found that **115** (Figure 5.27) can self-assemble in a mixed solvent of DMSO and H₂O (1 : 1) with the formation of hydrogel at a MGC of 0.5 wt%. Authors concluded that the unsubstituted amide moiety (–CONH–) is crucial for the formation of supramolecular hydrogel without a co-solvent.³¹⁷

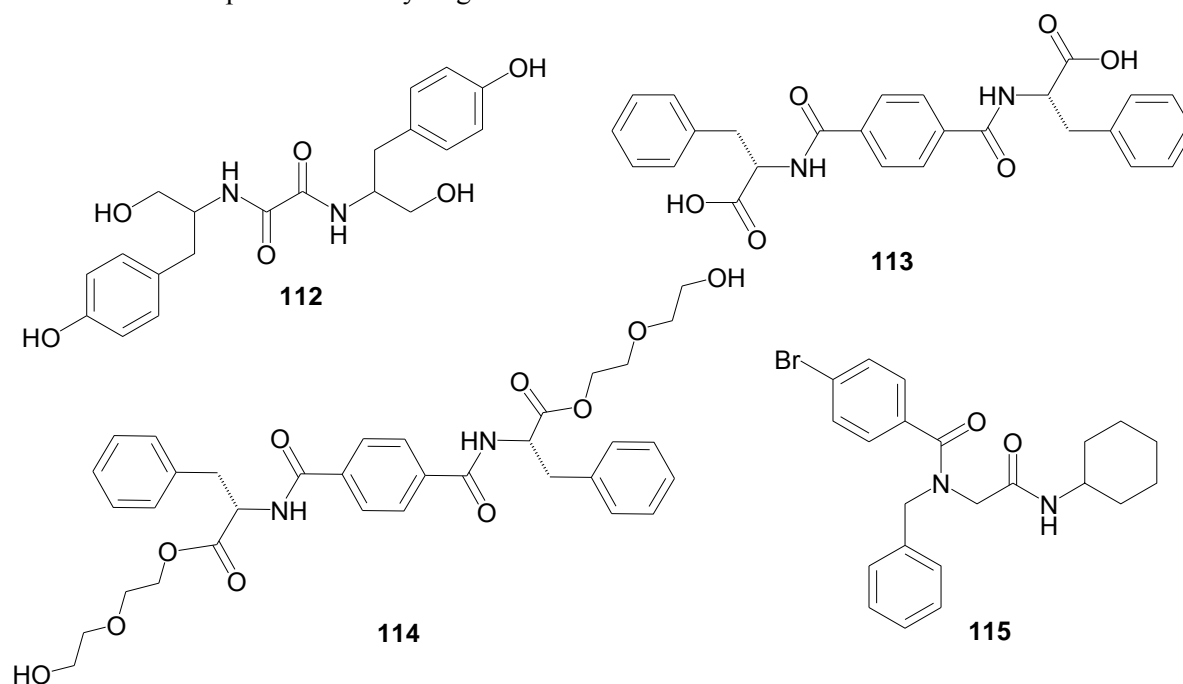


Figure 5.27. Representative molecular structures of other homotypic LMWHGs.

Interestingly, Szymanski and Feringa *et al.* have reported the photoswitch phenomenon of dichromonyl compound **116** that bears an azobenzene. Compound **116** forms a hydrogel in its *trans*-conformation with a MGC of 1.5 wt% (Figure 5.28). Compared to other reported photoswitchable hydrogelators,³¹⁸⁻³²¹ authors investigated that **116** exhibited much faster kinetics and is able to form a gel within 1 min upon photo irradiation of the *cis*-**116** form.³²²

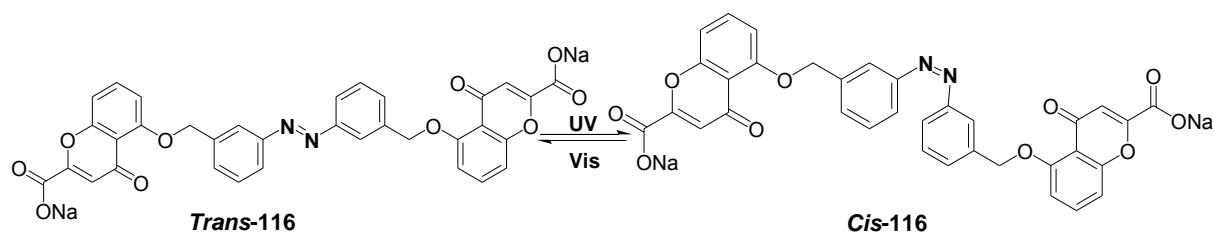


Figure 5.28. Representative molecular structures of the photosensitive LMWHG (**116**).

V.4.1.9. Hydrogelators Composed of Two Components

This family refers to hydrogelators that composed of two components in which usually the both constituents are not gelators by themselves, but together they can act as a gelator *via* intermolecular interactions. Two-component hydrogels have certain benefits over one-component small molecule hydrogels because the tunability of the individual components allows more versatile and dynamic reversibility, which may result in greater diversity in morphology and larger variation in mechanical and optical properties. Moreover, the gelation process and the properties of the gels can be easily tuned by changing the components, the compositions of the components or by functional modifications in one of the components. All these advantages should be beneficial for the applications of these hydrogels.⁵²

As shown in Figure 5.59, Tang *et al.* reported a supramolecular hydrogel consisting of two types of building blocks, 1,2,4,5-benzenetetracarboxylic acid **117** and 4-hydroxypyridine **118**, at a concentration of 2.5 wt%. On the basis of XRD and other spectroscopic techniques, the authors concluded that the hydrogen bonds between the carboxylic acid and pyridine units are strong enough to allow the fibers formation.³²³

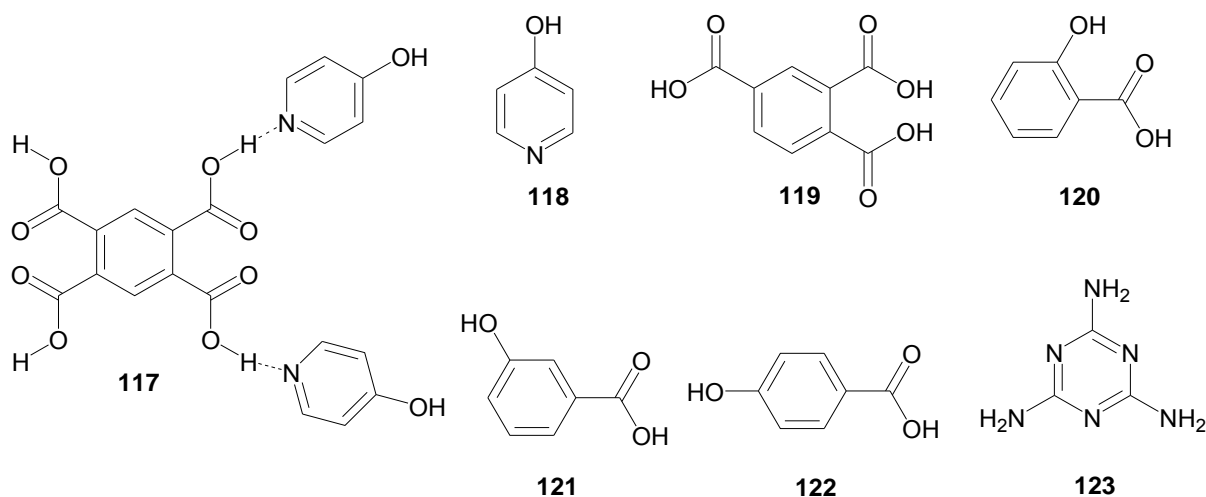


Figure 5.29. Representative molecular structures of two-component LMWHGs.

The same group have developed a number of two-component hydrogelators, including the two-component hydrogel with a MGC of 4.0 wt% upon mixing a branched gelator consisting of 1,2,4-benzenetricarboxylic acid **119** with 4-hydroxypyridine **118** (Figure 5.29). X-ray for a single crystal of the complex from **118** and **119** demonstrated that the molecules assemble into branched fibers *via* different hydrogen bonds.³²⁴ Authors reported that when the concentration of the mixture (*i.e.*, **118** and **119**) is 2.5 wt% and below the MGC, the gelators self-assemble in water to form macrospheres with diameters of millimeters.³²⁵

Nandi *et al.* succeeded to obtain two-component hydrogels by mixing the positional isomers of hydroxybenzoic acid (**120** – **122**) to interact with melamine **123** at (1 : 1) molar ratio (Figure 5.29).³²⁶ The MGC values are 0.5, 1.0 and 0.1 wt% for the hydrogels containing **120**, **121** and **122**, respectively. Based on the spectroscopic studies, the author suggested the contribution of the aromatic protons in the gels formation through π - π stacking interactions. They also found that the strength of π -stacking in the gels follows the order **122** (*para*) > **120** (*ortho*) \approx **121** (*meta*). Finally, they reported that the thermal stability, the storage moduli and the critical strain of the hydrogels follow the order **122** > **120** > **121**.

Bhattacharya *et al.* reported two-component hydrogels consisting of stearic acid (**124**) or eicosanoic acid with di- or oligomeric amines (**125**), (Figure 5.30). The authors demonstrated that **124** and **125** at a molar ratio of (2 : 7) with a total concentration of 5.0 wt%, result in a hydrogel consisting of a 3D network formed by the self-assembled nanofibers of **124** and **125**. The authors succeeded to obtain crystals from the salts of these hydrogelator which allowed them to have deeply insights into the molecular packed structure.³²⁷

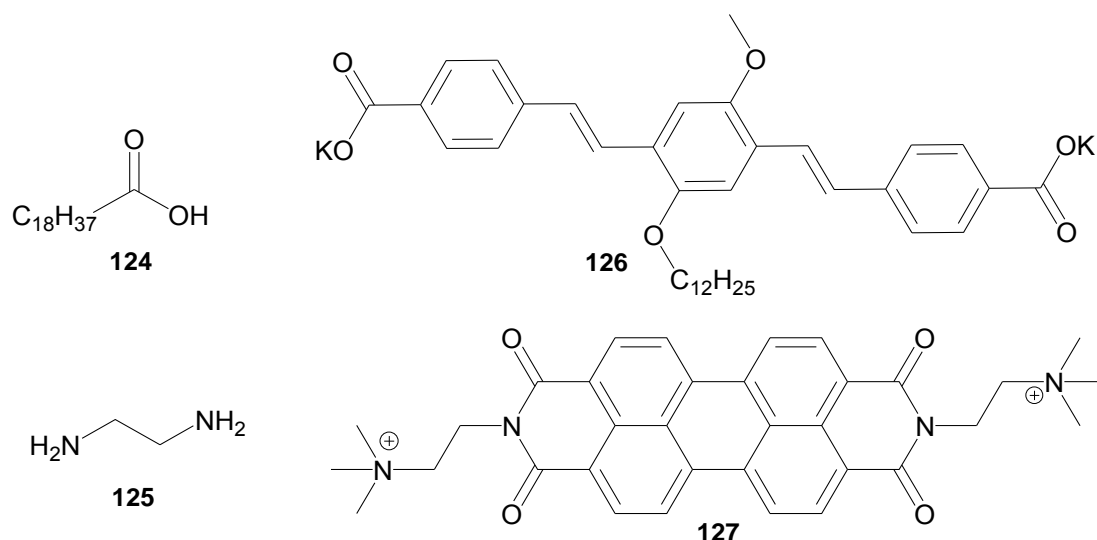


Figure 5.30. Representative molecular structures of other two components LMWHGs.

George *et al.* reported a two-component hydrogel that consists of an oligo(phenylenevinylene) derivative (**126**) and a perylenebisimide derivative (**127**), (Figure 5.30). The two molecules form a strong donor and acceptor interaction in water resulting in a hydrogel at a concentration of 0.4 wt%. Morphological study using TEM technique revealed that aggregation starts at very low concentration of 0.012 wt%.³²⁸

V.4.2. Inorganic–Organic Hybrid Hydrogels

Incorporation of inorganic components into the hydrogels is an effective way that may transfer the unique properties of the inorganic components, such as redox, catalytic, conductive, photoresponsive, photochemical, *etc.* into the soft materials. Development of metallohydrogels based on small organic molecules^{329,330} is mainly focused on the coordination between the organic molecules and metal ions. The organic molecules used in these hydrogel complexes should have functional groups (*e.g.*, carboxylic groups, electron-rich nitrogen atom, *etc.*) that serve as the ligands for metal ions.

V.4.2.1. Hydrogelators Containing Carboxylic Groups as Ligands

Suzuki *et al.*³³¹ reported that although *L*-lysine derivative **128**, (Figure 5.31) is insoluble in water and its alkali-metal salts are water soluble,³³² mixtures of these compounds (**128** and its lithium salt) can form hydrogels at MGC values from 0.5 to 1.7 wt% *via* hydrogen bonding and van der Waals interactions. Authors observed that while **128** forms spherical micelles, the mixtures of the hydrogelators self-assemble to form nanofibers.

Shen and Zhang *et al.*³³³ studied the effect of chirality of the ligand on the gelation process. They reported the supramolecular hydrogelation results from the coordination of phenylalanine (Phe, **129**) with Cu(II) at a MGC of 0.35 wt%, (Figure 5.31). The authors concluded that a decrease of the enantiomer excess of ligand *L*-Phe by *D*-Phe weakens the gelation ability of the Phe-Cu(II) complex. They also suggested that this complex is a promising hydrogelator for developing chiral sensing and recognition platforms.

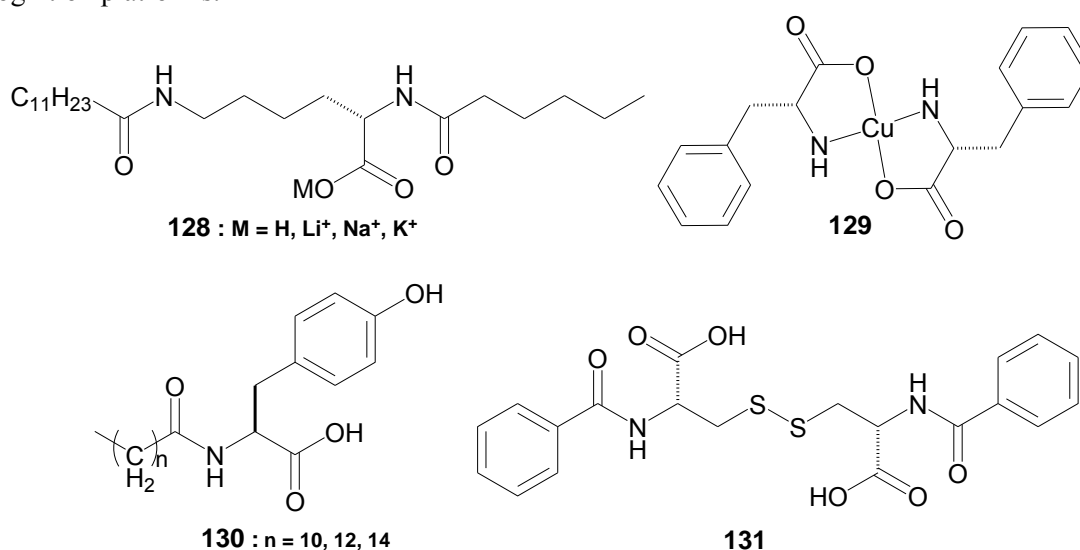


Figure 5.31. LMWHGs containing carboxylic group(s).

Banerjee *et al.*³³⁴ designed a series of tyrosine-based amphiphiles **130**, (Figure 5.31) which bind with Ni²⁺ ion selectively and result in hydrogels at MGC values of 0.78, 0.75 and 0.63 wt% when the chain length is 10, 12 and 14, respectively. Yang *et al.*³³⁵ reported a supramolecular hydrogel based on *N,N*-dibenzoyl-*L*-cystine (**131**) with a MGC of 0.2 wt%. The authors investigated that the interaction between Eu(III) ions and the hydrogelator molecules results in metallohydrogel with enhanced luminescence property.^{335,336}

V.4.2.2. Hydrogelators Coordinating *via* Nitrogen(s)

As illustrated in Figure 5.32, Escuder *et al.*³³⁷ reported the ability of **132** containing pyridine to form a supramolecular hydrogel at 0.5 wt%. They also found that **132** acts as organogelator and it binds with Pd(II) ion to create a functional material to catalyze the oxidation of benzyl alcohol. In the same category, Takaya and Nakamura *et al.*³³⁸ designed a supramolecular gel (**133**) coordinating Pd(II) ion for catalysis. The authors used the xerogel of **133** as a highly efficient catalyst for the intramolecular addition-cyclization of alkynoic acid in water.

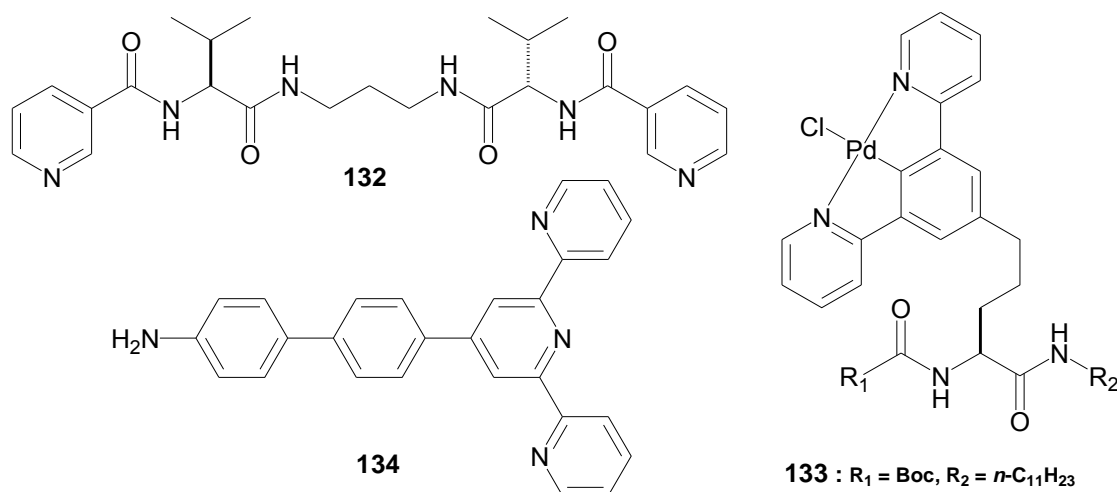


Figure 5.32. Hydrogels based on coordination *via* nitrogen(s).

Mal and Rissanen *et al.*³³⁹ found the formation of hydrogel upon the selective binding between the ligand of 40-[4-(4-aminophenyl)phenyl]-2,2':6',2''-terpyridine (**134**) and Hg²⁺ ion, (Figure 5.32). The interaction between benzo-18-crown-6 ether and the ammonium group on **134** is able to disrupt the hydrogelation, which can be partially recovered by the addition of K⁺ to bind competitively with the crown ether.

V.4.3. Hydrogels Based on Amino Acids, Peptides and their Derivatives

Besides the small organic and inorganic hydrogelators, the hydrogelators derived from amino acids or peptides are of great importance due to their inherent biocompatibility and biological activities. Peptide-based hydrogelators self-assemble *via* various noncovalent interactions, including hydrogen bonding, electrostatic interactions, aromatic-aromatic interactions and/or hydrophobic interactions.³⁴⁰ These intermolecular interactions lead to the formation of organized supramolecular structures that entrap water under appropriate stimuli.

In the following sections, we will present in brief different categories with representative molecules for hydrogelators-based amino acids, peptides and their derivatives which have been developed during the past decades. This summary may help researchers for better understanding the relationship between the peptide structures, conformation of the hydrogelators, and the morphologies of the matrices of the supramolecular hydrogels, and these will allow researchers for rational design of new supramolecular hydrogels.

V.4.3.1. Amino Acid Derivatives

V.4.3.1.1. Amino Acid Derivatives Containing Alkyl Chain(s)

Most amino acid derivatives containing alkyl chains are conventional amphiphiles, consisting of a polar head group and one or two hydrophobic tails.³⁴¹ Dey *et al.* developed a series of amino acid-based gelators *N*-(*n*-alkylcarbamoyl)-*L*-alanine, *e.g.*, molecule **135** (Figure 5.33). Authors observed that all the series can form stable organogels in the presence of water at a concentration of 1.0 (w/v)%. They concluded that water-mediated intermolecular hydrogen bonds between amphiphiles result in the formation of supramolecular self-assemblies. Moreover, the presence of urea moiety as a linkage in the molecular structure of the hydrogelators provides two hydrogen bond donors and one acceptor which support the formation of the supramolecular hydrogels.³⁴²

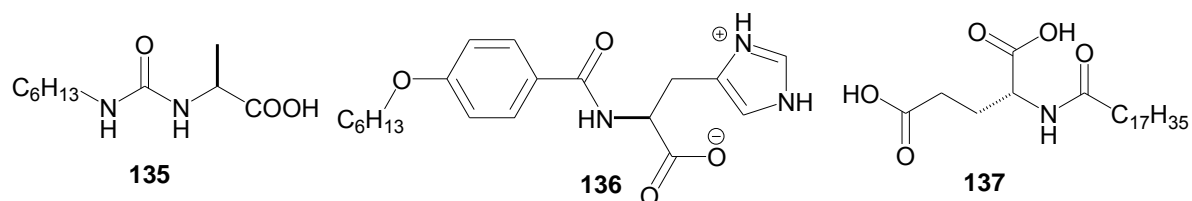


Figure 5.33. Hydrogelators based on amino acid bearing long alkyl chain.

The same group developed a thermoreversible hydrogels with the molecular structure N^{α} -[4-(*n*-alkyloxy)benzoyl]-*L*-histidine containing a hydrocarbon chain such as **136** (Figure 5.33). Authors reported that this molecular structure affords thermoreversible hydrogels in a wide range of pH at room temperature with MGC range of 2.5 - 5.0 (w/v)%.³⁴³

Liu *et al.* reported a multiple hydrogen bonding amphiphile, *N*-stearoyl-*L*-glutamic acid (**137**, Figure 5.33), which forms disk- and fiber-like nanostructures in hydrophilic and hydrophobic environments, respectively. They concluded that the self-assembly process is driven mainly by the intra- and intermolecular hydrogen bonds.³⁴⁴

V.4.3.1.2. Ionic Amino Acid Derivatives

Hydrogelation process occurs when the balance between the hydrophobic and hydrophilic ratio is achieved. Hydrophobic character is represented by the presence of long alkyl chains or aromatic rings segments that decrease the solubility of the hydrogelators in water, however introducing charges or polar groups in the hydrogelators increase their hydrophilic properties enhancing solubility and augment their self-assembly in water.³⁴⁵⁻³⁴⁷

Suzuki and Liu *et al.*³⁴⁸⁻³⁵⁰ developed hydrogelator *L*-lysine-based pyridinium bromide salt **138**. They reported the ability of **138** to form a hydrogels at a wide range of pH values and it reflects a low MGC of about 0.3 wt% at neutral pH, Figure 5.34.

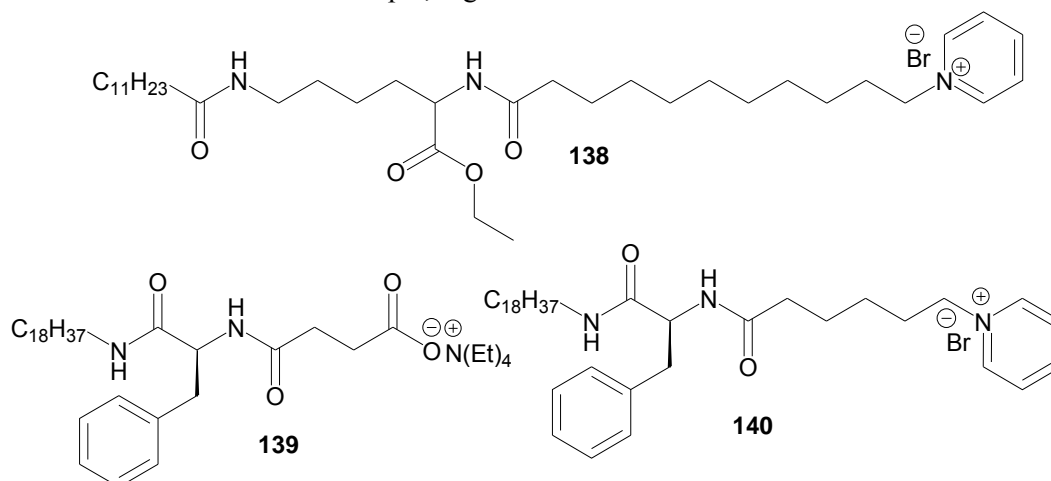


Figure 5.34. Hydrogelators based on ionic amino acid derivatives bearing long alkyl chain.

Yang *et al.* reported the ability of the two chiral *L*-phenylalanine-based salts (**139** and **140**) to act as hydrogelators.³⁵¹⁻³⁵³ Figure 5.34 illustrates the molecular structures of **139** containing an ammonium salt, while the hydrogelator **140** has a pyridinium salt. Both of them can self-assemble in aqueous media at different pH values to form supramolecular hydrogels with MGC values of 1.2 - 2.0 wt% and < 1.0 wt% for **139** and **140**, respectively.

V.4.3.1.3. Amino Acid Derivatives Containing Aromatic Group(s)

Introducing of aryl motifs (*e.g.*, ferrocenyl, fluorenyl, naphthyl or pyrenyl) in the molecular structures have an effective role in the self-assembly and hydrogelation process. The self-assembly is supported mainly by aromatic-aromatic interactions leading to the formation of mechanically strong and stable supramolecular hydrogels.³⁵⁴⁻³⁵⁶

As shown in Figure 5.35, Zhang *et al.* discovered that ferrocenoylphenylalanine (**141**) self-assembles in water to form a stable hydrogel. They reported that **141** is multiple responsive hydrogelator and it exhibits a sharp phase transition in response to different external stimuli (*i.e.*, oxidation-reduction reaction, guest-host interaction and pH changes).³⁵⁷

Fmoc-group is widely used as protecting group in peptide synthesis, it has become a popular *N*-terminal capping motif in peptidic hydrogelators for several reasons: (i) Fmoc-protected amino acids or peptides are commercially available or quite easy to be synthesized, (ii) can be easily incorporated into peptide/ amino acid derivatives, (iii) low cost, and (iv) excellent capacity to promote self-assembly which leads to hydrogels formation. Changing the pH is the common external stimuli to induce formation of supramolecular hydrogels from Fmoc-protected amino acids or peptides.⁵²

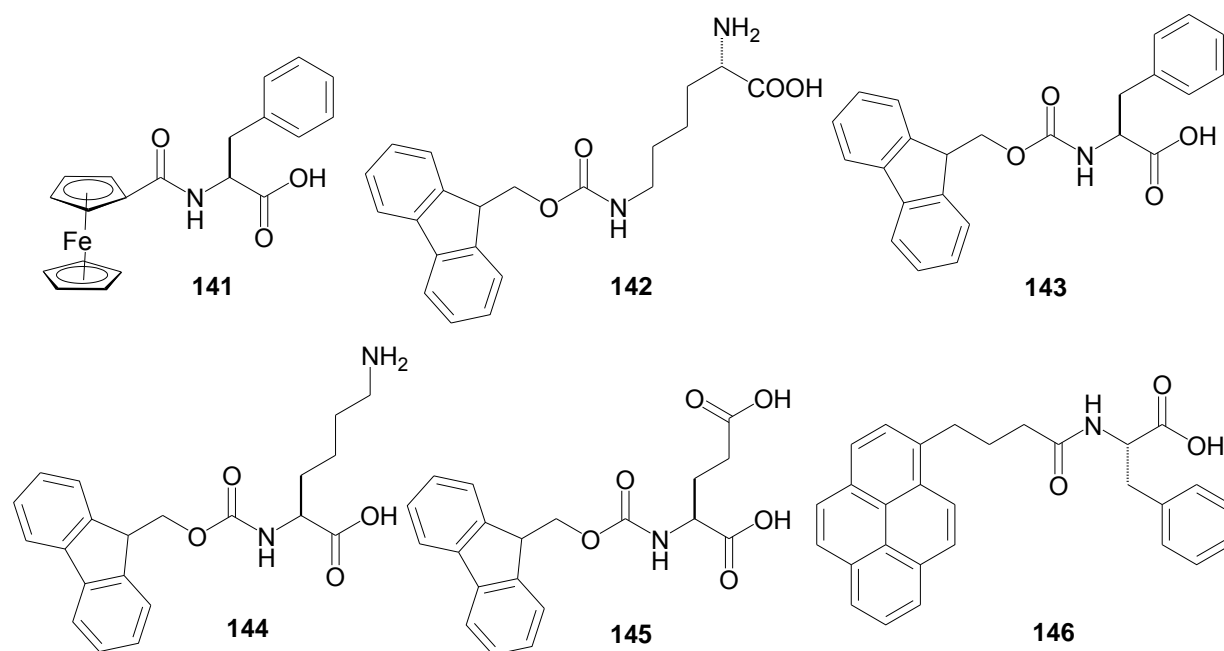


Figure 5.35. LMWHGs based on amino acid derivatives bearing aromatic moieties.

Xu *et al.* stated the first case of the use of Fmoc-amino acid derivatives to generate multicomponent supramolecular hydrogels (Figure 5.35).^{102,358,359} They reported that mixing and then heating (1.0 equiv.) of **142**, (1.0 equiv.) of **143** and (2.0 equiv.) of Na_2CO_3 in water eventually leads to the formation of hydrogel upon cooling the hot clear solution to room temperature. The authors declared that the hydrogel exhibits exceptionally high storage moduli and a rapid recovery of its original mechanical strength after removal of the external forces.^{358,359}

Banerjee *et al.* also reported that the co-assembling between the two oppositely charged Fmoc-amino acids (*i.e.*, Fmoc-Lys **144** and Fmoc-Glu **145**) gives rise to the formation of hydrogel with a MGC value of 1.8 wt% (Figure 5.35).³⁶⁰

Pyrene has become a popular moiety to be incorporated into supramolecular hydrogelators.^{277,361} Banerjee *et al.* designed and developed a hydrogelator (**146**) consisting of a single amino acid and a pyrene group (Figure 5.35). Authors reported that **146** can form hydrogels in a wide range of pH (7.5 – 14.0) in the aqueous phase. They also reported that increasing the the pH causes a distinct morphological change of the nanofibers of the hydrogel from helical to tape-like.³⁶²

As the π -surface area of aromatic-aromatic interactions increases, the ability of the molecules to self-assemble to afford gel increases. Although the aromatic-aromatic interaction between two phenyl groups is weaker than that exists between two fluorenyl or two pyrenyl groups, phenylalanine is often incorporated into peptides for increasing the tendency of self-assembly.⁵²

V.4.3.1.4. Amino Acid-Based Bolaamphiphiles

Liu *et al.* developed series of bolaamphiphiles such as **147** with head groups made of *L*-glutamic acid, and a hybrid linker composed of two rigid benzene rings and a butyl segment (Figure 5.36). They reported that by changing the pH of the solution, the hierarchical self-assemblies can be controlled. While the molecules of **147** form a hydrogel in water at a concentration of 0.5 wt% (MGC) at pH 3.0, the hydrogelator form vesicle-like aggregates at pH 12.0.³⁶³

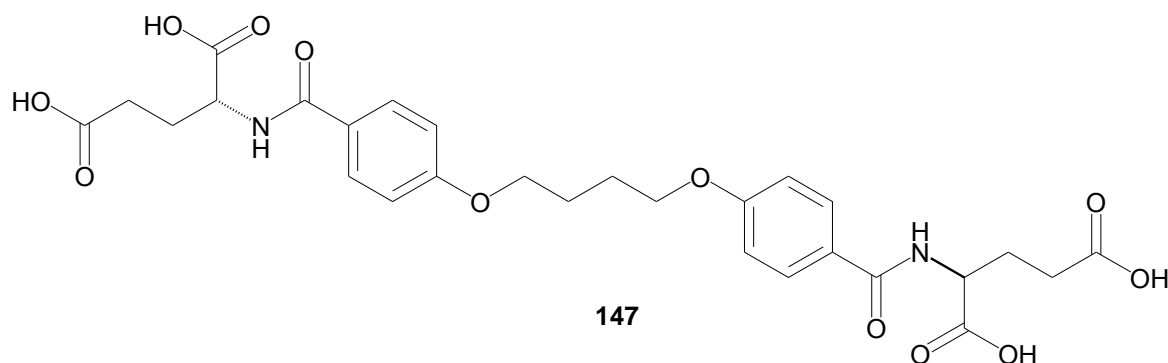


Figure 5.36. Amino acid-based amphiphile as LMWHG.

V.4.3.2. Peptides

Numerous low molecular weight hydrogelators based on small peptides,^{364,365} such as dipeptides have been designed and they showed their abilities to self-assemble in water yielding supramolecular hydrogels. Gazit *et al.* investigated that diphenylalanine (FF **148**, Figure 5.37)³⁶⁶⁻³⁷⁰ has the ability to self-assemble in water, and the nanofibers entangle to form 3D network trapping the solvent molecules leading to hydrogel formation.³⁷¹⁻³⁷⁴ Park *et al.* demonstrated that **148** self-assembles in water with the formation of nanowires and nanotubes with high thermal, chemical, and proteolytic stability. The authors confirmed the crystallinity of these nanowires and nanotubes using XRD study.³⁷¹

Ventura *et al.* reported that while the dipeptides Ile-Phe (IF **149**) can self-assemble at 1.5 wt% in water to give hydrogel consisting of persistent nanofibers with a diameter of about 55 nm, Val-Phe (VF **150**) can not self-assemble. Accordingly, the molecular structure affects greatly on inducing hydrogelation as the only difference between **149** and **150** is the presence of one methylene group which exerts its effective role in the self-assembly process in case of **149** (Figure 5.37).³⁷⁵

There are rare reports concerning the self-assembly of the cyclic peptides and this is attributed to the difficulty in their synthesis.^{376,377} As shown in Figure 5.37, Feng *et al.*³⁷⁸ reported that the cyclodipeptide **151** containing tyrosine and lysine residues acts as a hydrogelator and forms a hydrogel

at a MGC of 0.6 wt%. They demonstrated that the subsequent hydrogel has a relatively low mechanical strength formed with the assistance of ultrasound. They found that the MGC increases to 1.5 wt% when an alkyl chain attaches at the ϵ -amino group of the hydrogelator **151**.³⁷⁸

Marchesan *et al.* studied a series of tripeptides containing one *D*-amino acid moiety at the *N*-terminal and they reported the effect of the chirality on the morphology of the nanofiber networks that lead to hydrogels. They found that while the tripeptides VFF and FFV can not self-assemble at physiological pH, *D*-VFF (**152**) and *D*-FFV (**153**) in Figure 5.37 are able to self-assemble at a concentration of about 0.67 wt%. Authors observed that while hydrogelator **152** self-assembles into nanotapes, hydrogelator **153** results in twisted nanofibers.³⁷⁹ The same group confirmed their principle through another hydrogelator *D*-LFF (**154**, Figure 5.37), which forms a hydrogel at 0.67 wt%. They reported that the self-assembly of **154** affords mainly nanofiber networks, the self-assembly of LFF is rather polymorphic and fails to form a self-supporting hydrogel.⁸²

Cao *et al.* found that FFY (**155**, Figure 5.37) has the ability to self-assemble to form nanoparticles which convert into nanorods after photo-cross-linking. They also reported that Fmoc-FFY (**156**) forms weak hydrogel at 0.1 wt% consisting of nanofibers that turn into nanoparticles after photo-cross-linking.³⁸⁰

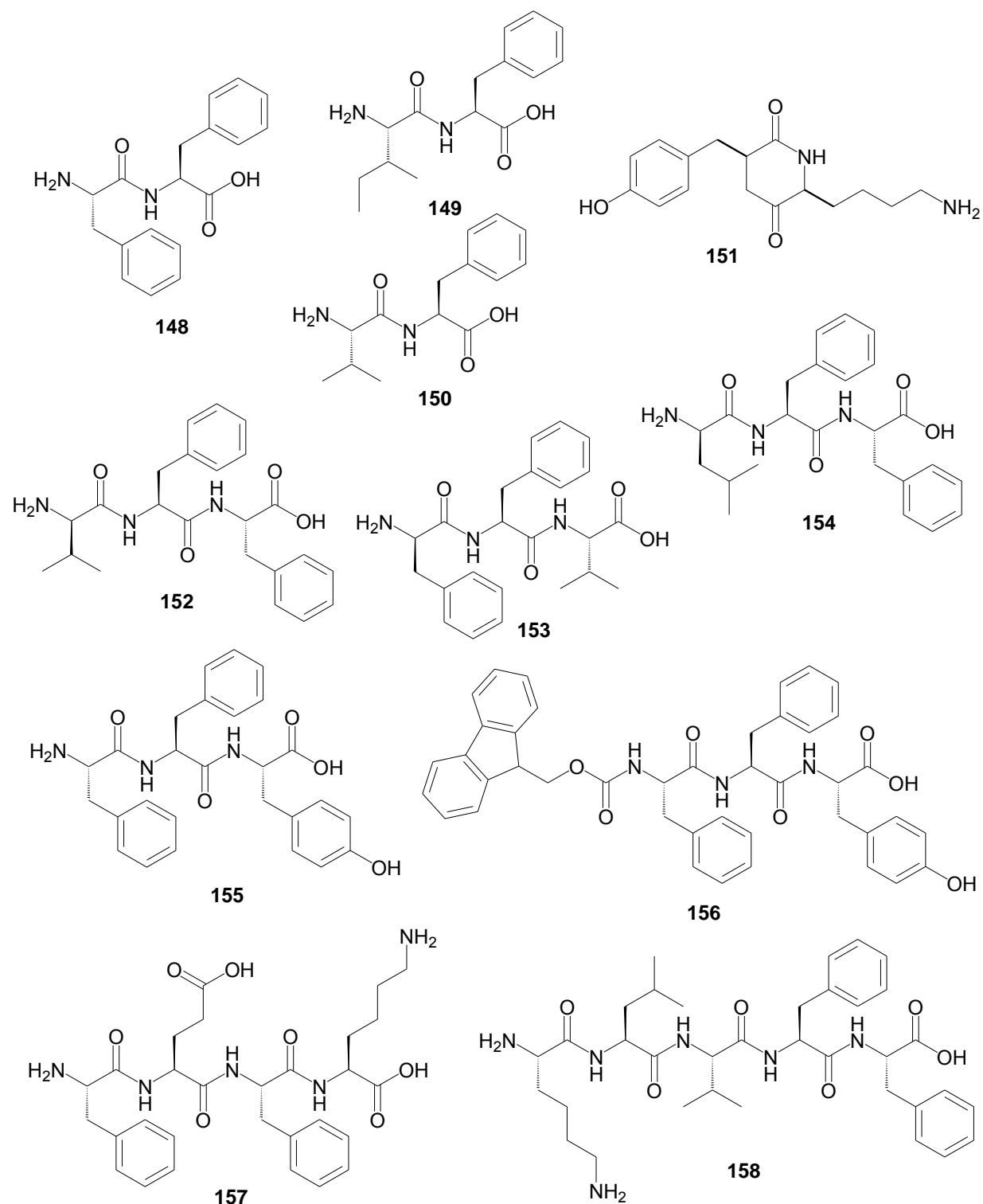


Figure 5.37. Representative molecular structures of LMWHGs based on different peptides.

Miller *et al.* reported that while the tetrapeptide (FEFK **157**, Figure 5.37) fails to induce hydrogelation even at high concentration of 10.0 wt%, **157** can serve as a substrate for thermolysin to undergo reverse hydrolysis for enzymatic hydrogelation by the formation of octapeptides as the final products.³⁸¹

Hamley *et al.* investigated the hydrogelation ability of the pentapeptide KLVFF (**158**, Figure 5.37). They reported that while (**158**) self-assembles at 2.5 % in water, it forms hydrogel at 3.0 % in phosphate-buffered saline. They confirmed the self-assembly process by the observation of fibrils of diameter 10 nm formed from aqueous solution using cryo-TEM and SAXS techniques.³⁸² More extensive overview about other examples concerning longer LMWHGs based-peptides have been reviewed.⁵²

V.4.3.3. Peptide Derivatives

V.4.3.3.1. Peptides with Capped *N*- and/or *C*-Terminals

Based on many previous studies, we could conclude that not only the native peptides can act as hydrogelators, but also peptide derivatives can self-assemble in water to form hydrogels. The most common way to modify a peptide is to block the *N*-terminal, the *C*-terminal or to cap both ends.³⁸³⁻³⁸⁵

Solaro *et al.* investigated the ability of the *N*-protected tetrapeptide Ac-RWDW-NH₂ (**159**) to form soft hydrogel at 0.026 wt% in PBS buffer (Figure 5.38). They observed that an increase in the concentration of **159** and the addition of CaCl₂ result in a transparent hydrogel.³⁸⁶

Furthermore, Xu and Lu *et al.* reported that the *N*-protected hexapeptide Ac-IIICGK-NH₂ (**160**, Figure 5.38) can act as hydrogelator since it self-assembles in water forming long nanofibers and results in a hydrogel at 0.53 wt%. Authors could not get any hydrogel upon replacing the Cys with a Met residue, although they reported the formation of nanofibers at 1.7 mM.³⁸⁷

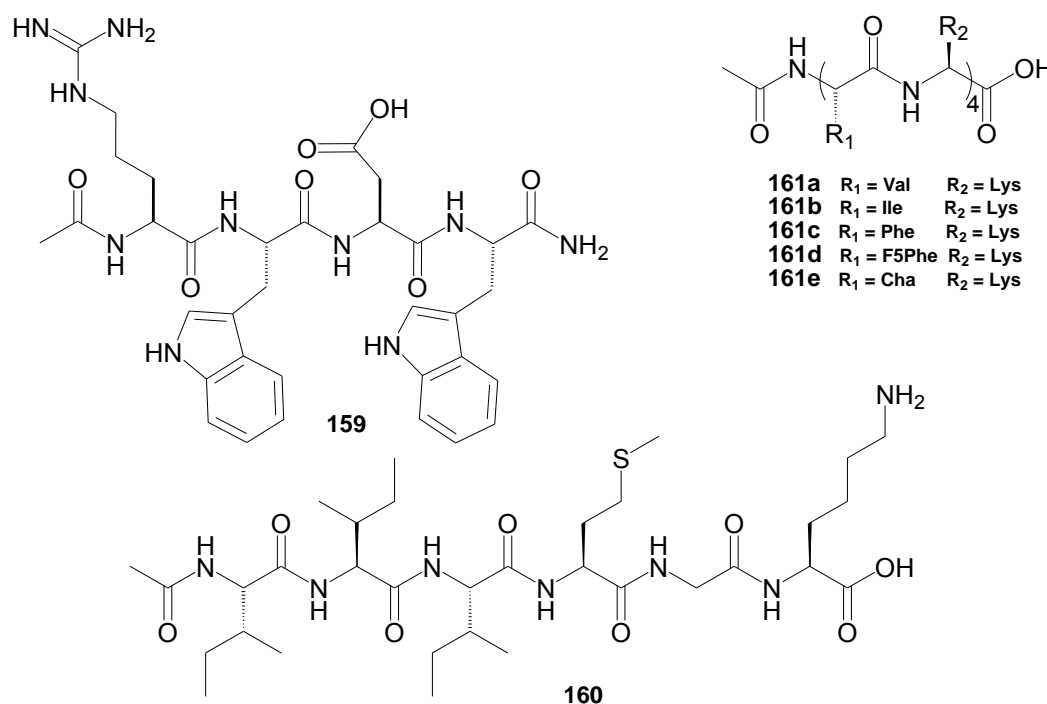


Figure 5.38. Representative molecular structures of peptidic LMWHGs with capped *N*-terminal.

Nilsson *et al.* synthesized a series of capped octapeptides [Ac-XKXKXKXK-NH₂; X = Val (**161a**), Ile (**161b**), Phe (**161c**), pentafluorophenylalanine F₅-Phe (**161d**) and cyclohexylalanine (Cha) (**161e**)] that are composed of alternating hydrophobic residues (X) and positively charged residue (Lys). At concentration of 8.0 mM, the authors reported that **161a** is unable to form hydrogel and it is too hydrophilic, in the contrary **161b**, **161c**, **161d** and **161e** self-assemble in water to form a

assembly is mediated by a counter ion and stabilized by van der Waals, hydrophobic forces, ionic bridging and hydrogen bonding interactions.⁴⁰⁴

Moreover, Stupp *et al.* developed hydrogels formed by co-assembly of amphiphiles with opposite peptide polarities. For example, authors reported that mixing the molecules **165** and **166** as shown in Figure 5.39 with complementary polarities, results in co-assembled structures possessing unusual thermal stability compared to the assemblies formed by only one of the both components.⁴⁰⁵

V.4.3.3.3. Peptide Derivatives Containing Aromatic Group(s)

LMWHGs based on *N*-terminal functionalized peptides with large aromatic groups have recently emerged as an interesting class of supramolecular hydrogelators.⁴⁰⁶⁻⁴⁰⁹ The most commonly used aromatic group is Fmoc.⁴¹⁰⁻⁴¹² In the past decades, several Fmoc-dipeptide derivatives have been reported.^{7,378,413-425} As shown in Figure 5.40, Ulijn *et al.* developed the low molecular weight hydrogelator Fmoc-diphenylalanine (Fmoc-FF, **167**).⁴²⁶⁻⁴²⁸ The authors reported that the molecules of **167** form hydrogels by adjusting the pH of the aqueous solution of **167**,^{426,429} or by the addition of water to a DMSO solution of **167**.^{430,431}

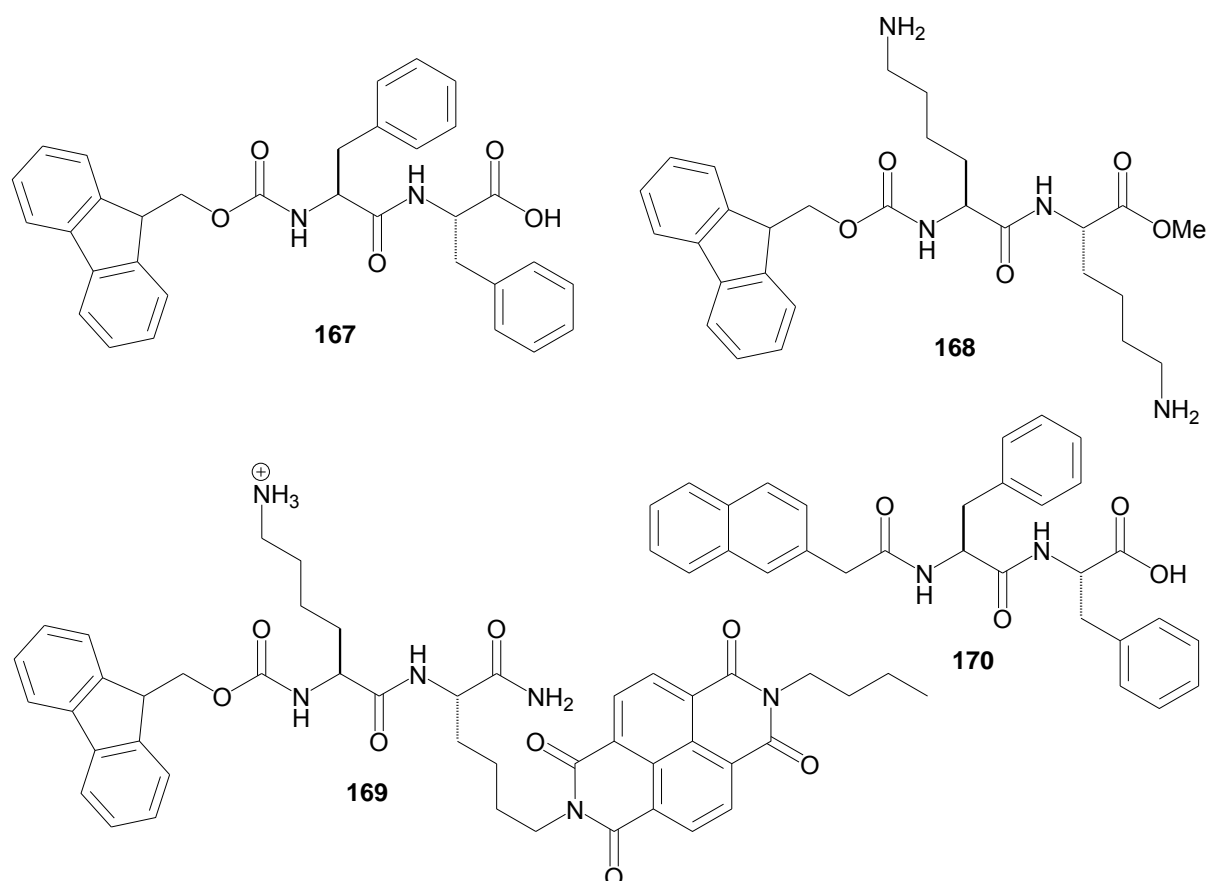


Figure 5.40. Representative molecular structures of LMWHGs based on peptide derivatives bearing aromatic moieties.

Fmoc-peptide derivatives with more than two amino acids are also excellent candidates for self-assembly to form hydrogels.^{432,433} These small molecules are obtained by both chemical approaches^{394,434-436} and enzymatic reactions.⁴³⁷⁻⁴⁴²

Part B

Chapter V. Bibliography of Gels and Low Molecular Weight Organo-/Hydro-Gelators

Parquette *et al.* reported that the functionalization of Fmoc-dipeptide Fmoc-KK (**168**) at the ϵ -amino position with a naphthalenediimide (NDI) chromophore leads to the formation of Fmoc-KK(NDI) (**169**), Figure 5.40. This molecule (**169**) forms a self-supporting hydrogel at a concentration of 1.5 wt% which exerts high thermal stability up to 75 °C.⁴⁴³

Naphthalene^{444,445} is another aromatic group frequently used in peptide derivatives to achieve strong intermolecular interaction for self-assembly through its π -aromatic surface.⁴⁴⁶

Figure 5.40, Xu *et al.* reported dipeptide derivative **170** obtained from conjugating 2-(naphthalen-2-yl)acetic acid with Phe-Phe. Authors found that the self-assembly of **170** in an aqueous environment is supported by the naphthalenyl group which provides the hydrophobic force, while the dipeptide backbone acts as both hydrogen bond acceptors and donors. They also mentioned that the hydrogelator **170** forms hydrogel at a concentration of 0.8 wt% with gel-to-sol transition temperature at about 323 K.⁴⁴⁷ Single crystals form **170** were grown from a mixed solvent of ethanol and water and the results revealed that the aromatic-aromatic and hydrogen bonding interactions are the main driving forces for the self-assembly.^{448,449}

In addition to Fmoc and naphthalene aromatic groups, the pyrene motif not only enhances aromatic-aromatic intermolecular interaction to promote self-assembly, but also exhibits fluorescence property that helps in studying the aggregation behaviors of the hydrogelators.^{450,451}

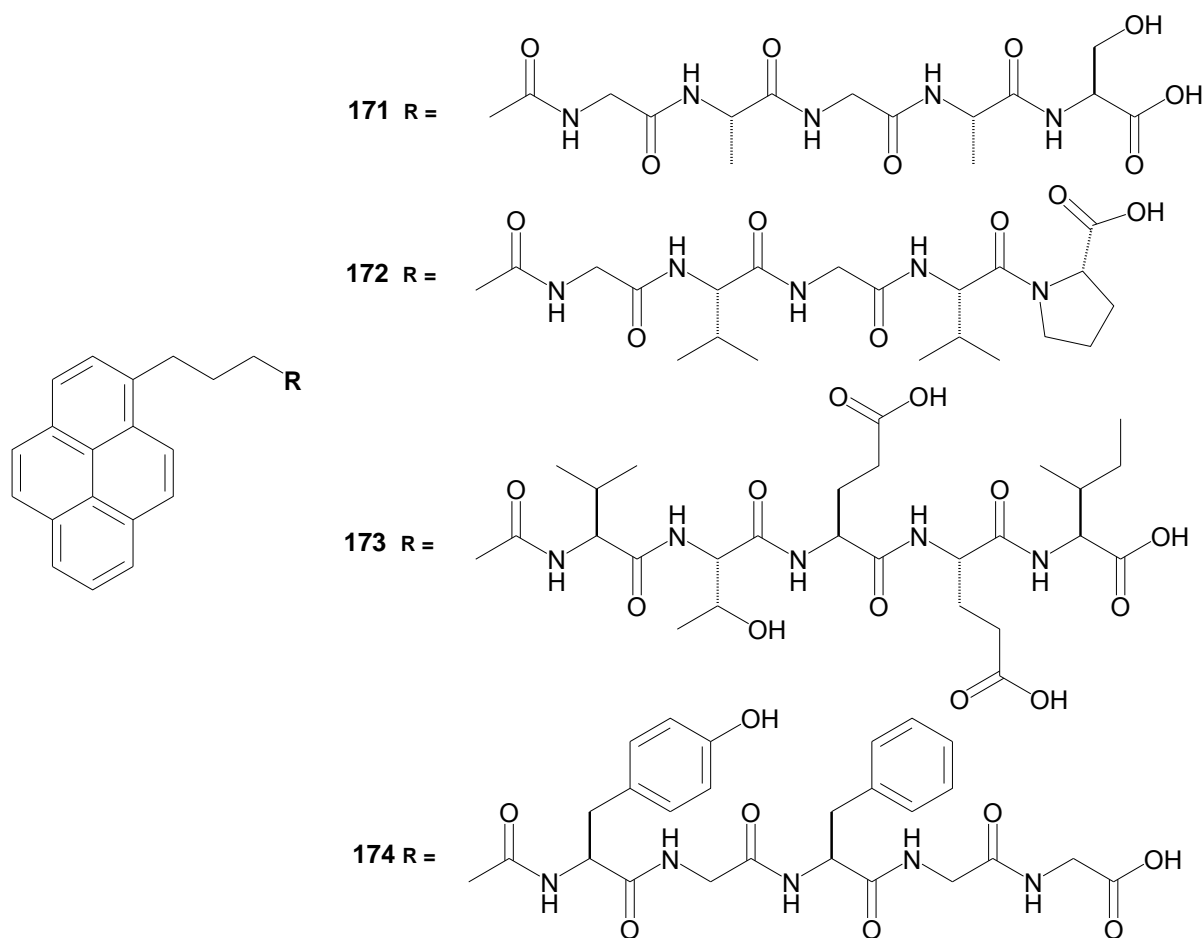


Figure 5.41. Representative molecular structures of LMWHGs based on peptide derivatives bearing pyrene as an aromatic moiety.

V.4.3.3.5. Peptide Bolaamphiphiles

Peptide-based bolaamphiphiles exhibit diverse self-assembly behaviors in responding to different external stimuli.⁴⁶⁰ As shown in Figure 5.43, Das *et al.* developed a series of bolaamphiphiles by changing the amino acids (*e.g.*, Phe, Tyr, Leu or Gly) as the head groups. The authors reported that changing the pH, triggers the hydrogelation of these peptide bolaamphiphiles. For example, **177** at concentration of 0.003 wt% can self-assemble affording hydrogel by pH triggering.

Recently, several studies have shown that replacing the alkyl chain (linker segment) in the peptide-based bolaamphiphiles with π -conjugated system, results in molecules exhibiting potential uses in organic electronic devices, such as photovoltaic cells.^{461,462} For example, Stupp *et al.* developed a peptide-based bolaamphiphile **178**, (Figure 5.43) which composed of three segments: (i) polar amino acids for solubility, (ii) β -sheet forming amino acids for self-assembly, and (iii) an oligothiophene core for conductivity. They reported that the self-assembly of the molecule **178** results in a hydrogel at low concentration of 1.0 wt%.

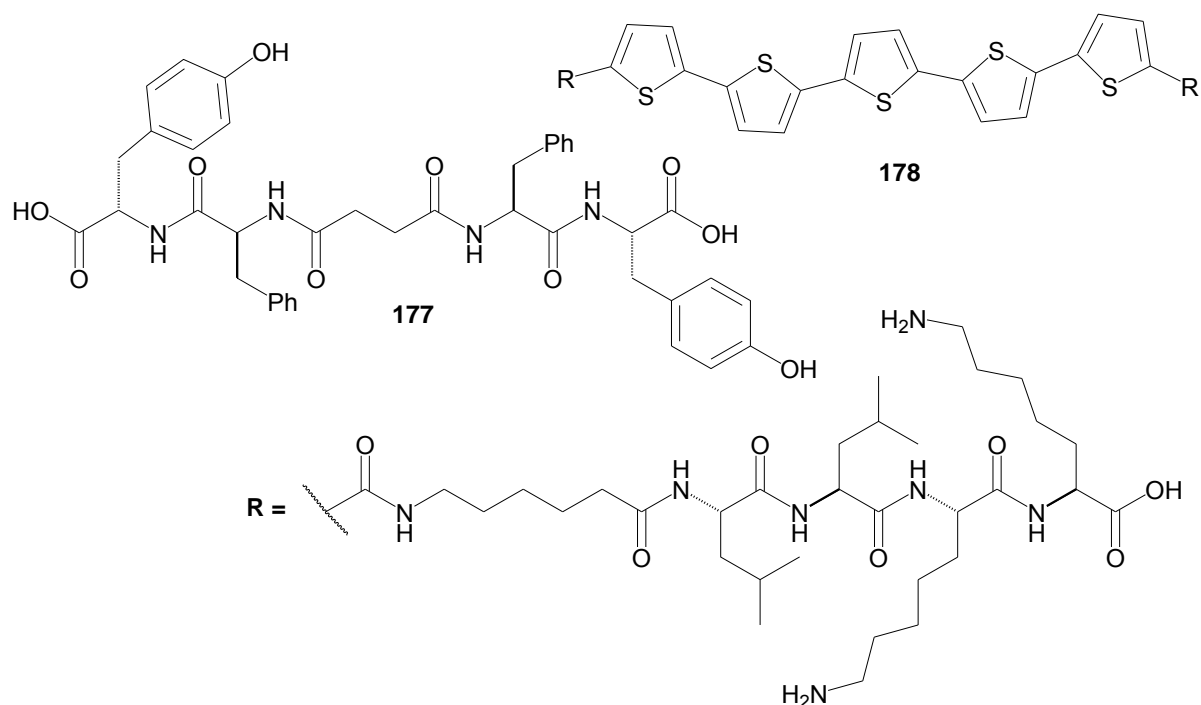


Figure 5.43. Representative molecular structures of peptide-based amphiphiles as LMWHGs.

V.4.4. Hydrogels Based on Nucleobase Derivatives

Design of new hydrogelators based on nucleobases has become an interesting subject of study in the fields of cell biology and supramolecular chemistry particularly after the discovery of the DNA double helix structure over 60 years ago and more deeply by the presence of specific interactions between the base pairs of the DNA.⁴⁶³ Nucleobase hydrogels have been classified into two main groups: (i) the homotypic, and (ii) the multicomponent hydrogels.

V.4.4.1. Homotypic Hydrogels Based on Nucleobases

As shown in Figure 5.44, Barthelemy *et al.* synthesized a family of new uridine phosphocholine hydrogelators (**179**). They reported that these hydrogelators self-assemble in water to form DNA-like helical nanofibers and result in hydrogels at concentration around 6.0 wt%.¹³⁷

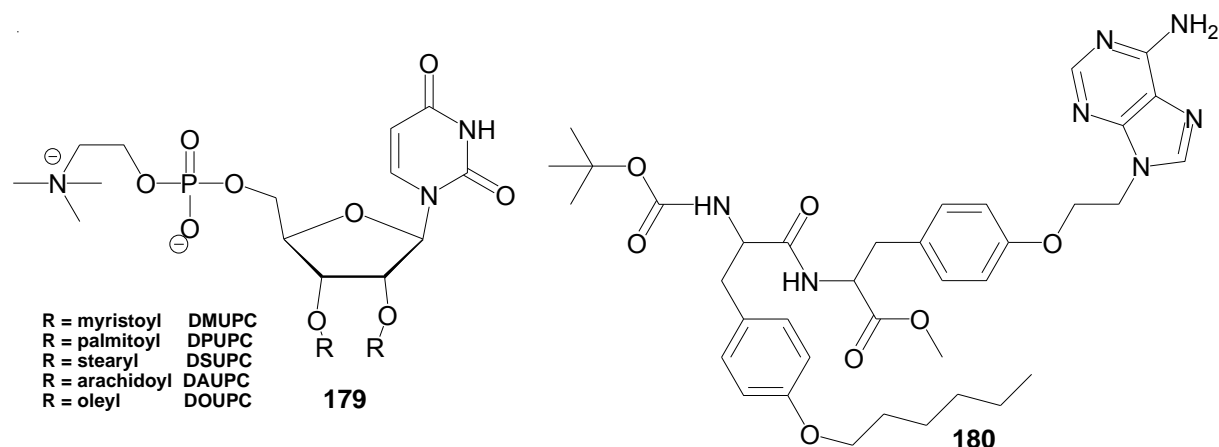


Figure 5.44. Examples of homotypic LMWHGs containing nucleobases.

Interestingly, they found that below the phase transition temperature (T_g), **179** self-assembles to form helical fibers which are transformed to compact bilayers above the T_g .¹³⁷

Sleiman *et al.* prepared a series of nucleobase peptide amphiphiles such as **180** (Figure 5.44) which self-assembles to form nanofibers and results in a hydrogel in water (5.0% DMSO) with a MGC of 0.5 wt%.⁴⁶⁴

V.4.4.2. Multicomponent Hydrogels Based on Nucleobases

Li *et al.* developed a new two-component hydrogel based on thymidine (**181**, Figure 5.45) and melamine **123** at a MGC of 0.1 wt%. Using FTIR and X-ray diffraction, the authors confirmed that the main driving force for the formation of supramolecular complex from thymidine and melamine is the intermolecular hydrogen bonding interactions.⁴⁶⁵

Adhikari and Kraatz *et al.* synthesized a hydrogelator of deoxyguanosine (**182**) that affords a hydrogel with a MGC of 0.57 wt% in the presence of Ag^+ , (Figure 5.45). The authors found that mixing the two hydrogelators **182** and **183** yields a co-gel which exhibits enhanced stability, an extended life-time and self-healing properties.⁴⁶⁶

Xu *et al.* designed two nucleopeptides (**184** and **185**, Figure 5.45) that alone are not able to form hydrogels, while mixing the two nucleopeptides supports the self-assembly process to form nanofibers and results in a hydrogel.⁴⁶⁷

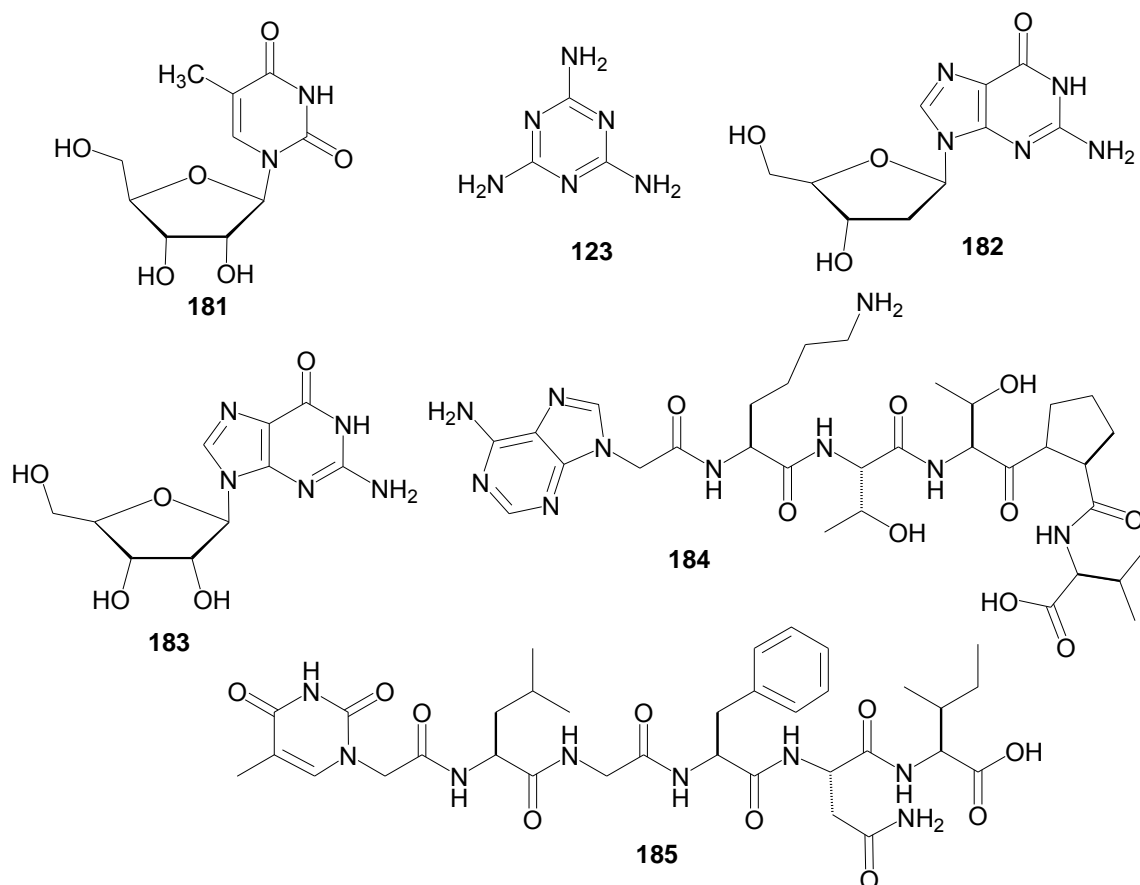


Figure 5.45. Examples of multicomponents LMWHGs based on nucleobases.

V.4.5. Hydrogels Based on Saccharides

Saccharides are characterized by possessing multiple hydroxyl groups in their molecular structures which increase the hydrophilicity of the saccharides and ease their dissolution in aqueous system prior to the triggering for hydrogelation by external stimuli (*i.e.*, pH, temperature, or ionic strength). Moreover, the hydrophilic structure of saccharides provides chance for a number of intermolecular interactions which play an essential role in the molecular self-assembly in water and results in hydrogelation. Saccharides-based hydrogelators have been categorized into monosaccharide- and oligosaccharide-based hydrogelators.⁵²

V.4.5.1. Monosaccharide-Based Hydrogelators

As shown in Figure 5.46 John and Shimizu *et al.* developed a series of low molecular weight gelators (**186** and **187**) based on simple glycolipids. They reported that **186** and **187** are capable of forming gels in a water/alcohol mixture at a concentration of 0.15 wt%. They found that the Tg of **186** is higher than of **187**.²⁰⁵

Bhattacharya *et al.* reported the hydrogelation phenomenon of the tetrameric *D*-xylofuranuronic acid derivative containing an azobenzene core (**188**, Figure 5.46).⁴⁶⁸ They investigated that **188** exhibits pronounced hydrogelation at 0.1 wt% assisted by initial dissolution in a small amount of DMSO. They also reported that the resulting hydrogel displays a remarkable photostability under UV irradiation since the hydrophobic azobenzene group is packed inside the gel state. Finally they found that addition of a salt (*e.g.*, CaCl₂) changes the morphology of the networks in the hydrogel from globular spongy to rod-like fibers.⁴⁶⁸

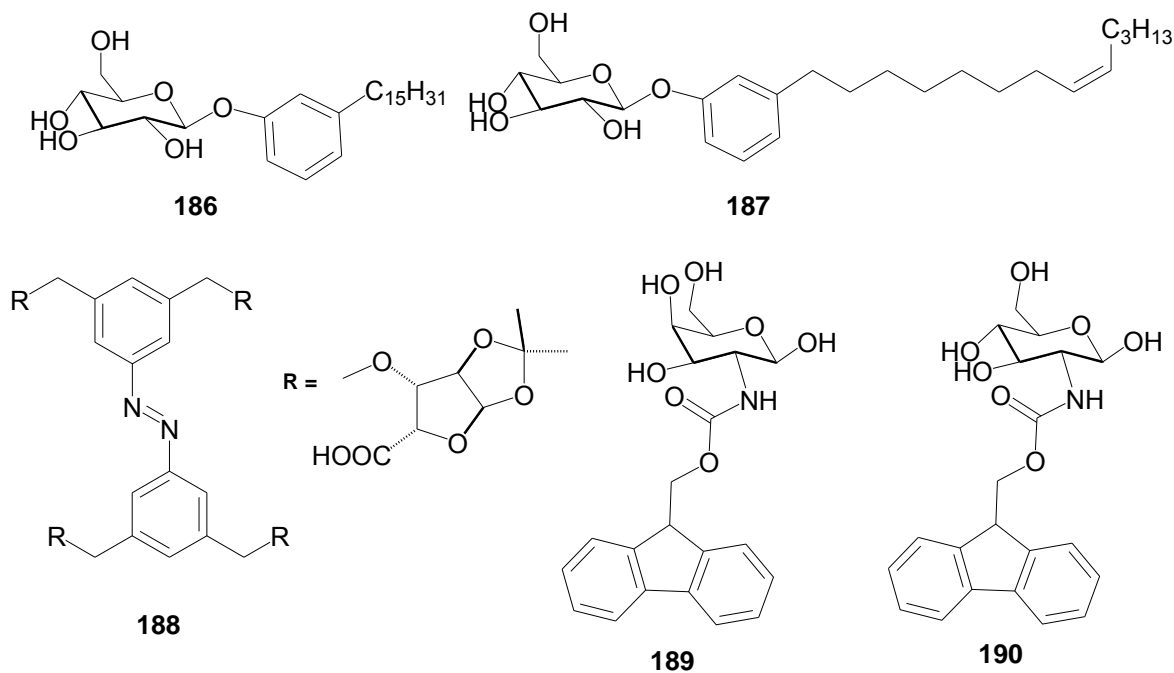


Figure 5.46. Representative molecular structures of monosaccharide based one-component LMWHGs.

Birchall and Edward *et al.* developed a class of supramolecular hydrogels (**189** and **190**, Figure 5.46) derived from glucosamine and Fmoc. The authors suggested that CH- π interaction, rather than π - π stacking and hydrogen bonding, is responsible for the self-assembly and subsequently hydrogelation.⁴⁶⁹

Bhuniya and Kim developed a series of monosaccharide based one-component hydrogelators using a methylene linker followed by a reverse amide group (Figure 5.47).

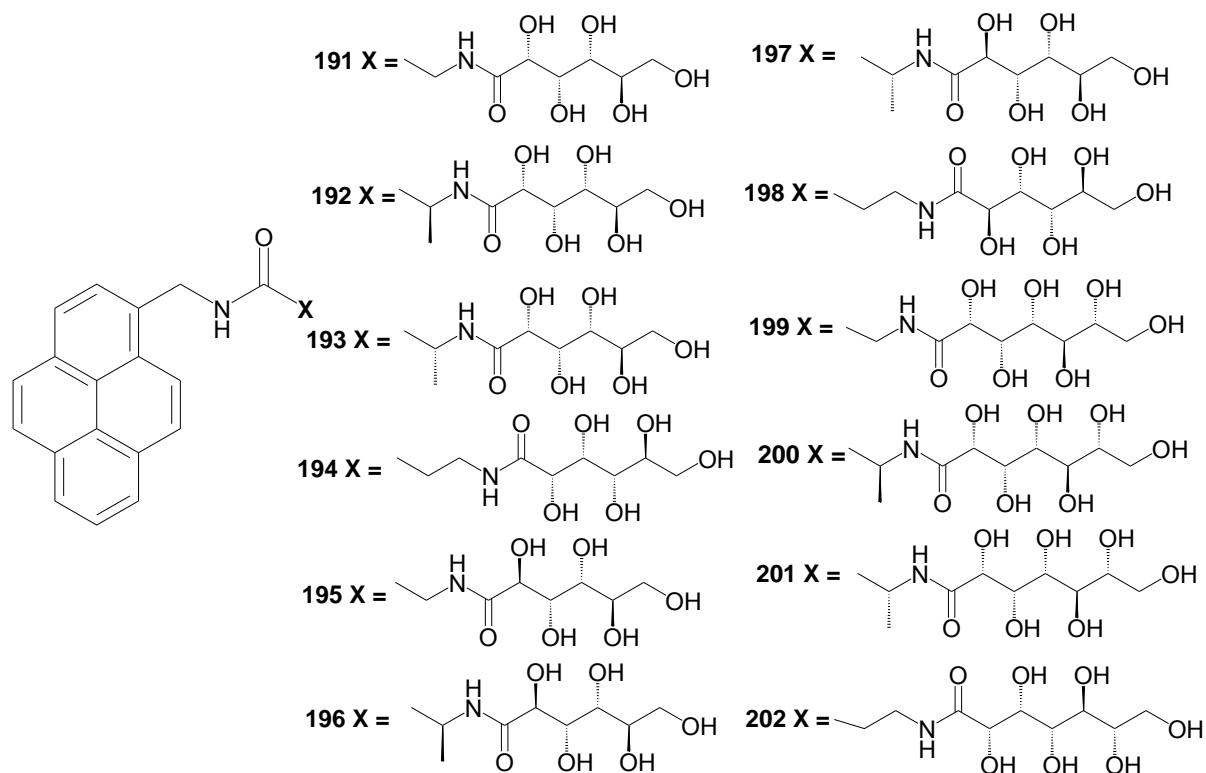


Figure 5.47. Other examples of monosaccharide based one-component LMWHGs.

Compounds **191**, **192**, **196 - 199** and **201** are able to form gels in water and the gelation ability is dependent on the nature of the amino acid and monosaccharide units. The most efficient hydrogelator **198** is able to gel water at 1.04 mM concentration (53400 water molecules/gelator molecule). The self-assembly of the gelators is driven by hydrogen bonding and π - π stacking interactions as indicated by FTIR and fluorescence spectroscopic studies.⁴⁷⁰

V.4.5.2. Oligosaccharide-Based Hydrogelators

As shown in Figure 5.48, Oriol *et al.* succeeded to synthesize a class of maltose-based supramolecular hydrogelators (**203 - 205**) by click chemistry.

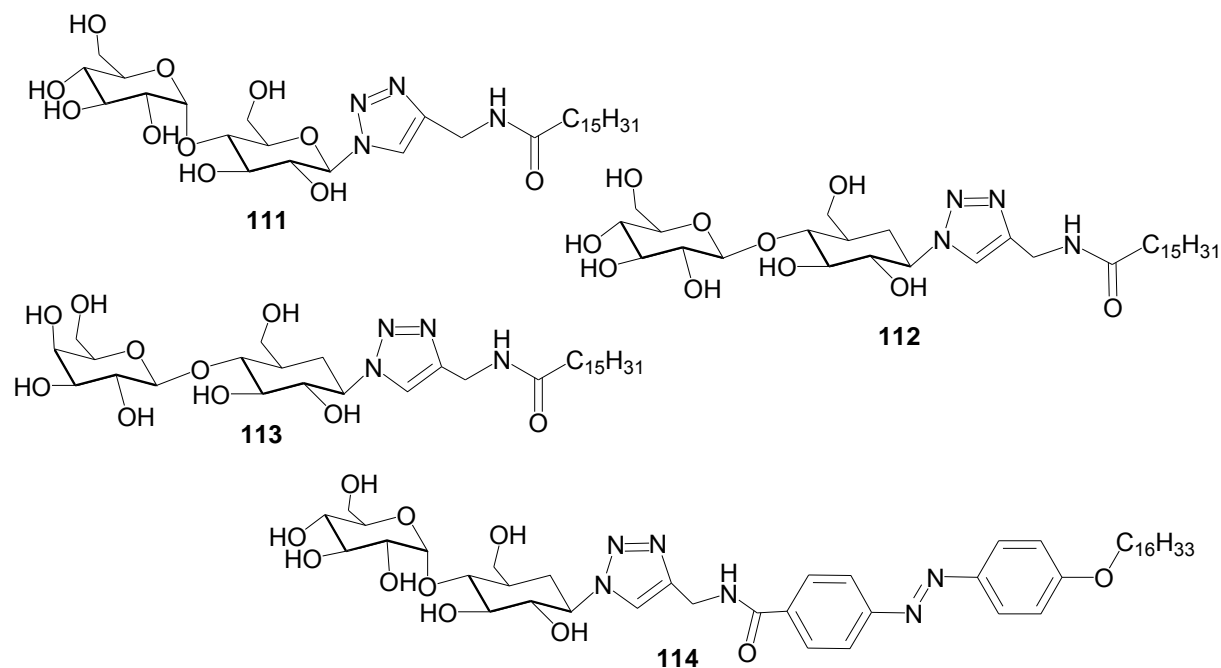


Figure 5.48. Representative molecular structures of some LMWHGs based on oligosaccharides.

Both hydrogelators (**203** and **205**) self-assemble in water to form typical ribbons with a left-handed twist and result in hydrogels with a MGC of 1.0 wt%. In the other hand, the authors found that hydrogelator **204** forms ribbons with a right-handed twist and affords a hydrogel with a MGC of 0.5 wt%.^{471,472}

Oriol *et al.* modified the hydrogelator **203** by incorporating azobenzene into its molecular structure resulting in a new hydrogelator (**206**) that forms a stable hydrogel with a MGC of 5.0 wt%. Interestingly, the authors reported that CD reveals that UV irradiation is unable to induce *cis* \rightleftharpoons *trans* isomerization of azobenzene and they attributed that due to the dense packing of azobenzene in the gel state which hinders the photoisomerization.⁴⁷³

Interestingly, in the current study the heterochiral cyclo-(*D*-Phe-azaPhe-Ala)₂-hexamer (**9b**) could self-assemble in some organic solvents (toluene, benzene, chlorobenzene and *p*-xylene). Furthermore, the gelator molecules undergo further cross-linking and entanglement to give 3D extended self-assembled network that immobilize solvent molecules leading to the formation of organogels (Chapter VI). The chapter will establish the characterizations of this LMWOG (**9b**) by studying its structure, morphology, and physico-chemical behaviors using several sophisticated techniques. In addition, studying the mechanical and thermal stabilities by the help of rheological measurements in different organic solvents will be also investigated.

Part B

Chapter V. Bibliography of Gels and Low Molecular Weight Organo-/Hydro-Gelators

In addition, modification in the molecular structure of 2:1-[α /aza]-oligomers could achieve supramolecular hydrogels from the two trimers: Fmoc-Phe-azaPhe-Ala-OH (**7a'**) and Fmoc-*D*-Phe-azaPhe-Ala-OH (**7b'**) at pHs (7.0 and 10.0). Characterizations of the two molecules at the molecular and supramolecular levels will be discussed using different techniques (Chapter VII). The rheological behaviors of the two hydrogels will be assessed through rheological experiments. Finally, the morphological study will also be established by utilizing scanning electronic microscopy (SEM) for imaging the dried hydrogels from **7a'** and **7b'**.

**Chapter VI. Supramolecular Organogels Based
Heterochiral Cyclo-(*D*-Phe-azaPhe-Ala)₂-
Hexamer**

VI.1. Introduction

Chapter IV described in details the synthesis and structural studies of homo- and heterochiral cyclo-(*L*- or *D*-Phe-azaPhe-Ala)₂-hexamers in solid and solution states.⁴⁷⁴ Interestingly, we have found that only heterochiral cyclo-(*D*-Phe-azaPhe-Ala)₂-hexamer (**9b**, Figure 6.1) could self-assemble in some aromatic solvents to form thermoreversible supramolecular organogels in which the gels exhibit the phenomenon of gel-to-sol phase transition reversibly by the influence of temperature.

In this chapter (VI), characterization of our LMWOG (**9b**) will be established by studying its molecular and supramolecular structures, morphology, chemical and physical behaviors using several sophisticated techniques including NMR, FTIR, SEM and TEM in order to emphasize the existence of certain conformation (β -turn, α -helix, β -sheet, *etc.*) and to obtain a virtual image for the 3D hierarchical structures of our gel system. Furthermore, studying the mechanical and thermal properties by the help of rheological measurements in different organic solvents will also be described.

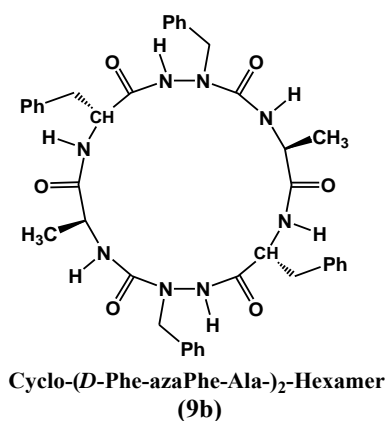


Figure 6.1. Molecular structure of heterochiral cyclo-(*D*-Phe-azaPhe-Ala)₂-hexamer (**9b**).

VI.2. Gelation Behaviors of Cyclo-(*D*-Phe-azaPhe-Ala)₂-Hexamer

It has been reported that gelation process can be achieved when the intermolecular forces (repulsion and attractive) in the system are so balanced⁶⁴ since gelation process is considered to be the equilibrium between solubility and phase separation.⁵¹

Gelation process is a consecutive mechanism starts from the molecular level until the formation of 3D network: (i) in solution, the primary structure from angstrom to nanometer scale (molecular level) is determined when the monomer molecules first assemble into dimers, and then oligomerization between these dimers lead to the formation of anisotropic aggregation in one or two dimensionally expanded structures called fibrils, (ii) the secondary structure from nano- to micrometer scale is defined as the morphology of the aggregates, which are formed from the bundling of the fibrils lead to the formation of micelles, vesicles, fibers, ribbons, or sheets which are further self-assemble supported by a number of non-covalent interactions yielding infinite highly organized 3D network structures, and (iii) the interconnected 3D network may trap and immobilize the solvent molecules leading to what is recognized at the macroscopic level as a gel.^{51,475}

The gelation properties of compound **9b** were first studied in various solvents. The minimum gelation concentrations (MGCs), which refer to the minimum concentrations that lead to gelation, are summarized in Table 6.1.⁴⁷⁶ Compound **9b** was found to form transparent gels (Figure 6.2) in all solvents including benzene, chlorobenzene, toluene and *p*-xylene, however the gels from these solvents become less transparent by increasing the concentrations.

Part B
Chapter VI. Supramolecular Organo-Gels Based Cyclo-(D-Phe-azaPhe-Ala)₂-Hexamer

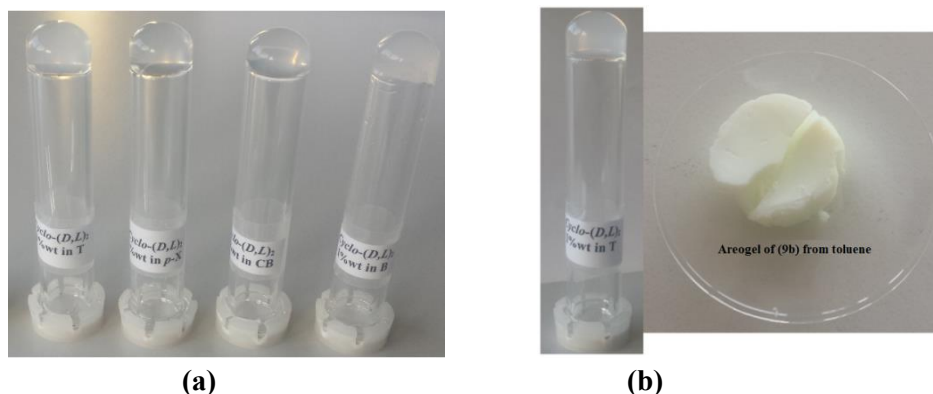


Figure 6.2. (a) Gelation tests in different solvents (T = toluene, *p*-X = *p*-xylene, CB = chlorobenzene and B = benzene), and (b) aerogel of **9b** from toluene obtained under supercritical CO₂-drying condition.

The highest gelation efficiency for **9b** was observed in toluene (MGC = 0.3 wt%) where a single molecule of **9b** can gel about ~ 2640 toluene molecules. The MGC of **9b** varies from 0.3 – 0.41 wt% in the different gelified solvents. The T_g values of organogels from **9b** at their MGCs were determined by the “falling ball” method^{3,28,69} recording the T_g range 38.3 – 45.3 °C (Table 6.1). All gels investigated their stabilities over a period of months at room temperature. These behaviors of gelator **9b** obey the criteria of a stable gel as reported by Abdallah and Weiss.³²

Table 6.1. Minimum gelation concentrations (MGCs, wt%), and gel-to-sol transition temperatures (T_gs, °C) of **9b** in different organic solvents

Solvent	MGC (wt%)	^d T _g at MGC (°C)	^e T _g (°C)	^f T _g (°C)	^g T _g (°C)
Benzene	^a G 0.41	38.3	65 - 70	55 - 60	47.8
Toluene	G 0.30	45.3	70 - 75	70 - 75	67.4
<i>p</i> -Xylene	G 0.34	40.7	70 - 75	75 - 80	87.2
Chlorobenzene	G 0.38	39.1	70 - 75	55 - 60	52.9
Solvents					State
<i>n</i> -Heptane / <i>n</i> -Hexane / <i>n</i> -Dodecane / Cyclohexane / Carbon tetrachloride / Carbon disulfide / Diethyl ether / Nitobenzene					^b I
Dichloromethane / Dichloroethane / Ethyl acetate / Methanol / Pentan-3-ol / Dioxane / THF / DMF / DMSO					^c S

^aG = Gel, ^bI = Insoluble, ^cS = Soluble, ^dGelation temperature at MGC determined by “falling ball” method, and ^{e-g}gelation temperatures at (0.5 wt%) determined by ^eNMR, ^fFTIR, and ^gRheology.

Gelator **9b** was found to be soluble in alcohols (such as methanol, ethanol, pentan-3-ol, *etc.*), dimethyl sulfoxide (DMSO), *N,N*-dimethyl formamide (DMF) and no gelation was observed even when the solutions were cooled in a refrigerator for several hours. In contrast, cyclopseudopeptide **9b** was insoluble in non-polar solvents like cyclohexane, *n*-hexane, and carbon tetrachloride (CCl₄), *etc.*, (Table 6.1).

Formation of LMW thermoreversible organogels is an evidence of the existence of self-assembly of the molecules in the solution state to form highly organized three-dimensional supramolecular structure which in turn has the ability to trap solvent molecules within the interconnected 3D network *via* non-covalent interactions.^{22,29,192,477,478} It was interesting before studying the supramolecular structure of gelator **9b** in the gel state, is to gain insight about the molecular structure of **9b** (monomeric state) in the gelified solvents, particularly toluene.

VI.3. NMR Spectroscopic Studies of Cyclo-(*D*-Phe-azaPhe-Ala)₂-Hexamer

VI.3.1. At Diluted Conditions

¹H NMR spectrum of compound **9b** has recorded in toluene-*d*₈ at low concentration (0.1 mmol. L⁻¹, 293 K) to avoid the intermolecular interactions; (toluene is considered to be the most practical solvent between the tested gelified solvents).⁴⁷⁹ The spectrum in toluene-*d*₈ shows a well resolved signals and the molecule **9b** behaves similarly as in CDCl₃ (chapter IV)⁴⁷⁴ where there are doubling of the signals confirming the presence of equilibrium between two conformers **V** and **W** (Appendix 3, Figure S6.1). Moreover, the chemical shifts of the NH protons of Ala moieties are located in the deshielding bound region (~ 6.3 ppm) in toluene-*d*₈, as well as the protons of methylene groups of the benzyl moieties are non-equivalent chemically. All these observations suggest that the two β-turn conformations which have been observed for **9b** in case of CDCl₃ (Chapter IV) are not disturbed in the toluene-*d*₈ for the both conformers **V** and **W**.⁴⁷⁴

In order to confirm the existence of β-turn in toluene-*d*₈, ROESY experiment (1.0 mmol. L⁻¹, 293 K) has been undertaken for compound **9b** (Appendix 3, Figure S6.2). In case of conformer **V**, the NH (*D*-Phe) signal is superimposed and overlapped with the aromatic protons of toluene and it was difficult to determine all the dipolar coupling constants associated with this proton.

Conformer **V** revealed moderate correlation between C^αH (*D*-Phe) and NH (azaPhe) and strong correlation between NH (azaPhe) and NH (Ala). Similarly, the protons of the C^αH (*D*-Phe), NH (azaPhe), and NH (Ala) of conformer **W** are well separated from conformer **V** showing strong correlation between C^αH (*D*-Phe) and NH (azaPhe) in addition to moderate correlation between NH (azaPhe) and NH (Ala). These correlations are characteristic of the presence of βII-turn conformation (Appendix 3, Figure S6.2).^{480,481} Based on the conformational studies of this molecule in chloroform (Chapter IV) and from the structural studies of acyclic series,⁴⁸² it was noticed that changing the absolute configuration of the Phe residue to (*R*) instead of (*S*), has led to change in the conformation from βII to βII'. So in our case both conformers **V** and **W** adopt βII'-turn conformation (Figure 6.3) which supports the 3D supramolecular organization. Based on X-ray results and NMR studies in chloroform (Chapter IV)⁴⁷⁴ or in toluene (current Chapter), we could suggest that molecule **9b** adopts majorly two βII'-turn conformations in solid and solution states.

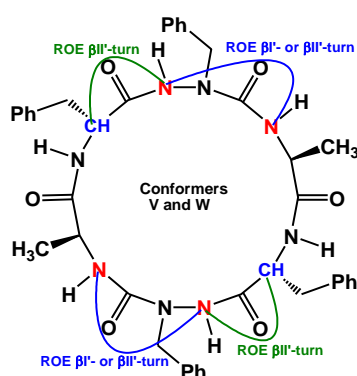


Figure 6.3. ROE correlations of β-turn conformations in the two conformers **V** and **W** from ROESY experiment in toluene-*d*₈; (1.0 mmol. L⁻¹, 293 K).

VI.3.2. Concentration-Dependent ¹H NMR Studies

Most of the known gelator molecules reported in the literature obey to the criterion of "dry gel" in which the NMR signals of gelator molecules completely disappear in the gel state and they are

Part B
Chapter VI. Supramolecular Organo-Gels Based Cyclo-(D-Phe-azaPhe-Ala)₂-Hexamer

only detected in the liquid state. This phenomenon has been explained by the fact that the gel fiber can be considered as a crystal of the gelator in which the molecular motion is very limited and the solvent molecules are excluded from the fiber.⁴⁸³

Concentration-dependent NMR study of **9b** has performed at 25 °C in toluene-*d*₈ from 0.1 mmol. L⁻¹ (solution state) to 6.0 mmol. L⁻¹ (gel state), (Figure 6.4). The spectra show that the signals of the gelator molecules are still visible even in the gel state. This result suggests that the gelator molecules are in a good thermal motion within the fibers and this behavior is consistent with the principle of "wet gel" as described by Sakurai *et al.* in which the molecules of solvent are incorporated into the gel fibers^{29,201,484,485} and the observed NMR signals correspond to discrete (non-associated) molecules.^{486,487}

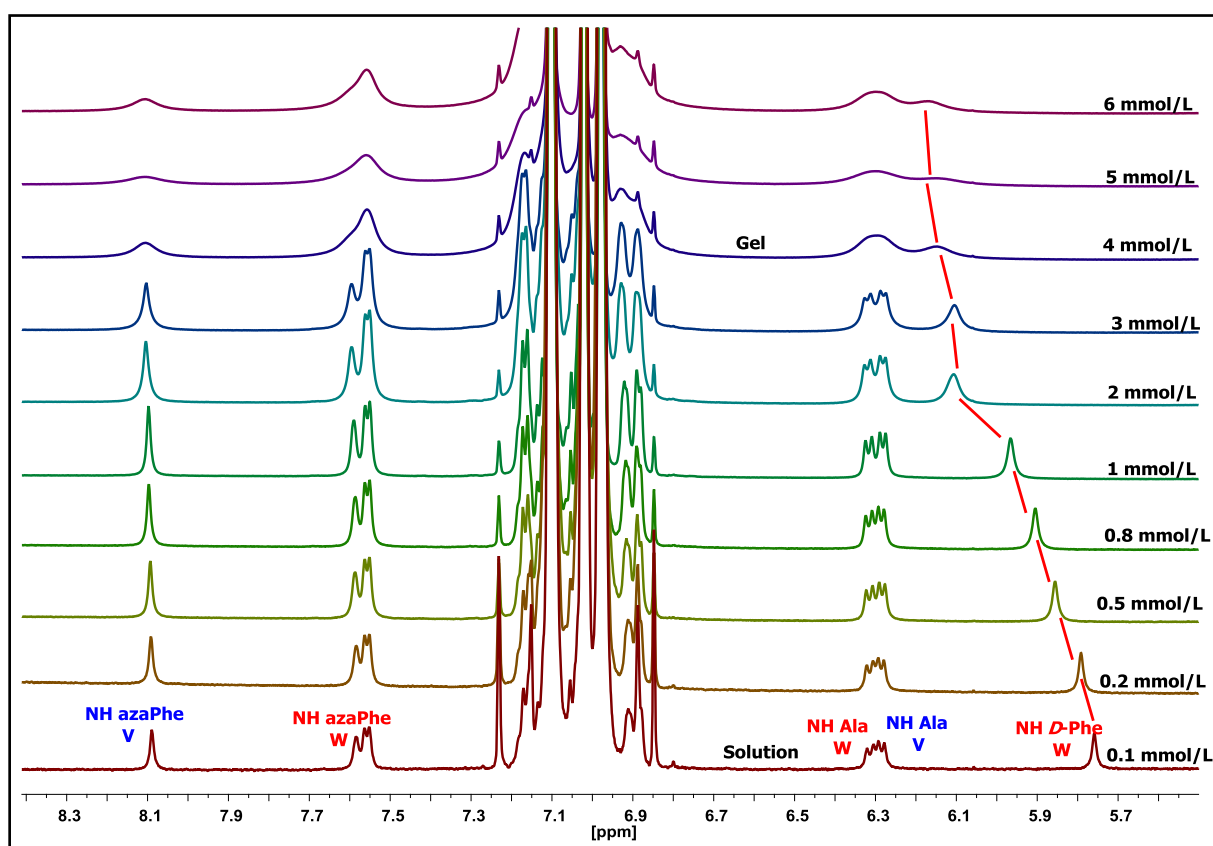


Figure 6.4. Concentration-dependent ¹H NMR (600 MHz) spectra show chemical shifts (δ ppm) of NH protons for compound **9b** in toluene-*d*₈; ($c = 0.1$ to 6.0 mmol. L⁻¹).

One can notice that the proton of the NH (*D*-Phe) of conformer **W** has deshielded from 5.76 ppm to 6.15 ppm and the signal became broad when the concentration exceeds the 3.0 mmol. L⁻¹ towards the formation of gel (Figure 6.4). Consequently, NMR observations confirm that the gel state of **9b** corresponds to molecules associated by hydrogen bonds (intermolecular interactions).^{73,167,265,314,488-490}

Unfortunately, the signal of the NH (*D*-Phe) of conformer **V** is overlapped with the toluene signals, so it was not possible to predict its contribution in the organogel formation. In addition, no chemical shift variations for the signals of the NH or the aromatic protons of the (azaPhe) moieties have been observed for both conformers which mainly stabilize the 3D supramolecular structure in case of CDCl₃ through π -stacking (Chapter IV).⁴⁷⁴

VI.3.3. Temperature-Dependent ¹H NMR Studies

Thermal reversibility of the self-assembly process is one of the key features of supramolecular gels.⁵² Studying the property of thermal reversibility of a gel provides more detailed information about the physical changes and the mechanism of the supramolecular formation.³ Temperature of gelation (T_g) is the most often reported parameter which can be determined by multiple methods, including the “falling ball” experiment, differential scanning calorimetry (DSC), rheological measurement, as well as spectroscopic techniques such as nuclear magnetic resonance (NMR), Uv-vis, circular dichroism (CD) and fourier transform infrared (FTIR).⁵² As we mentioned before that the transition temperatures determined by spectroscopic techniques are often different from those determined from rheometry, since they detect changes in primary rather than tertiary structure.^{3,73}

In order to gain further insight into the gelation phenomenon, the behavior of **9b** in all of the gelified solvents (toluene, benzene, chlorobenzene and *p*-xylene) were investigated using temperature-dependent NMR and FTIR spectroscopies from gel to solution states. Temperature-dependent NMR spectra for gelator **9b** in all gelified solvents reflected similar behaviors upon raising temperature (Figures 6.5a-d), and the gels showed close T_g at the same concentration (0.5 wt%), Table 6.1.

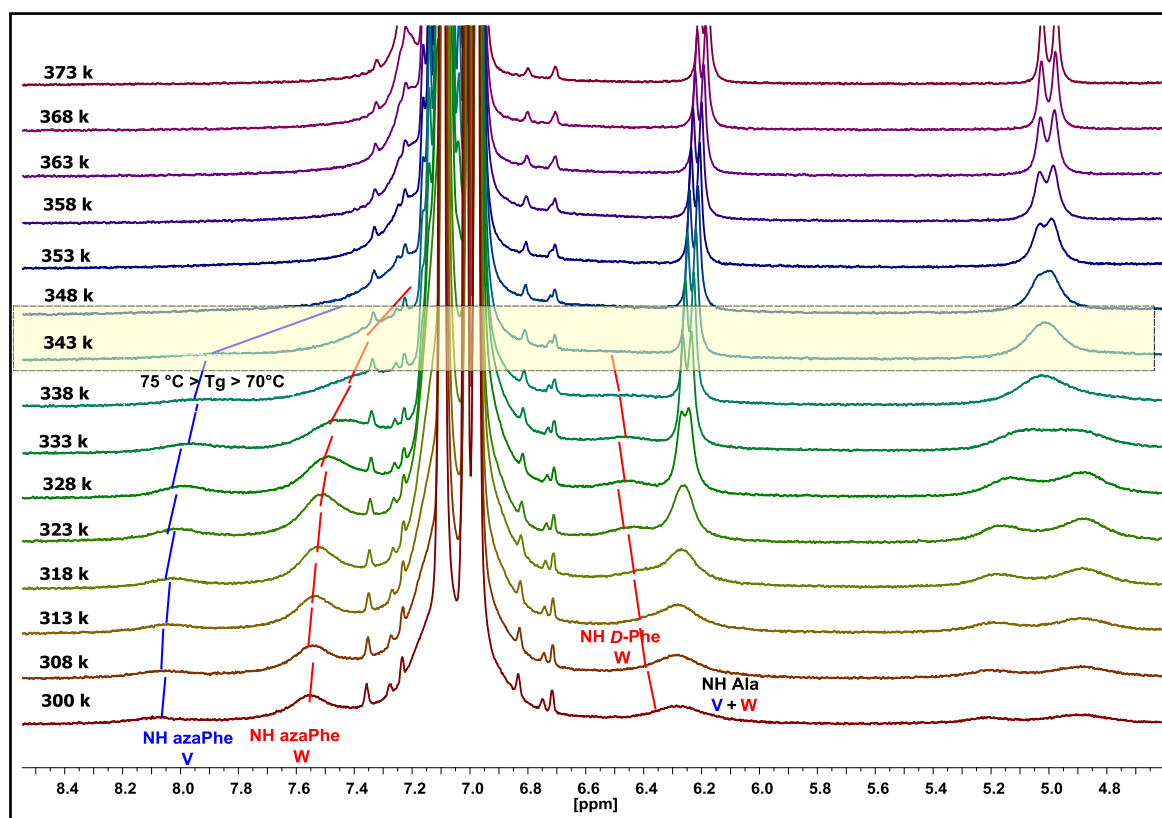


Figure 6.5a. Temperature-dependent ¹H NMR (300 MHz) of gelator **9b** in toluene-*d*₈; (c = 0.5 wt%).

In case of toluene-*d*₈, temperature-dependent ¹H NMR spectra of **9b** at 0.5 wt% were recorded in the temperature range from 27 °C to 100 °C in order to follow the evolution of the protons signals in transition from gel to solution state. Although the signals of the molecule in the gel state are less resolved and less visible in the ¹H NMR spectrum (Figure 6.5a), the peaks are still detected. This result suggests that some of the gelator molecules still keeping good thermal mobility in the fibers.^{22,29,192,483-485} When increasing the temperature, gradual improvement of the spectral resolution and sharpness (refinement) of signals are observed just after 65 °C which reflects the liquid behavior of the gelator molecules (Figure 6.5a).

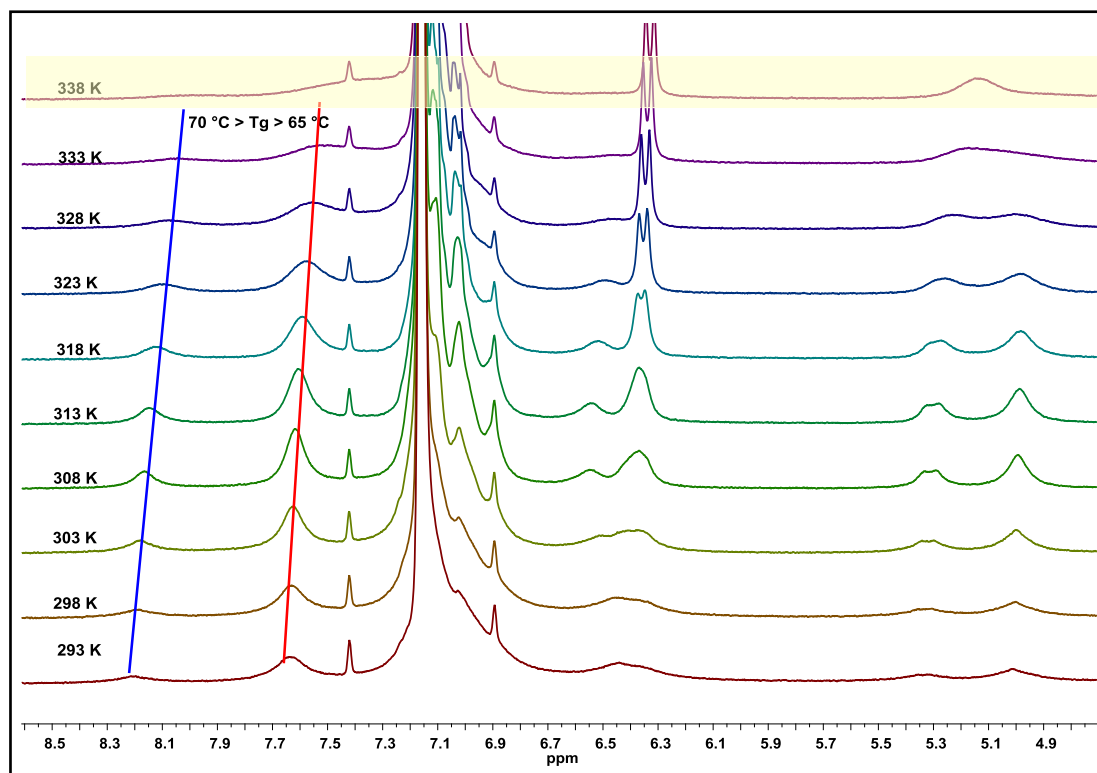


Figure 6.5b. Temperature-dependent ¹H NMR (300 MHz) of compound **9b** in gel state; (0.5 wt% in benzene-*d*₆).

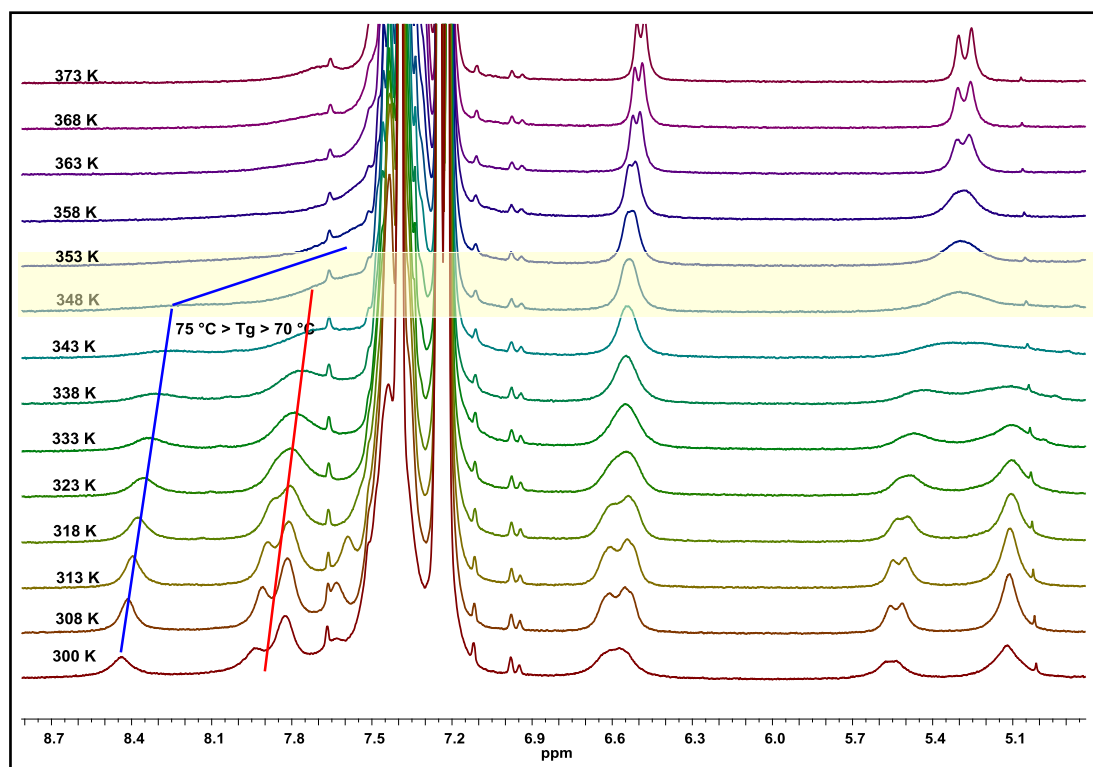


Figure 6.5c. Temperature-dependent ¹H NMR (300 MHz) of compound **9b** in gel state; (0.5 wt% in chlorobenzene-*d*₅).

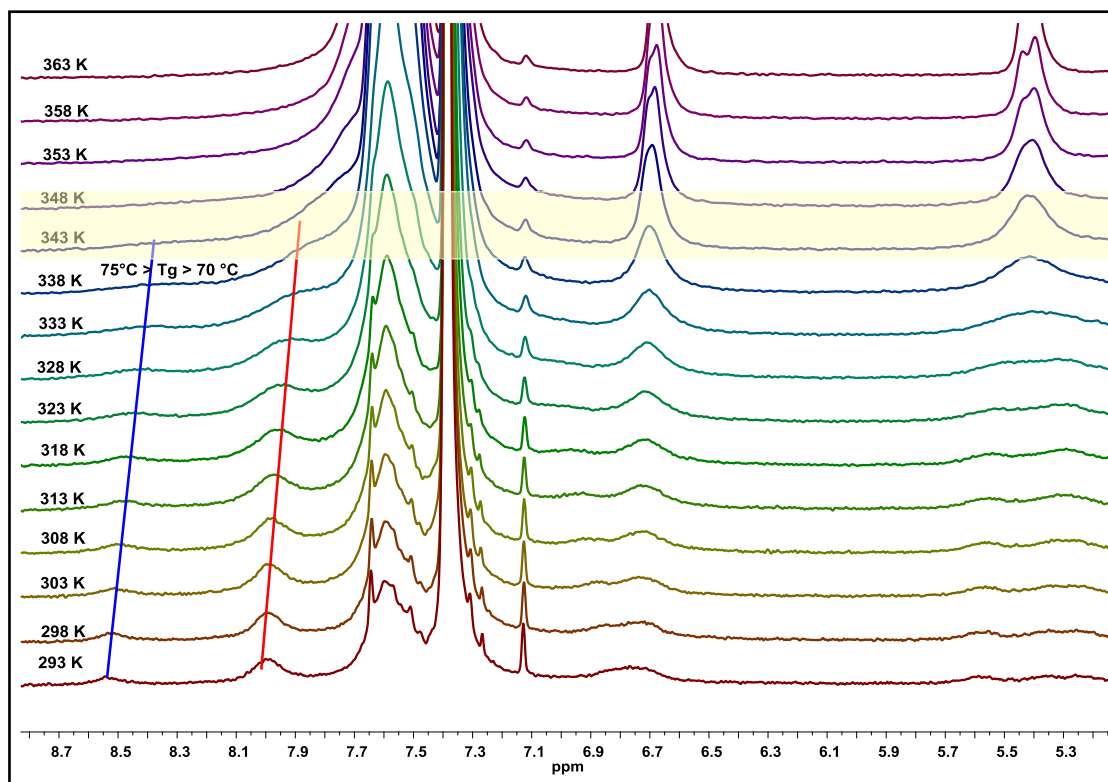


Figure 6.5d. Temperature-dependent ¹H NMR (300 MHz) of compound **9b** in gel state; (0.5 wt% in *p*-xylene-*d*₁₀).

In addition, the NH (azaPhe) chemical shifts of conformers **V** and **W** are shifted linearly upfield with increasing the temperature (Figure 6.5a). This shielding may result from the destruction of the supramolecular structure into small aggregates in which the protons become more shielded. So, we could propose that these NH (azaPhe) protons of both conformers are directly involved in the supramolecular construction (the behavior of NH protons of azaPhe moieties in the supramolecular construction were not obvious from the concentration-dependent experiment). Furthermore, the protons of NH (*D*-Phe) residues of conformer **W** suffer from weak deshielding (~ 0.15 ppm) upon increasing temperature from 27 °C to 100 °C, which may be attributed to the solvation effect of NH (*D*-Phe) protons by toluene-*d*₈ molecules (NH- π interaction).⁴⁹¹

Interestingly, coalescence of the signals of the CH₂ (azaPhe) protons for conformers **V** and **W** has been observed when the temperature rises over 65 °C and they become chemically equivalent in the solution state (Figure 6.5a). This can be interpreted as the fast equilibrium between the two conformers since the acquired thermal motion results in a difficulty in detection by NMR technique. Finally, NH (Ala) protons are not sensitive to the variations in the temperature which confirm that these NH (Ala) protons are involved in intramolecular hydrogen bonds as in the crystalline state.⁴⁷⁴

NMR studies of molecule **9b** at low concentrations (solution state) in toluene suggested that the two conformers exist under the form of β II'-turn conformation which favors the stacking mechanism upon increasing the concentration. At high concentrations (the gel state), β II'-turn conformation supported by a number of the intermolecular hydrogen bonds lead to the formation of the 3D supramolecular network structure. Unfortunately, NMR studies could not give approve about the contribution of the π - π stacking in the construction of the 3D network (the π -interactions were not visible in the NMR spectra).

VI.4. FTIR Spectroscopic Studies of Cyclo-(*D*-Phe-azaPhe-Ala)₂-Hexamer

In order to identify the role of the driving forces particularly hydrogen bonds in the construction of the supramolecular structure which led to gels formation, FTIR measurements were performed on gelator **9b**. Spectra were recorded on samples prepared from the gelified solvents at different concentrations and temperatures. Interestingly, all of the gelified solvents demonstrated similar behaviors reflecting that our gelator **9b** behaves similarly in these solvents. In the next two sections, we will present in details the behavior of the gel from toluene-*d*₈ as it is the most practical solvent compared with the other tested solvents.⁴⁷⁹

VI.4.1. Concentration-Dependent FTIR Studies

Concentration-dependent FTIR experiments for **9b** in toluene-*d*₈ at 25 °C have been recorded in the range from 0.8 mmol. L⁻¹ to 3.0 mmol. L⁻¹ (Figure 6.6). The spectra show two characteristic domains correspond to the NH and CO stretching regions. At low concentration (0.8 mmol. L⁻¹), the NH stretching spectrum reveals the presence of small free NH band around 3408 cm⁻¹ belongs to the free protons of NH (*D*-Phe) and NH (azaPhe) residues. In addition, a broad bound band around 3340 cm⁻¹ is observed which corresponds to the bound NH protons of Ala residues, and this band confirms the presence of intramolecular hydrogen bond in the monomeric state at low concentration (Figure 6.6a).⁴⁸² Moreover, the spectrum shows a new bound band at 3390 cm⁻¹ which was not exist at low concentration in case of CDCl₃ (Chapter IV)⁴⁷⁴ and we supposed that this band is due to NH- π interaction between the gelator molecules and toluene-*d*₈ molecules.⁴⁹¹⁻⁴⁹³ These results are consistent with the temperature-dependent NMR experiments (deshielding of the NH (*D*-Phe) with increasing temperature).

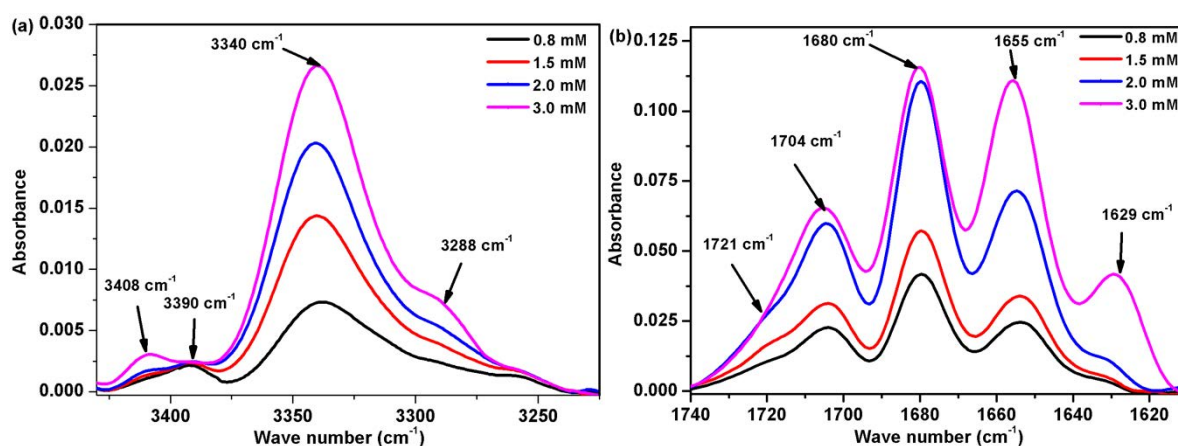


Figure 6.6. Concentration-dependent FTIR of **9b** in toluene-*d*₈; ($c = 0.8$ to 3.0 mmol. L⁻¹).

Regarding the CO region, there are 4 bands at 0.8 mmol. L⁻¹ and their assignments were based on their linear precursor (Figure 6.6b).^{474,482} Subsequently, the CO of Ala is involved in intramolecular hydrogen bond at $\tilde{\nu} = 1655$ cm⁻¹, while the other CO groups are in free states in toluene solution as noticed from their higher wave numbers at $\tilde{\nu} = 1721$ cm⁻¹, 1704 cm⁻¹, and 1680 cm⁻¹ correspond to the free CO of *D*-Phe, Ala, and azaPhe residues, respectively (Figure 6.6b).

The spectrum of **9b** in toluene-*d*₈ is similar to that observed in CDCl₃ (Chapter IV) and all the bands in the both spectra are nearly at the same positions with small variations in the wave numbers. These results support our suggestion that the conformation of **9b** in toluene-*d*₈ is similar to that observed in CDCl₃.^{474,482}

Increasing the concentration from 0.8 mmol. L⁻¹ to 3.0 mmol. L⁻¹ showed an increase in the intensity of the bound band at 3340 cm⁻¹ and appearance of one new band in the more bound NH region at 3288 cm⁻¹ (Figure 6.6a). These observations are consistent with the NMR studies which revealed deshielding of the proton of the NH (*D*-Phe) of conformer **W** with increasing concentration from which we could conclude that may be this NH proton is involved in intermolecular hydrogen bond. Unexpectedly the free band at 3408 cm⁻¹ corresponds to NH protons of the free states of (*D*-Phe) and (azaPhe) increases with increasing the concentration (Figure 6.6a). This confirms the NMR hypothesis that our gelator molecules at high concentration still mobile and possess thermal motion within the fibers as shown from the existence of the signals at high concentration. In contrast, the bound band at 3390 cm⁻¹ has no significant changes by increasing the concentration.

When the concentration of **9b** increases from 0.8 mmol. L⁻¹ to 2.0 mmol. L⁻¹, the intensities of all the CO bands increased which signify that most of the CO groups are involved in intermolecular hydrogen bonds (Figure 6.6b). Unfortunately, we have not observed any decrease in the intensity of the free CO bands from which we can not predict which CO group is bound intermolecularly with the NH *D*-Phe. Further increasing in the concentration to 3.0 mmol. L⁻¹, new band in the more bound CO region had been observed at 1629 cm⁻¹ which may be attributed to the self-assembly of the gelator molecules *via* intermolecular hydrogen bonds at the gel state (Figure 6.6b).

Consequently, concentration-dependent NMR and FTIR studies in the gel state suggested the presence of equilibrium between the monomeric state of **9b** and the supramolecular structure. In the solution state, the molecules are surrounded by huge number of toluene molecules that allowed for the NH- π interactions between the gelator and toluene molecules with the presence of certain number of free monomers. Increasing the concentration allows the gelator molecules to form intermolecular interactions with each other favoring the stacking mechanism to construct supramolecular structure but at the same time some of the NH- π interactions are broken to conserve the equilibrium.

Interestingly, comparison of the ATR-FTIR spectra of the aerogel, xerogel and the crystal of **9b** demonstrated similar IR signatures for the three states (Figure 6.7). Accordingly, we suggested that compound **9b** self-assembles in the same manner in the gel and in the crystal states and they have the same molecular packing.^{29,51,172,483,494}

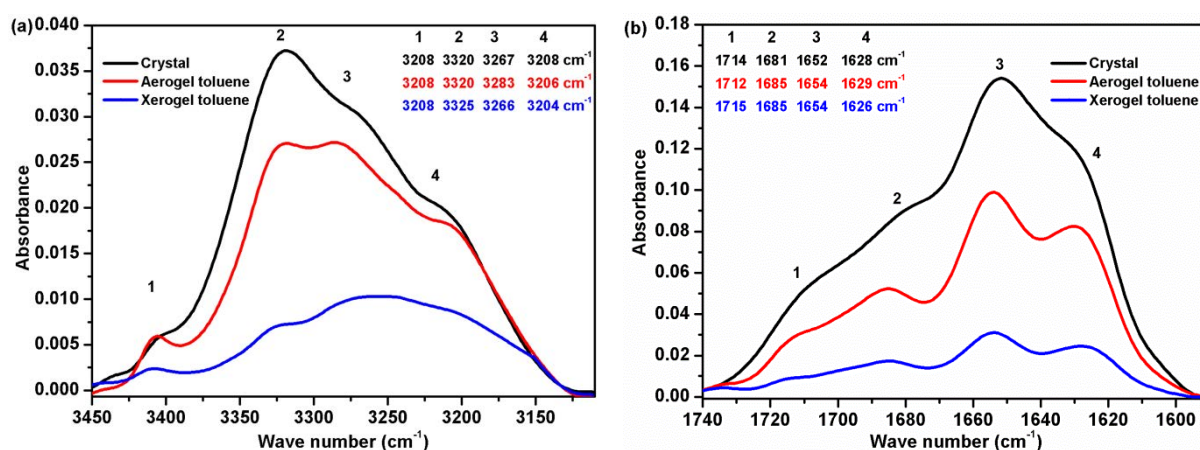


Figure 6.7. Comparison of the ATR-FTIR spectra in the crystal (black), aerogel (red), and xerogel (blue) states for **9b**: (a) NH stretching region, and (b) CO stretching region.

VI.4.2. Temperature-Dependent FTIR Studies

The physical behaviors of gelator **9b** in the different gelified solvents have been studied by following the changes which accompanied the CO and NH bands during raising the temperature sufficient to break the intermolecular interactions and obtaining solution state.

IR spectra have been recorded for gelator **9b** from all the gelified solvents (benzene-*d*₆, chlorobenzene-*d*₅, toluene-*d*₈ and *p*-xylene-*d*₁₀) at 0.5 wt% by heating the gel till solution state. This method is also a practical in the determination of the gel-to-sol transition temperature which corresponds to the collapsing of the physical interactions.³ The Tgs at 0.5 wt% were determined for each gelified solvents (Figures 6.8 and 6.9), and the values are summarized in Table 6.1.

Heating toluene-*d*₈ gel of **9b** from 25 °C to 90 °C led to a gradual collapse of all the four NH bands at 3202, 3286, 3325 and 3410 cm⁻¹ in favor of one band located at 3345 cm⁻¹ (Figure 6.8a).

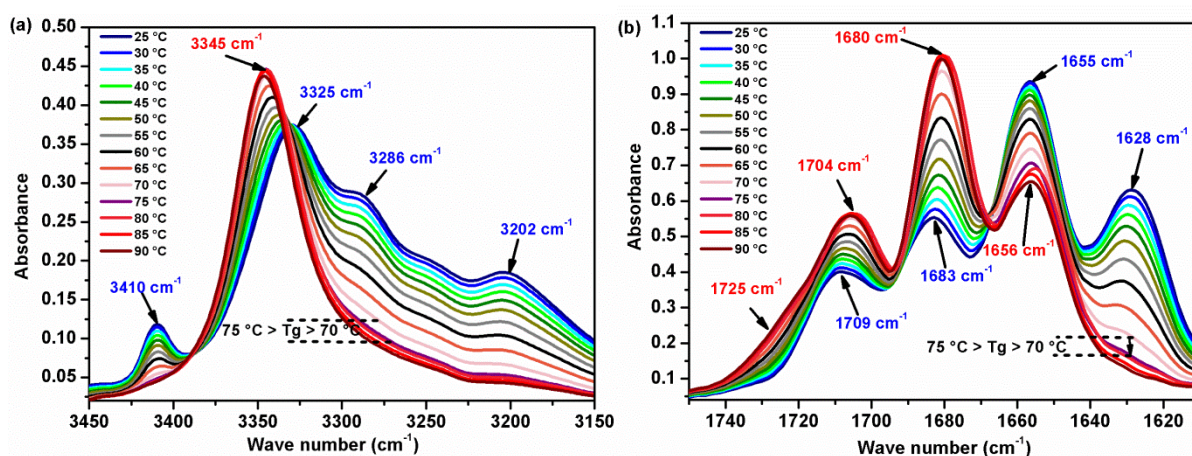


Figure 6.8. Temperature-dependent FTIR spectra from 25 °C to 90 °C of toluene-*d*₈ gel from **9b** at *c* = 0.5 wt%; (a) NH stretching region, and (b) CO stretching region.

This observation could be interpreted as the consequence disruption of the intermolecular hydrogen-bound network responsible for the gel formation.³⁰ The bound band at 3345 cm⁻¹ (Figure 6.8a) is close to the one which has been obtained in isotropic chloroform or toluene solutions, and was attributed to the intramolecular hydrogen bonds by the NH protons of Ala moieties.⁴⁷⁴

Studying the C=O stretching bands gave rise to the same conclusion realized from the NH stretching region, the gel state showed four CO bands (blue color) at 1628, 1655, 1683, and 1709 cm⁻¹ at 25 °C (Figure 6.8b). Heating the gel from 25 °C to 90 °C resulted in total disappearing of the band at 1628 cm⁻¹ and decreasing the intensity of the CO band located at 1655 cm⁻¹ confirming the involvement of these CO groups in intra- and intermolecular hydrogen bonds. Raising the temperature led to increase the intensities of the bands at 1683 and 1709 cm⁻¹ as well as evolution of new band at 1725 cm⁻¹ which has a close value from that observed in isotropic solutions of chloroform and toluene (free state).⁴⁷⁴ Since the spectra recorded at high temperatures are very similar to the one obtained for **9b** in isotropic solutions of chloroform or toluene, we could propose that the bands located at 1628 cm⁻¹ and 1655 cm⁻¹ result from intermolecular hydrogen bonds in the gel state. It is important to note that by passing the Tg around 72.5 °C, the band at 1656 cm⁻¹ still existing even at 90 °C, this band must correspond to the CO (Ala) which is involved in intramolecular hydrogen bond in solution state.⁴⁷⁴

Part B

Chapter VI. Supramolecular Organo-Gels Based Cyclo-(*D*-Phe-azaPhe-Ala)₂-Hexamer

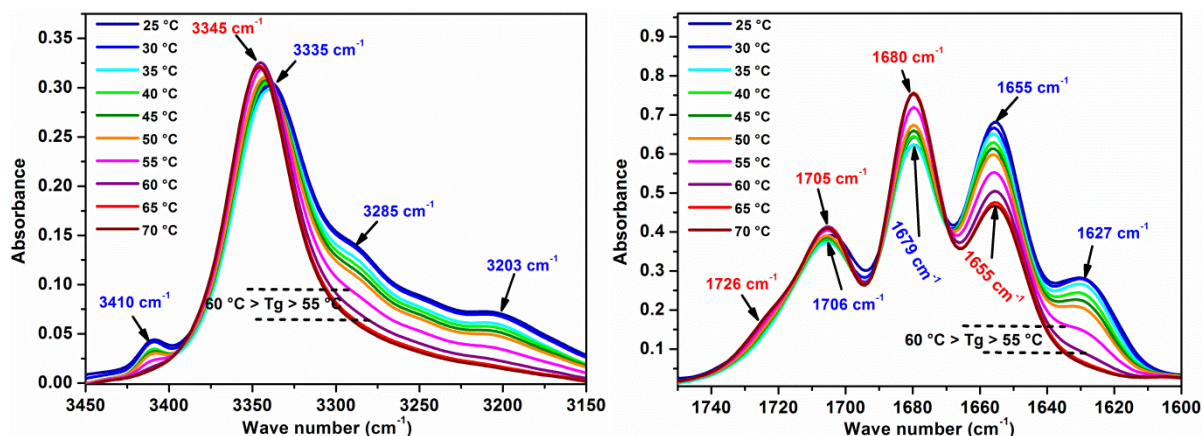


Figure 6.9a. Temperature-dependent FTIR spectra from 25 °C to 70 °C of benzene-*d*₆ gel from **9b** at *c* = 0.5 wt%; NH stretching region (left), and CO stretching region (right).

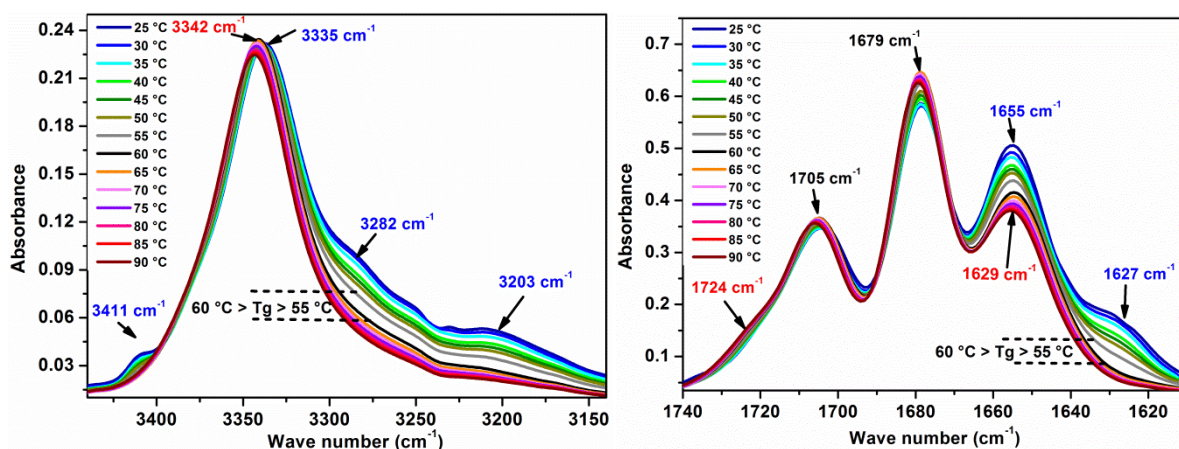


Figure 6.9b. Temperature-dependent FTIR spectra from 25 °C to 90 °C of chlorobenzene-*d*₅ gel from **9b** at *c* = 0.5 wt%; NH stretching region (left), and CO stretching region (right).

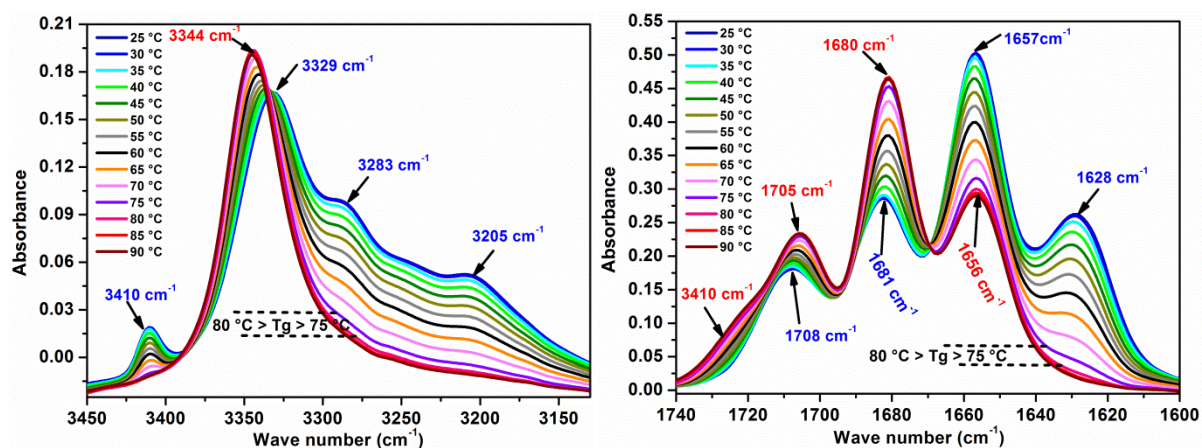


Figure 6.9c. Temperature-dependent FTIR spectra from 25 °C to 90 °C of *p*-xylene-*d*₁₀ gel from **9b** at *c* = 0.5 wt%; NH stretching region (left), and CO stretching region (right).

In order to determine the *T*_g at 0.5 wt%, we studied the change in the intensities of the free NH band at 3410 cm⁻¹ and the bound CO band at 1628 cm⁻¹ in which they showed total disappearance when heating (Figure 6.8a, b). As we can see in Figure 6.10, the intensities of the two bands decrease sharply when heating from 25 °C to 65°C, then the curves show weak changes in their intensities accompanied by semi-steady state behavior which correspond to collapsing of most of the physical

intermolecular interactions in the gel. The gel-to-sol transition can be considered at the inflection point of the two curves which records $T_g = 72.5\text{ }^\circ\text{C}$ for gel at 0.5 wt% from toluene.

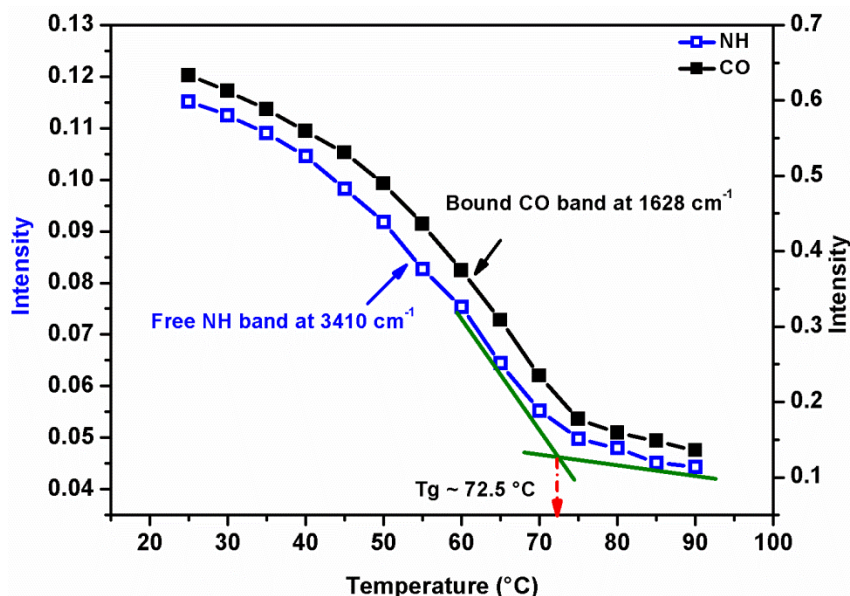


Figure 6.10. Gel-to-sol transition temperature (T_g) using FTIR for toluene-*d*₈ gel from **9b** at 0.5 wt%.

Temperature-dependent FTIR led us to suggest that all the formed gels from the different solvents are supported by involvement of the NH and CO groups in intermolecular hydrogen bonds stabilizing the gel fibers organization. In addition, gelator **9b** shows similar behaviors in the different gelified solvents which support our suggestion that the mechanism of the 3D supramolecular network structures are very similar in these solvents. Moreover, these supramolecular structures trap the solvent molecules within the spaces of the interconnected fibers leading to gel formation which is maintained by the same intermolecular forces mainly hydrogen bonds.

In addition to the previous structural studies using NMR and FTIR techniques, further characterizations (mechanical, thermal and morphological studies) for the different supramolecular organogels from **9b** will be discussed in the following sections.

VI.5. Rheological Studies

Rheological measurements provide information about the mechanical strength and rigidity of the gels through measuring two main parameters; storage (elastic) modulus (G') corresponds to the ability of the deformed material to store energy, and the loss (viscous) modulus (G'') which reflects the flowing behavior of the gels upon applying external stress.¹⁵ Generally, true physical gels reveal $G' > G''$ in gel state, and $G'' > G'$ in the solution state.^{77,83,360,495} Rheological measurements can also help to evaluate the thermal stability of gels by studying the transition temperature (T_g) at certain concentration through an oscillatory temperature sweep experiment.¹⁵

In the current work, organogels from **9b** were prepared in different organic solvents (benzene, chlorobenzene, toluene and *p*-xylene) at different concentrations. All the oscillatory experiments were performed within the LVR for all the gels starting with the oscillatory stress sweep experiments (OSS), where G' and G'' were measured as a function of oscillatory stress at a constant angular frequency, Figure 6.11.^{496,497} Initially, all the organogels of **9b** revealed that G' are higher than G'' . By gradual increase in the applied stress, the values of both G' and G'' remain nearly unaltered and get

Part B

Chapter VI. Supramolecular Organo-Gels Based Cyclo-(D-Phe-azaPhe-Ala)₂-Hexamer

deviated from linearity beyond a certain stress. This stress at which G'' becomes higher than G' is referred to the yield stress.^{496,497} All the gels at 0.5 wt% showed close yield stress at the crossover point within the range 38 - 48 Pa reflecting that these gels have very similar mechanical rigidity, Figure 6.11.

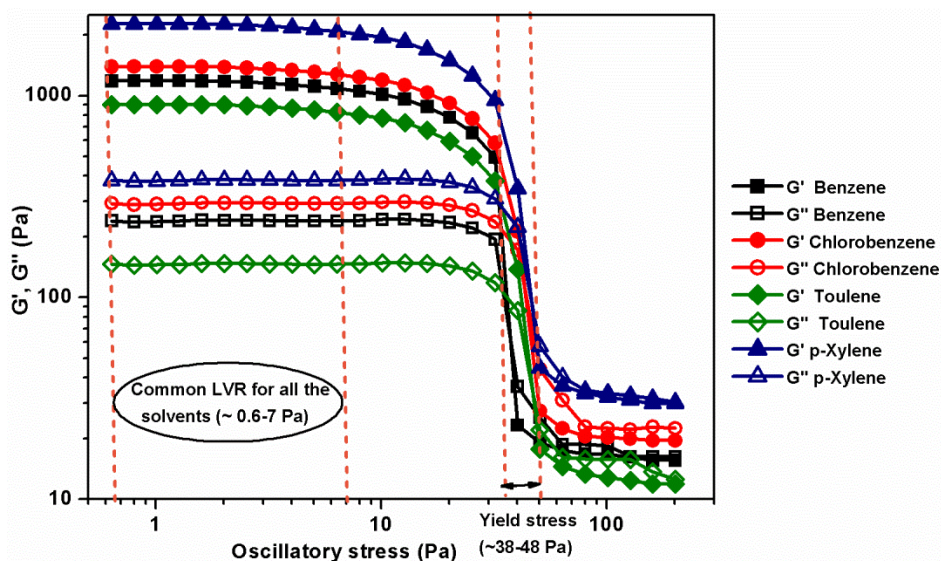


Figure 6.11. Oscillatory stress sweep experiments (OSS) for organogels of **9b**; ($c = 0.5$ wt%, $\omega = 0.63$ rad. s^{-1} , $T = 25$ °C).

Investigation of the LVR was continued through dynamic oscillatory time sweep (OTS) experiment, where each sample was subjected to shear stress (0.6 to 6.25 Pa) for 2 minutes followed by monitoring G' as a function of time at a constant angular frequency of $\omega = 0.628$ rad. s^{-1} and stress of $\sigma = 0.01$ Pa. The recovery of the gel represented by G' from the deformed state has been studied as a function of time (15 minutes) through oscillatory time sweep (OTS) experiment, Figure 6.12.

The plotted data in Figure 6.12 show that all the gels are mostly recovered within the time span of 100 seconds, hence the oscillatory experiments have been performed after 300 seconds within the LVR.

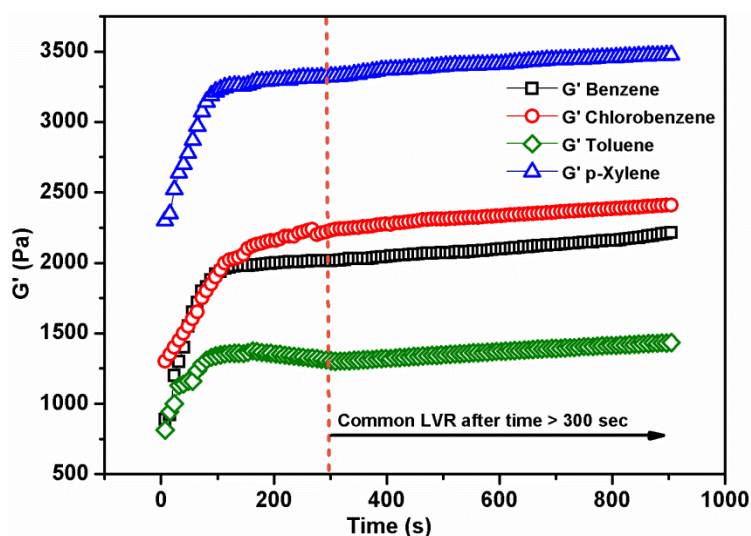


Figure 6.12. The rheogram shows the oscillatory time sweep experiments (OTS) for the organogels from **9b**; ($c = 0.5$ wt%, $\omega = 0.628$ rad. s^{-1} , $\sigma = 1.5$ Pa, $T = 25$ °C).

In order to evaluate the mechanical strength for the organogels, each gel sample of 0.5 wt% was subjected to oscillatory frequency sweep experiment (OFS). In this experiment, the variations of G' and G'' are regulated as a function of angular frequency (ω) at a constant applied stress.^{498,499} The results revealed that G' for all the organogels is higher than G'' by at least two orders of magnitude and they do not cross with each other over the entire ω range (0.1 – 62.83 rad. s⁻¹, Figure 6.13).

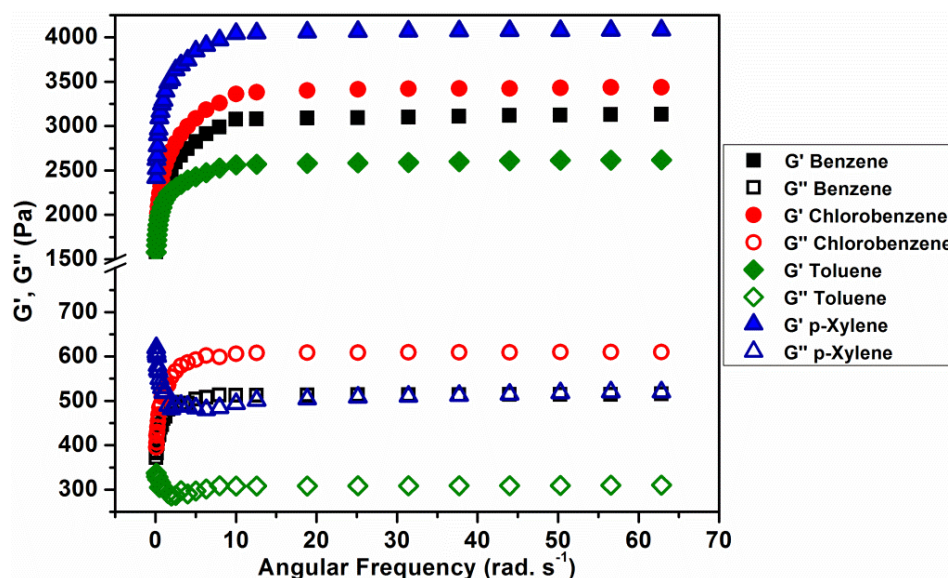


Figure 6.13. Oscillatory frequency sweep experiments (OFS) for organogels of **9b**; ($c = 0.5$ wt%, $\sigma = 1.5$ Pa, $T = 25$ °C).

Figure 6.13 shows that the storage modulus of the organogels (G') is in the order (p -xylene > chlorobenzene > benzene > toluene), and the gels reflect good mechanical strength ($10^4 > G' > 10^2$ Pa) compared with other previously reported supramolecular gels.⁵⁰⁰⁻⁵⁰⁶ At low frequencies, both G' and G'' ($G' > G''$) increase largely followed by a very weak dependence of G' and G'' on the applied angular frequency showing a plateau region suggesting that the gel matrices have excellent tolerance towards external forces indicating that **9b** forms effective organogels.

Interestingly, plotting of the average values of G' and G'' for a range of concentrations (0.4, 0.5, 0.6, 0.8 and 1.0 wt%) for all the solvents as a function of angular frequency at constant applied stress (Appendix 3, Figure S6.5) show the same trend of G' (p -xylene > chlorobenzene > benzene > toluene) as obtained for each concentration individually (Figure 6.13). This reflects that the mechanical strength of the gel vary in a constant definite way with concentration.

As we mentioned before that the temperature at which the gel-to-sol transition occurs is defined as the gelation temperature (T_g). Gel-to-sol transition takes place due to rupture of weak interactions during the course of heating. The T_g s of our organogels form **9b** have been determined by operating the oscillatory temperature sweep experiments for each gel sample at different concentrations (Appendix 3, Figure S6.6a-d). Transition temperature (T_g) corresponds to certain concentration could be obtained at the cross point between the G' and G'' curves when plotting against temperature.⁵⁰⁷ For example, the T_g for the gel of 0.5 wt% from toluene reveals ~ 67 °C (Figure 6.14). All the T_g s at 0.5 wt% from the gelified solvents are summarized in Table 6.1.

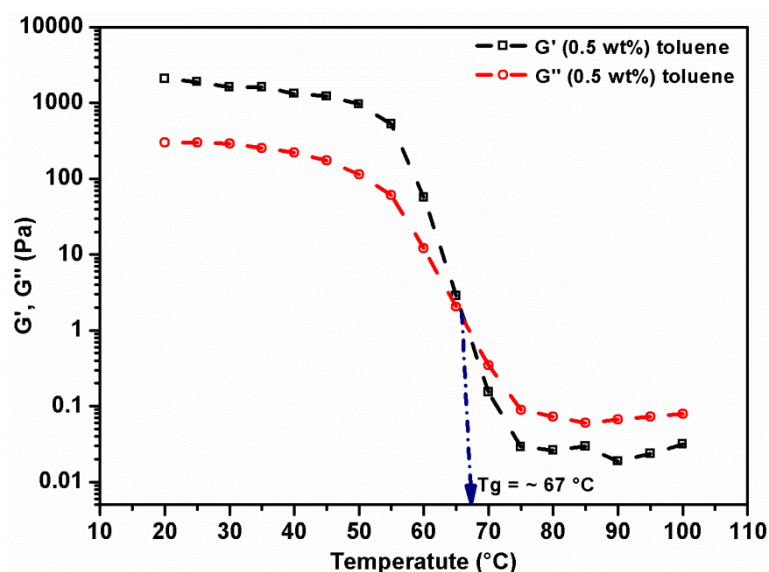


Figure 6.14. Oscillatory temperature sweep experiment shows the transition temperature of gel **9b** from toluene at ~ 67 °C; ($c = 0.5$ wt%, $\sigma = 1.5$ Pa, $\omega = 0.628$ rad. s^{-1}).

Further elucidation of the thermal stability of all the organogels from **9b** in the different solvents has been investigated. We examined the gel-to-sol transition temperature as a function of concentration by operating oscillatory temperature sweep experiment for each solvent individually at different concentrations (Appendix 3, Figure S6.6a-d). All the gels have the same trend in which their Tgs increase with increasing concentration (Figure 6.15), and this behavior is in concurrence with earlier reports.^{28,64,69}

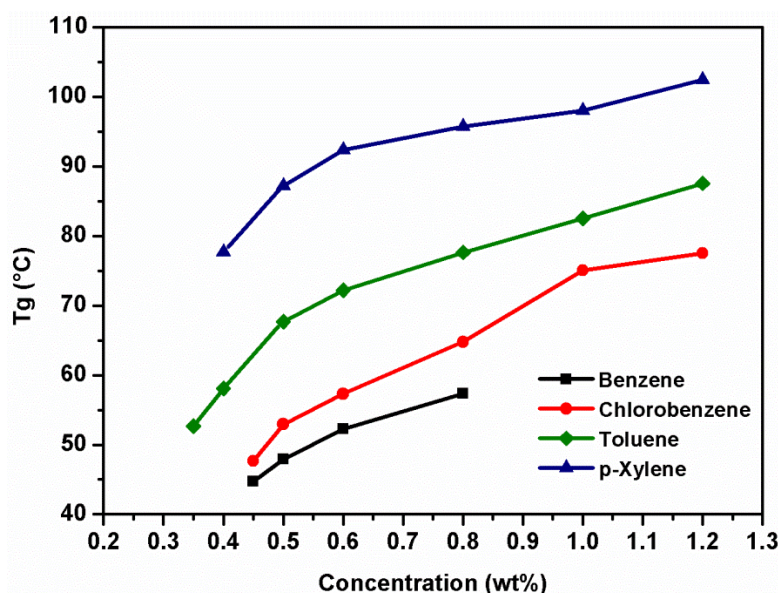


Figure 6.15. Variations of Tg (°C) as a function of concentration (wt%) for the organogels of **9b** from different gelified solvents.

Regarding the study case of gel in toluene, the OFS experiment for 0.5 wt% gel from **9b** was performed at the Tg = 65 °C. The plotted result in Figure 6.16 reveals that both G' and G'' increase linearly keeping $G' > G''$ over the entire range of the applied angular frequency confirming that the gel from toluene is true physical organogel and not viscoelastic fluid.^{83,360,495}

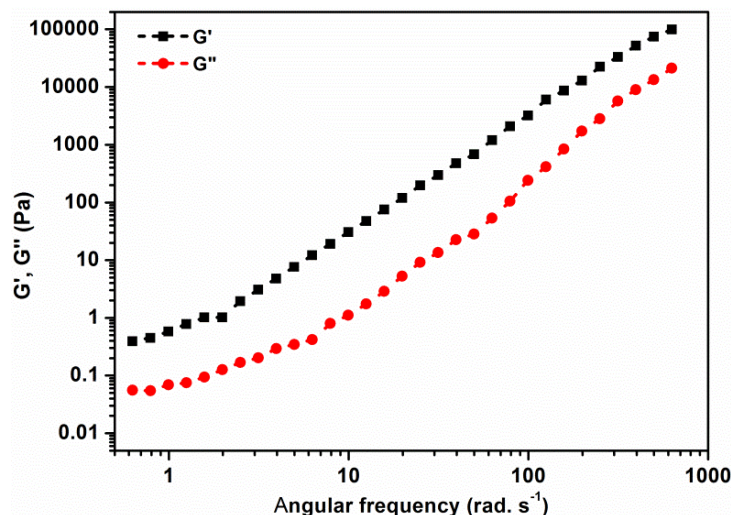


Figure 6.16. The rheogram of the oscillatory frequency sweep experiments (OFS), G' and G'' as a function of angular frequency at the T_g of toluene gel from **9b**; ($c = 0.5$ wt %, $T = 65$ °C, $\sigma = 1.5$ Pa).

Rheological studies showed that all the organogels from **9b** have nearly similar thermal and mechanical properties. Consequently, gelator **9b** self-assembles in the same way in all of the gelified solvents leading to the formation of nearly resemble supramolecular 3D arrangement which supported by almost the same intermolecular interactions that keep gel stability.

VI.6. Morphological Studies

Formation of organogels based new bis-nitrogen pseudopeptides (cyclic azapeptides) has deemed to be an interesting subject of study. The gelation process of **9b** reflects a great self-assembly abilities of this family to form fibrous network through the combination of non-covalent interactions, Figure 6.17.

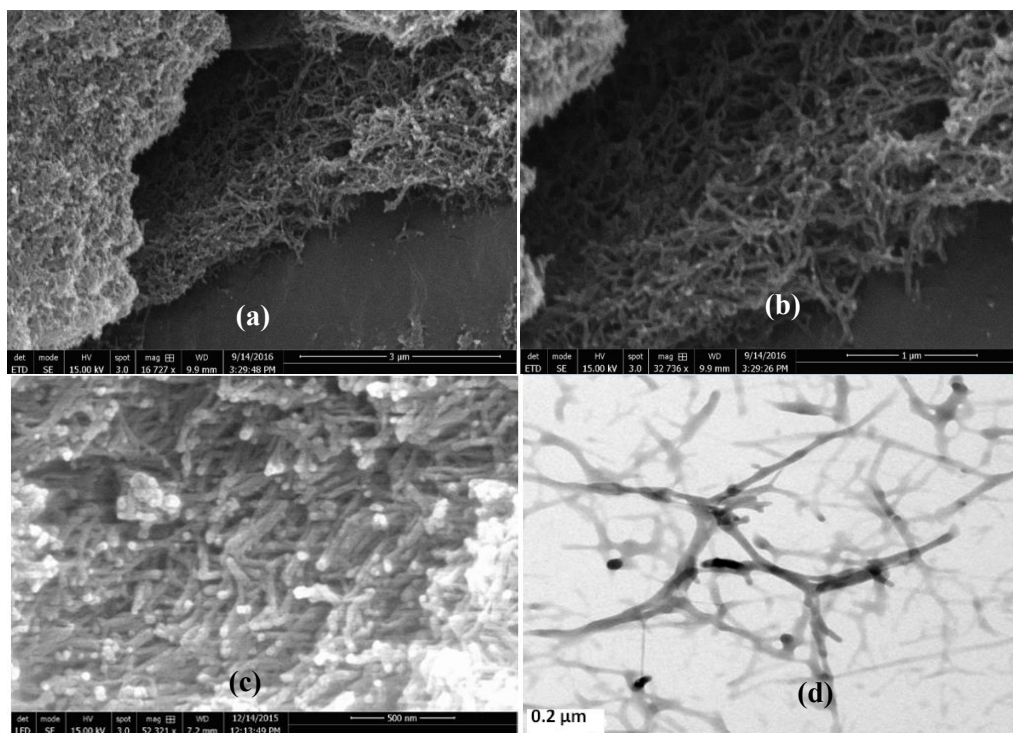


Figure 6.17. (a-c) SEM images, and (d) TEM image of aerogel of **9b** from toluene.

Part B

Chapter VI. Supramolecular Organo-Gels Based Cyclo-(*D*-Phe-azaPhe-Ala)₂-Hexamer

SEM images of the aerogel **9b** from toluene exhibited an interconnected network of thin non-twisted fibers-like structure with a thickness of a few tens of nanometers (Figures 6.17a-c). The morphology of the dried aerogel **9b** from toluene was also confirmed by TEM images (Figure 6.17d) which clearly showed the formation of self-assembled interconnected fibrillar networks (SAFINs). The thickness of the fibril in the supramolecular assembly ranges from 40 – 50 nm with variable lengths of about several micrometers, and this is consistent with the SEM result.

In the other hand, the SEM images of the xerogels of **9b** from *p*-xylene, benzene, chlorobenzene and toluene could not show a clear fiber structure from which we can easily suppose that xerogels could not conserve the self-assembly of compound **9b** (Figures 6.18a-d).

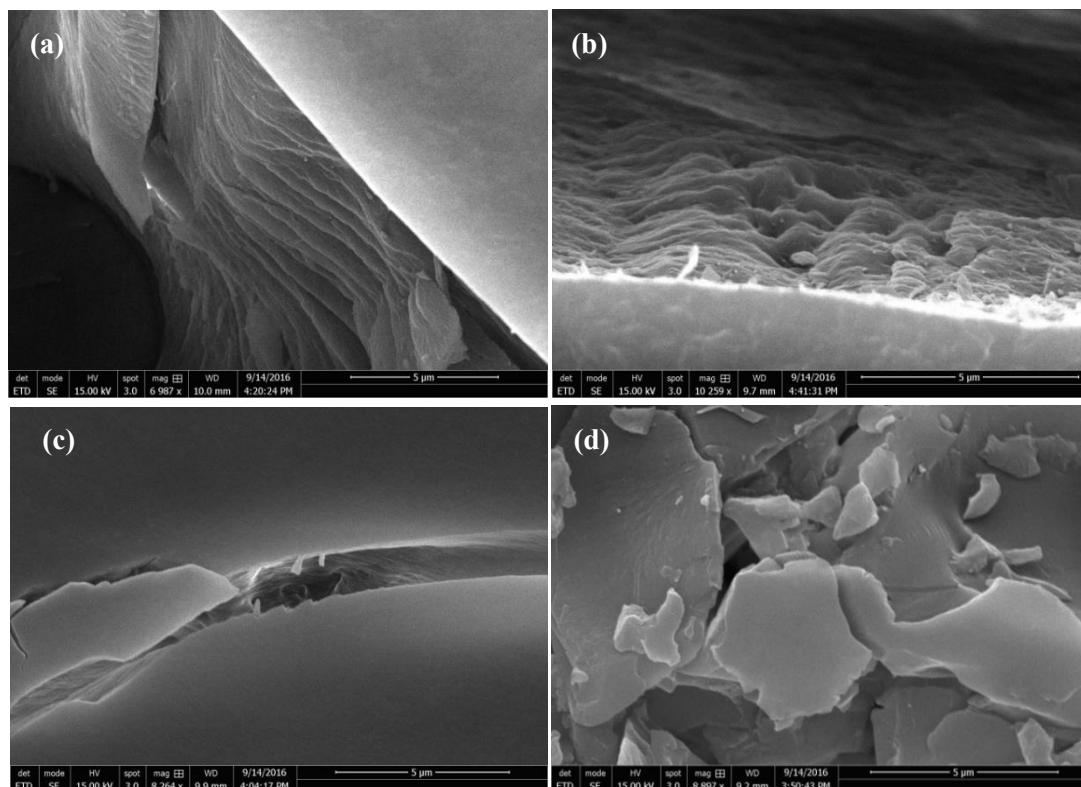


Figure 6.18. SEM images of xerogels obtained from air-drying of organogels of **9b** from: (a) toluene, (b) benzene, (c) chlorobenzene, and (d) *p*-xylene.

VI.7. Experimental Section

VI.7.1. Synthesis and characterization of Low Molecular Weight Organo-Gelator **9b**

The general stepwise strategy used to synthesize heterochiral cyclo-(*D*-Phe-azaPhe-Ala)₂-hexamer (**9b**) together with all the characteristics spectroscopic, X-ray diffraction and HRMS features have been described and reported in Chapter IV.^{474,482}

VI.7.2. Organogels Formation, Gelation Tests and Minimum Gelation Concentration (MGC) Measurements

The gelation ability of cyclic pseudopeptide-based-organogelator **9b** was tested in variety of aromatic and aliphatic organic solvents such as *n*-hexane, CCl₄, toluene, *etc.* by “stable-to-inversion of test tube” method.⁴⁷⁶ Gelation experiment for all the tested solvents was performed by weighing 10.0 mg of compound **9b** in a 7 mL transparent glass tube and then the solvent was added dropwise to

reach final weight of 1 g mixture ($c = 1.0$ wt%), the suspension was refluxed to form a clear solution which was kept to cool back to room temperature and the results of gelation tests were recorded for all tested solvents. The required concentrations in wt%, molarity, or w/v% to prepare gel or solution samples from compound **9b** have done by following the aforementioned procedure.

It is well established that the minimum gelation concentration (MGC) and the gel-to-sol phase transition temperature (T_g) are primary physical properties which should be determined in all the gelified solvents. By using “stable-to-inversion of test tube” method, MGC for each gelified solvent (benzene, chlorobenzene, toluene and *p*-xylene) was determined by continuous dilution of a gel sample of known concentration until a concentration below it, gravitational flow of the gel occurs from the inverted glass vial, this concentration is defined as the minimum gelation concentration (MGC).⁴⁷⁶

VI.7.3. Gel-to-Sol Transition Temperature (T_g) Measurement:

Determination of the gel-to-sol transition temperature (T_g) at the MGC for each solvent has been determined by the “falling ball method” through placing the gel-containing glass vial in a thermostatted oil bath and slowly raising the temperature of the bath at a rate of $2\text{ }^\circ\text{C min}^{-1}$. The T_g was defined by the temperature at which the gel melted and the ball breaks through the gel.^{3,69,73} The T_g value at MGC is the average of a triplicate measurements. Besides the aforementioned method for the determination of the T_g , there are several physico-chemical techniques have also been established to provide information about the T_g of the gel. Among these techniques that have been used herein in our study are NMR, FTIR and rheological measurements.³

VI.7.4. NMR and FTIR Spectroscopic Studies:

All NMR spectra (¹H, ROESY) were recorded using a Bruker Advance NMR spectrophotometer (300 or 600 MHz) in benzene-*d*₆, chlorobenzene-*d*₅, toluene-*d*₈, and *p*-xylene-*d*₁₀ as solvents. The chemical shifts were reported in ppm (δ) relative to tetramethylsilane (TMS) served as an internal standard ($\delta = 0$ ppm). Concentration-dependant NMR experiments for the organogel of **9b** from toluene-*d*₈, benzene-*d*₆, chlorobenzene-*d*₅, and *p*-xylene-*d*₁₀ have been performed.

FTIR spectra were recorded with Bruker Tensor 27 over 128 scans and referenced to the residual solvent resonances. The device is equipped with thermostatted controlled heating unit by which temperature-dependent FTIR experiments have been performed. In addition, attenuated total reflectance (ATR-FTIR) measurements have been operated on solids, xerogels (air-drying) and aerogel (CO₂-drying). All the spectra were recorded on Bruker Tensor 27 spectrometer equipped with a trough plate comprising of a germanium single crystal where the samples were loaded over it. Spectra were acquired in the $4000 - 400\text{ cm}^{-1}$ range with a resolution of 4.0 cm^{-1} over 128 scans, taken into consideration the background subtraction from each spectra to correct for atmospheric interference.

VI.7.5. Rheological Measurements:

The rheological experiments were carried out on Advanced Rheometer-AR2000 (TA instruments) operating in oscillatory mode with a 20 mm parallel plate geometry with serrated surfaces to prevent slidings due to the liquid film expelled by certain dilute samples (diameter gap was adjusted to $1000\text{ }\mu\text{m}$).⁷³ In order to determine the linear viscoelastic region (LVR) at which the oscillatory experiments were operated, each gel sample prepared from **9b** was subjected to an oscillatory stress sweep experiments (OSS); (G' and G'' were measured as a function of oscillatory stress ($0.6 - 6366\text{ Pa}$) at a constant angular frequency of 0.628 rad. s^{-1}).^{496,497} Then a dynamic oscillatory time sweep (OTS)

was performed for 15 minutes with an angular frequency of 0.628 rad s^{-1} , and applied stress of 1.5 Pa which has been chosen within the LVR from the OSS.⁵⁰⁸ After that, each sample was subjected to an oscillatory frequency sweep experiment (OFS) over a range of frequencies ($0.1 - 62.83 \text{ rad. s}^{-1}$) and applied stress of 1.5 Pa obtained from OSS step at $25 \text{ }^\circ\text{C}$.⁵⁰⁸ Finally, in order to obtain the gel-to-sol transition temperature (thermal properties of the gel), G' and G'' for each gel sample were studied over range of temperature sufficient for melting the gel to solution through oscillatory temperature sweep experiment, from which T_g can be determined at the cross point between the G' and G'' curves.⁵⁰⁷

VI.7.6. Morphological Studies:

Removal of toluene solvent from the organogel of **9b** using a supercritical CO_2 drying process led to the formation of the corresponding aerogel,⁷⁰ while xerogels from **9b** were obtained by slow evaporation of the trapped solvent molecules (benzene, toluene, chlorobenzene and *p*-xylene) from the 3D interconnected fibers in air.⁶⁹ To get a visual insight into the aggregation morphology of the formed gels from compound **9b** on a nanoscale, high-resolution scanning electron microscopy (HRSEM) (Environmental Quanta FEG 600-FEI, high vacuum, acceleration voltage of 15 kV, large field detector), and transmission electronic microscope (TEM) (Philips CM200 microscope, 200 kV, equipped with an EDXS spectrometer) were employed. While the dried samples (aerogel and xerogels) for SEM analysis were coated with gold (15 \AA) during 2 min by physical vapor deposition,⁶⁹ TEM image for the aerogel sample from toluene was recorded without pre-treatment.

Chapter VII. Supramolecular Hydrogels Based on 2:1- $[\alpha/\text{aza}]$ -Trimers

VII.1. Introduction

Developing of supramolecular hydrogels based on 2:1-[α /aza]-oligomers was a subject of great interest by our group due to their high potential applications. Furthermore, our interests were to investigate the ability of this family to self-assemble and form hydrogels. We focused mainly on testing the short azapeptides of the sequence 2:1-[α /aza]-trimers for hydrogelation. All the synthesized protected trimers (series A, Table 7.1) have been tested at different pHs (4.0, 7.0 and 10.0), unfortunately precipitations have been observed at the different pHs and no hydrogel has been achieved. We tried to increase the hydrophilicity of the final trimer by either carrying out deprotection of Boc-group (series B, Table 7.1), deprotection of methyl ester group (series C, Table 7.1), or even deprotection of the Z-group(s) for the trimers possessing lysine residue(s) (series D, Table 7.1). All these trials led to precipitations at pH 4.0, while solutions have been obtained at pHs 7.0 and 10.0.

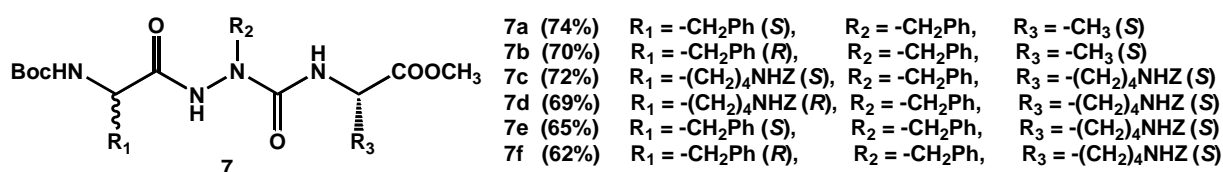


Table 7.1. All the trials for hydrogel formation based on 2:1-[α /aza]-trimers (7)

1- Protected trimers (series A)	2- Free N-terminal trimers (series B) (Boc-group deprotection)
<p>Boc-FazaFA-OMe Boc-D-FazaFA-OMe Boc-K(Z)azaFK(Z)-OMe Boc-D-K(Z)azaFK(Z)-OMe Boc-FazaFK(Z)-OMe Boc-D-FazaFK(Z)-OMe</p> <p style="text-align: center;">pH 4 & 7 & 10</p> <div style="text-align: center;"> <p>Precipitate or Emulsion</p> </div>	<p>H₂N-FazaFA-OMe H₂N-D-FazaFA-OMe H₂N-K(Z)azaFK(Z)-OMe H₂N-D-K(Z)azaFK(Z)-OMe H₂N-FazaFK(Z)-OMe H₂N-D-FazaFK(Z)-OMe</p> <div style="display: flex; justify-content: space-around;"> <div style="text-align: center;"> <p>pH 4</p> <p>Precipitate or Emulsion</p> </div> <div style="text-align: center;"> <p>pH 7 & 10</p> <p>Solution</p> </div> </div>
3- Free C-terminal trimers (series C) (Methyl ester deprotection)	4- Z-group deprotection (series D) (trimers containing lysine residue)
<p>Boc-FazaFA-OH Boc-D-FazaFA-OH Boc-K(Z)azaFK(Z)-OH Boc-D-K(Z)azaFK(Z)-OH Boc-FazaFK(Z)-OH Boc-D-FazaFK(Z)-OH</p> <div style="display: flex; justify-content: space-around;"> <div style="text-align: center;"> <p>pH 4</p> <p>Precipitate or Emulsion</p> </div> <div style="text-align: center;"> <p>pH 7 & 10</p> <p>Solution</p> </div> </div>	<p>Boc-KazaFK-OMe Boc-D-KazaFKOMe Boc-FazaFK-OMe Boc-D-FazaFK-OMe</p> <div style="display: flex; justify-content: space-around;"> <div style="text-align: center;"> <p>pH 4</p> <p>Precipitate or Emulsion</p> </div> <div style="text-align: center;"> <p>pH 7 & 10</p> <p>Solution</p> </div> </div>

After that and in order to induce hydrogelation, we thought to replace the Boc-group with Fmoc-moiety as fluorenyl group is known by its large π -surface area that has advantages of: (i) increasing stability through π - π aromatic interactions, (ii) increase the rigidity and reducing the flexibility, (iii) increasing hydrophobicity which is necessarily for hydrogel formation, and (iv) support the self-assembly which may lead to the hydrogel formation. Interestingly, replacing the Boc-group by Fmoc-group for the deprotected C-terminal 2:1-[α /aza]-trimers has achieved two new low molecular weight hydrogelators (LMWHGs) (7a' and 7b') which have led hydrogels at pHs 7.0 and 10.0.

In this chapter, two molecules Fmoc-Phe-azaPhe-Ala-OH (**7a'**) and Fmoc-*D*-Phe-azaPhe-Ala-OH (**7b'**) have been synthesized and showed their abilities to form hydrogels at pHs 7.0 and 10.0. Characterizations of the two molecules at the molecular and supramolecular levels have been investigated using X-ray diffraction, and number of spectroscopy techniques including NMR, FTIR, UV-visible absorption, fluorescence emission, and circular dichorism (CD). The rheological behaviors of the two hydrogels were assessed through rheological experiments. Finally, the morphological studies have been established by utilizing scanning electronic microscopy (SEM) for imaging the dried hydrogels from **7a'** and **7b'**.

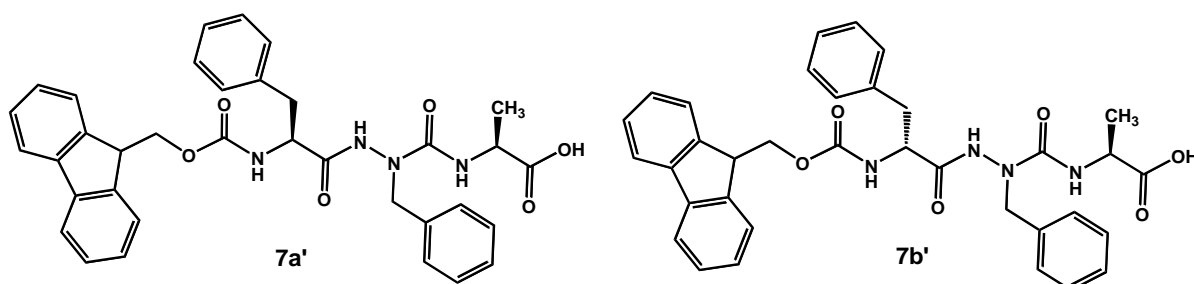
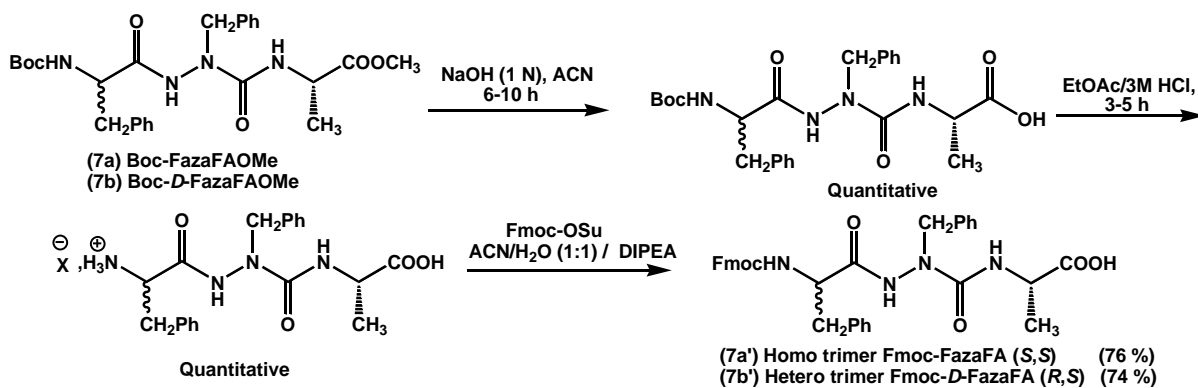


Figure 7.1. Molecular structures of Fmoc-FazaFA (**7a'**) and Fmoc-*D*-FazaFA (**7b'**).

VII.2. Synthesis and Characterizations of Fmoc-*L*- or *D*-Phe-azaPhe-Ala-OH

Compounds Fmoc-*L*-Phe-azaPhe-Ala-OH (**7a'**) and Fmoc-*D*-Phe-azaPhe-Ala-OH (**7b'**) have been synthesized in pure forms and good yields by carrying out three more additional steps on the general strategy that has been reported in Chapter II for the synthesis of 2:1-[α /aza]-oligomers.^{482,509} Fmoc-products **7a'** and **7b'** were obtained from the corresponding Boc-products in three consecutive steps: (i) Boc-deprotection, (ii) Methyl ester deprotection, and then (iii) coupling with the Fmoc-OSu to achieve the interested products as shown in Scheme 7.1.⁵¹⁰



Scheme 7.1. Stepwise synthesis of **7a'** and **7b'** from the corresponding Boc-precursors.⁵¹⁰

VII.3. Structural and Conformational Studies of Fmoc-*L*- or *D*-Phe-azaPhe-Ala-OH

VII.3.1. X-ray Crystallographic Data

Single crystals of compound **7b'** suitable for X-ray crystallographic analysis were grown by slow evaporation from EtOH. Compound **7b'** crystallizes in space group *P1* with two conformers in the asymmetric unit as shown in Figure 7.2 (two half-asymmetric units in the unit cell ($Z = 2$)), (Appendix 4, Figure S7.5 and Table S7.1).

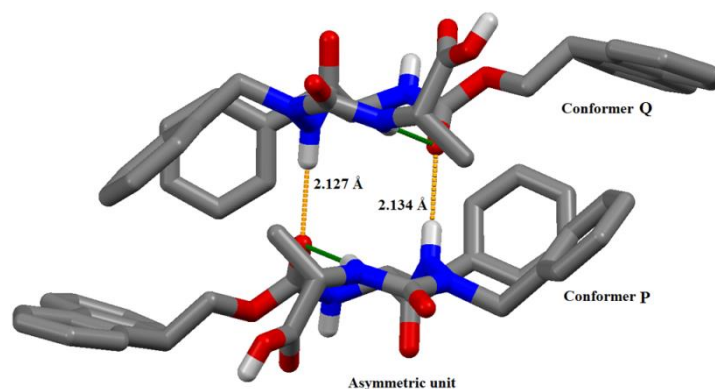


Figure 7.2. Crystal molecular structure (X-ray) of the asymmetric unit of compound **7b'**. The intramolecular and intermolecular hydrogen bonds are illustrated as dotted lines in green and orange colors, respectively. The H atoms, except those of the NH and OH groups, have been omitted for clarity.

X-ray results recorded interatomic distance between the polar sites ($O_i \cdots NH_{i+3}$) to be 3.060 Å and 3.049 Å for conformers **P** and **Q**, respectively (Table 7.2) which are adequate values for intramolecular hydrogen bond interactions^{118,511} closing pseudocycles of 10 atoms between NH_{i+3} (Ala) and the CO_i (Fmoc-group) of the type ($i+3 \cdots i$) as shown in Figure 7.3.

Table 7.2. Intramolecular hydrogen bond distances and bond angles in conformers **P** and **Q**

Conformer	Residue	Residue	Distance (Å)	Angle (°)	
P	CO (i)	NH (i + 3)	2.254	3.060	165.33
Q	CO (i)	NH (i + 3)	2.292	3.049	165.48

The distances between the C^α of residue (i) and C^α of residue (i + 3) in both conformers are less 7 Å which supports the existence of β -turn conformation.^{512,513} Moreover, each conformer is stabilized intramolecularly by orthogonal π -stacking between the phenyl groups of *D*-Phe and azaPhe as clear in Figure 7.3.

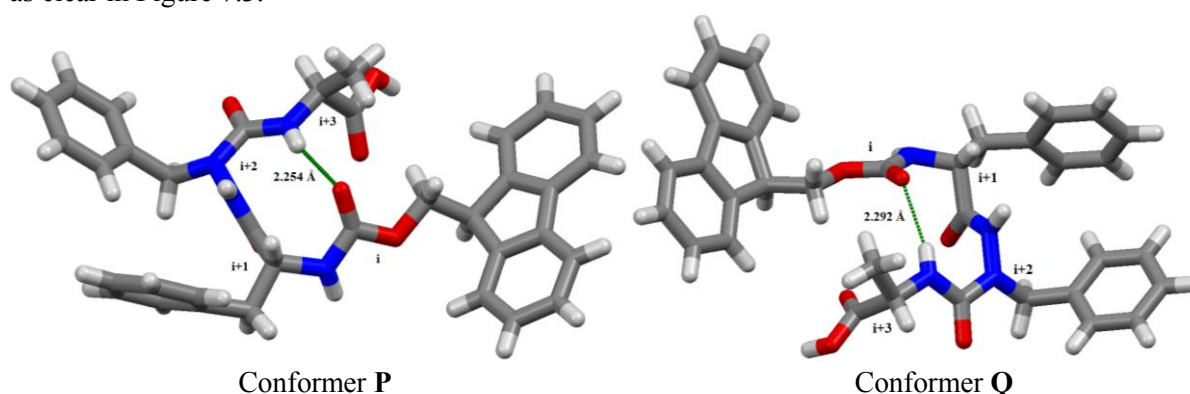


Figure 7.3. Crystal molecular structure (X-ray) of the conformers **P** (left), and **Q** (right). The intramolecular hydrogen bonds are illustrated as green dotted lines.

The two conformers (**P** and **Q**) in the asymmetric unit (Figure 7.2) form two intermolecular hydrogen bonds between CO_i (Fmoc-group) and NH_{i+2} (azaPhe) of conformer **P** with the NH_{i+2} (azaPhe) and CO_i (Fmoc-group) of conformer **Q** with a distance of 3.005 Å ($CO_i \cdots NH_{i+3}$), and bond angles of 175.84° and 175.10° for the both interactions, respectively (Table 7.3).

Moreover, Figure 7.3 indicates that the two conformers in the asymmetric unit are stabilized intermolecularly by orthogonal π -stacking between the benzyl groups (*D*-Phe and azaPhe) of one conformer and the fluorenyl group of the other conformer in an antiparallel mode.

Table 7.3. Intermolecular hydrogen bond distances and bond angles in the asymmetric unit of **7b'**

Conformer P	Conformer Q	Distance (Å)		Angle (°)
CO (i)	NH (i + 2)	2.127	3.005	175.84
NH (i + 2)	CO (i)	2.134	3.005	175.10

Whilst the values of the torsion angle $|\omega|$ range from 175.16° to 179.87° confirming *Z*-configuration for all the peptide bonds (Table 7.4), the torsion angles (ϕ , ψ) help in determination the nature of folding.^{480,481} The torsion angles recorded values of: ($\phi_{i+1} = 63.87^\circ$, $\psi_{i+1} = -125.12^\circ$) and ($\phi_{i+2} = -83.31^\circ$, $\psi_{i+2} = -8.2^\circ$) for conformer **P**, and ($\phi_{i+1} = 62.96^\circ$, $\psi_{i+1} = -122.06^\circ$) and ($\phi_{i+2} = -87.58^\circ$, $\psi_{i+2} = -7.68^\circ$) for conformer **Q** (Table 7.4). These values are close to classical β II'-turn angles in peptides, confirming that insertion of aza-amino acid in the peptide sequence supports the β -folding which is stabilized through intramolecular hydrogen bond of the type (i---i+3).^{480,481}

Table 7.4. Torsion angles in **7b'**

Conformer	Residue (i + 1)			Residue (i + 2)		
	ϕ	ψ	ω	ϕ	ψ	ω
P	63.87°	-125.12°	175.16°	-83.31°	-8.20°	-178.66°
Q	62.96°	-122.06°	175.36°	-87.58°	-7.68°	-179.87°
βII'-turn	60°	-120°	180°	-80°	0°	180°

Concerning the molecular packing of compound **7b'**, three of four carbonyl groups are oriented up and down perpendicularly, while the fourth carbonyl group projected pseudo-equatorially to the plane of the molecule as it is involved in intramolecular hydrogen bond. In contrast to the orientation of the Ala side chains in the asymmetric unit (Figure 7.2), the side chains of the Ala residues are oriented perpendicular to the plane of the molecules in opposite direction to the formed intermolecular hydrogen bonds and this supports the stacking of the molecules. Interestingly, we could recognize that each fluorenyl ring of conformer **P** or **Q** intercalates between the two phenyl rings of *D*-Phe and azaPhe residues of conformer **Q** or **P** through perpendicular and parallel π -stacking interactions, respectively (Figure 7.4a, b).

The alignment of the carbonyl groups allows the stacking of the molecules through four intermolecular hydrogen bonds between NH_{i+1} (*D*-Phe), CO_{i+1} (*D*-Phe), CO_{i+3} (Ala), and $\text{OH}_{\text{carboxylic}}$ of one molecule of conformer **P** with CO_{i+3} (Ala), $\text{OH}_{\text{carboxylic}}$ of one molecule of conformer **Q**, and NH_{i+1} (*D*-Phe), and CO_{i+1} (*D*-Phe) of another molecule of conformer **Q**, respectively. This means that each molecule of certain conformer forms 4 intermolecular hydrogen bonds with 2 molecules of the second conformer as shown in Figure 7.4b. The interatomic distances between the polar sites of these hydrogen bonds are 2.949 Å, 2.668 Å, 2.980 Å and 2.687 Å, while the bond angles are 162.02°, 165.22°, 161.40° and 162.28° for the four hydrogen bonds, respectively (Table 7.5), which are accepted values as hydrogen bonds.^{118,511} The arrangement of the carbonyl groups in this manner supports the formation of supramolecular structure held *via* an antiparallel hydrogen-bound network leading to an extended β -sheet like structure which is further stabilized by the stacking between the aromatic moieties (Figure 7.4b).^{413,429,514-518}

Part B
Chapter VII. Supramolecular Hydro-Gels Based on 2:1-[α /aza]-Trimers

Table 7.5. Intermolecular hydrogen bond distances and bond angles between conformers P and Q in packing mode

Conformer P	Conformer Q	Distance (Å)		Angle (°)
NH (i + 1) <i>D</i> -Phe	CO (i + 3) Ala	2.099	2.949	162.02
CO (i + 1) <i>D</i> -Phe	OH carboxylic	1.867	2.668	165.22
CO (i + 3) Ala	NH (i + 1) <i>D</i> -Phe	2.190	2.980	161.40
OH carboxylic	CO (i + 1) <i>D</i> -Phe	1.897	2.687	162.28

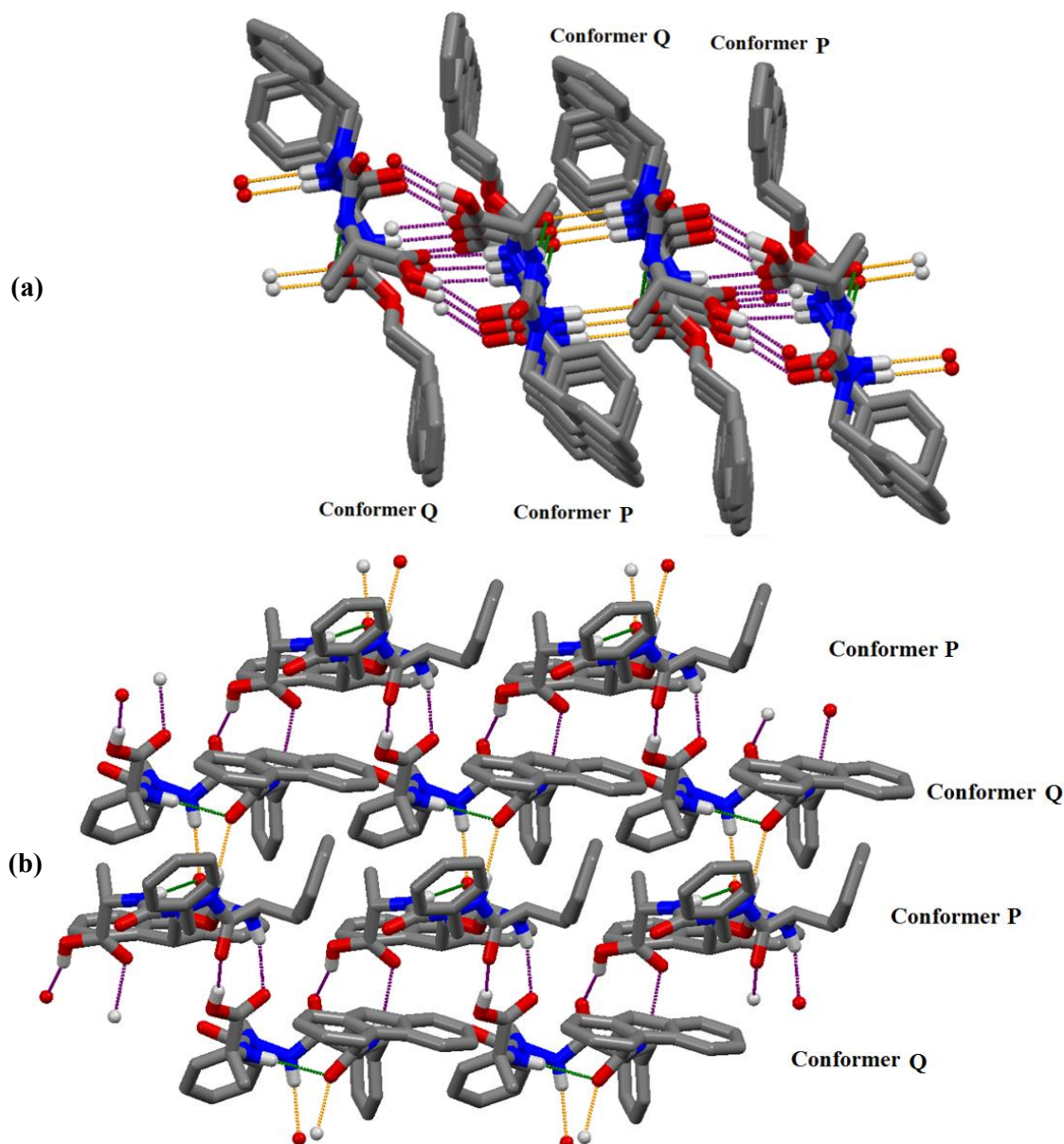


Figure 7.4. View of the packing mode in compound **7b'** in crystal state (X-ray) involving asymmetric units: (a) side view, and (b) top view. The intermolecular hydrogen bonds, (purple---packing, yellow---asymmetric unit) and intramolecular hydrogen bonds (green), are marked as dashed lines. The H atoms, except those of the NH and OH groups, have been omitted for clarity.

VII.3.2. NMR Spectroscopic Studies

^1H NMR studies of **7a'** and **7b'** were done in $\text{DMSO-}d_6$ (4.0 mmol. L^{-1} , 300 K) which provided high resolved signals compared with the resolution of the spectra recorded in CDCl_3 . The spectra of **7a'** and **7b'** are very similar except for the signals of the CH_2 protons of the residues (Phe) and (*D*-Phe) of compound **7a'** and **7b'**, respectively which appear chemically equivalent in case of compound **7a'** while they are non-equivalent in compound **7b'** (Appendix 4, Figures S7.1 – S7.4).

In order to gain an accurate insight into the conformation of both molecules in solution, 2D NMR (ROESY) experiments have been conducted on compounds **7a'** and **7b'** (4.0 mmol. L^{-1} , 300 K) to identify the most favorable conformation(s) (Appendix 4, Figures S7.7 and S7.8). Both molecules **7a'** and **7b'** adopt β -turn conformation in solution (Figure 7.5). The strong correlation between C^αH (Phe or *D*-Phe) and NH (azaPhe), and the moderate correlation between the NH (azaPhe) and NH (Ala), indicate that the both compounds adopt βII - and $\beta\text{I}'$ -turn conformations, respectively.^{480,481}

Furthermore, compounds **7a'** and **7b'** revealed the presence of weak correlation between the protons of NH (Phe or *D*-Phe) and NH (azaPhe) residues, suggesting that both compounds adopt partially βI - and $\beta\text{I}'$ -turn conformations, respectively (Figure 7.5).^{480,481}

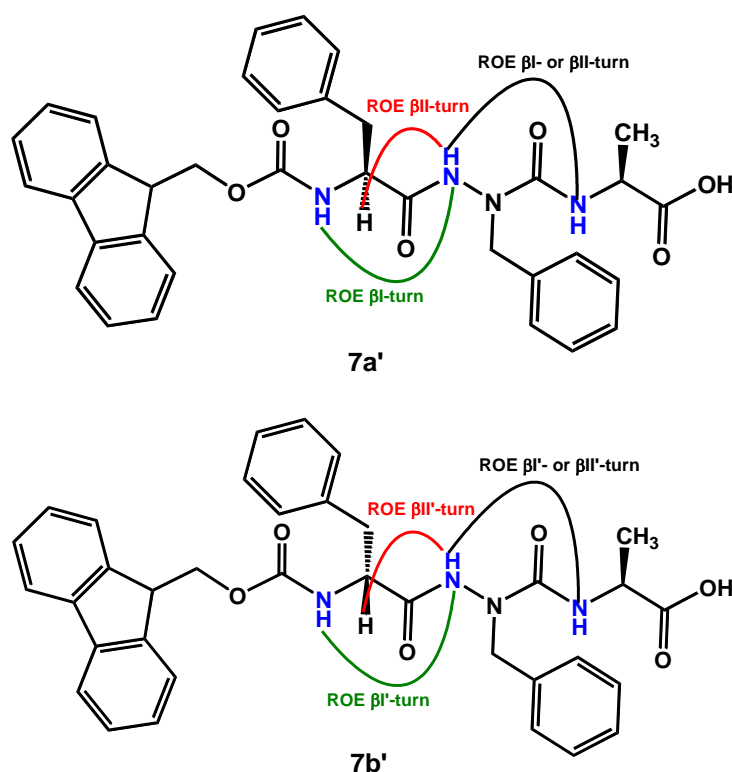


Figure 7. 5. ROE correlations of β -turn in compound **7a'** (left) and $\beta\text{I}'$ -turn conformation in compound **7b'** (right); (4.0 mmol. L^{-1} , $\text{DMSO-}d_6$).

Based on the structural studies of acyclic series⁴⁸² and on the X-ray studies of **7b'**, we could notice that changing the absolute configuration of the Phe residue from (*S*) in **7a'** to (*R*) in **7b'**, led to change in the conformation from β -type to $\beta\text{I}'$ -type, subsequently compound **7b'** exists mainly in $\beta\text{II}'$ -turn conformation.

We were interested to study if the β -turn conformations in the both compounds are supported by any intramolecular hydrogen bond. Hence, we studied the effect of solvent composition in which the method measures the sensitivity of the NH or OH protons through the change in their chemical shifts as a function of addition of polar solvent (*i.e.*, DMSO- d_6) to nonpolar (*i.e.*, CDCl₃).⁵¹⁹

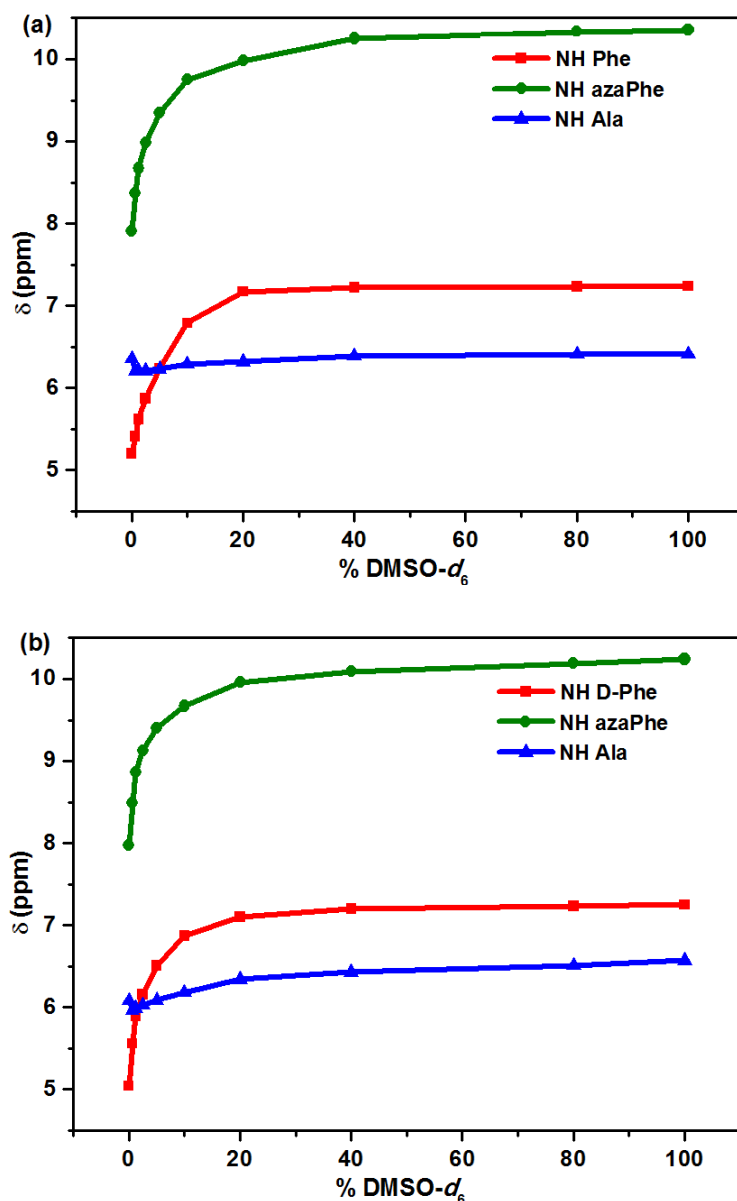


Figure 7.6. Chemical shift-variations (δ) of NH protons for: (a) **7a'**, and (b) **7b'** as a function of % [CDCl₃/DMSO- d_6] mixtures; (300 MHz, 4.0 mmol. L⁻¹).

Figure 7.6 shows that while the chemical shifts of the NH protons of Phe (**7a'**), D-Phe (**7b'**) and azaPhe in the two compounds are greatly sensitive to the addition of DMSO- d_6 , the NH protons of Ala residues are weakly affected by the addition of the DMSO- d_6 . Regarding the OH protons in both compounds, it was difficult to follow the variations in their chemical shifts due to broadening of the peak signals in presence of CDCl₃ (Appendix 4, Figure S7.9). These results reveal that only the NH proton of Ala may be involved in intramolecular hydrogen bond.⁵¹⁹ Interestingly, the aromatic protons suffer deshielding effect when increasing DMSO- d_6 percentage indicating that the conformation in chloroform is stabilized by π -stacking between the aromatic moieties (Figures 7.7a, b).

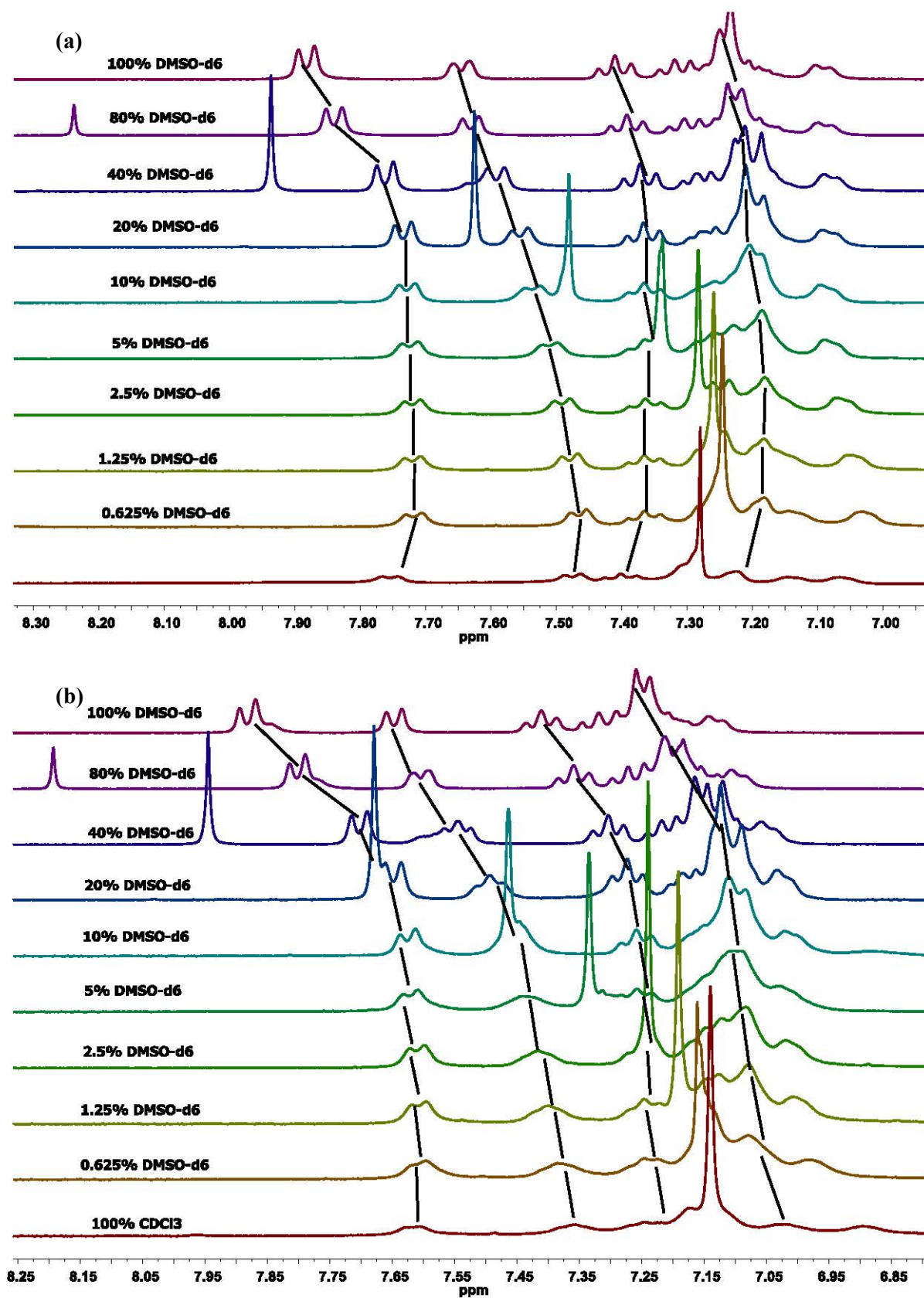


Figure 7.7. Chemical shift-variations (δ) ppm of aromatic protons for: (a) **7a'**, and (b) **7b'** as a function of % [$\text{CDCl}_3/\text{DMSO-}d_6$] mixtures; (300 MHz, 4.0 mmol. L^{-1}).

VII.3.3. FTIR Spectroscopic Studies

IR spectra were recorded for compounds **7a'** and **7b'** at dilute condition (2.0 mmol. L^{-1}) to avoid the intermolecular interactions. They showed two characteristic domains correspond to the stretching NH and CO regions (Figures 7.8 and 7.9). In compound **7a'**, the NH stretching region reveals the presence of free NH band around 3435 cm^{-1} belongs to the free NH_{i+1} (Phe) and NH_{i+2} (azaPhe), in addition to a broad bound band with two maxima around 3331 cm^{-1} and 3369 cm^{-1} in which one of them corresponds to the bound NH_{i+3} proton of Ala (Figure 7.8a). Similarly, the spectrum of compound **7b'** shows a band around 3432 cm^{-1} belongs to the free NH_{i+1} (*D*-Phe) and NH_{i+2} (azaPhe), as well as there are several bound bands centered at 3275 cm^{-1} , 3349 cm^{-1} and 3368 cm^{-1} in which one of these bands corresponds to the bound NH_{i+3} proton of Ala (Figure 7.8b). The additional bound NH bands in the FTIR spectra in both molecules could be assigned latter using molecular dynamic calculations (Next Section).

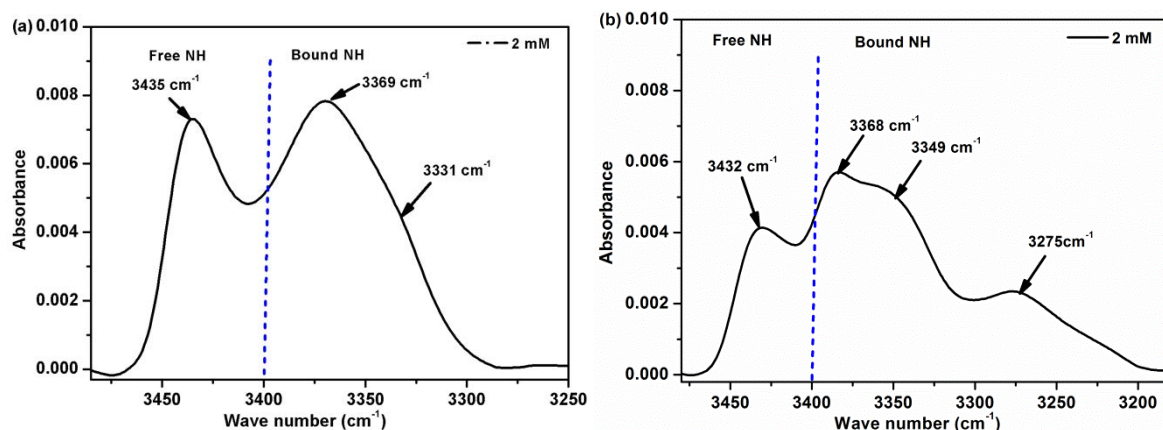


Figure 7.8. FTIR spectra belong to the NH stretching region for: (a) **7a'**, and (b) **7b'**; (2.0 mmol. L^{-1} , CDCl_3).

Regarding to the CO vibration region, both compounds (**7a'** and **7b'**) exhibited similar broad spectrum with 4 main bands in the amide I region (Figure 7.8). Thanks to 2nd derivative method which helped to obtain 7 deconvoluted bands. The assignments of these bands were done based on their shorted peptides as well as the previously reported oligomers belong to the same azapeptide series.⁴⁸²

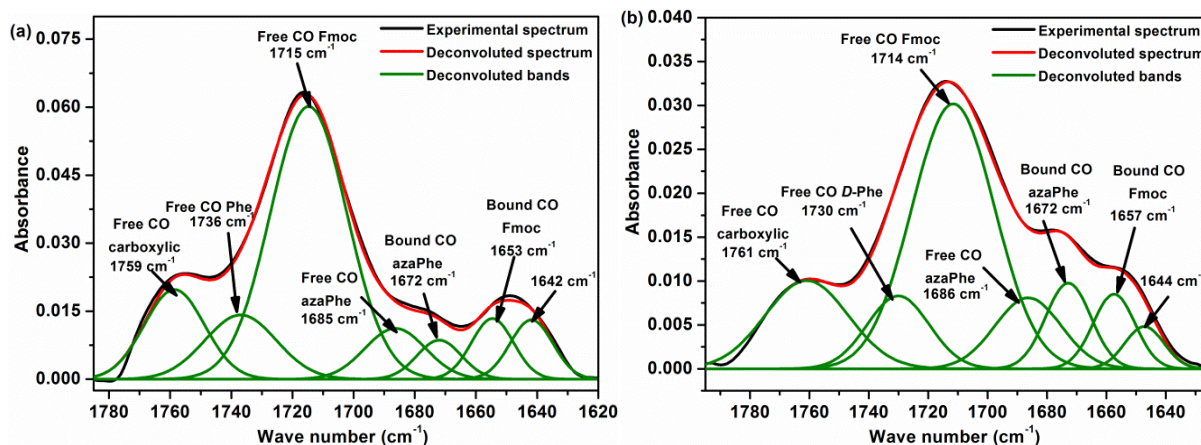


Figure 7.9. FTIR spectra belong to CO stretching region for: (a) **7a'**, and (b) **7b'**; (2.0 mmol. L^{-1} , CDCl_3).

Based on previous study, the bound CO band around 1655 cm^{-1} should be related to NH_{i+3} proton of Ala residue that is involved in intramolecular hydrogen bond in both molecules (Figure 7.9).⁴⁸² In contrast, the other CO groups are in free states in dilute solution as noticed from their higher wave numbers at $1685, 1715, 1736$ and 1759 cm^{-1} for molecule **7a'** (Figure 7.9a), and $1686, 1714, 1730$ and 1761 cm^{-1} for molecule **7b'** (Figure 7.9b); corresponding to the free CO of azaPhe, Fmoc, (Phe or *D*-Phe), and Ala residues, respectively. Based on the available data from NMR and FTIR spectroscopy, we could not succeed to assign the additional bound band obtained after deconvolution at 1672 cm^{-1} . Molecular dynamics calculations were recommended to have an idea about the possibility of other intramolecular interactions in both molecules (Next Section).

Other experimental studies in the literature indicated that infrared studies provide information about the secondary structures in peptides and proteins. Not only the zone $1690 - 1660\text{ cm}^{-1}$, but also the region $1645 - 1635\text{ cm}^{-1}$ are characteristics for β -turn conformation in small peptides.⁵²⁰ Accordingly, 2nd derivative method was helpful to confirm the presence of band at 1642 cm^{-1} (**7a'**) and 1644 cm^{-1} (**7b'**) from which we suggest that both compounds exist in a β -turn conformation in solution and these are in accordance with the 2D NMR results.

VII.3.4. Molecular Dynamic Calculations (AMBER 12)

In order to investigate the most dominant conformation(s) as well as the possible intramolecular hydrogen bonds in the two molecules **7a'** and **7b'**, molecular dynamic calculations were carried out according to the protocol described in experimental section.^{521,522} Ptraaj was employed for the analysis of 25,000 structures in order to assess the possibility of hydrogen bond formation and the average values of the torsion angles to have an idea about the most favorable conformations adopted by these oligomers.

Molecular dynamic simulation predicted that both molecules (**7a'** and **7b'**) possess a new intramolecular hydrogen bond between CO_{i+2} (azaPhe) and OH_{i+3} (Ala) closing a pseudocycle of 7 atoms (Figure 7.10) which structures the peptide backbone in γ -turn conformation. This bond could not be verified in NMR spectroscopy due to the broadening of the OH signals, however the modelling results is consistent with the FTIR results by interpreting the additional broad bound NH bands in both compounds. The difference in modelling and NMR results may be related to the different experimental conditions in both techniques.

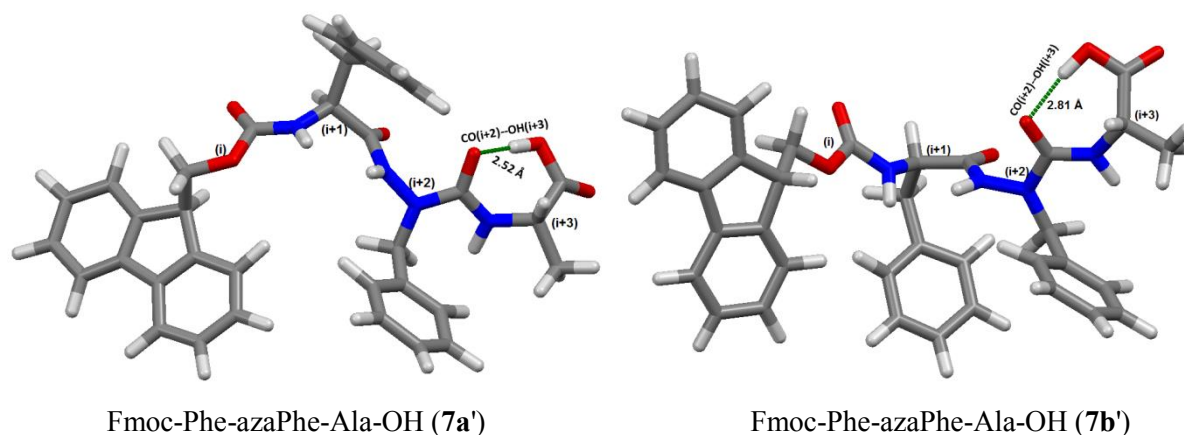


Figure 7.10. Selected frame for molecule: **7a'** (left), and **7b'** (right) issued of the molecular dynamic simulations showing the intramolecular hydrogen bond illustrated by green dots.

By applying the most favorable parameters for hydrogen bond formation in which the bond angle prefers to be greater than 120° and the bond distance to be less than 3.2 \AA .^{118,511} We could calculate that about 15353 (61.4%) and 8291 (33.2%) frames in case of **7a'** and **7b'**, respectively possess the same intramolecular hydrogen bond between CO_{i+2} (azaPhe) and the OH_{i+3} (Ala), (Table 7.6).

Table 7. 6. Average intramolecular hydrogen bond distances and angles in **7a'** and **7b'** issued of the molecular dynamic simulations

Molecule	Residue	Residue	Distance (\AA) O----OH	Angle ($^\circ$)	Intramolecular H-bond (%)
7a'	CO (i + 2)	OH (i + 3)	2.65	163.58	61.4
7b'	CO (i + 2)	OH (i + 3)	2.65	163.56	33.2

The secondary structures of azapeptides are based on their backbone structural elements which composed of the hydrazine as part of the hydrazide group and an urea constituent, in which the two parts are described by the torsion angles ϕ and ψ , respectively.⁴⁸¹ Dihedral angles were measured over the trajectories of molecular dynamic simulations for the molecules **7a'** and **7b'** (Table 7.7).

Table 7.7. Mean dihedral angles of molecules **7a'** and **7b'** calculated from 25,000 structures issued of the molecular dynamic simulations

Compound	ϕ_{i+1}	ψ_{i+1}	ϕ_{i+2}	ψ_{i+2}	ϕ_{i+3}	ψ_{i+3}
7a'	-125.18°	-15.45°	88.42°	-46.39°	-93.40°	71.02°
7b'	135.00°	12.46°	91.00°	-29.76°	-113.18°	84.97°
Classic γ-turn	--	--	80.00°	-65.00°	--	--
Inverse γ-turn	--	--	--	--	-80.00°	65.00°

Based on the average values of the torsion angles for all the simulated 25,000 structures in the two trimers **7a'** and **7b'** (Table 7.7), we could suppose that the residues (i+2) and (i+3) in both molecules induce classic and inverse γ -turn conformations, respectively. Only the inverse γ -turn is stabilized by the formation of intramolecular hydrogen bond between CO_{i+2} (azaPhe) and OH_{i+3} (Ala) closing a pseudocycle of 7 atoms as described previously.

Comparing with the previous study of the protected C-terminal trimer of the same azapeptide series,⁴⁸² we could conclude that the presence free carboxylic group (COOH) of Ala residue has not disturb the role of the aza-motif in structuring the peptide backbone in certain conformation. In addition, changing the chirality of the first residue (i+1) has no much effect on the conformation of both molecules.

VII.4. Characterization of Low Molecular Weight Hydrogels from **7a'** and **7b'**

VII.4.1. Gel Preparation and Minimum Gelation Concentrations (MGCs)

In the course of investigating the self-assembly behavior of Fmoc-Phe-azaPhe-Ala-OH (**7a'**) and Fmoc-D-Phe-azaPhe-Ala-OH (**7b'**), the two pseudopeptides showed a dual property. They could form hydrogels under pH trigger and the formed hydrogels exhibit thermoreversible behavior (Figure 7.11). These hydrogels are stable within the pH range 7.0 – 10.0, while precipitation occurs at pH 4.0.

We examined the gelation ability of gelators **7a'** and **7b'** in buffer solutions pH 7.0 and 10.0 by adopting the “stable-to-inversion” method.^{132,476} We deemed the sample to be a gel when it was not visually phase-separated and did not flow when the glass vial was inverted.

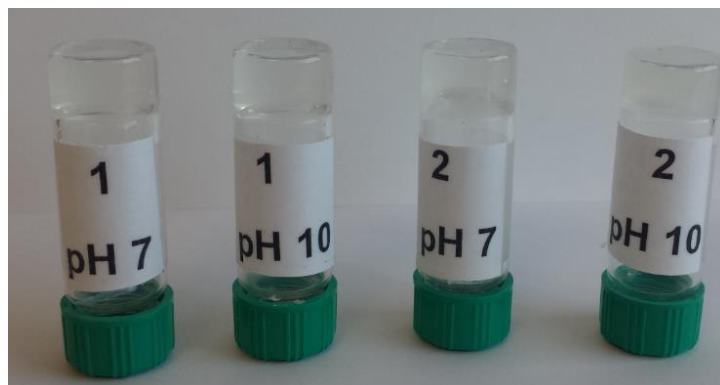


Figure 7.11. Supramolecular hydrogels from **7a'** (vials 1), and **7b'** (vials 2) induced by pH 7.0 and pH 10.0; ($c = 1.0$ wt%).

We observed that both gelators (**7a'** and **7b'**) revealed close behaviors in buffer solutions at the same concentration and this has been confirmed by studying the two gelators using spectroscopic techniques (NMR, FTIR, CD, UV-vis and fluorescence), rheological measurements and morphological studies, which gave indication that changing the chirality of the amino acid does not have much effect of the properties on the formed hydrogels.

MGC is the lowest gelator concentration at which gelation occurs and the flow of medium is restricted.⁵²³ The minimum gelation concentrations (MGCs) are in the ranges 0.6 – 0.8 wt% and 0.7 – 1.0 wt% for gelators **7a'** and **7b'**, respectively.

In order to investigate the role of aza-moiety on the gelation behavior, we synthesized the corresponding peptides possessing no aza-moiety. Interestingly, the MGCs increased to be in the range 1.2 – 1.4 wt% and the formed gels were not homogenous containing suspended particles (Figure 7.12) due to the poor solubility of the starting peptides (Table 7.8).



Figure 7.12. Effect of insertion of aza-amino acid on the MGCs. Hydrogels obtained from compounds **7a'** (vial 1), and **7b'** (vial 2) *versus* viscous solution from the corresponding peptides without aza-moiety, vial **N1**= Fmoc-FFA, and vial **N2** = Fmoc-*D*-FFA; (1.0 wt%, pH 7.0 and 10.0).

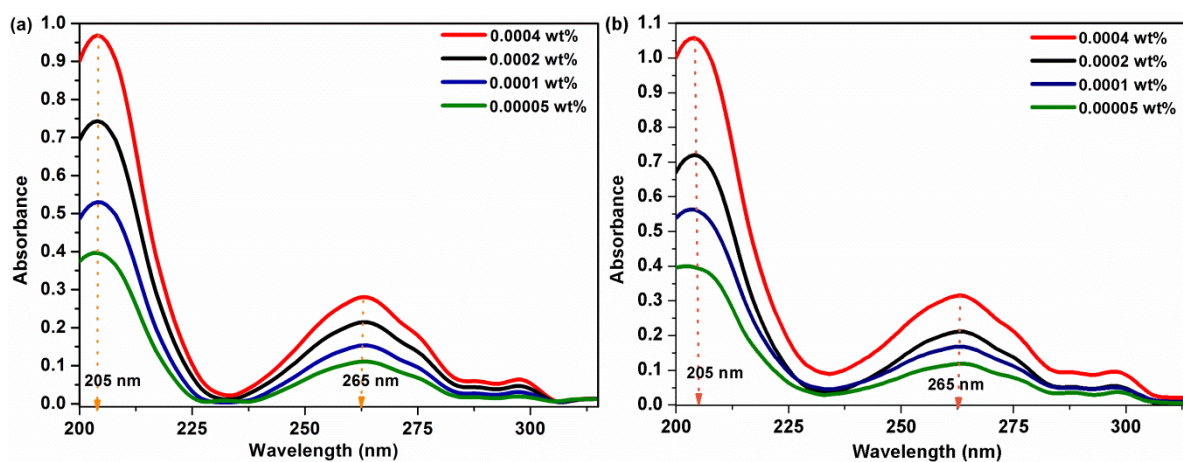
Table 7.8. Minimum gelation concentrations of azapeptides (**7a'** and **7b'**) versus normal peptides (N1 and N2)

		Gelator	MGC (wt%)
Vial	1	7a'	0.6 - 0.8
Vial	N1	Fmoc-FFA	1.2 - 1.3
Vial	2	7b'	0.7 - 1.0
Vial	N2	Fmoc-D-FFA	1.2 - 1.4

1D and 2D NMR studies of the hydrogels in presence of the buffer solution and also the unavailability of deuterated ethanol in our laboratory during that period, put difficulties to investigate the correlations existed in the gel state. We aimed in perspective studies to perform solid state NMR for these hydrogels to avoid the solvents interferences. Structural characterizations of the self-assembled structures for both hydrogels have been continued using UV absorption and fluorescence emission, circular dichroism (CD), infrared (IR), and the results will be overviewed in the following sections.

VII.4.2. UV-visible Absorption and Fluorescence Emission Spectroscopic Studies

Fmoc and phenyl groups were previously found to play inducing role in the self-assembly mechanism of Fmoc-peptides, enabling the gelator molecules to interact through hydrophobic π - π interactions.^{413,426} UV-absorption and fluorescence emission spectroscopy were used to investigate and probe π - π^* stacking interactions of aromatic units in Fmoc-FazaFA, and Fmoc-D-FazaFA at pH 7.0 as a function of concentration and temperature.

Figure 7.13. UV-visible spectra of: (a) Fmoc-FazaFA (**7a'**) and, (b) Fmoc-D-FazaFA (**7b'**).

The UV-absorption spectra of the hydrogelators Fmoc-FazaFA (**7a'**) and Fmoc-D-FazaFA (**7b'**) at dilute solutions showed two main broad peaks with maxima at 205 and 265 nm (Figure 7.13), which were previously assigned to the absorption of Phe residue and Fmoc-moiety, respectively.^{382,524,525} We could not follow the shift in the maxima of the two peaks from solution to gel state for both hydrogelators due to the saturation in the absorption spectra that accompanied the high concentrations.

Concentration gradient fluorescence spectroscopy for both hydrogelators **7a'** and **7b'** were studied from 0.025 wt% (sol) to 1.0 wt% (gel), Figure 7.14. In the solution state, the gelator molecules of **7a'** and **7b'** move freely and the fluorescence emission spectra for both hydrogelators exhibit a broad band with maxima centered at 312 - 314 nm and 322 - 326 nm which correspond to π -interactions of the monomeric states for the aromatic moieties (fluorenyl and phenyl groups).^{359,422}

Part B
Chapter VII. Supramolecular Hydro-Gels Based on 2:1-[α /aza]-Trimers

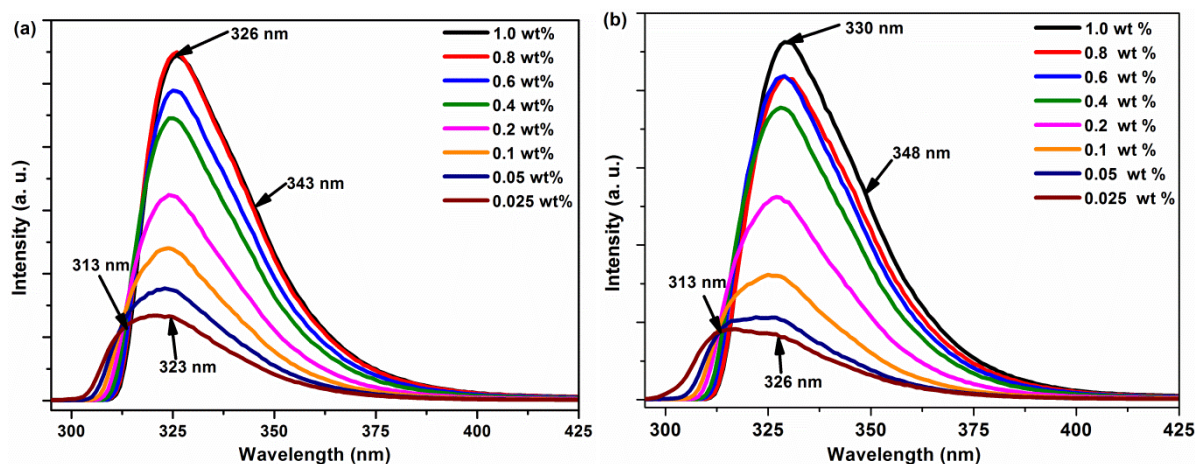


Figure 7.14. Concentration gradient fluorescence spectra of: (a) Fmoc-FazaFA (**7a'**) and, (b) Fmoc-D-FazaFA (**7b'**); ($\lambda_{\text{ex.}} = 265 \text{ nm}$).

Increasing the concentration to the gel state (1.0 wt%) causes a slight red shift recording a maximum peak around 325 - 330 nm in both hydrogels (Figure 7.14). This red shift has been interpreted as the aromatic groups are stacked in the gel state³⁵⁹ and stabilized through excimer (excited) π - π^* stacking interactions of fluorenyl units (Fmoc).^{102,413,526,527} In addition, broad shoulder centered around 343 - 348 nm is recognized when increasing the concentration than 0.1 wt% which suggests that the self-assembly is supported by further multiple π - π^* stacking interactions between the aromatic moieties in an antiparallel orientation.^{102,414,418,419,422,526,528}

Each hydrogel of concentration 0.7 wt% at pH 7.0 was subjected to temperature-dependent fluorescence over heating cycle from 25 °C to 90 °C at a rate of 5 °C/min (Figure 7.15).

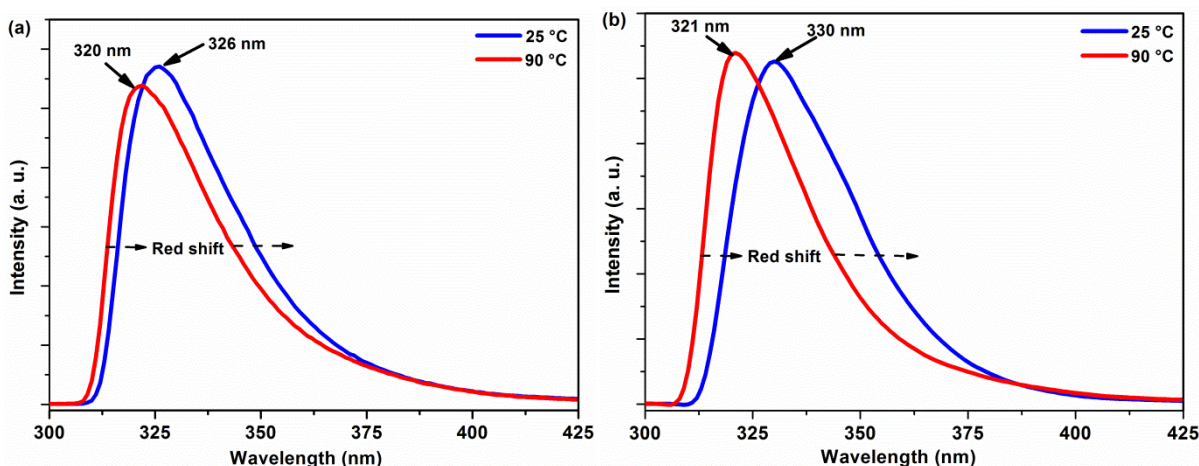


Figure 7.15. Temperature-dependent fluorescence spectra of: (a) Fmoc-FazaFA (**7a'**) and, (b) Fmoc-D-FazaFA (**7b'**); (25 °C and 90 °C, $\lambda_{\text{ex.}} = 265 \text{ nm}$).

The spectra in Figure 7.15 demonstrate only two measurements at the lowest and highest temperatures to focus on the change in the behaviors of the hydrogelators **7a'** and **7b'** when heating. The two spectra show distinct red shift to lower wavelengths at high temperature (90 °C, sol state) compared with the room temperature (25 °C, gel state) supposing that most of the intermolecular interactions (π -stacking and hydrogen bonds) are broken and the gelator molecules of **7a'** and **7b'** move freely in their solutions at high temperatures. Hydrogel **7b'** reflects more red shift than **7a'** proposing that the aromatic moieties are more overlapped in the gel state of **7b'** than in case of **7a'**.

Fluorescence study clearly emphasizes that hydrogelation phenomenon in both gelators is induced by the same intermolecular interactions mainly π -stacking between the fluorenyl and phenyl moieties. In addition, the two hydrogelators behave similarly since the spectra are very similar and they showed red-shift in the whole spectrum when increasing concentration or raising the temperature.

VII.4.3. Circular Dichroism (CD) Spectroscopic Studies

Circular dichroism (CD) spectroscopy is a powerful technique for studying molecular self-assembly.^{362,363,529-534} It is used to: (i) assess the nature of the secondary structure of the self-assembled materials,³⁷⁹ (ii) discriminate between monomer and supramolecular induced chirality, (iii) provide information about the handedness orientation of many aromatic molecules such as Fmoc-functionalized peptides and amino acids,^{1,7,382,460} in addition (iv) CD spectroscopy has been utilized to probe $n\text{-}\pi^*$ and $\pi\text{-}\pi^*$ stacking interactions within the self-assembled structures.³⁸²

It has been reported that the supramolecular chiral structures show more intense CD signals compared with the signal observed from either the chiral properties of the single chromophore or excitonic interaction between chromophores.^{415,535} In previous studies, Fmoc-peptides have shown their spontaneous molecular self-assembly in buffer solutions which could lead to hydrogels formation. Chiral organization of the resulting self-assembled hydrogel shows intense CD signals which originate principally from the supramolecular organization of the Fmoc moiety.^{426,429,536-539} Formation of hydrogels from aromatic peptide amphiphiles is driven by two major types of interaction: (i) aromatic π -stacking amongst the aromatic moieties, and (ii) hydrogen bond formation between the peptidic carbonyl and amide NH group, resulting in structures similar to the β -sheet observed in peptides and proteins.^{415,429,539}

The terminal COOH group plays a key role in self-assembly mechanism of this class of gelators. It has been observed that the apparent pKa of the terminal carboxylic acid is shifted several pH units from the expected value of around 3.5 – 4.0 due to the COOH group being presented in high hydrophobic environment upon self-assembly.^{429,538} Therefore, at pH 7.0 the gelator molecule is anionic and self-assembly can be induced by increasing the ionic strength of the solution, thereby shielding the unfavorable electrostatic repulsion.⁵⁴⁰

The CD spectra of our pseudotripeptides **7a'** and **7b'** at pH 7 are very similar in gel and viscous states (Figure 7.16).

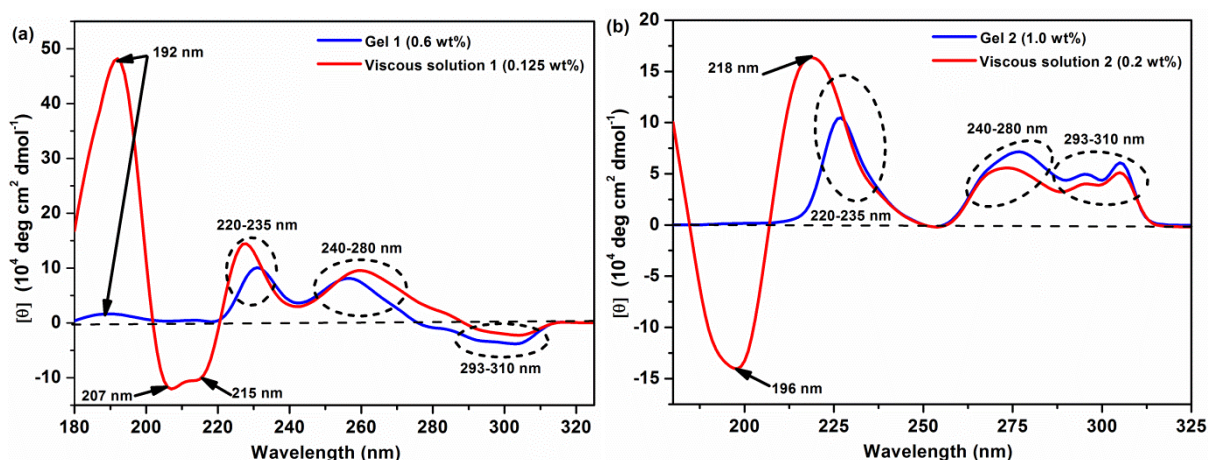


Figure 7.16. Normalized CD spectra of gel and viscous states for hydrogels from pH 7.0 of: (a) **7a'**, and (b) **7b'**.

While viscous solution **7a'** (2.0 mmol. L⁻¹, 0.125 wt%) demonstrates a maximum at 192 and minima peaks at 207 and 215 nm (Figure 7.16a), solution **7b'** (3.3 mmol. L⁻¹, 0.2 wt%) reflects a minimum at 196 nm and a maximum at 218 nm, (Figure 7.16b). These CD signatures of both gelators are characteristics of β -sheet structure in peptides and proteins.^{382,541} In previous studies, authors reported that the peak around 200 nm is associated with a π - π^* transition, and the peak around 217 nm is associated with a n - π^* transition.⁵⁴² Other studies assigned the minimum around 200 nm to the presence of cross- β assemblies stabilized by π -stacking of the aromatic side chains^{543,544} or due to the distortion of β -sheet structures.⁵⁴⁵

In the gel state (at MGCs) of **7a'** (9.9 mmol. L⁻¹, 0.6 wt%) and **7b'** (16.5 mmol. L⁻¹, 1.0 wt%), it was difficult to have detectable CD signals in the range 180 - 215 nm, and the spectra showed almost zero ellipticity, except the positive maximum shallow peak at 192 nm for gel from **7a'**. The zero response signals in the CD spectra in the range 180 - 215 nm (at gel state) of both **7a'** and **7b'** due to the saturation effect which has observed in the UV-absorption spectra in this region (Figure 7.16).

In the range 215 - 315 nm, the CD spectra of both hydrogelators in solution or gel states at pH 7.0 are very similar and they show the same interactions but they exhibit opposite signs of CD signals within the range 290 - 315 nm, (Figure 7.16). Indeed, the CD spectra of hydrogelators Fmoc-FazaFaA (**7a'**) and Fmoc-*D*-FazaFaA (**7b'**) at pH 7.0 in both gel and sol states show two successive positive maxima peaks: (i) the range 220 - 235 nm which indicative of π - π stacking of the aromatic phenylalanine residues, and (ii) the range 240 - 280 nm which can be attributed to interactions of phenylalanine residues with tertiary structure or π - π stacking interactions between phenyl and fluorenyl groups.^{7,379} Finally, the presence of cotton effect with opposite maxima signs for **7a'** and **7b'** in the range 293 - 315 nm have been assigned previously to π - π interactions of the fluorenyl groups as was observed by Xu and co-workers.^{102,526,539,546-548}

The different in the cotton effect associated with the fluorenyl groups from negative maxima in **7a'** to positive maxima in **7b'** imply that the Fmoc-groups in the two gels have different chiral orientation in the formed self-assembled nanostructures which may attributed to the different in the chirality of the first amino acid.³⁶² This observation has been previously reported, since the orientation of the supramolecular self-assembled structure has changed from right-handed to left-handed when changing the chirality of the first amino acid from *L*-Phe to *D*-Phe.^{7,420}

Based on CD results, we could suppose that the hydrogelators of **7a'** and **7b'** can self-assemble at pH = 7 into self-assembled nanostructures in which the molecules orient themselves in supramolecular structure displaying CD signatures characteristic of classical β -sheet arrangements stabilized by π - π stacking between the aromatic moieties.³⁸⁸ This supramolecular organization is still conserved in the gel state as most of the CD signals (215 - 315 nm) are the same in the both normalized spectra of viscous and gel states assuming β -sheet self-assembly by the gelator molecules within the fibrils in the gel state.^{3,40,225,285,424,549-556}

VII.4.4. ATR-FTIR Spectroscopic Studies

In order to investigate the driving forces particularly the role of the hydrogen bond interactions in the self-assembly and hydrogel formation, ATR-FTIR measurements have been performed on lyophilized hydrogel samples for **7a'** and **7b'**.

In previous studies, authors used the ATR-FTIR experiments to study the self-assembled structures in peptides and proteins focusing mainly on the amide A, amide I and amide II domains, which are informative regions concerning the secondary structures.³⁸²

Part B

Chapter VII. Supramolecular Hydro-Gels Based on 2:1-[α /aza]-Trimers

These studies reported that: peaks around 1690 and 1629 cm^{-1} are associated with a β -sheet structure,^{7,379,388,413,429,557-561} bands in the range 1643 - 1648 cm^{-1} have been assigned to random-coil or unordered structures,^{379,388,559-562} bands within the range 1673 - 1680 cm^{-1} are often associated with an antiparallel β -sheet structure,⁵⁶¹ although there is controversy in the literature about these ranges.^{382,563}

In previous studies on Fmoc-peptides, authors reported that the presence of phenylalanine residue and Fmoc group in the short peptide sequence cause relative rigidity in the whole structure and this support the self-assembly favoring the formation of extended β -sheet structures,⁵⁶⁴ where the rigidity facilitates the phenyl and fluorenyl groups to interlock into β -sheet arrangement.^{413,429}

The ATR-FTIR spectra for both lyophilized hydrogels at the two pH values showed similar behaviors in the amide I and amide II domains. Concerning the stretching CO region (amide I) and comparing with the solid states, most of the stretching CO groups in the lyophilized hydrogels spectra of **7a'** and **7b'** shift to lower frequencies indicating significantly to their participation in the co-assembled gel through hydrogen bonding interactions, Figure 7.17.¹

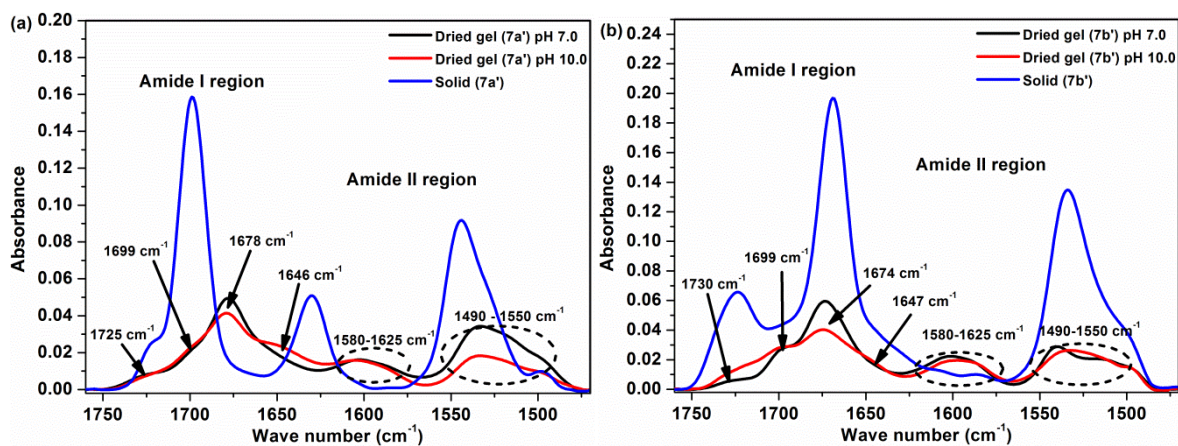


Figure 7.17. Comparison of the ATR-FTIR spectra in the CO stretching and NH bending regions for the dried gels from: (a) **7a'**, and (b) **7b'** at pH 7.0 and pH 10.0, versus their solid states.

The spectra of **7a'** at pH 7.0 and pH 10.0 (Figure 7.17a) show C=O stretching bands with maxima at 1725, 1699, 1678 and 1646 cm^{-1} for the carboxylic acid, amide, carbamidic and hydrazidic carbonyl groups, respectively. In the other side, ATR-FTIR spectra of **7b'** at pH 7.0 and pH 10.0 (Figure 7.17b) show C=O stretching bands with maxima at 1730, 1699, 1674 and 1647 cm^{-1} for the carboxylic acid, amide, carbamidic and hydrazidic carbonyl groups, respectively.

Moreover, in the co-assembled gels, the stretching CO band of -COOH group has decreased compared with solid state which may indicate its contribution in the gel formation through hydrogen bond formation. The spectra of all the lyophilized gels (**7a'** and **7b'**) demonstrate two distinct broad bands in the amide II region with ranges 1580 - 1625 cm^{-1} and 1490 - 1550 cm^{-1} .

In the literature, the bands within the ranges 1670 - 1685 cm^{-1} and 1580 - 1625 cm^{-1} are characteristics of carbonyl groups engaged in β -sheet hydrogen-bound network structure,^{388,415} and more particularly in β -sheet antiparallel arrangement. Accordingly we could assign the range 1580 - 1625 cm^{-1} to the presence of β -sheet like structure formed by the self-assembly of hydrogelator molecules in both **7a'** and **7b'**. In addition, the broad band at 1490 - 1550 cm^{-1} was assigned in the literature to the carboxylate ion (-COO⁻) of the Ala residue due to the deprotonation effect occurs at the tested pH values.⁶⁰

The observed negative bands in the NH stretching (amide A region) for the dried gels made us to compare between the solid and the solution (CDCl_3) states, Figure 7.18. The spectra of both solids demonstrate lower frequency values for all the NH protons and they occur in the bound NH region. Hence, strong participation of most of these NH protons in supramolecular construction in solid state through intermolecular hydrogen bonds with the CO groups should be expected.⁷

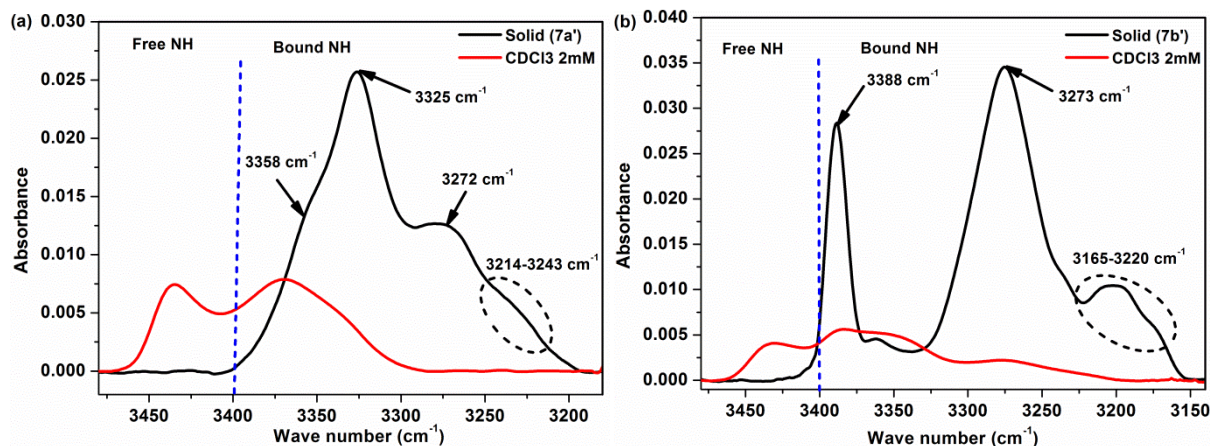


Figure 7.18. Comparison of the FTIR spectra in the NH stretching region between the solid states and solution states in CDCl_3 for: (a) **7a'**, and (b) **7b'**.

Infrared studies highlighted that the vibrators (CO, NH, and OH) belong to the carboxylic, amidic, carbamidic and hydrazidic are engaged as a part of the self-assembled antiparallel β -sheet like structure in the dried gels. The spectra showed strong shift towards the lower wave numbers which confirm the high propensity of the gelator molecules to construct supramolecular structure supported by network of intermolecular hydrogen bonds between the CO, OH and NH groups.¹⁵ These data indicate that hydrogen bonding interactions play a major role in self-association of the gelator molecules in gel formation.^{69,362,500}

For further characterization of the hydrogels from **7a'** and **7b'**, each hydrogel sample at pH 7.0 has been exposed to rheological measurements within the linear viscoelastic region as will be explained in the next section.

VII.4.5. Rheological Studies

Rheological measurements have performed to investigate the mechanical and thermal properties of the supramolecular hydrogels obtained from **7a'** and **7b'**.^{286,565,566} We focused on studying the hydrogel formed at pH 7.0 for determining its utility in biomedical applications. All the oscillation experiments have performed in the LVR (Appendix 4, Figure S7.12). In the OSS experiment at a constant angular frequency ($0.628 \text{ rad. s}^{-1}$) with stain of 1.0%, the plotted data in Figure 7.19 indicates the weak dependence of the storage modulus (G') and the loss modulus (G'') for both hydrogels on the applied stress until the yield stress is reached at which the gel begins to lose its solid-like behavior. The yield stress of hydrogel **7b'** is higher than for **7a'** which gives indication that gel **7b'** possesses more mechanical rigidity than **7a'**.

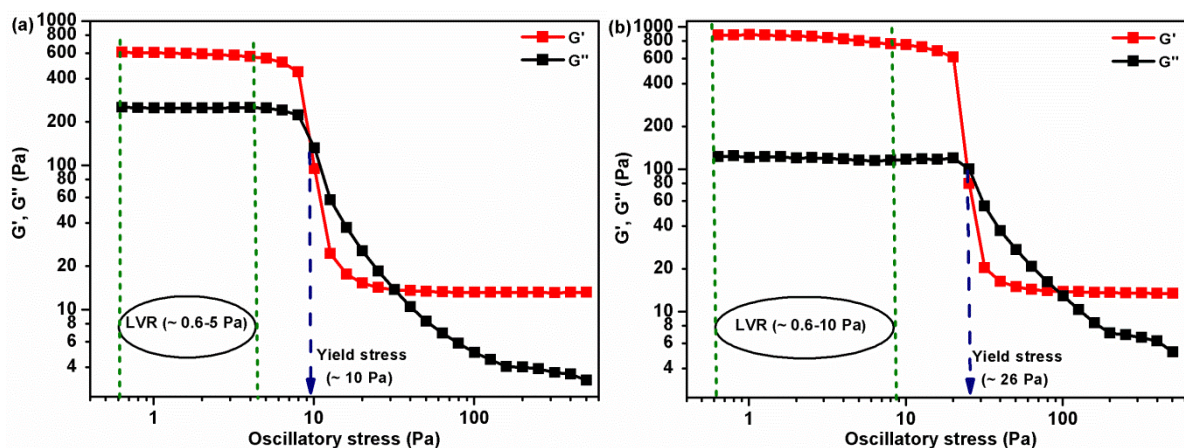


Figure 7.19. Oscillatory stress sweep experiments (OSS) for hydrogels from pH 7.0 of: (a) **7a'**, and (b) **7b'**; ($c = 2.0$ wt%, $\omega = 0.63$ rad. s^{-1} , $T = 25$ °C).

Both hydrogels at pH 7.0 have been subjected to shear stress of 0.6 - 6.25 Pa for 2 minutes to deform the gel, then the recovery of the gel from the deformed state has been studied at 0.01 Pa stress as a function of time (15 minutes) through oscillatory time sweep (OTS) experiment, Figure 7.20. The plotted data show a fast recovery behavior after removing the applied shear stress and gel formation starts immediately ($G' > G''$). Moreover, the gel strength is fully recovered within the time span of 100 seconds for gel **7a'** and 30 seconds for gel **7b'**. These results reflect the high re-healing property after the deformation of both hydrogels.

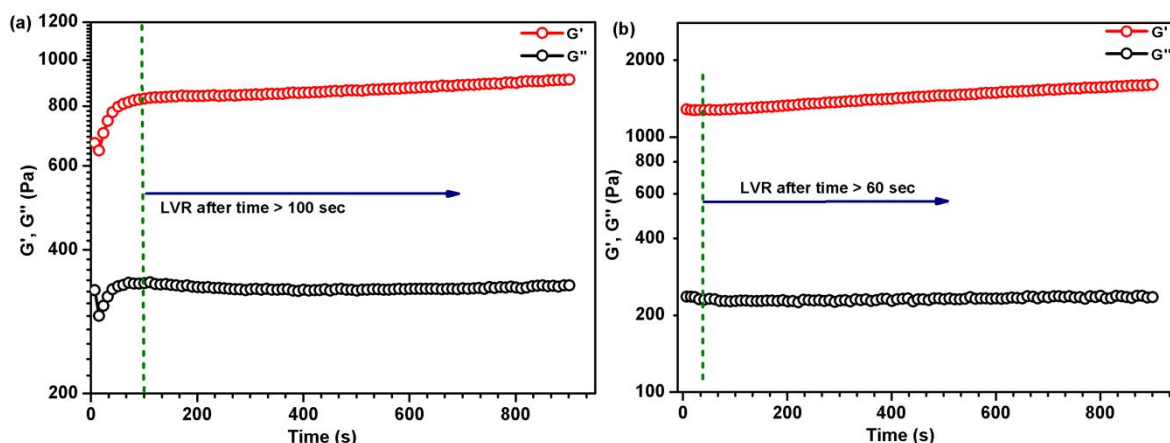


Figure 7.20. Oscillatory time sweep experiments (OTS) for hydrogels from pH 7.0 of: (a) **7a'**, and (b) **7b'**; ($c = 2.0$ wt%, $\omega = 0.63$ rad s^{-1} , $\sigma = 0.01$ Pa, $T = 25$ °C).

It has been reported that in the frequency sweep experiment (OFS) within the LVR, gel materials are characterized by G' greater than G'' ($G' < G''$) while viscous materials exhibit G'' greater than G' ($G'' < G'$).^{362,499,567-572} Regarding our hydrogels, the dynamic moduli (G' and G'') exhibit weak dependence on the applied low frequencies which consistent with entangled network structures.^{413,420} Then the moduli show strong upturns at higher frequencies which may be due to the gel instability resulting from gel thickening by displacing the water from gels (Figure 7.21).^{420,442} Interestingly, we suppose that the two hydrogels from **7a'** and **7b'** at the experimental condition exhibit a solid-like rheological behavior as G' dominating G'' over the investigated oscillating frequency range, Figure 7.21.^{362,499,567-572}

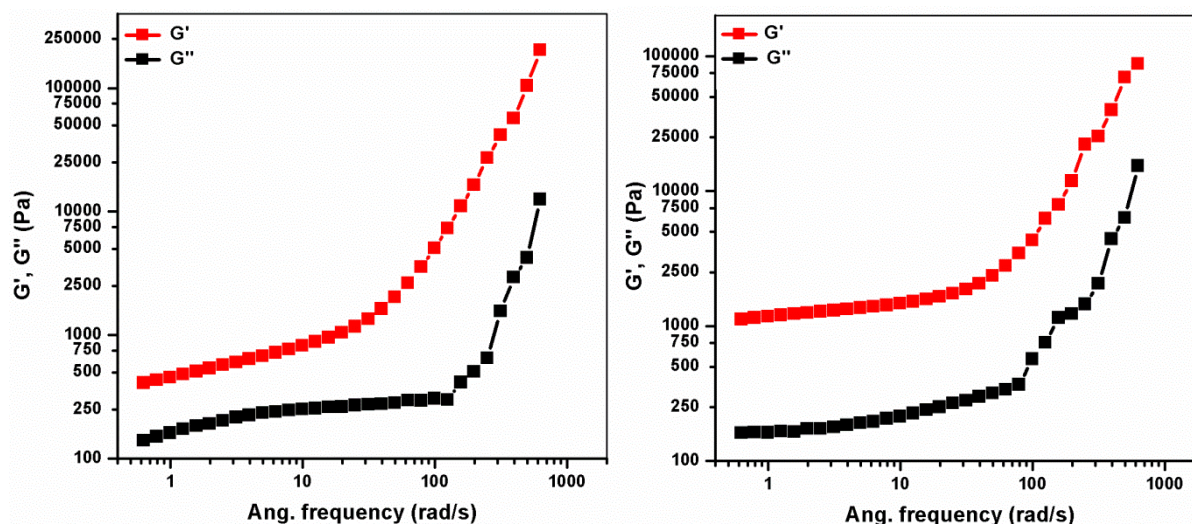


Figure 7.21. Oscillatory frequency sweep experiments (OFS) for hydrogels from pH 7.0 of: (a) **7a'**, and (b) **7b'**; ($c = 2.0$ wt%, $\sigma = 1.5$ Pa, $T = 25$ °C).

Concerning the thermal properties of the gel, as we mentioned before that the temperature at which the gel-to-sol transition occurs, is defined as the gelation temperature (T_g). Gel-to-sol transition takes place due to rupture of non-bonding interactions during the course of heating. In our case, the T_g s of the hydrogels from **7a'** and **7b'** could not be determined by operating the oscillatory temperature sweep experiments for each gel sample from pH 7.0 at concentration of 2.0 wt%, (Appendix 4, Figure S7.13). We suggest that the transition temperatures (T_g s) could not be reached due to the high concentration of the tested hydrogels and the T_g s are higher than the boiling point of the buffer solvent.

VII.4.6. Morphological Studies

In order to have deeply insight into the morphology of hydrogels from **7a'** and **7b'** on a nanoscale level, the freeze-dried hydrogels of **7a'** and **7b'** from pH 7.0 and pH 10.0 were inspected through high-resolution field emission scanning electron microscopy (HRSEM). While the FE-SEM images of the lyophilized gels at pH 7.0 for both gelators reveal that the gels are composed of randomly thin fibrous structure (Figure 7.22a, c), the FE-SEM images of the dried gels at pH 10.0 show interconnected thick fibers of agglomerated fibrils (Figure 7.22b, d).

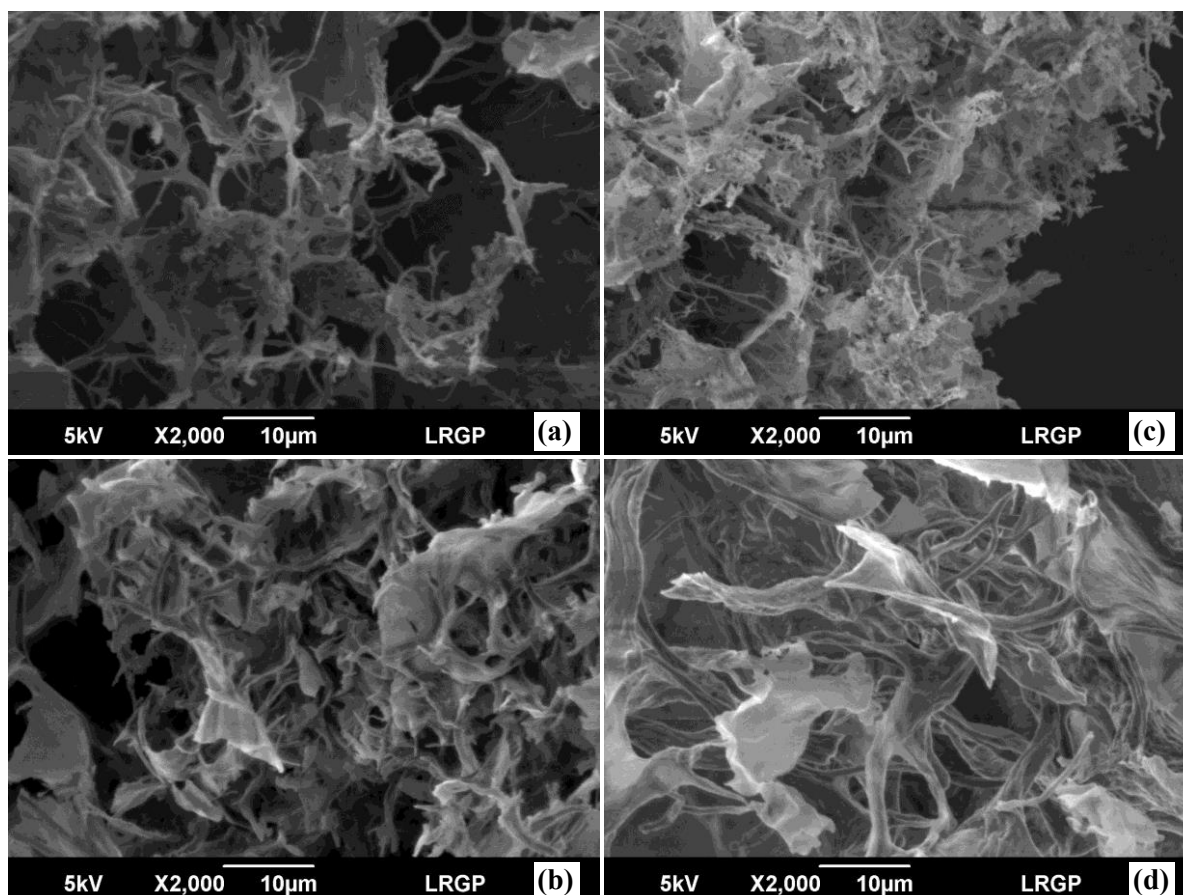


Figure 7.22. SEM images of the dried hydrogels from pH 7.0 (up) and pH 10.0 (bottom) for: (a & c) **7a'** and (b & d) **7b'**.

As seen from the FE-SEM images (Figure 7.22), both hydrogels have not significant difference in the morphology and they reflect fibrous structure. So we assume that gelator molecules of **7a'** and **7b'** self-organize in the same way and they possess almost the same supramolecular arrangement at the two different pH values. Firstly, they form one dimensional fibrils which undergo further organization resulting in the formation of randomly fibrous network structure. This 3D interconnected fibrous networks structure entrap the water molecules within the pores and spaces leading to the formation of hydrogels.⁴²²

These results are consistent with the CD, fluorescence, ATR-FTIR, rheology in which the gelator molecules are self-assemble in β -sheet like structure showing their very close physico-chemical and mechanical behaviors.

VII.5. Conclusions

This work opens the way for a new supramolecular hydrogels based on pseudopeptides and particularly azapeptide family. The study has investigated the synthesis and characterizations of two new Fmoc-*N*-functionalized-2:1-[α /aza]-trimers; Fmoc-FazaFA (**7a'**) and Fmoc-*D*-FazaFA (**7b'**). At the monomeric state in solution, spectroscopic and X-ray techniques demonstrated that both molecules adopt β -turn conformation. At the gel state, all the spectroscopic techniques established the idea that both gelator molecules at the tested pH values have the ability to self-assemble into 3D interconnected supramolecular β -sheet like structure. In addition, the techniques demonstrated that the intermolecular hydrogen bonding and the π -stacking interactions between the aromatic moieties are the main driving forces inducing the self-assembly and hydrogelation phenomena. The phenomenon of the self-assembly has been confirmed from the fibrous structure observed by SEM imaging. Rheological measurements confirmed the solid-like behavior of both hydrogels as G' greater than G'' over the investigated frequencies range. Finally, both hydrogels show similar behaviors pointing out that changing the chirality of the first amino acid from (*S*) in **7a'** to (*R*) in **7b'** has no much effect on the physico-chemical behaviors of the molecules in solution and gel states.

VII.6. Experimental Section

VII.6.1. Materials and Chemicals

Unless otherwise stated, all chemicals and reagents were purchased from commercial suppliers (Sigma-Aldrich, Fluka, Merck or Alfa-Aesar). All reagent-grade solvents were used without further purification as received. Buffer solutions (pH 7.0 = *potassium dihydrogen phosphate/disodium hydrogen phosphate*, pH 10.0 = *borax/sodium hydroxide*) were purchased from Fluka company. Reactions were monitored by thin layer chromatography (TLC) using aluminum-backed silica gel plates. TLC spots were viewed under UV light or/and by heating the plate after treatment with a staining solution of phosphomolybdic acid. Flash chromatography was carried out on silica gel 60 (0.04 - 0.063 μ m Mesh ASTM). All yields were calculated from pure isolated products. Electron spray ionization mass spectra (HRMS-ESI) were recorded with a Bruker MicroTof-Q HR spectrometer in the "Service commun de Spectrométrie de Masse", Faculté des Sciences et Technologies, Vandoeuvre-lès-Nancy, France. All melting points (mp) were uncorrected.

VII.6.2. Synthesis of 2:1-[α /aza]-Trimers

Compounds **7a'** and **7b'** have been synthesized in pure forms and good yields by carrying out three more additional steps on the general strategy that has been reported in our previous studies for the synthesis of 2:1-[α /aza]-oligomers.^{482,509} Fmoc-products **7a'** and **7b'** were obtained from the corresponding Boc-products in three consecutive steps⁵¹⁰:

General methyl ester deprotection procedure: To a solution of methyl ester-protected trimers (Boc-FazaFAOMe or Boc-*D*-FazaFAOMe) (1.0 equiv., 2.0 mmol.) in CH₃CN (10.0 mL), a solution of 1M NaOH (2.0 equiv., 4.0 mmol.) was added at 0 °C. The mixture was vigorously stirred for 6 - 10h at room temperature until reaction completion (as monitored by TLC). The aqueous phase was cooled to 0 °C and acidified with 2M HCl to pH 2 and extracted with CH₂Cl₂ (3 \times 10.0 mL). The combined organic layers were dried over MgSO₄, filtered, and evaporated in vacuum to give the corresponding carboxylic acid in quantitative yield which was used in the next step without further purification.

General Boc-deprotection procedure: To the Boc-protected compounds obtained from the previous step (1.0 equiv., 2.0 mmol.), EtOAc/3M HCl (10.0 equiv., 20.0 mmol.) was added. The mixture was stirred about 3 - 5 h at room temperature until reaction completion without any control by TLC. The

solution was concentrated under vacuum, and the excess of HCl was co-evaporated with DCM (4 times), affording the corresponding hydrochloride salt compounds as white solids in quantitative yields.

Synthesis of Fmoc-N-functionalized-2:1-[α /aza]-Trimers: The crude residue (deprotected trimer) from last step (1.0 equiv., 2.0 mmol.) was dissolved in 5.0 mL H₂O with the help of DIPEA (1.0 equiv., 2.0 mmol.). To this mixture a solution of re-crystallized^a Fmoc-OSu (Appendix 4, Note 1) in 5.0 mL ACN (0.95 equiv., 1.9 mmol.) was added one portion. The pH of the reaction mixture drops due to the liberation of the free *N*-hydroxy-succinimide, so the pH of the mixture should maintain at pH 8.5 - 9.0 by controlled addition of DIPEA. The reaction was stirred overnight for completion monitoring by TLC (20% EtOH : 80% DCM). The solution was concentrated, poured into 30.0 mL of 1.5M HCl in a separatory funnel, and then the product was extracted by ethyl acetate (10.0 mL x 3 times). The organic layer was washed with water, saturated NaCl, dried over MgSO₄, and then the solvent was evaporated under vacuum and the resulting product was crystallized from hexane yielding the corresponding Fmoc-product (**7a'** or **7b'**) as a white solid^b (Appendix 4, Note 2).

VII.6.3. Characteristic Properties of products **7a'** and **7b'**

Homochiral Trimer [Fmoc-Phe-azaPhe-Ala-OH or Fmoc-FazaFA] (7a'): Compound **7a'** was isolated as white powder (925 mg, yield 76%) after flash chromatography (0.04 – 0.063 μ m) using (20% EtOH : 80% CH₂Cl₂) as eluent. Characterization data: m.p. 196 - 197 °C. ¹H NMR (300 MHz, DMSO-*d*₆, 4.0 mmol. L⁻¹) δ _H 1.17 and 1.20 (d, 3H, CH₃), 2.85 and 2.87 (d, 2H, CH₂), 3.99 - 4.02 (m, 1H, C ^{α} H), 4.11 - 4.13 (br s, 1H, C ^{α} H), 4.14 - 4.26 (s, 3H: 1H, CH and 2H, CH₂), 4.27 and 4.69 (br s, 2H, NCH₂), 6.38 and 6.40 (d, 1H, NH), 7.07 – 7.90 (m, 19H: 18 H arom, and 1 H, NH), 10.36 (s, 1H, NH), 12.29 (br s, 1H, OH). ¹³C NMR (75 MHz, DMSO-*d*₆, 8.0 mmol. L⁻¹) δ _C 17.53 (CH₃), 36.29 (CH₂), 46.53 (CH), 48.92 (C ^{α} H), 51.01 (NCH₂), 54.53 (C ^{α} H), 65.67 (OCH₂), 120.07 (CH arom fluorenyl), 125.10, 126.16, 126.40, 126.89, 127.04, 127.24, 127.60, 128.00, 128.10, 128.87, and 129.18 (CH arom Ph), 137.75 and 143.62 (C arom fluorenyl), 137.10 and 140.63 (C arom Ph), 156.21 (O=C-NH, fluorenyl), 156.53 (HN-N-C=O), 170.96 (O=C-NH), 174.49 (O=C-OH). IR (CDCl₃) $\tilde{\nu}$ _{max} = 3331 cm⁻¹, 3369 cm⁻¹, 3435 cm⁻¹ (NH), 1642 cm⁻¹, 1653 cm⁻¹, 1672 cm⁻¹, 1685 cm⁻¹, 1715 cm⁻¹, 1736 cm⁻¹, 1759 cm⁻¹ (C=O). HRMS (ESI) (m/z) for [C₃₅H₃₄N₄O₆Na]: calculated 629.2376; found, 629.2398 [M+Na]⁺.

Heterochiral Trimer [Fmoc-D-Phe-azaPhe-Ala-OH or Fmoc-D-FazaFA] (7b'): Compound **7b'** was isolated as white powder (900 mg, yield 74%) after flash chromatography (0.04 – 0.063 μ m) using (20% EtOH : 80% CH₂Cl₂) as eluent. Characterization data: m.p. 176 - 177 °C; ¹H NMR (300 MHz, DMSO-*d*₆, 4.0 mmol. L⁻¹) δ _H 1.26 and 1.28 (d, 3H, CH₃), 2.80 - 2.96 (dd, 2H, CH₂), 3.92 - 3.99 (m, 1H, C ^{α} H), 4.11 - 4.14 (br s, 1H, C ^{α} H), 4.14 - 4.21 (s, 3H: 1H, CH and 2H, CH₂), 4.23 and 4.43 (br s, 2H, NCH₂), 6.55 and 6.58 (d, 1H, NH), 7.14 - 7.89 (m, 19H: 18 H arom, and 1 H, NH), 10.25 (s, 1H, NH), 12.28 (br s, 1H, OH). ¹³C NMR (75 MHz, DMSO-*d*₆, 8.0 mmol. L⁻¹) δ _C 18.24 (CH₃), 36.51 (CH₂), 46.50 (CH), 49.29 (C ^{α} H), 50.79 (NCH₂), 54.69 (C ^{α} H), 65.77 (OCH₂), 120.07 (CH arom fluorenyl), 125.23, 126.36, 126.94, 127.04, 127.61, 128.08, 128.15 and 129.21 (CH arom Ph), 140.65 and 143.82 (C arom fluorenyl), 137.86 and 143.63 (C arom Ph), 156.15 (O=C-NH, fluorenyl), 156.60 (HN-N-C=O), 170.82 (O=C-NH), 174.68 (O=C-OH). IR (CDCl₃) $\tilde{\nu}$ _{max} = 3275 cm⁻¹, 3349 cm⁻¹, 3368 cm⁻¹, 3432 cm⁻¹ (NH), 1644 cm⁻¹, 1657 cm⁻¹, 1672 cm⁻¹, 1686 cm⁻¹, 1714 cm⁻¹, 1730 cm⁻¹, 1761 cm⁻¹ (C=O). HRMS (ESI) (m/z) for [C₃₅H₃₄N₄O₆Na]: calculated 629.2376; found, 629.2384 [M+Na]⁺.

VII.6.4. NMR and FTIR Spectroscopic Studies

¹H and ¹³C NMR spectra were recorded using a Bruker Avance NMR spectrophotometer (300 MHz) in DMSO-*d*₆ as solvent at room temperature with chemical shift of 2.50 ppm. The

Part B

Chapter VII. Supramolecular Hydro-Gels Based on 2:1-[α /aza]-Trimers

chemical shifts were reported in ppm (δ) relative to tetramethylsilane (TMS) served as an internal standard ($\delta = 0$ ppm) for ^1H NMR, while DMSO- d_6 ($\delta = 39.5$ ppm) was used as an internal standard for ^{13}C NMR. Multiplicities are reported as follows: s = singlet, d = doublet, q = quartet, m = multiplet, br = broad, arom = aromatic.

FTIR spectra of **7a'** and **7b'** in diluted condition of CDCl_3 were recorded with Bruker Tensor 27 over 128 scans and referenced to the residual solvent resonances. In addition, attenuated total reflectance (ATR-FTIR) measurements have been performed on solids and lyophilized hydrogel samples for **7a'** and **7b'** prepared from buffer solutions pH 7.0 and pH 10.0. All the spectra were recorded on Bruker Tensor 27 spectrometer equipped with a trough plate comprising of a germanium single crystal where the samples were loaded over it. Spectra were acquired in the $400 - 4000\text{ cm}^{-1}$ range with a resolution of 4.0 cm^{-1} over 128 scans, taken into consideration the background subtraction from each spectra to correct for atmospheric interference.

VII.6.5. Molecular Dynamic Calculations (AMBER 12)

Calculations on molecules **7a'** and **7b'** were carried out according to the protocol: $0.5\mu\text{s}$ with 2fs steps molecular dynamics simulations were calculated in explicit solvent (dimethyl sulfoxide; DMSO box) without any ROE constraints under constant pressure periodic boundary conditions, pressure relaxation time of $0.5\mu\text{s}$, and constant temperature 300 K, using the package of molecular dynamics simulation programs AMBER 12. The starting molecules were constructed using MarvinSketch (ChemAxon), Antechamber and Xleap from AMBER program suite. Molecular dynamic simulations were done with Sander program with general AMBER force field (GAFF) and included amino acid parameters (ff99SB). Ptraj was employed for the analysis of 25,000 structures in order to assess the possibility of a hydrogen bond formation and the predicted conformation in solution.^{521,522}

VII.6.6. Hydrogels Preparation and Minimum Gelation Concentrations (MGCs)

Stock solutions of **7a'** and **7b'** were prepared by dissolving 100 mg of **7a'** or **7b'** in 0.6 g ethanol supported by gentle heating. (x) mg of this stock solution was transferred into a sealed glass tube and then diluted by buffer solution to a final calculated weight of (y) g to get the desired final concentration. The mixtures were mixed well by hand shake until obtaining homogenous solutions and then the tubes were maintained at room temperature gave rise to the formation of the corresponding transparent hydrogels. In order to determine the MGC, series of concentrations with the range (0.1 - 2.0 wt%) for each gelator (**7a'** & **7b'**) were prepared in the two tested buffer solutions. The tubes were kept to allow gelation at room temperature. The MGC for each hydrogelator in certain buffer was considered as the concentration that below it, no gelation occurs.⁴⁷⁶

VII.6.7. Circular Dichroism Spectroscopic studies

The CD spectra of viscous solutions and gels (at MGCs) for **7a'** and **7b'** from phosphate buffer (pH 7.0) were monitored on Chirascan-plus qCD spectrometer equipped with a temperature control and reported in molar ellipticity [θ]; spectra were recorded from 180 to 350 nm at $25\text{ }^\circ\text{C}$. Samples were loaded into a 0.1 mm path length quartz cover slip cuvette and spectra were measured at 50 nm min^{-1} with a 1.0 nm step size and a 1.0 nm bandwidth, taking two averages.

VII.6.8. UV-visible Absorption and Fluorescence Emission Spectroscopic studies

Absorption spectra were recorded on a UV-3600, UV-visible double beam spectrophotometer (SHIMADZU, MARNE LA VALLEE, France). Fluorescence spectra were recorded on a Fluorolog

FL3-222 spectrofluorimeter (HORIBA Jobin Yvon, LONGJUMEAU, France) equipped with 450 W Xenon lamp, a thermo-stated cell compartment (25°C), a UV-visible photomultiplier R928 (HAMAMATSU Japan). Excitation beam is diffracted by a double ruled grating SPEX monochromator (1200 grooves/mm blazed at 330 nm). Emission beam is diffracted by a double ruled grating SPEX monochromator (1200 grooves/mm blazed at 500 nm). All spectra were measured in 4 faces 1.0 cm path-length quartz cuvettes. In UV-absorption measurements, the reference cell was filled with phosphate buffer solution pH 7.0 to auto-zero the solvent effect in each measurement from the peptide solutions of Fmoc-FazaFA (**7a'**) and Fmoc-*D*-FazaFA (**7b'**). The absorption spectra for a series of concentrations for both hydrogelators (pH 7.0) were recorded in the UV-visible range 200 - 600 nm. The fluorescence emission spectra were measured for a series of concentrations from 1.0 wt% (gel state) to 0.025wt% (viscous state) for both hydrogelators (**7a'** and **7b'**) in phosphate buffer solution (pH 7.0) by excitation at 265 nm (slit width of 2.0 nm), and the emission spectra were recorded within the range 250 - 600 nm.

VII.6.9. Rheological Measurements

All hydrogels of Fmoc-FazaFA (**7a'**) and Fmoc-*D*-FazaFA (**7b'**) were prepared directly in 7 mL glass tubes and left overnight (~ 12 h) at room temperature to obtain a stable gels before the measurements.^{418,573} All rheological experiments were performed on Advanced Rheometer-AR2000 (TA instruments) operating in oscillatory mode with a 20 mm parallel plate geometry with serrated surfaces to prevent sliding due to the liquid film expelled by samples (diameter gap was adjusted to 1000 μm).²⁸ To keep the sample hydrated by minimizing the solvent evaporation, a solvent trap was used and the atmosphere within the sample chamber was saturated with water.^{413,425} In order to determine the linear viscoelastic region (LVR) at which the oscillatory experiments were operated, each gel sample (2.0 wt%, pH 7.0) was subjected to an oscillatory stress sweep experiments (OSS); (G' and G'' were measured as a function of oscillatory stress ($\sigma = 0.6 - 505 \text{ Pa}$) at a constant angular frequency of $\omega = 0.628 \text{ rad. s}^{-1}$).^{425,496,497} Then a dynamic oscillatory time sweep (OTS) was performed for 15 minutes with an angular frequency of $\omega = 0.628 \text{ rad. s}^{-1}$, and applied stress of $\sigma = 1.5 \text{ Pa}$ chosen within the LVR from the OSS.⁵⁰⁸ After that, each sample was subjected to an oscillatory frequency sweep experiment (OFS) over a range of frequencies ($\omega = 0.1 - 628.3 \text{ rad. s}^{-1}$) and applied stress of $\sigma = 1.5 \text{ Pa}$ obtained from OSS step at 20 °C.^{413,508} Finally, in order to determine the gel-to-sol transition temperature (T_g), G' and G'' for each gel sample (2.0 wt%) were studied over heating program ($T = 20 - 110 \text{ }^\circ\text{C}$ at a rate of $5^\circ/\text{min}$) sufficient for melting the gel to solution through oscillatory temperature sweep experiment, from which T_g can be determined at the cross point between the G' and G'' curves.^{418,507} Repeat measurements on fresh samples (three times) were also carried out to ensure reproducibility between samples.

VII.6.10. Morphological Studies

Lyophilized dried gel samples were obtained after the freeze-drying of hydrogels from **7a'** and **7b'** prepared from buffer solutions (pH 7.0 and pH 10.0). The dried gels from **7a'** and **7b'** have been inspected at the nanoscale level using high-resolution field emission scanning electron microscopy (HRSEM) (JEOL JSM-6490LV, France, high vacuum, acceleration voltage of 5 kV, large field detector) after treatment by gold coating.

Part B
Bibliographies

Part B

Bibliographies

Bibliographies

- (1) Reddy, S. M. M.; Shanmugam, G.; Duraipandy, N.; Kiran, M. S.; Mandal, A. B. *Soft Matter* **2015**, *11*, 8126-8140.
- (2) Terech, P.; Weiss, R. G. *Chem. Rev.* **1997**, *97*, 3133-3159.
- (3) Estroff, L. A.; Hamilton, A. D. *Chem. Rev.* **2004**, *104*, 1201-1217.
- (4) Adams, D. J. *Macromol. Biosci.* **2011**, *11*, 160-173.
- (5) Adhikari, B.; Palui, G.; Banerjee, A. *Soft Matter* **2009**, *5*, 3452-3460.
- (6) Ryan, D. M.; Anderson, S. B.; Senguen, F. T.; Youngman, R. E.; Nilsson, B. L. *Soft Matter* **2010**, *6*, 475-479.
- (7) Fleming, S.; Debnath, S.; Frederix, P. W. J. M.; Tuttle, T.; Ulijn, R. V. *Chem. Commun.* **2013**, *49*, 10587-10589.
- (8) Briseno, A. L.; Holcombe, T. W.; Boukai, A. I.; Garnett, E. C.; Shelton, S. W.; Frchet, J. J. M.; Yang, P. *Nano Lett.* **2010**, *10*, 334-340.
- (9) Gunes, S.; Neugebauer, H.; Sariciftci, N. S. *Chem. Rev.* **2007**, *107*, 1324-1338.
- (10) Murphy, R. J.; Frchet, M. *Chem. Rev.* **2007**, *107*, 1066-1096.
- (11) Briseno, L.; Mannsfeld, S. C.; Formo, E.; Xiong, Y.; Lu, X.; Bao, Z.; Jenekhe, S. A.; Xia, Y. *Mater. Chem.* **2008**, *18*, 5395-5398.
- (12) Kim, J. H.; Jung, Y.; Chung, J. W.; An, B. K.; Park, S. Y. *Small* **2009**, *5*, 804-807.
- (13) Kumar, R.; Katare, O. P. *AAPS Pharm. Sci. Tech.* **2005**, *6*, E298-E310.
- (14) Boekhoven, J.; Koot, M.; Wezendonk, T. A.; Eelkema, R.; van Esch, J. H. *J. Am. Chem. Soc.* **2012**, *134*, 12908-12911.
- (15) Kar, T.; Mukherjee, S.; Das, P. K. *New J. Chem.* **2014**, *38*, 1158-1167.
- (16) Banerjee, S.; Das, R. K.; Maitra, U. *J. Mater. Chem.* **2009**, *19*, 6649-6687.
- (17) Das, D.; Kar, T.; Das, P. K. *Soft Matter* **2012**, *8*, 2348-2365.
- (18) Ajayaghosh, A.; Praveen, V. K.; Vijayakumar, C. *Chem. Soc. Rev.* **2008**, *37*, 109-122.
- (19) Bernet, A.; Behr, M.; Schmidt, H.-W. *Soft Matter* **2012**, *8*, 4873-4876.
- (20) Xue, P.; Xu, Q.; Gong, P.; Qian, C.; Zhang, Z.; Jia, J.; Zhao, X.; Lu, R.; Ren, A.; Zhang, T. *RSC Adv.* **2013**, *3*, 26403-26411.
- (21) Sun, Z.; Li, Z.; He, Y.; Shen, R.; Deng, L.; Yang, M.; Liang, Y.; Zhang, Y. *J. Am. Chem. Soc.* **2013**, *135*, 13379-13386.
- (22) van Esch, J. H. *Langmuir* **2009**, *25*, 8392-8394.
- (23) Hughes, M.; Birchall, L. S.; Zuberi, K.; Aitkin, L. A.; Debnath, S.; Javid, N.; Ulijn, R. V. *Soft Matter* **2012**, *8*, 11565-11574.
- (24) Li, X.; Kuang, Y.; Xu, B. *Soft Matter* **2012**, *8*, 2801-2806.
- (25) Chakrabarti, A.; Maitra, U.; Devi Das, A. *J. Mater. Chem.* **2012**, *22*, 18268-18274.
- (26) Samanta, S. K.; Subrahmanyam, K. S.; Bhattacharya, S.; Rao, C. N. R. *Chem.-Eur. J.* **2012**, *18*, 2890-2901.
- (27) Banerjee, S.; Das, R. K.; Terech, P.; de Geyer, A.; Aymonier, C.; Serani, A. L.; Raffy, G.; Maitra, U.; Guerzon, A. D.; Desvergne, J.-P. *J. Mater. Chem. C* **2013**, *1*, 3305-3316.
- (28) Terech, P.; Pasquier, D.; Bordas, V.; Rossat, C. *Langmuir* **2000**, *16*, 4485-4494.
- (29) Allix, F.; Curcio, P.; Quoc, N. P.; Pickaert, G.; Jamart-Gregoire, B. *Langmuir* **2010**, *26*, 16818-16827.
- (30) Moussodia, R. O.; Acherar, S.; Romero, E.; Didierjean, C.; Jamart-Gregoire, B. *J. Org. Chem.* **2015**, *80*, 3022-3029.
- (31) Hanabusa, K.; Matsumoto, M.; Kimura, M.; Kakehi, A.; Shirai, H. *J. Colloid Interface Sci.* **2000**, *224*, 231-244.
- (32) Abdallah, D. J.; Weiss, R. G. *Langmuir* **2000**, *16*, 352-355.
- (33) Nguyen, M. K.; Lee, D. S. *Chem. Commun.* **2010**, *46*, 3583-3585.
- (34) Palui, G.; Nanda, J.; Banerjee, A. *Chem.-Eur. J.* **2009**, *15*, 6902-6909.
- (35) Kim, J.-H.; Lee, T. R. *Chem. Mater.* **2004**, *16*, 3647-3651.
- (36) Naskar, J.; Palui, G.; Banerjee, A. *J. Phys. Chem. B* **2009**, *113*, 11787-11792.
- (37) Chang, C.-H.; Lin, Y.-H.; Yeh, C.-L.; Chen, Y.-C.; Chiou, S.-F.; Has, Y.-M.; Chen, Y.-S.; Wang, C.-C. *Biomacromolecules* **2010**, *11*, 133-142.
- (38) Chen, Q.; Lv, Y.; Zhang, D.; Zhang, G.; Liu, C.; Zhu, D. *Langmuir* **2010**, *26*, 3165-3168.

Part B

Bibliographies

- (39) Fujita, N.; Sakamoto, Y.; Shirakawa, M.; Ojima, M.; Fujii, A.; Ozaki, M.; Shinkai, S. *J. Am. Chem. Soc.* **2007**, *129*, 4134-4152.
- (40) Xue, P. C.; Lu, R.; Chen, G. J.; Zhang, Y.; Nomoto, H.; Takafuji, M.; Ihara, H. *Chem.-Eur. J.* **2007**, *13*, 8231-8239.
- (41) de Jong, J. J. D.; Lucas, L. N.; Kellogg, R. M.; van Esch, J. H.; Feringa, B. L. *Science* **2004**, *304*, 278-281.
- (42) Bardelang, D. *Soft Matter* **2009**, *5*, 1969-1971.
- (43) Cravotto, G.; Cintas, P. *Chem. Soc. Rev.* **2009**, *38*, 2684-2697.
- (44) Hui, J. K. H.; Yu, Z.; Mirfakhrai, T.; MacLachlan, M. J. *Chem.-Eur. J.* **2009**, *15*, 13456-13465.
- (45) Lloyd, G. O.; Steed, J. W. *Nat. Chem. Biol.* **2009**, *5*, 437-442.
- (46) Yang, Z.; Liang, G.; Wang, L.; Xu, B. *J. Am. Chem. Soc.* **2006**, *128*, 3038-3043.
- (47) Zhao, F.; Ma, M. L.; Xu, B. *Chem. Soc. Rev.* **2009**, *38*, 883-891.
- (48) Zinic, M.; Vogtle, F.; Fages, F.: Low Molecular Mass Gelators: Design, Self-Assembly, Function. Fages, F., Ed.; Topics in Current Chemistry, **2005**; Vol. 256.
- (49) Weiss, R. G.; Terech, P. Molecular Gels: Materials with Self-Assembled Fibrillar Networks. *Springer* **2006**.
- (50) Sangeetha, N. M.; Maitra, U. *Chem. Soc. Rev.* **2005**, *34*, 821-836.
- (51) Piepenbrock, M. O. M.; Lloyd, G. O.; Clarke, N.; Steed, J. W. *Chem. Rev.* **2010**, *110*, 1960-2004.
- (52) Du, X. W.; Zhou, J.; Shi, J. F.; Xu, B. *Chem. Rev.* **2015**, *115*, 13165-13307.
- (53) von Lipowitz, A.; Liebig, P. *Ann. Chem. Pharm.* **1841**, *38*, 348-355.
- (54) Graham, T. *Phil. Trans. Roy. Soc.* **1861**, *151*, 183-224.
- (55) Lloyd, D. J.: The problem of gel structure. In *Colloid Chemistry*; Alexander, J., Ed.: The Chemical Catalogue Company, New York, U. S. A., **1926**; pp 767-782.
- (56) Dean, R. B. *Modern Colloids* **1948**, New York: D. Van Nostrand Co., p. 2.
- (57) Hermans, P. H.: In *Colloid Science, Chapter XII*; Kruyt, H. R., Ed.: Amsterdam: Elsevier, **1949**; Vol. 2; pp p. 484.
- (58) Ferry, J. D. Viscoelastic Properties of Polymers. *New York: Wiley* **1961**, p. 391.
- (59) Bachl, J.; Oehm, S.; Mayr, J.; Cativiela, C.; Marrero-Tellado, J. J.; Diaz, D. D. *Int. J. Mol. Sci.* **2015**, *16*, 11766-11784.
- (60) Bairi, P.; Roy, B.; Routh, P.; Sen, K.; Nandi, A. K. *Soft Matter* **2012**, *8*, 7436-7445.
- (61) Erdogan, H.; Sakalak, H.; Yavuz, M. S.; Demirel, G. *Langmuir* **2013**, *29*, 6975-6982.
- (62) Schmidt, R. H. *J. Am. Chem. Soc.* **1981**, 131-146.
- (63) Yu, S. L.; Dou, X. Q.; Qu, D. H.; Feng, C. L. *J. Mol. Liq.* **2014**, *190*, 94-98.
- (64) Zweep, N.; Hopkinson, A.; Meetsma, A.; Browne, W. R.; Feringa, B. L.; van Esch, J. H. *Langmuir* **2009**, *25*, 8802-8809.
- (65) Osada, Y.; Kajiwara, K., (Ed.); Fushimi, T.; Hirasa, O.; Hirokawa, Y.; Matsunaga, T.; Shimomura, T.; Wang, L., (Assoc. Ed.); Ishida, H., (Translator): Gels hand book. Academic Press, San Diego, **2001**; Vol. 1-3.
- (66) Mukhopadhyay, S.; Maitra, U. *Curr. Sci.* **2004**, *87*, 1666-1683.
- (67) Clark, A. H.: Gels and gelling. In *Physical Chemistry of Foods*; Schwartzberg, H. G., Hartel, R. W., Eds.: New York: Marcel Dekker, **1996**; pp 263-305.
- (68) Smith, D. K.; Atwood, J. L.; Steed, J. W. E. In *Organic Nanostructures, Wiley-VCH: Weinheim, Germany* **2008**, 111-154.
- (69) Feng, G. L.; Chen, H. H.; Cai, J. H.; Wen, J. W.; Liu, X. B. *Soft Mater.* **2014**, *12*, 403-410.
- (70) Placin, F.; Desvergne, J.-P.; Cansell, F. *J. Mater. Chem.* **2000**, *10*, 2147-2149.
- (71) Nakayama, M.; Okano, T.; Miyazaki, T.; Kohori, F.; Sakai, K.; Yokoyama, M. *J. Control Rel.* **2006** *115*, 46-56.
- (72) Gil, E. S.; Hudson, S. M. *Prog. Polym. Sci.* **2004**, *29*, 1173-1222.
- (73) Terech, P.; Rossat, C.; Volino, F. *J. Colloid Interface Sci.* **2000**, *227*, 363-370.
- (74) Tanaka, T. *Phys Rev A: Atomic Mol. Opt. Phys.* **1978**, *17*, 763-766.
- (75) Ajithkumar, S.; Patel, N. K.; Kansara, S. S. *Eur. Polym. J.* **2000**, *36*, 2387-2393.
- (76) Wang, C. S.; Wei, W.; Li, Z. Y.; Wang, X. H.; Shen, H.; Sui, Z. T. *Russ. J. Phys. Chem. A* **2012**, *86*, 45-49.
-

Part B

Bibliographies

- (77) Kleinsmann, A. J.; Nachtsheim, B. J. *Chem. Commun.* **2013**, *49*, 7818-7820.
- (78) Burke, S. E.; Barrett, C. J. *Biomacromolecules* **2003**, *4*, 1773-1783.
- (79) Benns, J. M.; Choi, J. S.; Mahato, R. I.; Park, J. S.; Kim, S. W. *Bioconjugate Chem.* **2000**, *11*, 637-645.
- (80) Park, J. S.; Han, T. H.; Lee, K. Y.; Han, S. S.; Hwang, J. J.; Moon, D. H.; al., e. *J. Control Release* **2006**, *115*, 37-45.
- (81) Grigoriou, S.; Johnson, E. K.; Chen, L.; Adams, D. J.; James, T. D.; Cameron, P. J. *Soft Matter* **2012**, *8*, 6788-6791.
- (82) Marchesan, S.; Waddington, L.; Easton, C. D.; Winkler, D. A.; Goodall, L.; Forsythe, J.; Hartley, P. G. *Nanoscale* **2012**, *4*, 6752-6760.
- (83) Nanda, J.; Banerjee, A. *Soft Matter* **2012**, *8*, 3380-3386.
- (84) Nonoyama, T.; Ogasawara, H.; Tanaka, M.; Higuchi, M.; Kinoshita, T. *Soft Matter* **2012**, *8*, 11531-11536.
- (85) Imura, Y.; Matsue, K.; Sugimoto, H.; Ito, R.; Kondo, T.; Kawai, T. *Chem. Lett.* **2009**, *38*, 778-779.
- (86) Liu, Y. F.; Yang, Y. L.; Wang, C.; Zhao, X. J. *Nanoscale* **2013**, *5*, 6413-6421.
- (87) Sershen, S.; West, J. *Adv. Drug. Deliv. Rev.* **2002**, *54*, 1225-1235.
- (88) Mathiowitz, E.; Cohen, M. D. *J. Membr. Sci.* **1989**, *40*, 1-26.
- (89) Xie, Z. G.; Zhang, A. Y.; Ye, L.; Feng, Z. G. *Soft Matter* **2009**, *5*, 1474-1482.
- (90) Pan, S. F.; Luo, S.; Li, S.; Lai, Y. S.; Geng, Y. Y.; He, B.; Gu, Z. W. *Chem. Commun.* **2013**, *49*, 8045-8047.
- (91) Roy, D.; Camber, J. N.; Sumerlin, B. S. *Prog. Polym. Sci.* **2010**, *35*, 278-301.
- (92) Lambeth, R. H.; Moore, J. S. *Macromolecules* **2007**, *40*, 1838-1842.
- (93) West, J. L.; Hubbell, J. A. *Proc. Natl. Acad. Sci. U.S.A.* **1996**, *93*, 13188-13193.
- (94) Elisseeff, J.; McIntosh, W.; Anseth, K.; Riley, S.; Ragan, P.; Langer, R. *J. Biomed. Mater. Res.* **2000**, *51*, 164-171.
- (95) van der Veen, G.; Prins, W. *Nature* **1971**, *230*, 70-72.
- (96) Irie, M.; Hirano, Y.; Hashimoto, S.; Hayashi, K. *Macromolecules* **1981**, *14*, 262-267.
- (97) Irie, M.; Menju, A.; Hayashi, K. *Macromolecules* **1979**, *12*, 1176-1180.
- (98) Irie, M.; Hayashi, K.; Menju, A. *Polym. Photochem.* **1981**, *1*, 233-242.
- (99) Ding, Y.; Li, Y.; Qin, M.; Cao, Y.; Wang, W. *Langmuir* **2013**, *29*, 13299-13306.
- (100) Poolman, J. M.; Boekhoven, J.; Besselink, A.; Olive, A. G. L.; van Esch, J. H.; Eelkema, R. *Nat. Protoc.* **2014**, *9*, 977-988.
- (101) Boekhoven, J.; Poolman, J. M.; Maity, C.; Li, F.; van der Mee, L.; Minkenberg, C. B.; Mendes, E.; van Esch, J. H.; Eelkema, R. *Nat. Chem.* **2013**, *5*, 433-437.
- (102) Yang, Z. M.; Gu, H. W.; Fu, D. G.; Gao, P.; Lam, J. K.; Xu, B. *Adv. Mater.* **2004**, *16*, 1440-1444.
- (103) Gao, Y.; Au-Yeung, S. C. F.; Wu, C. *Macromolecules* **1999**, *32*, 3674-3677.
- (104) Pich, A.; Bhattacharya, S.; Lu, Y.; Boyko, V.; Adler, H.-J. P. *Langmuir* **2004**, *20*, 10706-10711.
- (105) Qiu, Y.; Park, K. *Adv. Drug. Deliv. Rev.* **2001**, *53*, 321-339.
- (106) Shiga, T. *Adv. Polym. Sci.* **1997**, *134*, 131-163.
- (107) Osada, Y.; Okuzaki, H.; Hori, H. *Nature* **1992**, *355*, 242-244.
- (108) Shiga, T.; Yoshiharu Hirose, Y.; Okada, A.; Kurauchi, T. *J. Appl. Polym. Sci.* **1993**, *47*, 113-119.
- (109) Hench, L. L.; West, J. K. *Chem. Rev.* **1990**, *90*, 33-72.
- (110) Suzuki, M.; Hanabusa, K. *Chem. Soc. Rev.* **2010**, *39*, 455-463.
- (111) Nikiforidis, C. V.; Gilbert, E. P.; Scholten, E. *RSC Adv.* **2015**, *5*, 47466-47475.
- (112) Dastida, P. *Chem. Soc. Rev.* **2008**, *37*, 2699-2715.
- (113) van Oss, C. J.; Absolom, D. R.; Neumann, A. W. *Colloids Surf.* **1980**, *1*, 45-56.
- (114) Paulini, R.; Müller, K.; Diederich, F. *Angew. Chem., Int. Ed.* **2005**, *44*, 1788-1805.
- (115) Ma, J. C.; Dougherty, D. A. *Chem. Rev.* **1997**, *97*, 1303-1324.
- (116) Hoeben, F. J. M.; Jonkheijm, P.; Meijer, E. W.; Schenning, A. P. H. *Chem. Rev.* **2005**, *105*, 1491-1546.
- (117) Hunter, C. A.; Sanders, J. K. M. *J. Am. Chem. Soc.* **1990**, *112*, 5525-5534.

Part B

Bibliographies

- (118) Jeffrey, G. A.: Review of hydrogen bonding: An Introduction to Hydrogen Bonding. New York, Oxford University Press, **1997**.
- (119) Chung, Y. I.; Lee, S. Y.; Tae, G. *Colloids Surf. A* **2006**, 480–484.
- (120) Kurisawa, M.; Chung, J. E.; Yang, Y. Y.; Gao, S. J.; Uyama, H. *Chem. Commun.* **2005**, 94, 4312–4314.
- (121) Estroff, L. A.; Hamilton, A. D. *Angew. Chem., Int. Ed. Engl.* **2000**, 39, 3447-3450.
- (122) Shimizu, T.; Masuda, M. *J. Am. Chem. Soc.* **1997**, 119, 2812-2818.
- (123) Iwaura, R.; Yoshida, K.; Masuda, M.; Yase, K.; Shimizu, T. *Chem. Mater.* **2002**, 14, 3047-3053.
- (124) Wang, S. F.; Chen, T.; Zhang, Z. L.; Shen, X. C.; Lu, Z. X.; Pang, D. W.; Wong, K. Y. *Langmuir* **2005**, 21, 9260–9266.
- (125) Yokoi, H.; Kinoshita, T.; Zhang, S. G. *Proc. Natl. Acad. Sci. U. S. A.* **2005**, 102, 8414–8419.
- (126) Chen, J.; Park, H.; Park, K. *J. Biomed. Mater. Res.* **1999**, 44, 53–62.
- (127) Erni, R.; Rossell, M. D.; Kisielowski, C.; Dahmen, U. *Phys. Rev. Lett.* **2009**, 102, 1–4.
- (128) Kolbel, M.; Menger, F. M. *Chem. Commun.* **2001**, 275-276.
- (129) Kuehlbrandt, W. *Cryo-Em Enters a New Era. eLife* **2014**, 3, e03678.
- (130) Bhattacharya, S.; Acharya, S. N. G. *Chem. Mater.* **1999**, 11, 3504-3511.
- (131) Hanabusa, K.; Hirata, T.; Inoue, D.; Kimura, I.; Shirai, H. *Colloid Surf., A* **2000**, 169, 307-315.
- (132) Menger, F. M.; Caran, K. L. *J. Am. Chem. Soc.* **2000**, 122, 11679-11691.
- (133) Nowak, A. P.; Breedveld, V.; Pakstis, L.; Ozbas, B.; Pine, D. J.; Pochan, D.; Deming, T. J. *Nature* **2002**, 417, 424–428.
- (134) Ferry, J. D. *Viscoelastic Properties of Polymers. 3rd ed. Wiley: New York* **1980**.
- (135) Almdal, K.; Dyre, J.; Hvidt, S.; Kramer, O. *Polym. Gels Networks* **1993**, 1, 5-17.
- (136) Siepmann, J.; Peppas, N. A. *Adv. Drug Delivery Rev.* **2001**, 48, 139–157.
- (137) Moreau, L.; Barthelemy, P.; El Maataoui, M.; Grinstaff, M. W. *J. Am. Chem. Soc.* **2004**, 126, 7533-7539.
- (138) Anderson, K. M.; Day, G. M.; Paterson, M. J.; Byrne, P.; Clarke, N.; Steed, J. W. *Angew. Chem., Int. Ed.* **2008**, 47, 1058-1062.
- (139) Pochan, D. J.; Pakstis, L.; Ozbas, B.; Nowak, A. P.; Deming, T. J. *Macromolecules* **2002**, 35, 5358-5360.
- (140) Fukuda, H.; Goto, A.; Imae, T. *Langmuir* **2002**, 18, 7107-7114.
- (141) Roy, S.; Banerjee, A. *Soft Matter* **2001**, 7, 5300–5308.
- (142) Jung, J. H.; Shinkai, S.; Shimizu, T. *Chem.-Eur. J.* **2002**, 8, 2684-2690.
- (143) Estroff, L. A.; Leiserowitz, L.; Addadi, L.; Weiner, S.; Hamilton, A. D. *Adv. Mater.* **2003**, 15, 38-42.
- (144) Terech, P.; de Geyer, A.; Struth, B.; Talmon, Y. *Adv. Mater.* **2002**, 14, 495-498.
- (145) Wang, X. F.; Shen, Y. Z.; Pan, Y.; Liang, Y. Q. *Langmuir* **2001**, 17, 3162-3167.
- (146) David, W. I. F.; Shankland, K.; McCusker, L. B.; Baerlocher, C., Eds. *Structure Determination from Powder Diffraction Data. Oxford University Press: New York* **2002**, Vol. 13.
- (147) Azaroff, L. V.; Buerger, M. J. *The Powder Method in X-ray Crystallography. McGraw-Hill Book Company, Inc.: New York* **1958**.
- (148) Iton, L. E.; Trouw, F.; Brun, T. O.; Epperson, J. E.; White, J. W.; Henderson, S. J. *Langmuir* **1992**, 8, 1045–1048.
- (149) Meister, A.; Bastrop, M.; Koschoreck, S.; Garamus, V. M.; Sinemus, T.; Hempel, G.; Drescher, S.; Dobner, B.; Richtering, W.; Huber, K. *Langmuir* **2007**, 23, 7715-7723.
- (150) Hule, R. A.; Nagarkar, R. P.; Hammouda, B.; Schneider, J. P.; Pochan, D. J. *Macromolecules* **2009**, 42, 7137–7145.
- (151) Verma, G.; Aswal, V. K.; Hassan, P. *Soft Matter* **2009**, 5, 2919–2927.
- (152) Sakurai, K.; Ono, Y.; Jung, J. H.; Okamoto, S.; Sakurai, S.; Shinkai, S. *J. Chem. Soc., Perkin Trans. 2* **2001**, 108-112.
- (153) Sakurai, K.; Kimura, T.; Gronwald, O.; Inoue, K.; Shinkai, S. *Chem. Lett.* **2001**, 746-747.
- (154) Simmons, B. A.; Taylor, C. E.; Landis, F. A.; John, V. T.; McPherson, G. L.; Schwartz, D. K.; Moore, R. *J. Am. Chem. Soc.* **2001**, 123, 2414-2421.
- (155) Makarević, J.; Jokić, M.; Perić, B.; Tomišić, V.; Kojic-Prodić, B.; Žinić, M. *Chem.-Eur. J.* **2001**, 7, 3328-3341.

Part B

Bibliographies

- (156) Jung, J. H.; John, G.; Masuda, M.; Yoshida, K.; Shinkai, S.; Shimizu, T. *Langmuir* **2001**, *17*, 7229-7232.
- (157) Kim, H.; Ralph, J. *Org. Biomol. Chem.* **2010**, *8*, 576-591.
- (158) Fuhrhop, J. H.; Svenson, S.; Boettcher, C.; Rossler, E.; Vieth, H. M. *J. Am. Chem. Soc.* **1990**, *112*, 4307-4312.
- (159) Nakazawa, I.; Masuda, M.; Okada, Y.; Hanada, T.; Yase, K.; Asai, M.; Shimizu, T. *Langmuir* **1999**, *15*, 4757-4764.
- (160) Iwaura, R.; Yoshida, K.; Masuda, M.; Ohnishi-Kameyama, M.; Yoshida, M.; Shimizu, T. *Angew. Chem., Int. Ed.* **2003**, *42*, 1009-1012.
- (161) Suzuki, M.; Yumoto, M.; Kimura, M.; Shirai, H.; Hanabusa, K. *Chem.-Eur. J.* **2003**, *9*, 348-354.
- (162) Pan, K. M.; Baldwin, M.; Nguyen, J.; Gasset, M.; Serban, A.; Groth, D.; Mehlhorn, I.; Huang, Z. W.; Fletterick, R. J.; Cohen, F. E.; al., e. *Proc. Natl. Acad. Sci. U. S. A.* **1993**, *90*, 10962-10966.
- (163) Zhao, Y. L.; Stoddart, J. F. *Langmuir* **2009**, *25*, 8442-8446.
- (164) Raeburn, J.; McDonald, T. O.; Adams, D. J. *Chem. Commun.* **2012**, *48*, 9355-9357.
- (165) Nakayama, Y.; Takatsuka, M.; Matsuda, T. *Langmuir* **1999**, *15*, 1667-1672.
- (166) Rabindranath, A. R.; Maier, A.; Schafer, M. *Macromol. Chem. Phys.* **2009**, *210*, 659-666.
- (167) Schoonbeek, F. S.; van Esch, J. H.; Hulst, R.; Kellogg, R. M.; Feringa, B. L. *Chem.-Eur. J.* **2000**, *6*, 2633-2643.
- (168) Malik, S.; Maji, S. K.; Banerjee, A.; Nandi, A. K. *J. Chem. Soc. Perk. T.* **2002**, *2*, 1177-1186.
- (169) Bhattacharya, S.; Acharya, S. N. G. *Chem. Mater.* **1999**, *11*, 3121-3132.
- (170) Mikami, M.; Matsuzaki, T.; Masuda, M.; Shimizu, T.; Tanabe, K. *Comput. Mater. Sci.* **1999**, *14*, 267-276.
- (171) van Esch, J.; de Feyter, S.; Kellogg, R. M.; Schryver, F. D.; Feringa, B. L. *Chem.-Eur. J.* **1997**, *3*, 1238-1243.
- (172) Abdallah, D. J.; Sirchio, S. A.; Weiss, R. G. *Langmuir* **2000**, *16*, 7558-7561.
- (173) Abdallah, D. J.; Weiss, R. G. *Adv. Mater.* **2000**, *12*, 1237-1247.
- (174) Mieden-Gundert, G.; Klein, L.; Fischer, M.; Vögtle, F.; Heuzé, K.; Pozzo, J.-L.; Vallier, M.; Fages, F. *Angew. Chem., Int. Ed.* **2001**, *40*, 3164-3166.
- (175) Tachibana, T.; Mori, T.; Hori, K. *Bull. Chem. Soc. Jpn.* **1980**, *53*, 1714-1719.
- (176) Tachibana, T.; Mori, T.; Hori, K. *Bull. Chem. Soc. Jpn.* **1981**, *54*, 73-80.
- (177) Knight, D. W.; Morgan, I. R. *Tetrahedron Lett.* **2009**, *50*, 6610-6612.
- (178) Abdallah, D. J.; Lu, L.; Weiss, R. G. *Chem. Mater.* **1999**, *11*, 2907-2911.
- (179) George, M.; Weiss, R. G. *Langmuir* **2002**, *18*, 7124-7135.
- (180) Masunov, A.; Dannenberg, J. J. *J. Phys. Chem. B* **2000**, *104*, 806-810.
- (181) Masunov, A.; Dannenberg, J. J. *J. Phys. Chem. A* **1999**, *103*, 178-184.
- (182) George, M.; Tan, G.; John, V. T.; Weiss, R. G. *Chem.-Eur. J.* **2005**, *11*, 3243-3254.
- (183) Vemula, P. K.; John, G. *Chem. Commun.* **2006**, 2218-2220.
- (184) Wang, G.; Hamilton, A. D. *Chem.-Eur. J.* **2002**, *8*, 1954-1961.
- (185) de Loos, M.; Ligtenbarg, A. G. J.; van Esch, J.; Kooijman, H.; Spek, A. L.; Hage, R.; Kellogg, R. M.; Feringa, B. L. *Eur. J. Org. Chem.* **2000**, 3675-3678.
- (186) Yamanaka, M.; Nakagawa, T.; Aoyama, R.; Nakamura, T. *Tetrahedron Lett.* **2008**, *64*, 11558-11567.
- (187) Yamanaka, M.; Fujii, H. *J. Org. Chem.* **2009**, *74*, 5390-5394.
- (188) van Esch, J. H.; Schoonbeek, F.; de Loos, M.; Kooijman, H.; Spek, A. L.; Kellogg, R. M.; Feringa, B. L. *Chem.-Eur. J.* **1999**, *5*, 937-950.
- (189) Brinksma, J.; Feringa, B. L.; Kellogg, R. M.; Vreeker, R.; van Esch, J. *Langmuir* **2000**, *16*, 9249-9255.
- (190) Luo, X.; Li, C.; Liang, Y. *Chem. Commun.* **2000**, 2091-2092.
- (191) Ayerst, E. M.; Duke, J. R. C. *Acta Cryst.* **1954**, *7*, 588-590.
- (192) Hanabusa, K.; Yamada, M.; Kimura, M.; Shirai, H. *Angew. Chem., Int. Ed. Engl.* **1996**, *35*, 1949-1951.
- (193) Jung, J. H.; Ono, Y.; Hanabusa, K.; Shinkai, S. *J. Am. Chem. Soc.* **2000**, *122*, 5008-5009.
- (194) Schmidt, R.; Adam, F. B.; Michel, M.; Schmutz, M.; Decher, G.; Mésini, P. J. *Tetrahedron Lett.* **2003**, *44*, 3171-3174.
-

Part B

Bibliographies

- (195) Martin-Borret, O.; Ramasseul, R.; Rassat, R. *Bull. Soc. Chim. Fr.* **1979**, II-401, 7-8.
- (196) Lin, Y.; Weiss, R. G. *Macromolecules* **1987**, 20, 414-417.
- (197) Murata, K.; Aoki, M.; Suzuki, T.; Harada, T.; Kawabata, H.; Komori, T.; Ohseto, F.; Ueda, K.; Shinkai, S. *J. Am. Chem. Soc.* **1994**, 116, 6664-6676.
- (198) Murata, K.; Aoki, M.; Nishi, T.; Ikeda, A.; Shinkai, S. *J. Chem. Soc., Chem. Commun.* **1991**, 1715-1718.
- (199) Tian, H. J.; Inoue, K.; Yoza, K.; Ishi-i, T.; Shinkai, S. *Chem. Lett.* **1998**, 871-872.
- (200) Virtanen, E.; Kolehmainen, E. *Eur. J. Org. Chem.* **2004**, 3385-3399.
- (201) Geiger, C.; Stanescu, M.; Chen, L.; Whetten, D. G. *Langmuir* **1999**, 15, 2241-2245.
- (202) Mukkamala, R.; Weiss, R. G. *Langmuir* **1996**, 12, 1474-1482.
- (203) Smith, J. M.; Katsoulis, D. E. *J. Mater. Chem.* **1995**, 5, 1899-1903.
- (204) Hafkamp, R. J. H.; Feiters, M. C.; Nolte, R. J. M. *J. Org. Chem.* **1999**, 64, 412-426.
- (205) John, G.; Jung, J. H.; Masuda, M.; Shimizu, T. *Langmuir* **2004**, 20, 2060-2065.
- (206) Gronwald, O.; Shinkai, S. *Chem.-Eur. J.* **2001**, 7, 4329-4334.
- (207) Friggeri, A.; Gronwald, O.; van Bommel, K. J. C.; Shinkai, S.; Reinhoudt, D. N. *J. Am. Chem. Soc.* **2002**, 124, 10754-10758.
- (208) Luboradzki, R.; Pakulski, Z. *Tetrahedron* **2004**, 60, 4613-4616.
- (209) John, G.; Zhu, G.; Li, J.; Dordick, J. S. *Angew. Chem., Int. Ed.* **2006**, 45, 4772-4775.
- (210) Kida, T.; Kishimoto, K.; Hatano, K.; Muraoka, M.; Nakatsuji, Y.; Akashi, M. *Chem. Lett.* **2010**, 39, 1206-1208.
- (211) Thomas, P.; Sibi, M. *Comptes Rendus* **1926**, 183, 282.
- (212) Roehl, E. L.; Tan, H. B. Solid antiperspirant composition and process for its preparation U. S. 4154816 A.
- (213) Shepard, T. A. M.: North Carolina State University **1995**.
- (214) Yamamoto, S. *Bull. Chem. Soc. Jpn.* **1942**, 45, 695.
- (215) Watase, M.; Nakatani, Y.; Itagaki, H. *J. Phys. Chem. B* **1999**, 103, 2366-2373.
- (216) Clavier, G.; Mistry, M.; Fages, F.; Pozzo, J.-L. *Tetrahedron Lett.* **1999**, 40, 9021-9024.
- (217) Brotin, T.; Uttermöhlen, R.; Fages, F.; Bouas-Laurent, H.; Desvergne, J.-P. *J. Chem. Soc., Chem. Commun.* **1991**, 416-418.
- (218) Terech, P.; Bouas-Laurent, H.; Desvergne, J.-P. *J. Colloid Interface Sci.* **1995**, 174, 258-263.
- (219) Pozzo, J.-L.; Clavier, G. M.; Colomes, M.; Bouas-Laurent, H. *Tetrahedron* **1997**, 53, 6377-6390.
- (220) Clavier, G. M.; Brugger, J.-F.; Bouas-Laurent, H.; Pozzo, J.-L. *J. Chem. Soc., Perkin Trans.* **1998**, 2, 2527-2534.
- (221) Placin, F.; Desvergne, J.-P.; Belin, C.; Buffeteau, T.; Desbat, B.; Ducasse, L.; Lassègues, J.-C. *Langmuir* **2003**, 19, 4563-4572.
- (222) Li, X.-Q.; Stepanenko, V.; Chen, Z.; Prins, P.; Siebbeles, L. D. A.; Würthner, F. *Chem. Commun.* **2006**, 3871-3873.
- (223) Li, X. Ph.D. thesis: Hydrogen Bond-directed Self-assembly of Perylene Bisimide Organogelators. Julius-Maximilians-Universität Würzburg, **2009**.
- (224) Maitra, U.; VijayKumar, P.; Chandra, N.; D'Souza, L. J.; Prasanna, M. D.; Raju, A. R. *Chem. Commun.* **1999**, 595-596.
- (225) Babu, P.; Sangeetha, N. M.; Vijaykumar, P.; Maitra, U.; Rissanen, K.; Raju, A. R. *Chem.-Eur. J.* **2003**, 9, 1922-1932.
- (226) D'Souza, L. J.; Maitra, U. *J. Org. Chem.* **1996**, 61, 9494-9502.
- (227) Maitra, U.; Potluri, V. K.; Sangeetha, N. M.; Babu, P.; Raju, A. R. *Tetrahedron: Asymmetry* **2001**, 12, 477-480.
- (228) Das, R. K.; Kandaneli, R.; Linnanto, J.; Bose, K.; Maitra, U. *Langmuir* **2010**, 26, 16141-16149.
- (229) Sagawa, T.; Fukugawa, S.; Yamada, T.; H. Ihara, H. *Langmuir* **2002**, 18, 7223-7228.
- (230) Tamaru, S.; Uchino, S.; Takeuchi, M.; Ikeda, M.; Hatano, T.; Shinkai, S. *Tetrahedron Lett.* **2002**, 3751-3755.
- (231) Tanaka, S.; Shirakawa, M.; Kaneko, K.; Takeuchi, M.; Shinkai, S. *Langmuir* **2005**, 21, 2163-2172.

Part B

Bibliographies

- (232) van Nostrum, C. F.; Picken, S. J.; Schouten, A. J.; Nolte, R. J. M. *J. Am. Chem. Soc.* **1995**, *117*, 9957-9965.
- (233) Engelkamp, H.; Middelbeek, S.; Nolte, R. J. M. *Science* **1999**, *284*, 785-788.
- (234) Samorí, S.; Engelkamp, H.; de Witte, P.; Rowan, A. E.; Nolte, R. J. M.; Rabe, J. P. *Angew. Chem., Int. Ed.* **2001**, *40*, 2348-2350.
- (235) Piechocki, C.; Simon, J.; Skoulios, A.; Guillon, D.; Weber, P. *J. Am. Chem. Soc.* **1982**, *104*, 5245-5247.
- (236) Engel, M. K.; Bassoul, P.; Bosio, L.; Lehmann, H.; Hanack, M.; Simon, J. *Liq. Cryst.* **1993**, *15*, 709.
- (237) Cho, I.; Lim, Y. *Mol. Cryst. Liq. Cryst.* **1988**, *154*, 9-26.
- (238) van der Pol, J. F.; Neeleman, E.; Zwikker, J. W.; Nolte, R. J. M.; Drenth, W.; Aerts, J.; Visser, R.; Picken, S. J. *Liq. Cryst.* **1989**, *6*, 577-592.
- (239) van Nostrum, C. F.; Bosman, A. W.; Gelinck, G. H.; Schouten, P. G.; Warman, J. M.; Kentgens, A. P. M.; Meijerink, A.; Picken, S. J.; Devillers, M. A. C.; Sohling, U.; Schouten, A.-J.; Nolte, R. J. M. *Chem.-Eur. J.* **1995**, *1*, 171-182.
- (240) Cook, M. J.; Dunn, A. J.; Daniel, M. F.; Hart, R. C. O.; Richardson, R. M.; Roser, S. J. *Thin Solid Films* **1988**, *159*, 395-404.
- (241) Chester, M. A.; Cook, M. J.; Gallivan, S. L.; Simmons, J. M.; Slater, D. A. *Thin Solid Films* **1992**, *210/211*, 538-541.
- (242) Ogawa, K.; Yonehara, H.; Shoji, T.; Kinoshita, S.-I.; Maekawa, E.; Nakahara, H.; Fukuda, K. *Thin Solid Films* **1989**, *178*, 439-443.
- (243) Nakahara, H.; Fukuda, K.; Kitahara, K.; Nishi, H. *Thin Solid Films* **1989**, *178*, 361-366.
- (244) Schutte, W. J.; Sluyters-Rehbach, M.; Sluyters, J. H. *J. Phys. Chem.* **1993**, *97*, 6069-6073.
- (245) van Nostrum, C. F.; Nolte, R. J. M.; Devillers, M. A. C.; Oostergetel, G. T.; Teerenstra, M. N.; Schouten, A.-J. *Macromolecules* **1993**, *26*, 3306-3312.
- (246) Orthmann, E.; Wegner, G. *Angew. Chem.* **1986**, *98*, 1114-1115.
- (247) Piechocki, C.; Simon, J. *New J. Chem.* **1985**, *9*, 159-163.
- (248) Fujiki, M.; Tabei, H.; Kurihara, T. *J. Phys. Chem.* **1988**, *92*, 1281-1285.
- (249) Tai, S.; Hayashi, N. *J. Chem. Soc., Perkin Trans.* **1991**, *2*, 1275-1279.
- (250) Prasad, A.; Marand, H.; Bheda, M.; Gibson, H. W. *J. Am. Chem. Soc., Division of Polymer Chemistry* **1991**, *32*, 469.
- (251) Fages, F. *Angew. Chem., Int. Ed.* **2006**, *45*, 1680-1682.
- (252) Terech, P.; Chachaty, C.; Gaillard, J.; Giroud-Godquin, A. M. *J. Phys. Fr.* **1987**, *48*, 663-671.
- (253) Terech, P.; Gebel, G.; Ramasseul, R. *Langmuir* **1996**, *12*, 4321-4323.
- (254) Terech, P.; Scherer, C.; Demé, B.; Ramasseul, R. *Langmuir* **2003**, *19*, 10641-10647.
- (255) Liu, Q.; Wang, Y.; Li, W.; Wu, L. *Langmuir* **2007**, *23*, 8217-8223.
- (256) Kim, C.; Kim, K. T.; Chang, Y.; Song, H. H.; Cho, T.-Y.; Jeon, H.-J. *J. Am. Chem. Soc.* **2001**, *123*, 5586-5587.
- (257) Chow, H. F.; Zhang, J. *Chem.-Eur. J.* **2005**, *11*, 5817-5831.
- (258) Funkhouser, G. P.; Tonmukayakul, N.; Liang, F. *Langmuir* **2009**, *25*, 8672-8677.
- (259) George, M.; Weiss, R. G.: *Low Molecular-Mass Organic Gelators, In Molecular Gels. Materials with Self-Assembled Fibrillar Networks*; Springer: Dordrecht, Netherlands, **2006**.
- (260) Bhattacharya, S.; Pal, A. *J. Phys. Chem. B* **2008**, *112*, 4918-4927.
- (261) Pal, A.; Ghosh, Y. K.; Bhattacharya, S. *Tetrahedron* **2007**, *63*, 7334-7348.
- (262) Hanabusa, K.; Okui, K.; Karaki, K.; Koyama, T.; Shirai, H. *J. Chem. Soc., Chem. Commun.* **1992**, *18*, 1371-1373.
- (263) Makarević, J.; Jokić, M.; Frkanec, L.; Katalenić, D.; Žinić, M. *Chem. Commun.* **2002**, *19*, 2238-2239.
- (264) Jokić, M.; Makarević, J.; Žinić, M. *J. Chem. Soc., Chem. Commun.* **1995**, 1723-1724.
- (265) Duncan, D. C.; Whitten, D. G. *Langmuir* **2000**, *16*, 6445-6452.
- (266) Menger, F. M.; Yamasaki, Y.; Catlin, K. K.; Nishimi, T. *Angew. Chem., Int. Ed.* **1995**, *34*, 585-586.
- (267) Kar, T.; Debnath, S.; Das, D.; Shome, A.; Das, P. K. *Langmuir* **2006**, *25*, 8639-8648.
- (268) Luo, X.; Liu, B.; Liang, Y. *Chem. Commun.* **2001**, 1556-1557.
- (269) Dutta, A.; Chattopadhyay, D.; Pramanik, A. S. *Supramol. Chem.* **2010**, *22*, 95-102.

Part B

Bibliographies

- (270) Suzuki, M.; Nigawara, T.; Yumoto, M.; Kimura, M.; Shirai, H.; Hanabusa, K. *Tetrahedron Lett.* **2003**, *44*, 6841-6843.
- (271) Hanabusa, K.; Tange, J.; Taguchi, Y.; Koyama, T.; Shirai, H. *J. Chem. Soc., Chem. Commun.* **1993**, *4*, 390-392.
- (272) Becerril, J.; Burguete, M. I.; Escuder, B.; Luis, S. V.; Miravet, J. F.; Querol, M. *Chem. Commun.* **2002**, 738-739.
- (273) Brosse, N.; Barth, D.; Jamart-Grégoire, B. *Tetrahedron Lett.* **2004**, *45*, 9521-9524.
- (274) Pham, Q. N.; Brosse, N.; Frochet, C.; Dumas, D.; Hocquet, A.; Jamart-Gregoire, B. *New J. Chem.* **2008**, *32*, 1131-1139.
- (275) Lee, K. Y.; Mooney, D. J. *J. Chem. Rev.* **2001**, *101*, 1869-1879.
- (276) Tiller, J. C. *Angew. Chem., Int. Ed. Engl.* **2003**, *42*, 3072-3075.
- (277) Xing, B. G.; Yu, C. W.; Chow, K. H.; Ho, P. L.; Fu, D. G.; Xu, B. *J. Am. Chem. Soc.* **2002**, *124*, 14846-14847.
- (278) Kiyonaka, S.; Sugiyasu, K.; Shinkai, S.; Hamachi, I. *J. Am. Chem. Soc.* **2002**, *124*, 10954-10955.
- (279) Uhrich, K. E.; Cannizzaro, S. M.; Langer, R. S.; Shakesheff, K. M. *Chem. Rev.* **1999**, *99*, 3181-3198.
- (280) Yang, Z.; Xu, B. *Adv. Mater.* **2006**, *18*, 3043-3046.
- (281) Israelachvili, J. N. *Intermolecular and Surface Forces*, 2nd ed.; Academic Press: New York. **1991**.
- (282) Bernet, A.; Behr, M.; Schmidt, H. W. *Soft Matter* **2011**, *7*, 1058-1065.
- (283) Morita, C.; Kawai, C.; Kikuchi, A.; Imura, Y.; Kawai, T. *J. Oleo Sci.* **2012**, *61*, 707-713.
- (284) Soto Tellini, V. H.; Jover, A.; Meijide, F.; Vaquez Tato, J.; Galantini, L.; Pavel, N. V. *Adv. Mater.* **2007**, *19*, 1752-1756.
- (285) Galantini, L.; Leggio, C.; Jover, A.; Meijide, F.; Pavel, N. V.; Tellini, V. H. S.; Tato, J. V.; Di Leonardo, R.; Ruocco, G. *Soft Matter* **2009**, *5*, 3018-3025.
- (286) Wang, Y.; Xin, X.; Li, W.; Jia, C.; Wang, L.; Shen, J.; Xu, G. *J. Colloid Interface Sci.* **2014**, *431*, 82-89.
- (287) di Gregorio, M. C.; Pavel, N. V.; Miragaya, J.; Jover, A.; Meijide, F.; Tato, J. V.; Tellini, V. H. S.; Galantini, L. *Langmuir* **2013**, *29*, 12342-12351.
- (288) Kumar, D. K.; Jose, D. A.; Das, A.; Dastidar, P. *Chem. Commun.* **2005**, 4059-4061.
- (289) Adarsh, N. N.; Kumar, D. K.; Dastidar, P. *Tetrahedron* **2007**, *63*, 7386-7396.
- (290) Piepenbrock, M. O. M.; Lloyd, G. O.; Clarke, N.; Steed, J. W. *Chem. Commun.* **2008**, 2644-2646.
- (291) de Loos, M.; Friggeri, A.; van Esch, J.; Kellogg, R. M.; Feringa, B. L. *Org. Biomol. Chem.* **2005**, *3*, 1631-1639.
- (292) Li, J. J.; Fan, K. Q.; Niu, L. B.; Li, Y. C.; Song, J. *J. Phys. Chem. B* **2013**, *117*, 5989-5995.
- (293) Griffiths, P. C.; Knight, D. W.; Morgan, I. R.; Ford, A.; Brown, J.; Davies, B.; Heenan, R. K.; King, S. M.; Dalglish, R. M.; Tomkinson, J., et al. *J. Org. Chem. Commun.* **2010**, *6*, 1079-1088.
- (294) Ohsedo, Y.; Oono, M.; Saruhashi, K.; Watanabe, H. *RSC Adv.* **2014**, *4*, 43560-43563.
- (295) Ohsedo, Y.; Oono, M.; Saruhashi, K.; Watanabe, H. *RSC Adv.* **2014**, *4*, 48554-48558.
- (296) Kohler, K.; Forster, G.; Hauser, A.; Dobner, B.; Heiser, U. F.; Ziethe, F.; Richter, W.; Steiniger, F.; Drechsler, M.; Stettin, H., et al. *Angew. Chem., Int. Ed. Engl.* **2004**, *43*, 245-247.
- (297) Kohler, K.; Meister, A.; Forster, G.; Dobner, B.; Drescher, S.; Ziethe, F.; Richter, W.; Steiniger, F.; Drechsler, M.; Hause, G., et al. *Soft Matter* **2006**, *2*, 77-86.
- (298) Meister, A.; Drescher, S.; Garamus, V. M.; Karlsson, G.; Graf, G.; Dobner, B.; Blume, A. *Langmuir* **2008**, *24*, 6238-6246.
- (299) Bastrop, M.; Meister, A.; Metz, H.; Drescher, S.; Dobner, B.; Mader, K.; Blume, A. *J. Phys. Chem. B* **2009**, *113*, 574-582.
- (300) Meister, A.; Drescher, S.; Karlsson, G.; Hause, G.; Baumeister, U.; Hempel, G.; Garamus, V. M.; Dobner, B.; Blume, A. *Soft Matter* **2010**, *6*, 1317-1324.
- (301) Graf, G.; Drescher, S.; Meister, A.; Dobner, B.; Blume, A. *J. Phys. Chem. B* **2011**, *115*, 10478-10487.
- (302) Blume, A.; Drescher, S.; Meister, A.; Graf, G.; Dobner, B. **2013**, *161*, 193-213.

Part B

Bibliographies

- (303) Graf, G.; Drescher, S.; Meister, A.; Garamus, V. M.; Dobner, B.; Blume, A. *Soft Matter* **2013**, *9*, 9562–9571.
- (304) Blume, A.; Drescher, S.; Graf, G.; Köhler, K.; Meister, A. *Adv. Colloid Interface Sci.* **2014**, *208*, 264–278.
- (305) Drescher, S.; Meister, A.; Garamus, V. M.; Hause, G.; Garvey, C. J.; Dobner, B.; Blume, A. *Eur. J. Lipid Sci. Technol.* **2014**, *116*, 1205–1216.
- (306) Kohler, K.; Forster, G.; Hauser, A.; Dobner, B.; Heiser, U. F.; Ziethe, F.; Richter, W.; Steiniger, F.; Drechsler, M.; Stettin, H., et al. *J. Am. Chem. Soc.* **2004**, *126*, 16804–16813.
- (307) Song, B.; Wei, H.; Wang, Z. Q.; Zhang, X.; Smet, M.; Dehaen, W. *Adv. Mater.* **2007**, *19*, 416–420.
- (308) Cai, F.; Shen, J. S.; Wang, J. H.; Zhang, H.; Zhao, J. S.; Zeng, E. M.; Jiang, Y. B. *Org. Biomol. Chem.* **2012**, *10*, 1418–1423.
- (309) Roy, S.; Maiti, D. K.; Panigrahi, S.; Basak, D.; Banerjee, A. *RSC Adv.* **2012**, *2*, 11053–11060.
- (310) Datar, A.; Balakrishnan, K.; Zang, L. *Chem. Commun.* **2013**, *49*, 6894–6896.
- (311) Weingarten, A. S.; Kazantsev, R. V.; Palmer, L. C.; McClendon, M.; Koltonow, A. R.; Samuel, A. P. S.; Kiebal, D. J.; Wasielewski, M. R.; Stupp, S. I. *Nat. Chem.* **2014**, *6*, 964–970.
- (312) Molla, M. R.; Ghosh, S. *Chem.-Eur. J.* **2012**, *18*, 9860–9869.
- (313) End, N.; Macko, L.; Zehnder, M.; Pfaltz, A. *Chem.-Eur. J.* **1998**, *4*, 818–824.
- (314) Makarević, J.; Jokić, M.; Raza, Z.; Stefanić, Z.; Kojic-Prodić, B.; Žinić, M. *Chem.-Eur. J.* **2003**, *9*, 5567–5580.
- (315) Makarević, J.; Jokić, M.; Raza, Z.; Caplar, V.; Katalenić, D.; Stefanić, Z.; Kojic-Prodić, B.; Žinić, M. *Croat. Chem. Acta* **2004**, *77*, 403–414.
- (316) Dou, X. Q.; Li, P.; Zhang, D.; Feng, C. L. *Soft Matter* **2012**, 3231–3238.
- (317) Mangunuru, H. P. R.; Yang, H.; Wang, G. J. *Chem. Commun.* **2013**, *49*, 4489–4491.
- (318) Yamaguchi, H.; Kobayashi, Y.; Kobayashi, R.; Takashima, Y.; Hashidzume, A.; Harada, A. *Nat. Commun.* **2012**, *3*, 603–607.
- (319) Li, J.; Cvrtila, I.; Colomb-Delsuc, M.; Otten, E.; Otto, S. *Chem.-Eur. J.* **2014**, *20*, 15709–15714.
- (320) Yang, R.; Peng, S.; Wan, W.; Hughes, T. C. *J. Mater. Chem. C* **2014**, *2*, 9122–9131.
- (321) Yang, D.; Liu, C.; Zhang, L.; Liu, M. *Chem. Commun.* **2014**, *50*, 12688–12690.
- (322) Velema, W. A.; Stuart, M. C. A.; Szymanski, W.; Feringa, B. L. *Chem. Commun.* **2013**, *49*, 5001–5003.
- (323) Wang, Y. J.; Tang, L. M.; Wang, Y. *Chem. Lett.* **2006**, *35*, 548–549.
- (324) Jin, X.; Wang, Y. J.; Tang, L. M.; . *Acta Polym. Sin* **2010**, *1*, 462–467.
- (325) Wang, Y. J.; Chen, K.; Tang, L. M. *Chem. Lett.* **2009**, *38*, 472–473.
- (326) Roy, B.; Bairi, P.; Saha, A.; Nandi, A. K. *Soft Matter* **2011**, *7*, 8067–8076.
- (327) Basit, H.; Pal, A.; Sen, S.; Bhattacharya, S. *Chem.-Eur. J.* **2008**, *14*, 6534–6545.
- (328) Rao, K. V.; George, S. J. *Chem.-Eur. J.* **2012**, *18*, 14286–14291.
- (329) Xing, B.; Choi, M.-F.; Xu, B. *Chem. Commun.* **2002**, 362–363.
- (330) Xing, B.; Choi, M.-F.; Xu, B. *Chem.-Eur. J.* **2002**, *8*, 5028–5032.
- (331) Suzuki, M.; Yumoto, M.; Shirai, H.; Hanabusa, K. *Org. Biomol. Chem.* **2005**, *3*, 3073–3078.
- (332) Suzuki, M.; Yumoto, M.; Shirai, H.; Hanabusa, K. *Chem.-Eur. J.* **2008**, *14*, 2133–2144.
- (333) Shen, J. S.; Mao, G. J.; Zhou, Y. H.; Jiang, Y. B.; Zhang, H. W. *Dalton Trans.* **2010**, *39*, 7054–7058.
- (334) Basak, S.; Nanda, J.; Banerjee, A. *Chem. Commun.* **2014**, *50*, 2356–2359.
- (335) Wang, H.; Li, X.; Fang, F.; Yang, Y. J. *Dalton Trans.* **2010**, *39*, 7294–7300.
- (336) Zheng, Y. H.; Li, Y.; Tan, C. L.; Wang, Q. M. *Photochem. Photobiol.* **2011**, *87*, 641–645.
- (337) Miravet, J. F.; Escuder, B. *Chem. Commun.* **2005**, 5796–5798.
- (338) Ogata, K.; Sasano, D.; Yokoi, T.; Isozaki, K.; Seike, H.; Takaya, H.; Nakamura, M. *Chem. Lett.* **2012**, *41*, 498–500.
- (339) Ghosh, B. N.; Bhowmik, S.; Mal, P.; Rissanen, K. *Chem. Commun.* **2014**, *50*, 734–736.
- (340) Fu, I. W.; Markegard, C. B.; Nguyen, H. D. *Langmuir* **2015**, *31*, 315–324.
- (341) Jiang, J. A.; Wang, T. Y.; Liu, M. H. *Chem. Commun.* **2010**, *46*, 7178–7180.
- (342) Pal, A.; Dey, J. *Langmuir* **2011**, *27*, 3401–3408.
- (343) Patra, T.; Pal, A.; Dey, J. *Langmuir* **2010**, *26*, 7761–7767.

Part B

Bibliographies

- (344) Gao, P.; Zhan, C. L.; Liu, L. Z.; Zhou, Y. B.; Liu, M. H. *Chem. Commun.* **2004**, 1174–1175.
- (345) Roy, S.; Dasgupta, A.; Das, P. K. *Langmuir* **2007**, *23*, 11769–11776.
- (346) Dutta, S.; Shome, A.; Debnath, S.; Das, P. K. *Soft Matter* **2009**, *5*, 1607–1620.
- (347) Suzuki, M.; Owa, S.; Yumoto, M.; Kimura, M.; Shirai, H.; Hanabusa, K. *Tetrahedron Lett.* **2004**, *45*, 5399–5402.
- (348) Suzuki, M.; Yumoto, M.; Kimura, M.; Shirai, H.; Hanabusa, K. *Tetrahedron Lett.* **2004**, *45*, 2947–2950.
- (349) Gao, P.; Liu, L. Z.; Zhan, C. L.; Zhou, Y. B.; Liu, M. H. *Acta Chim. Sin.* **2004**, *62*, 895–900.
- (350) Suzuki, M.; Yumoto, M.; Kimura, M.; Shirai, H.; Hanabusa, K. *Chem. Lett.* **2004**, *33*, 1496–1497.
- (351) Fu, X. J.; Wang, N. X.; Zhang, S. Z.; Wang, H.; Yang, Y. J. *J. Colloid Interface Sci.* **2007**, *315*, 376–381.
- (352) Cao, S. Q.; Fu, X. J.; Wang, N. X.; Wang, H.; Yang, Y. J. *Int. J. Pharm.* **2008**, *357*, 95–99.
- (353) Fu, X. R.; Cao, S. Q.; Wang, N. X.; Zhang, S. Z.; Wang, H.; Yang, Y. J. *Chin. Chem. Lett.* **2007**, *18*, 1001–1004.
- (354) Chu, X.; Xing, P.; Li, S.; Ma, M.; Hao, J.; Hao, A. *RSC Adv.* **2015**, *5*, 1969–1978.
- (355) Huang, Z.; Luo, Q.; Guan, S.; Gao, J.; Wang, Y.; Zhang, B.; Wang, L.; Xu, J.; Dong, Z.; Liu, J. *Soft Matter* **2014**, *10*, 9695–9701.
- (356) Amarendar, R. M.; Srivastava, A. *Soft Matter* **2014**, *10*, 4863–4868.
- (357) Sun, Z. F.; Li, Z. Y.; He, Y. H.; Shen, R. J.; Deng, L.; Yang, M. H.; Liang, Y. Z.; Zhang, Y. J. *Am. Chem. Soc.* **2012**, *135*, 13379–13386.
- (358) Wang, Q. G.; Yang, Z. M.; Ma, M. L.; Chang, C. K.; Xu, B. *Chem.-Eur. J.* **2008**, *14*, 5073–5078.
- (359) Yang, Y.; Wang, L.; Wang, J.; Gao, P.; Xu, B. *J. Mater. Chem.* **2010**, *20*, 2128–2132.
- (360) Adhikari, B.; Nanda, J.; Banerjee, A. *Soft Matter* **2011**, *7*, 8913–8922.
- (361) Martari, M.; Sanderson, R. D. *S. Afr. J. Chem.* **2008**, *61*, 47–52.
- (362) Nanda, J.; Biswas, A.; Banerjee, A. *Soft Matter* **2013**, *9*, 4198–4208.
- (363) Wang, T. Y.; Jiang, J. A.; Liu, Y.; Li, Z. B.; Liu, M. *Langmuir* **2010**, *26*, 18694–18700.
- (364) Zhang, C.; Xue, X.; Luo, Q.; Li, Y.; Yang, K.; Zhuang, X.; Jiang, Y.; Zhang, J.; Liu, J.; Zou, G., et al. *ACS Nano* **2014**, *8*, 11715–11723.
- (365) Mu, Y.; Yu, M. *Soft Matter* **2014**, *10*, 4956–4965.
- (366) Reches, M.; Gazit, E. *Science* **2003**, *300*, 625–627.
- (367) Adler-Abramovich, L.; Reches, M.; Sedman, V. L.; Allen, S.; Tendler, S. J. B.; Gazit, E. *Langmuir* **2006**, *22*, 1313–1320.
- (368) Mahler, A.; Reches, M.; Rechter, M.; Cohen, S.; Gazit, E. *Adv. Mater.* **2006**, *18*, 1365–1370.
- (369) Reches, M.; Gazit, E. *Curr. Nanosci.* **2006**, *2*, 105–111.
- (370) Reches, M.; Gazit, E. *Phys. Biol.* **2006**, *3*, S10–S19.
- (371) Ryu, J.; Park, C. B. *Biotechnol. Bioeng* **2010**, *105*, 221–230.
- (372) Huang, R. L.; Qi, W.; Su, R. X.; Zhao, J.; He, Z. M. *Soft Matter* **2011**, *7*, 6418–6421.
- (373) Kumaraswamy, P.; Lakshmanan, R.; Sethuraman, S.; Krishnan, U. M. *Soft Matter* **2011**, *7*, 2744–2754.
- (374) Zhao, J.; Huang, R.; Qi, W.; Wang, Y.; Su, R.; He, Z. *Prog. Chem.* **2014**, *26*, 1445–1459.
- (375) de Groot, N. S.; Parella, T.; Aviles, F. X.; Vendrell, J.; Ventura, S. *Biophys. J.* **2007**, *92*, 1732–1741.
- (376) Chapman, R.; Danial, M.; Koh, M. L.; Jolliffe, K. A.; Perrier, S. *Chem. Soc. Rev.* **2012**, *41*, 6023–6041.
- (377) Qin, S. Y.; Jiang, H. F.; Liu, X. J.; Pei, Y.; Cheng, H.; Sun, Y. X.; Zhang, X. Z. *Soft Matter* **2014**, *10*, 947–951.
- (378) Xie, Z. G.; Zhang, A. Y.; Ye, L.; Feng, Z. G. *Acta Chim. Sin.* **2008**, *66*, 2620–2624.
- (379) Marchesan, S.; Easton, C. D.; Kushkaki, F.; Waddington, L.; Hartley, P. G. *Chem. Commun.* **2012**, *48*, 2195–2197.
- (380) Tie, Z. X.; Qin, M.; Zou, D. W.; Cao, Y.; Wang, W. *Chin. Phys. Lett.* **2011**, *28*, 028702.
- (381) Guilbaud, J. B.; Vey, E.; Boothroyd, S.; Smith, A. M.; Ulijn, R. V.; Saiani, A.; Miller, A. F. *Langmuir* **2010**, *26*, 11297–11303.
-

Part B

Bibliographies

- (382) Krysmann, M. J.; Castelletto, V.; Kellarakis, A.; Hamley, I. W.; Hule, R. A.; Pochan, D. J. *Biochemistry* **2008**, *47*, 4597–4605.
- (383) Colherinhas, G.; Fileti, E. *J. Phys. Chem. B* **2014**, *118*, 12215–12222.
- (384) Smadbeck, J.; Chan, K. H.; Khoury, G. A.; Xue, B.; Robinson, R. C.; Hauser, C. A.; Floudas, C. A. *PLoS Comput. Biol.* **2014**, *10*, e1003718.
- (385) Ruan, L. P.; Luo, H. L.; Zhang, H. Y.; Xing, Z. H. *J. Wuhan Univ. Technol., Mater. Sci. Ed.* **2013**, *28*, 622–626.
- (386) Desii, A.; Chiellini, F.; Di Stefano, R.; Tine, M. R.; Solaro, R. *J. Polym. Sci., Part A: Polym. Chem.* **2010**, *48*, 986–990.
- (387) Cao, C. H.; Cao, M. W.; Fan, H. M.; Xia, D. H.; Xu, H.; Lu, J. R. *Chin. Sci. Bull.* **2012**, *57*, 4296–4303.
- (388) Bowerman, C. J.; Liyanage, W.; Federation, A. J.; Nilsson, B. L. *Biomacromolecules* **2011**, *12*, 2735–2745.
- (389) Paramonov, S. E.; Jun, H. W.; Hartgerink, J. D. *Biomacromolecules* **2006**, *7*, 24–26.
- (390) Anderson, J. M.; Andukuri, A.; Lim, D. J.; Jun, H. W. *ACS Nano* **2009**, *3*, 3447–3454.
- (391) Xu, X.-D.; Jin, Y.; Liu, Y.; Zhang, X.-Z.; Zhou, R.-X. *Colloids Surf. B* **2010**, *81*, 329–335.
- (392) Mitra, R. N.; Das, P. K. *J. Phys. Chem. C* **2008**, *112*, 8159–8166.
- (393) Li, Y.; Li, B. Z.; Fu, Y. T.; Lin, S. W.; Yang, Y. G. *Langmuir* **2013**, *29*, 9721–9726.
- (394) Qin, S. Y.; Xu, S. S.; Zhuo, R. X.; Zhang, X. Z. *Langmuir* **2012**, *28*, 2083–2090.
- (395) Yelamaggad, C. V.; Shanker, G.; Rao, R. V. R.; Rao, D. S. S.; Prasad, S. K.; Babu, V. V. S. *Chem.-Eur. J.* **2008**, *14*, 10462–10471.
- (396) Gizzi, P.; Pasc, A.; Dupuy, N.; Parant, S.; Henry, B.; Gerardin, C. *Eur. J. Org. Chem.* **2009**, *2009*, 3953–3963.
- (397) Pasc, A.; Gizzi, P.; Dupuy, N.; Parant, S.; Ghanbaja, J.; Gerardin, C. *Tetrahedron Lett.* **2009**, *50*, 6183–6186.
- (398) Fu, X. J.; Zhang, H.; Zhou, S. K.; Liu, S. B.; Guo, F. Q.; Wang, H.; Yang, Y. J. *Helv. Chim. Acta* **2010**, *93*, 158–168.
- (399) Mitra, R. N.; Das, D.; Roy, S.; Das, P. K. *J. Phys. Chem. B* **2007**, *111*, 14107–14113.
- (400) Otsuka, T.; Maeda, T.; Hotta, A. *J. Phys. Chem. B* **2014**, *118*, 11537–11545.
- (401) Shundo, A.; Hoshino, Y.; Higuchi, T.; Matsumoto, Y.; Penaloza, D. P.; Matsumoto, K.; Ohno, M.; Miyaji, K.; Goto, M.; Tanaka, K. *RSC Adv.* **2014**, *4*, 36097–36100.
- (402) Pal, A.; Shrivastava, S.; Dey, J. *Chem. Commun.* **2009**, 6997–6999.
- (403) Pasc, A.; Akong, F. O.; Cosgun, S.; Gerardin, C. *Beilstein J. Org. Chem.* **2010**, *6*, 973–977.
- (404) Stendahl, J. C.; Rao, M. S.; Guler, M. O.; Stupp, S. I. *Adv. Funct. Mater.* **2006**, *16*, 499–508.
- (405) Behanna, H. A.; Donners, J.; Gordon, A. C.; Stupp, S. I. *J. Am. Chem. Soc.* **2005**, *127*, 1193–1200.
- (406) Bai, S.; Pappas, C.; Debnath, S.; Frederix, P. W. J. M.; Leckie, J.; Fleming, S.; Ulijn, R. V. *ACS Nano* **2014**, *8*, 7005–7013.
- (407) Nakayama, T.; Sakuraba, T.; Tomita, S.; Kaneko, A.; Takai, E.; Shiraki, K.; Tashiro, K.; Ishii, N.; Hasegawa, Y.; Yamada, Y., et al. *Asian J. Org. Chem.* **2014**, *3*, 1182–1188.
- (408) Chen, L.; McDonald, T. O.; Adams, D. J. *RSC Adv.* **2013**, *3*, 8714–8720.
- (409) Wall, B. D.; Tovar, J. D. *Pure Appl. Chem.* **2012**, *84*, 1039–1045.
- (410) Li, R.; Horgan, C. C.; Long, B.; Rodriguez, A. L.; Mather, L.; Barrow, C. J.; Nisbet, D. R.; Williams, R. J. *RSC Adv.* **2015**, *5*, 301–307.
- (411) Shi, Y.; Wang, J.; Wang, H.; Hu, Y.; Chen, X.; Yang, Z. *PLoS One* **2014**, *9*, e106968.
- (412) Zou, Y.; Razmkhah, K.; Chmel, N. P.; Hamley, I. W.; Rodger, A. *RSC Adv.* **2013**, *3*, 10854–10858.
- (413) Tang, C.; Ulijn, R. V.; Saiani, A. *Langmuir* **2011**, *27*, 14438–14449.
- (414) Adams, D. J.; Mullen, L. M.; Berta, M.; Chen, L.; Frith, W. J. *Soft Matter* **2010**, *6*, 1971–1980.
- (415) Roy, S.; Javid, N.; Frederix, P. W. J. M.; Lamprou, D. A.; Urquhart, A. J.; Hunt, N. T.; Halling, P. J.; Ulijn, R. V. *Chem.-Eur. J.* **2012**, *18*, 11723–11731.
- (416) Mu, X. J.; Eckes, K. M.; Nguyen, M. M.; Suggs, L. J.; Ren, P. Y. *Biomacromolecules* **2012**, *13*, 3562–3571.

Part B

Bibliographies

- (417) Fleming, S.; Frederix, P. W. J. M.; Sasselli, I. R.; Hunt, N. T.; Ulijn, R. V.; Tuttle, T. *Langmuir* **2013**, *29*, 9510–9515.
- (418) Chen, L.; Raeburn, J.; Sutton, S.; Spiller, D. G.; Williams, J.; Sharp, J. S.; Griffiths, P. C.; Heenan, R. K.; King, S. M.; Paul, A., et al. *Soft Matter* **2011**, *7*, 9721–9727.
- (419) Wang, W. P.; Yang, Z. M.; Patanavanich, S.; Xu, B.; Chau, Y. *Soft Matter* **2008**, *4*, 1617–1620.
- (420) Javid, N.; Roy, S.; Zelzer, M.; Yang, Z. M.; Sefcik, J.; Ulijn, R. V. *Biomacromolecules* **2013**, *14*, 4368–4376.
- (421) Johnson, E. K.; Chen, L.; Kubiak, P. S.; McDonald, S. F.; Adams, D. J.; Cameron, P. J. *Chem. Commun.* **2013**, *49*, 8698–8700.
- (422) Adhikari, B.; Banerjee, A. *Soft Matter* **2011**, *7*, 9259–9266.
- (423) Pappas, C. G.; Abul-Haija, Y. M.; Flack, A.; Frederix, P. W. J. M.; Ulijn, R. V. *Chem. Commun.* **2014**, *50*, 10630–10633.
- (424) Eckes, K. M.; Mu, X.; Ruehle, M. A.; Ren, P.; Suggs, L. J. *Langmuir* **2014**, *30*, 5287–5296.
- (425) Dudukovic, N. A.; Zukoski, C. F. *Soft Matter* **2014**, *10*, 7849–7856.
- (426) Smith, A. M.; Williams, R. J.; Tang, C.; Coppo, P.; Collins, R. F.; Turner, M. L.; Saiani, A.; Ulijn, R. V. *Adv. Mater.* **2008**, *20*, 37–41.
- (427) Helen, W.; de Leonardis, P.; Ulijn, R. V.; Gough, J.; Tirelli, N. *Soft Matter* **2011**, *7*, 1732–1740.
- (428) Truong, W. T.; Su, Y.; Gloria, D.; Braet, F.; Thordarson, P. *Biomater. Sci.* **2015**, *3*, 298–307.
- (429) Tang, C.; Smith, A. M.; Collins, R. F.; Ulijn, R. V.; Saiani, A. *Langmuir* **2009**, *25*, 9447–9453.
- (430) Kim, J. H.; Nam, D. H.; Lee, Y. W.; Nam, Y. S.; Park, C. B. *Small* **2013**, *10*, 1272–1277.
- (431) Raeburn, J.; Mendoza-Cuenca, C.; Cattoz, B. N.; Little, M. A.; Terry, A. E.; Cardoso, A. Z.; Griffiths, P. C.; Adams, D. J. *Soft Matter* **2015**, *11*, 927–935.
- (432) Milli, L.; Castellucci, N.; Tomasini, C. *Eur. J. Org. Chem.* **2014**, *2014*, 5954–5961.
- (433) Lopez-Perez, D. E.; Revilla-Lopez, G.; Hamley, I. W.; Aleman, C. *Soft Matter* **2013**, *9*, 11021–11032.
- (434) Ou, C. W.; Zhang, J. W.; Zhang, X. L.; Yang, Z. M.; Chen, M. S. *Chem. Commun.* **2013**, *49*, 1853–1855.
- (435) Rodriguez, A. L.; Parish, C. L.; Nisbet, D. R.; Williams, R. J. *Soft Matter* **2013**, *9*, 3915–3919.
- (436) Kuang, Y.; Gao, Y.; Shi, J.; Lin, H.-C.; Xu, B. *Chem. Commun.* **2011**, *47*, 8772–8774.
- (437) Williams, R. J.; Gardiner, J.; Sorensen, A. B.; Marchesan, S.; Mulder, R. J.; McLean, K. M.; Hartley, P. G. *Aust. J. Chem.* **2013**, *66*, 572–578.
- (438) Toledano, S.; Williams, R. J.; Jayawarna, V.; Ulijn, R. V. *J. Am. Chem. Soc.* **2006**, *128*, 1070–1071.
- (439) Hughes, M.; Frederix, P. W. J. M.; Raeburn, J.; Birchall, L. S.; Sadownik, J.; Coomer, F. C.; Lin, I. H.; Cussen, E. J.; Hunt, N. T.; Tuttle, T., et al. *Soft Matter* **2012**, *8*, 5595–5602.
- (440) Sadownik, J. W.; Ulijn, R. V. *Chem. Commun.* **2010**, *46*, 3481–3483.
- (441) Das, A. K.; Hirst, A. R.; Ulijn, R. V. *Faraday Discuss.* **2009**, *143*, 293–303.
- (442) Cheng, G.; Castelletto, V.; Moulton, C. M.; Newby, G. E.; Hamley, I. W. *Langmuir* **2010**, *26*, 4990–4998.
- (443) Shao, H.; Parquette, J. R. *Chem. Commun.* **2010**, *46*, 4285–4287.
- (444) Raeburn, J.; Alston, B.; Kroeger, J.; McDonald, T. O.; Howse, J. R.; Cameron, P. J.; Adams, D. J. *Mater. Horiz.* **2014**, *1*, 241–246.
- (445) Qin, S.-Y.; Jiang, H.-F.; Peng, M.-Y.; Lei, Q.; Zhuo, R.-X.; Zhang, X.-Z. *Polym. Chem.* **2015**, *6*, 519–524.
- (446) Rasale, D. B.; Maity, I.; Das, A. K. *Chem. Commun.* **2014**, *50*, 11397–11400.
- (447) Yang, Z. M.; Gu, H. W.; Du, J.; Gao, J. H.; Zhang, B.; Zhang, X. X.; Xu, B. *Tetrahedron* **2007**, *63*, 7349–7357.
- (448) Zhang, J.; Ou, C.; Shi, Y.; Wang, L.; Chen, M.; Yang, Z. *Chem. Commun.* **2014**, *50*, 12873–12876.
- (449) Mei, J. J.; Zhang, X. L.; Zhu, M. F.; Wang, J. N.; Wang, L.; Wang, L. Y. *RSC Adv.* **2014**, *4*, 1193–1196.

Part B

Bibliographies

- (450) Jones, S. L.; Wong, K. H.; Thordarson, P.; Ladouceur, F. *J. Phys-condens. Mater.* **2010**, *22*, 1-7.
- (451) Bhattacharjee, S.; Bhattacharya, S. *J. Mater. Chem. A* **2014**, *2*, 17889–17898.
- (452) Ma, M.; Kuang, Y.; Gao, Y.; Zhang, Y.; Gao, P.; Xu, B. *J. Am. Chem. Soc.* **2010**, *132*, 2719-2728.
- (453) Doran, T. M.; Ryan, D. M.; Nilsson, B. L. *Polym. Chem.* **2014**, *5*, 241–248.
- (454) Huang, Y. C.; Qiu, Z. J.; Xu, Y. M.; Shi, J. F.; Lin, H. K.; Zhang, Y. *Org. Biomol. Chem.* **2011**, *9*, 2149–2155.
- (455) Seliktar, D. *Science* **2012**, *336*, 1124–1128.
- (456) Ogawa, Y.; Yoshiyama, C.; Kitaoka, T. *Langmuir* **2012**, *28*, 4404–4412.
- (457) Lee, S.; Oh, S.; Lee, J.; Malpani, Y.; Jung, Y. S.; Kang, B.; Lee, J. Y.; Ozasa, K.; Isoshima, T.; Lee, S. Y. *Langmuir* **2013**, *29*, 5869–5877.
- (458) Lin, Y. Y.; Qiao, Y.; Tang, P. F.; Li, Z. B.; Huang, J. B. *Soft Matter* **2011**, *7*, 2762–2769.
- (459) Chen, C. S.; Xu, X. D.; Li, S. Y.; Zhuo, R. X.; Zhang, X. Z. *Nanoscale* **2013**, *5*, 6270–6274.
- (460) Bai, S.; Debnath, S.; Javid, N.; Frederix, P. W. J. M.; Fleming, S.; Pappas, C.; Ulijn, R. V. *Langmuir* **2014**, *30*, 7576–7584.
- (461) Sanders, A. M.; Dawidczyk, T. J.; Katz, H. E.; Tovar, J. D. *ACS Macro Lett.* **2012**, *1*, 1326–1329.
- (462) Wall, B. D.; Diegelmann, S. R.; Zhang, S. M.; Dawidczyk, T. J.; Wilson, W. L.; Katz, H. E.; Mao, H. Q.; Tovar, J. D. *Adv. Mater.* **2011**, *23*, 5009–5014.
- (463) Araki, K.; Yoshikawa, I.; Fages, F., Ed.: Springer: Berlin, **2005**; Vol. 256.
- (464) Serpell, C. J.; Barlog, M.; Basu, K.; Fakhoury, J. F.; Bazzi, H. S.; Sleiman, H. F. *Mater. Horiz.* **2014**, *1*, 348–354.
- (465) Yu, Z. X.; Bai, B. L.; Wang, H. T.; Ran, X.; Jin, G. B.; Sun, J.; Zhao, C. X.; Li, M. *Mater. Sci. Eng. C* **2011**, *31*, 880–884.
- (466) Adhikari, B.; Shah, A.; Kraatz, H.-B. *J. Mater. Chem. B* **2014**, *2*, 4802–4810.
- (467) Yuan, D.; Du, X.; Shi, J.; Zhou, N.; Zhou, J.; Xu, B. *Angew. Chem., Int. Ed.* **2015**, *54*, 5705–5708.
- (468) Srivastava, A.; Ghorai, S.; Bhattacharjya, A.; Bhattacharya, S. *J. Org. Chem.* **2005**, *70*, 6574–6582.
- (469) Birchall, L. S.; Roy, S.; Jayawarna, V.; Hughes, M.; Irvine, E.; Okorogheye, G. T.; Saudi, N.; De Santis, E.; Tuttle, T.; Edwards, A. A., et al. *Chem. Sci.* **2011**, *2*, 1349–1355.
- (470) Bhuniya, S.; Kim, B. H. *Chem. Commun.* **2006**, 1842-1844.
- (471) Clemente, M. J.; Fitremann, J.; Mauzac, M.; Serrano, J. L.; Oriol, L. *Langmuir* **2011**, *27*, 15236–15247.
- (472) Clemente, M. J.; Romero, P.; Serrano, J. L.; Fitremann, J.; Oriol, L. *Chem. Mater.* **2012**, *24*, 3847–3858.
- (473) Clemente, M. J.; Tejedor, R. M.; Romero, P.; Fitremann, J.; Oriol, L. *RSC Adv.* **2012**, *2*, 11419–11431.
- (474) Ibrahim, M. I. A.; Zhou, Z.; Deng, C.; Didierjean, C.; Vanderesse, R.; Bodiguel, J.; Averlant-Petit, M.-C.; Jamart-Grégoire, B. Impact of C^α-Chirality on Supramolecular Self-Assembly in Cyclo-2:1-[α /aza]-Hexamers (*D*/*L*-Phe-azaPhe-Ala)₂. *Eur. J. Org. Chem.* **2017**, 4703-4712.
- (475) Atwood, J. L.; Steed, J. W. Organic Nanostructures. *Wiley-VCH, Weinheim* **2008**, 111-154.
- (476) Chen, Y. Y.; Wang, H.; Zhang, D. W.; Hou, J. L.; Li, Z. T. *Chem. Commun.* **2015**, *51*, 12088-12091.
- (477) Ishi-i, T.; Shinkai, S. *Top. Curr. Chem.* **2005**, *258*, 119–160.
- (478) Melendez, R. E.; Carr, A. J.; Linton, B. R.; Hamilton, A. D. *Struct. Bonding (Berlin, Ger.)* **2000**, *96*, 31–61.
- (479) Housecroft, C. E.; Sharpe, A. G. *Inorganic Chemistry, 3rd ed.; Pearson Prentice Hall: New York* **2008**, 69-70.
- (480) Lee, H. J.; Park, H. M.; Lee, K. B. *Biophys. Chem.* **2007**, *125*, 117-126.
- (481) Thormann, M.; Hofmann, H. J. *J. Mol. Struct. (Theochem)* **1999**, *469*, 63-76.
- (482) Zhou, Z.; Deng, C.; Abbas, C.; Didierjean, C.; Averlant-Petit, M. C.; Bodiguel, J.; Vanderesse, R.; Jamart-Gregoire, B. *Eur. J. Org. Chem.* **2014**, 7643-7650.

Part B

Bibliographies

- (483) Cassin, G.; de Costa, C.; van Duynhoven, J. P. M.; Agterof, W. G. M. *Langmuir* **1998**, *14*, 5757–5763.
- (484) Sakurai, K.; Jeong, Y.; Koumoto, K.; Friggeri, A.; Gronwald, O.; Sakurai, S.; Okamoto, S.; Inoue, K.; Shinkai, S. *Langmuir* **2003**, *19*, 8211–8217.
- (485) Wang, R.; Geiger, C.; Chen, L.; Swanson, B.; Whitten, D. G. *J. Am. Chem. Soc.* **2000**, *122*, 2399–2400.
- (486) Escuder, B.; LLusar, M.; Miravet, J. F. *J. Org. Chem.* **2006**, *71*, 7747–7752.
- (487) Hirst, A. R.; Coates, I. A.; Boucheteau, T. R.; Miravet, J. F.; Escuder, B.; Castelletto, V.; Hamley, I. W.; Smith, D. K. *J. Am. Chem. Soc.* **2008**, *130*, 9113–9121.
- (488) Huang, B.; Hirst, A. R.; Smith, D. K.; Castelletto, V.; Hamley, I. W. *J. Am. Chem. Soc.* **2005**, *127*, 7130–7139.
- (489) Kral, V.; Pataridis, S.; Setnicka, V.; Zaruba, K.; Urbanova, M.; Volka, K. *Tetrahedron* **2005**, *61*, 5499–5506.
- (490) Sureshan, K. M.; Yamaguchi, K.; Sei, Y.; Watanabe, Y. *Eur. J. Org. Chem.* **2004**, 4703–4709.
- (491) Sebastien, D.; Jacques, B.; Axelle, A.; Brigitte, J. G. *Tetrahedron* **2012**, *68*, 4362–4367.
- (492) Nikolic, A. D.; Kobilarov, N. L.; Brzic, A. N. *J. Mol. Struct.* **1983**, *99*, 179–188.
- (493) Nikolic, A. D.; Tarjani, M.; Perisic-Janjic, N.; Petrovic, S. D. *J. Mol. Struct.* **1988**, *174*, 129–134.
- (494) George, M.; Weiss, R. G. *J. Am. Chem. Soc.* **2001**, *123*, 10393–10394.
- (495) Smith, A. M.; Turner, R. M. L.; Saianiand, A.; Ulijn, R. V. *Adv. Mater.* **2008**, *20*, 37–41.
- (496) Yang, Z.; Liang, G.; Xu, B. *Chem. Commun.* **2006**, 738–740.
- (497) Menger, F. M.; Peresyppkin, A. V. *J. Am. Chem. Soc.* **2003**, *125*, 5340–5345.
- (498) Mandal, S. K.; Kar, T.; Das, D.; Das, P. K. *Chem. Commun.* **2012**, *48*, 1814–1816.
- (499) Bhattacharya, S.; Srivastava, A.; Pal, A. *Angew. Chem., Int. Ed.* **2006**, *45*, 2934–2937.
- (500) Basak, S.; Nanda, J.; Banerjee, A. *J. Mater. Chem.* **2012**, *22*, 11658–11664.
- (501) Mukherjee, S.; Mukhopadhyay, B. *RSC Adv.* **2012**, *2*, 2270–2273.
- (502) Trivedi, D. R.; Dastidar, P. *Chem. Mater.* **2006**, *18*, 1470–1478.
- (503) Zhang, T.; Wu, Y.; Gao, L.; Song, Z.; Zhao, L.; Zhang, Y.; Tao, J. *Soft Matter* **2013**, *9*, 638–641.
- (504) Huertas, M. J.; Duque, E.; Molina, L.; Rossello-Mora, R.; Mosqueda, G.; Godoy, P.; Christensen, B.; Molin, S.; Ramos, J. L. *Environ. Sci. Technol.* **2000**, *34*, 3395.
- (505) Peng, J.; Liu, K.; Liu, X.; Xia, H.; Liu, J.; Fang, Y. *New J. Chem.* **2008**, *32*, 2218–2224.
- (506) Debnath, S.; Shome, A.; Dutta, S.; Das, P. K. *Chem.-Eur. J.* **2008**, *14*, 6870–6881.
- (507) Rogers, M. A.; Kim, J. H. *J. Food Res. Int.* **2011**, *44*, 1447–1451.
- (508) Sathaye, S.; Mbi, A.; Sonmez, C.; Chen, Y. C.; Blair, D. L.; Schneider, J. P.; Pochan, D. J. *Wiley Interdiscip. Rev. Nanomed. Nanobiotechnol.* **2015**, *7*, 34–68.
- (509) Abbas, C.; Pickaert, G.; Didierjean, C.; Gregoire, B. J.; Vanderesse, R. *Tetrahedron Lett.* **2009**, *50*, 4158–4160.
- (510) Ten Kortenaar, P. B. W.; Vandijk, B. G.; Peeters, J. M.; Raaben, B. J.; Adams, P. J. H. M.; Tesser, G. I. *Int. J. Pept. Protein Res.* **1986**, *27*, 398–400.
- (511) Horne, W. S.; Stout, C. D.; Ghadiri, M. R. *J. Am. Chem. Soc.* **2003**, *125*, 9372–9376.
- (512) Némethy, G.; Scheraga, H. A. *Biochem. Biophys. Res. Commun.* **1980**, *95*, 320–327.
- (513) Mantsch, H. H.; Perczel, A.; Hollósi, M.; Fasman, G. D. *Biopolymers* **1993**, *33*, 201–207.
- (514) Montenegro, J.; Ghadiri, M. R.; Granja, J. R. *Acc. Chem. Res.* **2013**, *46*, 2955–2965.
- (515) Karle, I. L.; Handa, B. K.; Hassall, C. H. *Acta Crystallogr., Sect. B* **1975**, *31*, 555–560.
- (516) Rosenthal-Aizman, K.; Svensson, G.; Unden, A. *J. Am. Chem. Soc.* **2004**, *126*, 3372–3373.
- (517) Ghadiri, M. R.; Granja, J. R.; Milligan, R. A.; McRee, D. E.; Khazanovich, N. *Nature* **1993**, *366*, 324–327.
- (518) Thomas, D. C.; Lukas, K. B.; Ghadiri, M. R. *J. Am. Chem. Soc.* **1998**, *20*, 651–656.
- (519) André, F.; Vicherat, A.; Boussard, G.; Aubry, A.; Marraud, M. *J. Pept. Res.* **1997**, *50*, 372–381.
- (520) Vass, E.; Kurz, M.; Konat, R. K.; Hollósi, M. *Spectrochim. Acta. A. Mol. Biomol. Spectrosc.* **1998**, 773–786.
- (521) Pearlman, D. A.; Case, D. A.; Caldwell, J. W.; Ross, W. S.; Cheatham, T. E.; DeBolt, S.; Ferguson, D.; Seibel, G.; Kollman, P. *Comp. Phys. Commun.* **1995**, *19*, 1–41.
-

Part B

Bibliographies

- (522) Case, D. A.; Cheatham, T.; Darden, T.; Gohlke, H.; Luo, R.; Merz, K. M. J.; Onufriev, A.; Simmerling, C.; Wang, B. J. *Computat. Chem.* **2005**, *26*, 1668-1688.
- (523) Bhuniya, S.; Park, S. M.; Kim, B. H. *Org. Lett.* **2005**, *7*, 1741-1744.
- (524) Kitagawa, T. *Prog. Biophys. Mol. Biol.* **1992**, *58*, 1-18.
- (525) Schmid, F. X. Macromolecular interactions: UV-visible spectrophotometry, in Encyclopedia of Life Sciences. *Nature* **2001**, Publishing, London, U.K.
- (526) Yang, Z.; Gu, H.; Zhang, Y.; Wang, L.; Xu, B. *Chem. Commun.* **2004**, 208-209.
- (527) Kang, H. K.; Kang, D. E.; Boo, B. H.; Yoo, S. J.; Lee, J. K.; Lim, E. C. *J. Phys. Chem. A* **2005**, *109*, 6799-6804.
- (528) Jayawarna, V.; Ali, M.; Jowitt, T. A.; Miller, A. E.; Saiani, A.; Gough, J. E.; Ulijn, R. V. *Adv. Mater.* **2006**, *18*, 611-614.
- (529) Luo, J.; Tong, Y. W. *ACS Nano* **2011**, *5*, 7739-7747.
- (530) Duan, P.; Qin, L.; Zhu, X.; Liu, M. *Chem.-Eur. J.* **2011**, *17*, 6389-6395.
- (531) Cao, H.; Jiang, J.; Zhu, X.; Duan, P.; Liu, M. *Soft Matter* **2011**, *7*, 4654-4660.
- (532) Zhu, X.; Li, Y.; Duan, P.; Liu, M. *Chem.-Eur. J.* **2010**, *16*, 8034-8040.
- (533) Bose, P. P.; Das, A. K.; Hegde, R. P.; Shamala, N.; Banerjee, A. *Chem. Mater.* **2007**, *19*, 6150-6157.
- (534) Haines, L. A.; Rajagopal, K.; Ozbas, B.; Salick, D. A.; Pochan, D. J.; Schneider, J. P. *J. Am. Chem. Soc.* **2005**, *127*, 17025-17029.
- (535) Keller, D.; Bustamante, C. *J. Chem. Phys.* **1986**, *84*, 2972-2980.
- (536) Adler-Abramovich, L.; Perry, R.; Sagi, A.; Gazit, E.; Shabat, D. *Chem. Bio. Chem.* **2007**, *8*, 859-862.
- (537) Williams, R. J.; Smith, A. M.; Collins, R. F.; Hodson, N.; Das, A. K.; Ulijn, R. V. *Nat. Nanotechnol.* **2009**, *4*, 19-24.
- (538) Chen, L.; Revel, S.; Morris, K.; Serpell, L. C.; Adams, D. J. *Langmuir* **2010**, *26*, 13466-13471.
- (539) Hirst, A. R.; Roy, S.; Arora, M.; Das, A. K.; Hodson, N.; Murray, P.; Marshall, S.; Javid, N.; Sefcik, J.; Boekhoven, J.; van Esch, J.; Santabarbara, S.; Ulijn, R. V. *Nat. Chem.* **2010**, *2*, 1089-1094.
- (540) Pochan, D. J.; Schneider, J. P.; Kretsinger, J.; Ozbas, B.; Rajagopal, K.; Haines, L. *J. Am. Chem. Soc.* **2003**, *125*, 11802-11803.
- (541) Woody, R. W.: Circular dichroism of peptides and proteins, in Circular Dichroism. Principles and Applications. Nakanishi, K., Berova, N., Woody, R. W., Eds.: VCH, New York, 1994; pp 473-496.
- (542) Gupta, M.; Bagaria, A.; Mishra, A.; Mathur, P.; Basu, A.; Ramakumar, S.; Chauhan, V. S. *Adv. Mater.* **2007**, *19*, 858-861.
- (543) Gazit, E. *FASEB J.* **2002**, *16*, 77-83.
- (544) Wang, K.; Keasling, J. D.; Muller, S. J. *Int. J. Biol. Macromol.* **2005**, *36*, 232-240.
- (545) Manavalan, P.; Johnson, W. C. *Nature* **1983**, *305*, 831-832.
- (546) Sreerama, N.; Woody, R. W.: Circular Dichroism: Principles and Applications. Wiley-VCH, Weinheim, Germany, 2000.
- (547) Zhang, Y.; Gu, H.; Yang, Z.; Xu, B. *J. Am. Chem. Soc.* **2003**, *125*, 13680-13681.
- (548) Roy, S.; Javid, N.; Sefcik, J.; Halling, P. J.; Ulijn, R. V. *Langmuir* **2012**, *28*, 16664-16670.
- (549) Gottarelli, G.; Lena, S.; Masiero, S.; Pieraccini, S.; Spada, G. P. *Chirality* **2008**, *20*, 471.
- (550) Jung, J. H.; Ono, Y.; Yoo, J. S.; Shinkai, S. *Chem.-Eur. J.* **2000**, *6*, 4552-4557.
- (551) Kawano, S.-I.; Tamaru, S.-I.; Fujita, N.; Shinkai, S. *Chem.-Eur. J.* **2004**, *10*, 343-351.
- (552) Kawano, S.-I.; Fujita, N.; Shinkai, S. *Chem.-Eur. J.* **2005**, *11*, 4735-4742.
- (553) Friggeri, A.; van der Pol, C.; van Bommel, K. J. C.; Heeres, A.; Stuart, M. C. A.; Feringa, B. L.; van Esch, J. *Chem.-Eur. J.* **2005**, *11*, 5353-5361.
- (554) Das, D.; Dasgupta, A.; Roy, S.; Mitra, R. N.; Debnath, S.; Das, P. K. *Chem.-Eur. J.* **2006**, *12*, 5068-5074.
- (555) Weiss, R. G.; Terech, P.: Molecular Gels. Materials with Self-Assembled Fibrillar Networks. Springer, Dordrecht, 2005.
- (556) Ghosh, S.; Li, X.-Q.; Stepanenko, V.; Würthner, F. *Chem.-Eur. J.* **2008**, *14*, 11343-11357.
- (557) Susi, H.; Byler, D. M. *Arch. Biochem. Biophys.* **1987**, *258*, 465-469.
- (558) Haris, P.; Chapman, D. *Biopolymers* **1995**, *37*, 251-263.
- (559) Stuart, B. Biological Applications of Infrared Spectroscopy. Wiley, Chichester, U.K. **1997**.
-

Part B

Bibliographies

- (560) Jackson, M.; Mantsch, H. H. *Crit. Rev. Biochem. Mol. Biol.* **1995**, *30*, 95-120.
- (561) Pelton, J. T.; McLean, L. R. *Anal. Biochem.* **2000**, *277*, 167-176.
- (562) Surewicz, W. K.; Mantsch, H. H. *Biochem. Biophys. Acta* **1998**, *952*, 115-130.
- (563) Barth, A.; Zscherp, C. *Q. Rev. Biophys.* **2002**, *35*, 369-430.
- (564) Chou, P. Y.; Fasman, G. D. *Trends Biochem. Sci.* **1977**, *2*, 128-131.
- (565) Xin, X.; Xu, G.; Gong, H.; Bai, Y.; Tan, Y. *Colloids Surf.* **2008**, *326*, 1-9.
- (566) Xu, L.; Xu, G.; Liu, T.; Chen, Y.; Gong, H. *Carbohydr. Polym.* **2013**, *92*, 516-522.
- (567) Srinivasan, S.; Babu, S. S.; Praveen, V. K.; Ajayaghosh, A. *Angew. Chem., Int. Ed.* **2008**, *47*, 5746-5749.
- (568) Pal, A.; Srivastava, A.; Bhattacharya, S. *Chem.-Eur. J.* **2009**, *15*, 9169-9182.
- (569) Sangeetha, N. M.; Bhat, S.; Raffy, G.; Belin, C.; Loppinet-Serani, A.; Aymonier, C.; Terech, P.; Maitra, U.; Desvergne, J.-P.; Guerso, A. D. *Chem. Mater.* **2009**, *21*, 3424-3432.
- (570) Palui, G.; Garai, A.; Nanda, J.; Nandi, A. K.; Banerjee, A. *J. Phys. Chem. B* **2010**, *114*, 1249-1256.
- (571) Roy, B.; Saha, A.; Esterrani, A.; Nandi, A. K. *Soft Matter* **2010**, *6*, 3337-3345.
- (572) Piepenbrock, M.-O. M.; Clarke, N.; Steed, J. W. *Soft Matter* **2011**, *7*, 2412-2418.
- (573) Raeburn, J.; Pont, G.; Chen, L.; Cesbron, Y.; Levy, R.; Adams, D. J. *Soft Matter* **2012**, *8*, 1168-1174.

Part C
Applications Based on 2:1-[α /aza]-Oligomers

Chapter VIII. Evaluation of the 2:1-[α /aza]- Oligomers in Two Potential applications

VIII.1. General Introduction

In this chapter, we summarize the preliminary results of the role of 2:1-[α /aza]-oligomers in two different environmental applications. While the first has concerned with testing different azapeptides in CO₂/N₂ gases separation upon incorporating them in commercial polymeric Pebax[®] membrane. The second was to evaluate the potential of the heterochiral cyclo-(D-Phe-azaPhe-Ala)₂-hexamer in water treatment through phase selective gelation (PSG) process.

VIII.2. Gases Separation

VIII.2.1. Introduction

We have investigated the use of our pseudopeptides as additives in the CO₂ membrane separation. In the literature, pseudopeptides showed preliminary promising results in this application.¹ The interest of the pseudopeptides particularly “azapeptides-based-lysine residues” comes from their amine-based nature which is well-known to be efficient for CO₂ separation.²⁻⁵ The evaluation of the CO₂ separation performances of the membranes containing pseudopeptide additives allowed to establish pseudopeptides nature-structure-performances relationships.

“Time lag” experiments were performed to characterize the membrane properties during the permeation of pure gases of CO₂, N₂ and CH₄ based on the solution-diffusion model.⁶ This model describes gas transport through dense polymer membranes in two main steps: (i) sorption of the gas molecules, and (ii) diffusion through the bulk. Desorption of the gas molecules at the membrane downstream side is usually considered as very rapid and non-limiting for the overall mass transfer. The sorption, accounting for the gas affinity for the membrane, is represented by S (sorption coefficient, in cm³(STP).cm⁻³. cmHg⁻¹). The diffusion, describing the mobility of gas through FFV (free fraction volume), is represented by D (diffusion coefficient, in cm². s⁻¹). The global separation performance is characterized by P (permeability, in Barrer = 10⁻¹⁰ cm³(STP).cm⁻¹.cmHg⁻¹. s⁻¹) and ideal selectivity $\alpha_{A/B}$ (for the permeation of pure gases A and B) according to equations (1) and (2).

$$P = D \times S \quad (1)$$

$$\alpha_{A/B} = \frac{P_A}{P_B} \quad (2)$$

Initially introduced by Daynes (1920),⁷ the “time lag” method is an “integral permeation method” based on continuous monitoring of the amount of gas crossing the membrane into a closed downstream vessel allowing direct determination of P and D and further deduction of S value by equation (2). The permeability coefficient P was calculated during the steady state by equation (3) assuming $p_{\text{upstream}} \gg p_{\text{downstream}}$

$$P = \frac{J_{st} \times l}{p_{\text{upstream}}} \quad (3)$$

where l is the sample thickness and J_{st} is the steady-state gas flux obtained from the slope of the steady-state part of the gas permeation curve. The time-lag diffusion coefficient D was calculated from the time-lag θ given by the intercept of the steady-state asymptote on the time axis by equation (4).

$$D = \frac{l^2}{6\theta} \quad (4)$$

In calculation, the diffusion coefficient was assumed to be time- and concentration-independent in the transient diffusion process, which is usually assumed for the diffusion of permanent

Part C

Chapter VIII. Evaluation of 2:1-[α /aza]-Oligomers in Two Potential Applications

gases through dense polymer membranes (because of relatively low sorption). The solubility coefficient S was then deduced by the ratio of the permeability P to the diffusion coefficient D by equation (1).

In order to assess the reproducibility of the data obtained for each gas, five measurements were carried out per gas and membrane sample. Two pure gases from MESSER Company were used for the gas permeation tests with the following commercial references CO₂ 4.5 and N₂ 5.0.

VIII.2.2. Results and Discussion

Seven azapeptides (**6b**, **6b'**, **7a**, **7c**, **7c'**, **8c**, and **8c'**) of the 2:1-[α /aza]-series have been tested for gases separation. The choice of the pseudopeptides was based on studying the effect of chain length and nature of the side chain (Table 8.1).

Table 8.1. Description of the 2:1-[α /aza]-oligomers tested for gases separation

Azapeptide	Description
6b	Dimer containing one protected Lys residue
*6b'	Deprotected dimer has one free Lys side-chain
7a	Trimer with Phe and Ala residues
7c	Trimer with two protected Lys residues
*7c'	Deprotected trimer has two free Lys side-chains
8c	Hexamer with four protected Lys residues
*8c'	Deprotected hexamer has four free Lys side-chains

*Deprotected azapeptides **6b'**, **7c'** and **8c'** have obtained from the corresponding protected analogs by catalytic hydrogenolysis (See Experimental Section).

Two strategies have been followed in preparation of membranes for testing gases separation including chemical and direct mixing pathways (Figure 8.1 and Scheme 8.1).

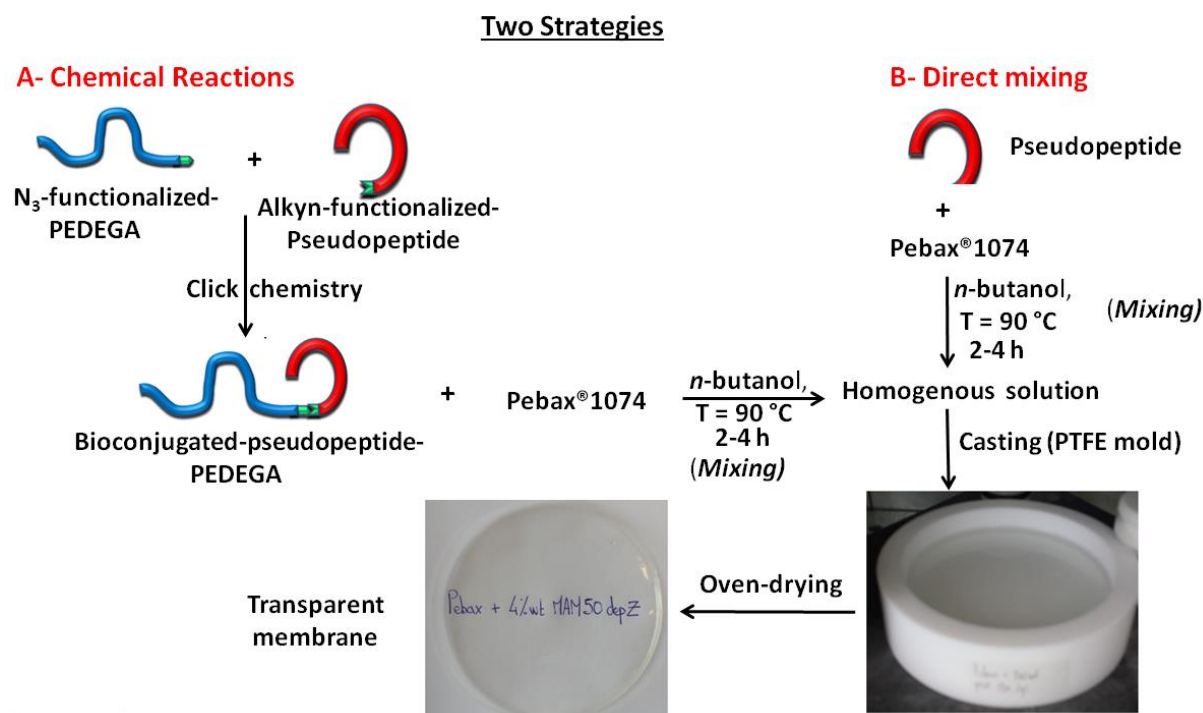


Figure 8.1. Representation of the two pathways followed in preparation of Pebax[®]-pseudopeptide membranes.

Part C

Chapter VIII. Evaluation of 2:1-[α /aza]-Oligomers in Two Potential Applications

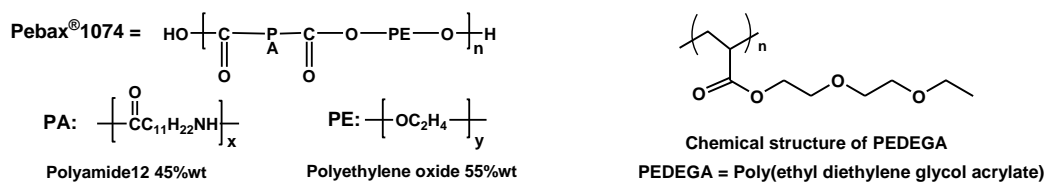
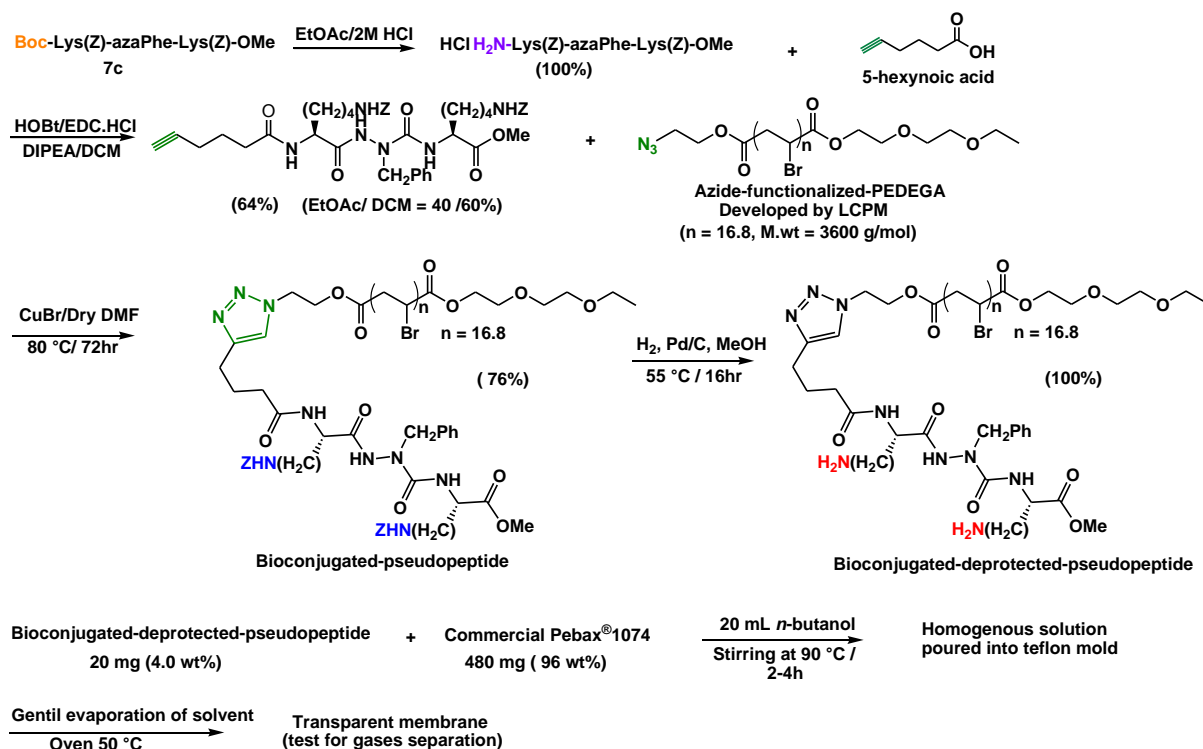
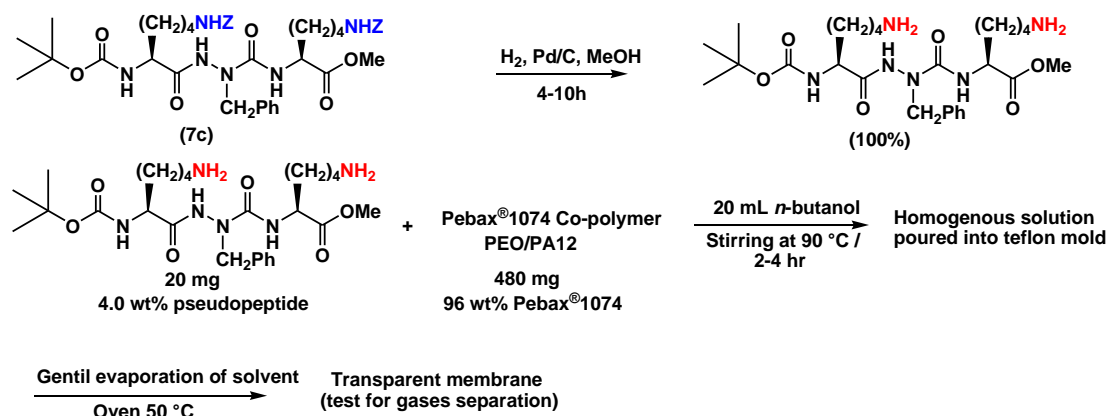


Figure 8.2. Chemical structures of the Pebax[®] co-polymer, and the PEDEGA polymer.

A- Chemical pathway:



B- Direct mixing:



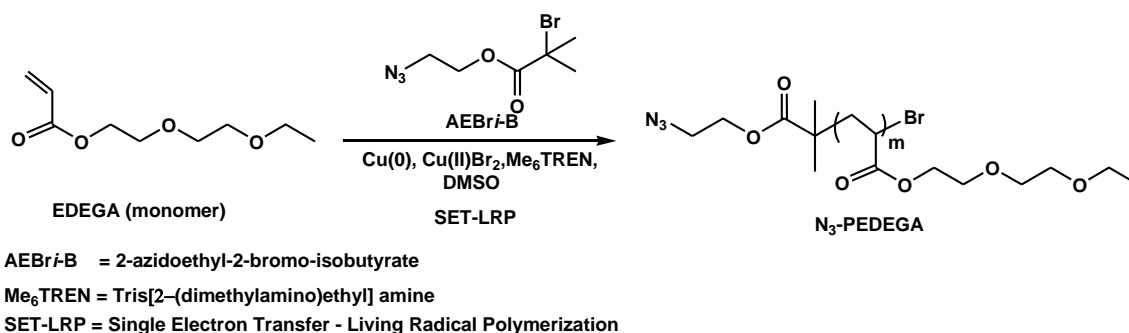
Scheme 8.1. Example for the preparation of Pebax[®]1074 membrane with an additive of azapeptide trimer (7c') after deprotection of the Z-groups using: (A) chemical pathway, and (B) direct mixing method.

We found that both strategies resulted in membranes with close behaviors in gases separation, so we continued our evaluations using the direct mixing method.

Part C

Chapter VIII. Evaluation of 2:1-[α /aza]-Oligomers in Two Potential Applications

Note: The azide-functionalized-PEDEGA has been developed by the LCPM polymeric group (Scheme 8.2) through single electron-transfer living radical polymerization (SET-LRP).¹



Scheme 8.2. Synthesis of the azide-functionalized-PEDEGA polymer as described by LCPM polymeric group.¹

The evolution of the CO₂ separation performances of the Pebax[®] in using additives of the chosen various pseudopeptides reflects several trends, Figure 8.3. First, the CO₂ permeability of the membrane strongly increases by deprotected lysine-containing-pseudopeptide (**6b'**, **7c'** and **8c'**). For example, the better enhancement is shown with the permeability of dimer-additive membrane (**6b'**) which increases by more than 20% (from 122 to 148 Barrer). Moreover, by adding deprotected pseudopeptides, the selectivity $\alpha_{\text{CO}_2/\text{N}_2}$ is maintained, overcoming the usual decreasing behavior of permeability *versus* selectivity widely observed in the literature^{8,9} and empirically theorized by Robeson.¹⁰ The release of the primary amine of the pseudopeptides by deprotection has a strong impact on the permeability as noticed by the trend of the deprotected analogs have higher permeability compared to the corresponding protected ones (**6b'** > **6b**, **7c'** > **7c**, and **8c'** > **8c**), Figure 8.3. Indeed, it is well known that free-amines have strong ability to interact with CO₂ and the incorporation of amine-based additives in polymer membrane increases the sorption coefficient $S(\text{CO}_2)$.²⁻⁵

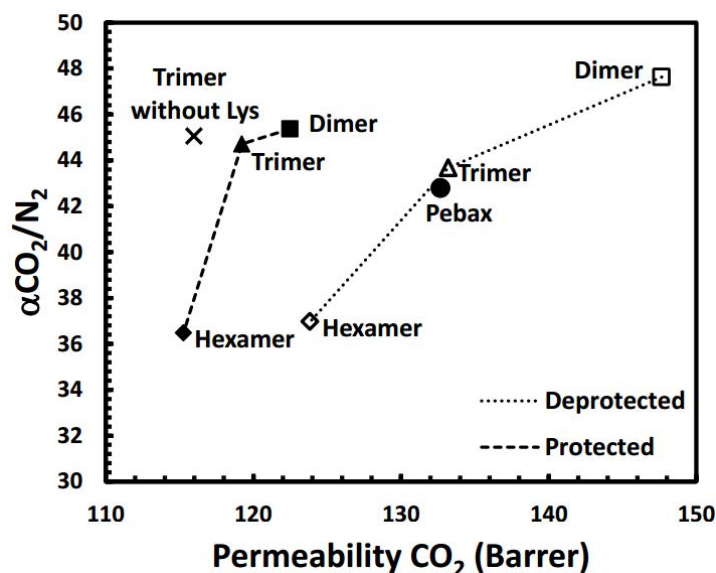


Figure 8.3. Permeability of CO₂ and selectivity $\alpha_{\text{CO}_2/\text{N}_2}$ for different Pebax[®] 1074 membranes with additives of protected and deprotected pseudopeptides dimer, trimer and hexamer, determined by time-lag method.

Secondly, we observed that the performances decreases with increasing the number of amino acid units in the pseudopeptides, *i.e.*, the dimer-based additives (**6b** & **6b'**) have better performances

than the trimer-based (**7c** & **7c'**) and the hexamer-based (**8c** & **8c'**). This trend may be explained as: increasing the chain length of peptide leads to increasing the folding possibility which usually supported by intramolecular hydrogen bonds between the amide groups. This has been confirmed from spectroscopic and molecular dynamic calculations, since several conformations have been investigated when increasing the chain length from 2 to 6 units (dimer > trimer > hexamer). Accordingly, the amine and amide nitrogen atoms in the longer chain (trimer and hexamer) are involved in intramolecular hydrogen bonds and the structures are more folded and have compact conformation compared with the structure of dimer that close to have a linear conformation. In this context, because part of the amine and amide functions are committed in the folding through intramolecular interactions, they are less available to interact with CO₂, resulting in lower performances in gases separation.

The study of the performances of the membranes using additives of trimer **7c** and trimer without lysine **7a** allows us to put evidence on the efficiency of the lysine unit for CO₂ separation. The plotted data illustrates that the membrane with protected lysine-based trimer (**7c**) shows better performance than membrane with non-lysine-based trimer (**7a**). Finally, even if the lysine unit is protected, it has benefits compared to trimer without lysine residue.

VIII.2.3. Conclusions

Different pseudopeptides were used as additives in Pebax[®] reference matrix membrane for CO₂ separation. The evaluation of the performances of the membranes using time lag permeation method, allows establishing pseudopeptides nature-structure-performances relationships. Particularly, the deprotected-lysine oligomers exhibit a great improvement in CO₂ separation, illustrating the strong interactions between CO₂ and free-amine. The conformation of the pseudopeptides has a strong influence on CO₂ separation ability mainly in azapeptides of longer chain length. Moreover, the effective role in incorporating lysine residues was clearly demonstrated by comparing the performances of trimer with and without lysine unit. Finally, the addition of 4.0 wt% of deprotected dimer additive in Pebax[®] allows increasing significantly the performances compared to the pristine Pebax[®] with an increase of more than 10% of the permeability and the selectivity α CO₂/N₂.

VIII.3. Phase Selective Gelation (PSG)

VIII.3.1. Introduction

In recent decades, water pollution has become a serious problem to mankind where the aquatic systems have suffered from several hazardous, mainly the organic contaminants that enter through several oil spill accidents and human activities.¹¹⁻¹⁴ Separation of the oil phase specifically the aromatic components which are very difficult to be decomposed naturally^{15,16} from water is essential because of their toxicity which brings a huge damage to aquatic ecosystems.¹¹ So, there was a great need to develop methods for managing this type of pollution.

In this context, bioremediation is a commonly available process which has used to clean up an oil spill.¹⁷ Chemical treatment has also suggested for oil recovery by using several chemical materials such as dispersants,¹⁸ sorbents,¹⁹⁻²² and solidifiers.²³ Unfortunately, some of these materials are toxic to aquatic life and/or not biodegradable naturally, and in certain cases, the recovery of the oil is really difficult.²⁴ Phase selective gelation (PSG) of organic phase from organic/water mixtures is being considered a promising tool in water purification.^{11,24}

Part C

Chapter VIII. Evaluation of 2:1-[α /aza]-Oligomers in Two Potential Applications

The ideal PSG treatment must fulfill some requirements: (a) the gelator exhibits efficient and selective gelation ability at room temperature, (b) the gelator can be easily synthesized from cheap starting materials, (c) the gel must have high mechanical stability to facilitate the separation of oil and gelator from a biphasic mixture, (d) easy recovery of the oil from the gel phase materials, and (e) the gelator should be recyclable for reuse.^{24,25}

One of the major drawbacks of some PSG described in the literature is the heating-cooling protocol necessary to induce gelation, which makes it impractical for the removal of oil spills due to the high flammability of most oil components (benzene, gasoline, diesel).¹¹ To overcome this problem, many methods have been reported by several research groups to trigger effective phase selective gelation process (PSG) at room temperature by: (a) using a change in the pH of the medium²⁶, (b) mechanical shaking,^{15,27} or sonication,²⁸ (c) addition of slightly pre-warmed concentrated solutions of the suitable gelator to an oil/aqueous mixture,¹¹ and recently phase selective gelation at room temperature can be achieved by (d) addition of pre-dissolved gelator in a co-solvent and it seems to be a practical procedure in real situations for water purification.^{13,24,29-31}

In this regard, Bhattacharya and Ghosh in 2001 reported the first phase selective gelation of oil by an alanine-based amphiphilic gelator in the presence of water.³² Then after, several other groups have reported very interesting LMWGs with PSG ability.^{12,14,27,33-35} John and co-workers recently demonstrated model solidifiers for oil spills by using an ethanolic solution of sugar based gelators in the oil/water mixture at room temperature.²⁵ In addition, sugar based gelators have also been used by Prathap and Sureshan for phase selective gelation by addition of pre-warmed solution of gelator into the biphasic oil/water mixture.³⁰

VIII.3.2. Results and Discussion

In order to demonstrate the potential of gelator **9b** for PSG process, two scenarios were followed as described in the experimental section.¹¹ Interestingly, gelator **9b** was found to be an appropriate molecule for phase selective gelation of several organic solvents including (benzene, toluene, chlorobenzene and *p*-xylene) from an organic/aqueous mixture within 2 minutes due to its: (i) excellent organogelation ability at room temperature, (ii) water insolubility, and (iii) high mechanical rigidity in the gelified organic solvents.

In order to evaluate the potential of **9b** for PSG process for natural polluted water with organic contaminants, comparative experiments using biphasic systems containing pure water and synthetic salty water (NaCl 3.5w/v%) have been done. Gelator **9b** could be triggered at room temperature by adding ethanol as co-solvent to dissolve the gelator before adding to the organic/aqueous mixture (Figures 8.4 and 8.5) or by adding a pre-warmed concentrated solution of the pseudopeptide **9b** in an organic phase to a mixture of the same compositions.

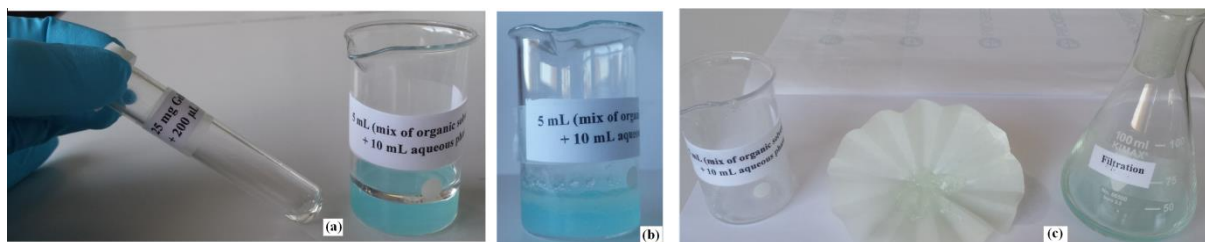


Figure 8.4. PSG by gelator **9b**; (a) addition of the concentrated ethanolic solution of **9b** ($c = 12.5$ w/v%) to organic/aqueous mixture, (b) gelation of the organic phase, and (c) separation of the organogel by filtration.

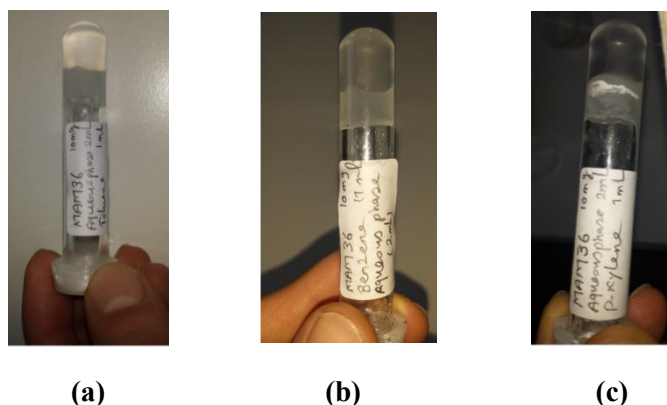


Figure 8.5. PSG by gelator **9b** for individual organic solvent: (a) Toluene, (b) benzene, and (c) *p*-xylene; (c = 0.5 wt% with respect to the organic solvent).

The results showed that gelator **9b** has good gelation ability at low concentration (~ 0.5 wt%) and the PSG by **9b** is independent on ionic strength of the water. Moreover, gelator **9b** has gelled the organic phases efficiently where the organic phases (aromatic solvents) recovered in high percentages after a simple distillation process (77 – 96 %), Table 8.2. The PSG method allowed the recovery and reuse of the gelator. These results led us to suggest that our LMWOG **9b** may be suitable for real use in oil spill recovery in the sea or river if the process can be scaled up.

Table 8.2. % of recovered organic solvent(s) from (water/organic) mixture by **9b** using phase selective gelation (PSG) method

Organic solvent	% Organic solvent recovered
Toluene	96
Benzene	94
<i>p</i> -Xylene	82
Chlorobenzene	77
Mixture	84

VIII.3.3. Conclusions

The low molecular weight organogelator **9b** is suitable for phase selective gelation (PSG) of an organic solvent(s) from (aqueous/organic) mixture with good recovery percent ranging from 77 – 96% which makes it under demand for water purification process if the process can be scaled up.

Subsequently, we can generally conclude from Chapter VIII that 2:1-[α /aza]-oligomers are promising candidates that may be involved in several potential applications if we can successfully functionalize them according to the desired fascinating properties they possess.

VIII.4. Experimental Section

Gases separation

Membrane preparation: For membrane casting, the Pebax[®] 1074 polymer and additives were dissolved in butanol during 2h at 80 °C to obtain a total concentration of 2.5 w/v%. After filtering on glass fibers, the solutions were cast on a PTFE mold. After butanol evaporation in thermal oven at 40 °C, the membranes were easily taken off the mold and were then dried under vacuum at 60 °C for 12h. The thicknesses of the membranes were measured by an Elcometer[™] micrometer after calibration in the thickness range of interest (measurement error: $\pm 1 \mu\text{m}$). The average thickness for the different membranes was *ca.* 80 μm with a maximum thickness difference between two membrane points of 5 μm . Different series of membranes were prepared using a precise concentration of 4.0 wt% for each pseudopeptide.

Synthesis of 6b', 7c' and 8c' by deprotection of Z-group from their protected analogs:

To a stirred solution of an appropriate protected side chain(s) azapeptide (200 mg) in methanol (5.0 mL), 10% Pd/C (X mg)* was added. The resulting reaction mixture was stirred under stream of H₂ gas at room temperature. After completion of the hydrogenolysis (4 – 12h), the mixture was filtered through celite bed and washed with methanol. The combined washings and filtrate were evaporated and then the residue was dried well under vacuum before verification by ¹H NMR in DMSO-*d*₆. The deprotection was considered to be successfully achieved if the signals belong to the CH₂ and the aromatic protons of Z-group disappeared in the ¹H NMR spectrum.

* The amount of Pd/C is dependent of the number of the Z-groups in the azapeptide analog (20 mg for each Z-group). This process has been carried out for the dimer (**6b**), trimer (**7c**) and hexamer (**8c**).

Phase selective gelation (PSG)

Two scenarios were followed to perform phase selective gelation (PSG) process.¹¹ First scenario, mixture of the gelified organic solvents including benzene, toluene, chlorobenzene and *p*-xylene (1.2 mL each solvent) was poured into salty water (NaCl 3.5 w/v%, 10 mL) which was stained with CuSO₄ for better visualization of the two-phases. The entire organic layer could be efficiently gelled by adding pre-warmed concentrated solution of gelator **9b** (12.5 w/v%) in a small volume of the same mixture (0.2 mL). This resulted in a gelator concentration of 0.5 w/v% with respect to the organic phase.¹¹ Second scenario, gelator **9b** is highly soluble in ethanol and can not gelate it even at high concentration. Subsequently, high concentrated solution (12.5 w/v%) of gelator **9b** in ethanol as a co-solvent at room temperature was prepared (25 mg of **9b** in 200 μL ethanol) and then added to a glass beaker containing a mixture of 4.8 mL and 10 mL organic and aqueous phases, respectively.^{11,35}

By taking the advantage of the thermoreversibility of our organogels and they are maintained by weak non-covalent interactions, so they can be easily broken by simple heating to get solutions. Accordingly, the organic phase was separated from aqueous phase by simple filtration and then the gel melts upon heating and the organic phase is subsequently distilled off in a round bottom flask.^{11,24}

Part C
Bibliographies

Part C

Bibliographies

Bibliographies

- (1) Solimando, X.; Lherbier, C.; Babin, J.; Arnal-Herault, C.; Romero, E.; Acherar, S.; Jamart-Gregoire, B.; Barth, D.; Roizard, D.; Jonquieres, A. *Polym. Int.* **2016**, 1464-1473.
- (2) Shen, J.; Liu, G.; Huang, K.; Li, Q.; Guan, K.; Li, Y.; Jin, W. *J. Membr. Sci.* **2016**, 513, 155-165.
- (3) Sridhar, S.; Smitha, B.; Aminabhavi, T. M. *Sep. Purif. Rev.* **2007**, 36, 113-174.
- (4) Nasir, R.; Mukhtar, H.; Man, Z. *J. Appl. Sci.* **2014**, 14, 1186-1191.
- (5) Chen, Y.; Zhao, L.; Wang, B.; Dutta, P.; Winston Ho, W. S. *J. Membr. Sci.* **2016**, 497, 21-28.
- (6) Wijmans, J. G.; Baker, R. W. The Solution-Diffusion Model: A Review. *J. Membr. Sci.* **1995**, 107, 1-21.
- (7) Daynes, H. A. *Proc. R. Soc. Lond. Math. Phys. Eng. Sci.* **1920**, 97, 286-307.
- (8) Liu, S. L.; Shao, L.; Chua, M. L.; Lau, C. H.; Wang, H.; Quan, S. *Prog. Polym. Sci.* **2013**, 38, 1089-1120.
- (9) Liu, J.; Hou, X.; Park, H. B.; Lin, H. *Chem. Weinh. Bergstr. Ger.* **2016**, 22, 15980-15990.
- (10) Robeson, L. M. *J. Membr. Sci.* **2008**, 320, 390-400.
- (11) Bachl, J.; Oehm, S.; Mayr, J.; Cativiela, C.; Marrero-Tellado, J. J.; Diaz, D. D. *Int. J. Mol. Sci.* **2015**, 16, 11766-11784.
- (12) Feng, G. L.; Chen, H. H.; Cai, J. H.; Wen, J. W.; Liu, X. B. *Soft Mater.* **2014**, 12, 403-410.
- (13) Konda, M.; Maity, I.; Rasale, D. B.; Das, A. K. *Chem. Plus. Chem.* **2014**, 79, 1482-1488.
- (14) Yu, S. L.; Dou, X. Q.; Qu, D. H.; Feng, C. L. *J. Mol. Liq.* **2014**, 190, 94-98.
- (15) Peng, J.; Liu, K.; Liu, X.; Xia, H.; Liu, J.; Fang, Y. *New J. Chem.* **2008**, 32, 2218-2224.
- (16) Huertas, M. J.; Duque, E.; Molina, L.; Rossello-Mora, R.; Mosqueda, G.; Godoy, P.; Christensen, B.; Molin, S.; Ramos, J. L. *Environ. Sci. Technol.* **2000**, 34, 3395.
- (17) Swannell, R. J.; Lee, K.; Mcdonagh, M. *Microbiol. Rev.* **1996**, 60, 342-365.
- (18) Fiocco, R. J.; Lewis, A. *Pure Appl. Chem.* **1999**, 71, 27-42.
- (19) Choi, H. M.; Cloud, R. M. *Environ. Sci. Technol.* **1992**, 26, 772-776.
- (20) Wang, F.; Yu, S.; Xue, M.; Ou, J.; Li, W. *New J. Chem.* **2014**, 38, 4388-4393.
- (21) Zhu, H.; Qiu, S.; Jiang, W.; Wu, D.; Zhang, C. *Environ. Sci. Technol.* **2011**, 45, 4527-4531.
- (22) Kizil, S.; Karadag, K.; Aydin, G. O.; Sonmez, H. B. *J. Environ. Manag.* **2015**, 149, 57-64.
- (23) Pelletier, É.; Siron, R. *Environ. Toxicol. Chem.* **1999**, 18, 813-818.
- (24) Basak, S.; Nanda, J.; Banerjee, A. *J. Mater. Chem.* **2012**, 22, 11658-11664.
- (25) Jadhav, S. R.; Vemula, P. K.; Kumar, R.; Raghavan, S. R.; G., J. *Angew. Chem., Int. Ed.* **2010**, 49, 7695-7698.
- (26) Kar, T.; Debnath, S.; Das, D.; Shome, A.; Das, P. K. *Langmuir* **2009**, 25, 8639-8648.
- (27) Xue, M.; Gao, D.; Liu, K.; Peng, J.; Fang, Y. *Tetrahedron* **2009**, 65, 3369-3377.
- (28) Suzuki, M.; Sato, T.; Shirai, H.; Hanabusa, K. *New J. Chem.* **2006**, 30, 1184-1191.
- (29) Mukherjee, S.; Shang, C.; Chen, X.; Chang, X.; Liu, K.; Yua, C.; Fang, Y. *Chem. Commun.* **2012**, 48, 5250-5252.
- (30) Prathap, A.; Sureshan, K. M. *Chem. Commun.* **2012**, 48, 5250-5252.
- (31) Yan, L.; Li, G.; Ye, Z.; Tian, F.; Zhang, S. *Chem. Commun.* **2014**, 50, 14839-14842.
- (32) Bhattacharya, S.; Krishnan-Ghosh, Y. *Chem. Commun.* **2001**, 185-186.
- (33) Debnath, S.; Shome, A.; Dutta, S.; Das, P. K. *Chem. Eur. J.* **2008**, 14, 6870-6881.
- (34) Trivedi, R. D.; Ballabh, A.; Dastidar, P. *Chem. Mater.* **2003**, 15, 3971-3973.
- (35) Kar, T.; Mukherjee, S.; Das, P. K. *New J. Chem.* **2014**, 38, 1158-1167.

General Conclusions and Perspectives

General Conclusions and Perspectives

This thesis which entitled “Synthesis, Structural and Supramolecular Studies of Linear and Cyclic 2:1-[α /aza]-Oligomers” succeeded to promote more area of research belongs to the azapeptide family. In this study, we could develop new azapeptide analogs possessing charged amino acid (lysine) using Boc chemistry. General strategy for the synthesis of new mixed cyclic 2:1-[α /aza]-oligomers has been investigated which is considered one of the few works concerning the structural and conformational studies of cyclic azapeptides in solution and solid states. The structural and conformational analyses at monomeric and 3D levels of some synthesized oligomers were main goal of this research. In addition, the study offers the possibility of modifying the *N*-terminal protecting group through three consecutive additional steps leading to the formation of supramolecular gels (*via* self-assembly) as new innovative soft materials involved in different disciplines. Characterization of supramolecular gels using different physico-chemical techniques has also been described. This work is presented in three main parts:

In **Part A** we have described the general strategy for the synthesis of linear and cyclic 2:1-[α /aza]-oligomers as well as their structural studies. NMR and FTIR spectroscopies have showed that all the synthesized oligomers, Boc-(*L*- or *D*-X-azaPhe-Y)_n-OMe; (X = Phe or Lys(Z), Y = Ala or Lys(Z), n = 1 trimer, n = 2 hexamer), could self-organize in solution adopting β -turn conformations. Molecular dynamic calculations for oligomers based lysine residues predicted that the side chains of lysine residues are involved in intramolecular hydrogen bonds with the amide groups of the backbone. This might affect the values of the backbone torsion angles of these oligomers and lead to adopting undefined conformations, particularly for longer sequences (hexamers).

Furthermore, in this part we have put the evidences using several techniques (X-ray, NMR and FTIR) that the homo- and heterochiral cyclo-(*L*- or *D*-Phe-azaPhe-Ala)₂-hexamers adopt β -turn conformations stabilized by intramolecular hydrogen bonds of the type (i---i+3) closing a pseudocycle of 10 atoms. Moreover, this conformation is stabilized not only by intramolecular hydrogen bonds, but also through π - π stacking interactions within the same macrocycle. In addition, both molecules have the ability to organize into 3D highly ordered tubular structures supported by non-covalent interactions mainly hydrogen bonding and π -stacking interactions between the stacked macrocycles.

In **Part B** we have demonstrated the spontaneous self-assembly of some 2:1-[α /aza]-oligomers in different solvents with the formation of supramolecular organo-/hydrogels which maintained *via* non-covalent interactions.

Interestingly, chirality and disorder have a great effect on the supramolecular organization of cyclo-(*L*- or *D*-Phe-azaPhe-Ala)₂-hexamer which permit only the heterocyclic analog to act as low molecular weight organogelator (LMWOG) and form supramolecular organogels from toluene, benzene, *p*-xylene and chlorobenzene. Spectroscopic and rheological studies of the organogels revealed good thermal and mechanical stability. SEM and TEM images of the aerogel from toluene confirm the self-organization of the monomers to give highly organized 3D fibrous structure.

Amazingly, the part has also offered new two low molecular weight hydrogelators (LMWHGs) based on 2:1-[α /aza]-oligomers. They were obtained through little structural modifications on the Boc-functionalized azapeptide structures. Replacing the Boc-group by Fmoc-group for a number of deprotected *C*-terminal 2:1-[α /aza]-trimers have achieved two hydrogels. Both trimers (Fmoc-*L*- or *D*-Phe-azaPhe-Ala-OH) have led to hydrogels at pH values of 7.0 and 10.0. X-ray, NMR and FTIR studies showed that 2:1-[α /aza]-*L*- or *D*-Phe-azaPhe-Ala molecules adopt β -turn conformation in solution and solid states supported by an intramolecular hydrogen bond and π -

General Conclusions and Perspectives

stacking between the aromatic moieties. UV-absorption and fluorescence emission demonstrated that the hydrogels are supported by the π -stacking between the aromatic moieties. CD analysis of the hydrogels (at MGCs) reflected that the two hydrogelators self-assemble into supramolecular β -sheet like structure in accordance with the ATR-FTIR results. Rheological studies on the hydrogels confirms the solid-like behavior of the hydrogels ($G' < G''$). SEM images of the xerogels showed interconnected fibrous structure confirming that the self-assembly phenomenon induces hydrogelation.

In **Part C** we have presented and evaluated the potentials of the linear and cyclic 2:1-[α /aza]-oligomers in certain applications based on their characteristic properties. Firstly, incorporating of 2:1-[α /aza]-oligomers with protected or deprotected lysine side chain(s) in the commercial polymeric Pebax[®] membranes revealed good performances for CO₂/N₂ separation compared with oligomers without lysine residue(s). In particular, the azapeptide (dimer) with deprotected lysine residue which reflected better selectivity and permeability than the reference Pebax[®] membrane. Secondly, heterochiral cyclo-(*D*-Phe-azaPhe-Ala)₂-hexamer showed high gelation ability. It has high efficiency in selective gelation of organic solvent(s) from (aqueous/organic) mixture with good recovery percentages which allows this gelator molecule to be under demand for water treatment if the process can be scaled up.

Based on the aforementioned behaviors of the azapeptide family, we could conclude that the aza-motif plays an important role in structuring the peptide backbone regardless the nature and chirality of the amino acids as well as the chain length of the peptide backbone. The study put the evidence that self-assembly phenomenon accompanied with non-covalent interactions provide supramolecular organo- or hydrogels from 2:1-[α /aza]-oligomers. We found that chirality and disorder have a principal role on the supramolecular organization of cyclo-(*L*- or *D*-Phe-azaPhe-Ala)₂-hexamer which lead only the heterocyclic analog to form organogels. In addition, the balance between hydrophobic and hydrophilic criteria in the 2:1-[α /aza]-oligomers may achieve hydrogels. Finally, linear and cyclic 2:1-[α /aza]-oligomers can be involved in certain application based on their characteristic properties.

General Conclusions and Perspectives

This study put the evidences that insertion of an aza-motif in peptide sequence leads to interesting phenomena from structuring the peptide backbone and gels formation. The below figure illustrates the relation between the three levels of organizations of the molecules (monomeric state, 3D organized structure and gel state).

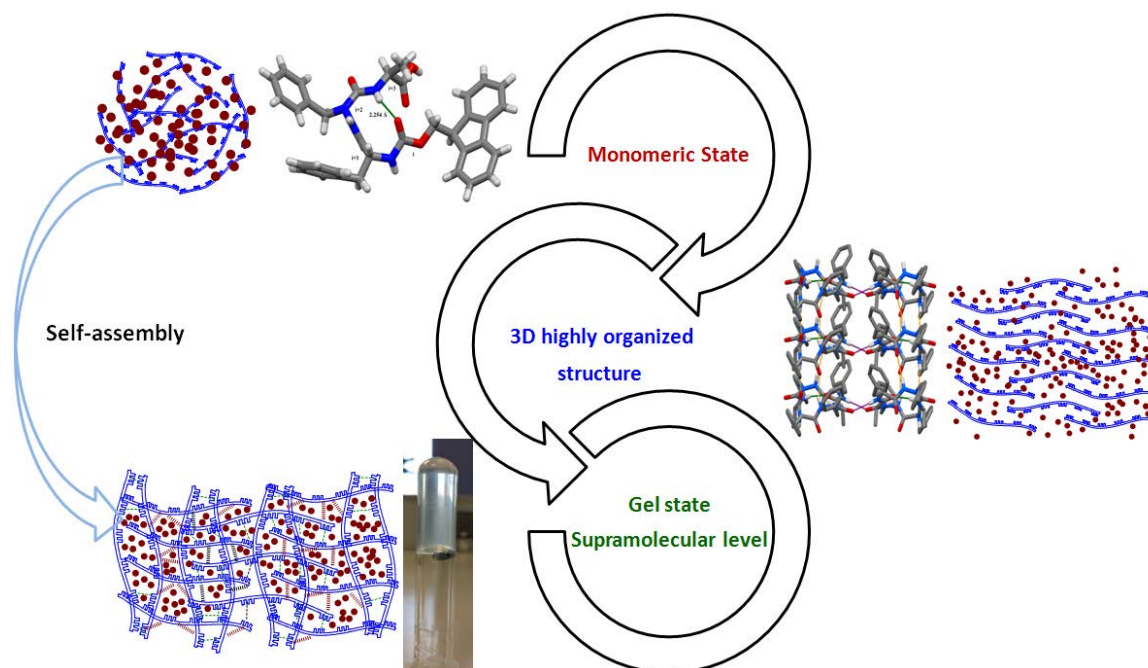
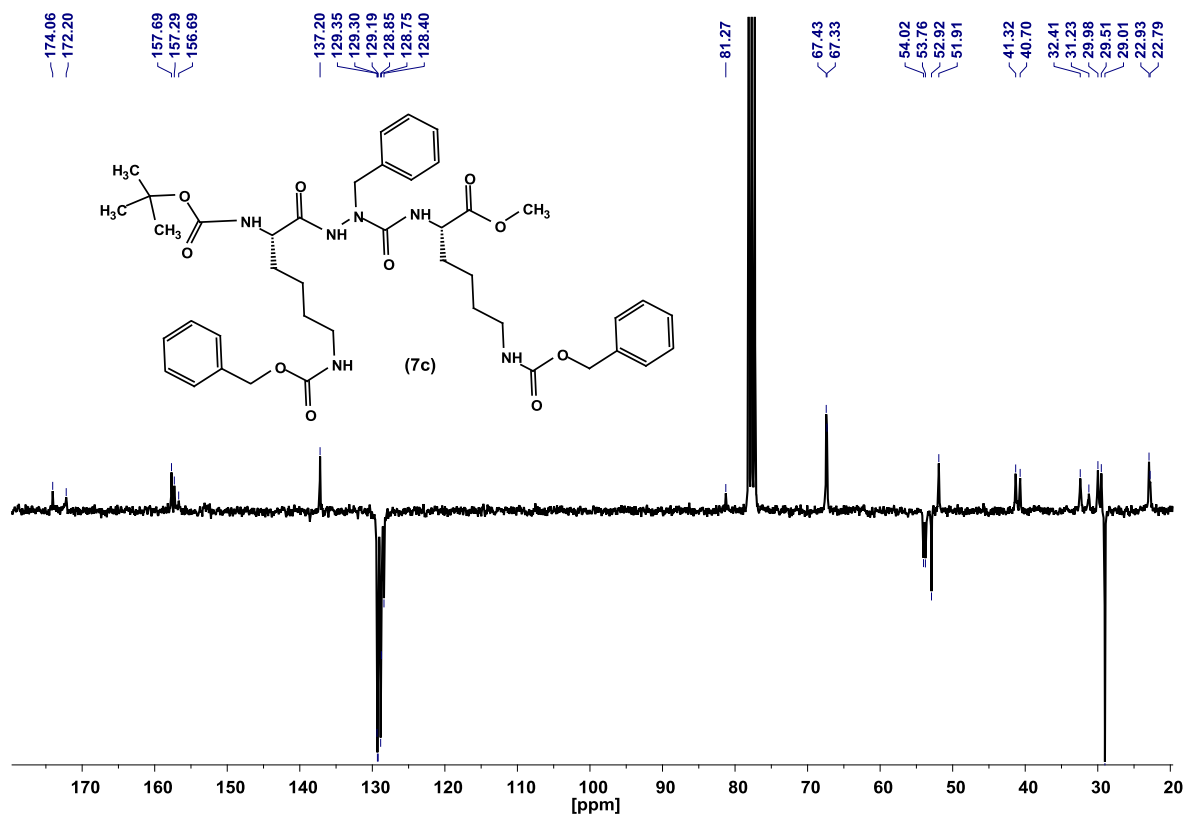
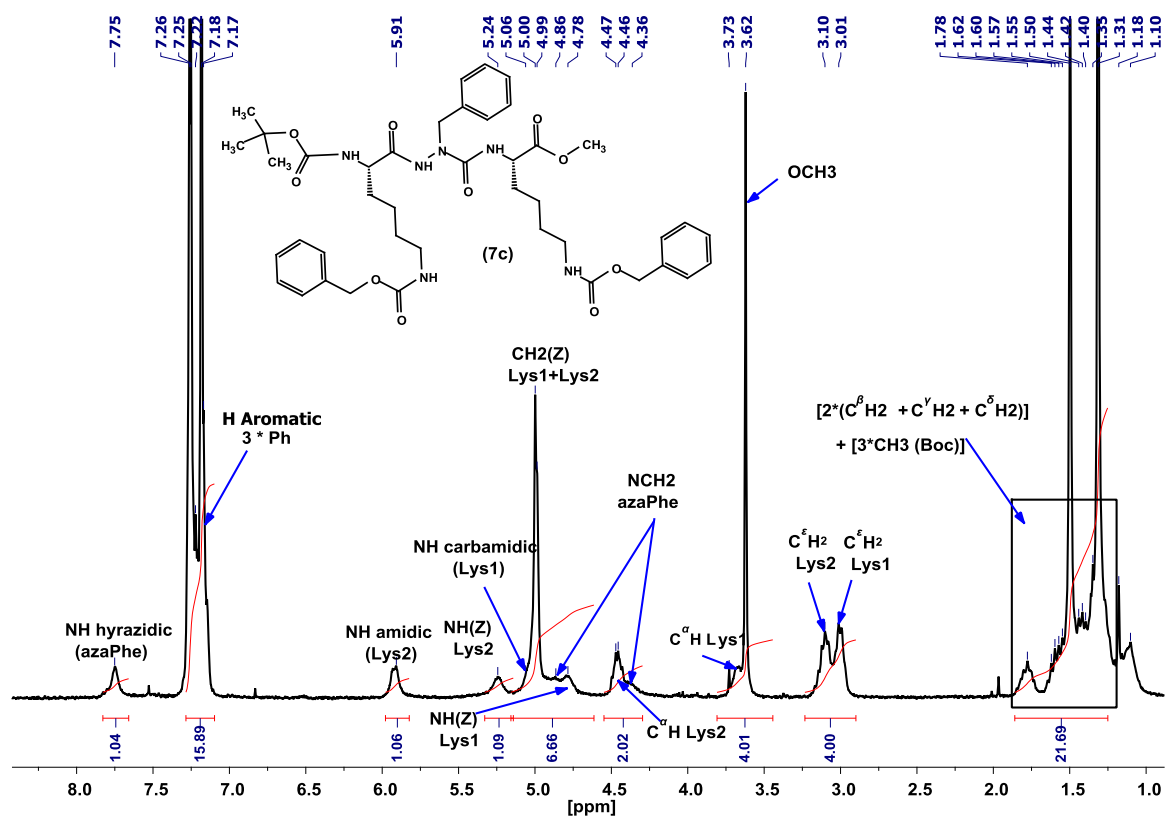


Figure illustrates the relation between three states of organization

Accordingly, the perspective studies will focus mainly on investigating other organogels with improved physico-chemical and mechanical properties. In addition to understanding the relation between gelators' structures and gelation phenomenon since the gel material texture will allow rational design of gels with different rheological properties and then afford different applications according to requirements specifications. To a further push in that direction, the group has planned the synthesis and formulation of other hydrogels and the correlation of structures, physico-chemical and mechanical properties (different side chain, backbone length, *etc.*). Finally, the group has started the evaluation of different hydrogels in stem cell culture with different hydrogels to optimize the required parameters to elaborate a media that promote a better cells expansion.

Appendices

APPENDIX 1
Chapter III. Structural Studies of 2:1-[a/aza]-Oligomers Possessing Lysine Residues



APPENDIX 1

Chapter III. Structural Studies of 2:1-[a/aza]-Oligomers Possessing Lysine Residues

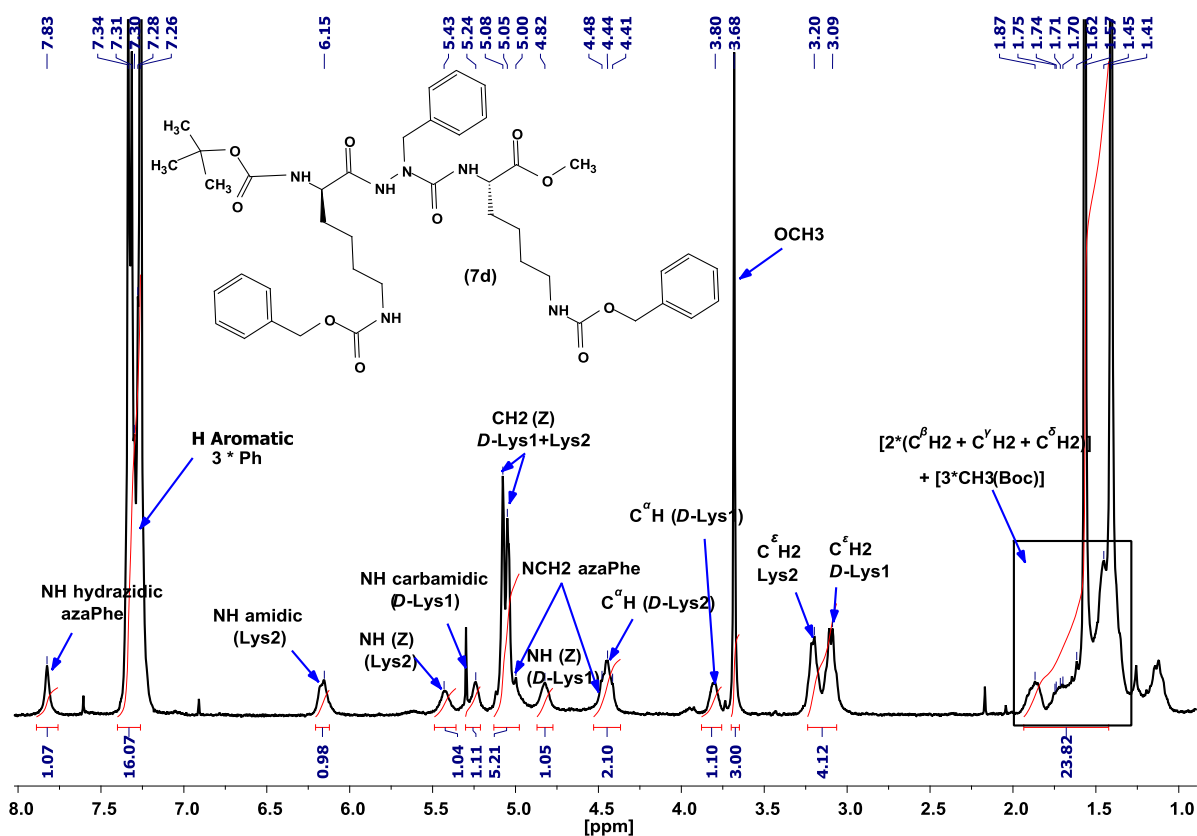


Figure S3.2a. ^1H spectrum of **7d**; (3.0 mmol. L^{-1} , CDCl_3 , 300 K).

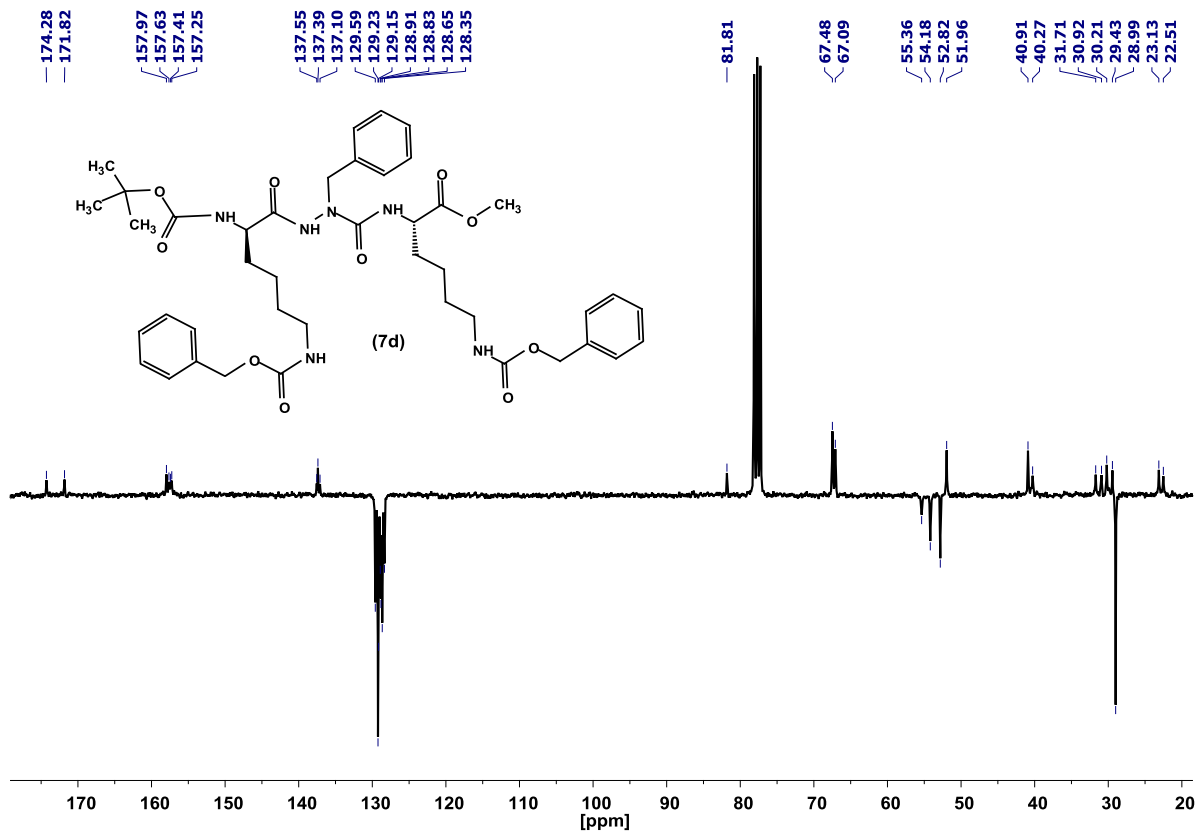


Figure S3.2b. ^{13}C spectrum of **7d**; (5.0 mmol. L^{-1} , CDCl_3 , 300 K).

APPENDIX 1

Chapter III. Structural Studies of 2:1-[a/aza]-Oligomers Possessing Lysine Residues

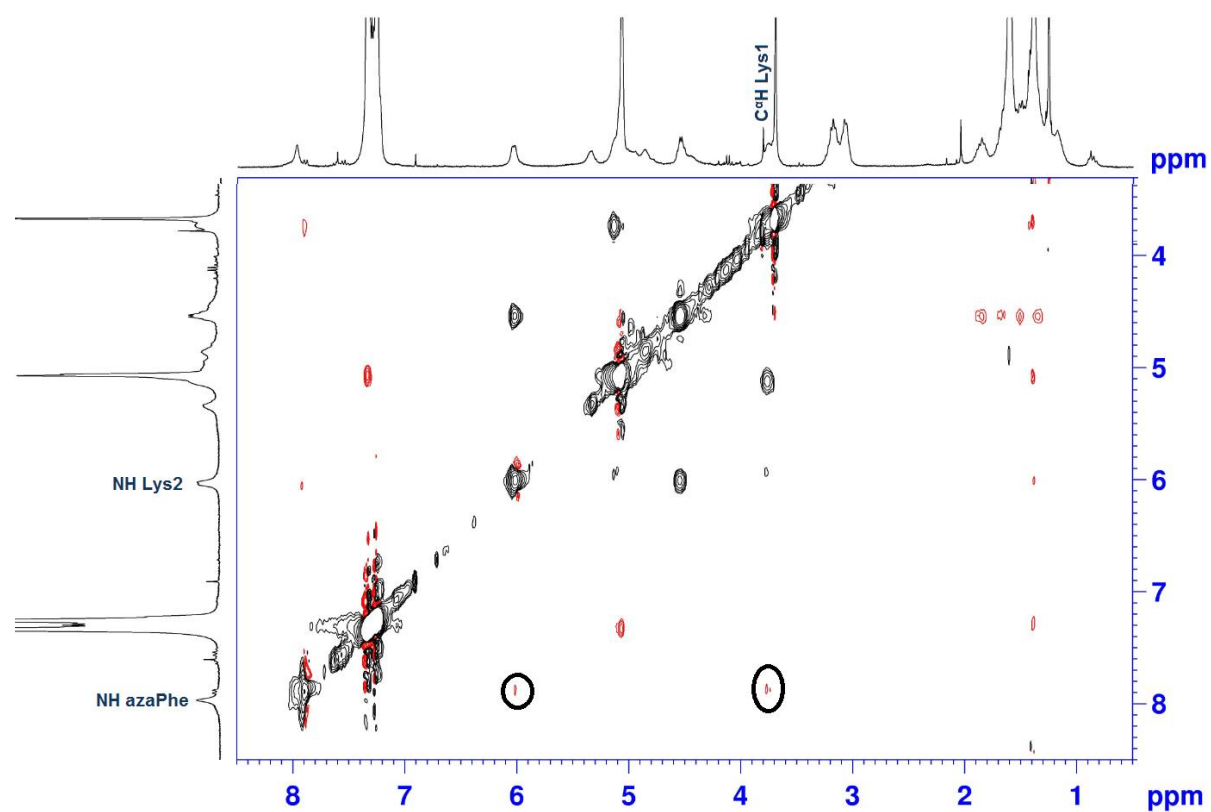


Figure S3.3. 2D ROESY spectrum illustrating the correlations of β II-turn conformation in **7c**; (300 MHz, 3.0 mmol. L⁻¹, CDCl₃, 300 K).

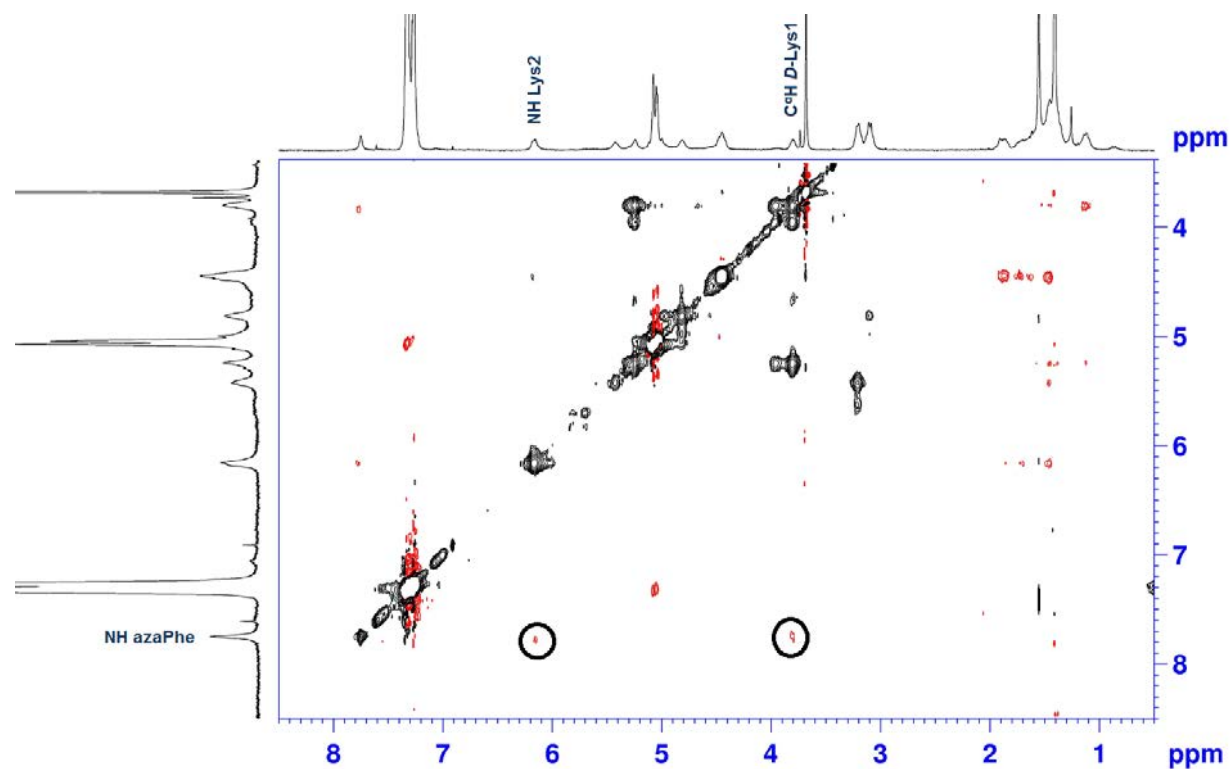


Figure S3.4. 2D ROESY spectrum illustrating the correlations of β II'-turn conformation in **7d**; (300 MHz, 3.0 mmol. L⁻¹, CDCl₃, 300 K).

APPENDIX 1

Chapter III. Structural Studies of 2:1-[a/aza]-Oligomers Possessing Lysine Residues

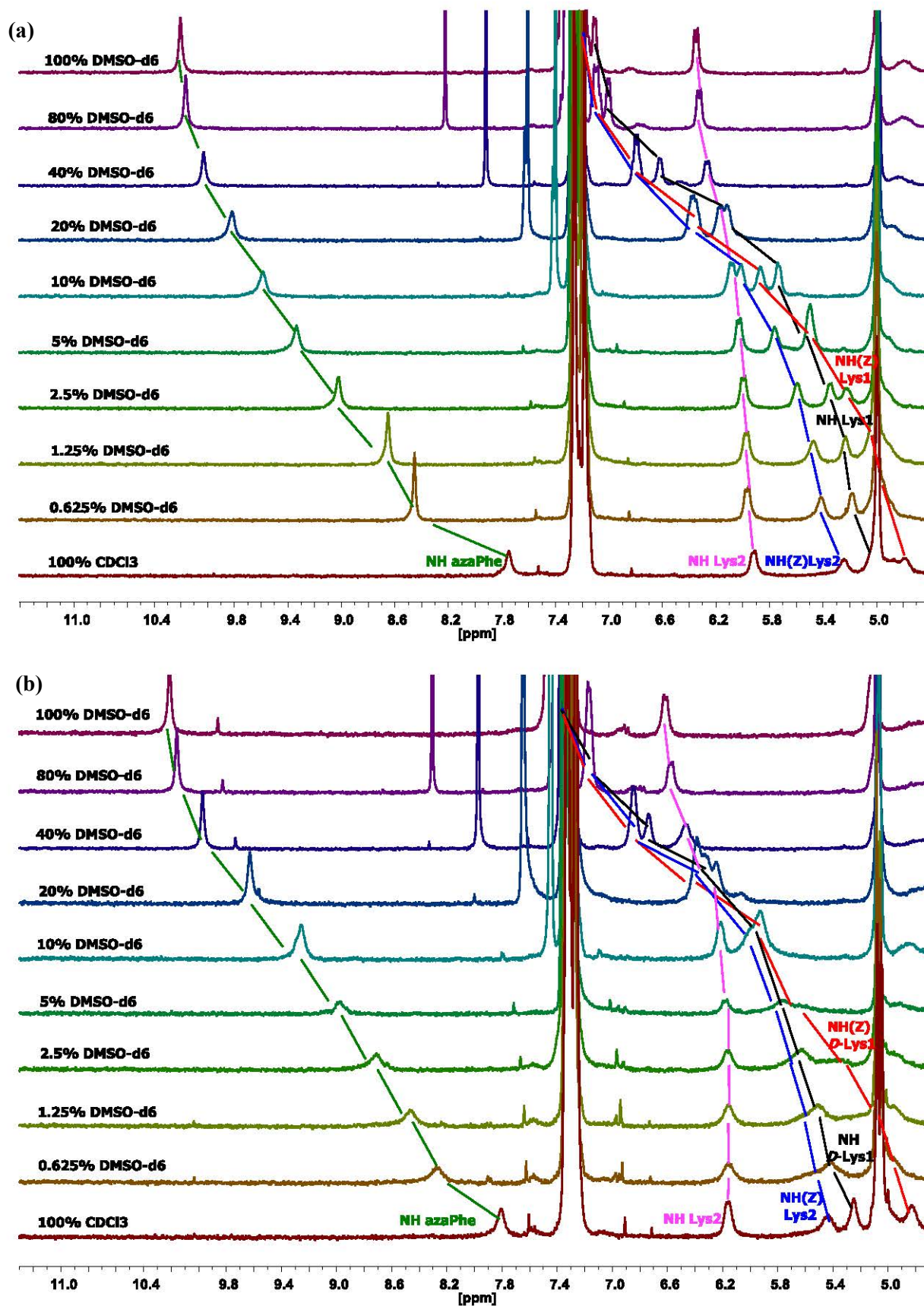


Figure S3.5. Chemical shift-variations (δ) ppm of NH protons for: (a) **7c**, and (b) **7d** as a function of % [CDCl₃/DMSO-*d*₆] mixtures; (300 MHz, 3.0 mmol. L⁻¹).

APPENDIX 1
Chapter III. Structural Studies of 2:1-[a/aza]-Oligomers Possessing Lysine Residues

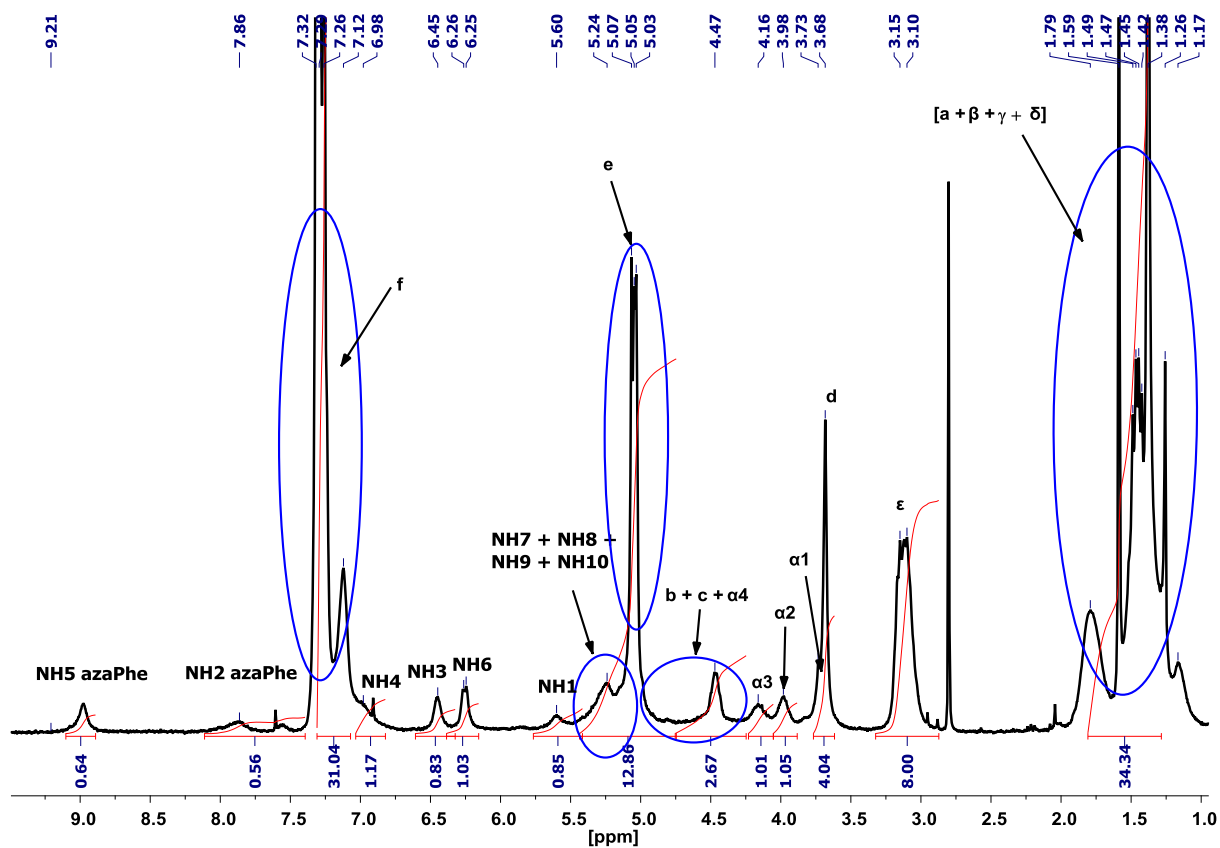
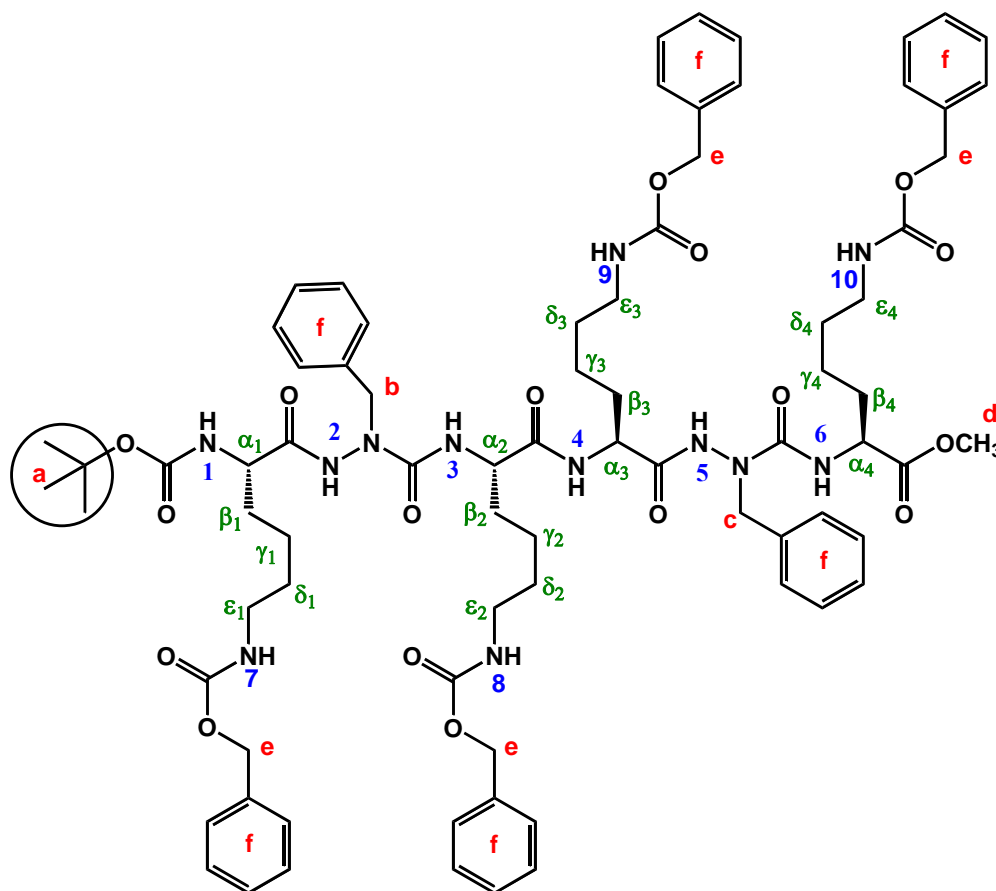


Figure S3.6. ^1H spectrum of **8c**; (4.0 mmol. L^{-1} , CDCl_3 , 300 K).



APPENDIX 1

Chapter III. Structural Studies of 2:1-[a/aza]-Oligomers Possessing Lysine Residues

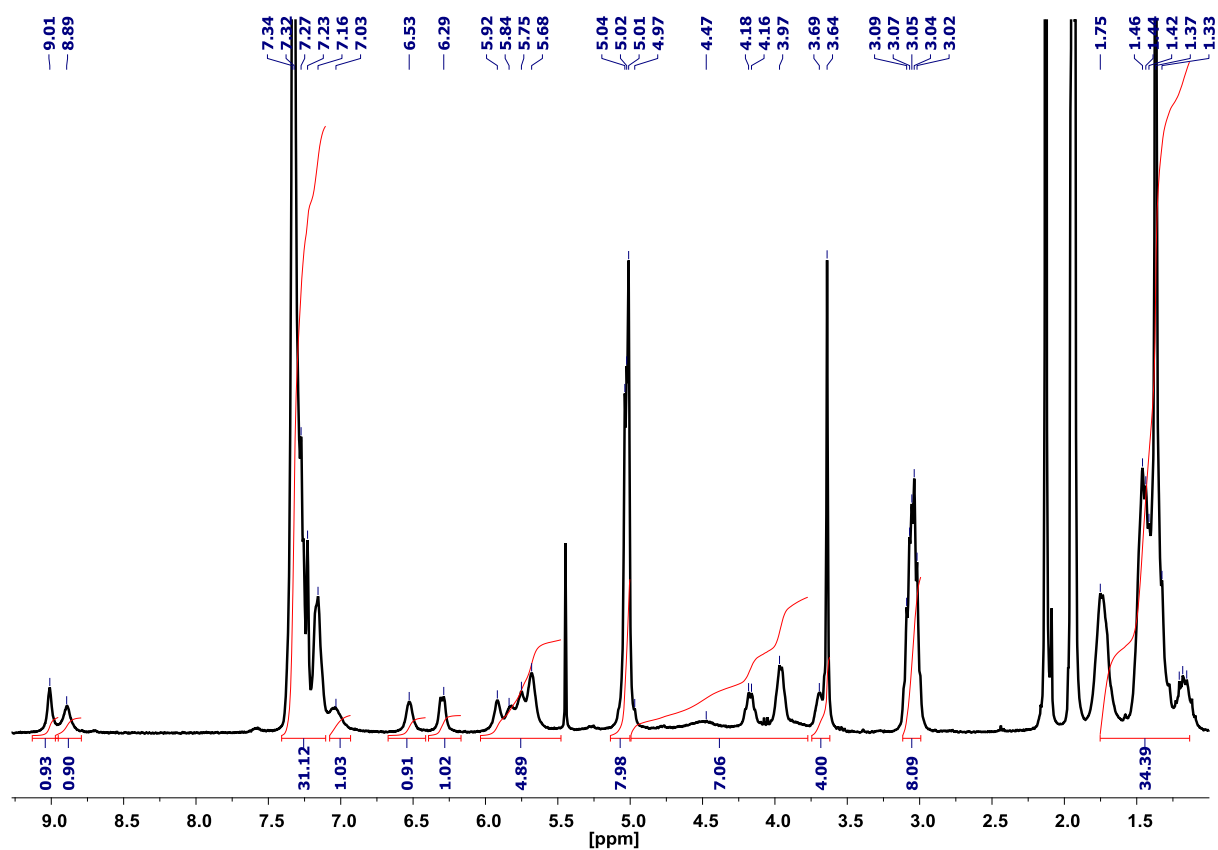


Figure S3.7a. ^1H spectrum of **8c**; (4.0 mmol. L^{-1} , CD_3CN , 300 K).

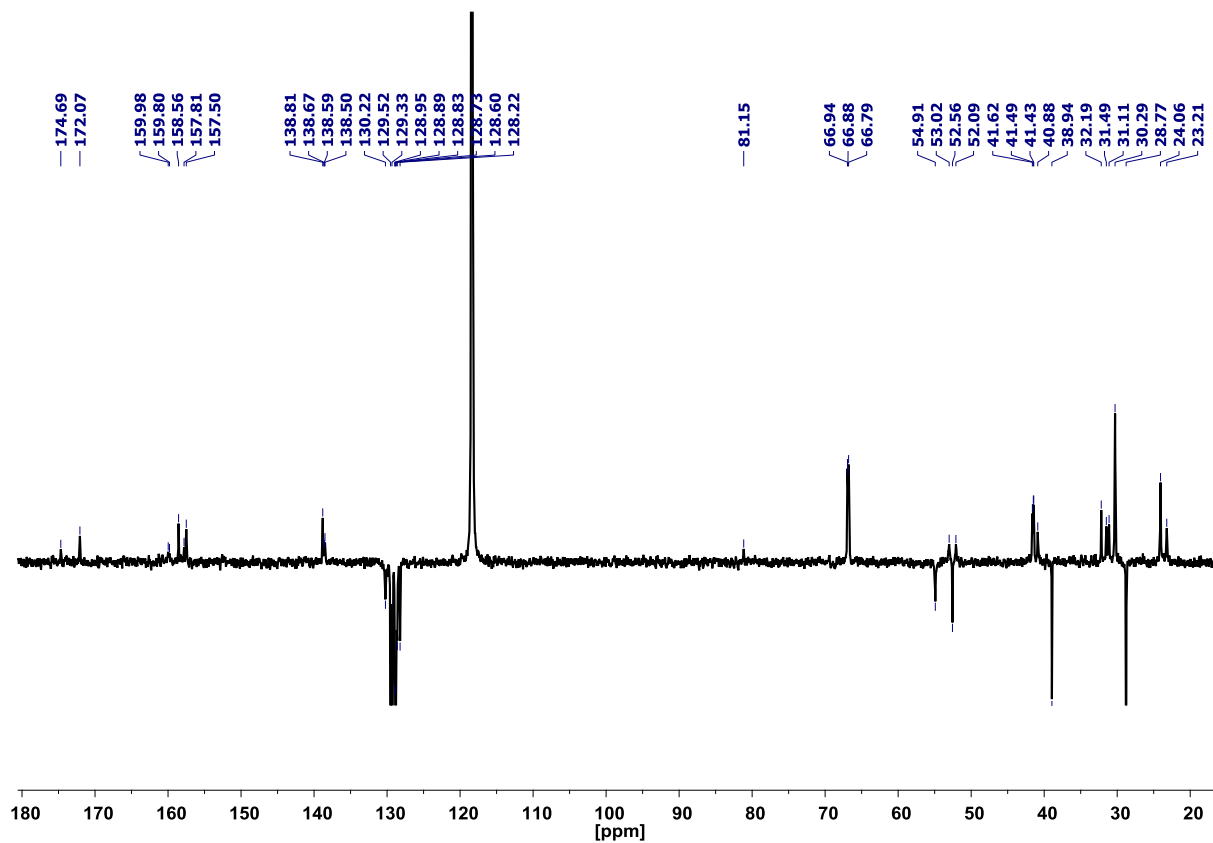


Figure S3.7b. ^{13}C spectrum of **8c**; (4.0 mmol. L^{-1} , CD_3CN , 300 K).

APPENDIX 1

Chapter III. Structural Studies of 2:1-[a/aza]-Oligomers Possessing Lysine Residues

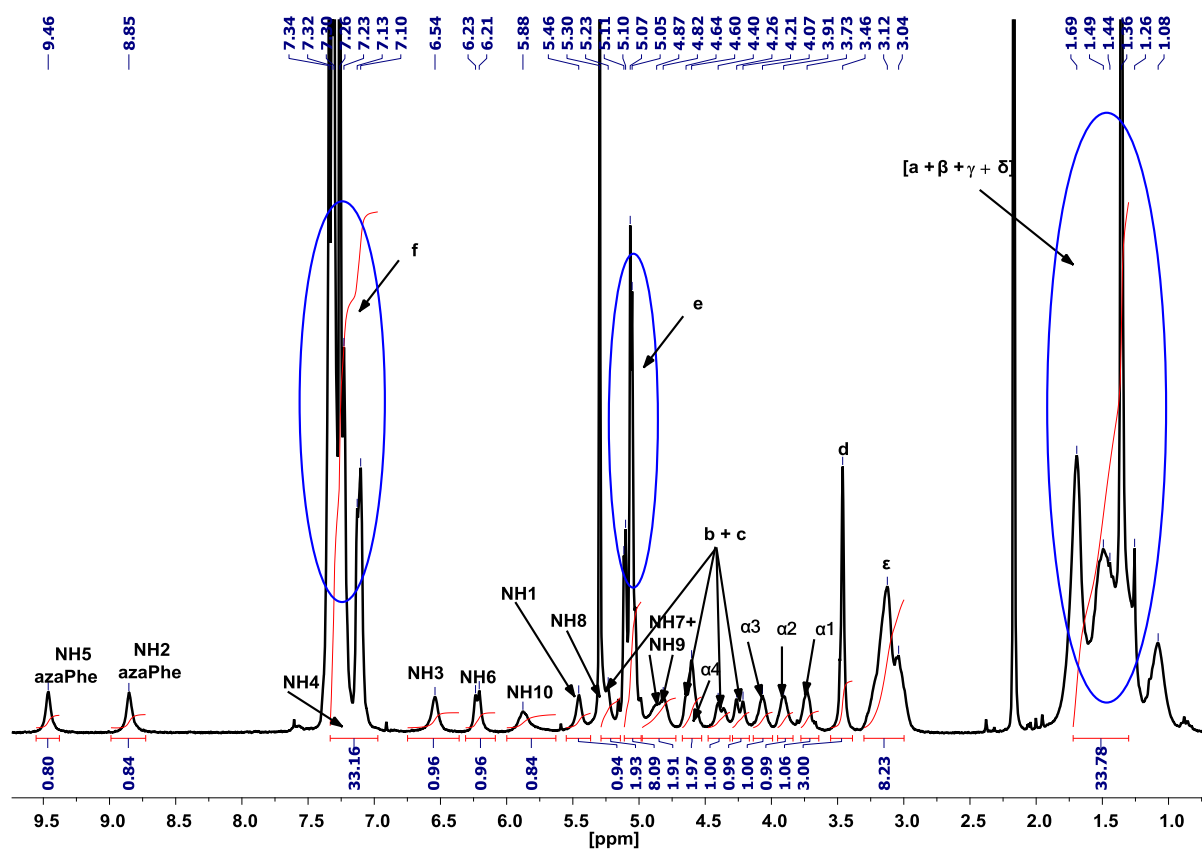
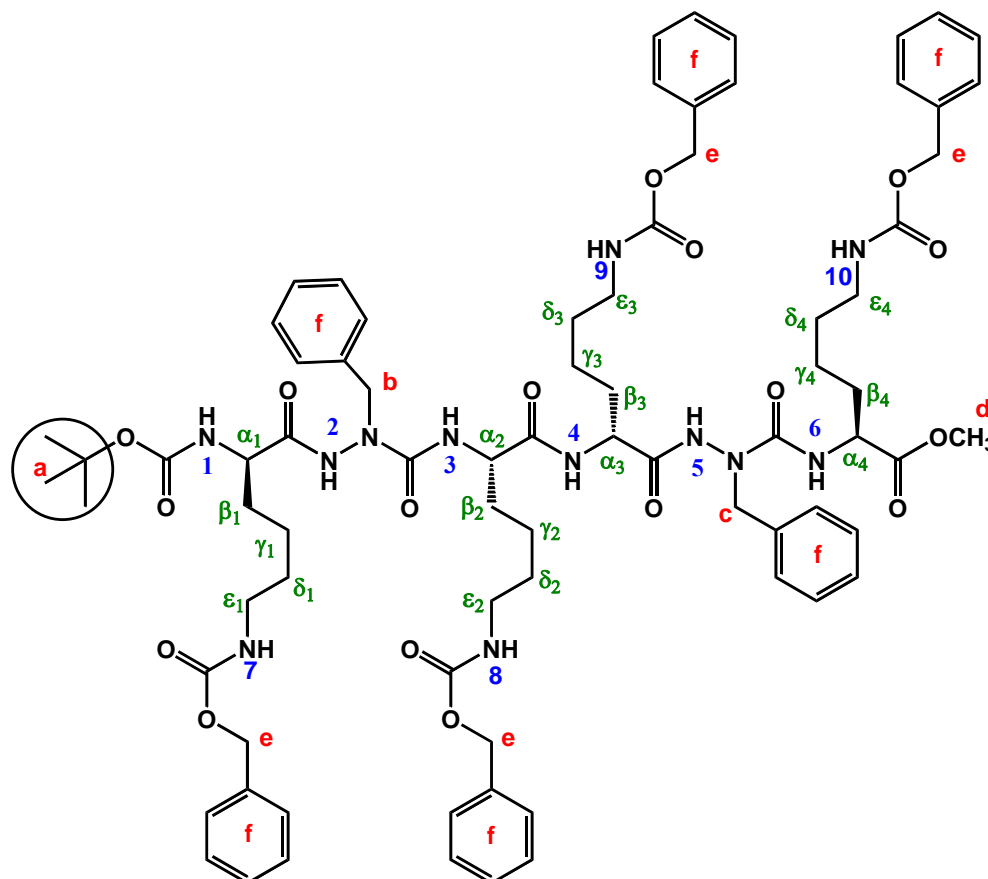


Figure S3.8a. ^1H spectrum of **8d**; (4.0 mmol. L^{-1} , CDCl_3 , 300 K).



APPENDIX 1

Chapter III. Structural Studies of 2:1-[a/aza]-Oligomers Possessing Lysine Residues

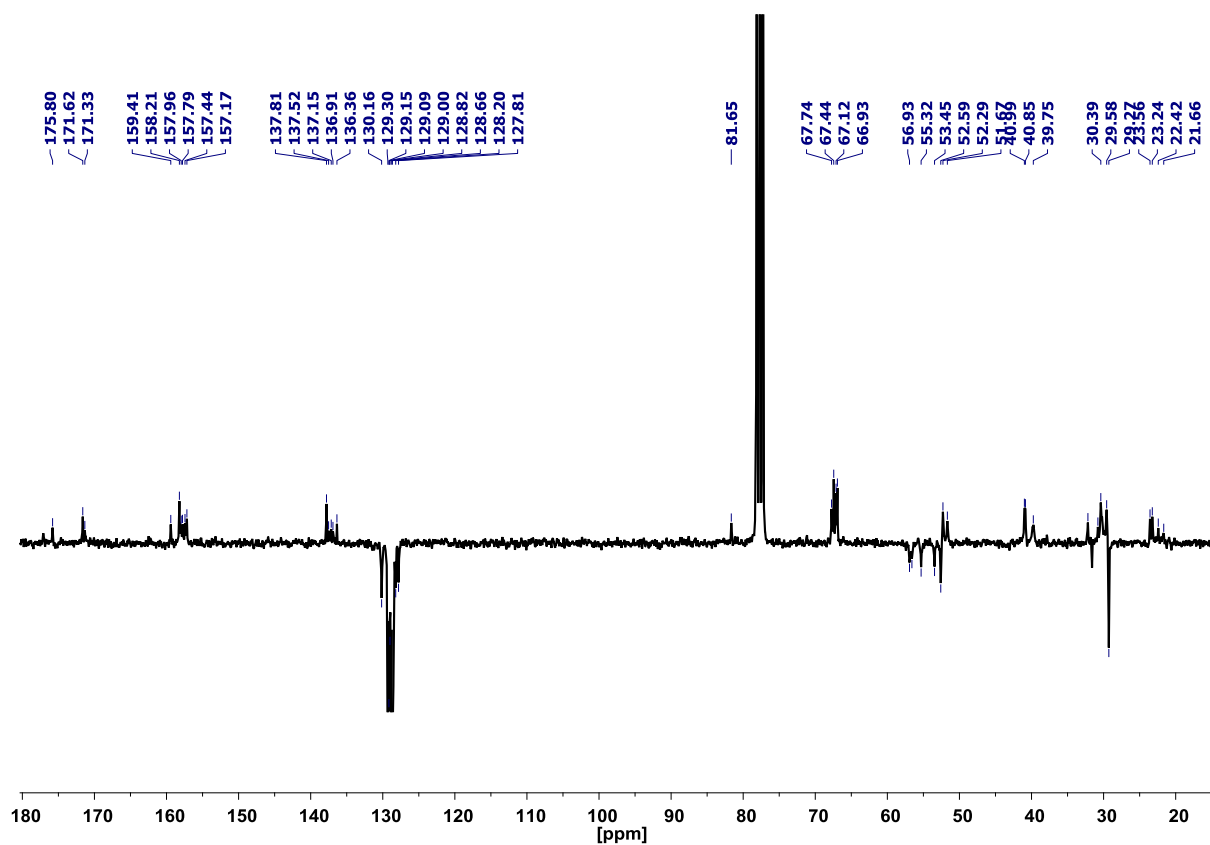


Figure S3.8b. ^{13}C spectrum of **8d**; (5.0 mmol. L $^{-1}$, CDCl $_3$, 300 K).

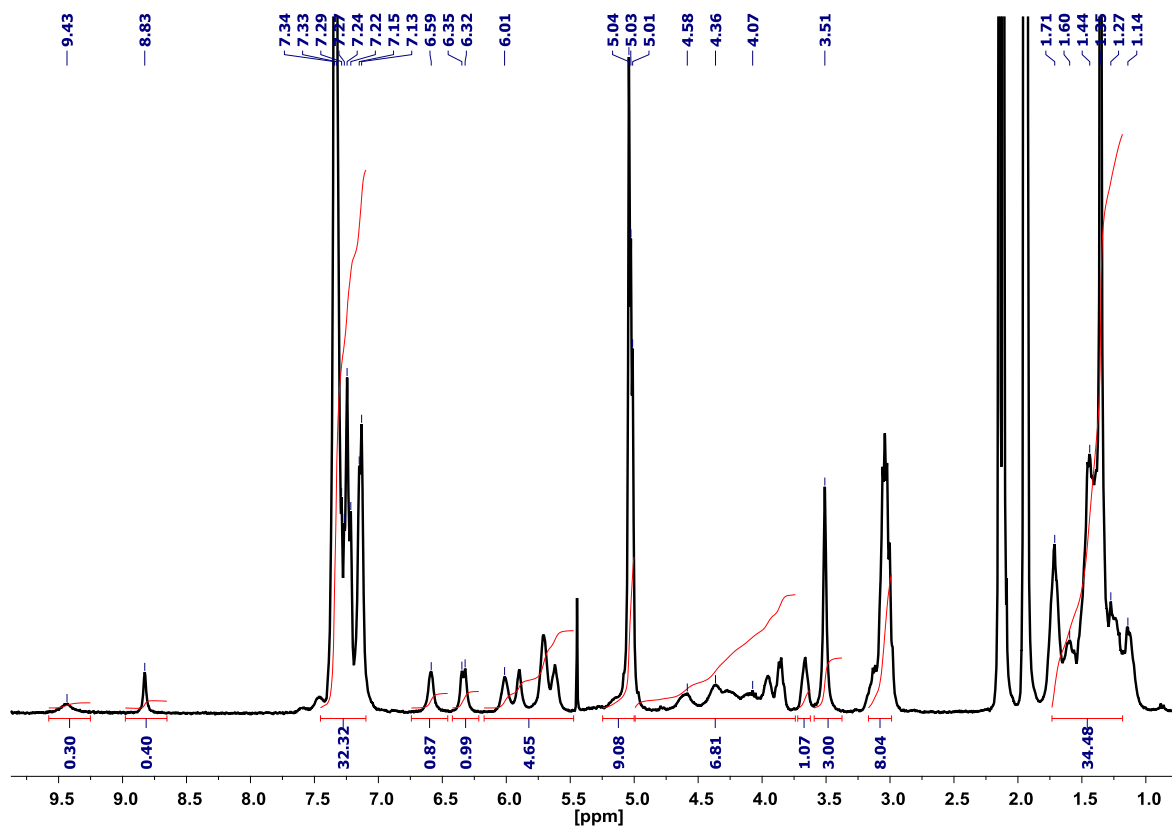


Figure S3.9. ^1H spectrum of **8d**; (4.0 mmol. L $^{-1}$, CD $_3$ CN, 300 K).

APPENDIX 1

Chapter III. Structural Studies of 2:1-[a/aza]-Oligomers Possessing Lysine Residues

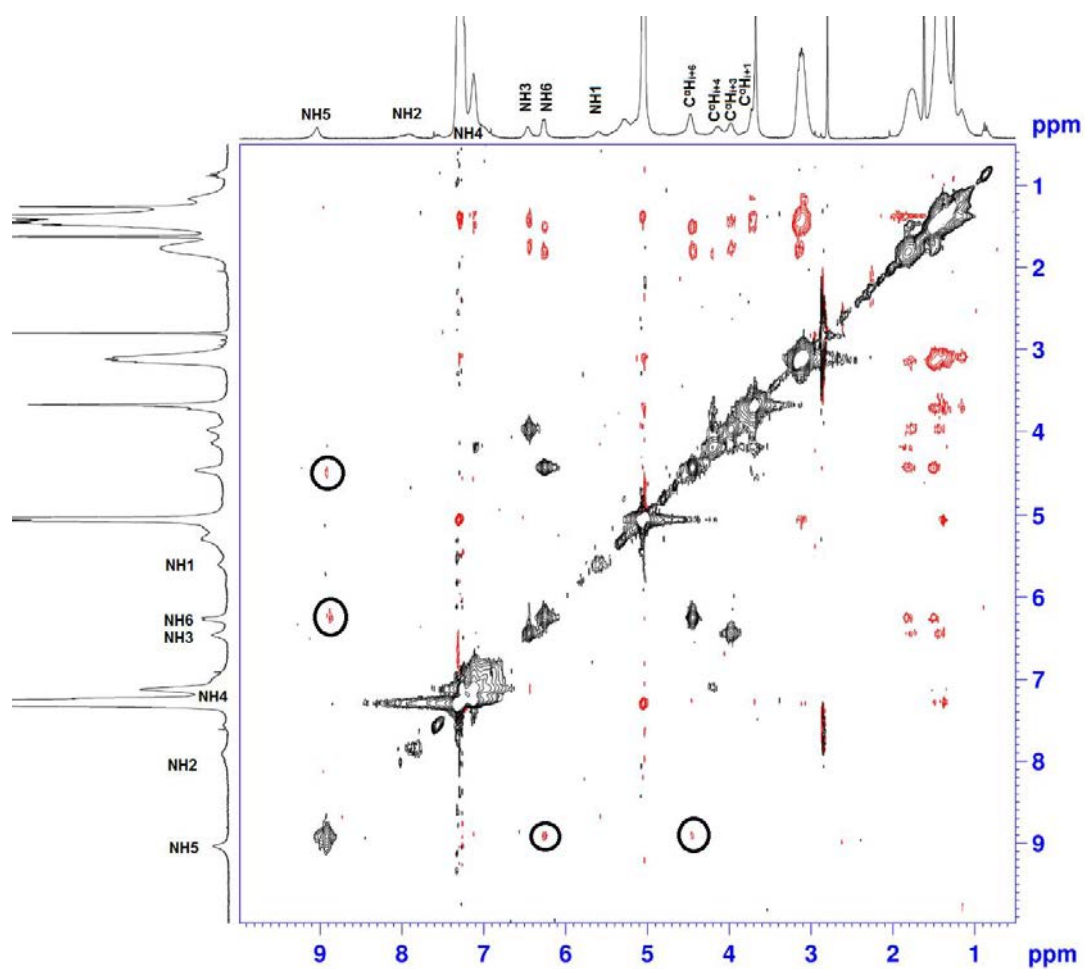


Figure S3.10. 2D ROESY spectrum illustrating the β -turn conformation in **8c**; (300 MHz, 4.0 mmol. L⁻¹, CDCl₃, 300 K).

APPENDIX 1

Chapter III. Structural Studies of 2:1-[a/aza]-Oligomers Possessing Lysine Residues

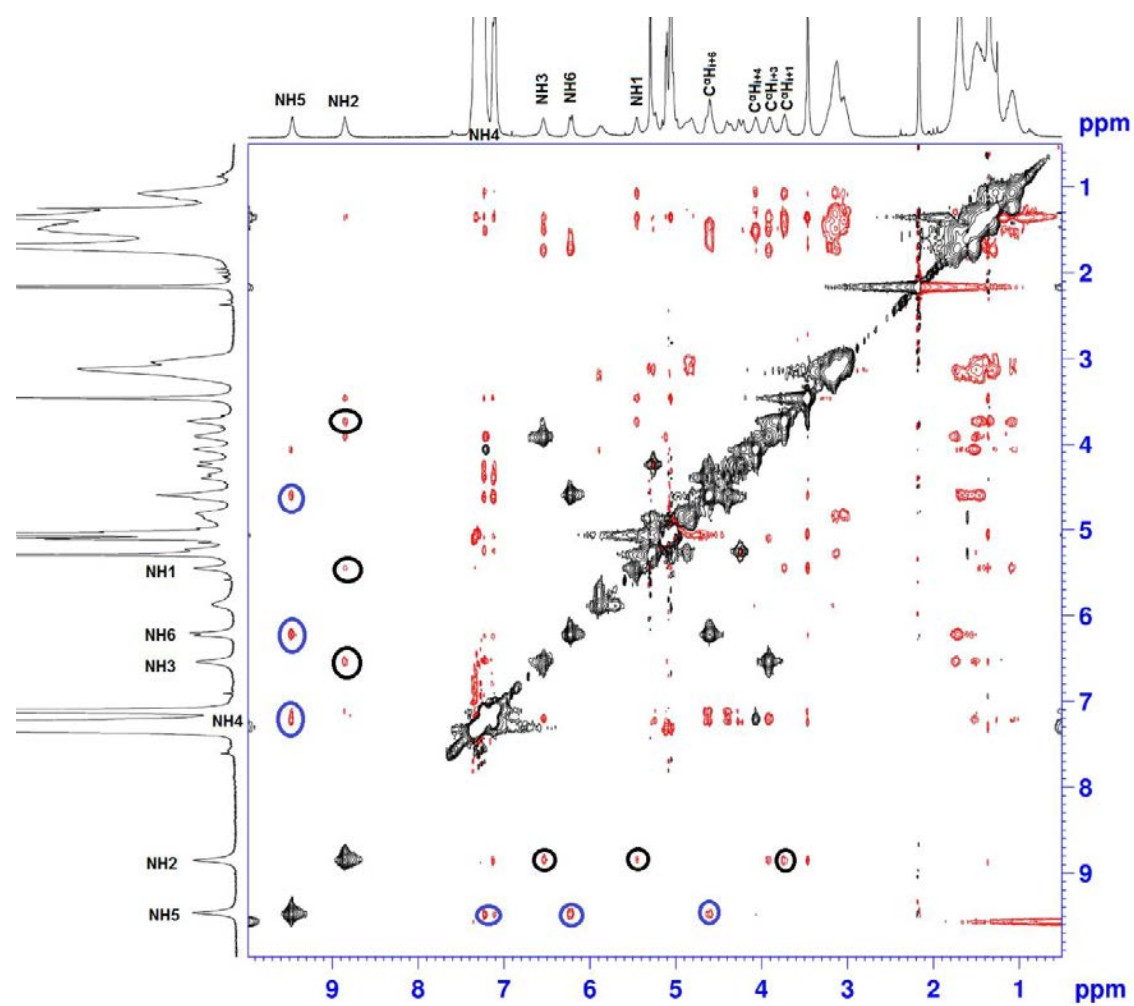


Figure S3.11. 2D ROESY spectrum illustrating the correlations of β -turn conformation in **8d**; (300 MHz, 4.0 mmol. L⁻¹, CDCl₃, 300 K).

APPENDIX 1

Chapter III. Structural Studies of 2:1-[a/aza]-Oligomers Possessing Lysine Residues

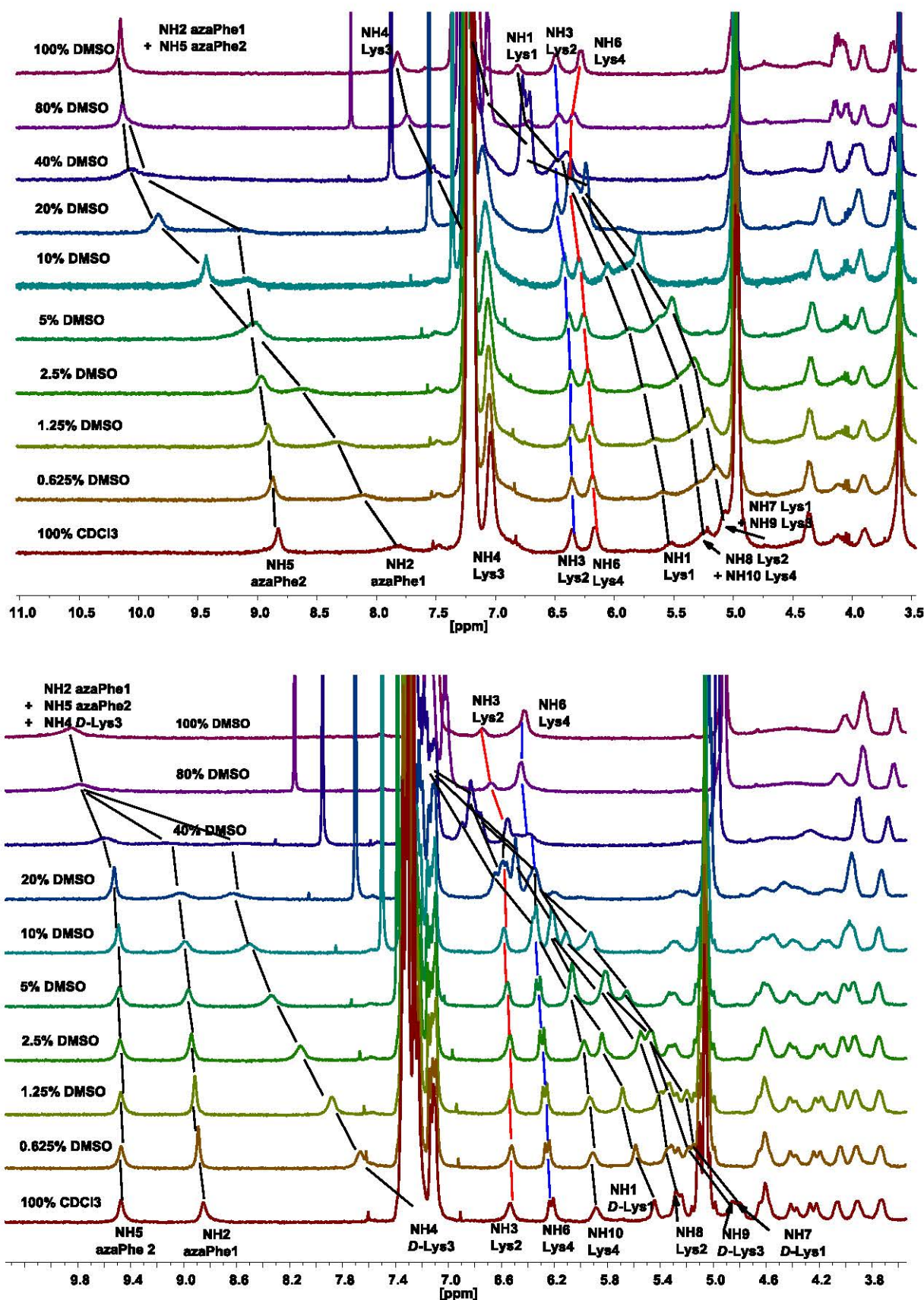


Figure S3.12. Chemical shift-variations (δ) of NH protons for: **8c** (up), and **8d** (bottom) as a function of % [CDCl₃/DMSO-*d*₆] mixtures.

APPENDIX 1

Chapter III. Structural Studies of 2:1-[a/aza]-Oligomers Possessing Lysine Residues

Table S3.1. Percentages of the expected intramolecular hydrogen bonds in **8c** issued of the molecular dynamic simulations

Molecule	Bond Ref.	No. of frames	Frames (%)	Bond Ref.	No. of frames	Frames (%)
8c	(i + ii)	15115	60.5	(i + ii + iii)	7368	29.5
	(i + iii)	11154	44.6	(i + iii + iv)	3607	14.4
	(i + iv)	6952	27.8	(i + ii + iv)	4282	17.3
	(ii + iii)	7892	31.8	(ii + iii + iv)	2560	10.2
	(ii + iv)	4921	19.7	(i + ii + iii + iv)	2259	9.0
	(iii + iv)	4215	16.9			

Table S3.2. Average percentages of the expected intramolecular hydrogen bonds in **8d** issued of the molecular dynamic simulations

Molecule	Bond Ref.	No. of frames	Frames (%)	Bond Ref.	No. of frames	Frames (%)
8d	(i + ii)	8941	35.8	(iv + v)	2614	10.5
	(i + iii)	3069	12.3	(iv + vi)	1775	7.1
	(i + iv)	5439	21.8	(v + vi)	1997	8.0
	(i + v)	4378	17.5	(i + ii + iii)	1862	7.5
	(i + vi)	2306	9.2	(i + iii + iv)	1142	4.5
	(ii + iii)	4257	17.0	(i + ii + iv)	2972	11.9
	(ii + iv)	4753	19.0	(ii + iii + iv)	1405	5.6
	(ii + v)	4363	17.4	(iv + v + vi)	766	3.0
	(ii + vi)	4219	16.9	(i + ii + iii + iv)	650	2.6
	(iii + iv)	2871	11.5	(ii + iii + iv + v)	582	2.3
	(iii + v)	2314	9.2	(i + iv + v + vi)	473	1.9
	(iii + vi)	2277	9.1	(i + ii + iii + vi + v)	402	1.6

APPENDIX 2

Chapter IV. Impact of C^α-Chirality on Supramolecular Self-Assembly in Cyclo-2:1-[α /aza]-Hexamers (*L*-/*D*-Phe-azaPhe-Ala)₂

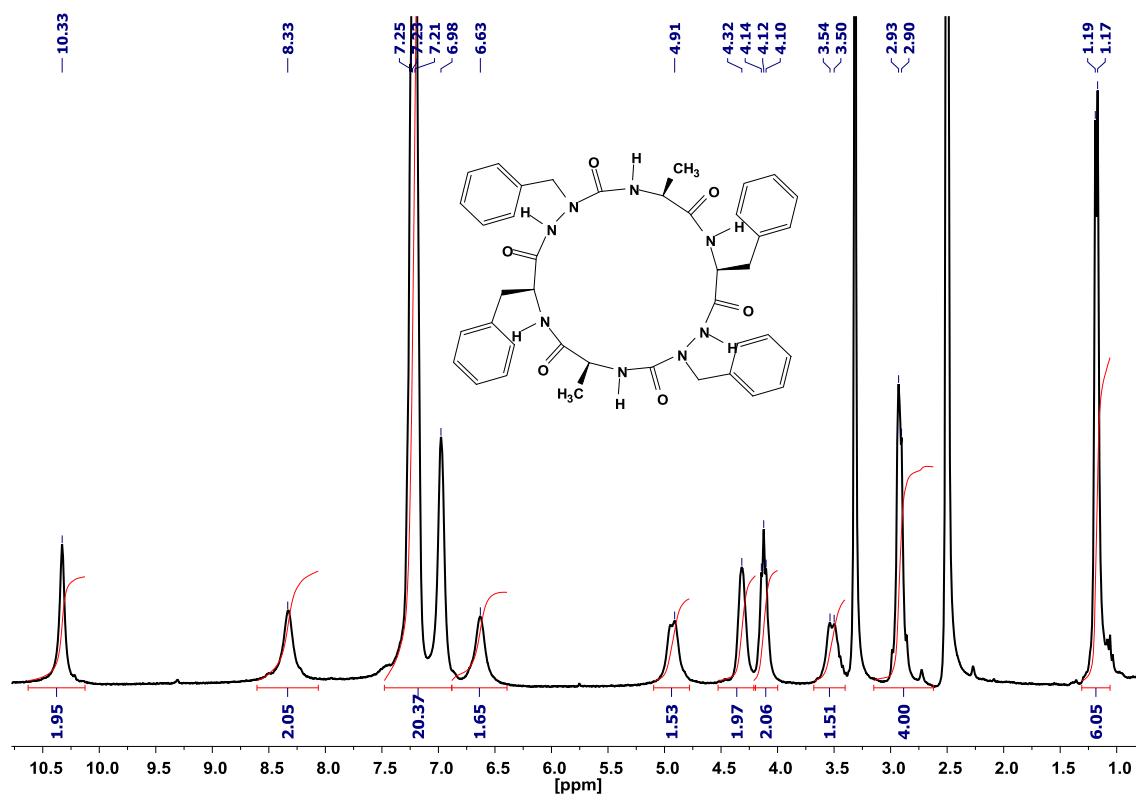


Figure S4.1. ¹H NMR spectrum for compound **9a** recorded in DMSO-*d*₆; (5.0 mmol. L⁻¹).

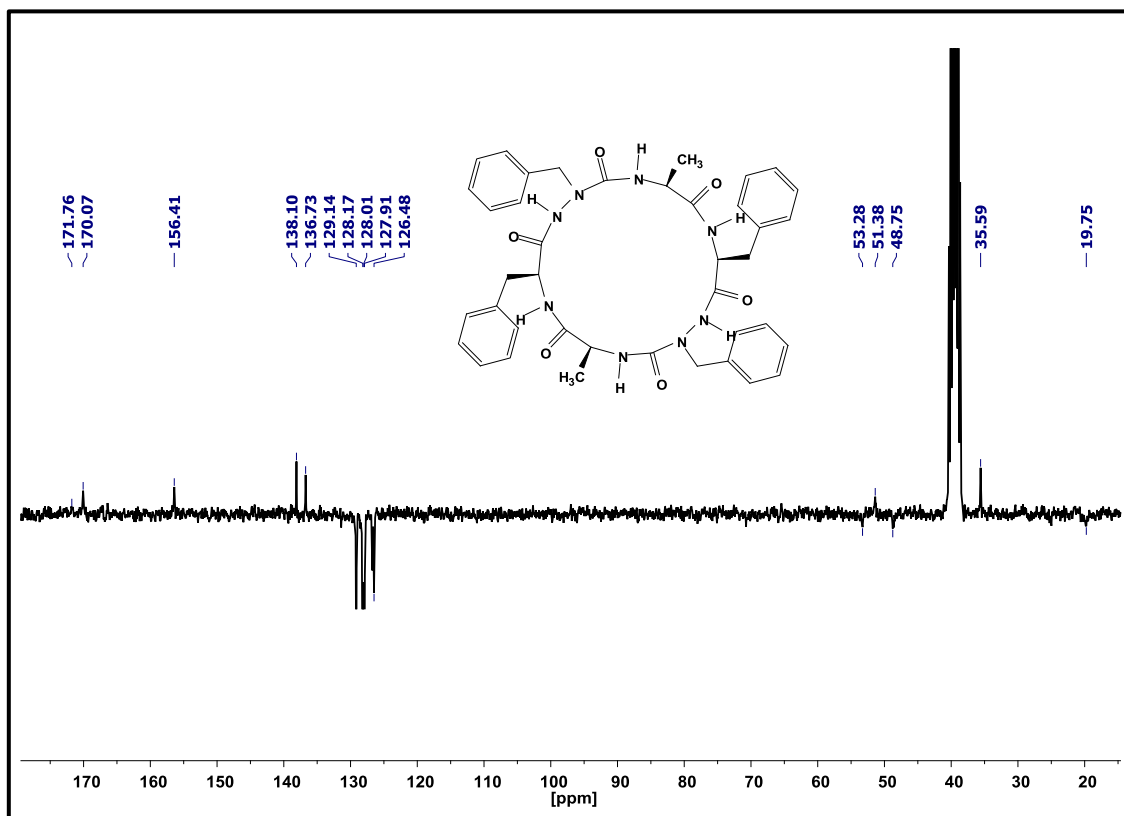


Figure S4.2. ¹³C NMR spectrum for compound **9a**; (DMSO-*d*₆, 8.0 mmol. L⁻¹).

APPENDIX 2

Chapter IV. Impact of C^α-Chirality on Supramolecular Self-Assembly in Cyclo-2:1-[α /aza]-Hexamers (*L*/*D*-Phe-azaPhe-Ala)₂

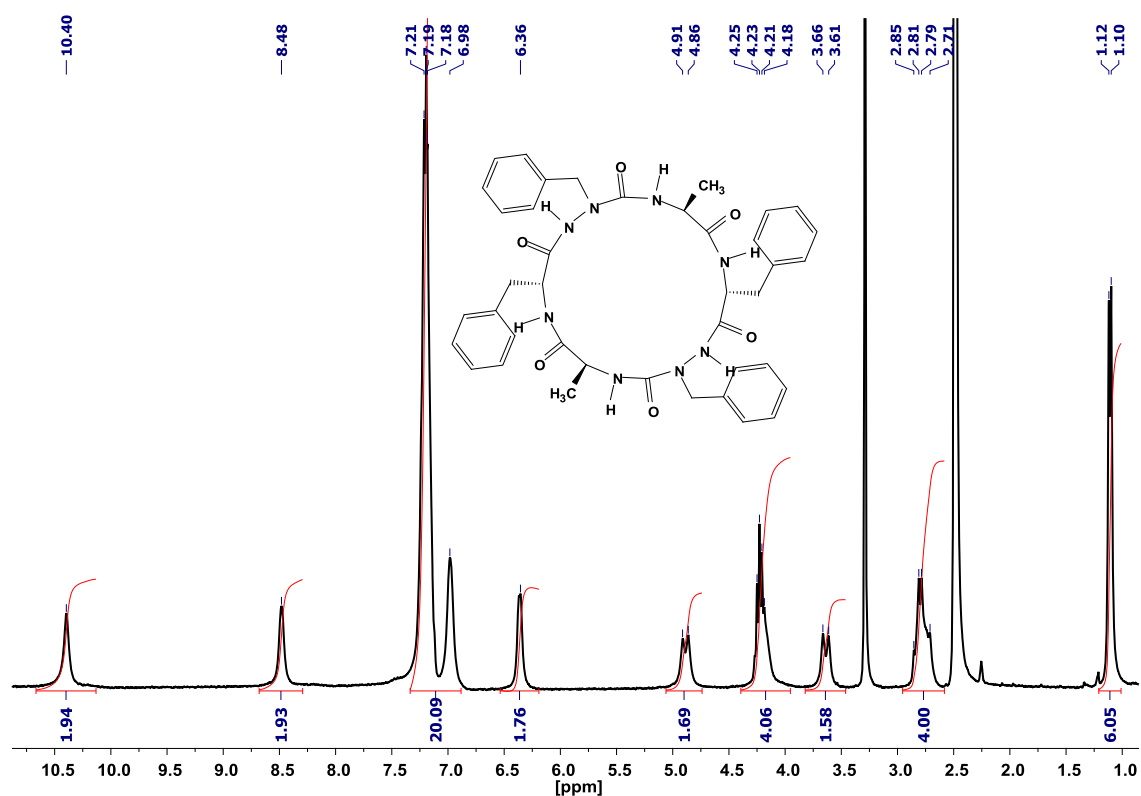


Figure S4.3. ¹H NMR spectrum for compound **9b** recorded in DMSO-*d*₆; (5.0 mmol. L⁻¹).

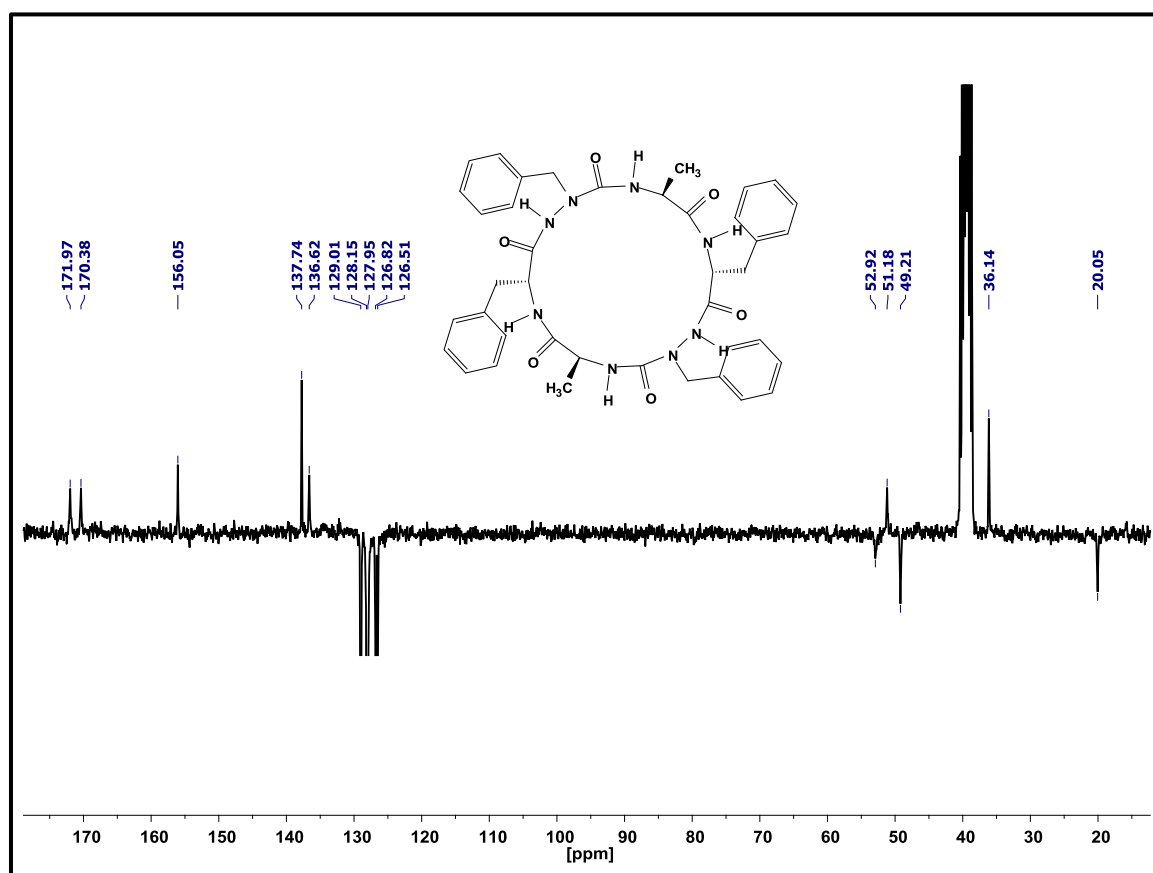
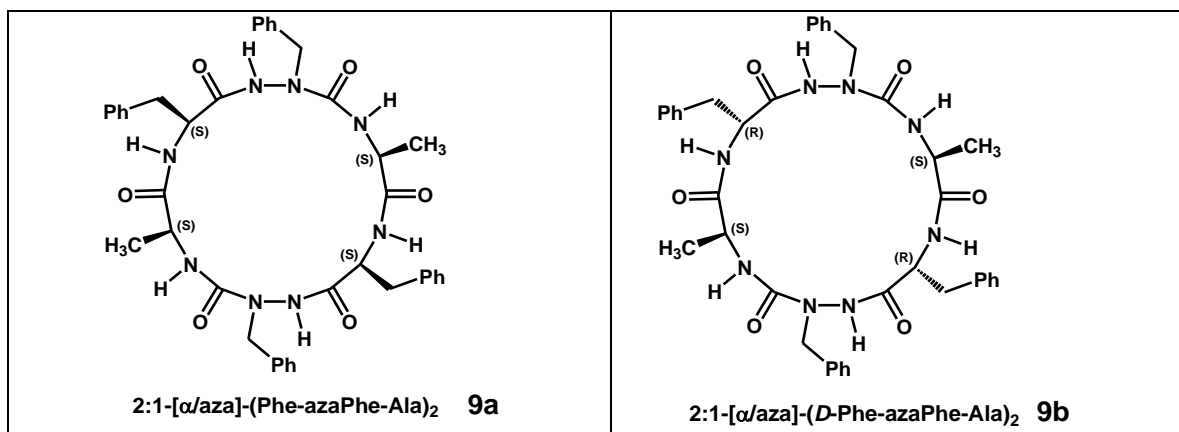


Figure S4.4. ¹³C NMR spectrum for compound **9b**; (DMSO-*d*₆, 8.0 mmol. L⁻¹).

APPENDIX 2

Chapter IV. Impact of C α -Chirality on Supramolecular Self-Assembly in Cyclo-2:1-[α /aza]-Hexamers (*L*-/*D*-Phe-azaPhe-Ala)₂

Crystallographic data for **9a** and **9b**



Cyclic oligomers **9a** and **9b** were recrystallized using diffusion in EtOAc/DIP mixture and EtOH/DIP mixture, respectively.

X-ray data for cyclic azapeptide **9a** were collected at 100 K with a Rigaku Diffraction Xcalibur 2 diffractometer equipped with copper high-intensity/low-power micro-source X-ray tube. Data were processed using CrysAlis PRO 1.171.38.41r^[1]. X-ray data for **9b** were collected at the synchrotron ESRF (Grenoble, France) on beamline Id30b dedicated to macromolecular biocrystallography^[2]. The beamline wavelength was 0.99187Å and the crystal-detector distance 151 mm. In these conditions, the resolution was 0.95Å in the corner of the detector. The diffraction data were processed with XDS^[3]. The precision of the unit cell parameters were estimated according the conclusions of the article of Dauter and Wlodawer on the accuracy of unit-cell parameters in protein crystallography^[4]. The structures of **9a** and **9b** were solved using SHELXT^[5] and Sir2014^[6], respectively. The crystallographic refinements were conducted with SHELXL^[5] using the graphical user interface ShelXle^[7]. Selected crystallographic data for **9a** and **9b** are provided in Table S1.

[1] Rigaku Oxford Diffraction **2015**.

[2] C. Mueller-Dieckmann, M. W. Bowler, P. Carpentier, D. Flot, A. A. McCarthy, M. H. Nanao, D. Nurizzo, P. Pernot, A. Popov, A. Round, A. Royant, D. de Sanctis, D. von Stetten, G. A. Leonard, *Eur. Phys. J. Plus* **2015**, 130, 70.

[3] W. Kabsch, *Acta Crystallographica Section D: Biological Crystallography* **2010**, 66, 125-132.

[4] Z. Dauter, A. Wlodawer, *Acta Crystallogr D Biol Crystallogr* **2015**, 71, 2217-2226.

[5] G. M. Sheldrick, *Acta crystallographica. Section A, Foundations and advances* **2015**, 71, 3-8.

[6] M. C. Burla, R. Caliandro, B. Carrozzini, G. L. Cascarano, C. Cuocci, C. Giacovazzo, M. Mallamo, A. Mazzone, G. Polidori, *Journal of Applied Crystallography* **2015**, 48, 306-309.

[7] C. B. Hubschle, G. M. Sheldrick, B. Dittrich, *Journal of Applied Crystallography* **2011**, 44, 1281-1284.

Details of the crystal structure have been deposited to the Cambridge Crystallographic Data Centre as supplementary publication numbers CCDC 1533841 (**9a**) and 1537325 (**9b**). Copies of the data can be obtained, free of charge, on application to CCDC, 12 Union Road, Cambridge CB2 1EZ, UK [fax: +44(0)-1223-336033 or e-mail: deposit@ccdc.cam.ac.uk].

APPENDIX 2

Chapter IV. Impact of C^α-Chirality on Supramolecular Self-Assembly in Cyclo-2:1-[α /aza]-Hexamers (*L*-/*D*-Phe-azaPhe-Ala)₂

Table S4.1. Selected crystallographic data for **9a** and **9b**

Parameter	Compound 9a	Compound 9b
Chemical formula	C ₄₀ H ₄₄ N ₈ O ₆	8(C ₄₀ H ₄₄ N ₈ O ₆), 9(H ₂ O)
<i>M</i> _r	732.34	6024.78
Crystal system, space group	Monoclinic, <i>P</i> 2	Triclinic, <i>P</i> 1
Unit cell dimensions	a = 17.8027(4) Å b = 5.23678(11) Å c = 20.8450(5) Å	a = 18.43(2) Å b = 20.39(2) Å c = 21.84(2) Å
α	90°	81.1(1)°
β	110.734(3)°	89.3(1)°
γ	90°	70.9(1)°
<i>V</i>	1817.49(8) Å ³	7656(14) Å ³
<i>Z</i>	2	1
<i>F</i> (000)	776.0	3194.0
<i>D</i> _x	1.338 mg. m ⁻³	1.307 mg. m ⁻³
Radiation type	Cu <i>K</i> α , λ = 1.54184 Å	(*) λ = 0.99187 Å
θ	4.1-76.5°	0.9 - 22.0°
μ	0.75 mm ⁻¹	0.20 mm ⁻¹
<i>T</i>	110 K	100 K
Crystal sizes	0.31 × 0.19 × 0.05 mm ³	0.2 × 0.2 × 0.05 mm ³
No. of measured reflections	31112	33740
<i>R</i> _{int}	0.041	0.084
θ_{\max} , θ_{\min}	77.0°, 2.8°	31.5°, 1.3°
<i>R</i> [<i>F</i> ² > 2 σ (<i>F</i> ²)]	0.034	0.086
<i>wR</i> (<i>F</i> ²)	0.108	0.216
<i>S</i>	0.91	1.54

(*) Synchrotron ESRF (Grenoble, France), beamline Id30b.

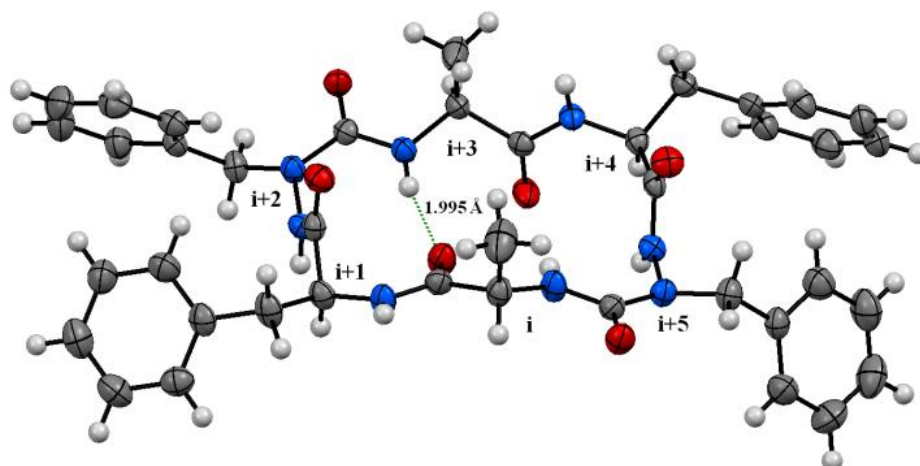


Figure S4.5. Crystal molecular structure of the asymmetric unit of compound **9a** (X-ray). The intramolecular hydrogen bonds (green) are illustrated as dotted lines.

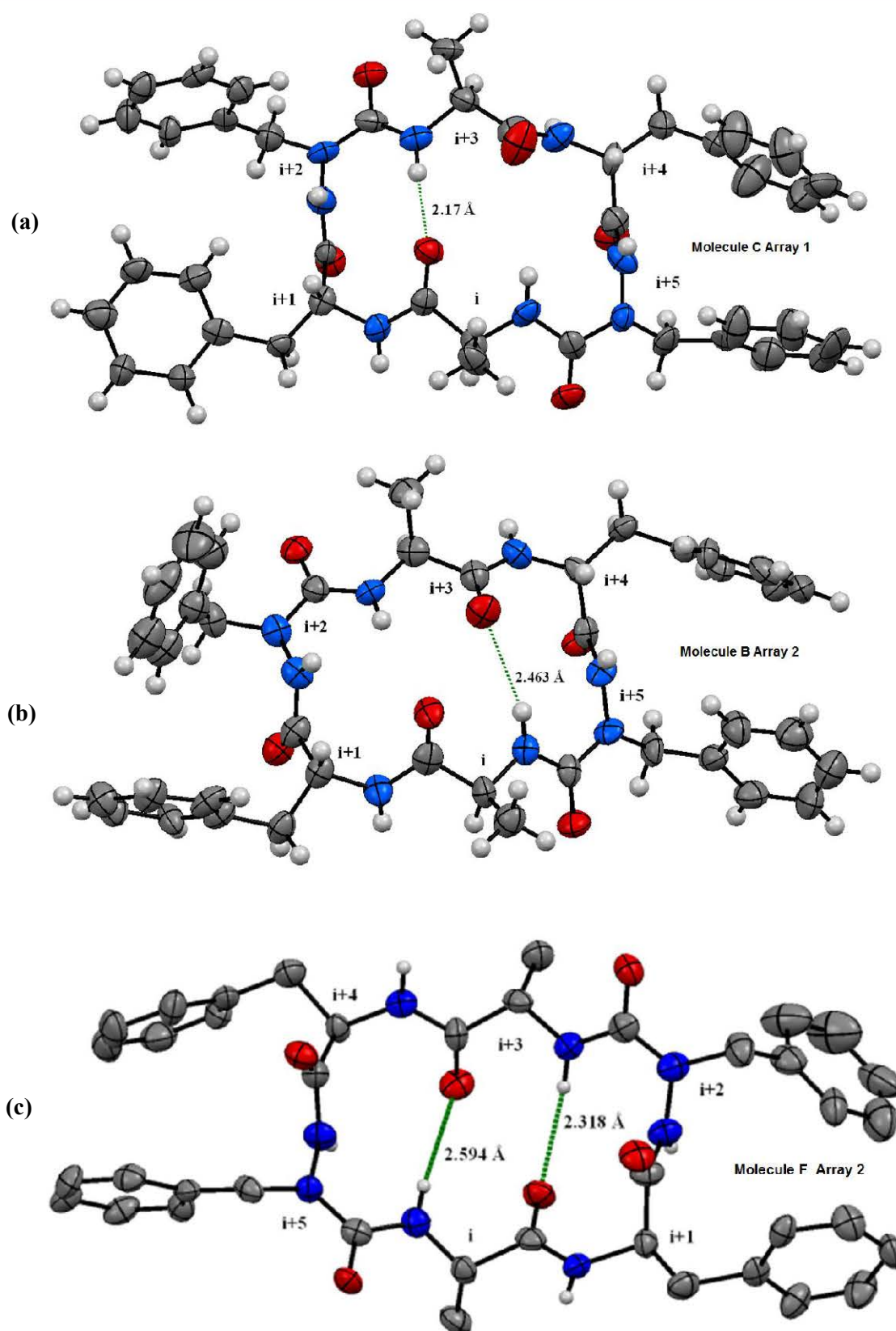


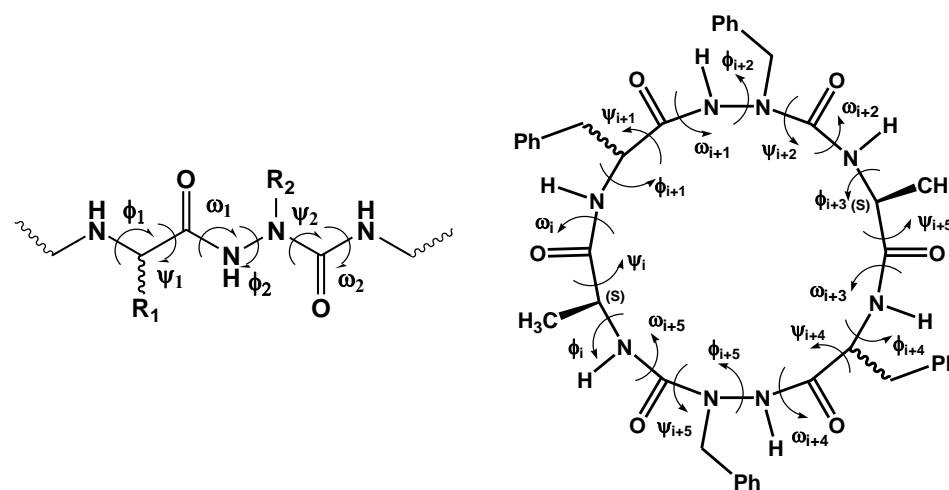
Figure S4.6. (a, b, and c) Selected molecular structures (X-ray) of **B**, **C**, and **F** conformers from the asymmetric unit of compound **9b**, respectively. The intramolecular hydrogen bonds (green) are illustrated as dotted lines.

APPENDIX 2

Chapter IV. Impact of C α -Chirality on Supramolecular Self-Assembly in Cyclo-2:1-[α /aza]-Hexamers (L-/D-Phe-azaPhe-Ala)₂

Table S4.2. Bond angle and intramolecular H-bond distances in **9a**

Intramolecular H-bond in compound 9a				
Residue	Residue	Distance (Å)		Angle (°)
CO (i)	NH (i + 3)	1.995	2.83	141.77



Nomenclature used for the backbone dihedral angles of two cyclic oligomers **9a** and **9b**.

Table S4.3. Torsion angles in **9a**

Parameter	Residue (i + 1)			Residue (i + 2)			Residue (i + 4)			Residue (i + 5)		
	ϕ	ψ	ω	ϕ	ψ	ω	ϕ	ψ	ω	ϕ	ψ	ω
Molecule 9a	-51.63°	125.9°	179.32°	77.71°	-5.93°	-169.78°	-100.67°	103.38°	-176.18°	81.52°	12.24°	-172.49°
β II-turn	-60°	120°	180°	80°	0°	180°	-60°	120°	180°	80°	0°	180°

APPENDIX 2

Chapter IV. Impact of α -Chirality on Supramolecular Self-Assembly in Cyclo-2:1- $[\alpha/\text{aza}]$ -Hexamers (L -/ D -Phe-azaPhe-Ala)₂

Table S4.4. Configuration of the N ^{α} atoms and their deviation from sp² in **9b**

Array 1	Residue	Distance from plane (Å)	Configuration	Array 2	Residue	Distance from plane (Å)	Configuration
Conformer A	(i + 2)	0.174	<i>L (S)</i> sp ³	Conformer B	(i + 2)	0.212	<i>L (S)</i> sp ³
	(i + 5)	0.059	<i>D (R)</i> sp ³		(i + 5)	0.077	<i>D (R)</i> sp ³
Conformer C	(i + 2)	0.07	<i>L (S)</i> sp ³	Conformer D	(i + 2)	0.094	<i>L (S)</i> sp ³
	(i + 5)	0.173	<i>D (R)</i> sp ³		(i + 5)	0.022	<i>D (R)</i> sp ³
Conformer E	(i + 2)	0.209	<i>L (S)</i> sp ³	Conformer F	(i + 2)	0.01	<i>D (R)</i> sp ³
	(i + 5)	0.046	<i>D (R)</i> sp ³		(i + 5)	0.05	<i>D (R)</i> sp ³
Conformer G	(i + 2)	0.113	<i>L (S)</i> sp ³	Conformer H	(i + 2)	0.072	<i>L (S)</i> sp ³
	(i + 5)	0.017	<i>D (R)</i> sp ³		(i + 5)	0.209	<i>D (R)</i> sp ³

Table S4.5. Bond angles and intramolecular H-bonds distances in **9b**

Molecule 9b	Residue	Residue	Distance (Å)		Angle (°)
Conformer A	CO (i)	NH (i + 3)	2.306	3.176	169.75
Conformer B	CO (i + 3)	NH (i)	2.463	3.308	160.97
Conformer C	CO (i)	NH (i + 3)	2.17	3.042	171.23
Conformer D	CO (i)	NH (i + 3)	2.552	3.418	168.4
Conformer E	CO (i + 3)	NH (i)	2.587	3.430	161.23
Conformer F	CO (i)	NH (i + 3)	2.318	3.192	171.55
	CO (i + 3)	NH (i)	2.594	3.471	174.17
Conformer G	CO (i)	NH (i + 3)	2.556	3.43	172.55
Conformer H	CO (i)	NH (i + 3)	2.174	3.043	169.66

APPENDIX 2

Chapter IV. Impact of C^α-Chirality on Supramolecular Self-Assembly in Cyclo-2:1-[α/aza]-Hexamers (L-/D-Phe-azaPhe-Ala)₂

Table S4.6. Torsion angles in **9b**

Array 1	Residue (i + 1)			Residue (i + 2)			Residue (i + 4)			Residue (i + 5)		
Torsion angle (°)	φ	ψ	ω	φ	ψ	ω	φ	ψ	ω	φ	ψ	ω
Conformer A	61.39°	-116.57°	-176.27°	-101.5°	1.01°	-175.30°	90.98°	-109.09°	173.45°	-118.52°	3.51°	-174.88°
Conformer C	66.42°	-112.72°	-179.52°	-105.43°	-3.08°	-170.67°	100.73°	-120.29°	176.50°	-94.256	-0.99°	-173.97°
Conformer E	87.6°	-110.47°	-179.17°	-112.47°	4.18°	178.98°	79.34°	-116.66°	177.49°	-113.98	-0.74°	-177.64°
Conformer G	77.7°	-105.46°	-178.63°	-111.86°	-1.67°	-175.74°	88.23°	-110.61°	174.51°	-120.69	5.73°	-171.54°
βII'-turn	60°	-120°	180°	-80°	0°	180°	60°	-120°	180°	-80°	0°	180°
Array 2	Residue (i + 1)			Residue (i + 2)			Residue (i + 4)			Residue (i + 5)		
Torsion angle	φ	ψ	ω	φ	ψ	ω	φ	ψ	ω	φ	ψ	ω
Conformer B	90.17°	-103.79°	-179.31°	-121.38°	-5.63°	175.60°	75.33°	-117.78	177.44°	-110.39°	-2.24°	-176.96°
Conformer D	72.54°	-106.35°	-177.54°	-108.44°	-0.65°	176.24°	88.81°	-109.45°	173.59°	-119.36°	5.40°	-172.78°
Conformer F	61.47°	-114.98°	-174.69°	-88.93°	-12.66°	-169.54°	86.59°	-104.61°	172.62°	-122.68°	4.22°	-173.18°
Conformer H	57.54°	-114.45°	-178.72°	-105.18°	7.60°	-175.74°	106.84°	-120.69°	173.87°	-92.00°	-5.53°	-172.56°
βII'-turn	60°	-120°	180°	-80°	0°	180°	60°	-120°	180°	-80°	0°	180°

APPENDIX 2

Chapter IV. Impact of C α -Chirality on Supramolecular Self-Assembly in Cyclo-(L-/D-Phe-azaPhe-Ala)₂-Hexamers

Table S4.7. Bond angles and intermolecular H-bond distances between the stacked macrocycles in **9a**

Molecule 9a	Molecule 3	Distance (Å)		Angle (°)
NH (i + 2)	CO (i + 1)	2.318	3.198	161.32
CO (i + 3)	NH (i + 4)	2.238	3.062	158.39
NH (i + 5)	CO (i + 4)	2.239	3.002	152.17

Table S4.8. Bond angles and intermolecular H-bond distances between the stacked macrocycles in **9b**

	Conformer A	Conformer C	Distance (Å)		Angle (°)
Array 1	CO (i + 2)	NH (i + 2)	2.046	2.862	154.08
	NH (i + 4)	CO (i + 3)	1.972	2.842	169.19
	CO (i+4)	NH (i + 5)	2.136	2.819	133.8
	Conformer E	Conformer G	Distance (Å)		Angle (°)
	CO (i + 2)	NH (i + 2)	2.022	2.884	165.77
	NH (i + 4)	CO (i + 3)	2.217	2.957	141.34
CO (i + 4)	NH (i + 5)	2.033	2.829	149.58	
Array 2	Conformer B	Conformer D	Distance (Å)		Angle (°)
	NH (i + 4)	CO (i + 3)	2.251	2.975	139.58
	CO (i + 4)	NH (i + 5)	2.086	2.869	147.87
	CO (i + 2)	NH (i + 2)	2.011	2.861	162.07
	Conformer D	Conformer F	Distance (Å)		Angle (°)
	NH (i + 4)	CO (i + 3)	2.122	2.969	160.74
	CO (i + 4)	NH (i + 5)	2.206	2.926	138.58
	CO (i + 2)	NH (i + 2)	1.973	2.791	153.89
	Conformer F	Conformer H	Distance (Å)		Angle (°)
	NH (i + 4)	CO (i + 3)	2.034	2.902	169.02
CO (i + 4)	NH (i + 5)	2.244	2.911	132.25	

APPENDIX 2

Chapter IV. Impact of C α -Chirality on Supramolecular Self-Assembly in Cyclo-(L-/D-Phe-azaPhe-Ala)₂-Hexamers

Table S4.9. Bond angles and intermolecular H-bond distances between each two adjacent molecules in 9a and 9b

Molecule 9a	Molecule 9a	Distance (Å)		Angle (°)
CO (i + 5)	NH (i + 1)	2.134	2.994	178
NH (i + 1)	CO (i + 5)	2.134	2.994	178
First Array 9b	Second array 9b	Distance (Å)		Angle (°)
Conformer A	Conformer B			
NH (i + 1)	CO (i + 5)	2.044	2.894	162.4
CO (i + 5)	NH (i + 1)	1.961	2.786	155.55
Conformer C	Conformer D	Distance (Å)		Angle (°)
NH (i + 1)	CO (i + 5)	2.121	2.995	171.81
CO (i + 5)	NH (i + 1)	2.011	2.858	160.84
Conformer E	Conformer F	Distance (Å)		Angle (°)
NH(i + 1)	CO (i + 5)	1.982	2.807	155.85
CO (i + 5)	NH (i + 1)	2.029	2.904	172.17
Conformer G	Conformer H	Distance (Å)		Angle (°)
NH (i + 1)	CO (i + 5)	2.003	2.852	161.63
CO (i + 5)	NH (i + 1)	2.097	2.969	171.11

APPENDIX 2

Chapter IV. Impact of α -Chirality on Supramolecular Self-Assembly in Cyclo-(L-/D-Phe-azaPhe-Ala)₂-Hexamers

Statistical analysis of hexacyclic peptides in the Cambridge Structural Database (CSD)

The CSD searches were performed using the program ConQuest and version 5.38 of the database. The search fragment was defined as shown in Figure S4.7. During the search the following filters were applied: 3D coordinates determined, R factor ≤ 0.1 , Not disordered, No errors and Only Organics. Among the 59 hits returned, the 4 bridged cyclohexamers were excluded. A total of 65 independent molecules (see below the list of the selected hits) were analyzed automatically using the “3D parameter” tool to evaluate in each case the angles between the carbonyl directions and the mean plane of the cyclohexamer. The average number of carbonyl groups per cycle in a pseudo-axial position was 2.7.

ID entries the selected hits:

UXOYEN; AAGAGG10; AHELEG; BIHTUH; BIHXUL10; BINJIR; BUNYEO10; BUYXOI; CAHWEN; CAMVES; CAMVES01; CGDLLL10; CGLEGL; CGLPGL; CLPGDH; CPRGCA20; CUBZEG; CYBGPP; DALPUC; DICWET; DUPKEE; DUYTIA; FALLIO; FAQYEC; FAQYIG; GAJFAY; GGAAGG; HEYZER; HXSARM; IJAQIV; IJAQOB; KINBAK; KIVDIC; MOCXUY; OGAZOM; OHUWUJ; OHUXAQ; OHUXEU; PANTOM; PAPRVA; PROGLY20; RAQVOU; SAVLOS; SAVLUY; VAWTAQ; VOKKAH; XINPAN; XINPAN; YEXJIV; YOMNOE; ZAJPAB; ZEWREA; ZOZTUD; ZUKRAY; CAMVES02.

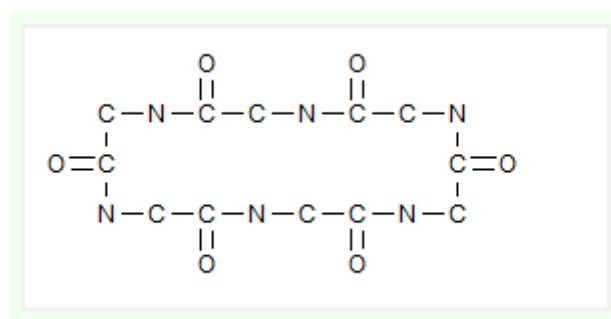


Figure S4.7. The search fragment input into the CSD.

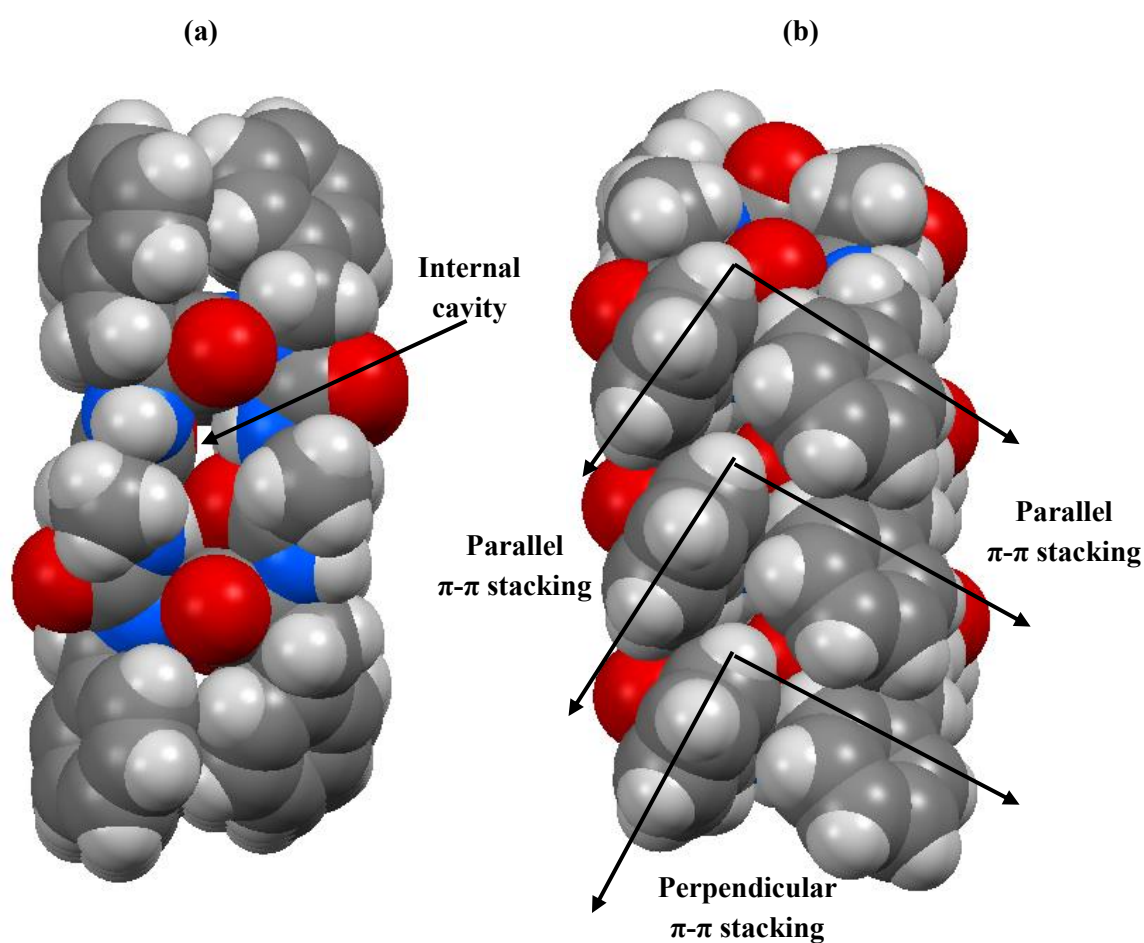


Figure S4.8a. Representation of supramolecular stacking in **9a** by considering the van der Waals radii between atoms: (a) top view shows the small internal cavity, and (b) side view shows the parallel and perpendicular π - π stacking between the benzyl groups.

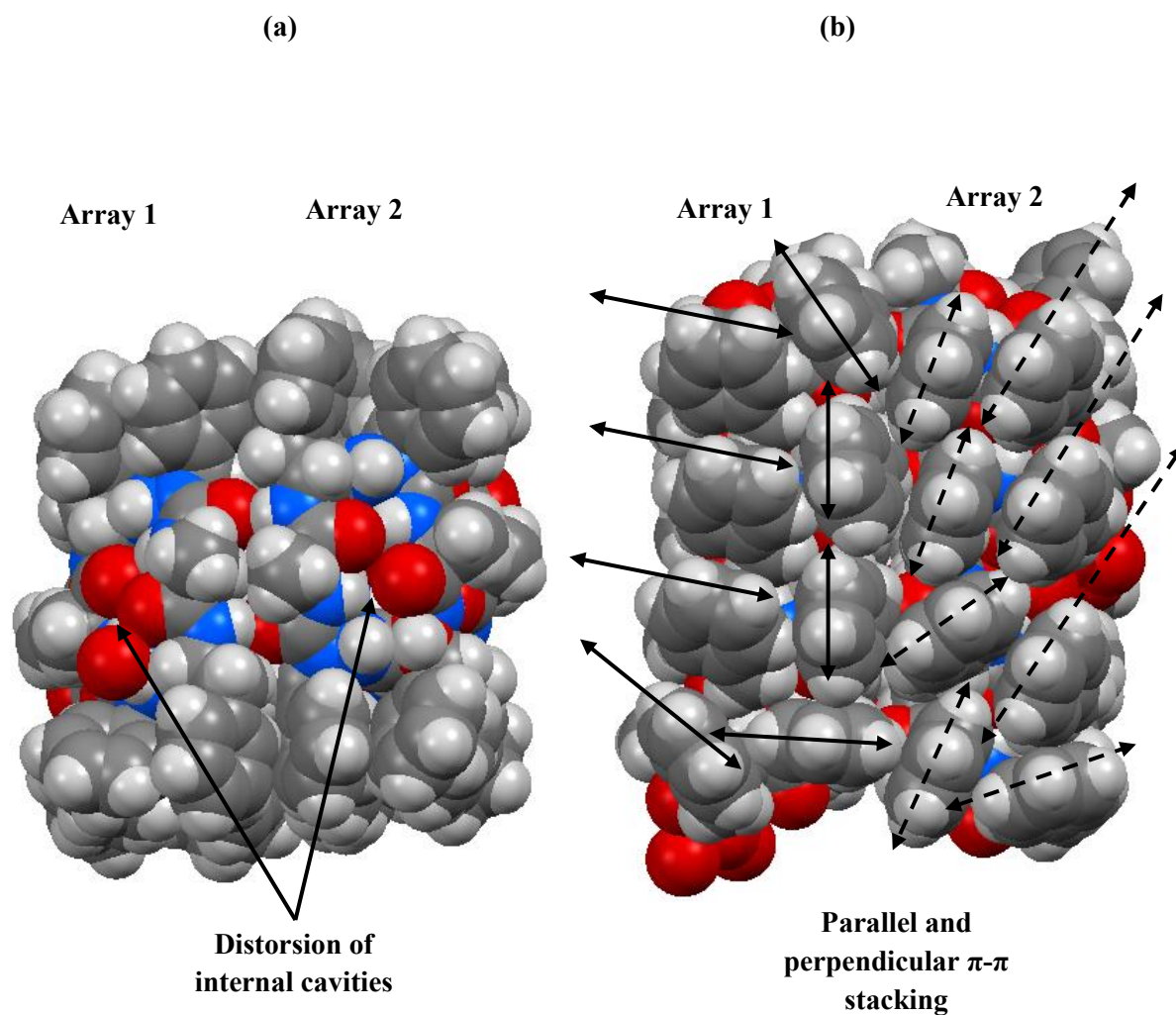


Figure S4.8b. Representation of supramolecular stacking in the asymmetric unit of **9b** by considering the van der Waals radius between atoms in the two arrays: (a) top view shows the distortion of the internal cavities; and (b) side view shows the parallel and perpendicular π - π stacking between the benzyl groups.

APPENDIX 2

Chapter IV. Impact of α -Chirality on Supramolecular Self-Assembly in Cyclo-(*L*-/*D*-Phe-azaPhe-Ala)₂-Hexamers

Spectroscopic data

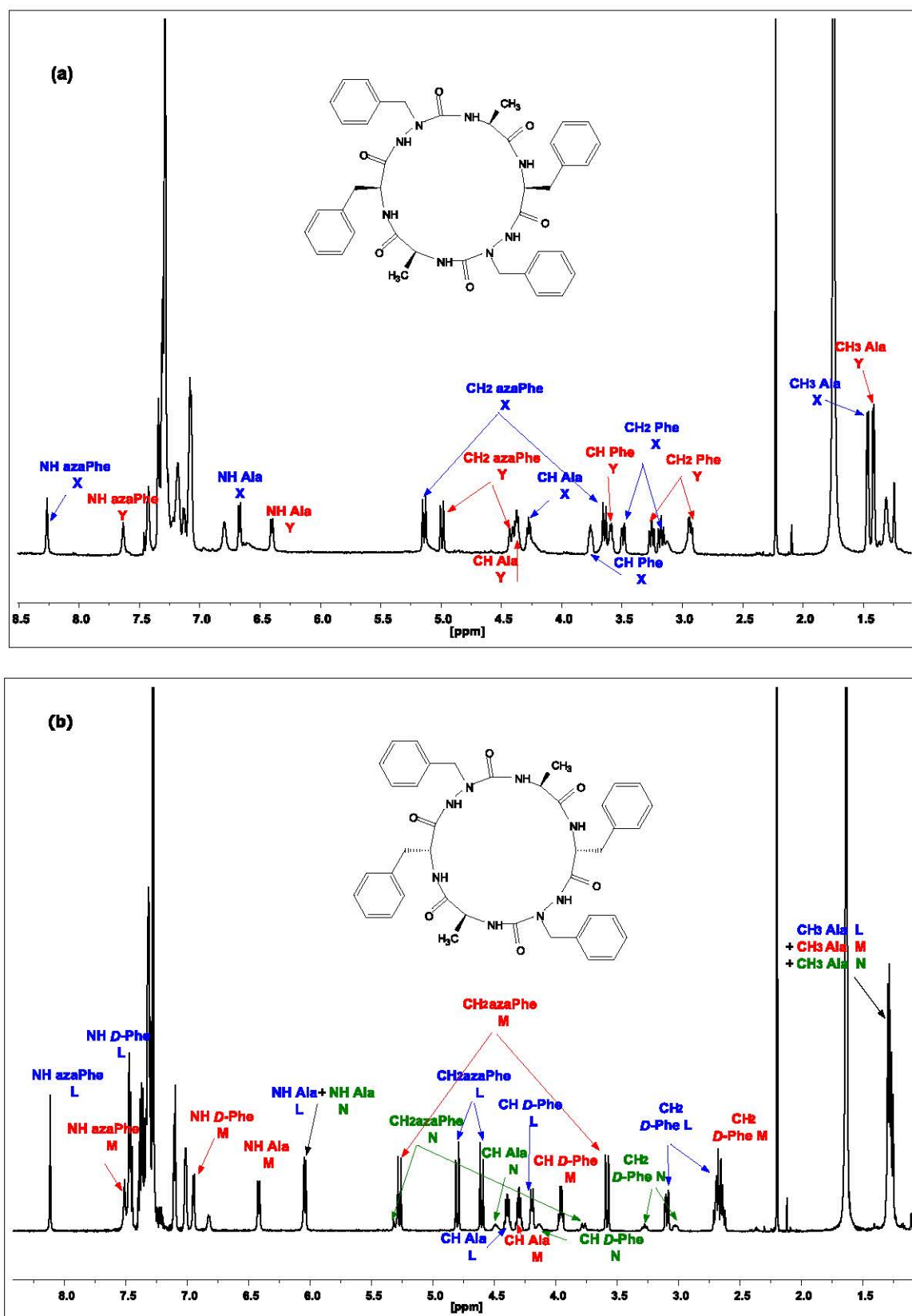


Figure S4.9. ¹H NMR (600 MHz): (a) compound **9a** (0.8 mmol L⁻¹ in CDCl₃, 253 K), and (b) compound **9b** (0.5 mmol L⁻¹ in CDCl₃, 278 K).

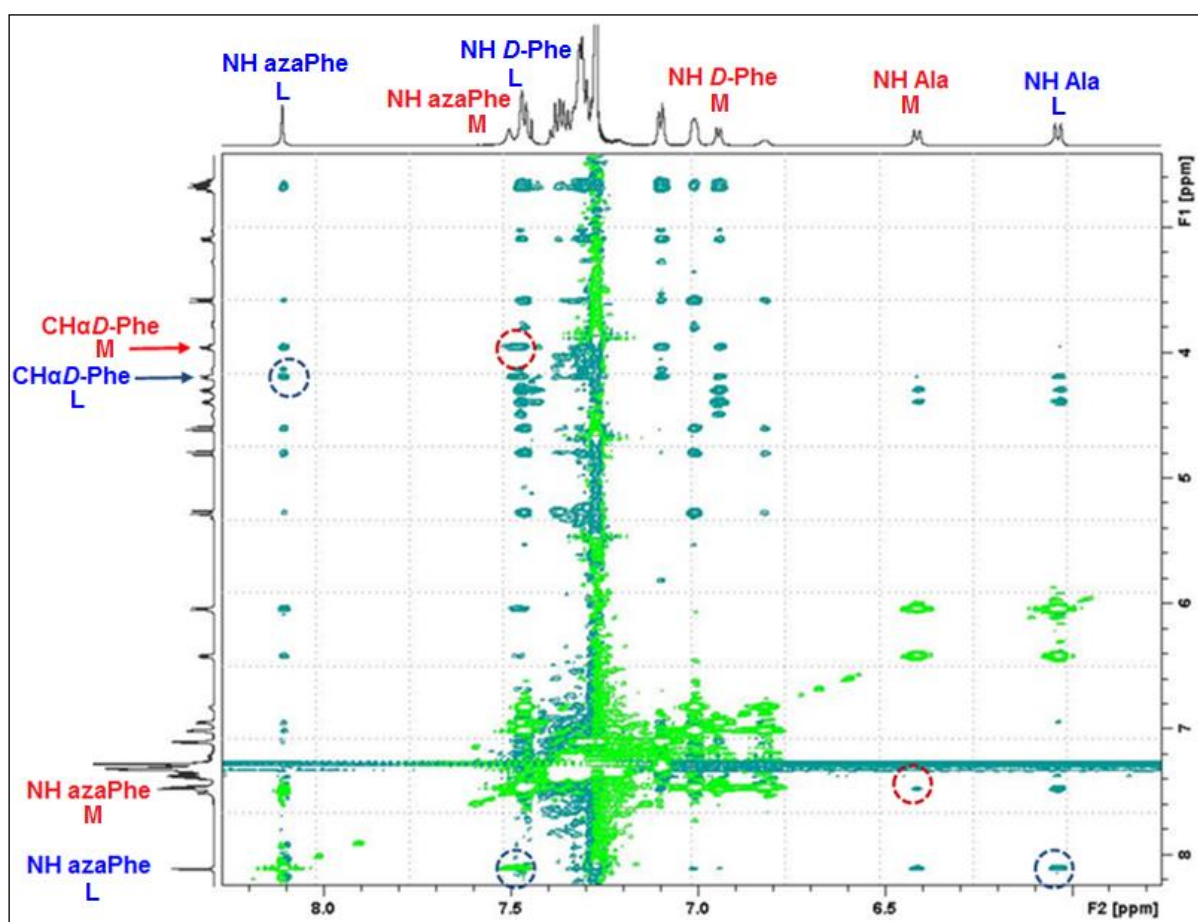


Figure S4.10. 2D ROESY spectrum illustrating the correlations of β -turn conformation in the two conformers **L** and **M** of compound **9b**; (600 MHz, 0.5 mmol. L⁻¹, CDCl₃).

APPENDIX 2

Chapter IV. Impact of α -Chirality on Supramolecular Self-Assembly in Cyclo-(*L*-/*D*-Phe-azaPhe-Ala)₂-Hexamers

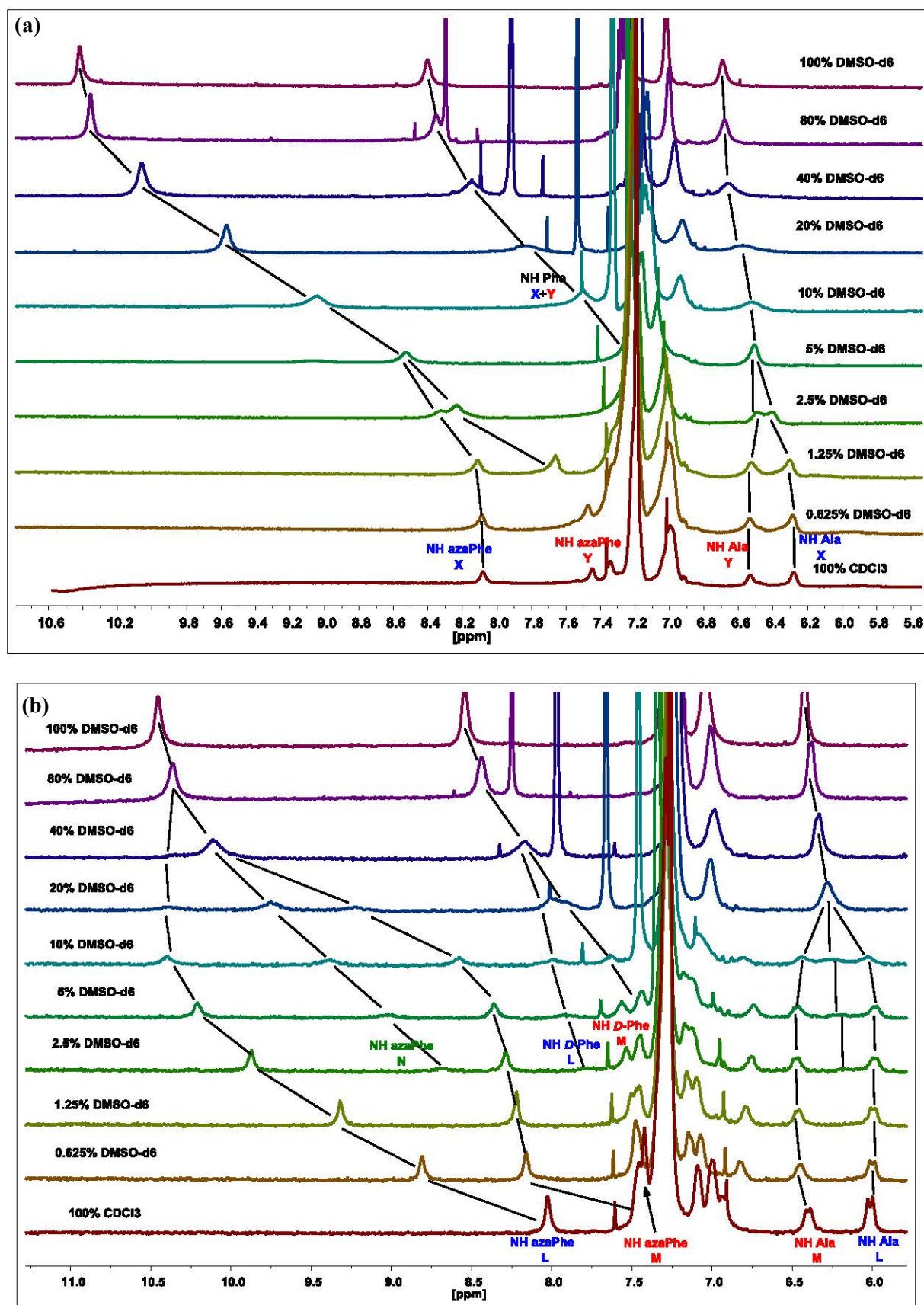


Figure S4.11. Chemical shift-variations (δ) ppm of NH protons for: (a) **9a**, and (b) **9b** as a function of % [CDCl₃/DMSO-*d*₆] mixtures; (600 MHz, 3.0 mmol. L⁻¹).

APPENDIX 2

Chapter IV. Impact of α -Chirality on Supramolecular Self-Assembly in Cyclo-(*L*-/*D*-Phe-azaPhe-Ala)₂-Hexamers

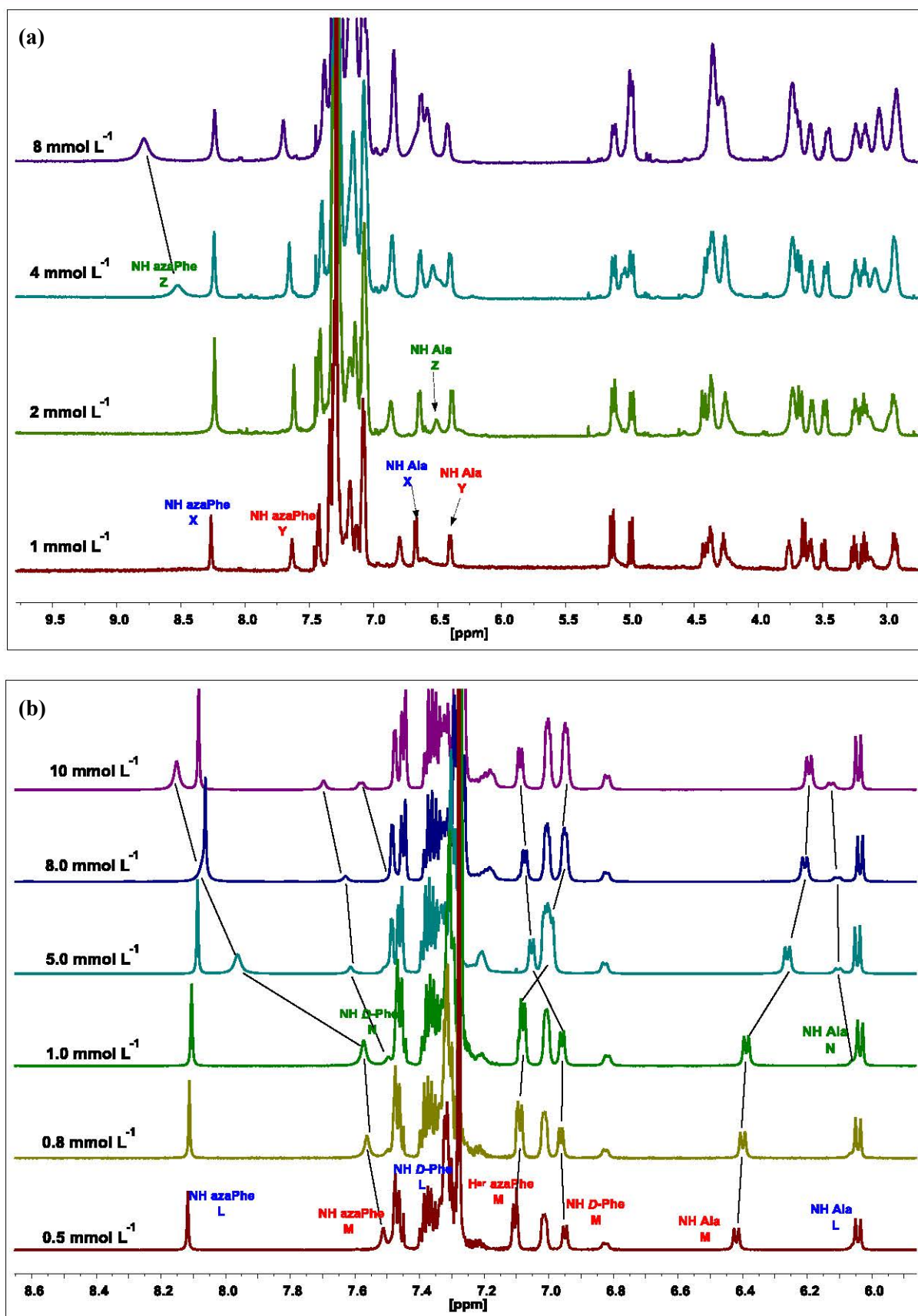


Figure S4.12. Concentration-dependent ¹H NMR (600 MHz) chemical shift (δ) ppm in CDCl₃ of NH protons for: (a) 9a (from 1.0 to 8.0 mmol L⁻¹), and (b) 9b (from 0.5 to 10.0 mmol L⁻¹).

APPENDIX 2

Chapter IV. Impact of α -Chirality on Supramolecular Self-Assembly in Cyclo-(*L*-/*D*-Phe-azaPhe-Ala)₂-Hexamers

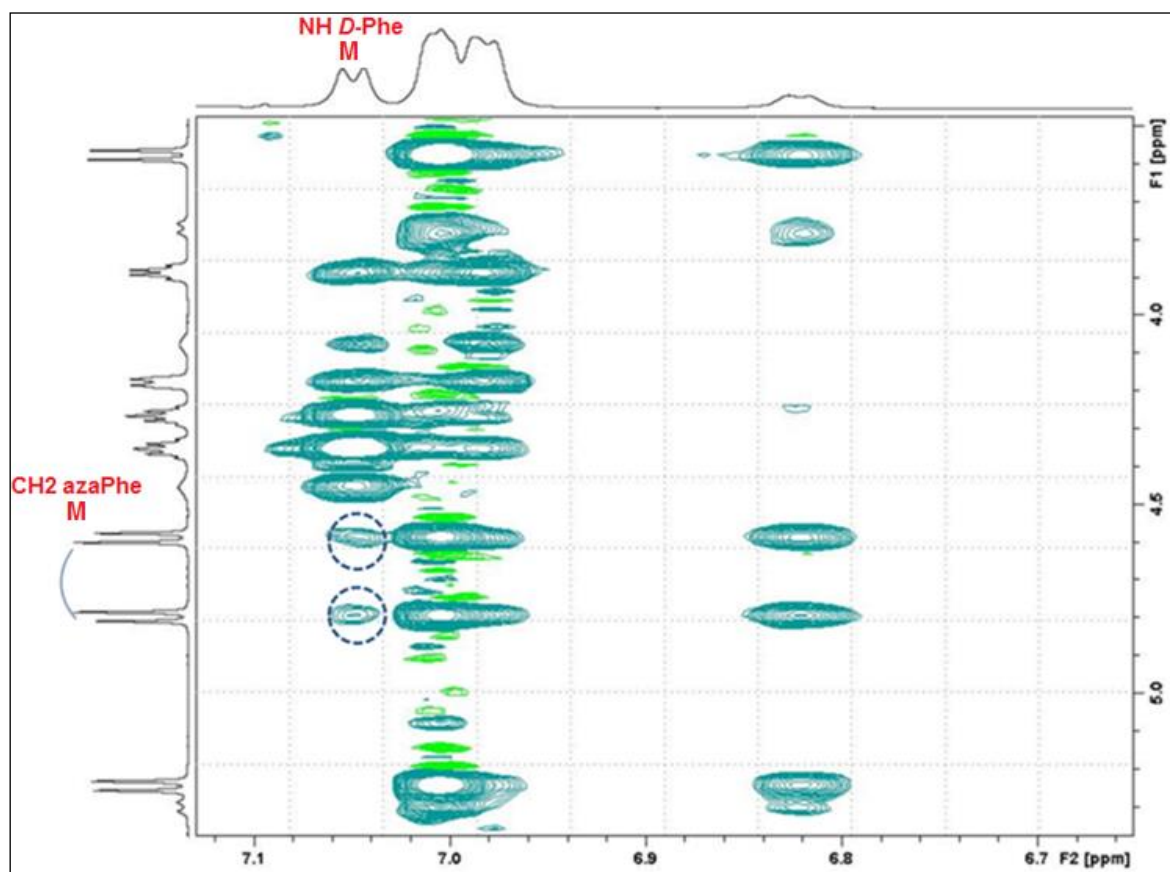


Figure S4.13. Portion of the 2D ROESY spectrum illustrating the conservation of β II'-turn conformation in the conformer **M** of compound **9b** in the supramolecular structure; (600 MHz, 5.0 mmol. L⁻¹, CDCl₃).

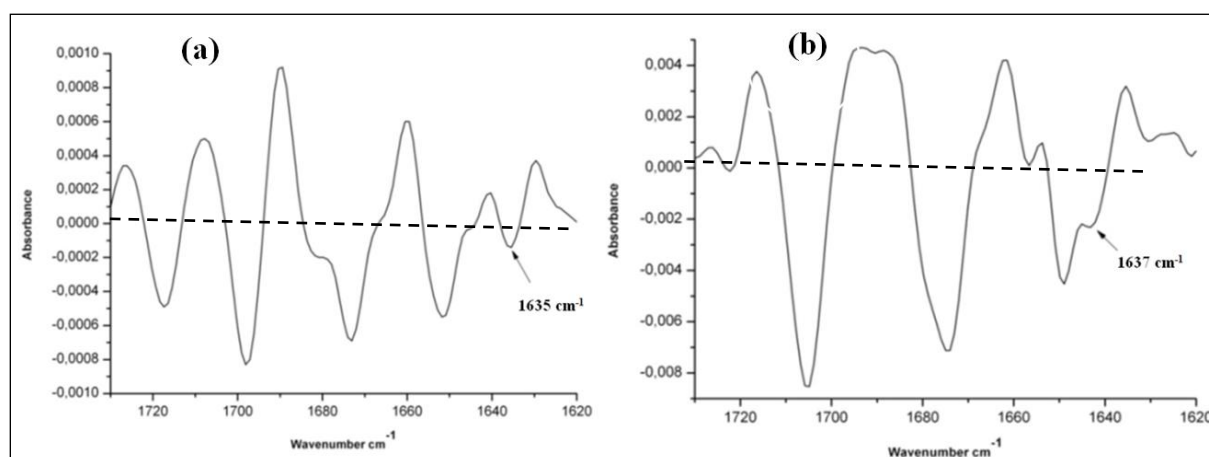


Figure S4.14. 2nd derivative FTIR spectra of: (a) **9a**, and (b) **9b**; (0.8 mmol. L⁻¹, CDCl₃).

APPENDIX 3

Chapter VI. Supramolecular Organo-Gels Based Cyclo-(D-Phe-azaPhe-Ala)₂-Hexamer

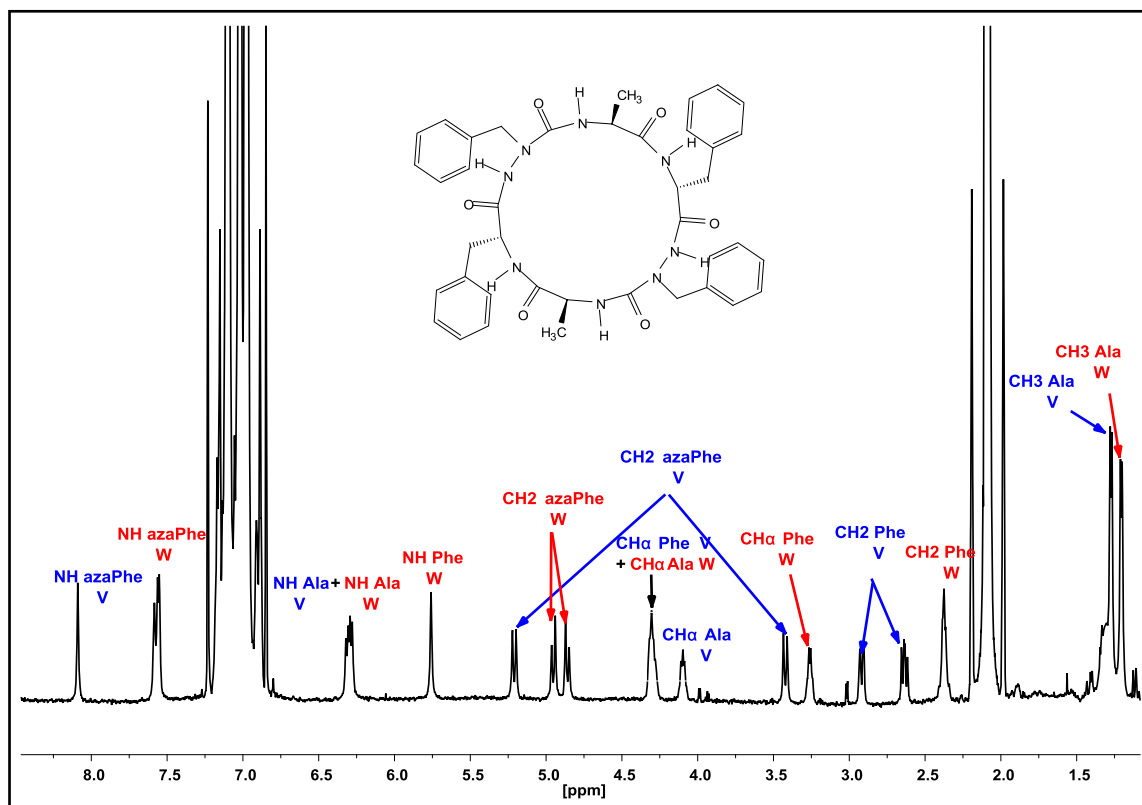


Figure S6.1. ¹H NMR (600 MHz) spectrum of compound **9b** in toluene-*d*₈; (0.1 mM at 293 K).

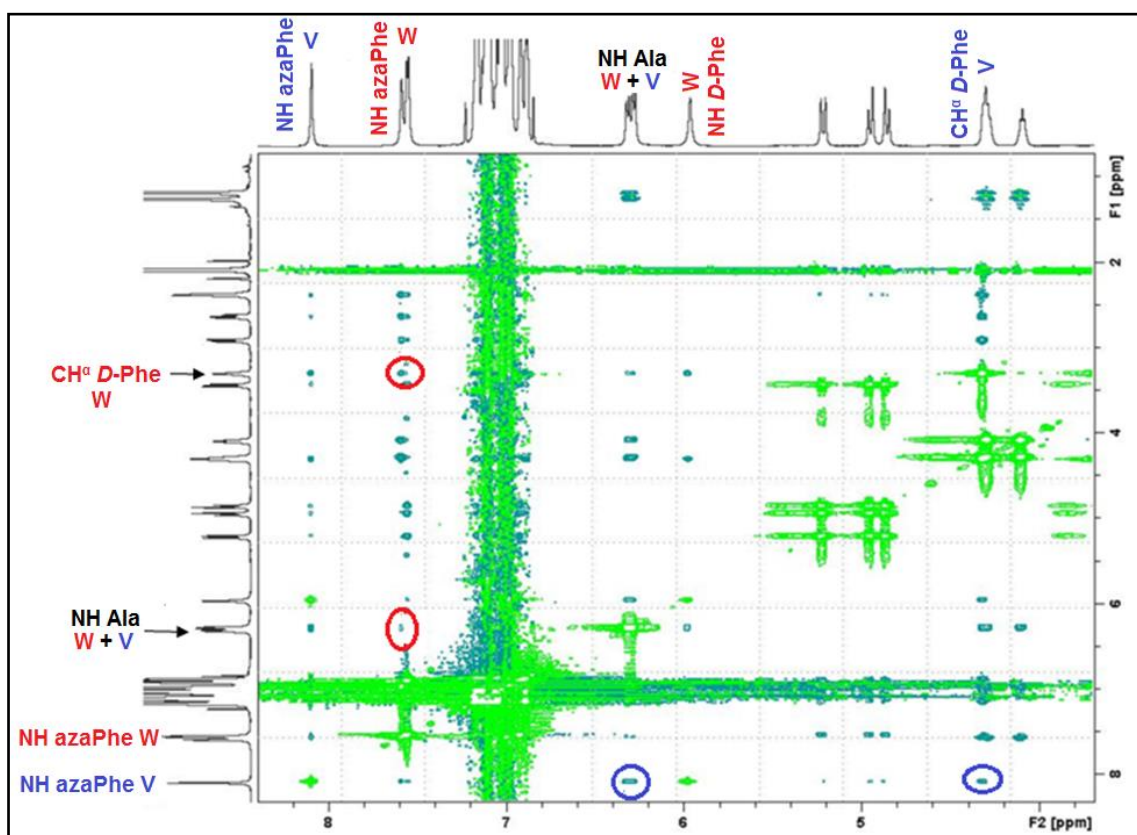


Figure S6.2. 2D ROESY spectrum of hetero cyclohexamer **9b** in toluene-*d*₈; (1.0 mM at 293 K) illustrating the ROE correlations of conformers **V** and **W**.

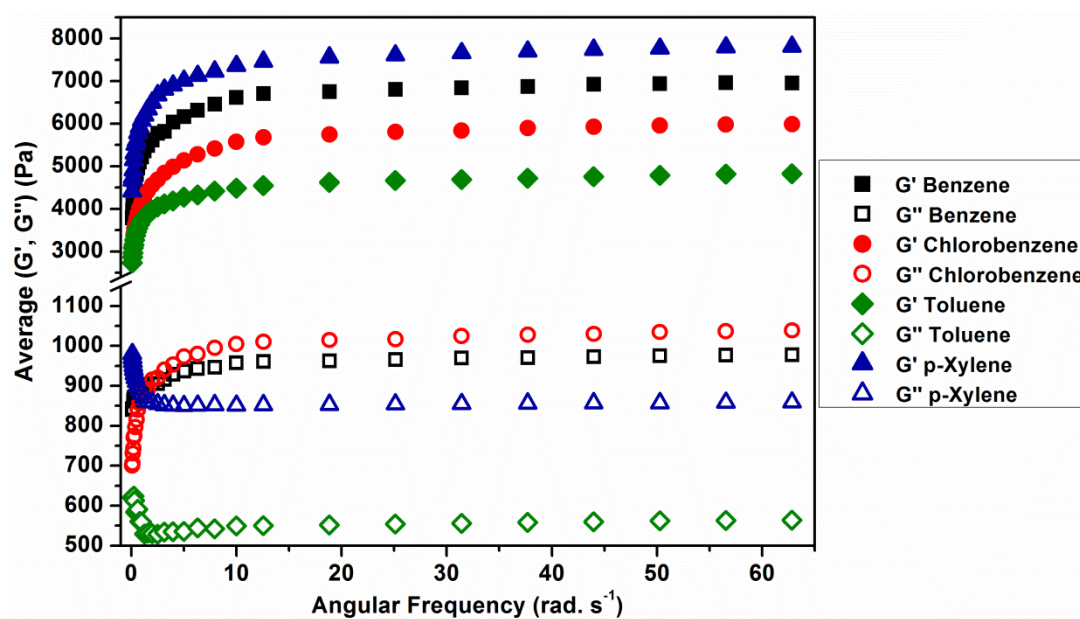


Figure S6.5. The rheogram shows the oscillatory frequency sweep experiments (OFS), plot of the average values of G' and G'' for a range of concentrations of **9b** in the different gelified solvents as a function of angular frequency (ω); ($c = 0.4 - 1.0$ wt%, $T = 25$ °C, $\sigma = 1.5$ Pa).

APPENDIX 3

Chapter VI. Supramolecular Organo-Gels Based Cyclo-(D-Phe-azaPhe-Ala)₂-Hexamer

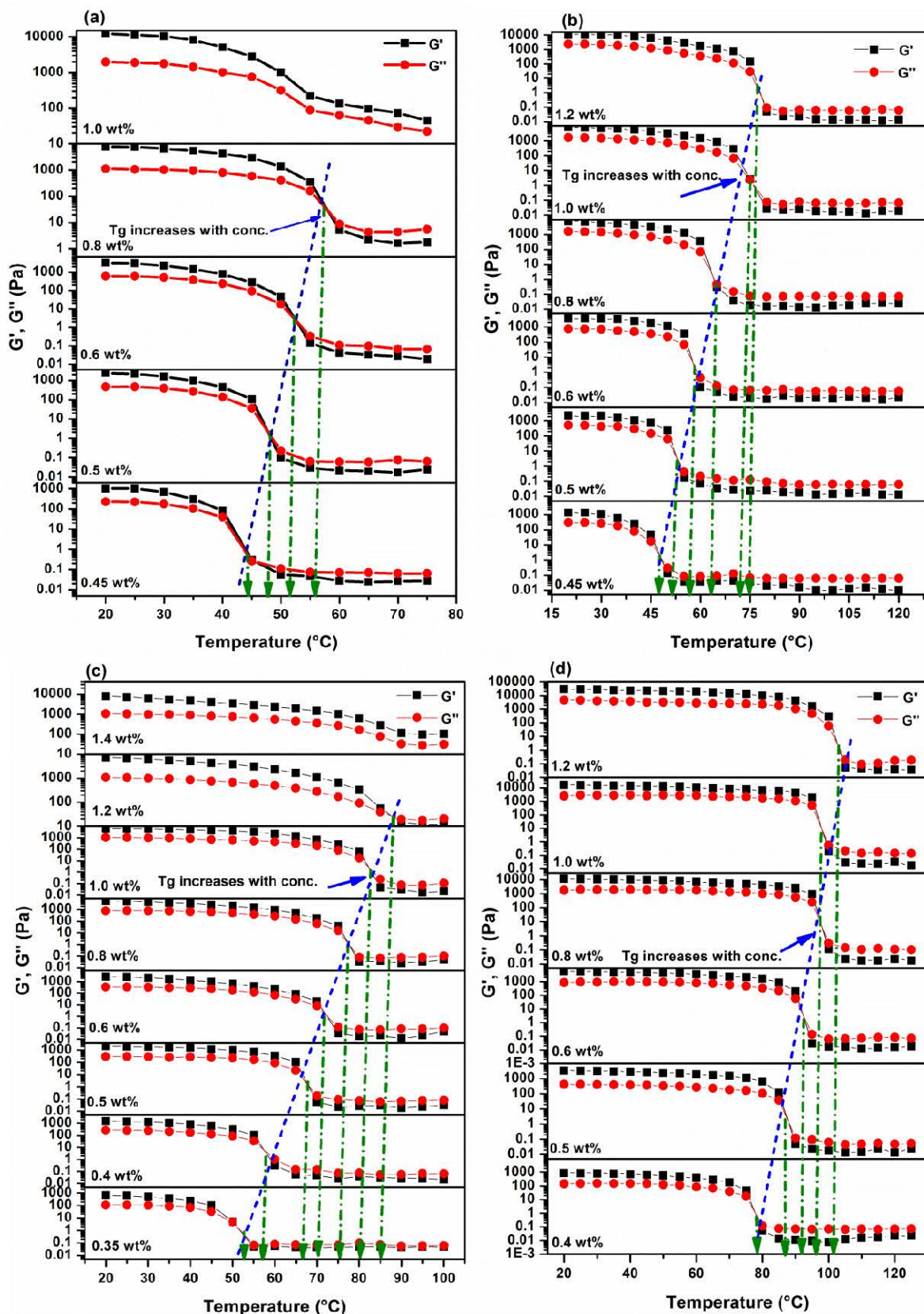


Figure S6.6. The rheograms for the oscillatory temperature sweep experiments, plot of the elastic (G') and viscous (G'') moduli as a function of temperature (T) for a range of concentrations of **9b** in the different gelified solvents: (a) benzene, (b) chlorobenzene, (c) toluene, and (d) *p*-xylene; ($\omega = 0.628 \text{ rad. s}^{-1}$, $\sigma = 1.5 \text{ Pa}$).

Synthesis of Fmoc-2:1-[α /aza]-Trimers:

^aNote 1: Fmoc-OSu has been crystallized before using: 0.05 mol commercially Fmoc-OSu is dissolved in 30 mL CHCl_3 and then it crystallizes by addition of 8.0 mL diethyl ether (72 % yield).

^bNote 2: If the products are not in pure form, flash chromatography on silica gel 60 (0.04 – 0.063 μm Mesh ASTM) is recommended using 20 % EtOH : 80 % DCM as eluent for both products **7a'** and **7b'**.

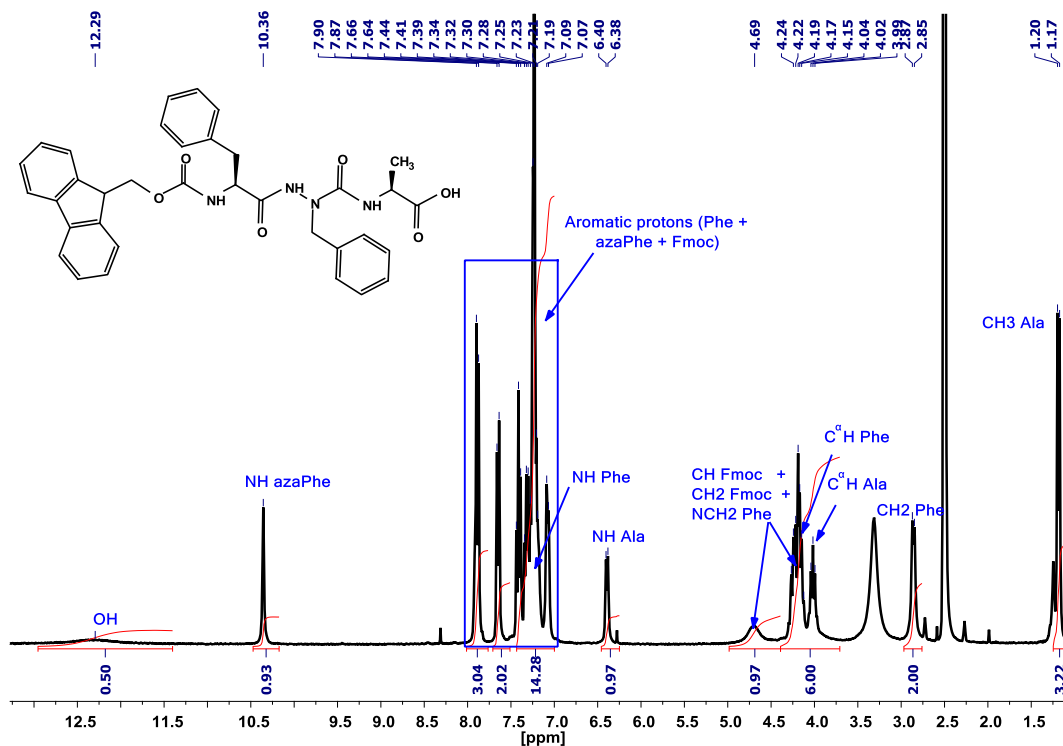


Figure S7.1. ¹H NMR spectrum for compound **7a'** recorded in $\text{DMSO}-d_6$; (4.0 mmol. L^{-1} , 300 K).

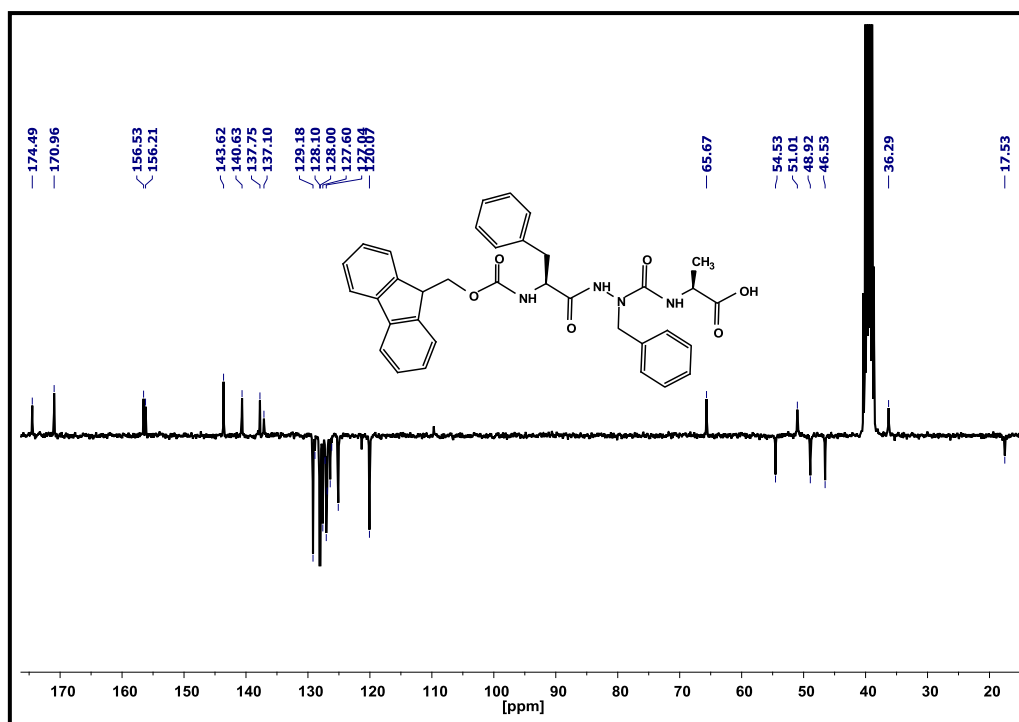
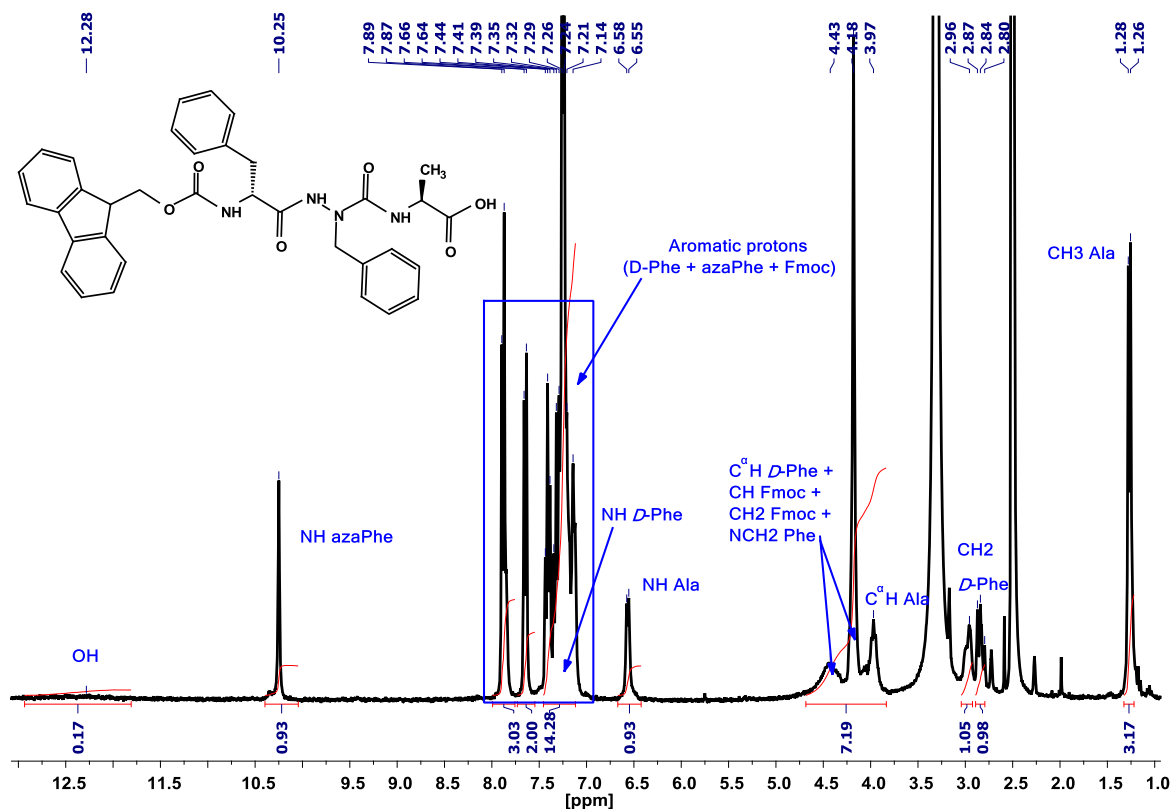
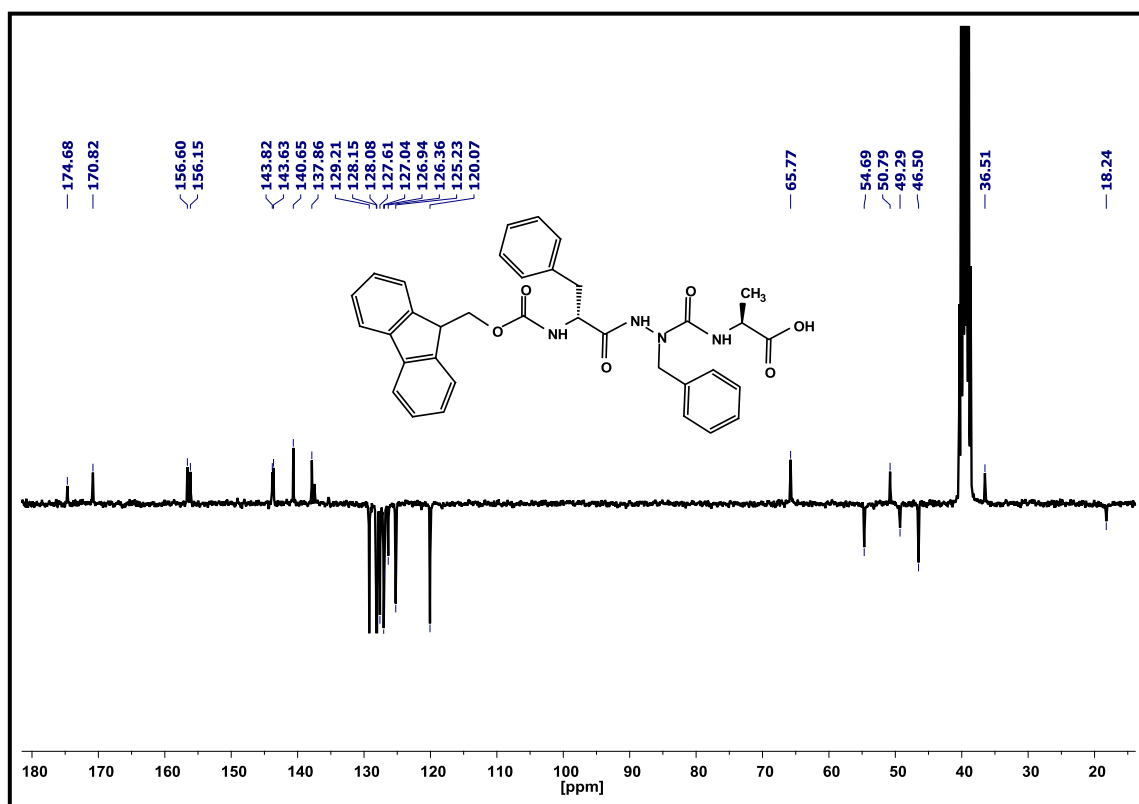


Figure S7.2. ¹³C NMR spectrum for compound **7a'**; ($\text{DMSO}-d_6$, 8.0 mmol. L^{-1} , 300 K).

Figure S7.3. ^1H NMR spectrum for compound **7b'** recorded in $\text{DMSO-}d_6$; (4.0 mmol. L^{-1} , 300 K).Figure S7.4. ^{13}C NMR spectrum for compound **7b'**; ($\text{DMSO-}d_6$, 8.0 mmol. L^{-1} , 300 K).

X-ray crystallographic data for **7b'**

Compound Fmoc-*D*-FazaFA (**7b'**) was recrystallized using diffusion in EtOH. X-ray data for azapeptide **7b'** were collected at 100 K with a Rigaku Diffraction Xcalibur 2 diffractometer equipped with molybdenum micro-source X-ray tube. Data were processed using CrysAlis PRO 1.171.38.43^[1]. The precision of the unit cell parameters were estimated according the conclusions of the article of Dauter and Wlodawer on the accuracy of unit-cell parameters in protein crystallography^[2]. The structures of **7b'** was solved using SHELXT^[3]. The crystallographic refinements were conducted with olex2.refine software^[4] using the graphical user interface Olex2^[5]. Selected crystallographic data for **7b'** are provided in Table S7.1.

[1] Rigaku Oxford Diffraction **2015**.

[2] Z. Dauter, A. Wlodawer, *Acta Crystallogr D Biol Crystallogr* **2015**, *71*, 2217-2226.

[3] G. M. Sheldrick, *Acta crystallographica. Section A, Foundations and advances* **2015**, *71*, 3-8.

[4] Bourhis, L. J., Dolomanov, O. V., Gildea, R. J., Howard, J. A. K. & Puschmann, H. *Acta Cryst.* **2015**, *A71*: 59-75

[5] Dolomanov, O. V., Bourhis, L. J., Gildea, R. J., Howard, J. A. K. & Puschmann, H. *J. Appl. Cryst.* **2009**, *42*, 339-341.

Details of the crystal structure have been deposited to the Cambridge Crystallographic Data Centre as supplementary publication number CCDC0000 (**7b'**). Copy of the data can be obtained, free of charge, on application to CCDC, 12 Union Road, Cambridge CB2 1EZ, UK [fax: +44(0)-1223-336033 or e-mail: deposit@ccdc.cam.ac.uk].

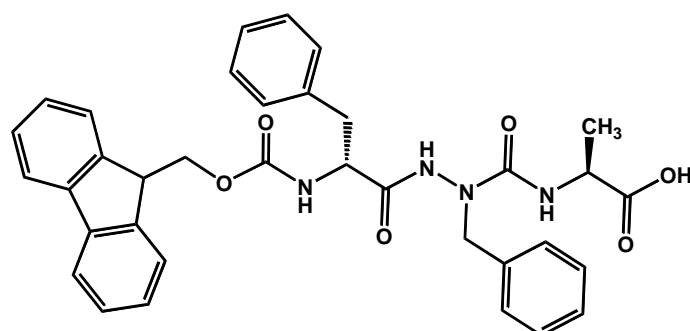
Fmoc-*D*-Phe-azaPhe-Ala-OH 7b'

Table S7.1. Selected crystallographic data for 7b'

Parameter	Compound 7b'
Chemical formula	2 C ₃₅ H ₃₄ N ₄ O ₆
M_r	606.68
Crystal system, space group	Triclinic, $P1$
Unit cell dimensions	a = 10.1083 (4) Å b = 11.2185 (11) Å c = 15.4760 (6) Å
α	99.653 (4)°
β	96.494 (3)°
γ	116.412 (4)°
V	1514.12 (14) Å ³
Z	2
$F(000)$	640.3243
D_x	1.331 mg m ⁻³
Radiation type	Mo $K\alpha$, $\lambda = 0.71073$ Å
θ	3.7 – 31.3°
μ	0.09 mm ⁻¹
T	100 K
Crystal size	0.34 × 0.14 × 0.07 mm
No. of measured reflections	32520
R_{int}	0.043
$\theta_{max}, \theta_{min}$	31.7°, 2.9°
$R[F^2 > 2\sigma(F^2)]$	0.054
$wR(F^2)$	0.120
S	1.05

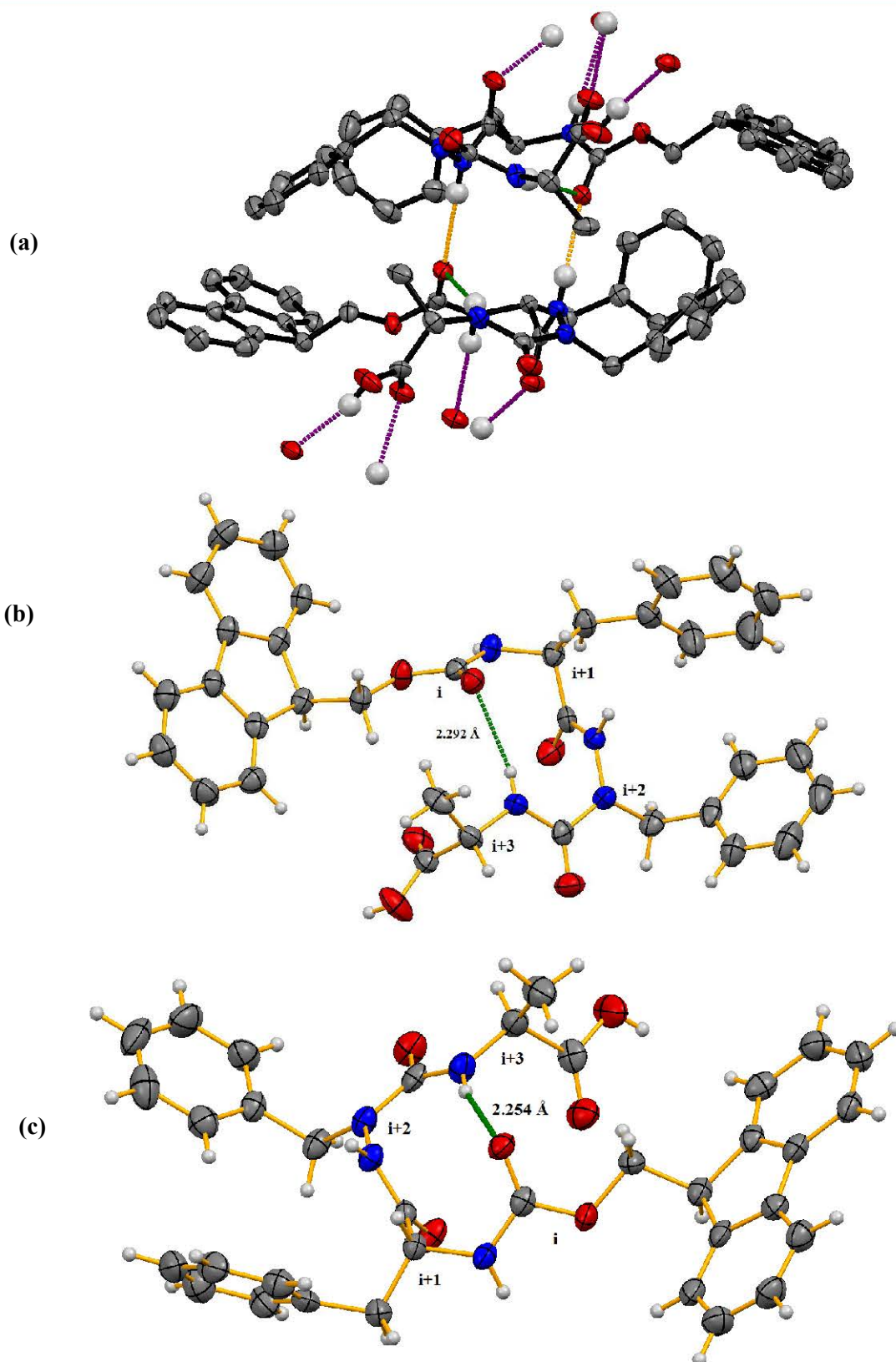
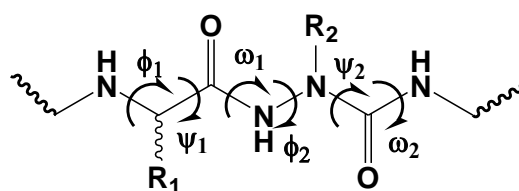


Figure S7.5. ORTEP views for the crystal molecular structures (X-ray) of: (a) asymmetric unit of compound **7b'**, (b) conformer **P**, and (c) conformer **Q**. The intramolecular and intermolecular hydrogen bonds are illustrated as dotted lines in green and orange colors, respectively. The H atoms in (a), except those of the NH and OH groups, have been omitted for clarity.



Nomenclature for the backbone dihedral angles of 2:1-[a/aza]-Fmoc-*D*-Phe-azaPhe-Ala (**7b'**)

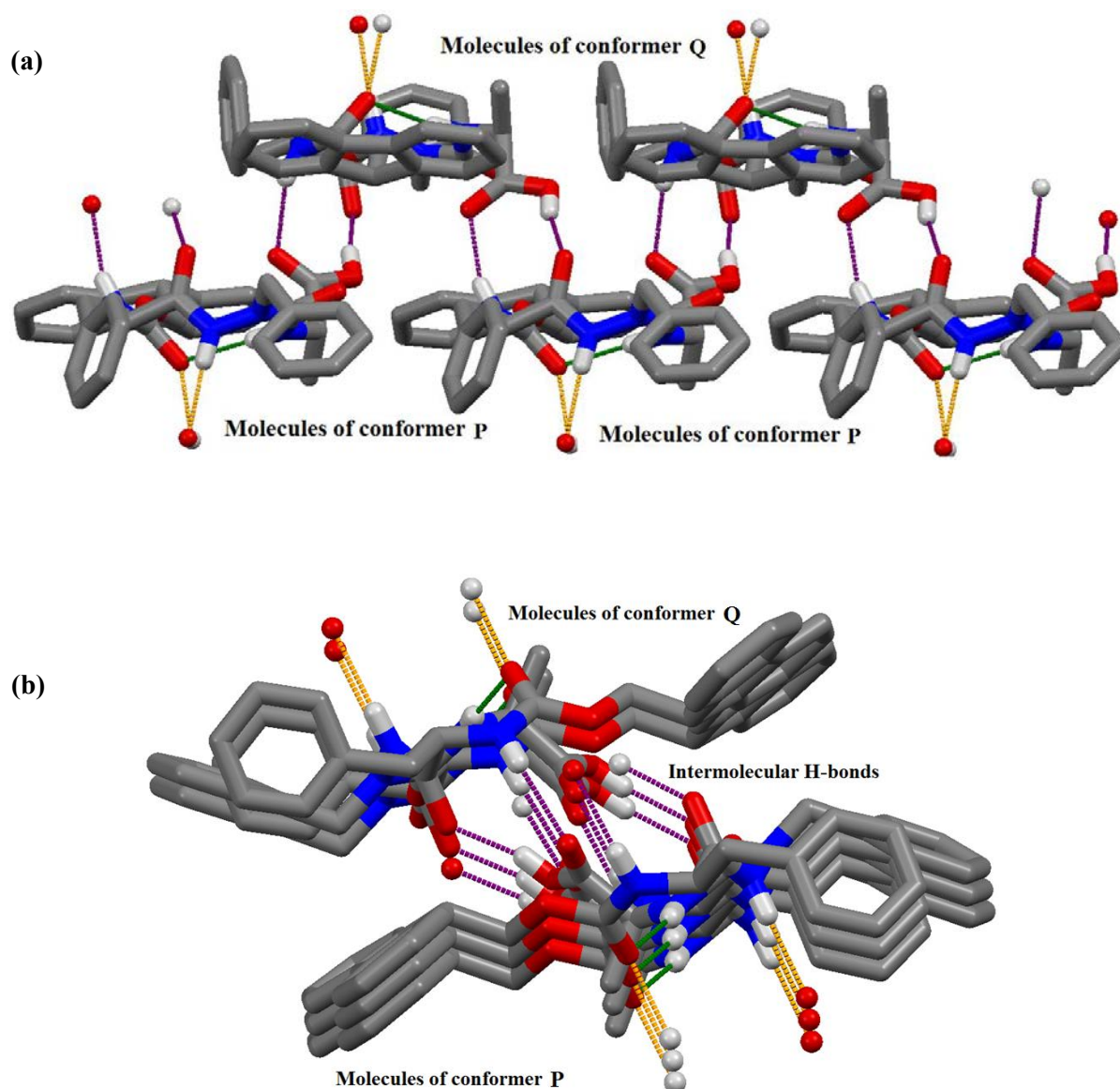


Figure S7.6. View of the packing mode in compound **7b'** in crystal state (X-ray): (a) side view, and (b) top view, the intermolecular hydrogen bonds (purple) and intramolecular hydrogen bonds (green) are marked as dashed lines. The H atoms, except those of the NH and OH groups, have been omitted for clarity.

NMR Spectroscopic data

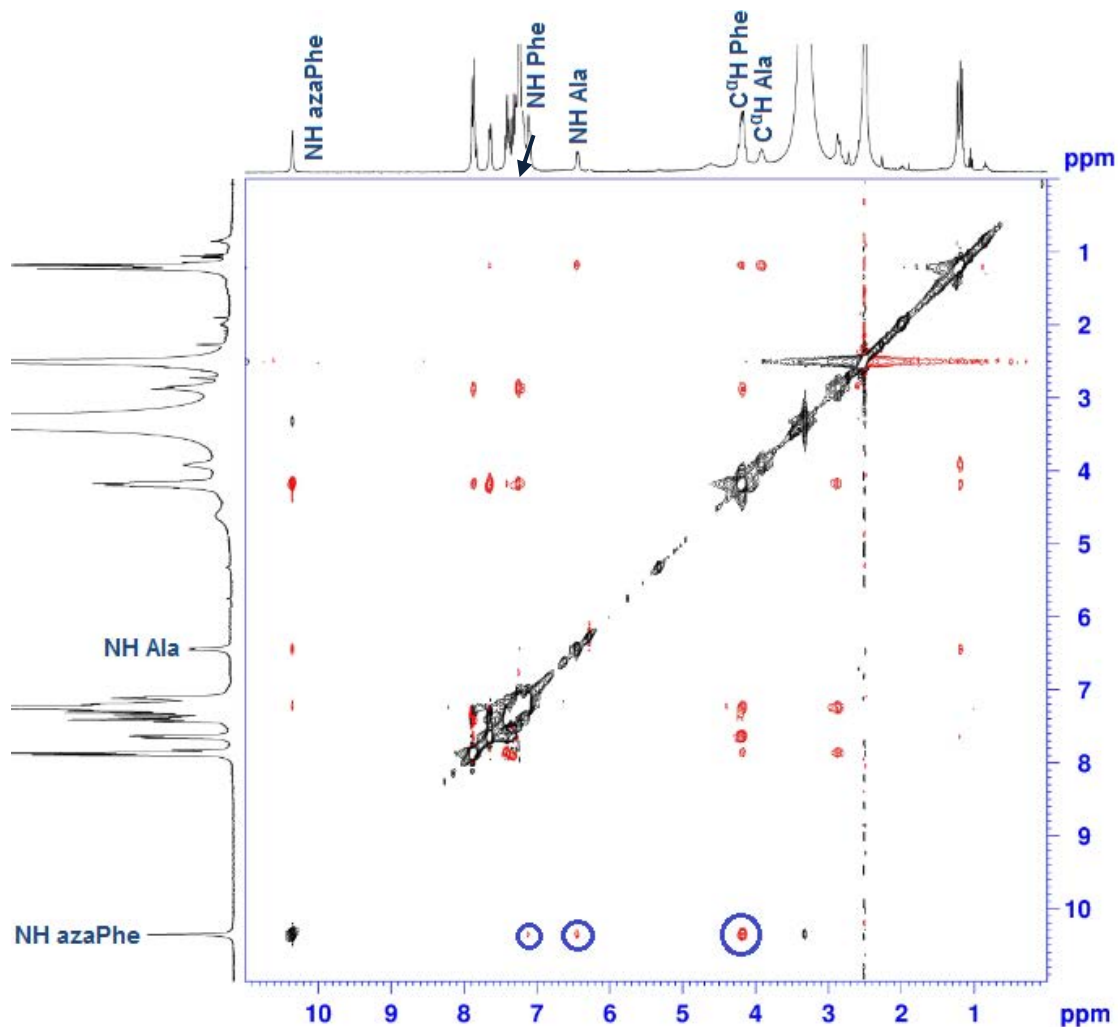


Figure S7.7. 2D ROESY spectrum illustrating the correlations of β -turn conformation in compound 7a'; (300 MHz, 4.0 mmol. L⁻¹, DMSO-*d*₆).

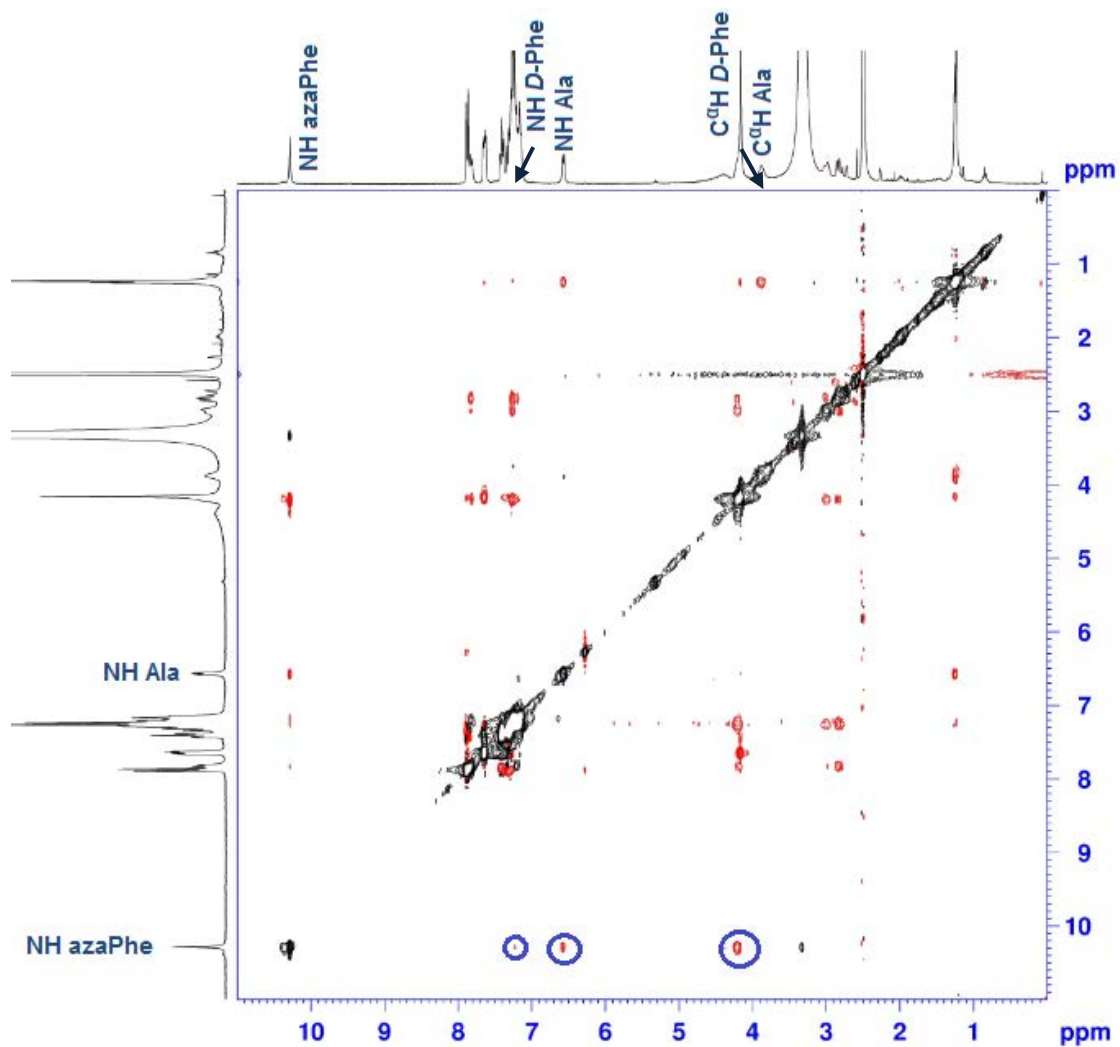


Figure S7.8. 2D ROESY spectrum illustrating the correlations of β' -turn conformation in compound **7b'**; (300 MHz, 4.0 mmol. L⁻¹, DMSO-*d*₆).

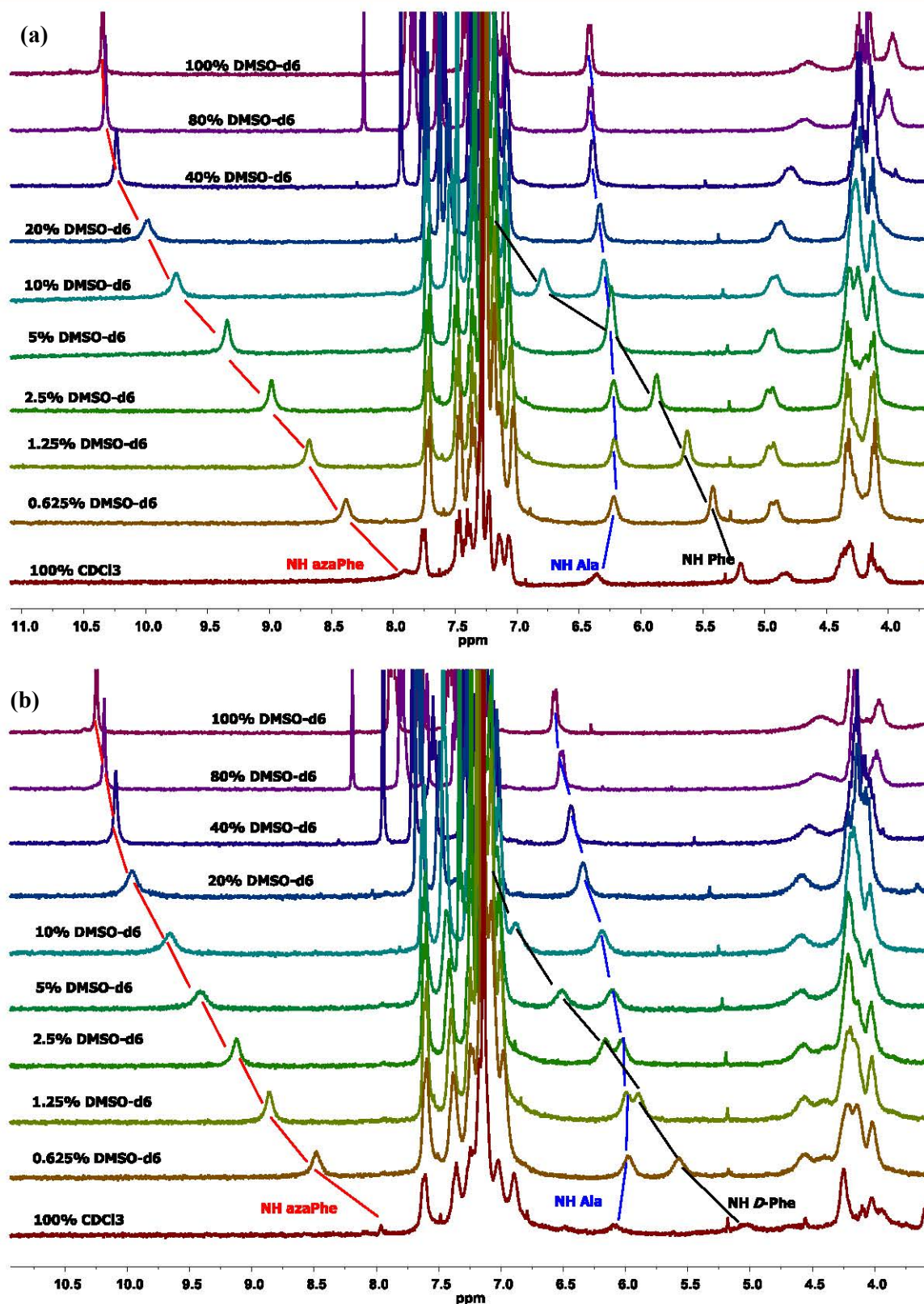


Figure S7.9. Chemical shift-variations (δ) ppm of NH protons for: (a) **7a'**, and (b) **7b'** as a function of % $[\text{CDCl}_3/\text{DMSO-}d_6]$ mixtures; (300 MHz, 4.0 mmol. L^{-1}).

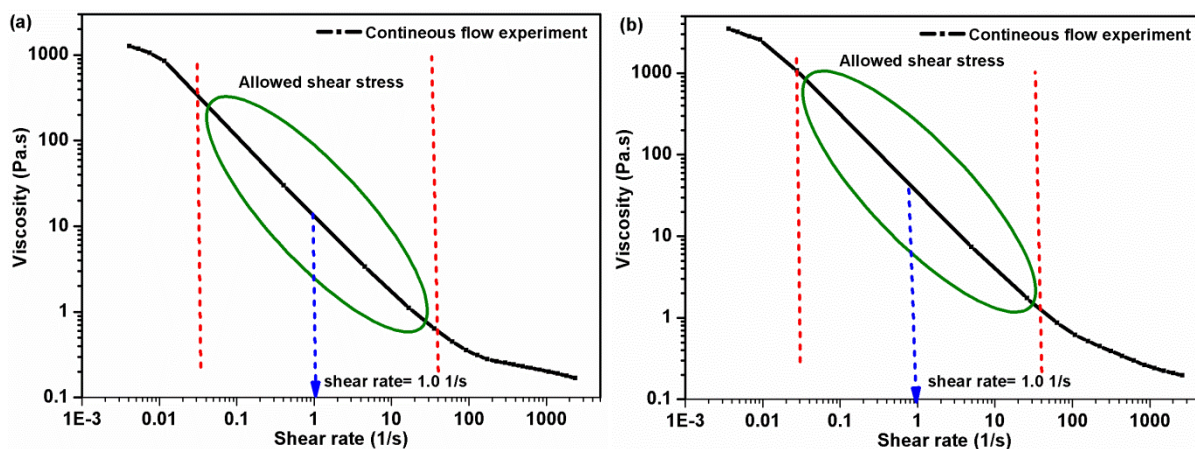
Rheological characterization of low molecular weight hydrogels from **7a'** and **7b'**

Figure S7.12. Determination of the pseudo-viscoelastic region through continuous flow experiment as a function of broad torque range (1 – 10,000 $\mu\text{N}\cdot\text{m}$) for hydrogels from pH 7.0 of: (a) **7a'**, and (b) **7b'**, ($c = 2.0 \text{ wt}\%$, $\omega = 0.63 \text{ rad}\cdot\text{s}^{-1}$, $T = 25 \text{ }^\circ\text{C}$).

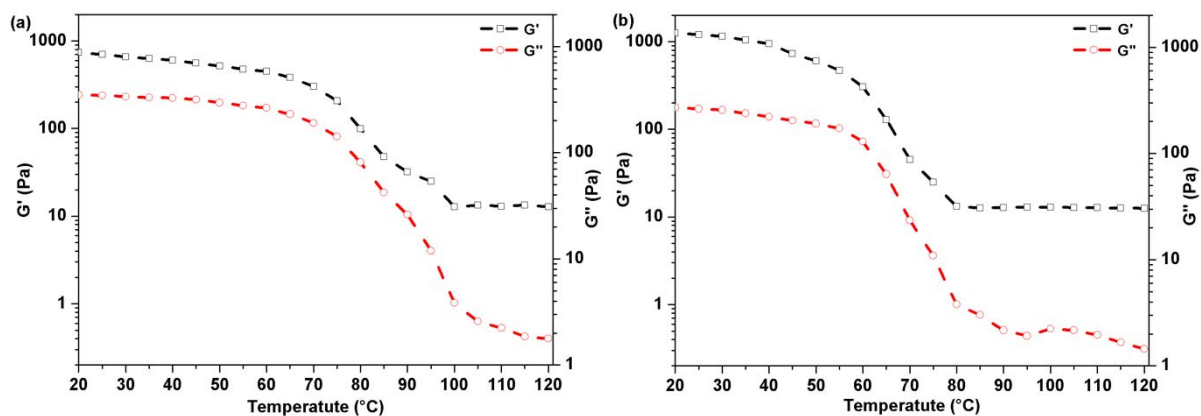


Figure S7.13. Oscillatory temperature sweep experiment performed on hydrogels from pH 7.0 of: (a) **7a'**, and (b) **7b'**; ($c = 2.0 \text{ wt}\%$, $\sigma = 1.5 \text{ Pa}$, $\omega = 0.628 \text{ rad}\cdot\text{s}^{-1}$).

Résumé

Résumé

Les peptides et protéines jouent des rôles essentiels dans le contrôle des fonctions biologiques des organismes vivants et sont, pour beaucoup, basées sur leurs structures tertiaire (3D) et quaternaire. Par conséquent, les études conformationnelles des chaînes polypeptidiques peuvent fournir une meilleure compréhension des relations structure-propriétés. Cependant, la difficulté à synthétiser des protéines et l'instabilité de peptides synthétisés limite leurs potentiels comme des candidats de médicament en raison de : (i) une dégradation rapide par protéases, (ii) une sélectivité basse due à leurs conformations flexibles qui permettent des réactions différents récepteurs et (iii) une faible perméabilité membranaire due à leur caractère hydrophile.

Depuis longtemps, la communauté scientifique s'est intéressée à concevoir de nouvelles petites molécules bio-organiques modifiées possédant des propriétés spécifiques : (i) elles imitent les éléments de structure secondaire des peptides naturels et de protéines telles que les coudes, les feuilles, les hélices, (ii) elles possèdent des propriétés biologiques comparables à celles des analogues naturels, et (iii) elles ont de meilleures propriétés physico-chimiques, cinétiques et thérapeutiques. En particulier, de nombreuses recherches se sont développées sur la synthèse d'oligomères fonctionnalisés possédant des propriétés d'auto-assemblage contrôlé en solution et possédant une structure définie, et des propriétés catalytiques et biologiques imitant les peptides naturels. Ces oligomères font partie de la famille des foldamères et ce champ de recherche initié par Samuel Gellman en 1991 a offert de nouvelles débouchées intéressantes pour les peptides et les mimes peptidiques et pseudopeptides c'est-à-dire qui contiennent des acides aminés modifiés ou des modifications dans le squelette peptidique. Les modifications pseudopeptidiques permettent d'introduire des contraintes qui stabilisent à leur tour des éléments de structures secondaires.

Récemment, au Laboratoire de Chimie Physique Macromoléculaire (LCPM) notre groupe s'est concentré sur le développement de motifs bis-azotés dans lesquels un atome de carbone est remplacé par un atome d'azote et conduisant à des hydrazinopeptides, des aza-peptides et des *N*-aminopeptides par exemple. En plus du développement de voies de synthèse, l'intérêt du groupe a été étendu aux études conformationnelles de ces analogues et pour notre travail de thèse à celles d'azapeptide dans lesquels un ou plusieurs carbones α est remplacé par un (des) atome(s) d'azote.

La conception de nouveaux oligomères [α -aza] a gagné l'intérêt de notre groupe pour plusieurs raisons : (i) le LCPM a montré que l'insertion d'un atome d'azote supplémentaire dans le squelette peptidique pour obtenir des hydrazinopeptides et des *N*-aminopeptides améliore la résistance vers la biodégradation, (ii) Kang-Bong Lee *et al.* ont montré que les aza-acides-aminés favorisent une conformation en coude β préférentielle qui conduit au repliement du pseudopeptide pour permettre dans certains cas le rapprochement des extrémités *N*- et des *C*-terminales et favoriser le processus de cyclisation, enfin (iii) si le squelette est modifié les chaînes latérales sont conservées ce qui est nécessaire pour la reconnaissance de site active dans la protéine.

Au LCPM, Michel Marraud a été le premier à incorporer un motif aza dans des peptides courts d'un, deux et trois résidus. Notre groupe a fait émerger deux familles d'azapeptides avec des propriétés structurales intéressantes : les 1:1- et de 2:1-[α /aza]-oligomères. Dans un premier temps, Cécile Abbas-Quinternet et d'autres ont optimisé une stratégie générale pour la synthèse d'azapeptides en solution, en utilisant la chimie Boc, qui a conduit à la synthèse de différents oligomères linéaires et cycliques. Ensuite, Zhou Zhou a, pendant sa thèse, étendu les études sur ces deux familles en se concentrant sur la synthèse et les études structurales d'oligomères linéaires et cycliques plus longs et permettant des constructions 3D hautement ordonnées et leur conférant des propriétés gélatrices.

La gélation est un phénomène qui reflète la capacité des molécules à s'associer dans des structures hiérarchiques hautement ordonnées (par ex. des fibres, des tubes, des rubans, des hélices, *etc.*). Ces nanostructures s'enchevêtrent et conduisent à un réseau interconnecté tridimensionnel qui est capable d'immobiliser une phase aqueuse ou organique dans les espaces inter-matriciels. Le processus d'auto-assemblage est conduit par de différentes interactions intermoléculaires chimiques et/ou physiques entre les molécules gélatrices ou entre les molécules gélatrices et molécules de solvant dans lesquelles les forces attractives et répulsives sont équilibrées. On peut ainsi considérer que la gélation est une compétition entre la séparation de phase et solubilisation.

Jusqu'à ces dernières années les gels étaient obtenus à partir de molécules polymères ayant un grand rayon hydrodynamique et répondant à des stimuli externes (par exemple la température, le pH, *etc.*). Ces chaînes interagissent les unes avec les autres et forment un réseau continu possédant des propriétés visco-élastiques de solide. Depuis peu de nouvelles familles de molécules gélatrices de faibles poids moléculaires (GFPMs) ont gagné en intérêt. En conséquence, les gels peuvent également être classifiés de plusieurs façons basées sur leur origine (naturel ou synthétique), leur constitution (macromoléculaire ou moléculaire), le type de liaisons inter-moléculaires à l'origine du réseau 3D (chimique ou physique) et les solvants piégés organiques pour organogels, aqueux pour hydrogel, ou séchés pour xero- et aérogels. Le processus d'assemblage qui mène aux gels moléculaires, est devenu un domaine d'étude de grand intérêt en chimie supramoléculaire en raison des applications attendues de ces gels en ingénierie tissulaire, comme agents anti-inflammatoires, matrice de délivrance de produits pharmaceutiques, matrices d'immobilisation d'enzyme ou encore le traitement d'eaux usées.

Plus de mille gélateurs de faible poids moléculaires (GFPMs) ont été reportés dans la littérature. Bien qu'il y ait une grande diversité chimiques et structurelle dans ces GFPMs, ils ont un trait commun, qu'ils piègent les molécules de solvant conduisant à un gel par des phénomènes d'auto-assemblage s'appuyant sur des interactions non-covalentes intermoléculaires électrostatiques, dipôle-dipôle, liaison hydrogène, hydrophobe, empilements π , interactions van der Waals et la balance hydrophylie/lipophilie. Les GFPMs sont dérivés de systèmes variés comme des hydrocarbures, des acides gras, des polysaccharides, des stéroïdes, des amide, des acides aminés, des peptides, des urées, des molécules aromatiques, des complexes de métaux et des dendrimères, *etc.*

En 2001, notre groupe a trouvé par sérendipité un nouveau matériau dérivé d'acides aminés gélifiant le toluène. Les études de conformations 3D et des mécanismes de gélation de ces organogels ont ensuite été établis. Notre groupe s'est alors investi dans la préparation de gels supramoléculaire de pseudo-peptides linéaires et macrocycliques pouvant gélifier différents solvants pour des applications potentielles dans le domaine des matériaux. Deux nouveaux oligomères 1:1- $[\alpha/\alpha\text{-N}^{\alpha}\text{-Bn-hydrazino}]$ cycliques ont montré leurs capacités à s'auto-associer dans le cyclohexane et le toluène, formant un réseau tridimensionnel et formant des organogels thermoréversibles. Les différentes études ont montré que ces organogels supramoléculaires sont stabilisés par des liaisons hydrogènes intermoléculaires et par des interactions π entre les noyaux aromatiques.

Dans la thèse de Zhou Zhou, soutenue au laboratoire en 2014, la synthèse et les études structurales de deux hexamères homo- et de hétéro-chiral cycliques dérivés de (*L*- ou *D*-Phe-azaPhe-Ala)₂ ont été investiguées. Les résultats ont montré qu'alors que l'analogue homochiral pouvait donner des monocristaux offrant ainsi l'accès à la détermination d'une structure 3D hautement ordonnée, aucun cristal de qualité suffisante pour la diffraction des rayons X n'avait pu être obtenu pour l'analogue hétérochiral mais il montrait une propriété fascinante de formation de gel dans le toluène. Ces comportements intéressants ont suscité quelques interrogations et idées pour le travail actuel :

Résumé

- (i) est-ce que c'est possible d'obtenir des monocristaux et résoudre la structure de l'analogue hétérochiral pour la comparer à celle de l'analogue homochiral ?
- (ii) comment la chiralité affecte-t-elle leur propriétés d'auto-association des deux macrocycles ? et pourquoi seul l'analogue hétérochiral conduit à des organogels ?
- (iii) est-il possible d'obtenir des organogels des deux macrocycles dans d'autres solvants ? et si oui
- (iv) quelles sont les propriétés caractéristiques de ces organogels d'un point de vue mécanique, thermique, morphologique, *etc.*
- (v) est-il possible d'obtenir des hydrogels en changeant les chaînes latérales par exemple ?
- (vi) est-ce que la famille 2:1-[α /aza]-pseudopeptides offre une promesse d'applications futures intéressantes ?

Ces questions ont constitué les objectifs et leurs réponses les apports de ce travail de thèse.

Après un état de l'art formulé à partir d'une recherche bibliographique fournie, les résultats ont été présentés en cinq points :

- (1) La synthèse de nouveaux oligomères 2:1-[α /aza] dans lesquels des résidus lysine sont incorporés.
- (2) Les études structurales des oligomères synthétisés, par Résonance Magnétique Nucléaire (RMN), spectroscopie infrarouge (IRTF), diffraction de rayons X (RDX) associés à des calculs de dynamique moléculaire, en se concentrant sur l'effet de chaînes latérales de la lysine et de la longueur du squelette sur les conformations de ces oligomères.
- (3) L'étude des corrélations entre les modifications structurales des azapeptides synthétisés et l'obtention de gels à partir de ces molécules de faible poids moléculaire.
- (4) L'étude des corrélations entre les conformations des gélateurs (par RMN, diffraction de rayons X et calculs de dynamique moléculaire), la caractérisation des gels formés par des techniques physico-chimiques telles que la RMN, la IRTF, le dichroïsme circulaire (CD), la spectroscopie UV visible, la fluorescence, et les caractéristiques visco-élastique et de morphologie des matériaux obtenus par rhéométrie et microscopies MEB et MET.
- (5) Enfin, quelques applications potentielles pour les 2:1-[α /aza]-oligomères ont été envisagées et les premiers tests réalisés.

Cette thèse intitulée “Synthèse et études structurales et supramoléculaires d'oligomères 2:1-[α /aza] linéaires et cycliques” a permis de mettre en évidence de nombreuses propriétés des molécules de la famille des azapeptides. De nouveaux composés ont été synthétisés en incorporant l'acide aminé lysine et en utilisant la chimie Boc pour protéger l'extrémité *N*-terminale. La stratégie générale de synthèse de nouveaux oligomères mixtes 2:1-[α /aza] cycliques s'est appuyée sur des travaux déjà réalisés au LCPM et a poursuivi des travaux sur les études structurale et conformationnelles d'azapeptides cycliques en solution et/ou en phase solide lorsque des monocristaux ont été obtenus. La modification de l'extrémité de *N*-terminale a conduit à l'obtention des hydrogels. Les caractérisations des gels supramoléculaires ont été établies en utilisant différentes techniques physico-chimiques et rhéologiques.

Résumé

La stratégie de synthèse choisie utilise la chimie de Boc pour la synthèse des nouveaux azapeptides, en particulier parce que les produits dérivés du Boc peuvent être facilement éliminés tout en permettant l'obtention des produits avec de bons rendements. Cette stratégie est également basée sur l'utilisation d'un noyau benzyle comme la chaîne latérale sur l'atome N^α ce qui présente plusieurs avantages : (i) soutien du repliement et de l'auto-assemblage, (ii) augmentation de la stabilité de l'assemblage peptidique par des interactions π , (iii) réduction de la flexibilité grâce à son noyau phényle et (iv) augmentation de l'hydrophobicité nécessaire au processus d'hydrogélation.

Seules de rares études rapportent dans la littérature, les effets de l'introduction d'un acide aminé chargé sur la conformation d'azapeptides et l'assemblage moléculaire des peptides, par conséquent, nous avons choisi d'introduire la lysine dans les oligomères 2:1-[α /aza]. Notre hypothèse étant que la chaîne latérale pouvait nous permettre d'optimiser le rapport hydrophilicité/lipophilicité et conduire à des hydrogels. Le choix d'obtenir des hydrogels a été motivé par la promesse d'applications médicales ou dans les domaines de l'environnement.

Dans **la partie A** de cette thèse, nous avons rapporté la synthèse en solution et aux études structurales de 2:1-[α /aza]-oligomères linéaires et cycliques. Les études par RMN et par spectroscopie infrarouge (IRTF) ont montré que tous les oligomères synthétisés, Boc-(*L*- ou *D*-X-azaPhe-Y)_n-OMe ; (X = Phe ou Lys (Z), Y = Ala ou Lys (Z), n = 1 trimère, n = 2 hexamère), pouvaient présenter des propriétés d'auto-assemblage en phase cristalline en partant d'un coude β en solution mais ils ne conduisent pas à des gels, des calculs de dynamique moléculaires sur ces mêmes oligomères ont également montré que les chaînes latérales des résidus lysines sont impliquées dans les liaisons hydrogènes intramoléculaires avec les groupes amides du squelette peptidique, ce qui entraînerait des angles de torsion du squelette peu favorables à un empilement régulier.

Dans les études précédemment réalisées au LCPM, les calculs de dynamiques moléculaires à partir de contraintes RMN ont montré que les hexamères linéaires Boc-(*L*- ou *D*-Phe-azaPhe-Ala)₂-OMe adoptent une forme cyclique presque fermée qui induit la proximité spatiale des extrémités *N*- et *C*-terminales favorisant la macrocyclization de ces oligomères linéaires. Nous avons poursuivi ce projet et étudié les composés macrocycliques correspondants afin d'évaluer leurs propensions à former des objets supramoléculaires hautement ordonnés. Cette partie a mis en évidence, en utilisant plusieurs techniques (rayons X, RMN et IRTF), que les hexamères homo- et hétérochiral cyclo-(*L*- ou *D*-Phe-azaPhe-Ala)₂ adoptent en solution des conformations, parmi lesquelles des coudes β stabilisés par des liaisons hydrogènes intramoléculaires en fermant un pseudo-cycle de 10 atomes. D'autre part il a été également observé sur les monocristaux des interactions de type empilements π intra- et intermoléculaire entre les cycles aromatiques. Par conséquence, les molécules ont la capacité de s'organiser en un réseau tubulaire tridimensionnel hautement ordonné soutenu par les interactions non-covalentes de type liaison hydrogène et empilements π . Ce travail a été publié avec le titre "Impact of C^α-Chirality on Supramolecular Self-Assembly in Cyclo-2:1-[α /aza]-Hexamers (*L*- / *D*-Phe-azaPhe-Ala)₂" dans European Journal of Organic Chemistry (2017), DOI : 10. 1002/ejoc. 201700555.

Dans **la partie B** nous avons exploré plus loin le phénomène d'auto-assemblage des oligomères 2:1-[α /aza] et analysé plusieurs milieux et la formation d'organogels ou d'hydrogels. Nous avons alors constaté que seul l'hexamère cyclo-(*D*-Phe-azaPhe-Ala)₂ pouvait présenter des propriétés d'auto-assemblage dans les solvants aromatiques (toluène, benzène, *p*-xylène et chlorobenzène) pour former des organogels supramoléculaires thermoréversibles. Afin de caractériser ces gels, leurs explorations à partir de méthodes spectroscopiques et rhéologiques ont permis de quantifier leurs propriétés thermiques et mécaniques. Les textures des différents gels ont été menées à partir d'image

MEB et MET sur des aérogels c'est-à-dire des gels séchés sous conditions supercritiques confirment l'organisation du matériau et révèle des fibres.

Le développement d'hydrogels supramoléculaires à partir des oligomères 2:1-[α /aza] présentait un intérêt pour notre groupe pour d'une part montrer, le caractère modulable des molécules et la possibilité d'obtenir des gels dans différentes conditions y compris aqueuses, et d'autre part pour leurs applications potentielles intéressantes dans le domaine biomédical ou en cosmétologie. Deux nouveaux hydrogélateurs de faible poids moléculaire (HGFPMs) ont été développés à partir des oligomères 2:1-[α /aza]. Seulement quelques modifications de l'azapeptides protégé en *N*-terminal ont été nécessaires, puisqu'il a suffi de remplacer le groupement Boc par le groupement Fmoc. En faisant varier les protections en *C*-terminal certains trimères 2:1-[α /aza] ont formé des hydrogels à pH 7 et 10. Le groupement Fmoc a été choisi en raison du groupe flourenyl qui contient et qui présente certains avantages comme : (i) une stabilité accrue par les interactions aromatiques π - π , (ii) une diminution de la flexibilité, et (iii) l'augmentation hydrophobicité nécessaire à la formation d'hydrogel. Les rayons X, la RMN et la spectroscopie infrarouge IRTF ont montré que les deux trimères (Fmoc-*L*- ou *D*-Phe azaPhe-Ala-OH) pouvaient adopter une conformation en coude β stabilisés par une liaison hydrogène intramoléculaire et des interactions d'empilements π , en solution et à l'état cristallin. Grâce à la spectroscopie UV et des spectres d'émission de fluorescence nous avons pu confirmer la présence d'empilements π entre les noyaux aromatiques. Une analyse par dichroïsme circulaire des hydrogels a reflété que deux des molécules hydrogélatrices s'organisent en feuillet β supramoléculaire conformément à ce qui a déjà été observé par ATR-IRTF. Enfin des études rhéologiques ont confirmé le comportement solide des hydrogels ($G' > G''$) et les images de MEB des xérogels ont montré la structure fibreuse.

La partie C est consacrée à l'évaluation du potentiel des oligomères 2:1-[α /aza] linéaires et cycliques dans certaines applications. Dans cette partie, nous résumons les résultats préliminaires dans deux applications liées à des questions environnementales : le premier concerne l'essai de différents azapeptides comme additifs à des membranes polymères pour la séparation du gaz CO₂/N₂. La fusion d'oligomères 2:1-[α /aza] contenant des résidus lysine protégés ou déprotégés sur la chaîne latérale, dans des membranes Pebax[®] commerciales a révélé de bonnes performances comparées à la membrane nue et à d'autres additifs en particulier des oligomères sans lysine. En particulier, l'azapeptide contenant une lysine déprotégée a montré sélectivité et perméabilité meilleure que la membrane Pebax[®] de référence.

La deuxième application a évalué le potentiel de l'héxamère hétérochiral cyclique (*D*-Phe-azaPhe-Ala)₂ pour le traitement des eaux polluées par gélation sélective de phases (GSP). L'héxamère hétérochiral cyclique (*D*-Phe-azaPhe-Ala)₂ présente de fortes propriétés de gélation. Il a été testé pour gélifier sélectivement des solvants organiques dans un mélange (aqueux/organique) avec des pourcentages de récupération variant de 77 à 96 %.

Toutes nos observations sur cette famille d'azapeptide nous permettent de conclure que le motif aza joue un rôle important dans la structuration du squelette peptidique malgré la nature et la chiralité des acides aminés ainsi que la longueur des pseudopeptides. L'étude a mis en évidence que le phénomène d'auto-assemblage est stabilisé par des interactions non-covalentes et conduit à des organogels ou hydrogels supramoléculaires. Nous avons constaté que la chiralité et le désordre jouent un rôle sur l'organisation supramoléculaire des héxamères cyclo-(*L*- ou *D*-Phe-azaPhe-Ala)₂ qui font que seul l'analogue hétérocyclique forme des organogels.

Résumé

Les peptides offrent également plusieurs points de variations qui permettent de jouer sur la balance entre les critères hydrophobes et hydrophiles et en modulant la structure primaire de nos pseudopeptides nous avons pu obtenir des hydrogels à partir des oligomères 2:1-[α /aza]. Cette variabilité permet un choix de modulation du matériau qui va depuis le solvant/milieu gélifié jusqu'aux propriétés rhéologiques des matériaux, offrant ainsi de nombreuses possibilités pour les applications. Les premiers résultats étant encourageants, ils nous permettent d'entrevoir de nombreuses applications, dont certaines sont déjà en cours.

Abstract

Synthesis, structural and supramolecular studies of linear and cyclic 2:1-[α /aza]-oligomers

Keywords: azapeptides, cyclooligomers, hydrogen bond, organogels, hydrogels, self-assembly

The first part of this thesis reported the synthesis and structural studies of linear and cyclic 2:1-[α /aza]-oligomers possessing hydrophobic and/or basic amino acids (lysine). NMR and FTIR results demonstrated that the oligomers could adopt β -turn conformations in solution. Molecular dynamic calculations for oligomers based lysine residues reflected the important role of the aza-motif(s) in structuring the backbones regardless the chirality and nature of the amino acids. In the other hand, X-ray, FTIR, and NMR studies showed that homo- and heterochiral cyclo-(*L*- or *D*-Phe-azaPhe-Ala)₂-hexamers adopt β -turn conformations in solution and solid states. Both molecules could organize into 3D highly ordered structures stabilized by hydrogen bonds and π -stacking. The second part reflected the propensity of some 2:1-[α /aza]-oligomers to self-assemble in some solvents to form supramolecular gels. Interestingly, the heterochiral cyclo-(*D*-Phe-azaPhe-Ala)₂-hexamer could form organogels. The spectroscopic and rheological studies of the organogels revealed good thermal and mechanical stability with solid-like behavior. SEM and TEM images of the aerogel showed fibrous structure. Furthermore, two hydrogelators, Fmoc-*D*- or *L*-Phe-azaPhe-Ala-OH, have been developed and they could achieve hydrogels at pHs 7.0 and 10.0. UV and Flu studies demonstrated that the hydrogels are supported by π -stacking between the aromatic groups. CD analysis reflected that the two hydrogelators self-assemble into β -sheet like structure in consistent with ATR-FTIR results. Both hydrogels exhibited solid-like behavior through rheological studies and the SEM analysis of the xerogels revealed fibrous structure. The third part offered two applications; (i) oligomers based lysine residues reflected good performances in CO₂/N₂ separation when used as additives in polymeric Pebax[®] membrane, and (ii) the heterochiral cyclo-(*D*-Phe-azaPhe-Ala)₂-hexamer is suitable for phase selective gelation with good recovery percentages.

Résumé

Synthèse, études structurales et supramoléculaires de 2:1-[α /aza]-oligomères linéaires et cycliques

Mots-clés: azapeptides, cyclooligomères, liaison hydrogène, organogels, hydrogels, auto-assemblage

La première partie de cette thèse concerne la synthèse et les études structurales de 2:1-[α /aza]-oligomères linéaires et cycliques possédant des acides aminés hydrophobes et/ou basiques. Les études RMN et IRTF ont démontré que les oligomères adopteraient des conformations de type coude β en solution. Les calculs de dynamiques moléculaires des oligomères à base de résidus lysine ont révélé l'importance du motif aza dans le repliement de ces oligomères indépendamment de l'impact de la chaîne latérale. Les études par DRX, IRTF et RMN ont révélé que les deux hexamères cycliques (*L*- ou *D*-Phe-azaPhe-Ala)₂ homo- et hétérochiraux adoptent des conformations de type coude β en solution et à l'état solide. Ils s'organisent en structures 3D très ordonnées, stabilisées par des ponts hydrogènes et des empilements π . La deuxième partie démontre l'auto-assemblage de quelques 2:1-[α /aza]-oligomères dans certains solvants pour former des gels supramoléculaires. Le cyclooligomère hétérochiral (*D*-Phe-azaPhe-Ala)₂ peut former des organogels. La spectroscopie et rhéologie des organogels ont révélé de bonnes stabilités thermique et mécanique avec un comportement de type solide. La MEB/MET de l'aérogel a montré une structure fibreuse 3D. De plus, deux hydrogels Fmoc-*D*- ou *L*-Phe-azaPhe-Ala-OH ont été obtenus aux pH 7.0 et 10.0. Les spectres UV et de fluorescence ont révélé une stabilisation des hydrogels par interaction π entre les groupes aromatiques. Leur analyse par CD montre que les trimères s'auto-assemblent sous forme de feuillet β en accord avec les résultats ATR/IRTF. Ainsi, leurs études rhéologiques ont révélé un comportement de type solide. La MEB des xérogels a montré une structure fibreuse. La troisième partie propose deux applications; (i) les oligomères à base de résidus lysine ont révélé de bonnes performances pour la séparation CO₂/N₂ dans des membranes polymères Pebax[®], et (ii) le cyclohexamère hétérochiral (*D*-Phe-azaPhe-Ala)₂ convient pour la gélification sélective avec un bon pourcentage de récupération.